

Imaging of Inflammation and Infection in Cardiovascular Diseases

Federico Caobelli
Editor

 Springer

Imaging of Inflammation and Infection in Cardiovascular Diseases

Federico Caobelli
Editor

Imaging of Inflammation and Infection in Cardiovascular Diseases

 Springer

Editor

Federico Caobelli
Clinic of Radiology and Nuclear Medicine
Department of Nuclear Medicine
University Hospital of Basel and University of Basel
Basel
Switzerland

ISBN 978-3-030-81130-3 ISBN 978-3-030-81131-0 (eBook)
<https://doi.org/10.1007/978-3-030-81131-0>

© The Editor(s) (if applicable) and The Author(s), under exclusive license to Springer Nature Switzerland AG 2021

This work is subject to copyright. All rights are solely and exclusively licensed by the Publisher, whether the whole or part of the material is concerned, specifically the rights of translation, reprinting, reuse of illustrations, recitation, broadcasting, reproduction on microfilms or in any other physical way, and transmission or information storage and retrieval, electronic adaptation, computer software, or by similar or dissimilar methodology now known or hereafter developed.

The use of general descriptive names, registered names, trademarks, service marks, etc. in this publication does not imply, even in the absence of a specific statement, that such names are exempt from the relevant protective laws and regulations and therefore free for general use.

The publisher, the authors, and the editors are safe to assume that the advice and information in this book are believed to be true and accurate at the date of publication. Neither the publisher nor the authors or the editors give a warranty, expressed or implied, with respect to the material contained herein or for any errors or omissions that may have been made. The publisher remains neutral with regard to jurisdictional claims in published maps and institutional affiliations.

This Springer imprint is published by the registered company Springer Nature Switzerland AG
The registered company address is: Gewerbestrasse 11, 6330 Cham, Switzerland

Preface

Imaging in the context of inflammatory and infectious cardiac disease is becoming more and more important in clinical practice. Besides known inflammatory and infectious diseases like endocarditis, pericarditis and myocarditis, increasing evidence supports the causal role of immune-inflammatory response in the occurrence of highly diverse cardiac diseases, also including atherosclerosis and post-ischaemic events.

Inflammation is a general reaction to any kind of tissue injury, which is needed for replacement of damaged cells and adequate repair. But as a matter of fact, suppressed or excessive inflammation also may contribute to further aggravation of damage and adverse outcome. In view of the importance of inflammation regarding prognosis, it may be that modification of the inflammatory response could be a crucial therapeutic strategy in the future, able to improve outcome.

In the previous years, many papers in the literature focused on this important topic, especially with regard to inflammatory and infectious cardiac disease, also leading to the draft of national and international guidelines, e.g., the Guidelines of the European Society of Cardiology for the diagnosis and management of infectious endocarditis, wherein a pivotal role for ^{18}F -fluorodeoxyglucose Positron Emission Tomography (PET)/Computed Tomography (CT) in the diagnostic workup is underscored.

Differently from imaging of infectious, granulomatous and infiltrative diseases, the use of cardiac imaging in post-ischaemic inflammation and of culprit, prone-to-rupture coronary plaques is to date still prevalent in a preclinical or research setting, but it is not unrealistic to foresee a more extensive use of non-invasive imaging in the next future, boosted by the need to provide a reliable and robust diagnostic and prognostic assessment.

To summarize the imaging approach in the broad field of inflammatory and infectious cardiac diseases, there is the need for an up-to-date textbook, comprising the most useful and used techniques such as cardiac magnetic resonance (CMR), positron emission tomography (PET), and single photon emission tomography (SPECT). With this book, we hope to cover these needs.

In this book, we specifically address the following important questions:

- Which are the most accurate methods to diagnose a particular inflammatory or infectious heart disease and to guide its appropriate therapeutic approach?

- Which are the most useful methods to risk stratify these patients?
- Which are the new targets and concepts toward which research is moving, allowing for an even better evaluation of the underlying pathophysiological mechanisms in these cardiac diseases?

To answer all these questions, top experts in cardiovascular imaging from leading institutions in Europe agreed to share their knowledge and experience on all the aspects of cardiac inflammation and infection by contributing chapters to this project. We would like to thank the authors for their kind contribution to this textbook.

In this book, the readers will find the most relevant and up-to-date information on this fascinating and challenging area of cardiac imaging. Hence, this book will be an invaluable guide for all professionals involved in the management of cardiac patients: cardiac imagers, nuclear medicine physicians, radiologists, cardiologists, cardiac surgeons, infectiologists, microbiologists, internal medicine specialists, pre-clinical scientists and other specialists who constitute a multidisciplinary team. Never like in the present time, an extensive collaboration among different experts driven by the same ideals should be pursued to provide early identification and treatment of infectious and inflammatory processes, responsible for the occurrence of major cardiac adverse events.

Basel, Switzerland
Basel, Switzerland

Federico Caobelli
Michael J. Zellweger

Contents

Part I Challenges in Patient Preparation

- 1 Challenges in Patient Preparation** 3
Cristina E. Popescu and Federico Caobelli

Part II Non-ischemic Diseases

- 2 Cardiac Sarcoidosis** 11
Philip Haaf, Assuero Giorgetti, Federico Caobelli,
and Michael J. Zellweger
- 3 Cardiac Amyloidosis** 37
Philip Haaf, Irene A. Burger, Michael J. Zellweger, Pankaj Garg,
and Cristina E. Popescu

Part III Ischemic Diseases

- 4 Molecular Imaging of Vulnerable Plaque** 73
Riccardo Laudicella, Kamani Christel, Irene A. Burger,
Sergio Baldari, and Pierpaolo Alongi
- 5 Post-Infarction Inflammatory Alterations** 109
Kim van der Heiden, Boudewijn J. Krenning, Daphne Merkus,
and Monique R. Bernsen

Part IV Infection

- 6 Infection: Pericarditis** 163
Tevfik F. Ismail, Philip Haaf, and Assuero Giorgetti
- 7 Infection: Myocarditis** 191
Tevfik F. Ismail, Alina Hua, Philip Haaf, and Assuero Giorgetti

8 Cardiac Devices Infection. 233
Ismaheel O. Lawal, Andor W. J. M. Glaudemans,
and Mike M. Sathekge

9 Endocarditis. 261
Antti Saraste and Federico Caobelli

Part I

Challenges in Patient Preparation



Challenges in Patient Preparation

1

Cristina E. Popescu and Federico Caobelli

Contents

1.1 Introduction.....	3
1.2 Prolonged Intervals of Fasting.....	4
1.3 Dietary Modifications.....	4
1.4 Pharmacologic Approaches.....	5
1.5 Conclusion.....	6
References.....	7

1.1 Introduction

When ^{18}F -fluorodeoxyglucose positron emission tomography (^{18}F -FDG PET) is performed to detect cardiac infection or inflammation, an adequate suppression of cardiac glucose metabolism plays a pivotal role to increase the interpretability and diagnostic reliability of ^{18}F -FDG PET studies. A challenge faced by this imaging technique is optimizing its ability to distinguish active inflammation lesions from physiological FDG uptake in the myocardium.

According to the Randle cycle, the uptake in normal myocardium is dependent mainly on insulin, blood glucose levels, and blood free fatty acid (FFA) levels. [1] In fact, dietary carbohydrate intake normally triggers insulin secretion, which

C. E. Popescu (✉)

Department of Nuclear Medicine, Kantonsspital Baden, Baden, Switzerland

Department of Health Sciences and Technology, ETH Zürich, Zürich, Switzerland

e-mail: cristina.popescu@ksb.ch

F. Caobelli

Clinic of Radiology and Nuclear Medicine, Department of Nuclear Medicine, University Hospital of Basel and University of Basel, Basel, Switzerland

© The Author(s), under exclusive license to Springer Nature
Switzerland AG 2021

F. Caobelli (ed.), *Imaging of Inflammation and Infection in Cardiovascular Diseases*, https://doi.org/10.1007/978-3-030-81131-0_1

3

activates the predominantly expressed glucose transporter GLUT4 in normal myocardium and allows glucose to enter cells. On the other hand, in inflammatory cells (such as neutrophils, monocytes, and macrophages), glucose enters the cell via type 1 and 3 cellular glucose transporters (GLUT1 and GLUT3) which are overexpressed [2, 3] and ^{18}F -FDG is trapped by phosphorylation [4]. As such, by manipulating the GLUT4 response it is possible to suppress physiologic myocardial glucose consumption independently of inflammatory process [2, 5].

In this regard, several methods to suppress physiological ^{18}F -FDG uptake in the myocardium and minimize false-positive results have been reported: prolonged intervals of fasting, dietary modification, or pharmacological approaches. However, to date no standard protocol has been adopted, although combinations of different protocols have been supported by some studies.

1.2 Prolonged Intervals of Fasting

As in the prolonged fasting state normal myocardial cells use free fatty acids (FFAs) for up to 90% of their oxygen consumption [6], many studies have suggested that using prolonged fasting (4–18 h) may allow to reduce physiologic myocardial ^{18}F -FDG uptake, thus increasing the specificity and sensitivity of PET imaging [7–10].

1.3 Dietary Modifications

A patient preparation including dietary modifications with a high-fat, low-carbohydrate, high-protein diet (HFLC) has also been suggested, in order to shift myocardial metabolism to fatty acid and suppress glucose utilization by normal myocardium [11]. Moreover, the superiority of a HFLC diet compared to fasting only has been demonstrated in a study by Coulden et al. [12], wherein patients following the prescribed dietary regimen showed a significantly lower myocardial FDG uptake. These findings were confirmed by Harisankar et al., wherein the physiologic ^{18}F -FDG uptake was more often adequately suppressed in the diet group (67%) than in a 12-h fast-alone group (52%). [13].

Some other studies expanded on this important topic also showing a significant improvement in myocardial glucose suppression if a prolonged HFLC diet was followed by the patients [14, 15]. In a recent retrospective study, a 72-h pre-test HFLC diet preparation protocol yielded higher rate of FDG uptake suppression than a 48-h dietary regimen [16]. A strategy of adding a high-fat beverage to the HFLC diet just before the ^{18}F -FDG has also been explored but does not appear to have additive benefit [17, 18].

A randomized trial conducted by Demeure et al. [19] compared the effectiveness of four different approaches in a group of 36 volunteers: a HFLC diet followed by

12 h fast, HFCLC diet followed by a high-fat drink 1 h prior to imaging, and a HFCLC meal followed by 12 h fast and oral verapamil. The rationale for adding verapamil is that intracellular calcium is known to increase glucose uptake, and calcium channel antagonism has reduced myocardial ^{18}F -FDG uptake in a mouse model [20]. In their study, the rate of suppression of cardiac glucose metabolism was higher in the group receiving HFCLC diet followed by 12 h fasting compare to the group with HFCLC diet together with a high-fat drink (89% vs 50%). Unfortunately, the use of calcium-channels antagonist did not translate into a significant higher rate of suppression, having no clear benefit over other preparations [19].

1.4 Pharmacologic Approaches

Pharmacologic approaches have also been employed with the aim of manipulating myocardial metabolism. Intravenous administration of unfractionated heparin (UFH) activates lipoprotein and hepatic lipases to increase plasma FFAs levels, causing a suppression of myocardial glucose utilization. In a Japanese study cohort after a fasting period of at least 6 h followed by 50 IU/kg of UFH injected 15 min before application of PET tracer, a robust suppression of cardiac FDG uptake was obtained [9].

A combination of different approaches to reduce physiologic myocardial ^{18}F -FDG uptake has been also used in a few studies, showing that the injection of heparin in addition to HFCLC diet preparation outperforms a dietary preparation without injection [21].

While intriguing due to its intrinsic advantages for the department's workflow, UFH injection alone seems to be less effective than an adequate dietary preparation. In fact, a study by Morooka et al. [22] reported that an 18-h fasting alone resulted in a higher rate of myocardial FDG uptake suppression than a 12-h fasting together with UFH injection. Furthermore, in another study of Manabe et al. [23] patients undergoing cardiac ^{18}F -FDG PET/CT after intravenous injection of UFH showed highest rate of suppression of glucose metabolism for 18 h-HFCLC prior to the examination than 6 h. (Fig. 1.1).

However, the same study also showed that intravenous UFH and a fast of more than 18 h were associated with a significantly lower rate of physiologic myocardial ^{18}F -FDG uptake (22%) than a fast of 18 h without UFH (38%) or a fast of less than 18 h without UFH (69%) [23].

Although there is currently no consensus on the best protocol for suppressing cardiac FDG-uptake, Genovesi et al. [24] provided a proposal for a preparatory schema including a high-fat, low-carbohydrate diet 72 h before the study, a fasting state for at least 6 h and intravenous heparin 15 min before PET tracer administration (Table 1.1).

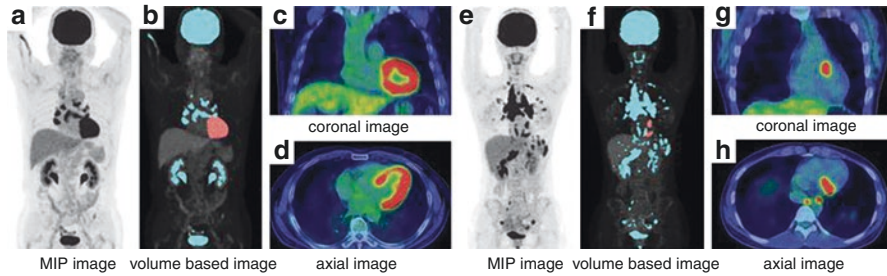


Fig. 1.1 Representative cases. (a–d) shows a 73-year-old man with diffuse LV FDG uptake, who was instructed to fast for a minimum of 6 h and whose FPG and FFA levels were 95 mg/dL and 464 μ Eq/L at baseline. Cardiac metabolic volume was estimated as 166.4 mL. There are multiple abnormal uptakes in mediastinal and hilar lymph nodes. (e–h) shows a 25-year-old woman without diffuse LV FDG uptake, who had over 18 h' fasting with a low-carbohydrate diet. Her FPG and FFA levels were 76 mg/dL and 1924 μ Eq/L at baseline. FDG PET/CT shows focal basal anterior wall uptake. Cardiac metabolic volume was estimated to be 8.3 mL. There are multiple lung uptakes and multiple lymph node uptakes in supraclavicular, mediastinal, hilar, and abdominal regions. Reprinted under the terms of the Creative Commons Attribution 4.0 International License (<https://creativecommons.org/licenses/by/4.0/>) from J Nucl Cardiology 2016; [23] MIP maximum intensity projection

Table 1.1 Proposal for a protocol for patient preparation before undergoing ^{18}F -FDG PET/CT for suspected cardiac sarcoidosis. Reprinted with permission of BJR Publications from Genovesi D et al., Br J Radiol 2019; 92 [24]. No changes were made. AC attenuation correction, ^{18}F -FDG ^{18}F -fludeoxyglucose, IU international unit; PET positron emission tomography, SUV_{max} maximum standardized uptake value, TLG total lesion glycolysis

Dietary preparation	High-fat, low-carbohydrate diet 72 h before the procedure
Fasting state	Min. 6 h before the procedure
Intravenous heparin	3×200 IU heparin at 0, 7 and 15 min
^{18}F -FDG administration	15 min after the last i.v. application of heparin. Dose: 3.5 MBq/kg (max 500 MBq)
Image acquisition	60 min after FDG administration, 90 s/bed position from skull to mid-thigh. Supplemental bed position over the heart (10 min, matrix 256×256). Low-dose CT based AC
Image interpretation	Comparison with ^{82}Rb PET/CT at rest or cardiac MR both AC and non-AC corrected images are separately evaluated. SUV_{max} and TLG are also determined.

1.5 Conclusion

^{18}F -FDG PET/CT is a valuable diagnostic tool in the evaluation of cardiac sites of inflammation and infection. Appropriate patient preparation plays a pivotal role as the diagnostic accuracy of this procedure is affected by the adequate suppression of physiologic glucose uptake of the cardiomyocyte before scanning

References

1. Randle PJ, Garland PB, Hales CN, Newsholme EA. The glucose fatty-acid cycle. Its role in insulin sensitivity and the metabolic disturbances of diabetes mellitus. *Lancet*. 1963;1(7285):785–9. [https://doi.org/10.1016/s0140-6736\(63\)91500-9](https://doi.org/10.1016/s0140-6736(63)91500-9).
2. Yamada S, Kubota K, Kubota R, Ido T, Tamahashi N. High accumulation of fluorine-18-fluorodeoxyglucose in turpentine-induced inflammatory tissue. *J Nucl Med*. 1995;36(7):1301–6.
3. Mochizuki T, Tsukamoto E, Kuge Y, Kanegae K, Zhao S, Hikosaka K, et al. FDG uptake and glucose transporter subtype expressions in experimental tumor and inflammation models. *J Nucl Med*. 2001;42(10):1551–5.
4. Nuutila P, Koivisto VA, Knuuti J, Ruotsalainen U, Teräs M, Haaparanta M, et al. Glucose-free fatty acid cycle operates in human heart and skeletal muscle in vivo. *J Clin Invest*. 1992;89(6):1767–74. <https://doi.org/10.1172/JCI115780>.
5. Miyagawa M, Yokoyama R, Nishiyama Y, Ogimoto A, Higaki J, Mochizuki T. Positron emission tomography-computed tomography for imaging of inflammatory cardiovascular diseases. *Circ J*. 2014;78(6):1302–10. <https://doi.org/10.1253/circj.cj-14-0250>.
6. Wisneski JA, Gertz EW, Neese RA, Mayr M. Myocardial metabolism of free fatty acids. Studies with ¹⁴C-labeled substrates in humans. *J Clin Invest*. 1987;79(2):359–66. <https://doi.org/10.1172/JCI112820>.
7. Blankstein R, Osborne M, Naya M, Waller A, Kim CK, Murthy VL, et al. Cardiac positron emission tomography enhances prognostic assessments of patients with suspected cardiac sarcoidosis. *J Am Coll Cardiol*. 2014;63(4):329–36. <https://doi.org/10.1016/j.jacc.2013.09.022>.
8. Ishida Y, Yoshinaga K, Miyagawa M, Moroi M, Kondoh C, Kiso K, et al. Recommendations for (18) F-fluorodeoxyglucose positron emission tomography imaging for cardiac sarcoidosis: Japanese Society of Nuclear Cardiology recommendations. *Ann Nucl Med*. 2014;28(4):393–403. <https://doi.org/10.1007/s12149-014-0806-0>.
9. Ishimaru S, Tsujino I, Takei T, Tsukamoto E, Sakaue S, Kamigaki M, et al. Focal uptake on 18F-fluoro-2-deoxyglucose positron emission tomography images indicates cardiac involvement of sarcoidosis. *Eur Heart J*. 2005;26(15):1538–43. <https://doi.org/10.1093/eurheartj/ehi180>.
10. Ambrosini V, Zompatori M, Fasano L, Nanni C, Nava S, Rubello D, et al. (18)F-FDG PET/CT for the assessment of disease extension and activity in patients with sarcoidosis: results of a preliminary prospective study. *Clin Nucl Med*. 2013;38(4):e171–7. <https://doi.org/10.1097/RLU.0b013e31827a27df>.
11. Lum DP, Wandell S, Ko J, Coel MN. Reduction of myocardial 2-deoxy-2-[¹⁸F]fluoro-D-glucose uptake artifacts in positron emission tomography using dietary carbohydrate restriction. *Mol Imaging Biol*. 2002;4(3):232–7. [https://doi.org/10.1016/s1095-0397\(01\)00062-0](https://doi.org/10.1016/s1095-0397(01)00062-0).
12. Coulden R, Chung P, Sonnex E, Ibrahim Q, Maguire C, Abele J. Suppression of myocardial 18F-FDG uptake with a preparatory “Atkins-style” low-carbohydrate diet. *Eur Radiol*. 2012;22(10):2221–8. <https://doi.org/10.1007/s00330-012-2478-2>.
13. Harisankar CN, Mittal BR, Agrawal KL, Abrar ML, Bhattacharya A. Utility of high fat and low carbohydrate diet in suppressing myocardial FDG uptake. *J Nucl Cardiol*. 2011;18(5):926–36. <https://doi.org/10.1007/s12350-011-9422-8>.
14. Williams G, Kolodny GM. Suppression of Myocardial 18F-FDG uptake by preparing patients with a high-fat, low-carbohydrate diet. *Am J Roentgenol*. 2008;190(2):W151–6. <https://doi.org/10.2214/ajr.07.2409>.
15. Balink H, Hut E, Pol T, Flokstra FJ, Roef M. Suppression of 18F-FDG myocardial uptake using a fat-allowed, carbohydrate-restricted diet. *J Nucl Med Technol*. 2011;39(3):185–9. <https://doi.org/10.2967/jnmt.110.076489>.
16. Lu Y, Grant C, Xie K, Sweiss NJ. Suppression of myocardial 18F-FDG uptake through prolonged high-fat, high-protein, and very-low-carbohydrate diet before FDG-PET/CT for evaluation of patients with suspected cardiac sarcoidosis. *Clin Nucl Med*. 2017;42(2):88–94. <https://doi.org/10.1097/RLU.0000000000001465>.

17. Kobayashi Y, Kumita S, Fukushima Y, Ishihara K, Suda M, Sakurai M. Significant suppression of myocardial (18)F-fluorodeoxyglucose uptake using 24-h carbohydrate restriction and a low-carbohydrate, high-fat diet. *J Cardiol*. 2013;62(5):314–9. <https://doi.org/10.1016/j.jjcc.2013.05.004>.
18. Cheng VY, Slomka PJ, Ahlen M, Thomson LEJ, Waxman AD, Berman DS. Impact of carbohydrate restriction with and without fatty acid loading on myocardial 18F-FDG uptake during PET: a randomized controlled trial. *J Nucl Cardiol*. 2010;17(2):286–91. <https://doi.org/10.1007/s12350-009-9179-5>.
19. Demeure F, Hanin F-X, Bol A, Vincent M-F, Pouleur A-C, Gerber B, et al. A randomized trial on the optimization of 18F-FDG myocardial uptake suppression: implications for vulnerable coronary plaque imaging. *J Nucl Med*. 2014;55(10):1629–35. <https://doi.org/10.2967/jnumed.114.138594>.
20. Gaeta C, Fernández Y, Pavía J, Flotats A, Artigas C, Deportos J, et al. Reduced myocardial 18F-FDG uptake after calcium channel blocker administration. Initial observation for a potential new method to improve plaque detection. *Eur J Nucl Med Mol Imaging*. 2011;38(11):2018–24. <https://doi.org/10.1007/s00259-011-1873-2>.
21. Scholtens AM, Verberne HJ, Budde RP, Lam MG. Additional heparin Preadministration improves cardiac glucose metabolism suppression over low-carbohydrate diet alone in ¹⁸F-FDG PET imaging. *J Nucl Med*. 2016;57(4):568–73. <https://doi.org/10.2967/jnumed.115.166884>.
22. Morooka M, Moroi M, Uno K, Ito K, Wu J, Nakagawa T, et al. Long fasting is effective in inhibiting physiological myocardial 18F-FDG uptake and for evaluating active lesions of cardiac sarcoidosis. *EJNMMI Res*. 2014;4(1):1. <https://doi.org/10.1186/2191-219X-4-1>.
23. Manabe O, Yoshinaga K, Ohira H, Masuda A, Sato T, Tsujino I, et al. The effects of 18-h fasting with low-carbohydrate diet preparation on suppressed physiological myocardial (18)F-fluorodeoxyglucose (FDG) uptake and possible minimal effects of unfractionated heparin use in patients with suspected cardiac involvement sarcoidosis. *J Nucl Cardiol*. 2016;23(2):244–52. <https://doi.org/10.1007/s12350-015-0226-0>.
24. Genovesi D, Bauckneht M, Altini C, Popescu CE, Ferro P, Monaco L, et al. The role of positron emission tomography in the assessment of cardiac sarcoidosis. *Br J Radiol*. 2019;92(1100):20190247. <https://doi.org/10.1259/bjr.20190247>.

Part II

Non-ischemic Diseases



Cardiac Sarcoidosis

2

Philip Haaf, Assuero Giorgetti, Federico Caobelli,
and Michael J. Zellweger

Contents

2.1	Introduction.....	12
2.2	Screening for Cardiac Sarcoidosis.....	12
2.3	Diagnosis.....	13
2.4	Endomyocardial Biopsy: Imaging Guidance.....	14
2.5	CMR for Diagnosis/CMR Imaging Protocol.....	15
2.6	Late Gadolinium Enhancement (LGE).....	17
2.7	Imaging Myocardial Inflammation and Quantitative Tissue Characterization with CMR T1 and T2 Mapping.....	17
2.8	Additional CMR Findings Suggestive of Cardiac Sarcoidosis.....	20
2.9	Differential Diagnosis.....	20
2.10	Treatment: Anti-Inflammatory Therapy.....	20
2.11	CMR for Arrhythmogenic Risk Stratification/ICD.....	22
2.12	Positron Emission Tomography.....	23
2.13	Positron Emission Tomography with Tracers Other than ¹⁸ F-FDG.....	23
2.14	Prognosis.....	27
2.15	Follow-up and Monitoring of Anti-Inflammatory Response.....	28
2.16	Hybrid PET-CMR Imaging.....	29

P. Haaf (✉) · M. J. Zellweger
Clinic of Cardiology, University Hospital Basel, Basel, Switzerland

Cardiovascular Research Institute Basel (CRIB), University Hospital Basel,
Basel, Switzerland
e-mail: Philip.haaf@usb.ch

A. Giorgetti
Nuclear Medicine Unit, Fondazione CNR/Regione Toscana “Gabriele Monasterio”,
Pisa, Italy

F. Caobelli
Clinic of Radiology and Nuclear Medicine, Department of Nuclear Medicine, University
Hospital of Basel and University of Basel, Basel, Switzerland

© The Author(s), under exclusive license to Springer Nature
Switzerland AG 2021

F. Caobelli (ed.), *Imaging of Inflammation and Infection in Cardiovascular
Diseases*, https://doi.org/10.1007/978-3-030-81131-0_2

2.17 Outlook.....	30
2.18 Conclusion.....	31
References.....	31

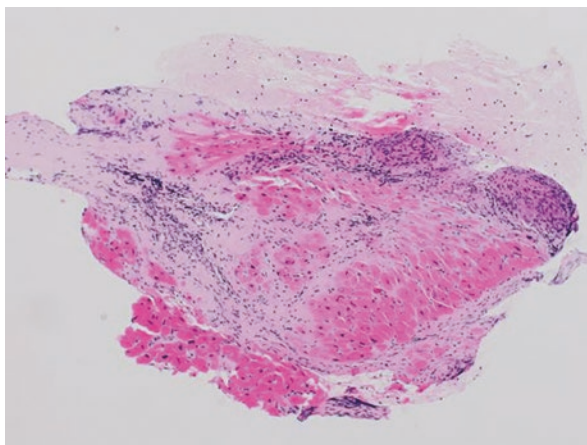
2.1 Introduction

Sarcoidosis is a multisystem inflammatory disorder of unknown aetiology resulting in the formation of non-caseating granulomas, primarily in the lungs, lymph nodes, skin, gastrointestinal system, eye, central nervous system and the heart (Fig. 2.1). Highest rates are reported in northern Europe and African Americans and in women with a worldwide prevalence of about 5 to 64 in 100.000 [1]. Cardiac involvement is clinically silent in the early stages and occurs in approximately a quarter of patients with extra-cardiac sarcoidosis in post-mortem studies and up to 40% in studies with advanced imaging (CMR/PET) [2–5]. Eventually, it may, in order of frequency, disrupt the cardiac electrical system leading to conduction abnormalities and arrhythmias, affect heart mechanics causing heart failure and lead to sudden cardiac death (Fig. 2.2). Thus, there is a clinical need to early identify patients with cardiac involvement of sarcoidosis.

2.2 Screening for Cardiac Sarcoidosis

Current guidelines recommend screening for silent cardiac sarcoidosis (CS) in patients with proven extra-cardiac sarcoidosis. Initial work-up for CS includes history, physical examination, as well as transthoracic echocardiography and ECG. In spite of their low sensitivity for CS, abnormal ECG or Holter monitoring findings (such as new atrioventricular block, frequent premature ventricular complexes and

Fig. 2.1 Myocardial sarcoidosis with partly granulomatous lymphohistiocytic myocardial inflammation and patchy fibrosis (100x, haematoxylin and eosin stain). There is usually no or only limited necrosis within sarcoid granulomas, unlike those associated with *Mycobacterium tuberculosis* infection. Courtesy of Prof. Katharina Glatz, Department of Pathology, University Hospital Basel, Switzerland



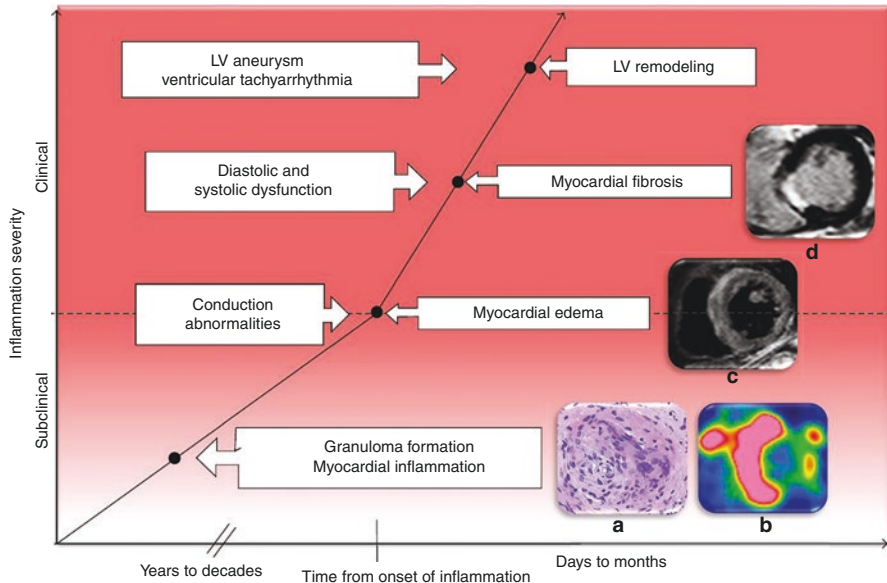


Fig. 2.2 Imaging and inflammation cascade. Schematic representation of disease progression with myocardial inflammation, oedema, fibrosis and remodelling. Granuloma formation (a), ^{18}F -FDG PET of myocardial inflammation (b), cardiac magnetic resonance imaging of myocardial oedema (c) and cardiac magnetic resonance imaging of myocardial fibrosis (d) are shown. ^{18}F -FDG PET: ^{18}F -fluorodeoxyglucose positron emission tomography. From Orii et al. [6]

ventricular tachycardia) should prompt further investigation. A high-resolution CT chest scan may detect or exclude mediastinal or bi-hilar lymphadenopathy. CMR and ^{18}F -FDG PET are the most sensitive and specific advanced imaging tests for the detection of CS.

2.3 Diagnosis

Angiotensin converting enzyme (ACE), serum amyloid A and adenosine deaminase have been tested with respect to their diagnostic value and their potential role in the context of disease monitoring. However, there was no clear evidence of their usefulness [7]. In untreated patients with sarcoidosis, ACE levels were elevated in 75% of patients. The sensitivity and specificity of high ACE for diagnosis of sarcoidosis were 41% (95% CI 35–48%) and 90% (95% CI 89–91%), respectively. The PPV and NPV in this population were 25% (95% CI 21–30%) and 95% (95% CI 85–87%) [8]. Elevated Interleukin-2 levels may help to identify patients with extra-pulmonary organ involvement [7]. Elevated high-sensitivity cardiac troponin levels can be observed in cardiac sarcoidosis patients. Troponin levels decrease after initiation of adequate therapy. Moreover, elevated troponin in CS patients is closely associated with future adverse events [9]. In 62 patients presenting with CS, high-sensitivity cardiac troponin was elevated in 52–58% of them [9].

Table 2.1 Adapted from Birnie et al. [14] LVEF denotes left ventricular ejection fraction, VT ventricular tachycardia, PET positron emission tomography, CS cardiac sarcoidosis and LGE late gadolinium enhancement

Heart rhythm society criteria for cardiac sarcoidosis diagnosis	
Histologic diagnosis-definite	Clinical diagnosis-probable
Positive endomyocardial biopsy (non-caseating granulomas) without alternate aetiology <i>NB: Endomyocardial biopsy for cardiac sarcoidosis only has a 20–30% sensitivity (sampling error)</i>	Extra-cardiac sarcoid (biopsy-proven) and ≥ 1 of the following (other causes excluded) <ul style="list-style-type: none"> • Steroid/immunosuppressant-responsive cardiomyopathy or heart block. • Unexplained LVEF <40%. • Unexplained sustained VT. • 2nd (type II) or third degree heart block • Focal uptake on cardiac PET (CS pattern). • LGE on CMR (CS pattern).

The diagnosis of CS is challenging in most cases. Guidelines recommend a combination of clinical, electrocardiographic and imaging findings (mainly CMR and PET/CT) if endomyocardial biopsy has not been done or cannot confirm the diagnosis.

The revised 2006 Japanese Ministry of Health and Welfare (JMH) diagnostic guidelines [10] require histologic confirmation of cardiac involvement or clinical confirmation via a combination of major and minor criteria. The JMH guidelines classify Gallium-67 uptake as a major imaging criterion even though this test is no longer performed at most centres due to its limited diagnostic accuracy. JMH criteria have performed poorly when compared to diagnostic accuracy by advanced imaging, reflecting that CMR and ^{18}F -FDG-PET have a higher sensitivity than these criteria [5, 11–13].

A more contemporary set of clinical criteria for the diagnosis of CS has been proposed by the Heart Rhythm Society (HRS) [14] (Table 2.1). The HRS 2014 criteria acknowledge the inherent uncertainty related to diagnosing CS and state that “it is probable that CS is present” (>50% likelihood) if there is a histological diagnosis of extra-cardiac sarcoidosis and that the patient meets one or more of several criteria (Table HRS Criteria for CS Diagnosis). These HRS criteria cannot be used for the diagnosis of isolated CS because an extra-cardiac biopsy-proven sarcoidosis is necessary. Accordingly, the absence of extra-cardiac sarcoidosis should not be used to exclude cardiac sarcoidosis.

Since no gold standard diagnostic criteria exist for the diagnosis of cardiac sarcoidosis, clinicians must combine clinical data suggesting elevated pre-test probability for CS together with advanced cardiac imaging (Fig. 2.3).

2.4 Endomyocardial Biopsy: Imaging Guidance

Endomyocardial biopsy (EMB) is the most specific detection method for CS, and only a positive endomyocardial biopsy can definitively establish the diagnosis of CS [14]. Yet, unless an endomyocardial biopsy is guided by imaging (CMR or PET)

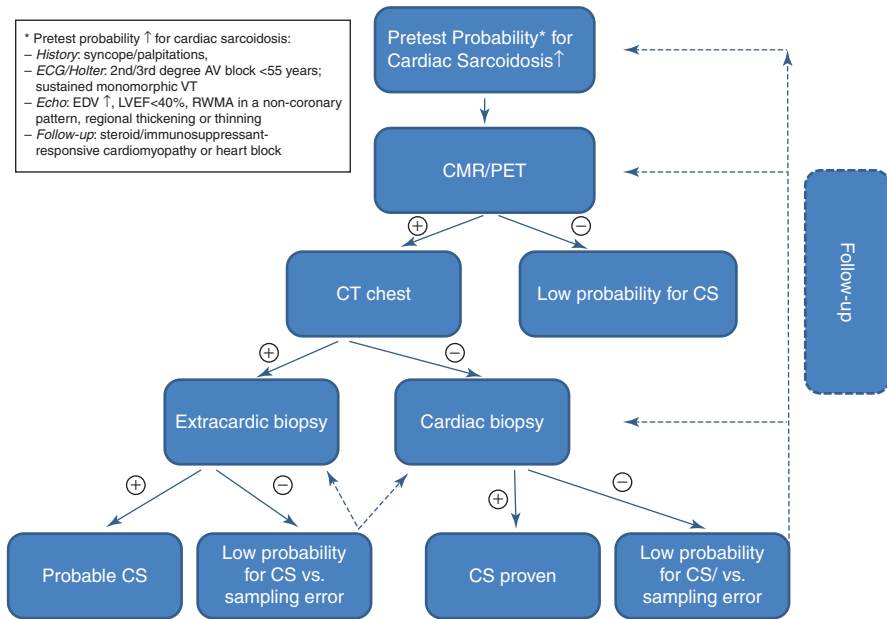


Fig. 2.3 Proposed algorithm for the diagnosis of cardiac sarcoidosis. CS denotes cardiac sarcoidosis, AV block atrioventricular block, VT ventricular tachycardia, EDV end-diastolic volume, LVEF left ventricular ejection fraction, RWMA regional wall motion abnormality

[15], the diagnostic yield of a sample taken blindly from a myocardium with patchy granulomatous infiltration only reaches 20% [15–18] precluding its routine usage (Fig. 2.4).

In a recent ^{18}F -FDG study of patients ($n = 70$) with a clinical diagnosis of CS, it was shown that patients with positive right ventricle FDG uptake had a significantly higher frequency of positive EMB than those without (42% vs. 6%, $p = 0.024$; overall 21% with positive EMB) (Fig. 2.5) [19].

The diagnostic yield of extra-cardiac biopsy (such as lymph nodes, lung biopsy, etc.) is much higher. Therefore, several criteria for CS have been proposed in the context of biopsy-proven extra-cardiac sarcoidosis (see Table 2.1).

2.5 CMR for Diagnosis/CMR Imaging Protocol

Cardiac sarcoidosis mainly involves three successive histological stages: oedema, granulomatous inflammation and fibrosis leading to post-inflammatory scarring. CMR imaging offers a non-invasive detection of biventricular morphology and function, myocardial oedema and minute regions of fibrosis even in patients with normal LV dimensions and systolic function [20–22]. Late gadolinium enhancement (LGE) is considered the most useful sequence in the diagnosis of CS.

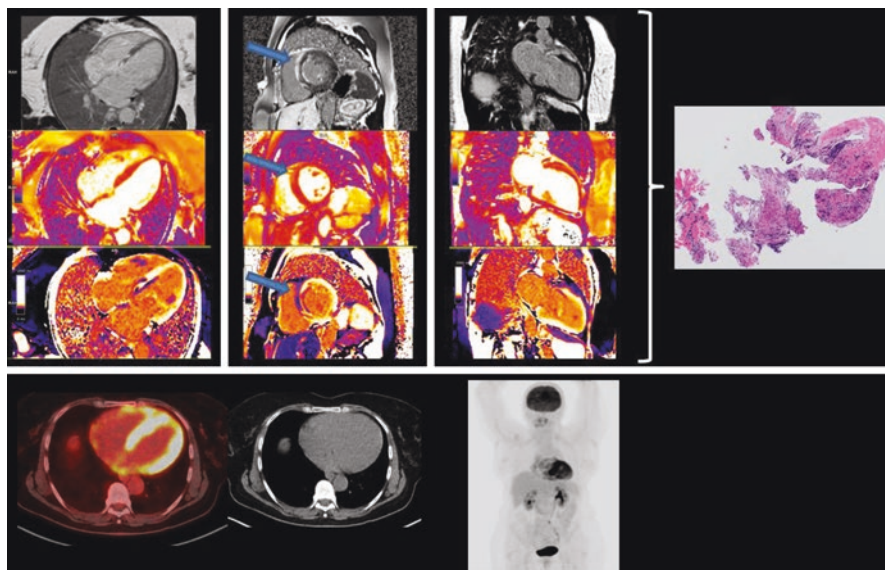
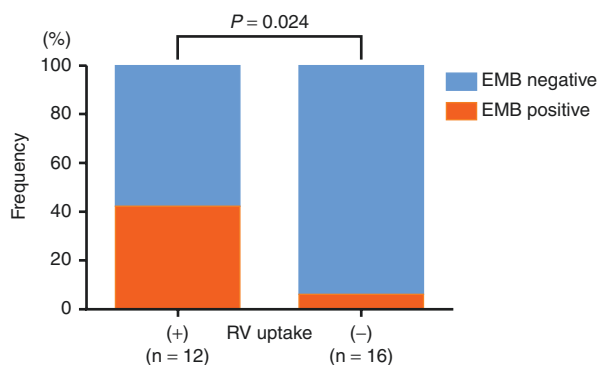


Fig. 2.4 MRI guided septal biopsy (blue arrow) in a patient with isolated cardiac sarcoidosis with complete atrioventricular block. Extensive diffuse fibrosis in the basal and mid septum, basal anterior and inferolateral wall, as well as both papillary muscles. Histopathology (haematoxylin and eosin stain x100) showing inflammation in 1 of 3 biopsies. ^{18}F FDG-PET (lower rows) show a diffuse, intense hypermetabolism within the myocardium but no other organ or lymph node manifestation (Images from University Hospital, Basel, Switzerland; Histopathology image courtesy of Prof. Katharina Glatz, University Hospital, Basel, Switzerland)

Fig. 2.5 Relationships between right ventricular ^{18}F FDG uptake and EMB results. From Omote et al. [19]. EMB denotes endomyocardial biopsy, ^{18}F FDG fluorodeoxyglucose, RV right ventricle



A CMR imaging protocol for CS should thus include (1) *cine imaging* (assessment of LV volume and mass, global and regional function, regional ventricular thickening and thinning), (2) assessment of *inflammation/oedema* (T2 mapping or T2w imaging), (3) *scar* (LGE, T1 mapping and ECV mapping) and (4) morphological images to detect *extra-cardiac findings* (mediastinal/bi-hilar lymphadenopathy) (Fig. 2.6) [23].

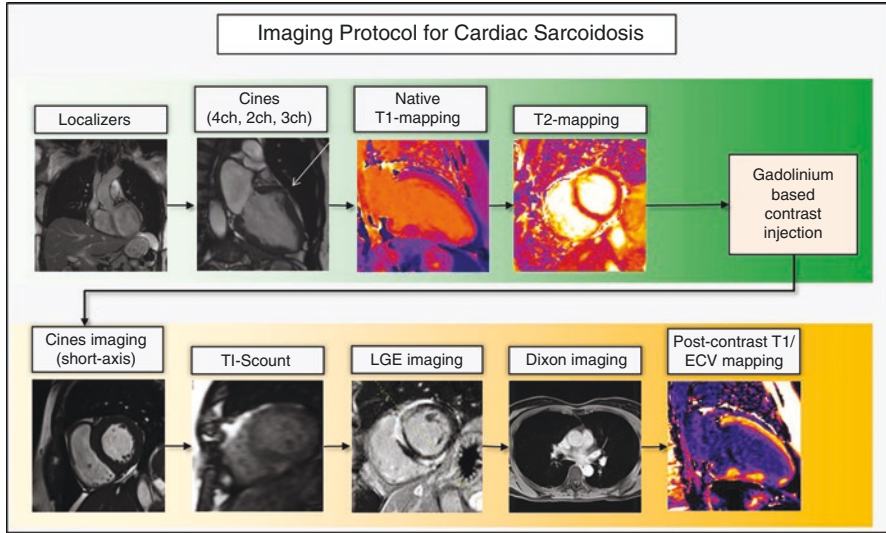


Fig. 2.6 CMR imaging protocol for cardiac sarcoidosis (Images from University Hospital, Basel, Switzerland)

2.6 Late Gadolinium Enhancement (LGE)

CMR allows non-invasive detection of focal fibrosis and scarring by LGE. Presence of focal LGE is the chief diagnostic finding on CMR scans and correlates to areas of dense fibrosis and granulomatous inflammation within patchy fibrosis [11]. Presence of scar on LGE has been shown to be up to twice as sensitive as the JMH criteria for identifying CS [11, 13]. While there is no specific pattern for CS, typical patterns of CS include sub-epicardial and mid-wall LGE along the basal and mid septum and inferolateral wall (Fig. 2.7) but also patchy LGE in a non-coronary pattern (Fig. 2.8) and LGE of the RV insertions points (hinge points) [24]. In 10–30% of patients with CS sub-endocardial or transmural hyper-enhancement patterns may be detected that mimic coronary artery disease. While the absence of LGE is associated with a high negative predictive value for excluding CS and with excellent cardiac prognosis, the “warranty period” of a normal CMR is unknown.

2.7 Imaging Myocardial Inflammation and Quantitative Tissue Characterization with CMR T1 and T2 Mapping

The intensity and size of focal LGE may decrease following immunosuppressive therapy [25]. Marked myocardial oedema also increases the interstitial space, but only profound myocardial oedema may occasionally result in diffuse LGE. In most cases, though, myocardial oedema will go undetected by LGE. Early gadolinium enhancement and T2-weighted images both have technical and methodological

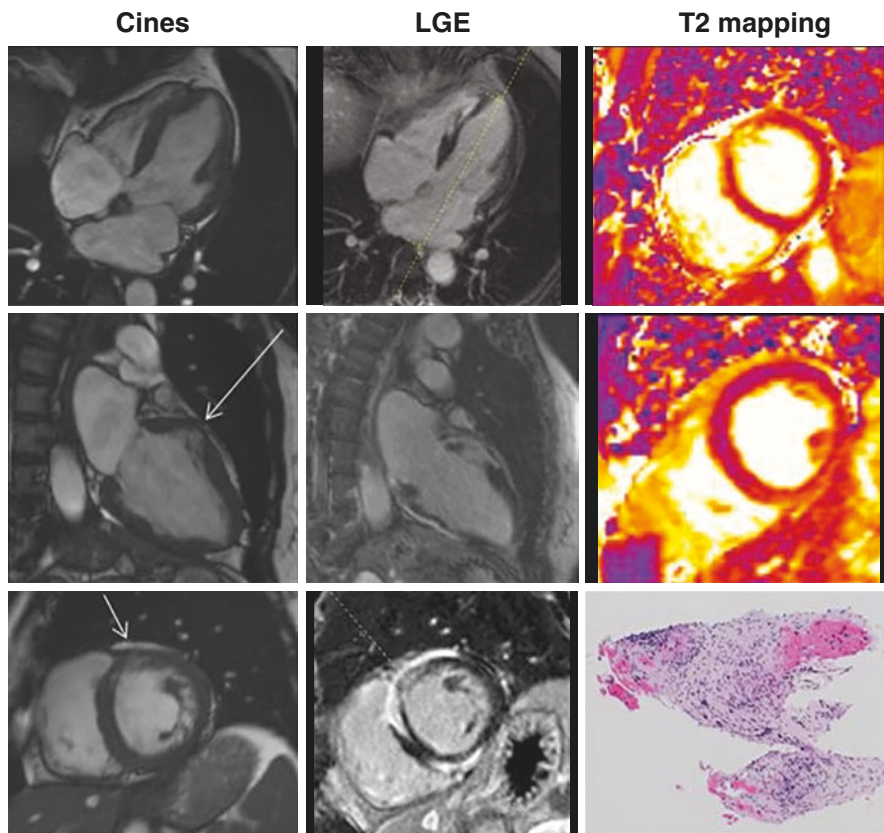


Fig. 2.7 Isolated cardiac sarcoidosis: LVEF 41%, antero-septal basal wall thinning (white arrow), pronounced LGE in a typical sub-epicardial and mid-wall LGE pattern along the basal and mid septum and evidence of myocardial oedema. No mediastinal or hilar lymphadenopathy. ^{18}F FDG-PET without evidence of systemic involvement (image not shown). Histopathology (haematoxylin and eosin stain $\times 100$) showing inflammation and patchy fibrosis (Images from University Hospital, Basel, Switzerland; Histopathology image courtesy of Prof. Katharina Glatz, University Hospital, Basel, Switzerland)

limitations and are increasingly being replaced by novel more accurate parametric tissue characterization mapping techniques (see also updated 2018 Lake Louise criteria [26]) [27].

Patients with sarcoidosis show higher native T1, T2 and ECV values and decreased post-contrast T1 values compared with healthy controls irrespective of the presence of LGE [28]. Significantly higher T2 mapping values expressing myocardial oedema occur in patients with CS compared to healthy controls and have been demonstrated in LGE negative patients with systemic sarcoidosis suggesting complementary information of T2 mapping to LGE [29]. While native T1 is sensitive to a wider spectrum of pathological signals from both intra- and extra-cellular spaces, T2 is more sensitive and specific to elevated water content and might,

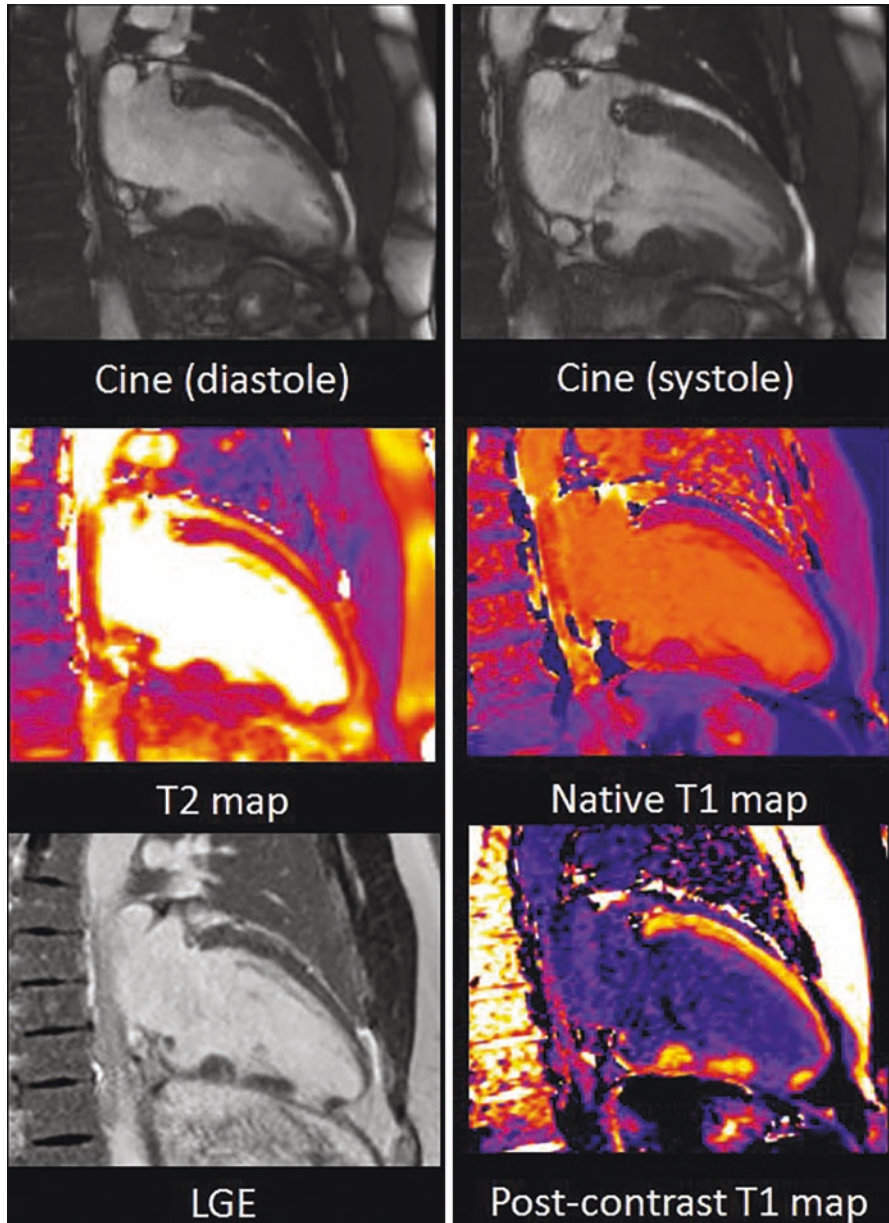


Fig. 2.8 Biopsy-proven pulmonary sarcoidosis with cardiac involvement: Regional thinning and thickening of the inferior wall. T2 and native T1 map without evidence of myocardial oedema. Patchy transmural late enhancement in a non-coronary pattern. (Images from University Hospital, Basel, Switzerland)

therefore, be particularly helpful in assessing myocardial oedema and inflammation in inflammatory cardiomyopathies. T2 cut off of 59 ms for myocardial oedema achieved a sensitivity of 54% and specificity of 100% for detection of myocardial oedema [29].

Established CMR imaging techniques (cine imaging and LGE) rely on detection of relatively gross and advanced abnormalities of function, structure or regional myocardial fibrosis. Novel quantitative approaches to CMR tissue characterization may be instrumental in earlier recognition of cardiac involvement, disease activity of myocardial inflammation and guidance of anti-inflammatory treatment response. In a recent study, both native T1 and T2 mapping outperformed LGE, HRS 2014 criteria as well as JMHW 2006 criteria in their discriminatory power between patients with systemic sarcoidosis and healthy controls [30].

T2 mapping—in contrast to ^{18}F -FDG PET—does not involve ionizing radiation, careful metabolic preparation and not even contrast agent and hence might become an alternative inflammatory biomarker once non-inferiority to ^{18}F -FDG PET has been shown.

2.8 Additional CMR Findings Suggestive of Cardiac Sarcoidosis

Left ventricular dilatation, regional thinning and/or thickening of the ventricular walls, regional wall motion abnormalities in a non-coronary pattern, restrictive filling pattern, focal oedema and pericardial effusion may also be suggestive of CS [29, 31]. CMR can also detect right-sided ventricular dysfunction due to elevated right heart pressures from pulmonary sarcoidosis or right ventricular granulomatous infiltration due to cardiac sarcoidosis.

2.9 Differential Diagnosis

Any patchy myocarditis including giant cell myocarditis, arrhythmogenic cardiomyopathy (patients with CS may formally fulfil arrhythmogenic cardiomyopathy criteria), dilated and hypertrophic cardiomyopathy, amyloidosis, Chagas disease, systemic lupus erythematosus and coronary artery disease may all mimic CS. This underlines the importance of the clinical context (i.e. pre-test probability of a disease) for image interpretation (Table 2.2).

2.10 Treatment: Anti-Inflammatory Therapy

The aims in the treatment of CS are to reduce inflammation and slower the evolution towards myocardial fibrosis and cardiac remodelling, while managing the eventual cardiac complications, such as heart failure and arrhythmias. Therefore, patients need a timely and accurate follow-up, in order to modulate the immunosuppressive

Table 2.2 MRI-based differential diagnosis of cardiac sarcoidosis *CS* cardiac sarcoidosis, *RWMA* regional wall motion abnormalities, *HCM* hypertrophic cardiomyopathy, *MI* myocardial infarction, *LGE* late gadolinium enhancement, *DCM* dilated cardiomyopathy, *AC/ARVC* arrhythmogenic (right ventricular) cardiomyopathy, *ECG* electrocardiogram, *LV* left ventricle; * ≥ 20 mm (African-American) and ≥ 13 mm (familial HCM); *ECG* electrocardiogram, *ECV* extra-cellular volume, *RV* right ventricle, *LV* left ventricle, *EDV* end-diastolic volume, *RBBB* right bundle branch block

Diagnosis	Clinical characteristics	MRI findings
CS	Multisystem disease, conduction abnormality, heart failure	Mediastinal and bi-hilar lymphadenopathy, LV dilatation, regional myocardial thickening or thinning, RWMA Myocardial oedema Sub-epicardial and mid-wall LGE predominantly at the basal septum, inferolateral wall or RV insertion site
Myocarditis	Recent history of symptoms from (viral) infection, fever and chills, chest pain mimicking MI, elevated cardiac enzymes, ECG repolarisation disorder	Myocardial oedema Sub-epicardial to mid-wall LGE in a non-coronary pattern commonly involving inferolateral wall
AC/ARVC	Syncope, palpitations/ventricular tachycardia, heart failure, ECG (T-wave inversion V_1 - V_3 in the absence of RBBB, epsilon wave), family history	RV, LV or biventricular involvement/dilatation Task force major criteria (see also [32]): Regional RV akinesia or dyskinesia or dyssynchronous RV contraction and • RV_{EDVi} ♂: ≥ 110 mL/m ² ♀: ≥ 100 mL/m ² or: • RV-ejection fraction $\leq 40\%$.
Idiopathic DCM	Heart failure, dyspnoea on exertion, palpitations, asymptomatic cardiomegaly, family history	Dilated ventricles and reduced systolic function, no LGE or septal mid-wall LGE (25% of DCM) in a non-coronary pattern
HCM	Wide spectrum from asymptomatic to sudden cardiac death, syncope, palpitations, family history	Increased LV wall thickness ≥ 15 mm*, LGE of hypertrophied segments or RV insertion site
Amyloidosis	Multisystem disease, heart failure and dyspnoea, ECG with low voltage QRS	Small thickened ventricles, large atria with interatrial thickening, restrictive physiology Global sub-endocardial or patchy LGE in a non-coronary pattern, atrial LGE Difficulty in nulling (TI-scout) ECV $\uparrow \uparrow > 0.40$

therapy and implement cardiac drug and device treatment. Although no randomized controlled trials for the treatment of cardiac sarcoidosis exist, recent studies demonstrated a prognostic benefit of early diagnosis and early initiation of corticosteroid therapy [33, 34]. Most experts advocate corticosteroid/anti-inflammatory treatment in patients with CS and active inflammation before LV systolic function declines

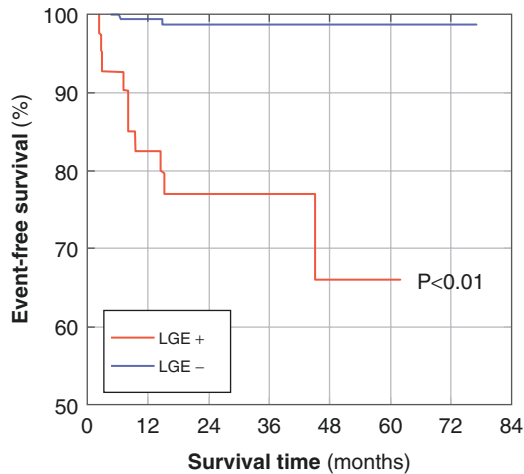
and nonresponsive fibrosis has occurred [35]. Steroids are believed to slow disease progression by re-establishing a normal T helper 1/T helper 2 (Th1/Th2) balance, reducing inflammation and, possibly, granuloma formation [36]. Corticosteroid taper or withdrawal may only be pursued in cases of absent (inflammatory) disease activity and therapy duration may be as long as 1–2 years. More recently, centres have recognized the role of steroid-sparing and immune-modulating agents to minimize steroid-induced side effects [37, 38]. Data to support their use in CS are limited, though.

2.11 CMR for Arrhythmogenic Risk Stratification/ICD

There is a growing body of data establishing the important role of CMR in the assessment and risk stratification of patients with suspected CS. Sudden cardiac death accounts for 30–65% of deaths in patients with CS [39]. Presence of scar on LGE imaging has been shown to be a potent independent risk factor for death, appropriate defibrillator discharge, ventricular arrhythmia and pacemaker requirement while the absence of LGE is associated with a low risk of death or sustained ventricular tachycardia (Fig. 2.9) [11, 40, 41].

According to the Heart Rhythm Society (HRS), CS patients who do not meet traditional criteria for ICD implantation but show imaging evidence of fibrosis or inflammation might be considered for ICD implantation if an electrophysiological study is positive. The results of a recent meta-analysis [42] may even justify device implantation without further electrophysiological testing in CS patients with

Fig. 2.9 Kaplan–Meier curves demonstrating the impact of cardiac sarcoidosis on event-free survival (free from sustained ventricular tachycardia) in the late gadolinium enhancement (LGE) + (red) and LGE– (blue) groups. P value refers to log rank test LGE+ vs LGE– survival. From Murtagh et al. [40] which is an open access article distributed under the terms of the Creative Commons CC BY license



Months	0	12	24	36	48	60	72	84
LGE +	41	32	21	12	5	1	0	0
LGE –	164	149	124	92	60	14	2	0

Number at risk

imaging evidence of fibrosis or inflammation who do not meet traditional ejection fraction based criteria for ICD implantation [14]. However, prospective studies have not been performed to definitively prove benefit versus harm of ICD implantation among such patients.

2.12 Positron Emission Tomography

Cardiac Positron Emission Tomography (PET) can be used to investigate both regional myocardial perfusion (using perfusion radiotracer like ^{82}Rb -Chloride and ^{13}N -ammonia) and glucose metabolism (using ^{18}F -Fluorodeoxyglucose, FDG). Of note, myocardial perfusion may also be obtained using single-photon emission tomography (SPECT) with radiotracers like ^{201}Tl -Chloride or $^{99\text{m}}\text{Tc}$ -Tetrofosmin/Sestamibi. As CS represents a cardiac manifestation of a multisystem inflammatory disease, an increased glucose metabolism of the myocardium represents the main finding in affected patients [43] (Fig. 2.10).

An accurate diagnosis of cardiac sarcoidosis can be effectively obtained by the comparison of perfusion and metabolic state within the myocardium. While a “mismatch pattern” characterized by reduced baseline perfusion and increased glucose metabolism within the same area is highly suggestive for cardiac sarcoidosis, other patterns can be identified as recently described in a position paper jointly drafted by the Society of Nuclear Medicine and Molecular Imaging (SNMMI) and the American Society of Nuclear Cardiology (ASNC) [44].

The various patterns of combined perfusion and metabolic images are summarized in Fig. 2.11. Several ^{18}F -FDG patterns of CS have been described including focal, diffuse and focal on diffuse [45]. In early stages of CS, regional areas of ^{18}F -FDG uptake are diagnostic of focal inflammation and in the same regions resting myocardial perfusion defects may be observed. With the progression of the disease, there could be a matched low-flow low-metabolism pattern, indicating the presence of scar without inflammation. Of note, higher ^{18}F -FDG myocardial uptake has been reported in patients with CS presenting with ventricular arrhythmias compared to those with advanced atrioventricular block or clinically silent [46, 47].

The clinical performance of ^{18}F -FDG PET/CT has been evaluated in a meta-analysis by Youssef and al [48], including 7 studies and 164 patients, most of whom with systemic sarcoidosis. Cardiac involvement was demonstrated in about half of the population and the diagnostic accuracy of ^{18}F -FDG PET resulted in 89% sensitivity, 78% specificity and AUC 0.93.

2.13 Positron Emission Tomography with Tracers Other than ^{18}F -FDG

As previously discussed, ^{18}F -FDG PET/CT imaging may be affected by non-specific myocardial uptake due to individual response to dietary preparation. Therefore, radiotracers other than ^{18}F -FDG have been investigated in CS.

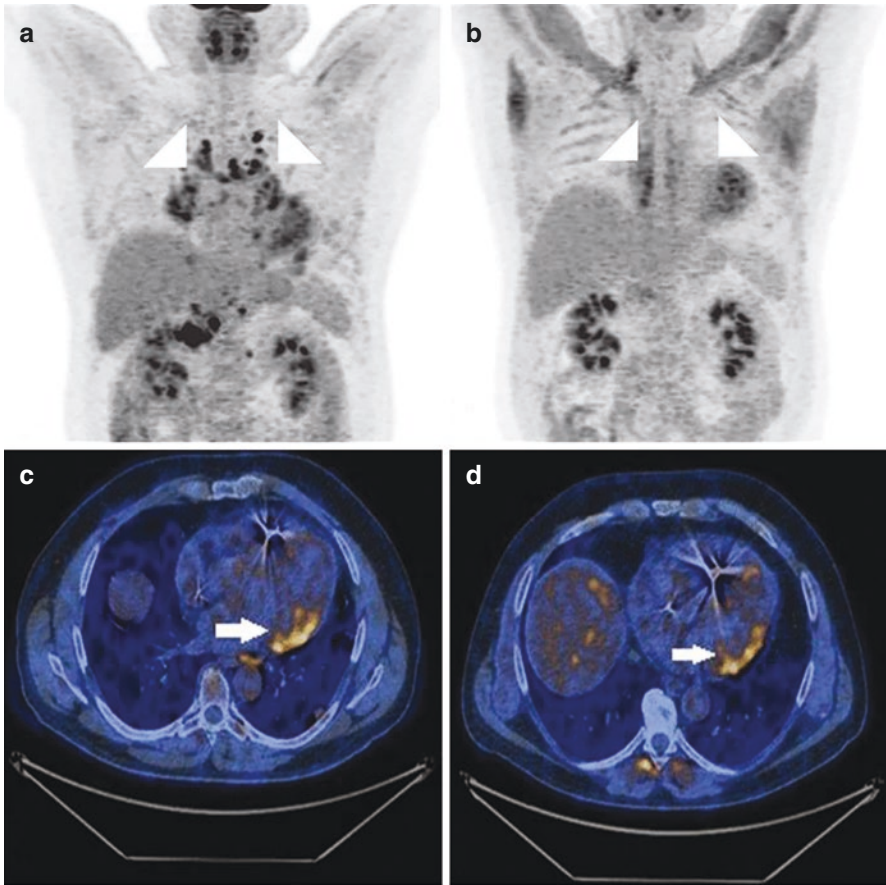


Fig. 2.10 A 54-year-old patient with sarcoidosis. Primary scan (**a** maximum intensity projection (MIP) and **c** axial) revealed increased uptake foci in the inferolateral segments of the left ventricle (concordant with prior magnetic resonance imaging findings) and active mediastinal lymph nodes. The follow-up scan (**b**, **d**) after 4 months of steroid treatment shows good response in lymph nodes, but no significant changes in the heart. Reprinted with permission of Springer from [43]

and corresponding perfusion defect (**D** and **E**) is highly suggestive for cardiac sarcoidosis in active phase. Finally, a perfusion defect without significant abnormalities on ^{18}F -FDG PET/CT is consistent with fibrosis/scar (**F**). Of note, pattern (**C**) isolated focal ^{18}F FDG uptake in the basal lateral wall in the absence of a perfusion defect, absence of abnormal wall motion or no delayed enhancement on CMR may have reduced specificity for active myocardial inflammation. Reprinted with permission of Springer Verlag from [45]

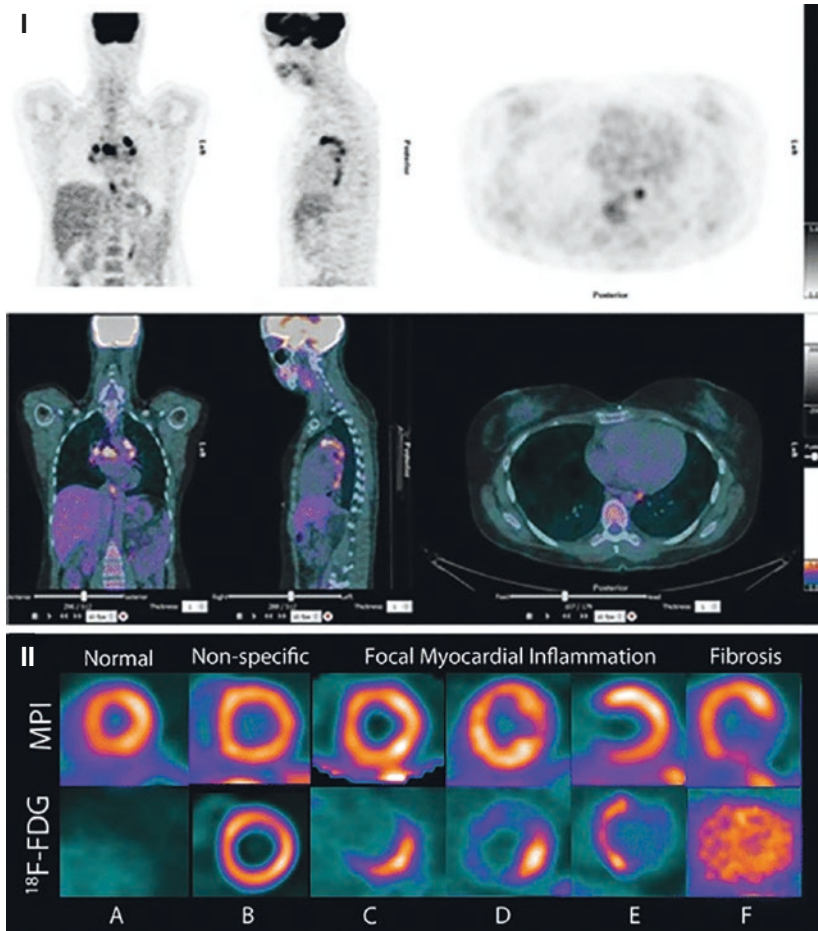


Fig. 2.11 (I) Example of ^{18}F FDG and myocardial perfusion PET in sarcoidosis. The whole body hybrid FDG-PET/CT study (I) showed multiple foci of inflammation in the mediastinum, but no active inflammation in the myocardium; hybrid imaging confirms regions of ^{18}F FDG uptake in the mediastinal lymph nodes and not in the myocardium. Assessment of systemic disease activity is an advantage of FDG- ^{18}F PET compared with echocardiography or CMR. (II) Patterns of myocardial perfusion imaging (MPI) and ^{18}F FDG imaging of myocardial inflammation. This figure shows rest MPI in the top row and ^{18}F FDG imaging of myocardial inflammation in the bottom row. A pattern of no myocardial ^{18}F FDG uptake and homogeneous perfusion is normal (A). A diffuse ^{18}F FDG uptake without perfusion abnormalities (B) is unspecific as often due to inadequate dietary preparation resulting in failed suppression of the physiological glucose metabolism of the heart. A focal ^{18}F FDG uptake without corresponding perfusion deficits may indicate an early disease, with active myocardial inflammation (C). A mismatch pattern (increased ^{18}F FDG uptake

Somatostatin receptors (SSTR) are abundant on the surface of activated inflammatory cells (macrophages, epithelioid cells and multinucleated giant cells) which are part of the sarcoid granuloma and absent in the normal myocardium. In the latest years, ^{68}Ga -labelled DOTA-peptides, which have high affinity for SSTR, have demonstrated to be promising in detecting CS although further studies are needed for their extensive clinical use [49–51] (Fig. 2.12).

Most recently, Weinberg et al. investigated the potential of ^{18}F -Natrium Fluoride (NaF) PET/CT in a small group of patients [52], but failed to image active inflammation related to cardiac sarcoidosis.

Markers of cell proliferation such as ^{18}F -fluorothymidine (FLT) and ^{11}C -thiothymidine have been investigated, as they have been proved to accumulate in chronic granulomatous lesions. While promising in view of their conceivably

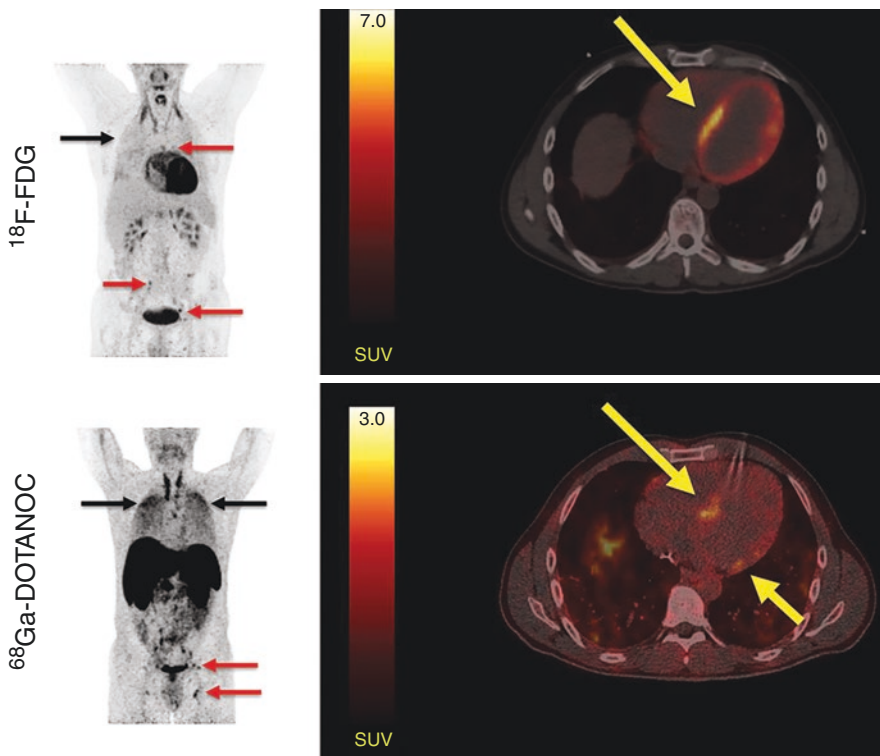


Fig. 2.12 Representative ^{18}F -FDG PET/CT and ^{68}Ga -DOTANOC PET/CT images in a patient with cardiac sarcoidosis. Left panel: MIPs showing dilated cardiomyopathy and multiple ^{18}F -FDG and ^{68}Ga -DOTANOC avid lymph nodes (red arrows). In addition, there is massive and diffusely increased activity in the lung parenchyma (black arrows) representing active pulmonary sarcoidosis. Right panel: while ^{18}F -FDG PET/CT was inconclusive due to failed suppression of tracer uptake from the myocardium (top), ^{68}Ga -DOTANOC images showed a clearly pathological uptake in the septum (bottom). Reprinted under the terms of the Creative Commons Attribution 4.0 International License (<https://creativecommons.org/licenses/by/4.0/>) from [51]

better specificity, preliminary reports failed to demonstrate an incremental clinical value over ^{18}F -FDG [53]. In a single instance, ^{11}C -thiothymidine (4DST) demonstrated diagnostic accuracy higher than ^{18}F -FDG and CMR, but its use is to date limited to research studies [54].

Finally, also markers of hypoxia have been investigated. The rationale of the use of these radiotracers relies in data from immune-chemistry examinations, showing that hypoxia-inducible factor HIF-1 α and vascular endothelial growth factor (VEGF) are expressed within granulomas in sarcoidosis [55]. Manabe et al. [56] showed a cardiac involvement of sarcoidosis by means of ^{18}F -Fluoromisonydazole (FMISO) PET/CT in a patient with histologically proven systemic sarcoidosis. Of note, the uptake of ^{18}F -FMISO was co-localized with FDG uptake within the myocardium.

2.14 Prognosis

Left ventricular ejection fraction and the occurrence of LGE are the most important clinical predictors of mortality among patients with CS. Advanced cardiac imaging findings (such as LGE with CMR, myocardial inflammation with ^{18}F -FDG-PET) have been studied in smaller trials [11, 12, 39, 57] and proved to be predictors of adverse clinical outcome. In a recent meta-analysis, it was shown that the presence of LGE on CMR imaging is associated with increased odds of both all-cause mortality and arrhythmogenic events, especially in the group of patients with LVEF $\geq 50\%$ [42]. The absence of LGE is associated with excellent cardiac prognosis (Fig. 2.13).

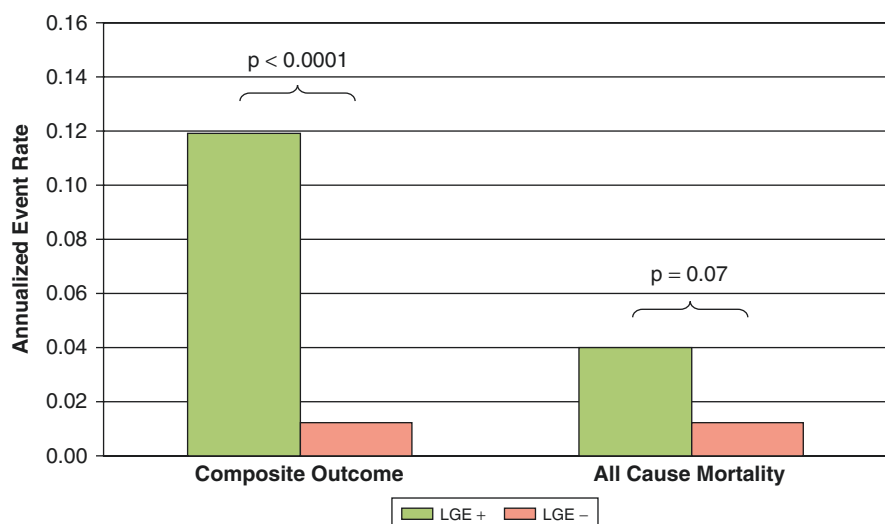


Fig. 2.13 Weighted mean annualized event rates (AERs) for the composite outcome of mortality plus arrhythmogenic events and all-cause mortality comparing patients with myocardial scarring as evidenced by the presence of LGE (green bars) with patients without LGE (pink bars). LGE denotes Late gadolinium enhancement. From Coleman et al. [42]

The metabolic information of ^{18}F -FDG PET/CT provides also important prognostic information. Blankstein and colleagues showed that perfusion/metabolic mismatch on cardiac PET identified patients at high risk of ventricular arrhythmias and death [58]. Moreover, semi-quantitative approaches such as standardized uptake value (SUV) calculation and FDG myocardial uptake localization seem to be significantly associated with risk stratification [59].

2.15 Follow-up and Monitoring of Anti-Inflammatory Response

Reduction in size and intensity of LGE may provide a method to assess for response to anti-inflammatory therapy [25]. Recent studies have shown significant reductions in native T1 and T2 in patients who received anti-inflammatory treatment associated with clinical improvement and lower C-reactive protein level [29, 30, 60]. Elevated T2w signal and elevated T2 mapping values have been shown to correspond to regional ^{18}F -FDG uptake, with reduced uptake following corticosteroids, indicating active inflammation and indicating a potentially reversible granulomatous inflammatory process with immune-suppressing therapy [21].

Nuclear imaging with ^{18}F -FDG-PET is able to directly image inflammation and macrophages activity and currently offers the most accurate imaging tool to monitor for anti-inflammatory therapy response. On the other hand, it should be considered that prolonged corticosteroid therapy may hamper the interpretation of ^{18}F -FDG PET/CT. In fact, steroids may increase serum glucose, insulin levels and ^{18}F -FDG uptake by normal myocytes, reducing test specificity [61]. Moreover, a reduction in myocardial ^{18}F -FDG uptake may either reflect resolution of inflammation or myocardial fibrosis. Therefore, the evaluation of the response to therapy is complex and always requires a comparison to a baseline ^{18}F -FDG PET/CT scan.

Studies including a limited number of patients have shown that variations in degree of inflammation can be assessed by serial ^{18}F -FDG PET/CT scans [62, 63] and these metabolic changes correlate with the improvements in symptoms and arrhythmias [64]. Furthermore, a reduction in both the intensity and extent of inflammation on a follow-up ^{18}F -FDG PET/CT was associated with an increase in left ventricular ejection fraction (Fig. 2.13) [65]. Conversely, increasing extension of myocardial inflammation as evidenced by ^{18}F -FDG PET/CT scan at follow-up as well as increased intensity of ^{18}F -FDG uptake associated with baseline heterogeneous radiotracer distribution are predictive for steroid therapy resistance [66]. It should also be noted that PET allows for whole body imaging that may identify extra-cardiac areas of metabolic activity and may guide the bioptic sampling (Fig. 2.14).

These evidences confirm the value of advanced imaging in the diagnosis and management of patients with CS and they have been considered in expert consensus recommendations, in which the identification of specific clinical scenarios may help to guide the appropriate utilization [44, 67].

Whether imaging-guided treatment improves outcome remains to be determined in multicentre collaboration trials.

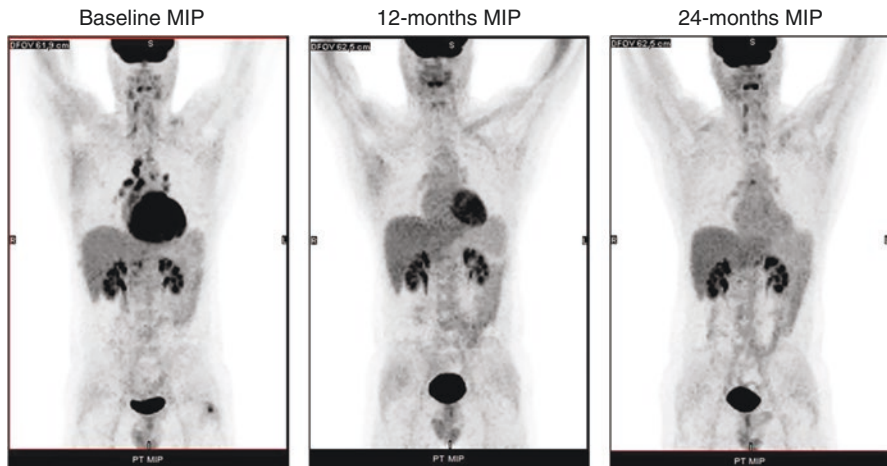


Fig. 2.14 Cardiac sarcoidosis. Patient admitted for recurrent episodes of ventricular tachycardia. Transthoracic echocardiography and CMR resulted in suggestive of infiltrative cardiomyopathy. After diet preparation, baseline ^{18}F FDG PET/CT (left) demonstrated a dramatic diffuse cardiac uptake of the radiotracer, mediastinal lymphadenopathy and bone disease indicative of sarcoidosis. Cardiac sarcoidosis was subsequently confirmed by endomyocardial biopsy. In the middle, PET Maximum Intensity Projection (MIP) images at 1-year follow-up following immunosuppressive therapy: there was a good metabolic response in the extra-cardiac areas of disease with low, persistent myocardial uptake of the radiotracer. On the right, PET MIP images at 24-months: there was a complete metabolic response. Patients were implanted with ICD that demonstrated recurrent episodes of ventricular tachycardia that required transcatheter ablation. Images from Nuclear Medicine Unit, Fondazione CNR/Regione Toscana “Gabriele Monasterio”, Pisa, Italy

2.16 Hybrid PET-CMR Imaging

Moreover, PET and CMR have a complementary value. While ^{18}F -FDG PET/CT has high sensitivity but suffers from lower specificity under certain metabolic conditions, LGE is more specific as it reflects the expression of myocardial damage or scar. Vita and co-workers retrospectively analysed data from 107 consecutive patients studied both with CMR and PET [68]. When PET imaging results were added to CMR data, 48/107 patients (45%) were reclassified as having a higher or lower likelihood of CS and most of the reclassified cases (80%) were concordant with the final diagnosis.

Using hybrid PET/MR scanners allows for a simultaneous acquisition of both ^{18}F -FDG PET and CMR, thus reducing artefacts due to misregistration of the images. Hanneman et al. validated the feasibility of this hybrid approach in CS and in myocarditis [69]. Dweck et al. studied 25 patients and 19 control subjects [70], showing incremental information about myocardial damage and disease activity if PET and CMR are simultaneously acquired. In their paper, semi-quantitative measures of target to background ratio resulted in 0.98 area under the ROC curves for the detection of CS. More recently, Wicks and colleagues compared the relative performance of PET/CMR vs. ^{18}F -FDG PET/CT and CMR as standalone modalities

in 51 consecutive patients with suspected CS [71]. Hybrid PET/MRI showed a superior sensitivity for detecting CS (0.94) than those of PET and CMR alone (0.85 and 0.82, respectively) (Fig. 2.15).

However, it should be noted that the comparison of the diagnostic accuracy of ^{18}F -FDG-PET vs. CMR has been limited due to an imperfect reference standard. Small areas of LGE on CMR not detected by ^{18}F -FDG-PET may represent false positive LGE or true disease. Similarly, small amounts of inflammation on ^{18}F -FDG-PET not detected by CMR could be false positive or early CS without fibrosis [72]. Although the evidence is limited, CMR (using fibrosis by LGE) and ^{18}F -FDG-PET (inflammation) are complementary, and CMR may be more sensitive for initial diagnosis, whereas ^{18}F -FDG-PET likely has greater utility for monitoring the anti-inflammatory response [72].

2.17 Outlook

While imaging with CMR and PET has been helpful for the diagnosis of CS and the identification of patients with a higher risk of adverse events, no randomized trials exist regarding the benefit of immunosuppressive therapies. Future studies are needed to prove better outcome and survival benefit from anti-inflammatory therapies and to determine the clinical benefit of imaging-guided therapies.

Novel CMR quantitative tissue characterization techniques have shown to be accurate and contribute to prognosis in inflammatory cardiomyopathies. They will likely emerge as biomarkers once trials on the impact on patient outcome and hybrid PET-CMR studies assessing detection of myocardial inflammation (^{18}F -FDG-PET vs. T2 mapping) have been published. Their accuracy, though, depends heavily on image quality, sophisticated image analysis and the advancing process of standardization of mapping methods and protocols [73]. Furthermore, the overlap of T1/T2

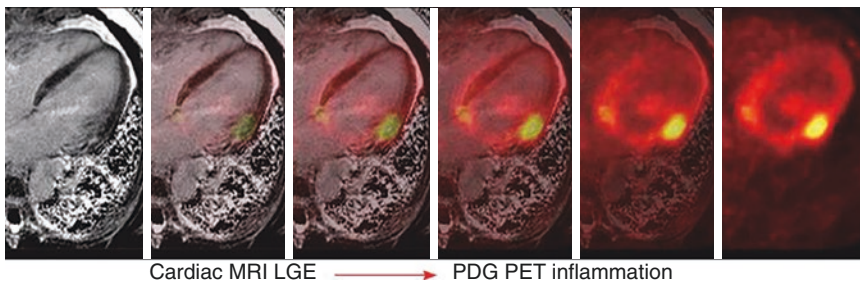


Fig. 2.15 Co-registration of separately acquired cardiac CMR, left panel with cardiac PET, right panel. The CMR was notable for a region of focal late gadolinium enhancement in the basal anterolateral wall. PET was significant for active inflammation in the same area in addition to an area of less intense inflammation in the basal antero-septum that did not have significant LGE. From Hulten et al. [72] which is an open access article distributed under the terms of the Creative Commons CC BY license. CMR denotes cardiac magnetic resonance, PET positron emission tomography, LGE late gadolinium enhancement

mapping values of patients vs. controls also often is substantial. Even if abnormal T1 and T2 values represent early disease, they currently carry uncertain clinical significance since LGE negative sarcoidosis patients are known to have an excellent prognosis [42]. To date, treatment of such abnormal T1 and T2 values is not warranted and should be studied in future trials.

2.18 Conclusion

Cardiac sarcoidosis remains an enigmatic disease with uncertain aetiology, challenging diagnostic and therapeutic concepts mainly based on expert consensus. Both CMR and PET have improved diagnostic accuracy for CS; its further impact on clinical management and outcome remains to be determined.

References

1. Hillerdal G, Nöu E, Osterman K, Schmekel B. Sarcoidosis: epidemiology and prognosis. A 15-year European study. *Am Rev Respir Dis.* 1984;130:29–32.
2. Schatka I, Bengel FM. Advanced imaging of cardiac sarcoidosis. *J Nucl Med Off Publ Soc Nucl Med.* 2014;55:99–106.
3. Silverman KJ, Hutchins GM, Bulkley BH. Cardiac sarcoid: a clinicopathologic study of 84 unselected patients with systemic sarcoidosis. *Circulation.* 1978;58:1204–11.
4. Iwai K, Takemura T, Kitaichi M, Kawabata Y, Matsui Y. Pathological studies on sarcoidosis autopsy. II. Early change, mode of progression and death pattern. *Acta Pathol Jpn.* 1993;43:377–85.
5. Mehta D, Lubitz SA, Frankel Z, Wisnivesky JP, Einstein AJ, Goldman M, Machac J, Teirstein A. Cardiac involvement in patients with sarcoidosis: diagnostic and prognostic value of outpatient testing. *Chest.* 2008;133:1426–35.
6. Orii M, Imanishi T, Akasaka T. Assessment of cardiac sarcoidosis with advanced imaging modalities. *Biomed Res Int.* 2014;2014:897956.
7. Gungor S, Ozseker F, Yalcinsoy M, Akkaya E, Can G, Eroglu H, Genc NS. Conventional markers in determination of activity of sarcoidosis. *Int Immunopharmacol.* 2015;25:174–9.
8. Ungprasert P, Carmona EM, Crowson CS, Matteson EL. Diagnostic utility of angiotensin-converting enzyme in sarcoidosis: a population-based study. *Lung.* 2016;194:91–5.
9. Kandolin R, Lehtonen J, Airaksinen J, Vihinen T, Miettinen H, Kaikkonen K, Haataja P, Kerola T, Kupari M. Usefulness of cardiac troponins as markers of early treatment response in cardiac sarcoidosis. *Am J Cardiol.* 2015;116:960–4.
10. Soejima K, Yada H. The work-up and management of patients with apparent or subclinical cardiac sarcoidosis: with emphasis on the associated heart rhythm abnormalities. *J Cardiovasc Electrophysiol.* 2009;20:578–83.
11. Patel MR, Cawley PJ, Heitner JF, et al. Detection of myocardial damage in patients with sarcoidosis. *Circulation.* 2009;120:1969–77.
12. Blankstein R, Osborne M, Naya M, et al. Cardiac positron emission tomography enhances prognostic assessments of patients with suspected cardiac sarcoidosis. *J Am Coll Cardiol.* 2014;63:329–36.
13. Smedema J-P, Snoep G, van Kroonenburgh MPG, van Geuns R-J, Dassen WRM, Gorgels APM, Crijns HJGM. Evaluation of the accuracy of gadolinium-enhanced cardiovascular magnetic resonance in the diagnosis of cardiac sarcoidosis. *J Am Coll Cardiol.* 2005;45:1683–90.

14. Birnie DH, Sauer WH, Bogun F, et al. HRS expert consensus statement on the diagnosis and management of arrhythmias associated with cardiac sarcoidosis. *Heart Rhythm*. 2014;11:1305–23.
15. Kandolin R, Lehtonen J, Graner M, Schildt J, Salmenkivi K, Kivistö SM, Kupari M. Diagnosing isolated cardiac sarcoidosis. *J Intern Med*. 2011;270:461–8.
16. Ratner SJ, Fenoglio JJ, Ursell PC. Utility of endomyocardial biopsy in the diagnosis of cardiac sarcoidosis. *Chest*. 1986;90:528–33.
17. Uemura A, Morimoto S, Hiramitsu S, Kato Y, Ito T, Hishida H. Histologic diagnostic rate of cardiac sarcoidosis: evaluation of endomyocardial biopsies. *Am Heart J*. 1999;138:299–302.
18. Ardehali H, Howard DL, Hariri A, Qasim A, Hare JM, Baughman KL, Kasper EK. A positive endomyocardial biopsy result for sarcoid is associated with poor prognosis in patients with initially unexplained cardiomyopathy. *Am Heart J*. 2005;150:459–63.
19. Omote K, Naya M, Koyanagawa K, et al. 18F-FDG uptake of the right ventricle is an important predictor of histopathologic diagnosis by endomyocardial biopsy in patients with cardiac sarcoidosis. *J Nucl Cardiol Off Publ Am Soc Nucl Cardiol*. 2019;27(6):2135–43. <https://doi.org/10.1007/s12350-018-01541-7>.
20. Cheong BYC, Muthupillai R, Nemeth M, Lambert B, Dees D, Huber S, Castriotta R, Flamm SD. The utility of delayed-enhancement magnetic resonance imaging for identifying nonischemic myocardial fibrosis in asymptomatic patients with biopsy-proven systemic sarcoidosis. *Sarcoidosis Vasc Diffuse Lung Dis Off J WASOG*. 2009;26:39–46.
21. Ohira H, Tsujino I, Ishimaru S, Oyama N, Takei T, Tsukamoto E, Miura M, Sakaue S, Tamaki N, Nishimura M. Myocardial imaging with 18F-fluoro-2-deoxyglucose positron emission tomography and magnetic resonance imaging in sarcoidosis. *Eur J Nucl Med Mol Imaging*. 2008;35:933–41.
22. Tadamura E, Yamamuro M, Kubo S, et al. Effectiveness of delayed enhanced MRI for identification of cardiac sarcoidosis: comparison with radionuclide imaging. *AJR Am J Roentgenol*. 2005;185:110–5.
23. Kramer CM, Barkhausen J, Bucciarelli-Ducci C, Flamm SD, Kim RJ, Nagel E. Standardized cardiovascular magnetic resonance imaging (CMR) protocols: 2020 update. *J Cardiovasc Magn Reson Off J Soc Cardiovasc Magn Reson*. 2020;22:17.
24. Vignaux O, Dhote R, Duboc D, Blanche P, Devaux J-Y, Weber S, Legmann P. Detection of myocardial involvement in patients with sarcoidosis applying T2-weighted, contrast-enhanced, and cine magnetic resonance imaging: initial results of a prospective study. *J Comput Assist Tomogr*. 2002;26:762–7.
25. Shimada T, Shimada K, Sakane T, et al. Diagnosis of cardiac sarcoidosis and evaluation of the effects of steroid therapy by gadolinium-DTPA-enhanced magnetic resonance imaging. *Am J Med*. 2001;110:520–7.
26. Ferreira VM, Schulz-Menger J, Holmvang G, et al. Cardiovascular magnetic resonance in nonischemic myocardial inflammation: expert recommendations. *J Am Coll Cardiol*. 2018;72:3158–76.
27. Thavendiranathan P, Walls M, Giri S, Verhaert D, Rajagopalan S, Moore S, Simonetti OP, Raman SV. Improved detection of myocardial involvement in acute inflammatory cardiomyopathies using T2 mapping. *Circ Cardiovasc Imaging*. 2012;5:102–10.
28. Greulich S, Kitterer D, Latus J, et al. Comprehensive cardiovascular magnetic resonance assessment in patients with sarcoidosis and preserved left ventricular ejection fraction. *Circ Cardiovasc Imaging*. 2016;9(11):e005022. <https://doi.org/10.1161/CIRCIMAGING.116.005022>.
29. Crouser ED, Ono C, Tran T, He X, Raman SV. Improved detection of cardiac sarcoidosis using magnetic resonance with myocardial T2 mapping. *Am J Respir Crit Care Med*. 2014;189:109–12.
30. Puntmann VO, Isted A, Hinojar R, Foote L, Carr-White G, Nagel E. T1 and T2 mapping in recognition of early cardiac involvement in systemic sarcoidosis. *Radiology*. 2017;285:63–72.
31. Schulz-Menger J, Wassmuth R, Abdel-Aty H, Siegel I, Franke A, Dietz R, Friedrich MG. Patterns of myocardial inflammation and scarring in sarcoidosis as assessed by cardiovascular magnetic resonance. *Heart Br Card Soc*. 2006;92:399–400.

32. Marcus FI, McKenna WJ, Sherrill D, et al. Diagnosis of arrhythmogenic right ventricular cardiomyopathy/dysplasia: proposed modification of the task force criteria. *Eur Heart J*. 2010;31:806–14.
33. Yazaki Y, Isobe M, Hiroe M, Morimoto S, Hiramitsu S, Nakano T, Izumi T, Sekiguchi M, Central Japan Heart Study Group. Prognostic determinants of long-term survival in Japanese patients with cardiac sarcoidosis treated with prednisone. *Am J Cardiol*. 2001;88:1006–10.
34. Lynch JP, Hwang J, Bradfield J, Fishbein M, Shivkumar K, Tung R. Cardiac involvement in sarcoidosis: evolving concepts in diagnosis and treatment. *Semin Respir Crit Care Med*. 2014;35:372–90.
35. Ayyala US, Nair AP, Padilla ML. Cardiac sarcoidosis. *Clin Chest Med*. 2008;29(3):493–508.
36. Youssef G, Beanlands RSB, Birnie DH, Nery PB. Cardiac sarcoidosis: applications of imaging in diagnosis and directing treatment. *Heart Br Card Soc*. 2011;97:2078–87.
37. Kim JS, Judson MA, Donnino R, Gold M, Cooper LT, Prystowsky EN, Prystowsky S. Cardiac sarcoidosis. *Am Heart J*. 2009;157:9–21.
38. Vorselelaars ADM, Cremers JP, Grutters JC, Drent M. Cytotoxic agents in sarcoidosis: which one should we choose? *Curr Opin Pulm Med*. 2014;20:479–87.
39. Roberts WC, McAllister HA, Ferrans VJ. Sarcoidosis of the heart. A clinicopathologic study of 35 necropsy patients (group 1) and review of 78 previously described necropsy patients (group 11). *Am J Med*. 1977;63:86–108.
40. Murtagh G, Laffin LJ, Beshai JF, et al. Prognosis of myocardial damage in sarcoidosis patients with preserved left ventricular ejection fraction: risk stratification using cardiovascular magnetic resonance. *Circ Cardiovasc Imaging*. 2016;9:e003738.
41. Greulich S, Deluigi CC, Gloekler S, et al. CMR imaging predicts death and other adverse events in suspected cardiac sarcoidosis. *JACC Cardiovasc Imaging*. 2013;6:501–11.
42. Coleman GC, Shaw PW, Balfour PC, Gonzalez JA, Kramer CM, Patel AR, Salerno M. Prognostic value of myocardial scarring on CMR in patients with cardiac sarcoidosis. *JACC Cardiovasc Imaging*. 2017;10:411–20.
43. Osiecki S, Sterliński M, Marciniak-Emmons M, Dziuk M. Feasibility of ¹⁸F-FDG PET in the cardiac inflammation. *Int J Cardiovasc Imaging*. 2021;37:1097–104.
44. Chareonthaitawee P, Beanlands RS, Chen W, Dorbala S, Miller EJ, Murthy VL, Birnie DH, Chen ES, Cooper LT, Tung RH, White ES, Borges-Neto S, Di Carli MF, Gropler RJ, Ruddy TD, Schindler TH, Blankstein R, NAME OF COLLAB GROUP. Joint SNMMI-ASNC expert consensus document on the role of ¹⁸F-FDG PET/CT in cardiac sarcoid detection and therapy monitoring. *J Nucl Med*. 2017;58:1341–53.
45. RHJA S, AWJM G, Lancellotti P, Hyafil F, Blankstein R, Schwartz RG, Jaber WA, Russell R, Gimelli A, Rouzet F, Hacker M, Gheysens O, Plein S, Miller EJ, Dorbala S, Donal E, Document Reading Group. A joint procedural position statement on imaging in cardiac sarcoidosis: from the Cardiovascular and Inflammation & Infection Committees of the European Association of Nuclear Medicine, the European Association of Cardiovascular Imaging, and the American Society of Nuclear Cardiology. *J Nucl Cardiol*. 2018;25:298–319.
46. Mc Ardle BA, Birnie DH, Klein R, de Kemp RA, Leung E, Renaud J, et al. Is there an association between clinical presentation and the location and extent of myocardial involvement of cardiac sarcoidosis as assessed by ¹⁸F-fluorodeoxyglucose positron emission tomography? *Circ Cardiovasc Imaging*. 2013;6:617–26.
47. Mc Ardle BA, Leung E, Ohira H, Cocker MS, deKemp RA, DaSilva J, et al. The role of F(18)-fluorodeoxyglucose positron emission tomography in guiding diagnosis and management in patients with known or suspected cardiac sarcoidosis. *J Nucl Cardiol*. 2013;20:297–306.
48. Youssef G, Leung E, Mylonas I, Nery P, Williams K, Wisenberg G, Gulenchyn KY, Dekemp RA, Dasilva J, Birnie D, Wells GA, Beanlands RS. The use of 18F-FDG PET in the diagnosis of cardiac sarcoidosis: a systematic review and metaanalysis including the Ontario experience. *J Nucl Med*. 2012;53:241–8.
49. Reiter T, Werner RA, Bauer WR, Lapa C. Detection of cardiac sarcoidosis by macrophage-directed somatostatin receptor 2-based positron emission tomography/computed tomography. *Eur Heart J*. 2015;36:2404.

50. Pizarro C, Klunker F, Dabir D, Thomas D, Gaertner FC, Essler M, et al. Cardiovascular magnetic resonance imaging and clinical performance of somatostatin receptor positron emission tomography in cardiac sarcoidosis. *ESC Heart Fail.* 2018;5:249–61.
51. Gormsen LC, Haraldsen A, Kramer S, Dias AH, Kim WY, Borghammer P. A dual tracer (68) Ga-DOTANOC PET/CT and (18)F-FDG PET/CT pilot study for detection of cardiac sarcoidosis. *EJNMMI Res.* 2016;6(1):52.
52. Weinberg RL, Morgenstern R, DeLuca A, Chen J, Bokhari S. F-18 sodium fluoride PET/CT does not effectively image myocardial inflammation due to suspected cardiac sarcoidosis. *J Nucl Cardiol.* 2017;24:2015–8.
53. Norikane T, Yamamoto Y, Maeda Y, Noma T, Dobashi H, Nishiyama Y. Comparative evaluation of 18 F-FLT and 18 F-FDG for detecting cardiac and extra-cardiac thoracic involvement in patients with newly diagnosed sarcoidosis. *EJNMMI Res.* 2017;7:69.
54. Hotta M, Minamimoto R, Kubota S, Awaya T, Hiroi Y. 11C-4DST PET/CT imaging of cardiac sarcoidosis: comparison with 18F-FDG and cardiac MRI. *Clin Nucl Med.* 2018;43:458–9.
55. Piotrowski WJ, Kiszalkiewicz J, Pastuszek-Lewandoska D, Górski P, Antczak A, Migdalska-Sęk M, et al. Expression of HIF-1A/VEGF/ING-4 Axis in pulmonary sarcoidosis. *Adv Exp Med Biol.* 2015;866:61–9.
56. Manabe O, Hirata K, Shozo O, Shiga T, Uchiyama Y, Kobayashi K, et al. ¹⁸F-fluoromisonidazole (FMISO) PET may have the potential to detect cardiac sarcoidosis. *J Nucl Cardiol.* 2017;24:329–31.
57. Tahara N, Tahara A, Nitta Y, et al. Heterogeneous myocardial FDG uptake and the disease activity in cardiac sarcoidosis. *JACC Cardiovasc Imaging.* 2010;3:1219–28.
58. Blankstein R, Osborne M, Naya M, Waller A, Kim CK, Murthy VL, Kazemian P, Kwong RY, Tokuda M, Skali H, Padera R, Hainer J, Stevenson WG, Dorbala S, Di Carli MF. Cardiac positron emission tomography enhances prognostic assessments of patients with suspected cardiac sarcoidosis. *J Am Coll Cardiol.* 2014;63:329–36.
59. Flores RJ, Flaherty KR, Jin Z, Bokhari S. The prognostic value of quantitating and localizing F-18 FDG uptake in cardiac sarcoidosis. *J Nucl Cardiol.* 2020;27:2003–10.
60. Crouser ED, Ruden E, Julian MW, Raman SV. Resolution of abnormal cardiac MRI T2 signal following immune suppression for cardiac sarcoidosis. *J Investig Med Off Publ Am Fed Clin Res.* 2016;64:1148–50.
61. Genovesi D, Bauckneht M, Altini C, Popescu CE, Ferro P, Monaco L, Borra A, Ferrari C, Caobelli F. The role of positron emission tomography in the assessment of cardiac sarcoidosis. *Br J Radiol.* 2019 Aug;92(1100):20190247.
62. Matthews R, Bench T, Meng H, Franceschi D, Relan N, Brown DL. Diagnosis and monitoring of cardiac sarcoidosis with delayed-enhanced MRI and 18F-FDG PETCT. *J Nucl Cardiol.* 2012;19:807–10.
63. Sobic-Saranovic DP, Grozdic IT, Videnovic-Ivanov J, Vucinic-Mihailovic V, Artiko VM, Saranovic DZ, Pavlovic SV, Obradovic VB. Responsiveness of FDG PET/CT to treatment of patients with active chronic sarcoidosis. *Clin Nucl Med.* 2013;38:516–21.
64. Yamagishi H, Shirai N, Takagi M, Yoshiyama M, Akioka K, Takeuchi K, Yoshikawa J. Identification of cardiac sarcoidosis with 13NH3/18FDG PET. *J Nucl Med.* 2003;44:1030–6.
65. Osborne MT, Hulten EA, Singh A, Waller AH, Bittencourt MS, Stewart GC, et al. Reduction in ¹⁸F-fluorodeoxyglucose uptake on serial cardiac positron emission tomography is associated with improved left ventricular ejection fraction in patients with cardiac sarcoidosis. *J Nucl Cardiol.* 2014;21:166–74.
66. Shelke AB, Aurangabadkar HU, Bradfield JS, Ali Z, Kumar KS, Narasimhan C. Serial FDG-PET scans help to identify steroid resistance in cardiac sarcoidosis. *Int J Cardiol.* 2017;228:717–22.
67. Nensa F, Bamberg F, Rischpler C, Menezes L, Poeppel TD, la Fougère C, Beitzke D, Rasul S, Loewe C, Nikolaou K, Bucnerius J, Kjaer A, Gutberlet M, Prakken NH, Vliegthart R, RHJA S, Nekolla SG, Lassen ML, Pichler BJ, Schlosser T, Jacquier A, Quick HH, Schäfers M, Hacker M, European Society of Cardiovascular Radiology (ESCR); European Association of Nuclear Medicine (EANM) Cardiovascular Committee. Hybrid cardiac imaging using PET/

- MRI: a joint position statement by the European Society of Cardiovascular Radiology (ESCR) and the European Association of Nuclear Medicine (EANM). *Eur Radiol.* 2018;28:4086–101.
68. Vita T, Okada DR, Veillet-Chowdhury M, Bravo PE, Mullins E, Hulten E, Agrawal M, Madan R, Taqueti VR, Steigner M, Skali H, Kwong RY, Stewart GC, Dorbala S, Di Carli MF, Blankstein R. Complementary value of cardiac magnetic resonance imaging and positron emission tomography/computed tomography in the assessment of cardiac sarcoidosis. *Circ Cardiovasc Imaging.* 2018;11:e007030.
 69. Hanneman K, Kadoch M, Guo HH, Jamali M, Quon A, Iagaru A, Herfkens R. Initial experience with simultaneous 18F-FDG PET/MRI in the evaluation of cardiac sarcoidosis and myocarditis. *Clin Nucl Med.* 2017;42:e328–34.
 70. Dweck MR, Abgral R, Trivieri MG, Robson PM, Karakatsanis N, Mani V, Palmisano A, Miller MA, Lala A, Chang HL, Sanz J, Contreras J, Narula J, Fuster V, Padilla M, Fayad ZA, Kovacic JC. Hybrid magnetic resonance imaging and positron emission tomography with Fluorodeoxyglucose to diagnose active cardiac sarcoidosis. *JACC Cardiovasc Imaging.* 2018;11:94–107.
 71. Wicks EC, Menezes LJ, Barnes A, Mohiddin SA, Sekhri N, Porter JC, Booth HL, Garrett E, Patel RS, Pavlou M, Groves AM, Elliott PM. Diagnostic accuracy and prognostic value of simultaneous hybrid 18F-fluorodeoxyglucose positron emission tomography/magnetic resonance imaging in cardiac sarcoidosis. *Eur Heart J Cardiovasc Imaging.* 2018;19:757–67.
 72. Hulten E, Aslam S, Osborne M, Abbasi S, Bittencourt MS, Blankstein R. Cardiac sarcoidosis-state of the art review. *Cardiovasc Diagn Ther.* 2016;6:50–63.
 73. Messroghli DR, Moon JC, Ferreira VM, et al. Clinical recommendations for cardiovascular magnetic resonance mapping of T1, T2, T2* and extracellular volume: a consensus statement by the Society for Cardiovascular Magnetic Resonance (SCMR) endorsed by the European Association for Cardiovascular Imaging (EACVI). *J Cardiovasc Magn Reson.* 2017;19:75.



Cardiac Amyloidosis

3

Philip Haaf, Irene A. Burger, Michael J. Zellweger,
Pankaj Garg, and Cristina E. Popescu

Contents

3.1 Introduction.....	38
3.2 Diagnosis.....	42
3.3 Treatment.....	60
3.4 Prognosis.....	60
3.5 Conclusion.....	62
References.....	63

P. Haaf · M. J. Zellweger

Clinic of Cardiology, University Hospital Basel, Basel, Switzerland

Cardiovascular Research Institute Basel (CRIB), University Hospital Basel,
Basel, Switzerland

I. A. Burger (✉)

Department of Nuclear Medicine, Kantonsspital Baden, Baden, Switzerland

Department of Nuclear Medicine, University Hospital Zürich, University of Zürich,
Zürich, Switzerland

e-mail: Irene.burger@ksb.ch

P. Garg

Sheffield Teaching Hospital NHS Foundation Trust, Sheffield, UK

Department of Infection, Immunity & Cardiovascular Disease, University of Sheffield,
Sheffield, UK

C. E. Popescu

Department of Nuclear Medicine, Kantonsspital Baden, Baden, Switzerland

Department of Health Sciences and Technology, ETH Zürich, Zürich, Switzerland

3.1 Introduction

Systemic amyloidosis is caused by an extracellular deposition (infiltration) of misfolded, insoluble protein with a characteristic β -sheet structure damaging the structure and function of various tissues and organs [1, 2]. Amyloid deposition can occur in multiple organs (e.g. heart, liver, kidney, skin, eyes, lungs, nervous system) resulting in a variety of clinical manifestations. Cardiac amyloid deposition may occur in the myocardium, pericardium, small vessels and conduction system. The result is an infiltrative restrictive cardiomyopathy with early diastolic and later systolic dysfunction, conduction disease including sudden death and occasionally ischaemia (with arterial involvement in mainly light chain (AL) CA) (Fig. 3.1).

Cardiac involvement drives the prognosis (ranging from less than 6 months for AL CA to up to 3–12 years for transthyretin (ATTR) CA) and treatment in systemic amyloidosis.

3.1.1 Different Phenotypes of Cardiac Amyloidosis

Clinical phenotype of the disease is determined by which protein is deposited (Table 3.1). Two types of amyloid commonly infiltrate the heart: immunoglobulin light chain (AL) amyloidosis and transthyretin (ATTR) amyloidosis. While ATTR fibrils are derived from transthyretin (a normal plasma *transport* protein of *thyroxine* and *retinol*; hence the name, *transthyretin*), AL fibrils are composed of unique monoclonal immunoglobulin AL proteins that differ in each patient.

3.1.1.1 AL Amyloidosis

AL amyloidosis is associated with clonal plasma cell or other B-cell dyscrasias and leads to a deposition of fibrils composed of monoclonal immunoglobulin light chains. Approximately 5–10% of patients with AL amyloidosis will have evidence

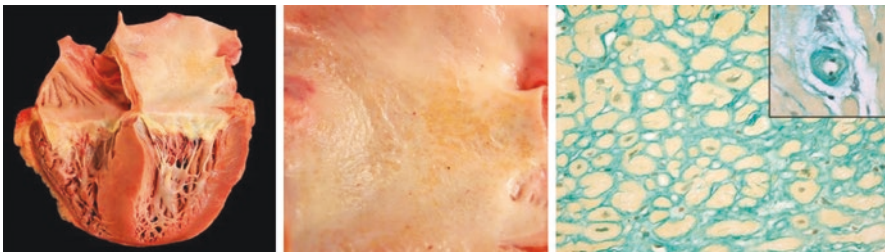


Fig. 3.1 (Left) Biatrial dilation with thickened atrial septum and extensive thickening of the left ventricle due to amyloid infiltration. (Middle) Close-up view of the atrium, showing the waxy, irregular surface due to amyloid deposition. Atrial infiltration leads to atrial dysfunction, and the irregular endocardial deposits can form a nidus for thrombus formation, accounting for the high prevalence of atrial thrombi in amyloid cardiomyopathy. (Right) Sulphated Alcian blue staining showing extensive amyloid deposits compressing myocytes and small vessels (inset): Adapted from Falk et al. [3]

Table 3.1 Summary of amyloid types with frequent cardiac involvement

Amyloid nomenclature	Amyloid type	Presentation	Cardiac involvement ^a	Other organ involvement	Treatment	Prognosis (median survival)
<i>Light-chain amyloidosis</i>						
AL	Primary systemic monoclonal light chain (AL) amyloidosis	Sixth to seventh decade $\delta \geq \text{♀}$	40–80%	Multorgan: Renal (nephrotic syndrome), liver, soft tissue, neuropathy, macroglossia	Chemotherapy (e.g. Bortezomib), peripheral blood stem cell transplantation	48 months, advanced-stage disease 4–6 months
<i>Transthyretin amyloidosis (ATTR)</i>						
ATTR _m	Hereditary (autosomal dominant) familial variant ATTR _m amyloidosis					
	<i>Mutant transthyretin^b</i>					
	ATTR _m (Val 1e 112)	> Fifth decade δ	Almost all	Carpal tunnel syndrome Peripheral and autonomic neuropathy	Supportive; Ivofersen, Patisiran, Diflunisal	3–12 years
	ATTR _m (T60 A)	6th decade $\delta > \text{♀}$	Up to 90%			Variable with liver transplantation
ATTR _{wt}	Non-hereditary variant ATTR _{wt} amyloidosis					
	<i>Wild-type (normal) transthyretin</i>					
	Senile wild-type ATTR _{wt} amyloidosis	Seventh decade $\delta \gg \text{♀}$ (>15:1)	Almost all	Carpal tunnel syndrome (preceding cardiac stenosis (other extracardiac involvement is unusual)	Supportive; Tafamidis, Diflunisal	2–6 years in the absence of treatment

^aIrrespective of the amyloid type, natriuretic peptide and high-sensitivity cardiac troponin usually are elevated and may be used for screening purposes

^bAbout 110 specific mutations have been described. Amyloid subtypes with only occasional cardiac involvement (such as acquired secondary serum amyloid A type (AA) amyloidosis, apolipoprotein AI (ApoA I), atrial natriuretic peptide (ANP) or ATTR (V30M) are not considered

of overt multiple myeloma. A similar proportion of multiple myeloma patients will have AL amyloidosis [3]. Many organs may be involved but cardiac involvement is sometimes the only presenting feature [4].

3.1.1.2 ATTR Amyloidosis

ATTR can be either hereditary (ATTR_m) or, more often, due to non-mutated wild-type TTR (ATTR_{wt}), also known as senile cardiac amyloidosis. ATTR is highly under-recognized within certain cardiovascular disorders and its reputation as a “rare disease” has recently been challenged: Recent autopsies have shown that cardiac amyloid deposits were present in 21% of heart failure with preserved ejection fraction (HFpEF) patients (mean age 76 years) [5] and in 5% of patients with presumed hypertrophic cardiomyopathy [6]. ATTR_{wt} has been shown to be prevalent in up to 16% of patients with low-flow low-gradient severe calcific aortic stenosis undergoing transcatheter aortic valve replacement (TAVR) and has been associated with a worse prognosis [7, 8]. In selected patients, exclusion of senile ATTR_{wt} may therefore be considered prior to TAVR.

3.1.2 Screening for Cardiac Amyloidosis

Amyloid cardiomyopathy should be included in the differential diagnosis of any patient who presents with HFpEF, in particular in patients with ventricular thickening without a history of hypertension or valvular disease. Other “red flags” to possible cardiac amyloidosis include progressive exercise intolerance, peripheral (limb leads) low voltage QRS (in contrast to markedly increased LV wall thickness) with poor R-wave progression in the chest leads (pseudoinfarct pattern) (Fig. 3.2), conduction disorder (atrioventricular, interventricular or sinoatrial), ventricular arrhythmia and typically exertional or postprandial syncope. Pleural and pericardial effusion is also frequently seen as well as atrial arrhythmias. Carpal tunnel syndrome and spinal canal stenosis may represent an early symptom of ATTR cardiomyopathy [9].

The typical constellation on echocardiography (concentric (bi-) ventricular hypertrophy, poor longitudinal ventricular contraction, restrictive filling with biatrial dilatation (“small ventricles, large atria”) and apical sparing in myocardial strain analysis), ECG abnormalities and elevated blood biomarkers (cardiac troponin and natriuretic peptides) is found mainly in advanced disease. Nevertheless, transthoracic echocardiography (TTE) remains the first-line test for patients with cardiovascular symptoms and hence the first suspicion of CA is often raised on TTE. Left ventricular ejection fraction is not a reliable indicator of systolic function in cardiac amyloidosis since ejection fraction and radial contraction are often preserved until end stage disease. In particular basal longitudinal contraction is typically affected earlier (apical sparing phenomenon of myocardial strain analysis) and the better disease [10] and prognostic marker [11] in cardiac amyloidosis (Fig. 3.3, top panel).

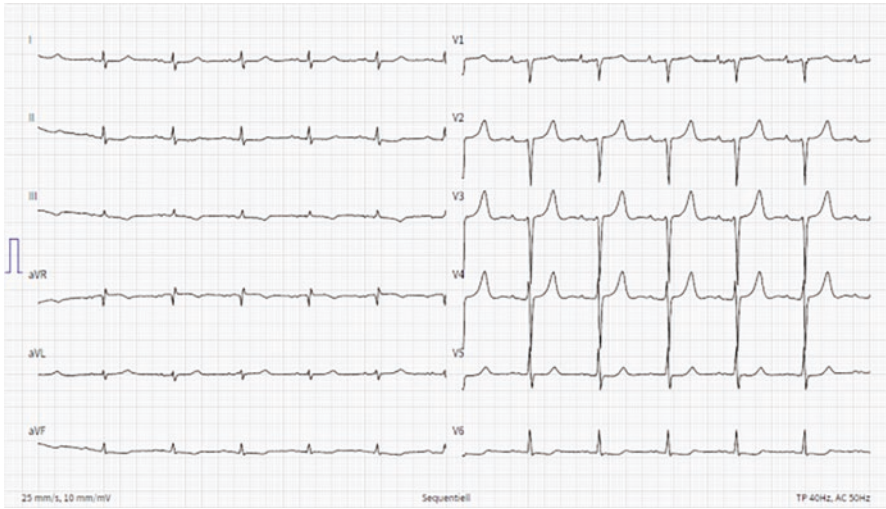


Fig. 3.2 Electrocardiogram of a patient with ATTR cardiac amyloidosis showing peripheral low voltage, pseudoinfarct pattern in the anterior leads and poor R-wave progression. (Image: University hospital Basel, Switzerland)

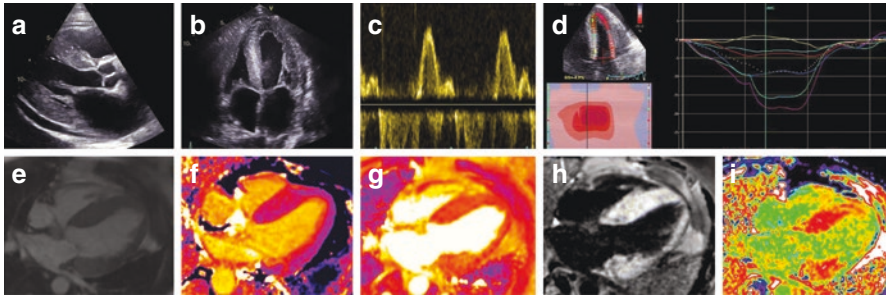


Fig. 3.3 Top Panel: Echocardiography findings in a patient with advanced cardiac amyloidosis. (a) Parasternal long axis view and (b) four chamber view showing concentric left ventricular hypertrophy (c) pulse wave Doppler showing restrictive left ventricular inflow pattern (d) strain pattern characteristic of an infiltrative process. Bottom Panel: CMR findings in a patient with advanced cardiac amyloidosis. (e) Four chamber steady state free precession cine, demonstrating left ventricular hypertrophy (f) corresponding native T1 map showing a T1 value of 1150 ms in the basal inferoseptum (g) corresponding T2 map showing a T2 value of 54 ms in the basal inferoseptum, within normal limits (h) corresponding phase-sensitive inversion recovery reconstruction showing transmural late gadolinium enhancement (i) corresponding extracellular volume map showing elevated value of 0.70. Images from [12], which is an open access article distributed under the terms of the Creative Commons CC BY license, which permits unrestricted use, distribution and reproduction in any medium, provided the original work is properly cited

Yet, TTE features are not specific to CA and are commonly seen in other hypertrophic phenocopies including heart failure with preserved ejection fraction (HFpEF) with high LV afterload (hypertension, aortic stenosis), infiltrative cardiomyopathies, hypertrophic cardiomyopathy or impaired LV relaxation due to metabolic disturbances (diabetes). Furthermore, the phenotypic heterogeneity of CA itself contributes to the under diagnosis of CA.

3.2 Diagnosis

3.2.1 Endomyocardial Biopsy

Endomyocardial biopsy (EMB) remains the gold standard for the diagnosis and subtyping of CA. In contrast to other diseases there is no issue with sampling errors in CA. Characteristically, β -pleated sheets of amyloid fibrils bind the Congo red stain, which when visualized under polarized light microscopy produces an abnormal yellow, orange or the characteristic “apple-green” birefringence colour (Figs. 3.1 and 3.4) [13]. Subtyping of CA has important therapeutic consequences.

3.2.2 Cardiac Magnetic Resonance (CMR) Imaging

CMR’s three-dimensional nature, excellent spatial resolution and high tissue contrast enable accurate measurement of cardiac function and morphology. Taken together with its unique possibilities of tissue characterization, CMR is the primary tool for the differential diagnosis of (hypertrophic) phenocopies of CA (Table 3.2; Fig. 3.3, bottom panel; Fig. 3.5).

3.2.2.1 CMR Diagnosis and Imaging Protocol

Amyloidosis can be regarded as the exemplar of an interstitial disease. CA is associated with a higher extracellular volume than any other cardiomyopathy (ECV $46.6 \pm 7.0\%$) due to the widespread and substantial extracellular infiltration [14]. A CMR imaging protocol (Fig. 3.6) for CA should include (1) cine imaging (assessment of LV volume and mass, global and regional function, regional ventricular thickening), (2) native T1 mapping, (3) assessment of inflammation/oedema (T2 mapping or T2w imaging), (4) assessment of early contrast uptake (early gadolinium enhancement/early post-contrast T1 mapping), (5) late contrast uptake (LGE) and (6) assessment of extracellular volume with post-contrast T1/ECV mapping and (7) morphological images to detect extracardiac findings (such as pericardial or pleural effusion).

3.2.2.2 Late Gadolinium Enhancement (LGE)

The most validated CMR technique for myocardial scar/fibrosis assessment remains LGE imaging. LGE imaging employs an inversion recovery T1-weighted (T1W) gradient-echo acquisition approximately 10 min after the intravenous

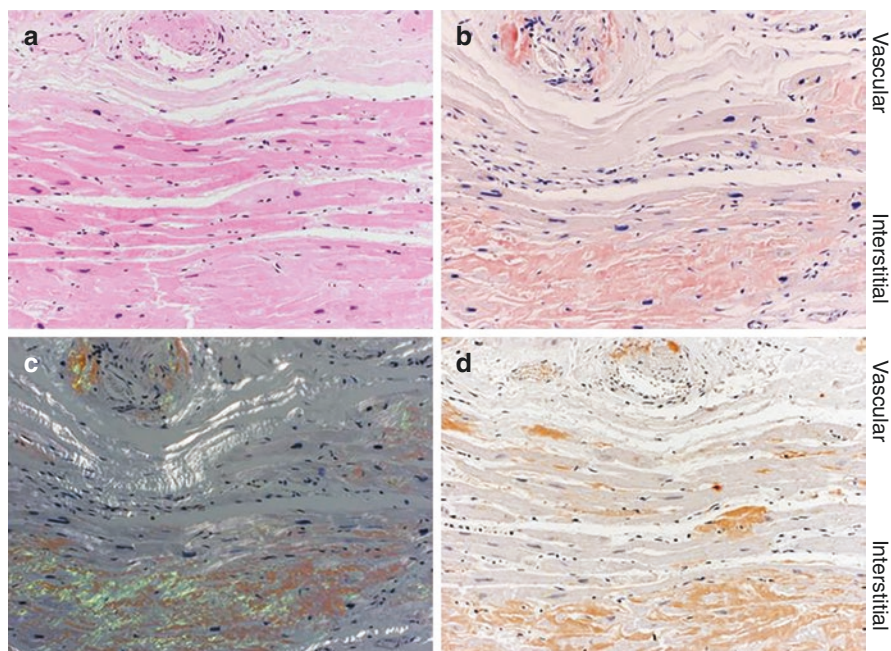


Fig. 3.4 Vascular wall (top) and myocardium (bottom) of a patient with ATTR cardiac amyloidosis with extensive and extracellular amyloid deposits compressing the cardiomyocytes. This leads to myocardial dysfunction, due to both stiffening of the extracellular space and direct myocyte damage. Amyloid surrounding small vessels may result in angina with normal-appearing epicardial coronary arteries on invasive coronary angiography. (a) Amorphous extracellular amyloid deposition (200 \times , haematoxylin and eosin stain). (b) Amyloid deposition with Congo red staining (200 \times , Congo red). (c) Amyloid deposition with apple-green birefringence (200 \times , Congo red, polarization filter). (d) Immunohistochemical classification of amyloid protein with an antibody against transthyretin (ATTR amyloid) (200 \times , ATTR). Courtesy of Prof. Katharina Glatz, Department of Pathology, University Hospital Basel, Switzerland

administration of the gadolinium contrast. With appropriate settings, normal myocardium appears black or nulled, whereas non-viable regions appear bright or hyper-enhanced. Gadolinium contrast distribution volume and tissue concentration are low in normal myocardium. Deposition of amyloid fibrils in the myocardium leads to expansion of extracellular interstitial space. As such, in CA compared to normal cardiac tissue, late gadolinium enhancement results from an increase in the concentration of gadolinium in the expanded extracellular interstitium. The characteristic diffuse LGE enhancement makes nulling of normal myocardium particularly difficult (Fig. 3.7); in the absence of normal myocardium the operator may erroneously null the abnormal myocardium carrying the risk of “false negative” or “mirror images” of the true pattern [12, 15].

Phase-sensitive inversion recovery (PSIR) sequence has reduced the need for optimal nulling, making LGE interpretation easier in cardiac amyloidosis. Myocardial amyloid deposition results in interstitial expansion which can be

Table 3.2 Phenocopies of amyloidosis. Cardiac Magnetic resonance imaging for differential diagnosis in LV hypertrophy

	Hypertensive heart disease	Hypertrophic CMP (1:5.000)	Cardiac amyloidosis	Anderson–Fabry disease (1:40.000)	Athlete's heart
	<i>Pathological LVH</i>				<i>Physiological LVH</i>
History	Long-lasting hypertension	Pos. Family history (40–60% sarcomeric protein gene mutation) Symptomatic LVOT obstruction (syncope, dyspnoea, chest pain) palpitations (SV/V arrhythmias)	Multiorgan disease (cardiac involvement with poor prognosis) heart failure	Multi-system lysosomal storage disease X-linked (men>women) Palpitations (SV/V arrhythmias)	No symptoms, high level sporting activity
ECG	High voltage QRS	Septal and lateral Q waves High voltage QRS Conduction disease Repolarization abnormalities (“giant T waves” in Yamaguchi)	Heart block Absence of high voltage QRS (despite LVH)	Young age: Short PR (no δ wave) Older age: AV block Prolonged, high voltage QRS	Resting bradycardia AV block I High voltage QRS Early repolarization

CMR ⁽⁴⁾	<p>Hypertensive heart disease</p> <p>Symmetric concentric LVH</p> <p>Wall thickness < 15 mm (Caucasian), <15–20 mm (black)</p> <p>Infrequently: SAM of ant. Mitral valve leaflet</p>	<p>Hypertrophic CMP (1:5,000)</p> <p>LVED wall thickness > 15 mm (Caucasian), >20 mm (black), >13 if familial HCM</p> <ul style="list-style-type: none"> • 60%: Asymmetric septal HCM → SAM/MR (inferolateral jet)HCM vs. HOCM • 25–30%: Symmetric concentric HCM • 10%: Apical HCM (Yamaguchi) → apical obliteration of LV cavity • Midcavity HCM → apical pouch with LGE, • 18%: RV hypertrophy <p>RWMA and longitudinal strain ↓ of hypertrophied segments</p> <p>Severe diastolic dysfunction</p> <p>Myocardial crypts, elongated mitral valve leaflets</p>	<p>Cardiac amyloidosis</p> <p>Global LV (and RV) hypertrophy</p> <p>Longitudinal contraction ↓</p> <p>Restrictive CMP: Small ventricles, large atria</p> <p>thickened interatrial septal walls in 20%</p> <p>Pericardial and pleural effusion</p> <p>DDAL vs. ATTR: (1) exclusion of serum/urine free light chains; (2) bone scintigraphy</p>	<p>Anderson–Fabry disease (1:40,000)</p> <p>Concentric LVH</p> <p>Patterns of hypertrophy often indistinguishable from HCM.</p>	<p>Athlete's heart</p> <p>Symmetric LVH</p> <ul style="list-style-type: none"> • <i>Concentric</i>: Isometric exercise • <i>Eccentric</i>: Isotonic exercise <p>Max. Wall thickness ≤ 12 mm (top athletes <14–16 mm)</p> <p>Normal diastolic function</p>
--------------------	--	---	---	---	--

(continued)

Table 3.2 (continued)

	Hypertensive heart disease	Hypertrophic CMP (1:5.000) Patchy mid-wall LGE of RV hinge points LGE localized to region of hypertrophy Extent of LGE correlates with risk of SCD	Cardiac amyloidosis Difficulty in nulling (1) Blood pool early darkening Global subendocardial distribution (non-coronary pattern!) Early forms: Patchy subendocardial LGE Base-apex LGE gradient	Anderson-Fabry disease (1:40.000) LGE in up to 50% of patients: Basal and/or apical inferolateral wall	Athlete's heart No LGE or non-specific pattern
CMR LGE pattern	No LGE or patchy LGE pattern				
T1/T2 mapping ECV		Native T1↑, post-contrast T1↓ ECV/T1 mapping may detect diffuse fibrosis that is not detected by LGE (subclinical/early stage of HCM) (ECV↑)	Oedema – Bright on T2w imaging, T2 levels upper normal range – Native T1↑ Amyloid burden – ECV↑↑ (> 0.40)	Native T1↓ – Septum <940 ms – Inferolateral LGE: Native T1 normal/↑	ECV↓ (true cellular hypertrophy)
Follow-up	LVH↓ under OMT for hypertension	Arrhythmia risk stratification SCD/ICD risk calculator (ESC 2014) doc2do.com/hcm/webHCM.html LGE: – Extensive LGE (≥15% of total LV mass): Consider ICD for primary prevention – Absence of LGE: Reassuring, low risk status	ECV potentially for monitoring myocardial amyloid burden and guiding treatment	Evaluate genetic testing Enzyme repl. Therapy	LVH↓ after deconditioning

^aEchocardiography remains the first-line imaging modality to assess left ventricular hypertrophy (LVH)

In most cases, LVH may be attributable to hypertension, valve disease (aortic stenosis), or obesity. Other rare causes of LV hypertrophy not considered in this table: mitochondrial myopathy, mucopolysaccharidosis, aortic coarctation

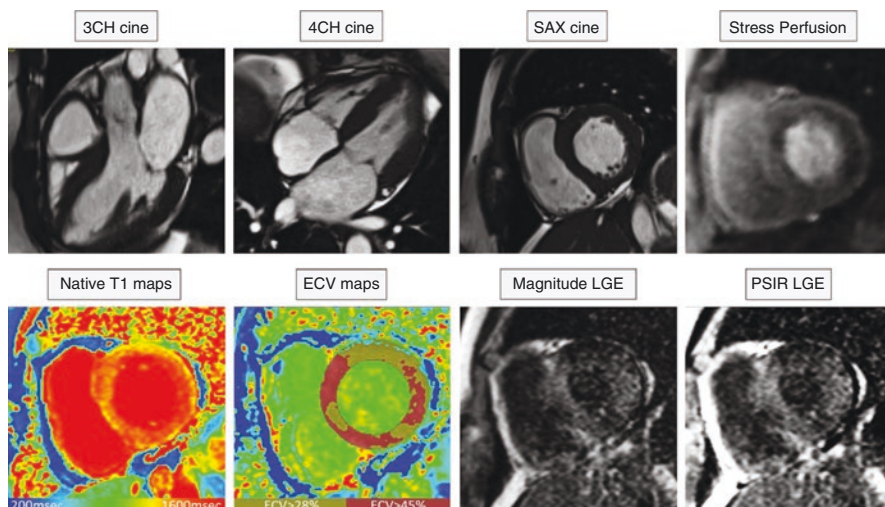


Fig. 3.5 This is an example of a patient with CA. On 3CH cine, septal hypertrophy is noted. In 4CH view, intra-atrial septum is thickened and the tips of mitral valve cups appear to be thicker than normal. There is concentric left ventricular hypertrophy in the short-axis cine view in the end-diastole. On first pass stress perfusion, there is evidence of subendocardial diffuse perfusion defects. Native T1 map demonstrates high native T1 values throughout. Extracellular volume (ECV) is above normal for the whole left ventricle, but, with extended areas of myocardium with $ECV > 45\%$. Magnitude LGE imaging is difficult to infer with a TI of 270 ms set manually. Magnitude LGE imaging demonstrates a similar pattern of diffuse fibrosis as PSIR LGE imaging. Courtesy of Dr. Pankaj Garg, Sheffield Teaching Hospital NHS Foundation Trust, Sheffield, United Kingdom

visualized by typically patchy LGE, subendocardial and/or transmural LGE in a non-coronary pattern with early blood pool darkening on Look-Locker/TI scout images [16]. Overall, LGE is an effective way of diagnosing patients with cardiac involvement in amyloidosis with a summary sensitivity of 85% and specificity of 92% for diagnosing CA in a recent systematic meta-analysis [17]. Atrial LGE is associated with atrial contractile dysfunction in CA and can rarely be seen in other cardiac diseases and therefore is a strong clue to the presence of CA.

3.2.2.3 Quantitative Tissue Characterization with CMR Native T1, T2 and ECV Mapping

T1 mapping measures the longitudinal relaxation time of tissue, which is determined by how rapidly proton spins re-equilibrate their longitudinal magnetization after being excited by a radiofrequency pulse [18]. It refers to pixel-wise measurement of absolute T1 relaxation times on a quantitative map. T1 mapping circumvents some of the issues of LGE imaging, namely the influence of windowing and nulling and provides quantitative assessment of diffuse extracellular expansion (Fig. 3.8).

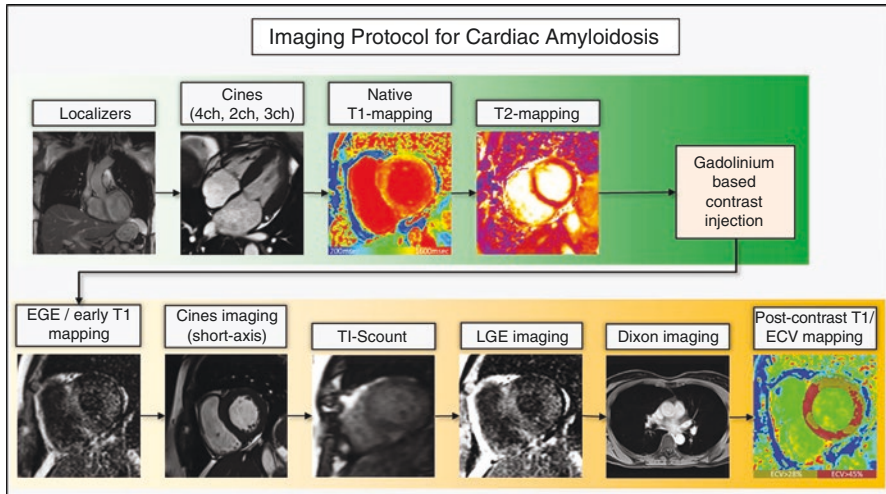


Fig. 3.6 CMR imaging protocol for cardiac amyloidosis (Images from University Hospital, Basel, Switzerland)

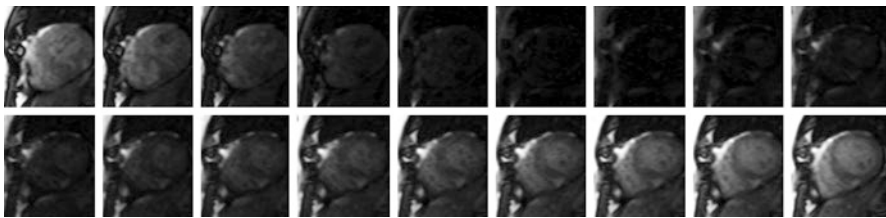


Fig. 3.7 One of the cornerstone to diagnose CA infiltration by CMR is no obvious difference in myocardial and blood pool signal intensity on T1 scout images resulting in difficult myocardial nulling. Courtesy of Dr. Pankaj Garg, Sheffield Teaching Hospital NHS Foundation Trust, Sheffield, United Kingdom

Native T1 mapping is a viable option in renal failure, which is common with amyloid. Conceptually, native T1 mapping measures a composite signal from both interstitium and myocytes and will be elevated both in cases of myocardial fibrosis and oedema. T1 mapping has the potential to detect diffuse myocardial structural alterations not accessible by other non-invasive methods and may be more sensitive than LGE in detecting diffuse myocardial fibrosis [18]. Normal native T1 values vary greatly between different field strengths, vendors and T1 mapping protocols. Cardiac amyloidosis is associated with a higher ECV ($ECV 46.6 \pm 7.0\%$) than any other cardiomyopathy due to widespread and substantial extracellular infiltration (Fig. 3.9) [14].

ECV is an imaging biomarker of myocardial tissue extracellular space (including interstitium and excluding myocytes) and provides a physiologically intuitive unit of measurement with normal ECV values of $25.3 \pm 3.5\%$ in normal myocardium

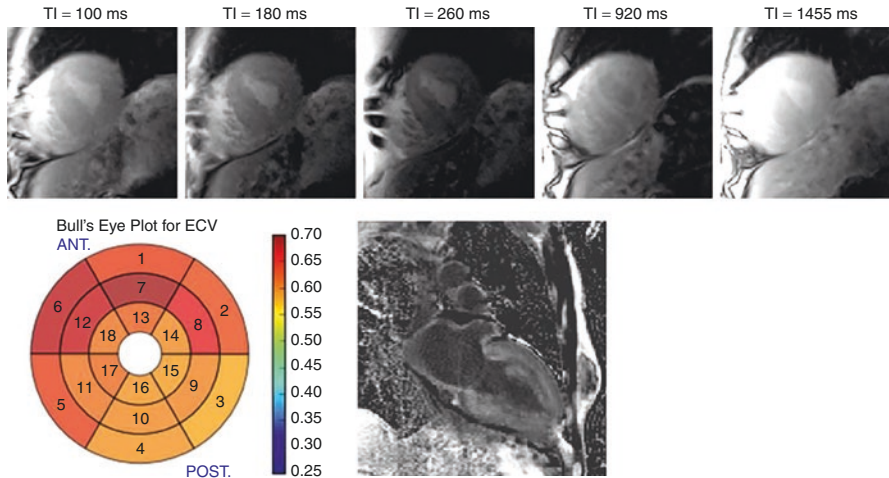


Fig. 3.8 (Top panel) Images from a modified Look-Locker acquisition in a patient with TTR cardiac amyloidosis, shown here in the order of increasing times after the magnetization inversion (TI). The images were acquired approximately 25 min after injection of 0.2 mmol/kg of gadolinium contrast, and the T1 in myocardium averaged 490 and 597 ms in the blood pool. The myocardial signal nulls characteristically early compared with the blood pool signal. (Bottom left panel) A bull’s-eye plot of extracellular volume (ECV) fraction in the same patient, calculated from pre- and post-contrast relaxation rate measurements for each of six myocardial segments in basal, mid, and apical slice locations, respectively. (Bottom right panel) Images of late gadolinium enhancement (LGE) in a two-chamber view for the same patient. Although ECV values in this patient approach the range measured for ECV in myocardial infarcts, the LGE image shows more muted enhancement than is seen for myocardial infarctions, which reflects the diffuse and global effect of cardiac amyloidosis in comparison to LGE in myocardial infarctions. LGE may therefore underestimate the severity of disease, whereas ECV provides an objective measure of extracellular space expansion. From: Falk et al. [3]

[14]. ECV is a more robust biomarker of pure infiltration than native or post-contrast T1. Since it is a ratio of change of T1 it is much less dependent on field strengths, vendors and T1 mapping protocols [18]. Estimation of ECV requires the measurement of myocardial and blood T1 before and after the administration of contrast agents as well as the patient’s haematocrit value:

$$ECV = (1 - \text{Haematocrit}) \frac{\frac{1}{\text{Post contrast T1 myo}} - \frac{1}{\text{Native T1 myo}}}{\frac{1}{\text{Post contrast T1 blood}} - \frac{1}{\text{Native T1 blood}}}$$

There is increasing evidence of a high correlation between synthetic ECV (derived by estimating haematocrit from native T1 blood values) and conventionally calculated ECV by using patient’s haematocrit [19, 20].

ECV can be regarded as the first non-invasive method for quantifying the cardiac amyloid burden. With the only differential being global oedema, high global ECV

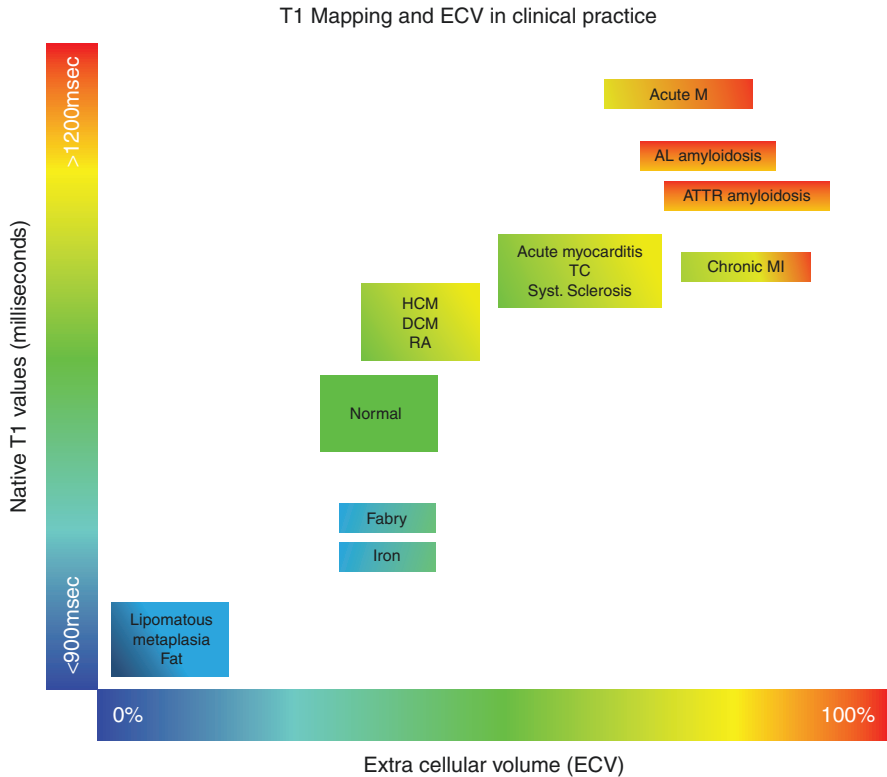


Fig. 3.9 Tissue characterisation using native T1 and extracellular volume fraction (ECV). Absolute values for native T1 depend greatly on field strength (1.5 T or 3 T), pulse sequence (MOLLI or ShMOLLI), scanner manufacturer and rules of measurements. For the purpose of comparability, only studies using 1.5 T scanners were considered in this figure. Figure from [18], which is an open access article distributed under the terms of the Creative Commons CC BY license, which permits unrestricted use, distribution and reproduction in any medium, provided the original work is properly cited

is very specific for cardiac amyloidosis. In CA, ECV is elevated before LGE or ventricular hypertrophy occurs [21–23]. In a large study of 250 patients, Fontana et al. demonstrated that there is a continuum of cardiac involvement in systemic AL and ATTR amyloidosis. Subsequently, this leads to further rise in ECV with subendocardial LGE enhancement and finally, often this leads to transmural LGE enhancement.

Myocardial oedema is present in cardiac amyloidosis by histology and CMR T2 mapping. It might have both important pathophysiological and prognostic roles in cardiac amyloidosis; T2 levels were more elevated in patients with untreated AL cardiac amyloidosis compared with treated AL and ATTR and a predictor of prognosis in AL amyloidosis. Additional to amyloid infiltration, myocardial oedema may therefore be contributing to mortality in amyloidosis [24].

As additional CMR findings suggestive of cardiac amyloidosis, pericardial and pleural effusion and ascites may be a further clue to cardiac amyloidosis.

3.2.2.4 Differential Diagnosis of AL vs. ATTR Amyloid

Efforts to differentiate between ATTR and AL have been made and showed more extensive LGE and higher LV mass in ATTR compared to less extensive more sub-endocardial LGE in AL (Fig. 3.10) [25]. The overlap between AL and ATTR amyloidosis, though, remains substantial.

Of note, more than 20% of patients with ATTR CA have an unrelated concomitant monoclonal gammopathy of undetermined significance (MGUS) [3]. Therefore, in patients suspected to have CA with monoclonal proteins, ATTR CA is still possible, and given the epidemiology, is even more likely than AL CA [26].

3.2.3 Scintigraphy

Radionuclide imaging plays an increasingly important role in the assessment of infiltrative heart disease. In this regard, several radiotracers targeting different components altered in the heart such as sympathetic innervation, perfusion, metabolism or amyloid deposits have been assessed for the detection of CA.

3.2.3.1 Bone Avid Radiotracers

Bone scintigraphy (BS) with ^{99m}Tc-3,3-diphosphono-1,2-propanodicarboxylic acid (^{99m}Tc-DPD), ^{99m}Tc-pyrophosphate (^{99m}Tc-PYP), or ^{99m}Tc-hydroxymethylene diphosphonate (^{99m}Tc-HMDP) has emerged as a sensitive tool for the identification of cardiac ATTR amyloidosis and differentiating it from AL type. Although the precise mechanism for accumulation of bone tracers in ATTR CA is not well known, it is hypothesized to this be related to different amounts of calcium ions available for the binding with the isotope [27].

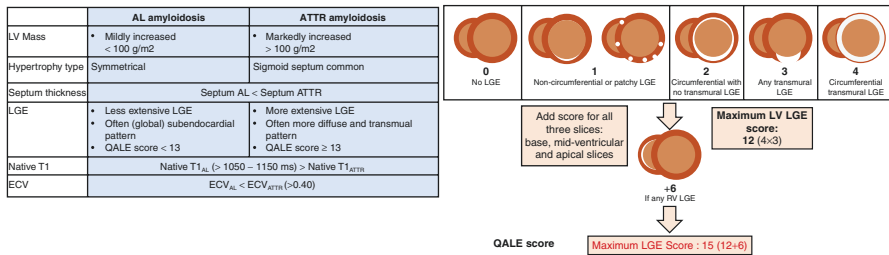


Fig. 3.10 CMR differences between AL and ATTR amyloidosis, figure adapted from [25]

Imaging Protocols and Interpretation

Studies on bone scan protocols for CA evaluation include planar and SPECT imaging routinely or planar imaging followed by SPECT if planar is positive. Planar imaging alone is limited as myocardial uptake cannot be distinguished from blood pool uptake, overlying rib uptake may add counts to the region of the heart, and attenuation correction is not feasible. SPECT overcomes these challenges.

Image interpretation of BS varies from visual, to semiquantitative methods and absolute quantification. According to the work of Perugini et al. [28], the most widely used method for *visual analysis* compares the myocardial uptake to bone (Perugini score), where grade 0 is absent myocardial uptake, grade 1 myocardial uptake lower than bone activity, grade 2 myocardial uptake equal or above bone activity and grade 3 is given if myocardial uptake is greater than bone activity with concomitant mild/absent bone uptake. Patients with ATTR CA showed increased DPD uptake (Perugini grade 2/3) in contrast to AL patients [28]. However, DPD uptake is not completely specific for this condition and some cardiac uptake does occur in a small proportion of patients with advanced AL CA. Examples of different myocardial uptake to bone scintigraphy are given in Fig. 3.11.

Several methods of measurement of bone scan uptake with *semiquantitative* indices, such as heart retention (HR), heart to whole-body retention (WBR) [29–31], heart-to-skull retention (HR/SR) [32] or heart-to-contralateral chest wall (H/CL) ratio, have been validated [33]. According to a multicentre study of Castano et al. [34], the diagnostic performance of the semiquantitative H/CL ratio is slightly better than the visual analysis. Moreover, Flaherty et al. [35] recently develop and validate a protocol for myocardial ^{99m}Tc -PYP uptake on a CZT scanner based on the established H/CL ratio. Using a diagnostic threshold H/CL ≥ 1.5 , the authors found a high correlation between CZT and planar H/CL ratios ($r = 0.92$, $P < 0.0001$) with a 100% agreement between both methods for the diagnosis of ATTR.

Finally, the diagnostic performance greatly increases when SPECT with *absolute quantification* of myocardial uptake is performed. In a study using ^{99m}Tc -HMDP in a small cohort of patients, myocardial maximum standardized

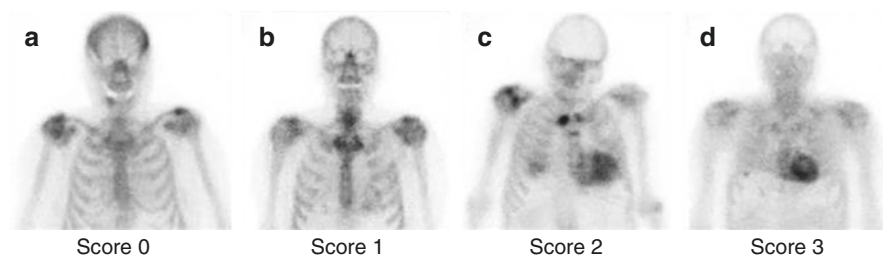


Fig. 3.11 Representative images illustrating the spectrum of ^{99m}Tc -DPD myocardial uptakes in four different cases. (a) No visually detectable myocardial uptake and normal bone activity (Score 0). (b) Low myocardial uptake lower than bone activity (Score 1). (c) Intense myocardial uptake equal or above bone activity (Score 2). (d) Intense myocardial uptake greater than bone with concomitant mild/absent bone uptake (Score 3). (Courtesy of Dr. Federico Caobelli, University Hospital Basel, Switzerland)

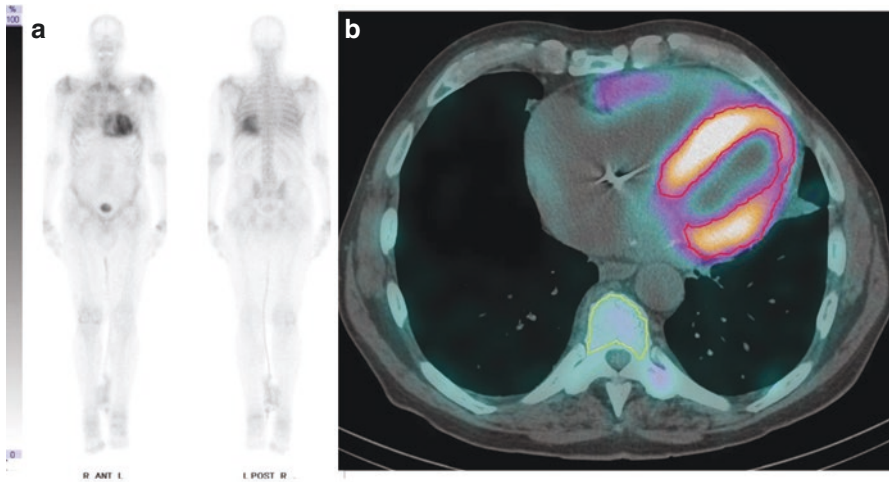


Fig. 3.12 Representative images of a patient with intensive myocardial uptake and concurrent reduced bone activity on planar imaging (**a**, Perugini score 3). On SPECT/CT imaging (**b**) isocontour VOIs were placed on the myocardium (red line), and on a vertebra (green line). Cardiac SUVmax was 15.6, cardiac SUVpeak was 14.8, cardiac SUVmax normalized to bone activity (nSUVmax) was 3.2, and SUVpeak normalized to bone activity (nSUVpeak) was 3.2. These findings were consistent with an ATTR amyloidosis. Reprinted with permission of Springer Nature from Caobelli F et al., *J. Nucl. Cardiol* 2020 [37]. No changes were made. SPECT/CT single-photon emission computed tomography/computed tomography, VOIs volume of interest, SUVmax maximum standardized uptake value

uptake value (SUVmax) accurately differentiated ATTR CA from other cardiac diseases. Of note, this measurement allowed the identification of a reference interval for individuals without ATTR CA, against which range a single potentially affected individual could be compared [36]. More recently, this concept was expanded by Caobelli et al. [37], showing that quantitative cardiac ^{99m}Tc -DPD SPECT is practical, allows the diagnosis of ATTR CA and provides a more accurate estimation of amyloid burden in patients with visual score grade 2 and 3. (Fig. 3.12).

Diagnostic Accuracy

Bone scintigraphy can be used to diagnose ATTR CA but not AL CA, with a sensitivity approaching ranged from 83% to 100% (with a pooled estimate of 92.2%), and the specificity ranged from 67% to 100% (with a pooled estimate of 95.4%) [28, 38]. However, not all bone tracers show equivalent diagnostic performance for CA. In fact, the use of ^{99m}Tc -methylene diphosphonate (^{99m}Tc -MDP) showed lower sensitivity and is considered inappropriate for patients with suspected ATTR CA [39].

^{99m}Tc -DPD and ^{99m}Tc -HMDP are the main bone-seeking tracers used for CA imaging in Europe. In the differential diagnosis, cardiac ^{99m}Tc -DPD uptake is strongly present in ATTR, absent in unaffected control subjects, and absent or weak

in AL CA (with a H/CL ratio < 1.5) [31, 33, 40, 41]. In the largest multicentre study, including 1217 patients with suspected CA, Gillmore et al. [28] proposed and validated a non-invasive algorithm to diagnose ATTR CA without the need of histology, but only with echocardiographic or CMR findings suggestive of CA, cardiac uptake at scintigraphy, and absence of monoclonal light chain gammopathy in serum and urine. They showed that the myocardial uptake on BS was $>99\%$ sensitive and 86% specific for cardiac ATTR amyloid, with false positives almost exclusively from uptake in patients with cardiac AL amyloidosis. Interestingly, when associated with the absence of a monoclonal protein in serum or urine, a bone scan with abnormal uptake (Grade 2 or 3) has a specificity and positive predictive value of 100% for a diagnosis of ATTR CA. On the contrary, if laboratory analysis detects monoclonal light chain gammopathy in serum and urine, extracardiac biopsy is required to confirm AL CA [28].

Among TTR mutation carriers, ^{99m}Tc -DPD uptake can be detected before clear echocardiographic and CMR phenotype development. Moreover, there seems to be a good correlation between ECV and cardiac uptake on ^{99m}Tc -DPD scintigraphy ($r = 0.533$; $p < 0.05$) (Fig. 3.13) [42]. Furthermore, in elderly patients with HFpEF, ^{99m}Tc -DPD scintigraphy is able to detect ATTR-wt [43, 44].

^{99m}Tc -HMDP showed similar diagnostic performance to detect cardiac ATTR amyloidosis prior to echocardiographic evidence of cardiac involvement. Various authors reported $90\text{--}100\%$ sensitivity and $81\text{--}96\%$ specificity for ATTR CA identification [45–47]. In addition, ^{99m}Tc -HMDP may aid differentiation between CA and other LV hypertrophy, provide prognostic information [46, 47], and assist in monitoring the progression of CA and the response to therapy [48].

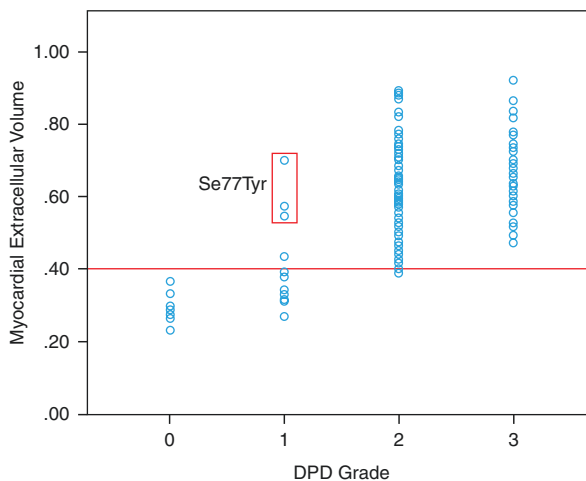


Fig. 3.13 ECV and cardiac uptake. As seen in this correlation between ECV and grade of abnormal cardiac uptake on ^{99m}Tc -DPD scintigraphy, only patients with the Se77Tyr variant had high ECV measurements with grade 1 abnormal uptake. DPD = 3,3-diphosphono-1,2-propanodicarboxylic acid; ECV = extracellular volume. From [42]

Another phosphate derivate extensively studied in the amyloid field that also showed to bind ATTR cardiac deposits with high affinity is $^{99m}\text{Tc-PYP}$. In fact, in a study conducted to validate the ability of $^{99m}\text{Tc-PYP}$ to distinguish between AL and ATTR CA, the authors found that subjects with ATTR CA had a significantly higher cardiac visual score than the AL type [33]. Moreover, the diagnostic performance is higher when a semiquantitative H/CL ratio is calculated (91–97% sensitivity and 92–100% specificity) [33, 34].

Finally, whole-body scan imaging with bone tracer provides information not only about cardiac involvement but also about other organs. Particularly, increased $^{99m}\text{Tc-DPD}$ uptake in the muscle has been described in ATTR CA on planar scintigraphy, as well as in the gluteal, shoulder, chest, and abdominal walls using SPECT/CT [27, 49]. However, this pattern of increased soft-tissue uptake has not been observed with $^{99m}\text{Tc-PYP}$ [50].

3.2.3.2 Innervation Radiotracers

Due to the amyloid infiltration into the myocardial and conduction tissue, patients with both AL and ATTR amyloidosis tend to develop cardiac dysautonomia [51, 52]. Scintigraphy with ^{123}I -metaiodobenzylguanidine ($^{123}\text{I-MIBG}$), an analogue of norepinephrine, is used for the indirect visualization of the sympathetic innervation of the heart [53]. The quantification of $^{123}\text{I-MIBG}$ uptake in the heart compared to the background (heart-to-mediastinum ratio, HMR) predicts clinical outcome of patients with chronic heart failure [54]. A reduced cardiac $^{123}\text{I-MIBG}$ uptake in patients with ATTR CA was described by several studies [55, 56]. Interestingly, $^{123}\text{I-MIBG}$ imaging can detect innervation changes earlier than other modalities, such as echocardiography [57] and bone scintigraphy [58]. Regarding the prognostic value of $^{123}\text{I-MIBG}$ uptake in ATTRm patients with familial amyloid polyneuropathy (FAP), a severe cardiac denervation at baseline is predictive of neurologic worsening after liver transplantation [59]. In fact, late HMR was identified as an independent prognostic predictor factor for 5-year all-cause mortality with a 42% mortality rate for those patients with late HMR <1.60 ($p < 0.001$). Therefore, $^{123}\text{I-MIBG}$ may be used to screen patients with TTR mutation allowing earlier CA detection before symptoms or function abnormalities occur [60].

In AL type patients, the myocardial uptake and turnover of $^{123}\text{I-MIBG}$ are heterogeneous and dependent on the presence or absence of congestive heart failure and cardiac autonomic dysfunction [61]. Of note, the presence of heart failure was associated with decreased HMR and increased washout rates. On the other hand, patients with autonomic dysfunction showed decreased HMR and washout rates. Recently, Noordzij et al. [57] demonstrated that $^{123}\text{I-MIBG}$ washout rate was higher irrespective of amyloid subtypes. Moreover, HMR was lower in ATTR patients without echocardiographic signs of amyloidosis than in patients with other types.

3.2.4 Positron Emission Tomography (PET)

In the last years, PET radiotracers, originally developed for imaging β -amyloid plaques in Alzheimer's disease have also demonstrated an affinity for amyloid fibrils and have gained an increased interest in the assessment of CA. Studies have reported the utility of ^{11}C -Pittsburgh compound B (PIB), ^{18}F -florbetapir, and ^{18}F -florbetaben for imaging AL and ATTR CA. Contrary to SPECT with bone agents, PET imaging with amyloid tracers seems to be the first to specifically image AL CA, with a high target-to-background ratio, with the potential to quantify amyloid cardiac and extracardiac burden and the response to therapy. Though, the role of PET/CT in cardiac amyloidosis is still limited.

^{11}C -PIB myocardial uptake was found to be elevated in both cardiac AL and ATTR with no uptake in control subjects [62, 63]. Furthermore, patients with ATTRm V30M type has myocardial PIB uptake on PET scan, but with significantly higher PIB retention in patients with full-length fibril type, generally associated with less cardiac involvement. (Fig. 3.14) [64].

Similar results were obtained using ^{18}F -florbetapir and ^{18}F -florbetaben [65–67]. Furthermore, an autopsy study showed that all myocardial sections of patients with CA (10AL, 10ATTR, 10 non-amyloid controls) had elevated uptake of ^{18}F -florbetapir compared to controls, interestingly with uptake greater in AL than ATTR ($p < 0.001$) [67]. Another study showed increased liver uptake of ^{18}F -Florbetapir in AL and normal liver uptake in ATTR CA, suggesting that ^{18}F -Florbetapir may preferentially bind AL fibrils [68]. ^{18}F -Florbetapen PET imaging can also identify and differentiate between CA and left ventricular hypertrophy secondary to longstanding hypertension [66].

Using semiquantitative parameters such as target-to-background ratio (TBR) [69], retention index (RI) [64, 65], SUV [66] or dynamic parameters [68], PET imaging has shown preliminary promise in quantifying amyloid disease burden. In a recent systematic review, including six studies, PET imaging with amyloid tracers demonstrated a pooled sensitivity of 0.95% and a pooled specificity of 0.98% for the detection of AL and ATTR CA. Importantly, the semiquantitative parameters showed significantly higher values for AL than ATTR patients (pooled standardized mean difference SMD = 0.96; $P < 0.001$) [70].

Amyloid specific agents may also provide information on the cardiac uptake and the response of therapy in patients with AL CA. In fact, some authors suggested that treatment-naïve AL patients might have higher cardiac uptake than those after chemotherapy [69, 71, 72].

Finally, whole-body PET/CT with ^{18}F -Florbetaben and ^{18}F -Florbetapir provides important structural and functional information regarding the extracardiac sites of amyloid deposition [73, 74] and may guide the management with novel fibril-resorbing therapies [75]. However, multicentre studies are required to evaluate the clinical utility as well as the potential of amyloid PET in the (early) therapy monitoring.

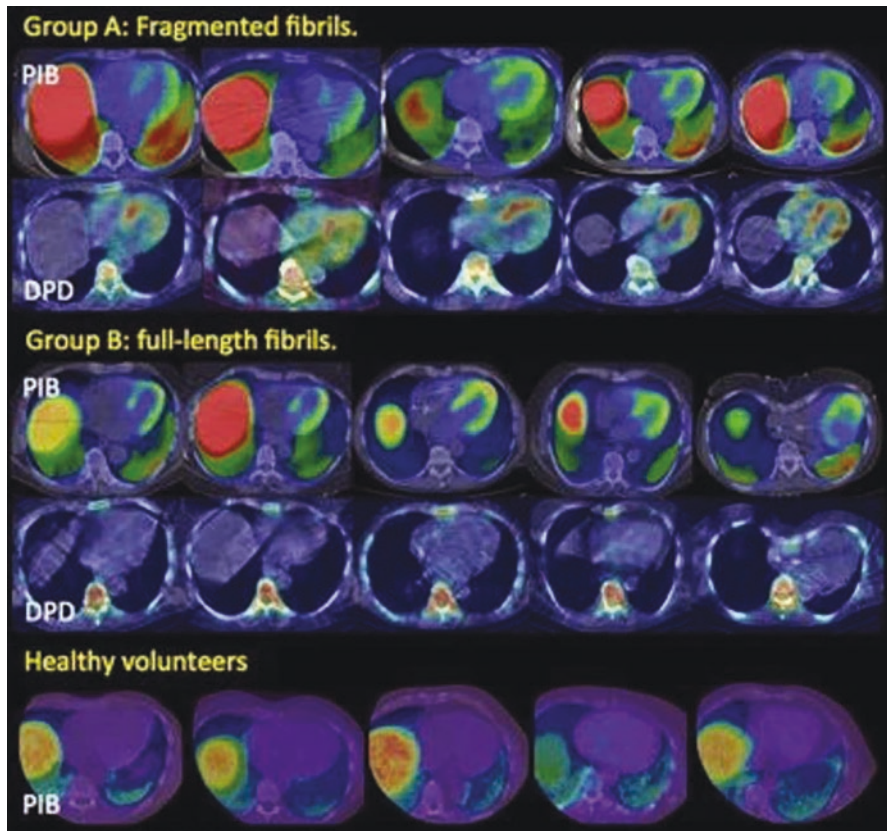


Fig. 3.14 Matched ^{11}C -PIB-PET (upper) and DPD SPECT (lower) images of patients with type A fibrils (group A) and type B fibrils (group B). At the bottom is ^{11}C -PIB-PET images from healthy volunteers. Reprinted under the terms of the Creative Commons Attribution 4.0 International License (<http://creativecommons.org/licenses/by/4.0/>). From Pilebro et al. [64] No changes were made. ^{11}C -PIB-PET Pittsburgh compound B- Positron Emission Tomography, DPD 3,3-diphosphono-1,2-propanodicarboxylic acid, SPECT single-photon emission computed tomography

Other PET tracers able to differentiate ATTR CA from AL CA include ^{18}F -Sodium fluoride (NaF). The use of a bone-seeking PET tracer could lead to an increase in diagnostic performance by improving imaging properties and allowing accurate quantification. In fact, some authors suggested that PET/CT with ^{18}F -NaF is more efficient than conventional $^{99\text{m}}\text{Tc}$ -diphosphonates imaging as it demonstrates faster kinetics and faster imaging time [76]. It was also noticed that type of ATTR mutation might influence ^{18}F -NaF tracer uptake [77]. Preliminary data showed increased uptake of ^{18}F -NaF in ATTR CA and no significant uptake in controls and AL patients [78, 79]. More recently, Martineau et al. [80] proved that the diagnostic accuracy for ATTR is higher when using quantitative analysis (sensitivity/specificity of 75%/100% for a target-to-background ratio using a cut-off value of 0.89).

3.2.5 Hybrid Imaging: PET/MRI

Novel trends in hybrid imaging, such as PET-magnetic resonance imaging (PET/MRI) are recently under investigation. Due to its higher spatial-temporal resolution, PET/MRI could constitute a one-stop-shop evaluation of amyloid load and cardiac function in patients needing rapid work-up. To date, only a few studies investigated the role of PET/MRI in CA. In particular, hybrid PET/MRI with ^{18}F -NaF is able to distinguish ATTR from AL/no CA patients, with equivalent performance compared with $^{99\text{m}}\text{Tc}$ -HMDP, but only when semi-quantification (myocardium-to-blood pool ratios) is used [81]. Though, contrast is low and visual interpretation may be challenging in routine. In another pilot study of patients with suspected CA, PET/MRI with ^{18}F -Florbetaben was performed for delimitation of systemic extent of amyloid deposition. The authors concluded that PET/MRI with amyloid tracer may provide important structural and functional information regarding the organs involved by the disease, with potential to guide biopsy and evaluate response to treatment [82] (Fig. 3.15).

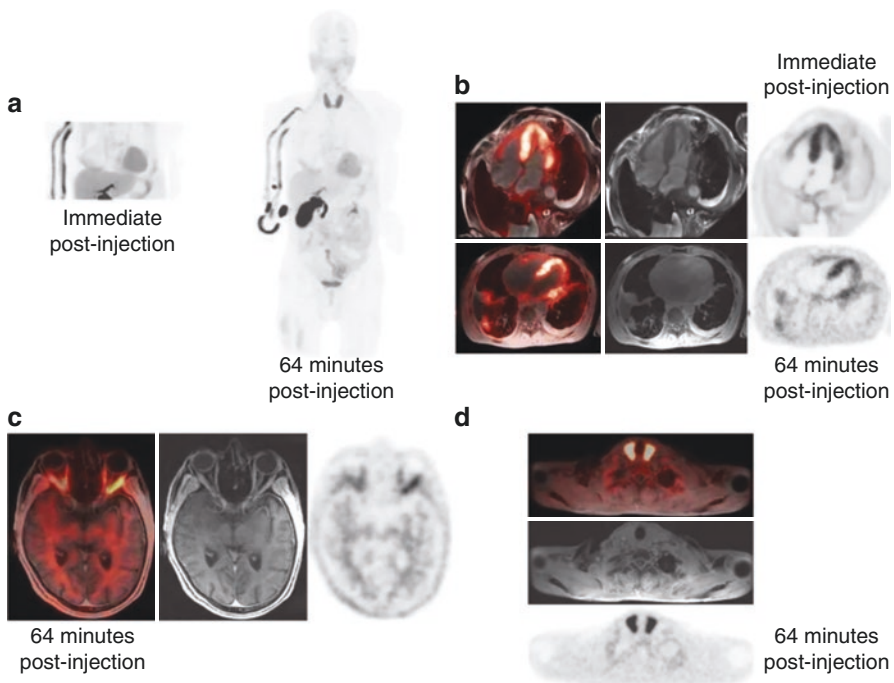


Fig. 3.15 Findings in a patient with systemic amyloidosis: (a) MIP and (b) cardiac bed images show intense myocardial ^{18}F -florbetaben uptake, suspicious for amyloid. Intense uptake was also demonstrated in the extraocular muscles, consistent with recent orbital MRI findings that were concerning for amyloid involvement (c). Although such manifestation is rare, intense uptake was noted in the thyroid glands (d). The patient had mild or subclinical hypothyroidism, with low free thyroxine (1.1 $\mu\text{g}/\text{dl}$) and upper limit of the TSH normal range (3.85–4.6 mIU/L). Physical examination of the neck also revealed discomfort on palpation. Images from Baratto et al. [82]. Reprinted under the terms of the Creative Commons Attribution 4.0 International License (<http://creativecommons.org/licenses/by/4.0/>)

However, future prospective studies are warranted on the role of integrated PET/MRI system for the diagnosis and progression of systemic amyloidosis, as well as highlighting technical issues due to the presence of device implantation artefacts, which may impair image interpretation, thus posing a challenge in evaluation with PET/MRI. In addition, with the promise of high spatial/temporal resolution and 3D coverage, MRI will be an important tool in the diagnosis and monitoring the benefits of new therapies.

3.2.6 Diagnostic Algorithm for Diagnosis and Sub-Typing of Cardiac Amyloidosis

A proposal for an algorithm using multi-modality imaging for diagnosis of CA and differentiation between AL and ATTR subtype is provided in Fig. 3.16.

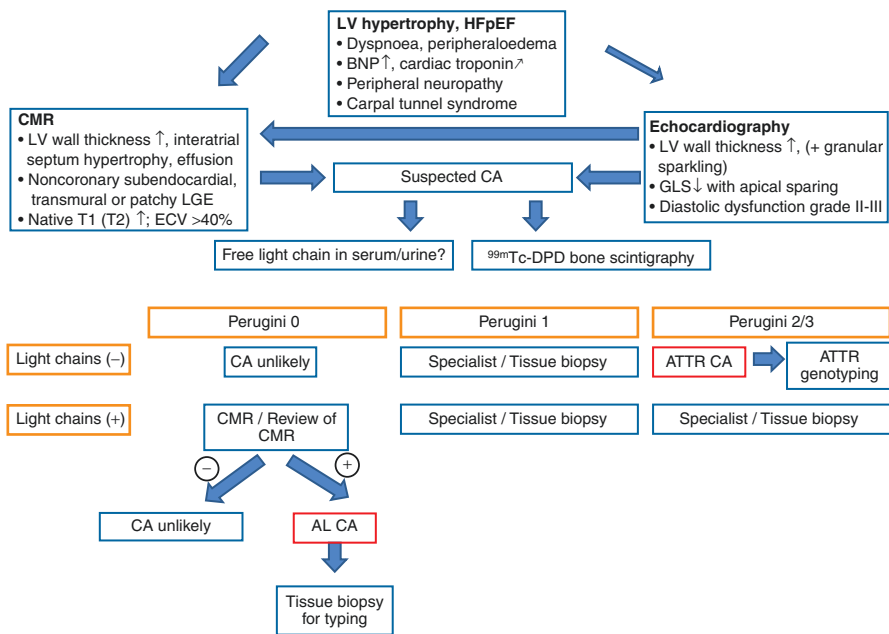


Fig. 3.16 Diagnostic algorithm for diagnosis and subtyping of cardiac amyloidosis. Histological confirmation should be pursued in all cases with inconclusive imaging results. *HFpEF* heart failure with preserved ejection fraction, *BNP* brain natriuretic peptide, *LV* left ventricular, *GLS* global longitudinal strain, *CMR* cardio magnetic resonance, *LGE* late gadolinium enhancement, *ECV* extracellular volume, *CA* cardiac amyloidosis; ^{99m}Tc-DPD technetium-99 m-3,3-diphosphono-1,2 propanodicarboxylic acid. As any algorithm, this algorithm may only cover the majority of patients with presumed cardiac amyloidosis. In all patients with unclear results interdisciplinary discussion between cardiologists, specialists in nuclear medicine, pathologists and geneticists is recommended

3.3 Treatment

The treatment to cardiac amyloidosis is two-fold: (1) optimal modified medical heart failure therapy including device therapy with careful titration of diuretics as cornerstone of therapy to avoid hypovolaemia and maintain adequate filling pressures; betablockers, angiotensin-converting enzyme inhibitors and angiotensin receptor blockers are poorly tolerated in cardiac amyloidosis; (2) treatment of the underlying disease.

Central to the treatment of AL amyloidosis is cytotoxic chemotherapy (e.g. bortezomib) [83]. Owing to age, renal function and advanced cardiac involvement (i.e. poor prognosis) the majority of patients are considered ineligible for stem cell transplantation [84].

Several pharmacotherapeutical options are now available for disease modification of ATTR amyloidosis: (1) *silencers* for reduction/elimination of the production of transthyretin [inotersen [85], patisiran [86]]; (2) *stabilizers* [tafamidis [87], diflunisal [88]] and (3) *degraders* for disruption of already disrupted amyloid fibrils are currently under study (Table 3.1).

3.4 Prognosis

The prognosis of virtually all cardiac diseases deteriorates with the presence of LGE. As regards, cardiac amyloidosis, there are some conflicting data in single-centre studies. A recent systematic review and meta-analysis, though, supported the prognostic role of LGE in risk stratification of patients with CA irrespective of cardiac biopsy results [89], and there is increasing evidence to use ECV as a prognostic marker [42, 90, 91]. Myocardial ECV remains an independent predictor of prognosis in cardiac ATTR after adjusting for known predictors and is the earliest disease marker to track amyloid regression [91, 92] (Fig. 3.17).

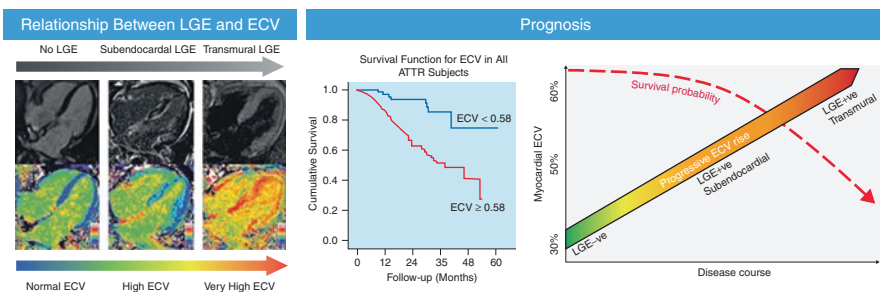


Fig. 3.17 The relationship between late gadolinium enhancement (LGE) patterns and ECV shows a typical correlation of very high ECV values and subendocardial or transmural LGE. In patients with ATTR, ECV was independently correlated with mortality. Adapted from [42]

ATTR CA despite showing more and more often transmural LGE than AL amyloidosis has a better prognosis [25]. This suggests additional processes contributing to cardiac dysfunction and mortality in AL CA not detectable by LGE such as a direct cardiotoxic effect of soluble light chain in AL CA which might also explain higher troponin level in AL CA [3]. Due to its diffuse uptake of gadolinium focal LGE may be less often detectable and ECV might be the better prognosticator in cardiac amyloidosis. ECV >45% carried a hazard ratio for death of 3.84 for mortality and was significant in a multivariate analysis with traditional prognostic factors (natriuretic peptides and grade of diastolic dysfunction) [90].

ECV can also be used to measure the myocyte response; detecting differences between AL and ATTR with an apparent relative (compensatory) hypertrophy response in ATTR not present in AL highlighting that amyloidosis is not just an interstitial disease [93]. In AL CA, all of the increase in left ventricular indexed mass is extracellular volume, whereas in patients with ATTR CA, the increase in mass is extracellular, with an additional 18% increase in the intracellular space [93].

Performed serially, CMR might be a means to follow response to treatment and changes in myocardial burden. ECV has been proposed to become a non-invasive test to quantify cardiac amyloid burden [14] and could be used as a tool to guide and monitor treatment [21]. Regression of ECV has been demonstrated in patients with AL cardiac amyloidosis and good clonal response to chemotherapy (Fig. 3.18) [92].

The prognostic value of nuclear imaging has also been evaluated in patients with CA. A few studies support the ability of semiquantitative parameters such as H/WB retention or H/CL ratio to identify higher risk of major adverse cardiac events, acute heart failure and mortality. In a study of 63 patients with ATTR CA, H/WB retention was used to quantify the degree of myocardial ^{99m}Tc -DPD uptake and was a prognostic “determinant” of outcome, either alone or in combination with left ventricle wall thickness. Interestingly, a wall thickness > 12 mm in combination with H/WB ratio ≥ 7.5 was associated with the highest event rate [94]. In a multicentre, retrospective study including 229 patients, Castano et al. [34] highlighted the prognostic value of ^{99m}Tc -PYP activity as quantified by H/CL. Over a 5-years follow-up period, a H/CL ≥ 1.6 was associated with a significantly worse survival, among patients with ATTR CA and was considered an independent predictor of poor outcome [34]. In addition, an apical sparing of tracer uptake pattern similar across ATTR-wt and ATTR-m subtypes was identified on myocardial scintigraphy with bone tracers, in accordance with echocardiographic and CMR findings, with similar prognostic value [95, 96]. However, there are no significant data on whether ^{99m}Tc -PYP scintigraphy could be used for reliable quantification of amyloid burden over time in ATTR CA. In fact, some research did not show any significant change during a 1.5-year follow-up despite obvious clinical progression [97]. Finally, Minamimoto et al. [98] showed that uptake of ^{11}C -PIB may be related to progressive amyloid deposition to the heart and can predict patient prognosis.

Apart from imaging, blood biomarkers such as cardiac troponin and brain natriuretic peptide levels have also been shown to provide important and easily obtainable prognostic information in patients with CA [99].

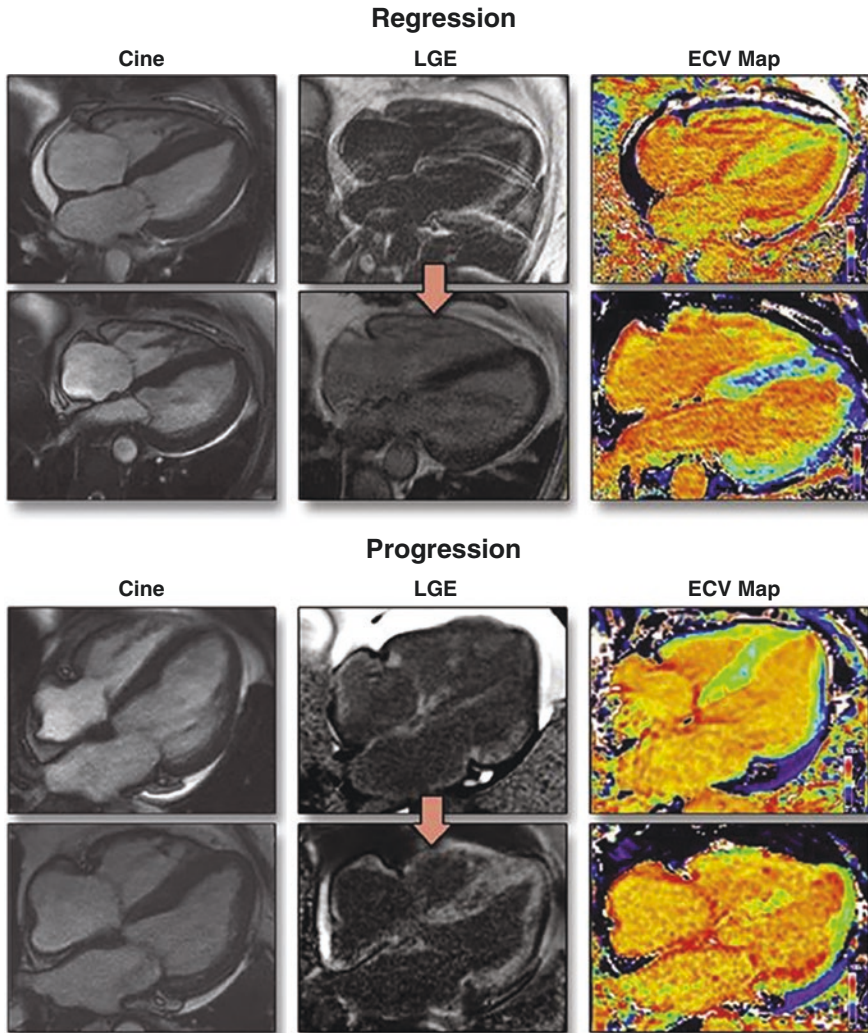


Fig. 3.18 Four chamber cine (left), corresponding LGE (middle) and ECV (right) mapping before and after chemotherapy in 2 patients with cardiac AL amyloidosis: 1 regressor (top) and 1 that progressed (bottom). *ECV* extracellular volume, *LGE* late gadolinium enhancement. From [92]

3.5 Conclusion

CA is an underdiagnosed cause of heart failure, significantly more common than previously thought. With specific treatments now available, diagnosing cardiac amyloidosis early and reliably with multi-modality cardiac imaging is possible and more important than ever. Recent advances in both CMR and nuclear imaging have

largely replaced the need for invasive cardiac biopsy in diagnosing CA. Future studies will have to prove the true clinical benefit of (earlier) diagnosis of CA and their role in monitoring the benefit of still very costly new therapeutic options.

References

1. Westermark P, Benson MD, Buxbaum JN, Cohen AS, Frangione B, Ikeda S, et al. A primer of amyloid nomenclature. *Amyloid*. 2007;14(3):179–83. <https://doi.org/10.1080/13506120701460923>.
2. Falk RH. Diagnosis and management of the cardiac amyloidoses. *Circulation*. 2005;112(13):2047–60. <https://doi.org/10.1161/CIRCULATIONAHA.104.489187>.
3. Falk RH, Alexander KM, Liao R, Dorbala S. AL (light-chain) cardiac amyloidosis: a review of diagnosis and therapy. *J Am Coll Cardiol*. 2016;68(12):1323–41. <https://doi.org/10.1016/j.jacc.2016.06.053>.
4. Kyle RA, Gertz MA. Primary systemic amyloidosis: clinical and laboratory features in 474 cases. *Semin Hematol*. 1995;32(1):45–59.
5. Mohammed SF, Mirzoyev SA, Edwards WD, Dogan A, Grogan DR, Dunlay SM, et al. Left ventricular amyloid deposition in patients with heart failure and preserved ejection fraction. *JACC Heart Fail*. 2014;2:113–22. <https://doi.org/10.1016/j.jchf.2013.11.004>.
6. Maurer MS, Bokhari S, Damy T, Dorbala S, Drachman BM, Fontana M, et al. Expert consensus recommendations for the suspicion and diagnosis of transthyretin cardiac amyloidosis. *Circ Heart Fail*. 2019;12(9):e006075. <https://doi.org/10.1161/CIRCHEARTFAILURE.119.006075>.
7. Treibel TA, Fontana M, Gilbertson JA, Castelletti S, White SK, Scully PR, et al. Occult transthyretin cardiac amyloid in severe calcific aortic stenosis: prevalence and prognosis in patients undergoing surgical aortic valve replacement. *Circ Cardiovasc Imaging*. 2016;9(8):e005066. <https://doi.org/10.1161/CIRCIMAGING.116.005066>.
8. Castaño A, Narotsky DL, Hamid N, Khaliq OK, Morgenstern R, DeLuca A, et al. Unveiling transthyretin cardiac amyloidosis and its predictors among elderly patients with severe aortic stenosis undergoing transcatheter aortic valve replacement. *Eur Heart J*. 2017;38:2879–87. <https://doi.org/10.1093/eurheartj/ehx350>.
9. Sekijima Y, Uchiyama S, Tojo K, Sano K, Shimizu Y, Imaeda T, et al. High prevalence of wild-type transthyretin deposition in patients with idiopathic carpal tunnel syndrome: a common cause of carpal tunnel syndrome in the elderly. *Hum Pathol*. 2011;42(11):1785–91. <https://doi.org/10.1016/j.humpath.2011.03.004>.
10. Phelan D, Collier P, Thavendiranathan P, Popović ZB, Hanna M, Plana JC, et al. Relative apical sparing of longitudinal strain using two-dimensional speckle-tracking echocardiography is both sensitive and specific for the diagnosis of cardiac amyloidosis. *Heart*. 2012;98(19):1442–8. <https://doi.org/10.1136/heartjnl-2012-302353>.
11. Hirata Y, Kusunose K, Miki H, Yamada H. Improvement of global longitudinal strain following high-dose chemotherapy and autologous peripheral blood stem cell transplantation in patients with amyloid light-chain cardiac amyloidosis: a case report. *Eur Heart J Case Rep*. 2019;3(4):1–6. <https://doi.org/10.1093/ehjcr/ytz225>.
12. Chacko L, Martone R, Cappelli F, Fontana M. Cardiac amyloidosis: updates in imaging. *Curr Cardiol Rep*. 2019;21(9):108. <https://doi.org/10.1007/s11886-019-1180-2>.
13. Banyersad SM, Moon JC, Whelan C, Hawkins PN, Wechalekar AD. Updates in cardiac amyloidosis: a review. *J Am Heart Assoc*. 2012;1(2):e000364. <https://doi.org/10.1161/JAHA.111.000364>.
14. Sado DM, Flett AS, Banyersad SM, White SK, Maestrini V, Quarta G, et al. Cardiovascular magnetic resonance measurement of myocardial extracellular volume in health and disease. *Heart*. 2012;98(19):1436–41. <https://doi.org/10.1136/heartjnl-2012-302346>.

15. Maceira AM, Joshi J, Prasad SK, Moon JC, Perugini E, Harding I, et al. Cardiovascular magnetic resonance in cardiac amyloidosis. *Circulation*. 2005;111(2):186–93. <https://doi.org/10.1161/01.CIR.0000152819.97857.9D>.
16. Syed IS, Glockner JF, Feng D, Araoz PA, Martinez MW, Edwards WD, et al. Role of cardiac magnetic resonance imaging in the detection of cardiac amyloidosis. *JACC Cardiovasc Imaging*. 2010;3(2):155–64. <https://doi.org/10.1016/j.jcmg.2009.09.023>.
17. Zhao L, Tian Z, Fang Q. Diagnostic accuracy of cardiovascular magnetic resonance for patients with suspected cardiac amyloidosis: a systematic review and meta-analysis. *BMC Cardiovasc Disord*. 2016;16:129. <https://doi.org/10.1186/s12872-016-0311-6>.
18. Haaf P, Garg P, Messroghli DR, Broadbent DA, Greenwood JP, Plein S. Cardiac T1 mapping and extracellular volume (ECV) in clinical practice: a comprehensive review. *J Cardiovasc Magn Reson*. 2016;18(1):89. <https://doi.org/10.1186/s12968-016-0308-4>.
19. Fent GJ, Garg P, Foley JRJ, Swoboda PP, Dobson LE, Erhayiem B, et al. Synthetic myocardial extracellular volume fraction. *JACC Cardiovasc Imaging*. 2017;10(11):1402–4. <https://doi.org/10.1016/j.jcmg.2016.12.007>.
20. Treibel TA, Fontana M, Maestrini V, Castelletti S, Rosmini S, Simpson J, et al. Automatic measurement of the myocardial Interstitium: synthetic extracellular volume quantification without hematocrit sampling. *JACC Cardiovasc Imaging*. 2016;9(1):54–63. <https://doi.org/10.1016/j.jcmg.2015.11.008>.
21. Banyersad SM, Sado DM, Flett AS, Gibbs SD, Pinney JH, Maestrini V, et al. Quantification of myocardial extracellular volume fraction in systemic AL amyloidosis: an equilibrium contrast cardiovascular magnetic resonance study. *Circ Cardiovasc Imaging*. 2013;6(1):34–9. <https://doi.org/10.1161/CIRCIMAGING.112.978627>.
22. Fontana M, Banyersad SM, Treibel TA, Maestrini V, Sado DM, White SK, et al. Native T1 mapping in transthyretin amyloidosis. *JACC Cardiovasc Imaging*. 2014;7(2):157–65. <https://doi.org/10.1016/j.jcmg.2013.10.008>.
23. Karamitsos TD, Piechnik SK, Banyersad SM, Fontana M, Ntusi NB, Ferreira VM, et al. Noncontrast T1 mapping for the diagnosis of cardiac amyloidosis. *JACC Cardiovasc Imaging*. 2013;6(4):488–97. <https://doi.org/10.1016/j.jcmg.2012.11.013>.
24. Kotecha T, Martinez-Naharro A, Treibel TA, Francis R, Nordin S, Abdel-Gadir A, et al. Myocardial edema and prognosis in amyloidosis. *J Am Coll Cardiol*. 2018;71(25):2919–31. <https://doi.org/10.1016/j.jacc.2018.03.536>.
25. Dungu JN, Valencia O, Pinney JH, Gibbs SD, Rowczenio D, Gilbertson JA, et al. CMR-based differentiation of AL and ATTR cardiac amyloidosis. *JACC Cardiovasc Imaging*. 2014;7(2):133–42. <https://doi.org/10.1016/j.jcmg.2013.08.015>.
26. Rubin J, Maurer MS. Cardiac amyloidosis: overlooked, underappreciated, and treatable. *Annu Rev Med*. 2020;71:203–19. <https://doi.org/10.1146/annurev-med-052918-020140>.
27. Kula RW, Engel WK, Line BR. Scanning for soft-tissue amyloid. *Lancet*. 1977;309(8002):92–3. [https://doi.org/10.1016/s0140-6736\(77\)91102-3](https://doi.org/10.1016/s0140-6736(77)91102-3).
28. Gillmore JD, Maurer MS, Falk RH, Merlini G, Damy T, Dispenzieri A, et al. Nonbiopsy diagnosis of cardiac transthyretin amyloidosis. *Circulation*. 2016;133(24):2404–12. <https://doi.org/10.1161/CIRCULATIONAHA.116.021612>.
29. Gallini C, Tutino F, Martone R, Ciaccio A, Costanzo EN, Taborchi G, et al. Semi-quantitative indices of cardiac uptake in patients with suspected cardiac amyloidosis undergoing ^{99m}Tc-HMDP scintigraphy. *J Nucl Cardiol*. 2019;28(1):90–9. <https://doi.org/10.1007/s12350-019-01643-w>.
30. Pradel S, Brun S, Victor G, Pascal P, Fournier P, Ribes D, et al. Pattern of myocardial ^{99m}Tc-HMDP uptake and impact on myocardial function in patients with transthyretin cardiac amyloidosis. *J Nucl Cardiol*. 2018;27(1):96–105. <https://doi.org/10.1007/s12350-018-1316-6>.
31. Rapezzi C, Quarta CC, Guidalotti PL, Longhi S, Pettinato C, Leone O, et al. Usefulness and limitations of ^{99m}Tc-3, 3-diphosphono-1, 2-propanodicarboxylic acid scintigraphy in the aetiological diagnosis of amyloidotic cardiomyopathy. *Eur J Nucl Med Mol Imaging*. 2011;38(3):470–8. <https://doi.org/10.1007/s00259-010-1642-7>.
32. Glaudemans AWJM, van Rheenen RWJ, van den Berg MP, Noordzij W, Koole M, Blokzijl H, et al. Bone scintigraphy with ^{99m}technetium-hydroxymethylene diphosphonate allows early

- diagnosis of cardiac involvement in patients with transthyretin-derived systemic amyloidosis. *Amyloid*. 2014;21(1):35–44. <https://doi.org/10.3109/13506129.2013.871250>.
33. Bokhari S, Castaño A, Pozniakoff T, Deslisle S, Latif F, Maurer MS. (99m)Tc-pyrophosphate scintigraphy for differentiating light-chain cardiac amyloidosis from the transthyretin-related familial and senile cardiac amyloidoses. *Circ Cardiovasc Imaging*. 2013;6(2):195–201. <https://doi.org/10.1161/CIRCIMAGING.112.000132>.
 34. Castano A, Haq M, Narotsky DL, Goldsmith J, Weinberg RL, Morgenstern R, et al. Multicenter study of planar technetium 99m pyrophosphate cardiac imaging: predicting survival for patients with ATTR cardiac amyloidosis. *JAMA Cardiol*. 2016;1(8):880–9. <https://doi.org/10.1001/jamacardio.2016.2839>.
 35. Flaherty KR, Morgenstern R, Pozniakoff T, DeLuca A, Castano A, Maurer MS, et al. ^{99m}Tc-pyrophosphate scintigraphy with cadmium zinc telluride cameras is a highly sensitive and specific imaging modality to diagnose transthyretin cardiac amyloidosis. *J Nucl Cardiol*. 2019;27(2):371–80. <https://doi.org/10.1007/s12350-019-01831-8>.
 36. Ramsay SC, Lindsay K, Fong W, Patford S, Younger J, Atherton J. Tc-HDP quantitative SPECT/CT in transthyretin cardiac amyloid and the development of a reference interval for myocardial uptake in the non-affected population. *Eur J Hybrid Imaging*. 2018;2(1):17. <https://doi.org/10.1186/s41824-018-0035-1>.
 37. Caobelli F, Braun M, Haaf P, Wild D, Zellweger MJ. Quantitative ^{99m}Tc-DPD SPECT/CT in patients with suspected ATTR cardiac amyloidosis: Feasibility and correlation with visual scores. *J Nucl Cardiol*. 2019;27(5):1456–63. <https://doi.org/10.1007/s12350-019-01893-8>.
 38. Treglia G, Glaudemans AWJM, Bertagna F, Hazenberg BPC, Erba PA, Giubbini R, et al. Diagnostic accuracy of bone scintigraphy in the assessment of cardiac transthyretin-related amyloidosis: a bivariate meta-analysis. *Eur J Nucl Med Mol Imaging*. 2018;45(11):1945–55. <https://doi.org/10.1007/s00259-018-4013-4>.
 39. Aljaroudi WA, Desai MY, Tang WH, Phelan D, Cerqueira MD, Jaber WA. Role of imaging in the diagnosis and management of patients with cardiac amyloidosis: state of the art review and focus on emerging nuclear techniques. *J Nucl Cardiol*. 2014;21(2):271–83. <https://doi.org/10.1007/s12350-013-9800-5>.
 40. Glaudemans AW, Slart RH, Zeebregts CJ, Veltman NC, Tio RA, Hazenberg BP, et al. Nuclear imaging in cardiac amyloidosis. *Eur J Nucl Med Mol Imaging*. 2009;36(4):702–14. <https://doi.org/10.1007/s00259-008-1037-1>.
 41. Perugini E, Guidalotti PL, Salvi F, Cooke RM, Pettinato C, Riva L, et al. Noninvasive etiologic diagnosis of cardiac amyloidosis using ^{99m}Tc-3,3-diphosphono-1,2-propanodicarboxylic acid scintigraphy. *J Am Coll Cardiol*. 2005;46(6):1076–84. <https://doi.org/10.1016/j.jacc.2005.05.073>.
 42. Martínez-Naharro A, Treibel TA, Abdel-Gadir A, Bulluck H, Zumbo G, Knight DS, et al. Magnetic resonance in transthyretin cardiac amyloidosis. *J Am Coll Cardiol*. 2017;70(4):466–77. <https://doi.org/10.1016/j.jacc.2017.05.053>.
 43. Bennani Smires Y, Victor G, Ribes D, Berry M, Cognet T, Méjean S, et al. Pilot study for left ventricular imaging phenotype of patients over 65 years old with heart failure and preserved ejection fraction: the high prevalence of amyloid cardiomyopathy. *Int J Cardiovasc Imaging*. 2016;32(9):1403–13. <https://doi.org/10.1007/s10554-016-0915-z>.
 44. González-López E, Gallego-Delgado M, Guzzo-Merello G, de Haro-Del Moral FJ, Cobo-Marcos M, Robles C, et al. Wild-type transthyretin amyloidosis as a cause of heart failure with preserved ejection fraction. *Eur Heart J*. 2015;36(38):2585–94. <https://doi.org/10.1093/eurheartj/ehv338>.
 45. Cappelli F, Gallini C, Di Mario C, Costanzo EN, Vaggelli L, Tutino F, et al. Accuracy of ^{99m}Tc-Hydroxymethylene diphosphonate scintigraphy for diagnosis of transthyretin cardiac amyloidosis. *J Nucl Cardiol*. 2019;26(2):497–504. <https://doi.org/10.1007/s12350-017-0922-z>.
 46. Cariou E, Bennani Smires Y, Victor G, Robin G, Ribes D, Pascal P, et al. Diagnostic score for the detection of cardiac amyloidosis in patients with left ventricular hypertrophy and impact on prognosis. *Amyloid*. 2017;24(2):101–9. <https://doi.org/10.1080/13506129.2017.1333956>.

47. Galat A, Rosso J, Guellich A, Van Der Gucht A, Rappeneau S, Bodez D, et al. Usefulness of (99m)Tc-HMDP scintigraphy for the etiologic diagnosis and prognosis of cardiac amyloidosis. *Amyloid*. 2015;22(4):210–20. <https://doi.org/10.3109/13506129.2015.1072089>.
48. Damy T, Judge DP, Kristen AV, Berthet K, Li H, Aarts J. Cardiac findings and events observed in an open-label clinical trial of tafamidis in patients with non-Val 30Met and non-Val 122Ile hereditary transthyretin amyloidosis. *J Cardiovasc Transl Res*. 2015;8(2):117–27. <https://doi.org/10.1007/s12265-015-9613-9>.
49. Hutt DF, Quigley AM, Page J, Hall ML, Burniston M, Gopaul D, et al. Utility and limitations of 3,3-diphosphono-1,2-propanodicarboxylic acid scintigraphy in systemic amyloidosis. *Eur Heart J Cardiovasc Imaging*. 2014;15(11):1289–98. <https://doi.org/10.1093/ehjci/jeu107>.
50. Sperry BW, Gonzalez MH, Brunken R, Cerqueira MD, Hanna M, Jaber WA. Non-cardiac uptake of technetium-99m pyrophosphate in transthyretin cardiac amyloidosis. *J Nucl Cardiol*. 2019;26(5):1630–7. <https://doi.org/10.1007/s12350-017-1166-7>.
51. Falk RH, Comenzo RL, Skinner M. The systemic amyloidoses. *N Engl J Med*. 1997;337(13):898–909. <https://doi.org/10.1056/NEJM199709253371306>.
52. Goldstein DS. Cardiac Dysautonomia and survival in hereditary transthyretin amyloidosis. *JACC Cardiovasc Imaging*. 2016;9(12):1442–5. <https://doi.org/10.1016/j.jcmg.2016.08.003>.
53. Bokhari S, Shahzad R, Castaño A, Maurer MS. Nuclear imaging modalities for cardiac amyloidosis. *J Nucl Cardiol*. 2014;21(1):175–84. <https://doi.org/10.1007/s12350-013-9803-2>.
54. Chen W, Cao Q, Dilsizian V. Variation of heart-to-mediastinal ratio in (123)I-MIBG cardiac sympathetic imaging: its affecting factors and potential corrections. *Curr Cardiol Rep*. 2011;13(2):132–7. <https://doi.org/10.1007/s11886-010-0157-y>.
55. Delahaye N, Dinanian S, Slama MS, Mzabi H, Samuel D, Adams D, et al. Cardiac sympathetic denervation in familial amyloid polyneuropathy assessed by iodine-123 metaiodobenzylguanidine scintigraphy and heart rate variability. *Eur J Nucl Med*. 1999;26(4):416–24. <https://doi.org/10.1007/s002590050406>.
56. Tanaka M, Hongo M, Kinoshita O, Takabayashi Y, Fujii T, Yazaki Y, et al. Iodine-123 metaiodobenzylguanidine scintigraphic assessment of myocardial sympathetic innervation in patients with familial amyloid polyneuropathy. *J Am Coll Cardiol*. 1997;29(1):168–74. [https://doi.org/10.1016/s0735-1097\(96\)00438-x](https://doi.org/10.1016/s0735-1097(96)00438-x).
57. Noordzij W, Glaudemans AW, van Rheenen RW, Hazenberg BP, Tio RA, Dierckx RA, et al. (123)I-labelled metaiodobenzylguanidine for the evaluation of cardiac sympathetic denervation in early stage amyloidosis. *Eur J Nucl Med Mol Imaging*. 2012;39(10):1609–17. <https://doi.org/10.1007/s00259-012-2187-8>.
58. Piekarski E, Chequer R, Algalarrondo V, Eliahou L, Mahida B, Vigne J, et al. Cardiac denervation evidenced by MIBG occurs earlier than amyloid deposits detection by diphosphonate scintigraphy in TTR mutation carriers. *Eur J Nucl Med Mol Imaging*. 2018;45(7):1108–18. <https://doi.org/10.1007/s00259-018-3963-x>.
59. Delahaye N, Rouzet F, Sarda L, Tamas C, Dinanian S, Plante-Bordeneuve V, et al. Impact of liver transplantation on cardiac autonomic denervation in familial amyloid polyneuropathy. *Medicine*. 2006;85(4):229–38. <https://doi.org/10.1097/01.md.0000232559.22098.c3>.
60. Coutinho MC, Cortez-Dias N, Cantinho G, Conceição I, Oliveira A, Bordalo e Sá a et al. reduced myocardial 123-iodine metaiodobenzylguanidine uptake: a prognostic marker in familial amyloid polyneuropathy. *Circ Cardiovasc Imaging*. 2013;6(5):627–36. <https://doi.org/10.1161/CIRCIMAGING.112.000367>.
61. Hongo M, Urushibata K, Kai R, Takahashi W, Koizumi T, Uchikawa S, et al. Iodine-123 metaiodobenzylguanidine scintigraphic analysis of myocardial sympathetic innervation in patients with AL (primary) amyloidosis. *Am Heart J*. 2002;144(1):122–9. <https://doi.org/10.1067/mhj.2002.123115>.
62. Antoni G, Lubberink M, Estrada S, Axelsson J, Carlson K, Lindsjö L, et al. In vivo visualization of amyloid deposits in the heart with 11C-PIB and PET. *J Nucl Med*. 2013;54(2):213–20. <https://doi.org/10.2967/jnumed.111.102053>.

63. Ezawa N, Katoh N, Oguchi K, Yoshinaga T, Yazaki M, Sekijima Y. Visualization of multiple organ amyloid involvement in systemic amyloidosis using ¹¹C-PiB PET imaging. *Eur J Nucl Med Mol Imaging*. 2018;45(3):452–61. <https://doi.org/10.1007/s00259-017-3814-1>.
64. Pilebro B, Arvidsson S, Lindqvist P, Sundström T, Westermark P, Antoni G, et al. Positron emission tomography (PET) utilizing Pittsburgh compound B (PiB) for detection of amyloid heart deposits in hereditary transthyretin amyloidosis (ATTR). *J Nucl Cardiol*. 2018;25(1):240–8. <https://doi.org/10.1007/s12350-016-0638-5>.
65. Dorbala S, Vangala D, Semer J, Strader C, Bruyere JR, Di Carli MF, et al. Imaging cardiac amyloidosis: a pilot study using ¹⁸F-florbetapir positron emission tomography. *Eur J Nucl Med Mol Imaging*. 2014;41(9):1652–62. <https://doi.org/10.1007/s00259-014-2787-6>.
66. Law WP, Wang WY, Moore PT, Mollee PN, Ng AC. Cardiac amyloid imaging with ¹⁸F-Florbetaben PET: a pilot study. *J Nucl Med*. 2016;57(11):1733–9. <https://doi.org/10.2967/jnumed.115.169870>.
67. Park MA, Padera RF, Belanger A, Dubey S, Hwang DH, Veeranna V, et al. ¹⁸F-Florbetapir binds specifically to myocardial light chain and transthyretin amyloid deposits: autoradiography study. *Circ Cardiovasc Imaging*. 2015;8(8):e002954. <https://doi.org/10.1161/CIRCIMAGING.114.002954>.
68. Osborne DR, Acuff SN, Stuckey A, Wall JS. A routine PET/CT protocol with streamlined calculations for assessing cardiac amyloidosis using (18)F-Florbetapir. *Front Cardiovasc Med*. 2015;2:23. <https://doi.org/10.3389/fcvm.2015.00023>.
69. Lee SP, Lee ES, Choi H, Im HJ, Koh Y, Lee MH, et al. ¹¹C-Pittsburgh B PET imaging in cardiac amyloidosis. *JACC Cardiovasc Imaging*. 2015;8(1):50–9. <https://doi.org/10.1016/j.jcmg.2014.09.018>.
70. Kim YJ, Ha S, Kim YI. Cardiac amyloidosis imaging with amyloid positron emission tomography: a systematic review and meta-analysis. *J Nucl Cardiol*. 2018;27(1):123–32. <https://doi.org/10.1007/s12350-018-1365-x>.
71. Kircher M, Ihne S, Brumberg J, Morbach C, Knop S, Kortüm KM, et al. Detection of cardiac amyloidosis with ¹⁸F-Florbetaben-PET/CT in comparison to echocardiography, cardiac MRI and DPD-scintigraphy. *Eur J Nucl Med Mol Imaging*. 2019;46(7):1407–16. <https://doi.org/10.1007/s00259-019-04290-y>.
72. Manwani R, Page J, Lane T, Burniston M, Skillen A, Lachmann HJ, et al. A pilot study demonstrating cardiac uptake with ¹⁸F-florbetapir PET in AL amyloidosis patients with cardiac involvement. *Amyloid*. 2018;25(4):247–52. <https://doi.org/10.1080/13506129.2018.1552852>.
73. Mestre-Torres J, Lorenzo-Bosquet C, Cuberas-Borrós G, Gironella M, Solans-Laqué R, Fernández-Codina A, et al. Utility of the ¹⁸F-Florbetapir positron emission tomography in systemic amyloidosis. *Amyloid*. 2018;25(2):109–14. <https://doi.org/10.1080/13506129.2018.1467313>.
74. Wagner T, Page J, Burniston M, Skillen A, Ross JC, Manwani R, et al. Extracardiac ¹⁸F-florbetapir imaging in patients with systemic amyloidosis: more than hearts and minds. *Eur J Nucl Med Mol Imaging*. 2018;45(7):1129–38. <https://doi.org/10.1007/s00259-018-3995-2>.
75. Ehman EC, El-Sady MS, Kijewski MF, Khor YM, Jacob S, Ruberg FL, et al. Early detection of multiorgan light-chain amyloidosis by whole-body ¹⁸F-Florbetapir PET/CT. *J Nucl Med*. 2019;60(9):1234–9. <https://doi.org/10.2967/jnumed.118.221770>.
76. Van Der Gucht A, Galat A, Rosso J, Guellich A, Garot J, Bodez D, et al. [¹⁸F]-NaF PET/CT imaging in cardiac amyloidosis. *J Nucl Cardiol*. 2016;23(4):846–9. <https://doi.org/10.1007/s12350-015-0287-0>.
77. Gagliardi C, Tabacchi E, Bonfiglioli R, Diodato S, Nanni C, Guidalotti P, et al. Does the etiology of cardiac amyloidosis determine the myocardial uptake of [¹⁸F]-NaF PET/CT. *J Nucl Cardiol*. 2017;24(2):746–9. <https://doi.org/10.1007/s12350-016-0457-8>.
78. Morgenstern R, Yeh R, Castano A, Maurer MS, Bokhari S. ¹⁸Fluorine sodium fluoride positron emission tomography, a potential biomarker of transthyretin cardiac amyloidosis. *J Nucl Cardiol*. 2018;25(5):1559–67. <https://doi.org/10.1007/s12350-017-0799-x>.

79. Trivieri MG, Dweck MR, Abgral R, Robson PM, Karakatsanis NA, Lala A, et al. ¹⁸F-sodium fluoride PET/MR for the assessment of cardiac amyloidosis. *J Am Coll Cardiol*. 2016;68(24):2712–4. <https://doi.org/10.1016/j.jacc.2016.09.953>.
80. Martineau P, Finnerty V, Giraldeau G, Authier S, Harel F, Pelletier-Galarneau M. Examining the sensitivity of ¹⁸F-NaF PET for the imaging of cardiac amyloidosis. *J Nucl Cardiol*. 2019;28(1):209–18. <https://doi.org/10.1007/s12350-019-01675-2>.
81. Abulizi M, Sifaoui I, Wuliya-Gariepy M, Kharoubi M, Israël JM, Emsen B, et al. ¹⁸F-sodium fluoride PET/MRI myocardial imaging in patients with suspected cardiac amyloidosis. *J Nucl Cardiol*. 2019;2019:31512197. <https://doi.org/10.1007/s12350-019-01885-8>.
82. Baratto L, Park SY, Hatami N, Gulaka P, Vasawala S, Yohannan TK, et al. ¹⁸F-florbetaben whole-body PET/MRI for evaluation of systemic amyloid deposition. *EJNMMI Res*. 2018;8(1):66. <https://doi.org/10.1186/s13550-018-0425-1>.
83. Wechalekar AD, Gillmore JD, Hawkins PN. Systemic amyloidosis. *Lancet*. 2016;387(10038):2641–54. [https://doi.org/10.1016/S0140-6736\(15\)01274-X](https://doi.org/10.1016/S0140-6736(15)01274-X).
84. Gertz MA. Immunoglobulin light chain amyloidosis diagnosis and treatment algorithm 2018. *Blood Cancer J*. 2018;8(5):44. <https://doi.org/10.1038/s41408-018-0080-9>.
85. Benson MD, Waddington-Cruz M, Berk JL, Polydefkis M, Dyck PJ, Wang AK, et al. Inotersen treatment for patients with hereditary transthyretin amyloidosis. *N Engl J Med*. 2018;379(1):22–31. <https://doi.org/10.1056/NEJMoa1716793>.
86. Adams D, Gonzalez-Duarte A, O’Riordan WD, Yang CC, Ueda M, Kristen AV, et al. Patisiran, an RNAi therapeutic, for hereditary transthyretin amyloidosis. *N Engl J Med*. 2018;379(1):11–21. <https://doi.org/10.1056/NEJMoa1716153>.
87. Maurer MS, Schwartz JH, Gundapaneni B, Elliott PM, Merlini G, Waddington-Cruz M, et al. Tafamidis treatment for patients with transthyretin amyloid cardiomyopathy. *N Engl J Med*. 2018;379(11):1007–16. <https://doi.org/10.1056/NEJMoa1805689>.
88. Ikram A, Donnelly JP, Sperry BW, Samaras C, Valent J, Hanna M. Diflunisal tolerability in transthyretin cardiac amyloidosis: a single center’s experience. *Amyloid*. 2018;25(3):197–202. <https://doi.org/10.1080/13506129.2018.1519507>.
89. Raina S, Lensing SY, Nairouz RS, Pothineni NV, Hakeem A, Bhatti S, et al. Prognostic value of late gadolinium enhancement CMR in systemic amyloidosis. *JACC Cardiovasc Imaging*. 2016;9(11):1267–77. <https://doi.org/10.1016/j.jcmg.2016.01.036>.
90. Banyersad SM, Fontana M, Maestrini V, Sado DM, Captur G, Petrie A, et al. T1 mapping and survival in systemic light-chain amyloidosis. *Eur Heart J*. 2015;36(4):244–51. <https://doi.org/10.1093/eurheartj/ehu444>.
91. Martinez-Naharro A, Kotecha T, Norrington K, Boldrini M, Rezk T, Quarta C, et al. Native T1 and extracellular volume in transthyretin amyloidosis. *JACC Cardiovasc Imaging*. 2019;12(5):810–9. <https://doi.org/10.1016/j.jcmg.2018.02.006>.
92. Martinez-Naharro A, Abdel-Gadir A, Treibel TA, Zumbo G, Knight DS, Rosmini S, et al. CMR-verified regression of cardiac AL amyloid after chemotherapy. *JACC Cardiovasc Imaging*. 2018;11(1):152–4. <https://doi.org/10.1016/j.jcmg.2017.02.012>.
93. Fontana M, Banyersad SM, Treibel TA, Abdel-Gadir A, Maestrini V, Lane T, et al. Differential myocyte responses in patients with cardiac transthyretin amyloidosis and light-chain amyloidosis: a cardiac MR imaging study. *Radiology*. 2015;277(2):388–97. <https://doi.org/10.1148/radiol.2015141744>.
94. Rapezzi C, Quarta CC, Guidalotti PL, Pettinato C, Fanti S, Leone O, et al. Role of ^{99m}Tc-DPD scintigraphy in diagnosis and prognosis of hereditary transthyretin-related cardiac amyloidosis. *JACC Cardiovasc Imaging*. 2011;4(6):659–70. <https://doi.org/10.1016/j.jcmg.2011.03.016>.
95. Sperry BW, Vranian MN, Tower-Rader A, Hachamovitch R, Hanna M, Brunken R, et al. Regional variation in technetium pyrophosphate uptake in transthyretin cardiac amyloidosis and impact on mortality. *JACC Cardiovasc Imaging*. 2018;11(2 Pt 1):234–42. <https://doi.org/10.1016/j.jcmg.2017.06.020>.
96. Van Der Gucht A, Cottureau AS, Abulizi M, Guellich A, Blanc-Durand P, Israel JM, et al. Apical sparing pattern of left ventricular myocardial ^{99m}Tc-HMDP uptake in patients with

- transthyretin cardiac amyloidosis. *J Nucl Cardiol*. 2018;25(6):2072–9. <https://doi.org/10.1007/s12350-017-0894-z>.
97. Castaño A, DeLuca A, Weinberg R, Pozniakoff T, Blaner WS, Pirmohamed A, et al. Serial scanning with technetium pyrophosphate (^{99m}Tc -PYP) in advanced ATTR cardiac amyloidosis. *J Nucl Cardiol*. 2016;23(6):1355–63. <https://doi.org/10.1007/s12350-015-0261-x>.
 98. Minamimoto R, Awaya T, Iwama K, Hotta M, Nakajima K, Hirai R, et al. Significance of ^{11}C -PIB PET/CT in cardiac amyloidosis compared with ^{99m}Tc -aprotinin scintigraphy: a pilot study. *J Nucl Cardiol*. 2018;27(1):202–9. <https://doi.org/10.1007/s12350-018-1260-5>.
 99. Grogan M, Scott CG, Kyle RA, Zeldenrust SR, Gertz MA, Lin G, et al. Natural history of Wild-type transthyretin cardiac amyloidosis and risk stratification using a novel staging system. *J Am Coll Cardiol*. 2016;68(10):1014–20. <https://doi.org/10.1016/j.jacc.2016.06.033>.

Part III

Ischemic Diseases



Molecular Imaging of Vulnerable Plaque

4

Riccardo Laudicella, Kamani Christel, Irene A. Burger,
Sergio Baldari, and Pierpaolo Alongi

Contents

4.1 Introduction.....	74
4.2 Biology and Pathogenesis of Atherosclerosis.....	75
4.3 Metabolism of Glucose in Atherosclerosis.....	83
4.4 Targeting Chemokine Receptor Expression in Vulnerable Plaque.....	87
4.5 Targeting Microcalcification in Atherosclerosis.....	90
4.6 Targeting Neovascularization in Atherosclerosis.....	93

Riccardo Laudicella and Kamani Christel contributed equally with all other contributors.

R. Laudicella

Nuclear Medicine Unit, Department of Biomedical and Dental Sciences and Morpho-Functional Imaging, University of Messina, Messina, Italy

K. Christel

Nuclear Medicine and Molecular Imaging Department, Lausanne University Hospital, Lausanne, Switzerland

e-mail: Christel-Hermann.Kamani@chuv.ch

I. A. Burger

Department of Nuclear Medicine, University Hospital Zurich, University of Zurich, Zürich, Switzerland

Department of Nuclear Medicine, Kantonsspital Baden, Baden, Switzerland

e-mail: irene.burger@usz.ch

S. Baldari

Nuclear Medicine Unit, Department of Biomedical and Dental Sciences and Morpho-Functional Imaging, University of Messina, Messina, Italy

e-mail: Sergio.baldari@unime.it

P. Alongi (✉)

Nuclear Medicine Unit, Fondazione Istituto G.Giglio, Contrada Pietrapollastra-Pisciotto, Cefalù, Italy

4.7 Targeting SSRT-2 Receptor Expression in Atherosclerosis with DOTA-Derivatives-PET.....	96
4.8 Summary.....	96
References.....	98

4.1 Introduction

The knowledge of vulnerable plaque is evolving rapidly in the last decade from the pioneering studies uncovering the pivotal role of plaque rupture and coronary thrombosis as the major cause of acute myocardial infarction and sudden cardiac death to the developing of new imaging modality and treatments. Many cellular and molecular pathways are involved in the pathogenesis of vulnerable plaque, including monocyte mobilization, the transformation of monocytes to phagocytic, tissue macrophages at the site of the atheroma, toxic interaction of phagocytized lipids, and cellular debris that result in the necrotic core, the structure of the atheroma (particularly the thin cap of atheroma), and the dual role of calcification [1].

New biological mechanisms beyond the simple accumulation of lipids have been demonstrated at the basis of lesion vulnerability such as tissue proteolysis by matrix metalloproteinases, recognized an essential factor responsible for rupture of the fibrous cap. A post-mortem study finally defined the role of necrotic core size, flogosis, and fibrous cap thickness. However, the diagnosis *in vivo* of vulnerable plaque remains still theoretic in the clinical scenario.

Nowadays, the developing role of new nuclear medicine imaging techniques, through the ongoing advancements in molecular imaging and new radiopharmaceutical compounds, surpassed the conventional morphological evaluation, permitting the assessment of specific bio-molecular targets involved in the plaque pathogenesis.

The first molecular imaging technique to study atheroma utilized ^{14}C and ^3H cholesterol administered to 13 patients (either orally or intravenously or both) to determine the turnover of cholesterol in atheroma that was confirmed by the arterial specimens [2]. Subsequently in the 1980s *in vivo* images of the carotid arteries were also described using autologous radioiodine-labeled or Tc-99 m- low-density lipoprotein (LDL) showing a greater uptake in parts of the lesions with foam cells and macrophages [3].

Positron emission tomography (PET) using different radiopharmaceutical agents has become a validated molecular imaging technique for the characterization of atherosclerotic plaque and for non-invasive quantification of plaque inflammation following therapeutic interventions targeted at reducing atherosclerotic inflammation [4–6]. In this regard, ^{18}F -fluorodeoxyglucose (FDG) PET/CT was demonstrated to be an accurate tool in the evaluation of the inflammatory activity of blood vessels, reflecting the glucose metabolism of intraplaque macrophage infiltration [7].

Furthermore, other novel radiopharmaceutical agents have been developed focusing on the evaluation of inflammatory processes in the arterial wall [5–7]. The most relevant application regards ^{18}F -sodium fluoride (NaF) PET as an emerging

tool in the assessment of ongoing microcalcification [8], but other more radiotracers may provide crucial information on specific metabolic targets involved in the pathophysiology of plaque, such as chemokine receptor CXCR4-expression [9] or amyloid- β deposition [10].

This chapter will focus on the biological and clinical correlates of arterial radiotracer uptake using new relevant emerging radiotracers in PET (fused with CT or MRI) and single photon emission tomography (SPECT), to highlight recent evidence in the evaluation of vulnerable plaque.

4.2 Biology and Pathogenesis of Atherosclerosis

Atherosclerosis is a multifocal disease resulting from the accumulation of fatty and/or fibrous material in the subendothelial space (intima) of medium and large-sized arteries. Atherosclerosis is initiated by the interplay between endothelial cells (ECs) and atherogenic stimuli, such as hyperlipidemia and disturbed blood flow [8, 9] (Fig. 4.1). Over time, a chronic inflammatory response occurs and involves numerous cellular components of the immune system, leading to the progression of atherosclerotic plaques, with numerous complications [8, 10]. Obstruction of the arterial lumen can occur, leading to tissue ischemia. In addition, rupture or erosion of a clinically silent atherosclerotic plaque can also occur, leading to acute thrombotic occlusion of the vessel, with life-threatening clinical conditions such as coronary syndrome or stroke. Atherosclerosis is by far the leading cause of cardiovascular

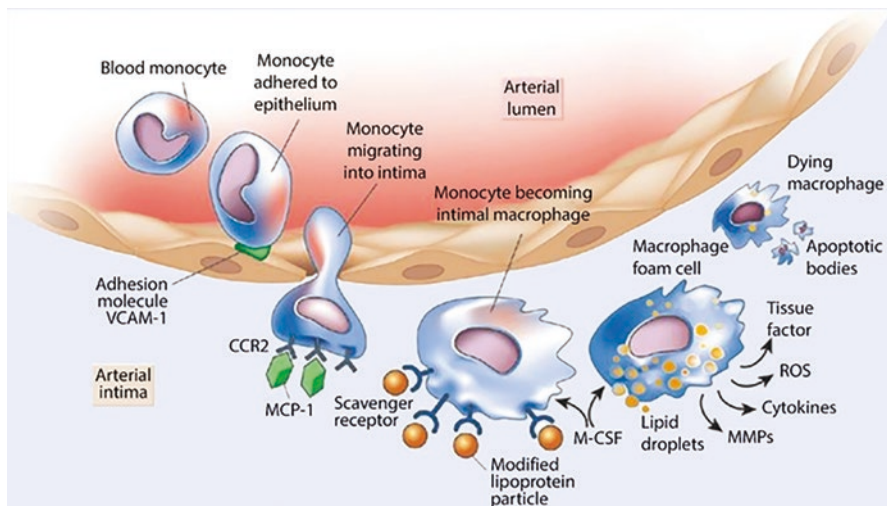


Fig. 4.1 Representation of intracellular and extracellular features in Atherosclerosis (adapted from: Mayer F.J., Binder C.J. (2019) Atherosclerosis. In: Geiger M. (eds) *Fundamentals of Vascular Biology*. Learning Materials in Biosciences. Springer, Cham. https://doi.org/10.1007/978-3-030-12,270-6_10. Under the licence of Springer)

diseases (CVDs) worldwide. Atherosclerotic CVDs remain the leading cause of death globally, with coronary artery disease and stroke being the most prevalent cause of death [11]. Tremendous efforts have been made in the understanding of the physiopathology of atherosclerotic CVDs as well as in their prevention and treatment. These measures help to counteract this global burden, even though a certain heterogeneity exists between populations. Indeed, more than 75% of death are from low and middle-income countries and more than 10% of country-based disability-adjusted life years lost result from atherosclerotic CVDs, with a significant impact on the economy of developing countries [12].

4.2.1 History

In 1952, von Rokitansky proposed the “thrombogenic theory,” based on the postulate that fibrin deposition in the intima of arterial wall preceded the development of atherosclerotic lesion and might contribute to this process [13]. This theory was challenged by the “inflammatory theory” of Rudolf Virchow in his publication “Cellular Pathology” in 1858. Virchow postulated that atherosclerotic lesion results from a dynamic process of tissue reaction rather than a passive deposition of lipid material. He also postulated that atherosclerotic lesion, called “endarteritis deformans,” resulted from an active inflammatory process within the intima. These theories built the basics of our contemporary understanding of atherosclerosis. In parallel, in the nineteenth century, the fundamentals concepts of modern immunology were established. First, work from Paul Ehrlich on antibodies demonstrated the interaction between antigens and antibodies, building the basics of the adaptive immunity field [14]. Then, the discovery of phagocytosis by Ilya Mechnikov allowed advances in the field of innate immunity field [15]. Further discoveries brought more light to the complex pathophysiologic process of atherosclerosis. In 1973, Ross and Glomset demonstrated the implication of vascular smooth muscle cells (SMCs) in the development and progression of atherosclerotic lesions [16]. In 1976, Ross and Harker proposed the “response to injury theory” as a mechanism for the development of atherosclerotic lesions. Furthermore, they demonstrated that hyperlipidemia solely can cause endothelial lesions as well as the initiation and progression of atherosclerotic plaques [17]. Later, Brown and Goldstein identified the major pathway of the low-density lipoprotein cholesterol (LDL-C) homeostasis [18], allowing the development of therapeutics targeting cholesterol metabolism. In 1981, Gerrity showed the critical role of foam cells derived from monocytes in atherogenesis, a still valid concept in our modern comprehension of atherosclerosis as an inflammatory disease [19]. In 1983, Erling Falk identified in human autopsy specimens the causative role of plaque rupture in the incidence of acute coronary thrombosis [20]. Davies identifies later on human autopsy studies the features of the vulnerable plaque, prone to rupture [21]. In 1987, Glagov proposed the concept of vascular remodeling during the progression of atherosclerotic plaque. In his observation, there was an excentric expansion of the arterial wall at the early stage of coronary heart disease (<40% stenosis) with relative preservation of the coronary

lumen. With the progression of the atherosclerotic lesion (>40% of stenosis), a significant reduction of the coronary lumen occurred [22]. Based on the knowledge of modern immunology, Hansson and Libby demonstrated the critical implication of the immune system in the development and progression of atherosclerosis, further consolidating the evidence that atherosclerosis is a chronic inflammatory disease [10, 23].

4.2.2 Mechanisms of Atherosclerosis

Based on our current understanding, the pathogenesis of atherosclerosis can be divided into three phases: initiation, progression, and complications.

4.2.2.1 Initiation of Atherosclerosis

Vascular Endothelium and Atherosclerosis

Vascular endothelium was initially considered as a simple cellular barrier between blood and interstitial space without relevant specific functions. Nowadays, the endothelium is well recognized as a dynamic adaptive interface between blood and arterial tissue with an essential function in the regulation of the homeostasis of the cardiovascular system [24]. Indeed, the endothelium mediates the selective transport of fluids and macromolecules. It also regulates coagulation and local vascular tone (through the synthesis of vasoactive molecules such as nitric oxide and prostaglandins) as well as inflammation through the expression of cytokines and cell adhesion molecules. The endothelium can also act as a sensor and transducer of the shear stress, the mechanical forces applied on the surface of ECs by the blood flow. Shear stress is known to influence endothelial cell morphology and function and is one key factor of atherogenesis [21]. The alteration of the endothelial function by pathological stimuli, such as conventional cardiovascular risk factors, pro-inflammatory processes, or pathological hemodynamic forces, is one of the earliest processes in the initiation of atherosclerosis [23].

Hemodynamics Forces in Atherosclerosis

Advancement in computational fluid dynamics helped to understand the relationship between blood flow and the development of atherosclerosis [25, 26]. Indeed, the rate and the velocity of blood flow vary along the vascular tree. While straight arteries experience a physiological high laminar flow, bifurcations and curvatures experience a low and turbulent flow. The preferential development of atherosclerosis in areas of disturbed flow has led to the hypothesis that shear stress-induced endothelial cell dysfunction could precede the disease onset [27]. In high shear stress regions of arteries, ECs are quiescent, elongated, and possess atheroprotective properties. They express anti-inflammatory and anti-thrombotic genes [28, 29]. ECs at bifurcations and curvatures have a cobblestone shape and a high turnover (high apoptosis and cell proliferation), a typical feature of endothelial dysfunction. They also display a pro-atherogenic phenotype as they express pro-inflammatory and

pro-thrombotic genes [30]. Altogether, the evidence demonstrates the key role of hemodynamic forces in atherogenesis.

Low-Density Lipoprotein Cholesterol

As already demonstrated by Nikolai Anitschkow in 1913 in a murine model with a cholesterol-rich diet, “without cholesterol, there is no atherosclerosis” [10]. More than a century later, these observations are still verified in different studies, showing that at the physiological level of LDL-C (10–20 mg/dl), atherosclerotic lesions would not develop [31]. However, this range is far exceeded in most of our contemporary societies [32]. Two populations particularly gained attention in the attempt to understand the impact of the chronic high levels of LDL-C blood concentration. Indeed, in patients with familial hypercholesterolemia, chronic exposure of the arteries to high LDL-C already at the early ages leads to premature atherosclerotic lesions [33]. On the contrary, patients with proprotein convertase subtilisin/kexin type 9 (PCSK9) loss-of-function mutations, who have chronically low LDL-C blood concentration, exhibit a significant reduction of cardiovascular events [34]. From these observations, the cumulative exposure of an artery to LDL-C over time seems to be one of the major determinants for the disease initiation and progression as well as a very promising pharmacological target.

Endothelial cell dysfunction (ECD) is linked with the impairment of its barrier function, promoting the infiltration of LDL-C particles in the intima, which get trapped into the extracellular matrix (ECM) [35]. The trapped lipoproteins bind to proteoglycan after biochemical modification by proteases and lipases, and form aggregates [36]. Subsequently, oxidized LDL (oxLDL) is formed by oxidative modification of LDL through myeloperoxidase, lipoxygenase and reactive oxygen species. OxLDL has the capacity to trigger the innate and adaptive immune system [37, 38].

Surface Adhesion Molecules

In response to the accumulation of oxLDL in the intimal space and in the presence of pathological blood flow, ECs express adhesion molecules, such as vascular cell adhesion protein 1 (VCAM-1), intercellular adhesion molecule-1, E, and P-selectin [24]. Interestingly, loss-of-function mutation in the gene encoding VCAM-1 led to a significant reduction of the atherosclerotic lesion in mice after 8 weeks of cholesterol-enriched diet [39]. Furthermore, it has been shown that the blood concentration of the soluble isoforms of VCAM-1 correlates with the maximum intima-media thickness at the carotid bifurcation, a well-recognized marker of atherosclerosis in the carotids [40]. Therefore, the pathogenic function of VCAM-1 in the initiation of atherosclerosis is a marker of ECD.

Monocytes and T-lymphocytes bind selectively to VCAM-1. Once bounded, the circulating mononuclear cells require the presence of chemotactic chemokines to stimulate their migration into the intima. Monocyte chemoattractant protein-1 (MCP-1), which is produced by ECs as well as by SMCs and macrophages, contribute significantly to this process [41]. MCP-1 binds with high affinity to its receptor CCR2. During plaque formation, CCR2 on monocytes can be upregulated by more

than 20-fold in comparison to the resting state [42]. In addition to MCP-1, three interferon- γ chemokines are also implicated in the recruitment of T-Lymphocytes to the nascent atherosclerotic plaque [43].

Foam Cells Formation

Activated and infiltrated monocytes further differentiate into macrophages. This process is induced by stimuli such as macrophage colony-stimulating factor and granulocyte-macrophage colony-stimulating factor, which is synthesized by ECs among others [44, 45]. Macrophages express high capacity scavenger receptors (SRs), of which SR-A and CD36 are the most important variants for the oxLDL uptake [46]. In contrast to other LDL-C receptors, SRs evade the negative feedback loop in response to increased intracellular cholesterol. Thus, SRs allow the overloading of the subendothelial resident macrophages with oxLDL, leading to the formation of lipid-loaded macrophages, named foamed cells, which are the hallmark of early atherosclerosis [8].

Progression of Atherosclerosis

Once initiated, atherosclerotic lesion progresses as a result of chronic inflammation. Accumulation of inflammatory cells within the atherosclerotic plaque is also mediated by their local proliferation. Various factors, such as semaphorins synthesized by macrophages, lead to the alteration of their migration capacity, contributing to their retention in the intimal space [47, 48]. During the progression of the atherosclerotic plaque, macrophages and SMCs are prone to apoptosis, leading to the formation of a lipid-rich or necrotic core [49, 50]. It has been shown that the normal process of dead cell removal, termed efferocytosis, is 20-fold reduced in atherosclerotic lesions in comparison to normal tissues [51]. This in turn also contributes to the formation of an atheromatous core consisting of apoptotic debris, lipid, and foam cells.

Smooth Muscle Cells and Atherosclerosis

The progressive accumulation of lipoproteins and inflammatory cells in atherosclerotic lesions leads to an expansion of the intima space with the subsequent disruption of the endothelium. Some authors suggested that this endothelial disruption may lead to the activation of SMCs [52]. However, this mechanism has to be better elucidated. Nevertheless, the inflammatory process occurring in the atherosclerotic plaque leads to the synthesis of different chemoattractant proteins. Platelet-derived growth factor (PDGF) is likely the dominant factor in fibrous cap formation [53]. Vascular SMCs, which usually reside in a quiescent state in the medial layer of normal arteries, respond to the PDGF stimulation through migration into the intima [54]. Under the stimulation of transforming growth factor (TGF)- β , SMCs trigger a fibro-proliferative response and synthesize ECM components among which elastin, proteoglycans, glycosaminoglycans, and fibrillar collagen [54]. This collagen-rich matrix contributes to the trapping of lipoproteins, promoting their accumulation within the intima. Fibrillar collagen also forms a dense tissue barrier that counteracts the release of the thrombogenic plaque material into the circulation. The strength of the fibrous cap is, therefore, determinant for plaque stability.

Interestingly, contrary to previous thoughts, the process of foam cell formation is not an exclusivity of monocytes-derived macrophages. It has been shown that under various stimuli, intimal SMCs can differentiate into a macrophage-like phenotype, with the expression of SRs at their surface, contributing to the formation of foam cells [55].

Calcification

Atherosclerotic plaque calcification is a common process seen during disease progression [56]. It is an active process, resulting from the alteration of the regulation and the clearance of calcium mineral. Of note, this process is similar to the mineralization process observed during bone formation [57]. Interestingly, diffuse calcification of the atherosclerotic plaque tends to consolidate the biomechanical stability of the fibrous cap, leading to fewer thrombotic events associated with plaque rupture [58]. However, the presence of small focal nodules of calcification, called spotty calcifications, leads to biomechanical instability of the plaque and is associated with increased cardiovascular events [59]. Nevertheless, the evaluation of the total amount of coronary calcification, termed coronary artery calcium score, is nowadays a well-established prognostic marker of atherosclerotic disease beyond traditional risk factors, as it reflects the extent of the disease [60]. Furthermore, assessment of the calcification activity within the coronary plaque is becoming a strong independent predictor of fatal or nonfatal myocardial infarction beyond the solely anatomical evaluation of the plaque burden [61].

Plaque Neoangiogenesis

Increasing wall thickness during atherosclerosis results in reduced oxygen availability for vascular cells. This hypoxic condition is further exacerbated by the increased oxygen consumption of high metabolic active immune cells [62]. In response to the hypoxic condition, vascular cells induce adaptive changes mediated by the oxygen-sensitive transcription factor, the hypoxia-inducible factor (HIF)-1. This results in the synthesis of hypoxia-responsive genes such as vascular endothelial growth factor (VEGF), fibroblast growth factor, cytokines, and angiopoietins [63]. VEGF promotes the shift of adventitial vasa vasorum ECs from a quiescent to an active migratory and proliferative state, leading to neovessels sprouting towards the base of the plaque [64]. The forming vessels are immature and prone to leakage, favoring the extravasation of plasma proteins, erythrocytes, and inflammatory cells. Consequently, pro-inflammatory processes as well as plaque progression and destabilization are exacerbated [65]. Therefore, plaque neovascularization in atherosclerosis could be a marker of inflammatory activity as well as a promising diagnostic and therapeutic target.

Innate Immunity Cells in Atherosclerosis

Histological examinations of atherosclerotic plaques led to the identification of three subsets of macrophages. M1 macrophages, with pro-inflammatory activity, are activated by IFN γ and lipopolysaccharides. M2 macrophages, with pro-regenerative activity, are activated by interleukin (IL)-4 or IL-13 [66, 67]. M1

macrophages appear to uptake more lipids in comparison to M2 macrophages, which are mostly located away from the lipid core [68]. Finally, oxidized phospholipids lead to the formation of Mox cells, which constitute 30% of the macrophage population, and display less phagocytic and chemotactic function in comparison to M1 and M2 macrophages [69]. This classification is not rigid, as macrophages have a high degree of plasticity with complex interaction with their environment [70].

Recently, the CANTOS study clearly established a relationship between cholesterol metabolism and the activation of the innate immune system, involving the NLRP3 inflammasome [37]. Indeed, oxLDL uptake by macrophages is followed by the precipitation of cholesterol, forming microcrystals in the cytosol. This results in the synthesis of the precursor form of IL-1 β and the activation of different enzymes, such as PYD domains containing protein 3 (NLRP3) inflammasome. The activated NLRP3 inflammasome gives rise to the active form of IL-1 β through caspase-1 cleavage [71]. In this randomized, double-blind secondary prevention study [37], inhibition of IL-1 β through canakinumab led to a significant reduction of cardiovascular events in patients with prior myocardial infarction and high levels of inflammatory markers, such as high sensitive c-reactive protein (hs-CRP). This study further validates inflammation as a potential therapeutic target, as previously demonstrated, using hs-CRP as a prognostic and therapeutic marker [72].

Macrophages are involved in the weakening of the protective fibrous cap, through the overproduction of matrix metalloproteinases (MMPs) that degrade the ECM components [73]. Moreover, macrophages contribute to the thrombogenic milieu in atherosclerotic plaque through high expression of tissue factor, a potent procoagulant mediator [74].

Other cells of the innate immune system, such as mast cells, neutrophils, natural killers are also involved in atherosclerosis. Mast cells, for example, contribute to ECM degradation through the synthesis of MMPs [75]. Nevertheless, monocyte-derived macrophages remain the main effector cell type of the innate immune system [10].

Adaptive Immunity in Atherosclerosis

Cells of the adaptive immunity are numerically less present in atherosclerotic plaques in comparison to cells of the innate immune system. Nevertheless, it is known that adaptive immune cells, especially T-cells, play an important regulatory role in the inflammatory process in atherosclerosis [10]. Indeed, severe T and B-lymphocytes immunodeficient mice had a delay in the development of atherosclerosis, in comparison to immunocompetent mice [76, 77]. Consistently, the transfer of specific T-lymphocytes in immunodeficient mice led to an exacerbation of atherosclerosis [76]. CD4+ T Helpers cells (TH) represent the main effector lymphocyte cell type [78] in atherosclerosis and highlight conflicting roles [10]. TH1 subset has a pro-atherosclerotic function. They synthesize IFN γ , which in addition promote foam cell formation, downregulate SMCs proliferation, leading to vulnerable plaque. TH2 subset has a complex function, promoting as well as limiting atherosclerosis progression. Regulatory T-cells play a role in plaque stabilization. They secrete TGF- β that promotes collagen-rich extracellular matrix synthesis by

SMCs. Evidence shows a link between cholesterol metabolism and TH cells activation through the interaction between the ApoB-derived T-cell epitopes of oxLDL and LDL lipoprotein, and the T-lymphocytes, leading to the T-cell activation [38]. B-cells are rare in the atherosclerotic plaque. While B2 cells enhance atherosclerosis, B1 cells prevent their progression [10].

Thus, the balance between the T and B-cell subpopulation in the atherosclerotic plaque has an impact on the progression and severity of the disease.

4.2.3 Complication of Atherosclerosis

4.2.3.1 Inducible Ischemia

Atherosclerosis can remain for a long time clinically silent until the vascular lumen is severely stenosed, or the thrombogenic plaque material is no more isolated from the blood circulation. As initially demonstrated by Glagov [22], atherosclerotic plaque initially expands away from the arterial lumen, with no significant flow-limiting effect on the organ perfusion at early stages. However, with increased plaque growth, the arterial lumen progressively reduces, leading to impaired organ perfusion. The imbalance in oxygen demand and supply can lead to clinical manifestations of tissue ischemia, such as angina pectoris.

4.2.3.2 Plaque Rupture

The stability of atherosclerotic plaque depends on its composition. The production of the collagen-rich fibrous cap by the SMCs helps to stabilize the plaque. However, under various stimuli, matrix degradation processes can take over, leading to a weakening of the protective cap, prone to rupture [73, 79]. Specific features of the atherosclerotic plaques have been proposed as a marker of vulnerability for plaque rupture. Vulnerable plaque is characterized by the presence of a large lipid core, low SMC and high macrophage content, resulting in high inflammatory, and protease activity. It also exhibits a thin fibroatheroma cap (<60 μm). In opposite, stable plaque displays a thick fibrous cap with reduced inflammation and lipid accumulation in the atheroma core and is less prone to rupture [80]. The plaque rupture leads to the exposure of its thrombogenic material, such as tissue factor, to the bloodstream. Tissue factor, a potent procoagulant mediator synthesized by macrophages and SMCs [74], induces the formation of thrombosis with the resulting occlusion of the arterial lumen. This complication constitutes the most common mechanism of acute thrombosis in myocardial infarction, leading to life-threatening complications such as ventricular arrhythmias [80, 81]. Different outcomes have been observed between patients experiencing acute coronary thrombotic occlusion. Patients with an obstructive disease with associated inducible ischemia before the thrombotic occlusion occurs seem to have a better outcome in comparison to patients with non-obstructive disease and no inducible ischemia. Indeed, data from autopsy studies revealed a correlation between angiographic discrete and moderate coronary stenosis (40–69% reduction of the coronary lumen), unlikely to induce myocardial ischemia in absence of thrombotic occlusion, and the occurrence of sudden cardiac

death in a significant number of studied patients [82]. On the other hand, data from catheterization laboratories revealed that a significant number of culprit lesion responsible for ST-segment elevation myocardial ischemia exhibits an angiographic severe coronary stenosis (>70% reduction of the coronary lumen) [83]. The theory of myocardial preconditioning has been proposed to explain the difference in the prognosis of these patients [84]. Indeed, in patients experiencing repetitive inducible ischemia before the occurrence of acute thrombotic occlusion, cellular myocardial adaptation may occur, conferring them relative protection against the development of ventricular arrhythmias [85, 86]. Therefore, they are more likely to reach the catheterization laboratory for emergent re-vascularization. On the contrary, in absence of inducible ischemia prior to acute thrombotic occlusion, this protective myocardial adaptation in response to intermittent ischemia does not take place, rendering the heart much vulnerable to fatal ventricular arrhythmia [84]. In the same line, other studies have shown that a majority of acute coronary syndromes occur in patients with non-obstructive disease [87, 88]. All these evidences suggest that other criteria than the solely angiographic stenosis should be considered, regarding the overall risk of death. In this regard, nuclear cardiology seems to be a promising field for the identification of atherosclerotic lesion prone to rupture, as discussed in the present chapter.

4.2.3.3 Plaque Erosion

Effective treatment with anti-inflammatory statins over years led to the modification of the plaque profile, with less inflammation, reduced lipid accumulation, and consolidation of the fibrous cap, potentially rendering them less prone to rupture [89]. However, there is still a residual risk of acute coronary events in patients treated with statins. In this particular setting, superficial plaque erosion, nowadays accounting for about one-third of acute coronary syndromes, has been proposed as the involved mechanism [90]. The exact underlying mechanism of thrombus formation following superficial plaque erosion remains to be better elucidated. Nevertheless, accumulating evidence pointed out the activation of the innate immune system as a possible pathway contributing to this process [90].

4.3 Metabolism of Glucose in Atherosclerosis

4.3.1 Glucose and Immune Cells

During the time course of atherosclerosis, immune cells undergo changes at the transcriptional and cellular level. They acquire higher migratory, proliferative, and secretory properties. These adaptations are concomitant with increased bioenergetic demand. Consequently, constant availability of metabolic substrate to provide sufficient ATP is fundamental for the efficient participation of immune cells in atherosclerosis.

Glucose constitutes an energy reservoir for a wide range of organisms and is the major fuel for lymphocytes and macrophages [91, 92]. It enters cells through

specific glucose transporters (GLUTs), and undergoes successive enzymatic transformations in aerobic or anaerobic conditions, leading to the formation of ATP [92]. Despite the increased vasa vasorum, the hypoxic condition in the interior of the plaque makes glucose the preferential source of energy used by inflammatory cells [93]. Once activated, these cells upregulate the expression of the GLUT1, GLUT3, and GLUT4 isoforms on their surface, favoring an increased uptake of glucose [91, 92]. Activation of immune cells also leads to downstream modification of the enzymatic cascade of the glycolytic pathway. Interestingly, it has been shown that activated macrophages display a ten-fold higher level of hexokinase activity in comparison to resting cells [94]. Therefore, the increased expression of GLUTs isoforms and the increased enzymatic activity of the glucose catabolism induce an increased uptake and utilization of glucose through activated inflammatory cells.

4.3.2 Imaging Inflammation in Atherosclerosis Using Glucose Metabolism

Increased glucose metabolism of the activated inflammatory cells constitutes the basic concept of the non-invasively evaluation of the inflammatory activity in atherosclerosis, using 2-deoxy-2-[^{18}F]fluoro-glucose (^{18}F -FDG), a glucose-based positron emission tomography/computed tomography (PET/CT) radiotracer [95]. As an analog to glucose, this radiotracer competes for uptake into cells. Once entry, ^{18}F -FDG is phosphorylated to ^{18}F -FDG-6-phosphate by hexokinase, and is trapped into the cells since it cannot be further metabolized. ^{18}F -FDG 6-phosphate can be dephosphorylated and release from the cell. However, this happens at a negligible rate. Therefore, the accumulated amount of ^{18}F -FDG 6-phosphate inside the cell is directly proportional to its glycolytic activity. Thus, the intensity of the emitted signal can be quantified using PET/CT and correlates with the intensity of the cellular metabolic activity (Fig. 4.2, [96]). A recent study investigated in vitro the cellular basis of the emitted ^{18}F -FDG signal by leukocyte subpopulations [97]. Interestingly, pro-inflammatory M1-macrophages exhibit the highest accumulation level of ^{18}F -FDG, reinforcing the evidence of the preferential accumulation of ^{18}F -FDG in pro-inflammatory cells (Fig. 4.3, [97]). Nowadays, among the inflammatory cells involved in atherosclerosis, activated macrophages are the most extensively studied. The first evidence of the use of ^{18}F -FDG PET/CT to image atherosclerosis comes from cholesterol-fed murine models. Indeed, Vallabojosula et al. demonstrated the quantifiable accumulation of FDG in atherosclerotic lesions, positively correlating with their macrophage content [98], results which were confirmed later by other studies [99]. Furthermore, the use of a positron-sensitive fiber optic probe allowed the differentiation between healthy from atherosclerotic damaged vascular wall in a mice model, based on the detected FDG accumulation [100]. Rudd et al. provide the first direct evidence for the non-invasively assessment of inflammation in human atherosclerotic plaque, using ^{18}F FDG-PET [101]. In this study, the authors demonstrated higher FDG accumulation in symptomatic carotid lesions, with no quantifiable FDG uptake into normal carotid arteries.

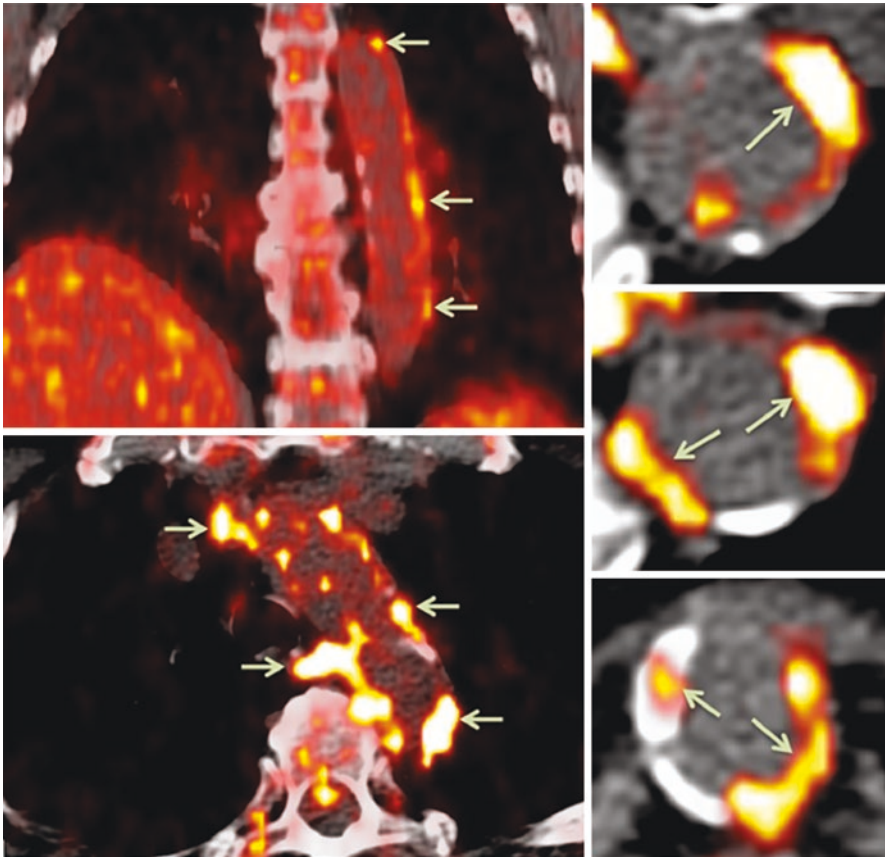


Fig. 4.2 ^{18}F -FDG PET/CT imaging of vulnerable plaques in descending aorta (adapted from: Giannakou S, Angelidis G, Tsougos I, Valotassiou V, Kappas K, Georgoulas P. Pet tracers for vulnerable plaque imaging. *Ann Nucl Med.* 2020 May; 34(5): 305–313. <https://doi.org/10.1007/s12149-020-01458-7>. Epub 2020 Mar 20. PMID: 32193790. Under the licence of Springer)

Given its capacity for detection of the inflammatory activity in atherosclerotic plaque, ^{18}F -FDG PET/CT also displays the predictive value for upcoming cardiovascular events. Indeed, accumulating evidence demonstrated a correlation between the vascular accumulation of FDG and the presence of atherosclerosis risk factors, such as circulating MMP-1, CRP, LDL-C as well as arterial hypertension, smoking, and age [101, 102]. Moreover, some authors demonstrated the complementary value of arterial FDG activity in the prediction of upcoming cardiovascular events, beyond conventional risk factor score such as Framingham risk score [103]. In addition, ^{18}F -FDG-PET/CT has been shown to be an independent predictive factor for the patient outcome with carotid artery disease [104, 105].

^{18}F -FDG-PET has also shown promising potential in the therapy monitoring of atherosclerotic plaque. Indeed, treatment with statin appeared to decrease the FDG

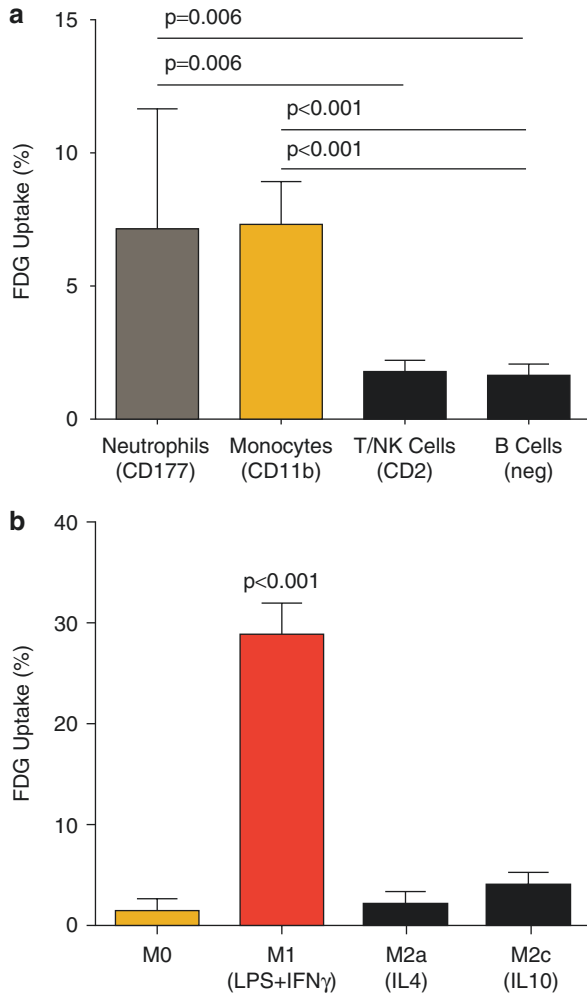


Fig. 4.3 Uptake of ^{18}F -FDG by peripheral blood leukocyte subtypes and polarized macrophages. **(a)** ^{18}F -FDG uptake in leukocyte subpopulations isolated from peripheral human blood by magnetic immunoseparation. **(b)** ^{18}F -FDG uptake by THP-1-derived macrophages with no polarization (M0) and following polarization to pro-inflammatory (M1) and anti-inflammatory M2a (IL-4) and angiogenic M2c (IL-10) subtypes. Data are shown as percent of total activity retained by cells at 60 min of incubation. T/NK, T- and natural killer cells; LPS, lipopolysaccharide, IFN- γ , interferon- γ ; IL-4, interleukin-4; IL-10, interleukin-10. Adapted from: Borchert T, Beitar L, Langer LBN, Polyak A, Wester HJ, Ross TL, Hilfiker-Kleiner D, Bengel FM, Thackeray JT. Dissecting the target leukocyte subpopulations of clinically relevant inflammation radiopharmaceuticals. *J Nucl Cardiol.* 2019 Oct 28. <https://doi.org/10.1007/s12350-019-01929-z>. Epub ahead of print. PMID: 31659697. Under the licence of Springer)

uptake in plaques, a finding that correlates with a better patient outcome [106, 107]. Moreover, risk factor modifications also result in a significant reduction in the number of vascular regions accumulating FDG [108].

Despite these promising potentials, ^{18}F FDG-PET has some limitations, especially for the evaluation of coronary plaque. Indeed, there is a physiological myocardial FDG uptake, which can alter the evaluation of coronary plaque uptake due to the increased background activity [101]. Nevertheless, this limitation can be overcome through a specific low carbohydrate, high-fat diet preparation for the suppression of the physiological uptake of FDG [109].

In summary, ^{18}F FDG-PET has the potential to diagnose and monitor the inflammatory activity of macrophages within the atherosclerotic plaque and could serve for the prognostic evaluation of these lesions.

4.4 Targeting Chemokine Receptor Expression in Vulnerable Plaque

Chemokine receptors (CXCR) are a class of transmembrane GTP-protein-coupled receptors physiologically expressed on cell membranes able to intercede the chemokines functions (i.e., immune cells and endothelial cells). The CX ligand 12 (CXCL12), also known as stromal derived factor 1 (SDF-1), is the main ligand of CXCR4 [110]. The CXCR4-CXCL12 axis has several functions in physiological and pathological processes. The CXCL12/CXCR4 complex stimulates the migration of hematopoietic progenitor and stem cells, endothelial cells, and most leukocytes. In particular, CXCR4 stimulates the platelet activation and adhesion [111], as well as the endothelial barrier function. Moreover, CXCR4 endothelial deficiency may determine inflammatory leukocyte recruitment and arterial leakage during atherogenesis [112]. Interestingly, LDL-C stimulates the CXCR4 expression, leading to leukocyte chemotaxis and macropinocytosis [111, 113]. In vascular SMCs, CXCR4-CXCL12 axis regulates the normal contractile responses as well as the vascular tone [112]. Therefore, tracking chemokine function may emerge as a suitable diagnostic as well as therapeutic target through modulation of the monocyte recruitment [114] as already demonstrated [115].

Two main radiopharmaceuticals have been developed to non-invasively evaluate the CXCL12/CXCR4 axis using PET/CT: ^{68}Ga -labeled Pentixafor as well as ^{18}F -labeled 1,4,7-triazacyclononane-triacetic acid (NOTA) analog of pentixather (^{18}F -AIF-NOTA-pentixather), that is still mainly under preclinical evaluation. Both compounds have been assessed in several clinical indications such as the diagnosis of solid tumors, hematological malignancies, traumatic splenosis, complicated urinary tract infections, and cardiovascular diseases [116–121]. In cardiology, ^{68}Ga -Pentixafor has been initially assessed in the post-infarct period, targeting the myocardial healing process following myocardial infarction, and therefore assessing the progression of disease and the response to therapy [122, 123]. In contrary to FDG, dietary manipulations and fasting conditions are unnecessary, since ^{68}Ga -Pentixafor highlighted lower accumulation in non-inflammatory cardiomyocytes as well as in cardiac fibroblasts. Due to this favorable physiological biodistribution of ^{68}Ga -Pentixafor, excluding significant accumulation in parenchyma adjacent to the vessel wall (i.e., myocardium and brain), the target-to-background

ratio (TBR) is enhanced, increasing the reader's confidence in assessing the atherosclerotic plaque [124]. Borchert et al. in a preliminary experience shown a ^{68}Ga -Pentixafor wide uptake by leukocyte subpopulations and polarized macrophages; the authors described the highest uptake in B-cells and T-cells/natural killer compared to neutrophils [97]. Therefore, CXCR4-directed imaging seems able to elucidate the nature of the involved inflammatory cells in atherosclerotic process. Thus, ^{68}Ga -Pentixafor may provide more insights into the underlying coronary atherosclerotic biology of inflammatory active plaque as well as the efficacy of therapeutics procedure on the inflammatory atherosclerotic processes [125]. Indeed, intense ^{68}Ga -Pentixafor accumulation was exclusively observed in patients with carotid stenosis greater than 50% in atherosclerotic plaque samples obtained from carotid endarterectomy, and linked with their CD68-macrophage content [124]. Similar results have been reported by Grosse et al. in ex-vivo analyses [126]. Furthermore, ^{68}Ga -Pentixafor uptake provided additional information concerning plaque composition, correlating with intraplaque hemorrhage, and potentially platelets content [126]. In a 51 patients cohort CXCR4-directed imaging demonstrated focal arterial uptake in correlation with calcified plaque burden ($P < 0.0001$), cardiovascular risk factors ($P < 0.0001$), or prior cardiovascular events ($P = 0.0004$) [127]. In a study by Kircher et al., in comparison with ^{18}F -FDG, ^{68}Ga -Pentixafor identified significantly more atherosclerotic lesions with higher radiotracer accumulation, which may impact on reader's confidence for overall detection rate [128]. However, PET/CT assessment may be challenging due to several issues, i.e., the small size of the target, partial volume effects, and blurring from cardiac/respiratory motion [125]. Nonetheless, motion-correction techniques have been advocated to overcome these limitations. Derlin et al. conducted CXCR4-targeted PET/CT combined with novel motion-correction techniques in a patient cohort that had undergone PET early after reperfusion for acute myocardial infarction [125]. The authors demonstrated that after applying this novel motion-correction techniques, ^{68}Ga -Pentixafor PET/CT uptake was linked to CD68+ macrophages at immunofluorescence. Moreover, ^{68}Ga -Pentixafor PET/CT identified a broad spectrum of coronary plaques, including stented culprit, stented non-culprit, non-stented non-culprit coronary lesions [125]. Therefore, a precise assessment of the CXCR4-expressing plaque burden of the vessel wall may allow for more reliable identification of patients that would most likely benefit from innovative CXCR4-targeting therapies.

4.4.1 Technological Advancements: PET/MRI and Chemokine Receptor

A potential opportunity in molecular imaging in cardiology may be represented by PET/Magnetic Resonance Imaging (MRI), especially for the characterization of the internal structure of atherosclerotic artery walls due to the excellent soft tissue contrast of MRI [129]. Comprehensive characterization of atherosclerosis might benefit from hybrid PET/MRI to delineate the vessel wall and the activity of atherosclerotic

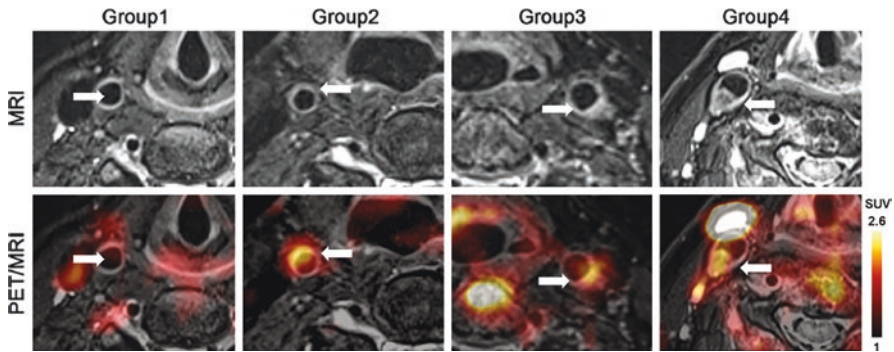


Fig. 4.4 Example transaxial [68Ga]Pentixafor PET/MRI images of carotid lesions within different groups. Focal uptake was observed in a mildly atherosclerotic carotid artery showing a slightly eccentric thickening (Group 1) and in a moderately (Group 3) and severely (Group 4) atherosclerotic carotid showing significant eccentric thickening, increased tracer uptake was absent at non-significantly eccentric control carotid (Group 1). Arrows indicate the arterial regions of interest. (Adapted from: Li X, Yu W, Wollenweber T, Lu X, Wei Y, Beitzke D, Wadsak W, Kropf S, Wester HJ, Haug AR, Zhang X, Hacker M. [68Ga]Pentixafor PET/MR imaging of chemokine receptor 4 expression in the human carotid artery. *Eur J Nucl Med Mol Imaging*. 2019 Jul;46(8): 1616–1625. <https://doi.org/10.1007/s00259-019-04322-7>. Under the licence of Springer)

lesions. In their experience of Li et al. [72] oncologic patients scheduled for CXCR4 imaging were investigated using PET/MRI (Fig. 4.4), showing increased ^{68}Ga Pentixafor uptake in eccentric carotids as mild, moderate, and severe [130]. They also assessed the overall diagnostic performance of ^{68}Ga -Pentixafor PET/MRI in the atherosclerotic plaque burden of seven arterial segments per subject. Namely, they found a higher TBR in men along with greater evidence of cardiovascular risk factors [131] but the authors underlined the significant limitation of partial volume effects in small-sized atherosclerotic lesions and MRI-based attenuation correction in PET imaging. In addition, the availability of PET/MRI systems is rather limited at present, which questions broader clinical applicability.

^{68}Ga -Pentixafor PET could serve as an *in vivo* imaging tool for the identification of inflammatory atherosclerosis and, together with dedicated MRI, might provide new insights into the pathobiology of atherosclerosis.

4.4.2 Radiopharmaceutical Agents Advancements: Theragnostic and Chemokine Receptor

Another great challenge of personalized medicine is related to theragnostics. Through the administration of a single radiopharmaceutical dose, simultaneous diagnostic purpose as well as therapeutic effects could be achieved. ^{68}Ga -Pentixafor could serve as imaging tool to identify the suitable patients for CXCR4-directed therapies with the beta emitter-labeled antagonists such as $^{177}\text{Lu}/^{90}\text{Y}$ -Pentixather, as described by Li et al. in high-risk individuals with atherosclerosis [132]. Another

CXCR4 targeting treatment option is represented by targeting the small antagonist molecule AMD3465, to prevent re-stenosis after re-vascularization by reducing neointimal lesion size and smooth muscle progenitor mobilization [133]. Further interesting preliminary results have been described by the group of Osl et al. [¹⁷⁷Lu] DOTA-r-a-ABA-CPCR4 has emerged from this study as a powerful second-generation therapeutic CXCR4 ligand with improved tumor retention and targeting efficiency [134].

4.5 Targeting Microcalcification in Atherosclerosis

Another clinical prominent characteristic of atherosclerosis is the presence of calcium deposition due to the association between microcalcification and high-risk atherosclerotic plaque rupture [135]. The calcification process in the atherosclerotic plaque involves arterial bone cells (osteoblasts and osteoclasts) as well as glycoproteins of the cellular matrix (osteopontin), which binds calcium at hydroxyapatite and mediates inflammation in myeloid cells and [136–140] able to further stimulate osteogenesis [141, 142]. Also, NaF uptake has been shown to microscopically correlate with calcification (instead of inflammation) [143, 144]. Several studies have confirmed that NaF accumulation is linked to vascular calcification; specifically, fluoride ions may be incorporated into the hydroxyapatite by ion-exchange mechanism with hydroxyl groups at the crystal surface [145].

4.5.1 Atherosclerotic Plaque Calcium Deposition

As above-mentioned, NaF is an established PET tracer for the assessment of new bone formation, and Thorsten et al. were the first who demonstrated its feasibility for imaging the mineral deposition in atherosclerotic plaque [146]. Also, vascular NaF uptake is inversely associated with bone metabolism, as described by Derlin et al. in a 304 patients cohort; namely, NaF uptake significantly increased with patients' age ($P < 0.001$), while regional bone metabolism decreased ($P < 0.001$), and both parameters resulted significantly associated with cardiovascular events and other risk factors [147]. In a comparison study, 77.1% of lesions with significant NaF uptake (active mineral deposition) and only 14.5% of lesions with FDG uptake (inflammation) were colocalized with arterial calcification defined by CT (coincident uptake was rarely observed). Therefore, both tracers depict distinct pathophysiological processes in atherosclerotic lesions and provide different information about the formation and progression of atherosclerotic plaque [148]. In a recent study by Kwiecinski et al., an automated assessment of disease activity in the whole coronary vasculature resulted feasible using ¹⁸F-NaF, in stronger agreement with CT markers of plaque vulnerability than the more traditional measures of plaque activity (SUV or TBR; Fig. 4.5, [149]).

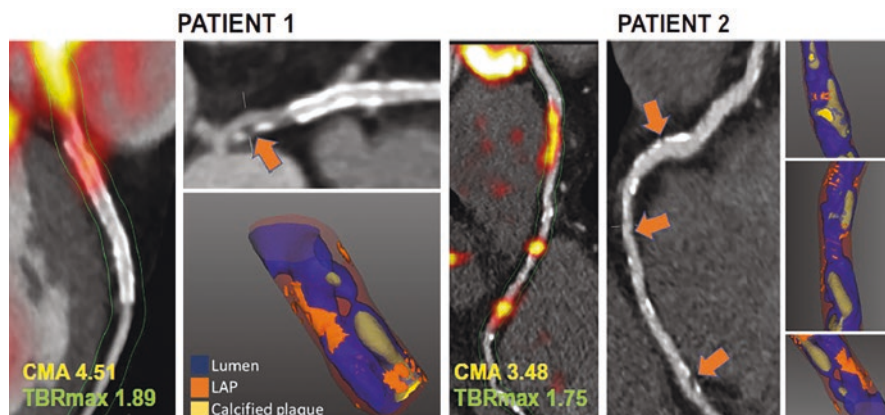


Fig. 4.5 Case examples of coronary ^{18}F -sodium fluoride uptake, low attenuation plaque (LAP) on CT angiography, and LAP (orange arrows, II) on 3D CTrendering (III). Right (Patient 1) and left anterior descending (Patient 2) coronary arteries. Areas of increased ^{18}F -NaF activity. While maximum target-to-background ratio (TBRmax) reflects single hot-spot activity coronary microcalcification activity (CMA) values represent the whole-vessel ^{18}F -sodium fluoride burden. (adapted from: Kwiecinski J, Cadet S, Daghm M, Lassen ML, Dey D, Dweck MR, Berman DS, Newby DE, Slomka PJ. Whole-vessel coronary ^{18}F -sodium fluoride PET for assessment of the global coronary microcalcification burden. *Eur J Nucl Med Mol Imaging.* 2020 Jul;47(7): 1736–1745. <https://doi.org/10.1007/s00259-019-04667-z>. Under the licence of Springer)

4.5.2 Cardiovascular Risk Quantification

Several studies have demonstrated that frequency and/or uptake of lesions are linked to cardiovascular risk. Namely, in a large retrospective study by Derlin et al., NaF uptake in carotid plaque resulted significantly associated with age ($P < 0.0001$, confirmed by [150, 151]), male gender ($P < 0.0001$), hypertension ($P < 0.002$), hypercholesterolemia ($P < 0.05$), and increased with the number of cardiovascular risk factors ($P < 0.0001$, [146]). Similar results have been described by Morbelli et al. who demonstrated a higher relation for NaF instead of CT [152]. However, other studies showed conflicting results [146, 150]. In a study by Janssen et al. in a cohort of 409 patients, linear NaF uptake in the femoral arteries significantly and proportionally correlated with cardiovascular risk factors (increasing NaF uptake as the number of cardiovascular risk factors increased, $P < 0.0001$) (Fig. 4.6, [153]). Similar results have been reported by the group of Dweck et al. in which patients with increased coronary NaF uptake showed higher Framingham Risk Score and higher rates of prior cardiovascular events and angina [154]. Also, Fitz et al. reported that in 78 patients, thoracic wall aorta NaF uptake correlated with cardiovascular risk and was able to describe patients' risk class. Interestingly, descending aorta TBR was the most significant parameter in cardiovascular risk determination [155]. Finally, in a cohort including 32 patients followed-up for 2 years after an NaF PET/

Fig. 4.6 MIP PET images of a 74-year-old woman demonstrating bilateral diffuse ^{18}F -sodium fluoride uptake in the femoral arteries. (Adapted from: Janssen T, Bannas P, Herrmann J, Veldhoen S, Busch JD, Treszl A, Münster S, Mester J, Derlin T. Association of linear ^{18}F -sodium fluoride accumulation in femoral arteries as a measure of diffuse calcification with cardiovascular risk factors: a PET/CT study. *J Nucl Cardiol.* 2013 Aug; 20(4): 569–77. <https://doi.org/10.1007/s12350-013-9680-8>. Under the licence of Springer)



CT scan, patients with coronary events had higher TBRmax than those without ($P = 0.0034$, [156]).

4.5.3 High/Risk Coronary Plaque Evaluation

Beyond being associated with general cardiovascular risk, NaF PET has demonstrated promising results to identify high-risk and localize ruptured plaque. In a prospective clinical trial by Joshi et al., patients with myocardial infarction and stable angina underwent NaF PET and invasive coronary angiography: in 93% of patients with myocardial infarction, the highest coronary NaF uptake was seen in the culprit plaque with statistically significant higher uptake (median maximum TBR: culprit 1.66 vs highest non-culprit 1.24, $P < 0.0001$). Histology specimen analysis demonstrated that all carotid plaque ruptures were associated with NaF uptake and with the presence of active calcification, macrophage infiltration, apoptosis, and necrosis [157].

In their experience, Vesey et al. investigated patients after a recent transient ischemic attack or minor ischemic stroke, finding that carotid NaF uptake was higher in symptomatic culprit plaques compared with asymptomatic contralateral plaques ($P = 0.001$), and with control patients ($P = 0.001$) [82]; also other studies confirmed that high-risk plaque has higher NaF uptake [158–160].

Lee et al. compared before coronary angiography the NaF uptake with optical coherence tomography (OCT), intravascular ultrasound (IVUS), and coronary CT angiography, prospectively in 51 patients cohort. The NaF TBR in plaques with high-risk characteristics was significantly higher than in those without ($P < 0.001$ for IVUS; $P = 0.014$ for OCT). Also, in 14/15 lesions that met both IVUS and OCT criteria for high-risk plaque, authors observed the presence of NaF uptake [159].

4.5.4 Atherosclerotic Plaque Composition/Activity Assessment

The available data on the role of arterial NaF uptake and subsequent evolving changes in plaque activity or composition is still limited. In a 19 oncologic patients experience, the NaF uptake measured as TBRmax, significantly increased from baseline (2.5 ± 0.8) to follow-up (2.8 ± 0.7 , $P < 0.05$) with a corresponding increased calcium density increased [161]. Ishiwata et al. reported a significant correlation between baseline calcification vessel wall NaF uptake activity and the change after 1 year in terms of calcification volumetric score also as a predictor of future cardiovascular disease risk, in absence of new macrocalcification [162]. Further longitudinal studies are crucially needed to explore whether NaF accumulation precedes the development of overt arterial calcification, and to define the reproducibility and stability of NaF signal in coronary and carotid arteries, also in the coronary stenosis severity assessment (Fig. 4.7) [163].

4.6 Targeting Neovascularization in Atherosclerosis

Angiogenesis is a highly regulated fundamental process involved in various physiological processes such as wound repair, reproduction, and response to ischemia, but also with pathological processes such as cancer, arthritis, and cardiovascular diseases [164, 165]. Specific local and circulating biomarkers, such as matrix metalloproteinases, vascular endothelial growth factor, and integrins alpha-v beta-3 ($\alpha v \beta 3$) have been shown to play an important role in the modulation of the angiogenic cascade. Therefore, these potential biomarkers have been identified as favorable targets for in vivo imaging of angiogenesis, and recent research has focused on the development of smart imaging radiotracers targeting these specific agents [166]. Among these agents, the integrin family has shown promising potential with translation from preclinical to clinical studies. The integrin family is a group of transmembrane glycoprotein comprised of 19 α - and 8 β -subunits, that are expressed in 25 different α/β heterodimeric combinations on the cell surface. Among 25 members of the integrin family, the integrin $\alpha v \beta 3$ has been most extensively studied for

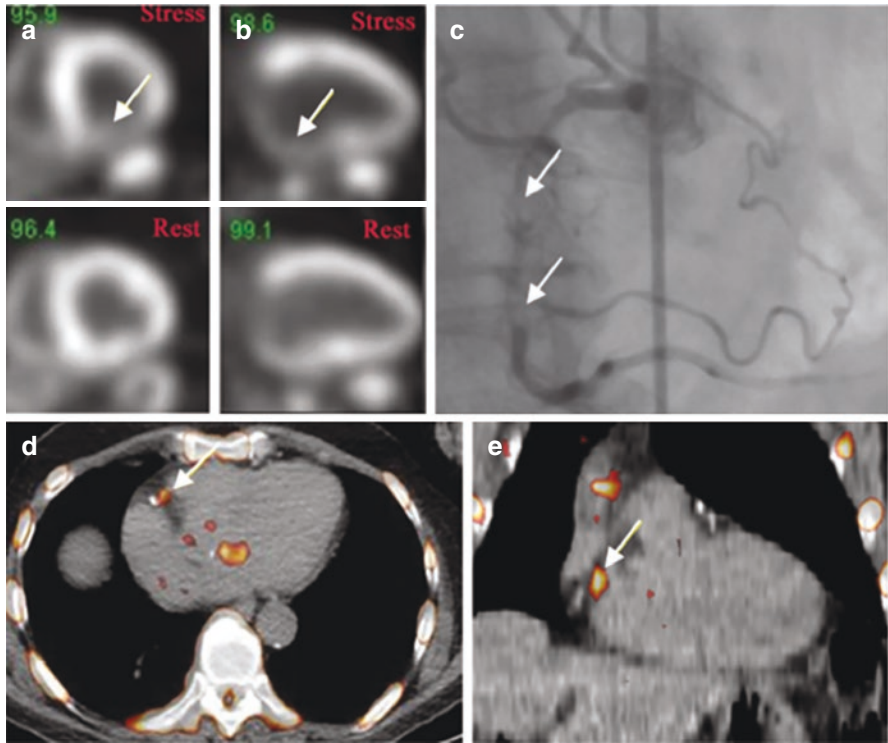


Fig. 4.7 Images from a 71-year-old male with stable angina who underwent regadenoson stress Rb-82 PET myocardial perfusion study show reversible perfusion defects in the proximal to mid inferior wall (**a**, short axis view; **b**, long axis view). Coronary angiogram (**c**) shows severe stenosis at proximal to mid RCA. He also received a 18F-NaF PET/CT scan within 2 months of the myocardial perfusion imaging study. The fused PET/CT axial (**c**) and coronal (**d**) views demonstrate increased 18F-NaF uptake at proximal to mid-RCA. 18F-NaF uptake is also noted in the area with mitral annular calcification (**e**). (Adapted from: Hayrapetian A, Berenji GR, Nguyen KL, Li Y. 18F-Sodium fluoride uptake is associated with severity of atherosclerotic stenosis in stable ischemic heart disease. *J Nucl Cardiol.* 2020 Jul 16. <https://doi.org/10.1007/s12350-020-02238-6>. Under the licence of Springer)

its role in tumor growth, progression, and angiogenesis. The restricted expression profile and good accessibility of cell adhesion molecule integrin $\alpha v \beta 3$ make it an attractive imaging target for angiogenesis given its major role in several pathophysiological processes, such as for coronary disease (Fig. 4.8), tumor angiogenesis, and metastasis [167, 168]. As previously demonstrated, intraplaque angiogenesis and neovascularization are implicated in the process leading to growth and instability of the atherosclerotic plaque [63–65]. The integrin $\alpha v \beta 3$ cell surface receptor is overexpressed on activated endothelial cells in state of angiogenesis. Interestingly, it is also overexpressed in macrophages at site of increased vascular inflammation.

The last decade has seen the development of new PET tracers for in vivo imaging of integrin $\alpha v \beta 3$ receptor expression based on arginine–glycine–aspartic acid

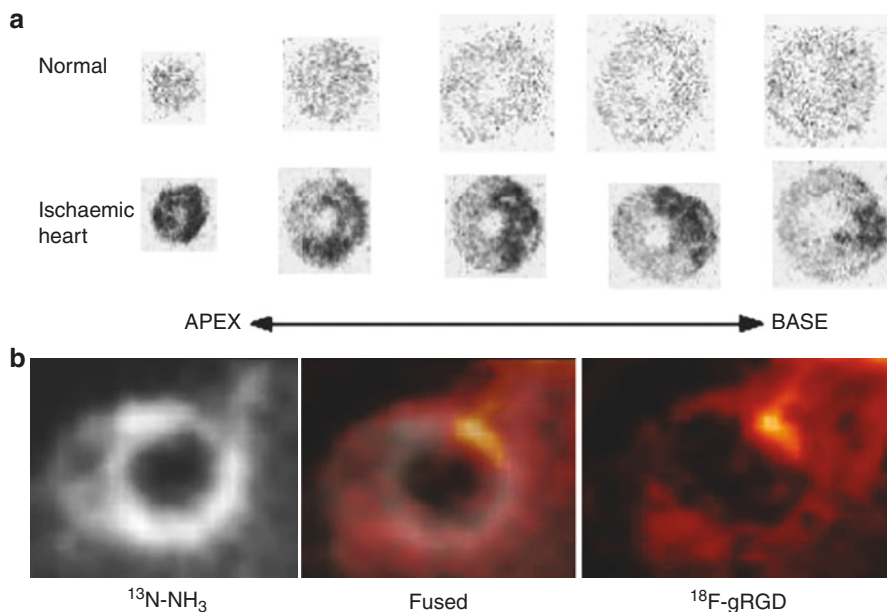


Fig. 4.8 Imaging of $\alpha v \beta 3$ integrin expression in a rat model of coronary occlusion (20 min)/reperfusion using ^{18}F -galacto- RGD. (a) Autoradiographic images of a non-operated normal heart and an ischemic heart with occlusion/reperfusion at 1 week. Focal tracer accumulation is seen in the ischemic heart. (b) In vivo short axis PET images demonstrating focal uptake of ^{18}F -galacto-RGD in the corresponding area, with a decrease in perfusion on ^{13}N -ammonia. PET, 1 week after the ischemic event. (adapted from: Higuchi T, Wester HJ, Schwaiger M. Imaging of angiogenesis in cardiology. *Eur J Nucl Med Mol Imaging*. 2007 Jun; 34 Suppl 1: S9–19. <https://doi.org/10.1007/s00259-007-0436-z>. Under the licence of Springer)

(RGD) peptide, a specific amino-sequence contains in the cell–ligand interaction site of the $\alpha v \beta 3$ -receptor on cell surface. Several studies have been published presenting the recent advancements in preparations of ^{18}F -labeled, ^{64}Cu -labeled, and ^{68}Ga -labeled RGD tracers, RGD-based PET multivalent probes, and RGD-based PET multimodality probes for imaging receptor integrin $\alpha v \beta 3$ expression but the translation in clinical practice is still limited [169]. The major use of these tracers has been presented in the assessment of tumor neoangiogenesis, but few papers described the potential role in atherosclerosis. Indeed, preclinical studies depicted promising potential in the assessment of the atherosclerotic disease activity in mice-models [170–172]. Recently, Jenkins et al. published the largest multimodality imaging study evaluating the clinical significance of RGD-based $\alpha v \beta 3$ integrin receptor radiotracer (^{18}F -fluciclatide) in the atherosclerotic process in human [173]. The authors demonstrated a positive correlation between the in vivo expression of $\alpha v \beta 3$ integrin receptor in human aortic atheroma and the atherosclerotic plaque burden, with an increase expression in patients with recent myocardial infarction. Therefore, quantification of $\alpha v \beta 3$ integrin expression using ^{18}F -fluciclatide PET could be seen as a promising non-invasive radiotracer to evaluate the disease

activity as well as the atherosclerotic plaque instability. Despite these very promising pre-clinical and clinical studies, large clinical trials are still needed to better elucidate the clinical importance of RGD-based radiotracers in our pathophysiological understanding of atherosclerotic process as well as in the identification of patients at increased risk of adverse cardiovascular events.

4.7 Targeting SSRT-2 Receptor Expression in Atherosclerosis with DOTA-Derivatives-PET

One particular target of the atherosclerosis is the macrophage, which is an abundant cell type in the plaque and highly active in inflammation. As previously demonstrated, the macrophage migrates into the arterial intima as a monocyte where it matures to become a phagocytic macrophage [42, 44, 45]. Various processes and cellular targets related to macrophages have been investigated and identified as potential target for non-invasive PET imaging. Among these, somatostatin receptor, a G-protein-coupled 7-transmembrane protein has been well studied. Indeed, from the five human somatostatin receptors subtypes, the subtype 2 has been shown to be upregulated on the surface of pro-inflammatory M1 macrophages [174]. Preclinical studies on mice [175, 176] as well as retrospective studies [177–179] suggest the potential utility of DOTA-peptide-based PET imaging in the assessment of atherosclerotic disease activity (Fig. 4.9). Hence, DOTA-derivatives-PET targeting SSRT-2 receptor expression might be potential tracers for molecular imaging of atherosclerosis [7, 8]. Recently, Tarkin et al. [180] provide genetic, cellular, plaque- and patient-level evidences on the utility of ^{68}Ga -DOTATATE PET/CT in the cell-specificity quantification of inflammatory activity in atherosclerotic plaque in the coronary arteries, outperforming ^{18}F -FDG PET/CT. This opens further perspectives for theranostics. Indeed, Schatka et al. investigated an oncological cohort treated with SSTR peptide receptor radionuclide therapy (PRRT), reporting the reduction of plaque burden by a subsequent SSTR-targeting endoradiotherapy [179]. Despite these promising results, further investigations are needed to confirm these results in a large cohort.

4.8 Summary

The concept of vulnerable plaque has been accurately studied and extensively recognized as one of the major cause of acute myocardial infarction and sudden cardiac death. Many cellular and molecular pathways have been demonstrated as crucial in the pathogenesis of vulnerable plaque. The role of nuclear medicine imaging techniques, through the ongoing advancements, surpassed the conventional morphological evaluation, permitting the assessment of specific bio-molecular targets involved in the plaque pathogenesis for a panel of application able to characterize the intraplaque inflammatory processes, the necrotic core, flogosis, and related receptor expression and fibrous cap thickness with the evaluation of calcification as

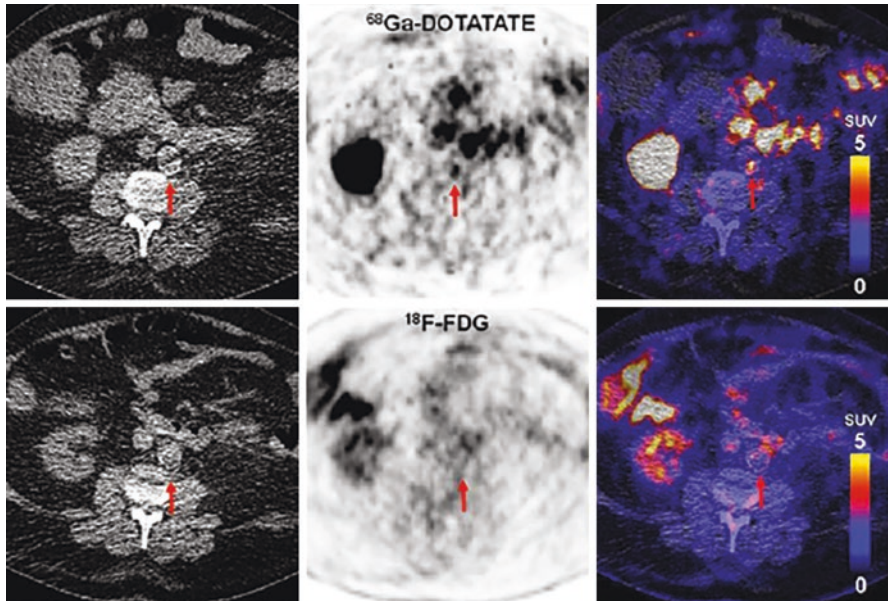


Fig. 4.9 Focal vascular uptake of ^{68}Ga -DOTATATE without corresponding focal ^{18}F -FDG uptake. Transverse PET/CT images of a 73-year-old male patient with hypertension, hypercholesterolemia, and smoking. Intense focal uptake of ^{68}Ga -DOTATATE can be observed in the aortic arch (upper row), whereas no focally increased ^{18}F -FDG uptake was seen (lower row). TBRDOTATATE was 7.60, while TRBFDG was 1.74. (Adapted from: i X, Samnick S, Lapa C, Israel I, Buck AK, Kreissl MC, Bauer W. ^{68}Ga -DOTATATE PET/CT for the detection of inflammation of large arteries: correlation with ^{18}F -FDG, calcium burden and risk factors. *EJNMMI Res.* 2012 Sep 27; 2(1): 52. <https://doi.org/10.1186/2191-219X-2-52>. Under the licence of Springer)

well as marker of neoangiogenesis. ^{18}F FDG-PET has the potential to diagnose and monitor the inflammatory activity of macrophages within the atherosclerotic plaque, with promising potential in the therapy monitoring of atherosclerotic plaque as well as in risk stratification. However, ^{18}F FDG-PET shows limitations, due to the physiological myocardial FDG uptake, which can alter the evaluation of coronary plaque uptake. This limitation can be overcome through a specific dietary preparation. Furthermore, SSRT-2 receptor expression PET imaging, which also targets activated inflammatory cells, appears to be a possible valuable alternative to ^{18}F -FDG PET/CT, with a more specific signal and without need for dietary preparation.

^{68}Ga -Pentixafor is a promising candidate for detecting high-risk atherosclerotic plaques. Precise assessment of CXCR4-expressing plaque burden of the vessel wall may allow for more reliable identification of patients that would most likely benefit from innovative CXCR4-targeting therapies. This PET application, together with dedicated MRI in a simultaneous PET/MRI examination, might provide new insights into the pathobiology of atherosclerosis. Further researches are warranted to determine the clinical role of CXCR4-directed molecular imaging and therapy in atherosclerosis and in other scenarios due to the CXCR4-related cell-type potential targeting.

Despite the described promising results, the potential role of NaF PET in prospective risk prediction remains to be determined. Indeed, it has been suggested that the observed high uptake of NaF in culprit lesions may be a consequence of plaque rupture rather than a hallmark of vulnerable plaque. Future observational studies relying on baseline PET scans in asymptomatic patients will help to clarify this question.

Promising results in the role of markers of intraplaque neovascularization in the evaluation of atherosclerotic disease activity are available, but further large studies are needed to better elucidate their utility.

Finally, the detection of atherosclerotic luminal stenosis is by far insufficient to give insights on the vulnerability of the plaque. Pathophysiological processes which built our current understanding of the pathogenesis of atherosclerosis have to be better address in the non-invasive imaging field, to provide a better assessment of the disease activity, and therefore the risk of cardiovascular events.

References

1. Finn AV, Nakano M, Narula J, et al. Concept of vulnerable/unstable plaque. *Arterioscler Thromb Vasc Biol.* 2010;30:1282–92.
2. Jagannathan SN, Connor WE, Baker WH, Bhattacharyya AK. The turnover of cholesterol in human atherosclerotic arteries. *J Clin Invest.* 1974;54:366–77. <https://doi.org/10.1172/JCI107772>.
3. Lees AM, Lees RS, Schoen FJ, et al. Imaging human atherosclerosis with 99mTc-labeled low density lipoproteins. *Arteriosclerosis.* 1988;8:461–70. <https://doi.org/10.1161/01.atv.8.5.461>.
4. Tawakol A, Fayad ZA, Mogg R, et al. Intensification of statin therapy results in a rapid reduction in atherosclerotic inflammation: results of a multicenter fluorodeoxyglucose-positron emission tomography/computed tomography feasibility study. *J Am Coll Cardiol.* 2013;62:909–17. <https://doi.org/10.1016/j.jacc.2013.04.066>.
5. Emami H, Vucic E, Subramanian S, et al. The effect of BMS-582949, a P38 mitogen-activated protein kinase (P38 MAPK) inhibitor on arterial inflammation: a multicenter FDG-PET trial. *Atherosclerosis.* 2015;240:490–6. <https://doi.org/10.1016/j.atherosclerosis.2015.03.039>.
6. Rudd JHF, Myers KS, Bansilal S, et al. 18Fluorodeoxyglucose positron emission tomography imaging of atherosclerotic plaque inflammation is highly reproducible. Implications for atherosclerosis therapy trials. *J Am Coll Cardiol.* 2007;50:892–6. <https://doi.org/10.1016/j.jacc.2007.05.024>.
7. Tawakol A, Migrino RQ, Bashian GG, et al. In vivo 18F-Fluorodeoxyglucose positron emission tomography imaging provides a noninvasive measure of carotid plaque inflammation in patients. *J Am Coll Cardiol.* 2006;48:1818–24. <https://doi.org/10.1016/j.jacc.2006.05.076>.
8. Libby P, Buring JE, Badimon L, et al. Atherosclerosis. *Nat Rev Dis Prim.* 2019;5(1):56. <https://doi.org/10.1038/s41572-019-0106-z>.
9. Mayer FJ, Binder CJ. *Atherosclerosis.* Cham: Springer; 2019. p. 195–233.
10. Gisterà A, Hansson GK. The immunology of atherosclerosis. *Nat Rev Nephrol.* 2017;13:368–80.
11. Benjamin EJ, Blaha MJ, Chiuve SE, et al. Heart disease and stroke Statistics'2017 update: a report from the American Heart Association. *Circulation.* 2017;135:e146–603.
12. James SL, Abate D, Hassen Abate K, et al. Global, regional, and national incidence, prevalence, and years lived with disability for 354 diseases and injuries for 195 countries and territories, 1990–2017: a systematic analysis for the global burden of disease study 2017. *Lancet.* 2018;392(10159):1789–858.

13. Mayerl C, Lukasser M, Sedivy R, et al. Atherosclerosis research from past to present - on the track of two pathologists with opposing views, Carl von Rokitsansky and Rudolf Virchow. *Virchows Arch*. 2006;449:96–103. <https://doi.org/10.1007/s00428-006-0176-7>.
14. Virchow R. As based upon physiological and pathological histology. *Nutr Rev*. 2009;47:23–5. <https://doi.org/10.1111/j.1753-4887.1989.tb02747.x>.
15. Bosch F, Rosich L. The contributions of Paul Ehrlich to pharmacology: a tribute on the occasion of the centenary of his Nobel prize. *Pharmacology*. 2008;82:171–9.
16. Karnovsky ML. Metchnikoff in Messina: a century of studies on phagocytosis - PubMed. *N Engl J Med*. 1981;7:1178–80.
17. Ross R, Glomset JA. Atherosclerosis and the arterial smooth muscle cell. *Science*. 1973;180:1332–9.
18. Brown MS, Goldstein JL. A receptor-mediated pathway for cholesterol homeostasis. *Science*. 1986;232:34–47. <https://doi.org/10.1126/science.3513311>.
19. Gerrity RG. The role of the monocyte in atherogenesis. I. Transition of blood-borne monocytes into foam cells in fatty lesions. *Am J Pathol*. 1981;103:181–90.
20. Falk E. Plaque rupture with severe pre-existing stenosis precipitating coronary thrombosis. Characteristics of coronary atherosclerotic plaques underlying fatal occlusive thrombi. *Br Heart J*. 1983;50:127–34. <https://doi.org/10.1136/hrt.50.2.127>.
21. Davies PF. Flow-mediated endothelial mechanotransduction. *Physiol Rev*. 1995;75:519–60.
22. Glagov S, Weisenberg E, Zarins CK, et al. Compensatory enlargement of human atherosclerotic coronary arteries. *N Engl J Med*. 1987;316:1371–5. <https://doi.org/10.1056/nejm198705283162204>.
23. Libby P. Inflammation in atherosclerosis. *Arterioscler Thromb Vasc Biol*. 2012;32:2045–51. <https://doi.org/10.1161/ATVBAHA.108.179705>.
24. Gimbrone MA, García-Cardeña G. Endothelial cell dysfunction and the pathobiology of atherosclerosis. *Circ Res*. 2016;118:620–36. <https://doi.org/10.1161/CIRCRESAHA.115.306301>.
25. Bussolari SR, Dewey CF, Gimbrone MA. Apparatus for subjecting living cells to fluid shear stress. *Rev Sci Instrum*. 1982;53:1851–4. <https://doi.org/10.1063/1.1136909>.
26. Dewey CF, Bussolari SR, Gimbrone MA, Davies PF. The dynamic response of vascular endothelial cells to fluid shear stress. *J Biomech Eng*. 1981;103:177–85. <https://doi.org/10.1115/1.3138276>.
27. Chiu JJ, Chien S. Effects of disturbed flow on vascular endothelium: pathophysiological basis and clinical perspectives. *Physiol Rev*. 2011;91:327–87.
28. Levesque MJ, Nerem RM. The elongation and orientation of cultured endothelial cells in response to shear stress. *J Biomech Eng*. 1985;107:341–7. <https://doi.org/10.1115/1.3138567>.
29. Topper JN, Cai J, Falb D, Gimbrone MA. Identification of vascular endothelial genes differentially responsive to fluid mechanical stimuli: Cyclooxygenase-2, manganese superoxide dismutase, and endothelial cell nitric oxide synthase are selectively up-regulated by steady laminar shear stress. *Proc Natl Acad Sci U S A*. 1996;93:10417–22. <https://doi.org/10.1073/pnas.93.19.10417>.
30. Cunningham KS, Gotlieb AI. The role of shear stress in the pathogenesis of atherosclerosis. *Lab Invest*. 2005;85:9–23.
31. Goldstein JL, Brown MS. A century of cholesterol and coronaries: from plaques to genes to statins. *Cell*. 2015;161:161–72.
32. Hopstock LA, Bønaa KH, Eggen AE, et al. Longitudinal and secular trends in total cholesterol levels and impact of lipid-lowering drug use among Norwegian women and men born in 1905–1977 in the population-based Tromsø Study 1979–2016. *BMJ Open*. 2017;7(8):e015001.
33. Nordestgaard BG, Chapman MJ, Humphries SE, et al. Familial hypercholesterolaemia is underdiagnosed and undertreated in the general population: Guidance for clinicians to prevent coronary heart disease. *Eur Heart J*. 2013;34(45):3478–90. <https://doi.org/10.1093/eurheartj/ehd273>.
34. Cohen JC, Boerwinkle E, Mosley TH, Hobbs HH. Sequence variations in PCSK9, low LDL, and protection against coronary heart disease. *N Engl J Med*. 2006;354:1264–72. <https://doi.org/10.1056/nejmoa054013>.

35. Borén J, Williams KJ. The central role of arterial retention of cholesterol rich apolipoprotein-B-containing lipoproteins in the pathogenesis of atherosclerosis: a triumph of simplicity. *Curr Opin Lipidol.* 2016;27:473–83.
36. Pentikäinen MO, Öörni K, Ala-Korpela M, Kovanen PT. Modified LDL - trigger of atherosclerosis and inflammation in the arterial intima. *J Intern Med.* 2000;247(3):359–70.
37. Ridker PM, Everett BM, Thuren T, et al. Antiinflammatory therapy with Canakinumab for atherosclerotic disease. *N Engl J Med.* 2017;377:1119–31. <https://doi.org/10.1056/nejmoa1707914>.
38. Stemme S, Faber B, Holm J, et al. T lymphocytes from human atherosclerotic plaques recognize oxidized low density lipoprotein. *Proc Natl Acad Sci U S A.* 1995;92:3893–7. <https://doi.org/10.1073/pnas.92.9.3893>.
39. Cybulsky MI, Iiyama K, Li H, et al. A major role for VCAM-1, but not ICAM-1, in early atherosclerosis. *J Clin Invest.* 2001;107:1255–62. <https://doi.org/10.1172/JCI11871>.
40. De Caterina R, Basta G, Lazzerini G, et al. Soluble vascular cell adhesion molecule-1 as a biohumoral correlate of atherosclerosis. *Arterioscler Thromb Vasc Biol.* 1997;17:2646–54. <https://doi.org/10.1161/01.ATV.17.11.2646>.
41. Gu L, Okada Y, Clinton SK, et al. Absence of monocyte chemoattractant protein-1 reduces atherosclerosis in low density lipoprotein receptor-deficient mice. *Mol Cell.* 1998;2:275–81. [https://doi.org/10.1016/S1097-2765\(00\)80139-2](https://doi.org/10.1016/S1097-2765(00)80139-2).
42. Falk E. Pathogenesis of atherosclerosis. *J Am Coll Cardiol.* 2006;47(8 Suppl): C7–C12.
43. Mach F, Sauty A, Iarossi AS, et al. Differential expression of three T lymphocyte-activating CXC chemokines by human atheroma-associated cells. *J Clin Invest.* 1999;104:1041–50. <https://doi.org/10.1172/JCI6993>.
44. Clinton SK, Underwood R, Hayes L, et al. Macrophage colony-stimulating factor gene expression in vascular cells and in experimental and human atherosclerosis. *Am J Pathol.* 1992;140:301–16.
45. Rosenfeld ME, Yla-Herttuala S, Lipton BA, et al. Macrophage colony-stimulating factor mRNA and protein in atherosclerotic lesions of rabbits and humans. *Am J Pathol.* 1992;140:291–300.
46. Kunjathoor VV, Febbraio M, Podrez EA, et al. Scavenger receptors class A-I/II and CD36 are the principal receptors responsible for the uptake of modified low density lipoprotein leading to lipid loading in macrophages. *J Biol Chem.* 2002;277:49982–8. <https://doi.org/10.1074/jbc.M209649200>.
47. Wanschel A, Seibert T, Hewing B, et al. Neuroimmune guidance cue semaphorin 3E is expressed in atherosclerotic plaques and regulates macrophage retention. *Arterioscler Thromb Vasc Biol.* 2013;33:886–93. <https://doi.org/10.1161/ATVBAHA.112.300941>.
48. Park YM, Drazba JA, Vasanji A, et al. Oxidized LDL/CD36 interaction induces loss of cell polarity and inhibits macrophage locomotion. *Mol Biol Cell.* 2012;23:3057–68. <https://doi.org/10.1091/mbc.E11-12-1051>.
49. Geng YJ, Libby P. Evidence for apoptosis in advanced human atheroma: Colocalization with interleukin-1 β -converting enzyme. *Am J Pathol.* 1995;147:251–66.
50. Clarke MCH, Talib S, Figg NL, Bennett MR. Vascular smooth muscle cell apoptosis induces interleukin-1-directed inflammation: effects of hyperlipidemia-mediated inhibition of phagocytosis. *Circ Res.* 2010;106:363–72. <https://doi.org/10.1161/CIRCRESAHA.109.208389>.
51. Tabas I. Macrophage death and defective inflammation resolution in atherosclerosis. *Nat Rev Immunol.* 2010;10:36–46.
52. Faggionato A, Ross R. Studies of hypercholesterolemia in the nonhuman primate II Fatty streak conversion to fibrous plaque. *Arteriosclerosis.* 1984;4:341–56. <https://doi.org/10.1161/01.atv.4.4.341>.
53. Sano H, Ueda Y, Takakura N, et al. Blockade of platelet-derived growth factor receptor- β pathway induces apoptosis of vascular endothelial cells and disrupts glomerular capillary formation in neonatal mice. *Am J Pathol.* 2002;161:135–43. [https://doi.org/10.1016/S0002-9440\(10\)64165-X](https://doi.org/10.1016/S0002-9440(10)64165-X).

54. Schwartz SM, Virmani R, Rosenfeld ME. The good smooth muscle cells in atherosclerosis. *Curr Atheroscler Rep.* 2000;2:422–9.
55. Bennett MR, Sinha S, Owens GK. Vascular smooth muscle cells in atherosclerosis. *Circ Res.* 2016;118:692–702. <https://doi.org/10.1161/CIRCRESAHA.115.306361>.
56. Stary HC. Natural history of calcium deposits in atherosclerosis progression and regression. *Z Kardiol.* 2000;89(Suppl 2):28–35. <https://doi.org/10.1007/s003920070097>.
57. Ruiz JL, Weinbaum S, Aikawa E, Hutcheson JD. Zooming in on the genesis of atherosclerotic plaque microcalcifications. *J Physiol.* 2016;594:2915–27.
58. Huang H, Virmani R, Younis H, et al. The impact of calcification on the biomechanical stability of atherosclerotic plaques. *Circulation.* 2001;103:1051–6. <https://doi.org/10.1161/01.CIR.103.8.1051>.
59. Ehara S, Kobayashi Y, Yoshiyama M, et al. Spotty calcification typifies the culprit plaque in patients with acute myocardial infarction: an intravascular ultrasound study. *Circulation.* 2004;110:3424–9. <https://doi.org/10.1161/01.CIR.0000148131.41425.E9>.
60. Pletcher MJ, Tice JA, Pignone M, Browner WS. Using the coronary artery calcium score to predict coronary heart disease events: a systematic review and meta-analysis. *Arch Intern Med.* 2004;164:1285–92.
61. Kwiecinski J, Dey D, Cadet S, et al. Predictors of 18F-sodium fluoride uptake in patients with stable coronary artery disease and adverse plaque features on computed tomography angiography. *Eur Heart J Cardiovasc Imaging.* 2020;21:58–66. <https://doi.org/10.1093/ehjci/jez152>.
62. Parathath S, Mick SL, Feig JE, et al. Hypoxia is present in murine atherosclerotic plaques and has multiple adverse effects on macrophage lipid metabolism. *Circ Res.* 2011;109:1141–52. <https://doi.org/10.1161/CIRCRESAHA.111.246363>.
63. Gao L, Chen Q, Zhou X, Fan L. The role of hypoxia-inducible factor 1 in atherosclerosis. *J Clin Pathol.* 2012;65:872–6.
64. Celletti FL, Waugh JM, Amabile PG, et al. Vascular endothelial growth factor enhances atherosclerotic plaque progression. *Nat Med.* 2001;7:425–9. <https://doi.org/10.1038/86490>.
65. De Vries MR, Quax PHA. Plaque angiogenesis and its relation to inflammation and atherosclerotic plaque destabilization. *Curr Opin Lipidol.* 2016;27:499–506.
66. Mills CD, Kincaid K, Alt JM, et al. M-1/M-2 macrophages and the Th1/Th2 paradigm. *J Immunol.* 2000;164:6166–73. <https://doi.org/10.4049/jimmunol.164.12.6166>.
67. Stremmel C, Stark K, Schulz C. Heterogeneity of macrophages in atherosclerosis. *Thromb Haemost.* 2019;119:1237–46. <https://doi.org/10.1055/s-0039-1692665>.
68. Chinetti-Gbaguidi G, Colin S, Staels B. Macrophage subsets in atherosclerosis. *Nat Rev Cardiol.* 2015;12:10–7.
69. Kadl A, Meher AK, Sharma PR, et al. Identification of a novel macrophage phenotype that develops in response to atherogenic phospholipids via Nrf2. *Circ Res.* 2010;107:737–46. <https://doi.org/10.1161/CIRCRESAHA.109.215715>.
70. Martinez FO, Gordon S. The M1 and M2 paradigm of macrophage activation: time for reassessment. *F1000Prime Rep.* 2014;6:13. <https://doi.org/10.12703/P6-13>.
71. Libby P, Ridker PM, Hansson GK. Progress and challenges in translating the biology of atherosclerosis. *Nature.* 2011;473:317–25.
72. Libby P, Ridker PM, Hansson GK. Inflammation in atherosclerosis. From pathophysiology to practice. *J Am Coll Cardiol.* 2009;54:2129–38.
73. Galis ZS, Sukhova GK, Lark MW, Libby P. Increased expression of matrix metalloproteinases and matrix degrading activity in vulnerable regions of human atherosclerotic plaques. *J Clin Invest.* 1994;94:2493–503. <https://doi.org/10.1172/JCI117619>.
74. Mach F, Schönbeck U, Bonnefoy JY, et al. Activation of monocyte/macrophage functions related to acute atheroma complication by ligation of CD40: induction of collagenase, stromelysin, and tissue factor. *Circulation.* 1997;96:396–9. <https://doi.org/10.1161/01.CIR.96.2.396>.
75. Kovanen PT, Kaartinen M, Paavonen T. Infiltrates of activated mast cells at the site of coronary atheromatous erosion or rupture in myocardial infarction. *Circulation.* 1995;92:1084–8. <https://doi.org/10.1161/01.CIR.92.5.1084>.

76. Zhou X, Robertson AKL, Hjerpe C, Hansson GK. Adoptive transfer of CD4+ T cells reactive to modified low-density lipoprotein aggravates atherosclerosis. *Arterioscler Thromb Vasc Biol.* 2006;26:864–70. <https://doi.org/10.1161/01.ATV.0000206122.61591.ff>.
77. Zhou X, Nicoletti A, Elhage R, Hansson GK. Transfer of CD4+ T cells aggravates atherosclerosis in immunodeficient apolipoprotein E knockout mice. *Circulation.* 2000;102:2919–22. <https://doi.org/10.1161/01.CIR.102.24.2919>.
78. Jonasson L, Holm J, Skalli O, et al. Regional accumulations of T cells, macrophages, and smooth muscle cells in the human atherosclerotic plaque. *Arteriosclerosis.* 1986;6:131–8. <https://doi.org/10.1161/01.atv.6.2.131>.
79. Galis ZS, Muszynski M, Sukhova GK, et al. Enhanced expression of vascular matrix metalloproteinases induced in vitro by cytokines and in regions of human atherosclerotic lesions. *Ann N Y Acad Sci.* 1994;748:501–7.
80. Bentzon JF, Otsuka F, Virmani R, Falk E. Mechanisms of plaque formation and rupture. *Circ Res.* 2014;114:1852–66. <https://doi.org/10.1161/CIRCRESAHA.114.302721>.
81. Libby P. Mechanisms of acute coronary syndromes and their implications for therapy. *N Engl J Med.* 2013;368:2004–13. <https://doi.org/10.1056/nejmra1216063>.
82. Farb A, Burke AP, Tang AL, et al. Coronary plaque erosion without rupture into a lipid core: a frequent cause of coronary thrombosis in sudden coronary death. *Circulation.* 1996;93:1354–63. <https://doi.org/10.1161/01.CIR.93.7.1354>.
83. Manoharan G, Ntalianis A, Muller O, et al. Severity of coronary arterial Stenoses responsible for acute coronary syndromes. *Am J Cardiol.* 2009;103:1183–8. <https://doi.org/10.1016/j.amjcard.2008.12.047>.
84. Murry CE, Jennings RB, Reimer KA. Preconditioning with ischemia: a delay of lethal cell injury in ischemic myocardium. *Circulation.* 1986;74:1124–36. <https://doi.org/10.1161/01.CIR.74.5.1124>.
85. Walsh SR, Tang TY, Kullar P, et al. Ischaemic preconditioning during cardiac surgery: systematic review and meta-analysis of perioperative outcomes in randomised clinical trials. *Eur J Cardio-Thoracic Surg.* 2008;34:985–94.
86. Wu ZK, Iivainen T, Pehkonen E, et al. Ischemic preconditioning suppresses ventricular tachyarrhythmias after myocardial revascularization. *Circulation.* 2002;106:3091–6. <https://doi.org/10.1161/01.CIR.0000041430.32233.5B>.
87. Hoffmann U, Ferencik U, Udelson JE, et al. Prognostic value of noninvasive cardiovascular testing in patients with stable chest pain: insights from the PROMISE trial (prospective multicenter imaging study for evaluation of chest pain). *Circulation.* 2017;135:2320–32. <https://doi.org/10.1161/CIRCULATIONAHA.116.024360>.
88. Chang HJ, Lin FY, Lee SE, et al. Coronary atherosclerotic precursors of acute coronary syndromes. *J Am Coll Cardiol.* 2018;71:2511–22. <https://doi.org/10.1016/j.jacc.2018.02.079>.
89. Pasterkamp G, Den Ruijter HM, Libby P. Temporal shifts in clinical presentation and underlying mechanisms of atherosclerotic disease. *Nat Rev Cardiol.* 2016;14:21–9.
90. Quillard T, Franck G, Mawson T, et al. Mechanisms of erosion of atherosclerotic plaques. *Curr Opin Lipidol.* 2017;28:434–41.
91. Calder PC, Dimitriadis G, Newsholme P. Glucose metabolism in lymphoid and inflammatory cells and tissues. *Curr Opin Clin Nutr Metab Care.* 2007;10:531–40.
92. Palmer CS, Ostrowski M, Balderson B, et al. Glucose metabolism regulates T cell activation, differentiation, and functions. *Front Immunol.* 2015;6:1.
93. Sluimer JC, Daemen MJ. Novel concepts in atherogenesis: angiogenesis and hypoxia in atherosclerosis. *J Pathol.* 2009;218:7–29.
94. Newsholme P, Curi R, Gordon S, Newsholme EA. Metabolism of glucose, glutamine, long-chain fatty acids and ketone bodies by murine macrophages. *Biochem J.* 1986;239:121–5. <https://doi.org/10.1042/bj2390121>.
95. Pacák J, Tořk Z, Erný M. Synthesis of 2-deoxy-2-fluoro-D-glucose. *J Chem Soc D Chem Commun.* 1969;2:77. <https://doi.org/10.1039/C29690000077>.
96. Basu S, Hess S, Nielsen Braad PE, et al. The basic principles of FDG-PET/CT imaging. *PET Clin.* 2014;9:355–70.

97. Borchert T, Beitar L, Langer LBN, et al. Dissecting the target leukocyte subpopulations of clinically relevant inflammation radiopharmaceuticals. *J Nucl Cardiol*. 2019; <https://doi.org/10.1007/s12350-019-01929-z>. Epub ahead of print. PMID: 31659697.
98. Vallabhajosula SFV. Atherosclerosis: imaging techniques and the evolving role of nuclear medicine - PubMed. *J Nucl Med*. 1997;38:1788–96.
99. Ogawa MISMTADTNWH, et al. (18)F-FDG accumulation in atherosclerotic plaques: immunohistochemical and PET imaging study - PubMed. *J Nucl Med*. 2004;45:1245–50.
100. Lederman RJ, Raylman RR, Fisher SJ, et al. Detection of atherosclerosis using a novel positron-sensitive probe and 18-fluorodeoxyglucose (FDG). *Nucl Med Commun*. 2001;22:747–53.
101. Rudd JHF, Narula J, Strauss HW, et al. Imaging atherosclerotic plaque inflammation by Fluorodeoxyglucose with positron emission tomography. Ready for prime time? *J Am Coll Cardiol*. 2010;55:2527–35.
102. Yun M, Jang S, Cucchiara A, et al. 18F FDG uptake in the large arteries: a correlation study with the atherogenic risk factors. *Semin Nucl Med*. 2002;32:70–6. <https://doi.org/10.1053/snuc.2002.29279>.
103. Figueroa AL, Abdelbaky A, Truong QA, et al. Measurement of arterial activity on routine FDG PET/CT images improves prediction of risk of future CV events. *JACC Cardiovasc Imaging*. 2013;6:1250–9. <https://doi.org/10.1016/j.jcmg.2013.08.006>.
104. Kelly PJ, Camps-Renom P, Giannotti N, et al. Carotid plaque inflammation imaged by 18F-Fluorodeoxyglucose positron emission tomography and risk of early recurrent stroke. *Stroke*. 2019;50:1766–73. <https://doi.org/10.1161/STROKEAHA.119.025422>.
105. Arauz A, Hoyos L, Zenteno M, et al. Carotid plaque inflammation detected by 18F-fluorodeoxyglucose-positron emission tomography. Pilot study. *Clin Neurol Neurosurg*. 2007;109:409–12. <https://doi.org/10.1016/j.clineuro.2007.02.012>.
106. Kang MK, Kim CJ, Choo EH, et al. Anti-inflammatory effect of statin is continuously working throughout use: a prospective three time point 18F-FDG PET/CT imaging study. *Int J Cardiovasc Imaging*. 2019;35:1745–53. <https://doi.org/10.1007/s10554-019-01584-y>.
107. Kim CJ, Han EJ, Chu E-H, et al. Effect of moderate-intensity statin therapy on plaque inflammation in patients with acute coronary syndrome: a prospective interventional study evaluated by 18F-FDG PET/CT of the carotid artery. *Cardiol J*. 2013;27(6):762–71. <https://doi.org/10.5603/cj.a2018.0069>.
108. Su JL, Young KO, Eun JL, et al. Reversal of vascular 18F-FDG uptake with plasma high-density lipoprotein elevation by atherogenic risk reduction. *J Nucl Med*. 2008;49:1277–82. <https://doi.org/10.2967/jnumed.108.052233>.
109. Osborne MT, Hulten EA, Murthy VL, et al. Patient preparation for cardiac fluorine-18 fluorodeoxyglucose positron emission tomography imaging of inflammation. *J Nucl Cardiol*. 2017;24:86–99. <https://doi.org/10.1007/s12350-016-0502-7>.
110. Hughes CE, Nibbs RJB. A guide to chemokines and their receptors. *FEBS J*. 2018;285:2944–71.
111. Döring Y, Pawig L, Weber C, Noels H. The CXCL12/CXCR4 chemokine ligand/receptor axis in cardiovascular disease. *Front Physiol*. 2014;5:212. <https://doi.org/10.3389/fphys.2014.00212>.
112. Döring Y, Noels H, Van Der Vorst EPC, et al. Vascular CXCR4 limits atherosclerosis by maintaining arterial integrity: evidence from mouse and human studies. *Circulation*. 2017;136:388–403. <https://doi.org/10.1161/CIRCULATIONAHA.117.027646>.
113. Gupta SK, Pillarisetti K, Lysko PG. Modulation of CXCR4 expression and SDF-1 α functional activity during differentiation of human monocytes and macrophages. *J Leukoc Biol*. 1999;66:135–43. <https://doi.org/10.1002/jlb.66.1.135>.
114. Koenen RR, Von Hundelshausen P, Nesselova IV, et al. Disrupting functional interactions between platelet chemokines inhibits atherosclerosis in hyperlipidemic mice. *Nat Med*. 2009;15:97–103. <https://doi.org/10.1038/nm.1898>.
115. Saederup N, Chan L, Lira SA, Charo IF. Fractalkine deficiency markedly reduces macrophage accumulation and atherosclerotic lesion formation in CCR2 $^{-/-}$ mice: evidence for independent chemokine functions in atherogenesis. *Circulation*. 2008;117:1642–8. <https://doi.org/10.1161/CIRCULATIONAHA.107.743872>.

116. Philipp-Abbrederis K, Herrmann K, Knop S, et al. In vivo molecular imaging of chemokine receptor CXCR 4 expression in patients with advanced multiple myeloma. *EMBO Mol Med.* 2015;7:477–87. <https://doi.org/10.15252/emmm.201404698>.
117. Werner RA, Kircher S, Higuchi T, et al. CXCR4-directed imaging in solid tumors. *Front Oncol.* 2019;9:770. <https://doi.org/10.3389/fonc.2019.00770>.
118. Haug AR, Leisser A, Wadsak W, et al. Prospective non-invasive evaluation of CXCR4 expression for the diagnosis of MALT lymphoma using [68Ga]Ga-Pentixafor-PET/MRI. *Theranostics.* 2019;9:3653–8. <https://doi.org/10.7150/thno.31032>.
119. Derlin T, Wester HJ, Bengel FM, Hueper K. Visualization of posttraumatic splenosis on chemokine receptor CXCR4-targeted PET/CT. *Clin Nucl Med.* 2017;42:e317–8. <https://doi.org/10.1097/RLU.0000000000001590>.
120. Derlin T, Gueler F, Bräsen JH, et al. Integrating MRI and chemokine receptor CXCR4-targeted PET for detection of leukocyte infiltration in complicated urinary tract infections after kidney transplantation. *J Nucl Med.* 2017;58:1831–7. <https://doi.org/10.2967/jnumed.117.193037>.
121. Poschenrieder A, Osl T, Schottelius M, Hoffmann F, et al. First 18F-labeled Pentixafor-based imaging agent for PET imaging of CXCR4 expression in vivo. *Tomography.* 2016;2:85–93. <https://doi.org/10.18383/j.tom.2016.00130>.
122. Thackeray JT, Derlin T, Haghikia A, et al. Molecular imaging of the chemokine receptor CXCR4 after acute myocardial infarction. *JACC Cardiovasc Imaging.* 2015;8:1417–26. <https://doi.org/10.1016/j.jcmg.2015.09.008>.
123. Reiter T, Kircher M, Schirbel A, et al. Imaging of C-X-C motif chemokine receptor CXCR4 expression after myocardial infarction with [68 Ga]Pentixafor-PET/CT in correlation with cardiac MRI. *JACC Cardiovasc Imaging.* 2018;11:1541–3.
124. Hyafil F, Pelisek J, Laitinen I, et al. Imaging the cytokine receptor CXCR4 in atherosclerotic plaques with the radiotracer 68Ga-Pentixafor for PET. *J Nucl Med.* 2017;58:499–506. <https://doi.org/10.2967/jnumed.116.179663>.
125. Derlin T, Sedding DG, Dutzmann J, et al. Imaging of chemokine receptor CXCR4 expression in culprit and nonculprit coronary atherosclerotic plaque using motion-corrected [68Ga]pentixafor PET/CT. *Eur J Nucl Med Mol Imaging.* 2018;45:1934–44. <https://doi.org/10.1007/s00259-018-4076-2>.
126. Grosse GM, Bascuñana P, Schulz-Schaeffer WJ, et al. Targeting chemokine receptor CXCR4 and translocator protein for characterization of high-risk plaque in carotid stenosis ex vivo. *Stroke.* 2018;49:1988–91. <https://doi.org/10.1161/STROKEAHA.118.021070>.
127. Weiberg D, Thackeray JT, Daum G, et al. Clinical molecular imaging of chemokine receptor CXCR4 expression in atherosclerotic plaque using 68 Ga-pentixafor PET: correlation with cardiovascular risk factors and calcified plaque burden. *J Nucl Med.* 2018;59:266–72. <https://doi.org/10.2967/jnumed.117.196485>.
128. Kircher M, Tran-Gia J, Kemmer L, et al. Imaging inflammation in atherosclerosis with CXCR4-directed 68Ga-Pentixafor PET/CT: correlation with 18F-FDG PET/CT. *J Nucl Med.* 2020;61:751–6. <https://doi.org/10.2967/jnumed.119.234484>.
129. Li X, Heber D, Rausch I, et al. Quantitative assessment of atherosclerotic plaques on 18F-FDG PET/MRI: comparison with a PET/CT hybrid system. *Eur J Nucl Med Mol Imaging.* 2016;43:1503–12. <https://doi.org/10.1007/s00259-016-3308-6>.
130. Li X, Yu W, Wollenweber T, et al. [68Ga]Pentixafor PET/MR imaging of chemokine receptor 4 expression in the human carotid artery. *Eur J Nucl Med Mol Imaging.* 2019;46:1616–25. <https://doi.org/10.1007/s00259-019-04322-7>.
131. Li X, Heber D, Leike T, et al. [68Ga]Pentixafor-PET/MRI for the detection of chemokine receptor 4 expression in atherosclerotic plaques. *Eur J Nucl Med Mol Imaging.* 2018;45:558–66. <https://doi.org/10.1007/s00259-017-3831-0>.
132. Li X, Kemmer L, Zhang X, et al. Anti-inflammatory effects on atherosclerotic lesions induced by CXCR4-directed Endoradiotherapy. *J Am Coll Cardiol.* 2018;72:122–3.
133. Karshovska E, Zagorac D, Zerneck A, et al. A small molecule CXCR4 antagonist inhibits neointima formation and smooth muscle progenitor cell mobilization after arterial injury. *J Thromb Haemost.* 2008;6:1812–5.

134. Osl T, Schmidt A, Schwaiger M, et al. A new class of pentixa for and pentixa ther-based theranostic agents with enhanced CXCR4-targeting efficiency. *Theranostics*. 2020;10:8264–80. <https://doi.org/10.7150/thno.45537>.
135. Vengrenyuk Y, Carlier S, Xanthos S, et al. A hypothesis for vulnerable plaque rupture due to stress-induced debonding around cellular microcalcifications in thin fibrous caps. *Proc Natl Acad Sci U S A*. 2006;103:14678–83. <https://doi.org/10.1073/pnas.0606310103>.
136. Jeziorska M, McCollum C, Woolley DE. Observations on bone formation and remodelling in advanced atherosclerotic lesions of human carotid arteries. *Virchows Arch*. 1998;433:559–65. <https://doi.org/10.1007/s004280050289>.
137. Schinke T, McKee MD, Karsenty G. Extracellular matrix calcification: where is the action? *Nat Genet*. 1999;21:150–1.
138. Ge Q, Ruan CC, Ma Y, et al. Osteopontin regulates macrophage activation and osteoclast formation in hypertensive patients with vascular calcification. *Sci Rep*. 2017;7:40253. <https://doi.org/10.1038/srep40253>.
139. Addison WN, Masica DL, Gray JJ, McKee MD. Phosphorylation-dependent inhibition of mineralization by osteopontin ASARM peptides is regulated by PHEX cleavage. *J Bone Miner Res*. 2010;25:695–705. <https://doi.org/10.1359/jbmr.090832>.
140. Koltsova EK, Hedrick CC, Ley K. Myeloid cells in atherosclerosis: a delicate balance of anti-inflammatory and proinflammatory mechanisms. *Curr Opin Lipidol*. 2013;24:371–80.
141. Aikawa E, Nahrendorf M, Figueiredo JL, et al. Osteogenesis associates with inflammation in early-stage atherosclerosis evaluated by molecular imaging in vivo. *Circulation*. 2007;116:2841–50. <https://doi.org/10.1161/CIRCULATIONAHA.107.732867>.
142. New SEP, Goetsch C, Aikawa M, et al. Macrophage-derived matrix vesicles : an alternative novel mechanism for microcalcification in atherosclerotic plaques. *Circ Res*. 2013;113:72–7. <https://doi.org/10.1161/CIRCRESAHA.113.301036>.
143. Irlke A, Vesey AT, Lewis DY, et al. Identifying active vascular microcalcification by 18F-sodium fluoride positron emission tomography. *Nat Commun*. 2015;6:7495. <https://doi.org/10.1038/ncomms8495>.
144. Zhang Y, Li H, Jia Y, et al. Noninvasive assessment of carotid plaques calcification by 18F-sodium fluoride accumulation: correlation with pathology. *J Stroke Cerebrovasc Dis*. 2018;27:1796–801. <https://doi.org/10.1016/j.jstrokecerebrovasdis.2018.02.011>.
145. Czernin J, Satyamurthy N, Schiepers C. Molecular mechanisms of bone 18F-NaF deposition. *J Nucl Med*. 2010;51:1826–9.
146. Derlin T, Wisotzki C, Richter U, et al. In vivo imaging of mineral deposition in carotid plaque using 18F-sodium fluoride PET/CT: correlation with atherogenic risk factors. *J Nucl Med*. 2011;52:362–8. <https://doi.org/10.2967/jnumed.110.081208>.
147. Derlin T, Janssen T, Salamon J, et al. Age-related differences in the activity of arterial mineral deposition and regional bone metabolism: a 18F-sodium fluoride positron emission tomography study. *Osteoporos Int*. 2014;26:199–207. <https://doi.org/10.1007/s00198-014-2839-6>.
148. Derlin T, Richter U, Bannas P, et al. Feasibility of 18F-sodium fluoride PET/CT for imaging of atherosclerotic plaque. *J Nucl Med*. 2010;51:862–5. <https://doi.org/10.2967/jnumed.110.076471>.
149. Kwiecinski J, Cadet S, Daghm M, et al. Whole-vessel coronary 18F-sodium fluoride PET for assessment of the global coronary microcalcification burden. *Eur J Nucl Med Mol Imaging*. 2020;47:1736–45. <https://doi.org/10.1007/s00259-019-04667-z>.
150. Blomberg BA, Thomassen A, De Jong PA, et al. Coronary fluorine-18-sodium fluoride uptake is increased in healthy adults with an unfavorable cardiovascular risk profile: results from the CAMONA study. *Nucl Med Commun*. 2017;38:1007–14. <https://doi.org/10.1097/MNM.0000000000000734>.
151. Beheshti MSBMNTDWTMEWRNABSLWAA. Detection and global quantification of cardiovascular molecular calcification by fluoro18-fluoride positron emission tomography/computed tomography--a novel concept - PubMed. *Hell J Nucl Med*. 2011;14:114–20.

152. Morbelli S, Fiz F, Piccardo A, et al. Divergent determinants of 18F-NaF uptake and visible calcium deposition in large arteries: relationship with Framingham risk score. *Int J Cardiovasc Imaging*. 2014;30:439–47. <https://doi.org/10.1007/s10554-013-0342-3>.
153. Janssen T, Bannas P, Herrmann J, et al. Association of linear 18F-sodium fluoride accumulation in femoral arteries as a measure of diffuse calcification with cardiovascular risk factors: a PET/CT study. *J Nucl Cardiol*. 2013;20:569–77. <https://doi.org/10.1007/s12350-013-9680-8>.
154. Dweck MR, Chow MWL, Joshi NV, et al. Coronary arterial 18F-sodium fluoride uptake: a novel marker of plaque biology. *J Am Coll Cardiol*. 2012;59:1539–48. <https://doi.org/10.1016/j.jacc.2011.12.037>.
155. Fiz F. Correlation between thoracic aorta 18F-natrium fluoride uptake and cardiovascular risk. *World J Radiol*. 2016;8:82. <https://doi.org/10.4329/wjr.v8.i1.82>.
156. Kitagawa T, Yamamoto H, Nakamoto Y, et al. Predictive value of 18F-sodium fluoride positron emission tomography in detecting high-risk coronary artery disease in combination with computed tomography. *J Am Heart Assoc*. 2018;7(20):e010224. <https://doi.org/10.1161/JAHA.118.010224>.
157. Joshi NV, Vesey AT, Williams MC, et al. 18F-fluoride positron emission tomography for identification of ruptured and high-risk coronary atherosclerotic plaques: a prospective clinical trial. *Lancet*. 2014;383:705–13. [https://doi.org/10.1016/S0140-6736\(13\)61754-7](https://doi.org/10.1016/S0140-6736(13)61754-7).
158. Marchesseau S, Seneviratna A, Sjöholm AT, et al. Hybrid PET/CT and PET/MRI imaging of vulnerable coronary plaque and myocardial scar tissue in acute myocardial infarction. *J Nucl Cardiol*. 2018;25:2001–11. <https://doi.org/10.1007/s12350-017-0918-8>.
159. Lee JM, Bang JI, Koo BK, et al. Clinical relevance of 18F-sodium fluoride positron-emission tomography in noninvasive identification of high-risk plaque in patients with coronary artery disease. *Circ Cardiovasc Imaging*. 2017;10(11):e006704. <https://doi.org/10.1161/CIRCIMAGING.117.006704>.
160. Li L, Li X, Jia Y, et al. Sodium-fluoride PET-CT for the non-invasive evaluation of coronary plaques in symptomatic patients with coronary artery disease: a cross-correlation study with intravascular ultrasound. *Eur J Nucl Med Mol Imaging*. 2018;45:2181–9. <https://doi.org/10.1007/s00259-018-4122-0>.
161. Li X, Heber D, Gonzalez JC, et al. Association between osteogenesis and inflammation during the progression of calcified plaque evaluated by 18F-fluoride and 18F-FDG. *J Nucl Med*. 2017;58:968–74. <https://doi.org/10.2967/jnumed.116.182790>.
162. Ishiwata Y, Kaneta T, Nawata S, et al. Quantification of temporal changes in calcium score in active atherosclerotic plaque in major vessels by 18F-sodium fluoride PET/CT. *Eur J Nucl Med Mol Imaging*. 2017;44:1529–37. <https://doi.org/10.1007/s00259-017-3680-x>.
163. Hayrapetian A, Berenji GR, Nguyen KL, Li Y. 18F-sodium fluoride uptake is associated with severity of atherosclerotic stenosis in stable ischemic heart disease. *J Nucl Cardiol*. 2020; <https://doi.org/10.1007/s12350-020-02238-6>.
164. Folkman J. Angiogenesis in cancer, vascular, rheumatoid and other disease. *Nat Med*. 1995;1:27–30.
165. Cao Y, Arbiser J, D'Amato RJ, et al. Forty-year journey of angiogenesis translational research. *Sci Transl Med*. 2011;3(114):114rv3.
166. Stollman TH, Ruers TJM, Oyen WJG, Boerman OC. New targeted probes for radioimaging of angiogenesis. *Methods*. 2009;48:188–92. <https://doi.org/10.1016/j.ymeth.2009.03.006>.
167. Higuchi T, Wester HJ, Schwaiger M. Imaging of angiogenesis in cardiology. *Eur J Nucl Med Mol Imaging*. 2007;34:S9–S19.
168. Dunphy MPS, Strauss HW. Molecular imaging of atherosclerosis. *Curr Cardiol Rep*. 2008;10:121–7.
169. Cai H, Conti PS. RGD-based PET tracers for imaging receptor integrin α v β 3 expression. *J Label Compd Radiopharm*. 2013;56:264–79.
170. Su H, Gorodny N, Gomez LF, et al. Atherosclerotic plaque uptake of a novel integrin tracer 18F-Flotegatide in a mouse model of atherosclerosis. *J Nucl Cardiol*. 2014;21:553–62. <https://doi.org/10.1007/s12350-014-9879-3>.

171. Vancraeynest D, Roelants V, Bouzin C, et al. $\alpha V\beta 3$ integrin-targeted microSPECT/CT imaging of inflamed atherosclerotic plaques in mice. *EJNMMI Res.* 2016;6(1):29. <https://doi.org/10.1186/s13550-016-0184-9>.
172. Laitinen I, Saraste A, Weidl E, et al. Evaluation of $\alpha V\beta 3$ integrin-targeted positron emission tomography tracer ^{18}F -galacto-RGD for imaging of vascular inflammation in atherosclerotic mice. *Circ Cardiovasc Imaging.* 2009;2:331–8. <https://doi.org/10.1161/CIRCIMAGING.108.846865>.
173. Jenkins WS, Vesey AT, Vickers A, et al. In vivo alpha-V beta-3 integrin expression in human aortic atherosclerosis aortic and vascular disease. *Heart.* 2019;105:1868–75. <https://doi.org/10.1136/heartjnl-2019-315103>.
174. Dalm VASH, Van Hagen PM, Van Koetsveld PM, et al. Expression of somatostatin, cortistatin, and somatostatin receptors in human monocytes, macrophages, and dendritic cells. *Am J Physiol-Endocrinol Metab.* 2003;285:E344–53. <https://doi.org/10.1152/ajpendo.00048.2003>.
175. Li X, Bauer W, Kreissl MC, et al. Specific somatostatin receptor II expression in arterial plaque: ^{68}Ga -DOTATATE autoradiographic, immunohistochemical and flow cytometric studies in apo E-deficient mice. *Atherosclerosis.* 2013;230:33–9. <https://doi.org/10.1016/j.atherosclerosis.2013.06.018>.
176. Rinne P, Hellberg S, Kiugel M, et al. Comparison of somatostatin receptor 2-targeting PET tracers in the detection of mouse atherosclerotic plaques. *Mol Imaging Biol.* 2016;18:99–108. <https://doi.org/10.1007/s11307-015-0873-1>.
177. Rominger A, Saam T, Vogl E, et al. In vivo imaging of macrophage activity in the coronary arteries using ^{68}Ga -DOTATATE PET/CT: correlation with coronary calcium burden and risk factors. *J Nucl Med.* 2010;51:193–7. <https://doi.org/10.2967/jnumed.109.070672>.
178. Li X, Sannick S, Lapa C, et al. ^{68}Ga -DOTATATE PET/CT for the detection of inflammation of large arteries: correlation with ^{18}F -FDG, calcium burden and risk factors. *EJNMMI Res.* 2012;2:1–10. <https://doi.org/10.1186/2191-219X-2-52>.
179. Schatka I, Wollenweber T, Haense C, et al. Peptide receptor-targeted radionuclide therapy alters inflammation in atherosclerotic plaques. *J Am Coll Cardiol.* 2013;62:2344–5.
180. Tarkin JM, Joshi FR, Evans NR, et al. Detection of atherosclerotic inflammation by ^{68}Ga -DOTATATE PET compared to ^{18}F FDG PET imaging. *J Am Coll Cardiol.* 2017;69:1774–91. <https://doi.org/10.1016/j.jacc.2017.01.060>.



Post-Infarction Inflammatory Alterations

5

Kim van der Heiden, Boudewijn J. Krenning,
Daphne Merkus, and Monique R. Bernsen

Contents

5.1	General Introduction.....	109
5.2	Biology of Ventricular Remodeling.....	110
5.3	The Role of Molecular Imaging.....	120
5.4	Imaging Targets.....	124
5.5	Hybrid Imaging: The Added Value of Hybrid Imaging.....	142
5.6	Concluding Remarks.....	143
	References.....	144

5.1 General Introduction

Coronary artery disease is one of the most common cardiovascular diseases and associated with significant mortality and morbidity. Atherosclerosis is the most common cause of myocardial infarction (MI), most often through the rupture of an atherosclerotic plaque, resulting in obstruction of coronary flow to distal

K. van der Heiden

Department of Biomedical Engineering, Thorax Center, Erasmus MC,
Rotterdam, The Netherlands

B. J. Krenning

Department of Cardiology, Thorax Center, Erasmus MC, Rotterdam, The Netherlands

D. Merkus

Department of Experimental Cardiology, Thorax Center, Erasmus MC,
Rotterdam, The Netherlands

M. R. Bernsen (✉)

Walter-Brendel Centre of Experimental Medicine, University Hospital, LMU Munich,
Munich, Germany

e-mail: m.bernsen@erasmusmc.nl

myocardium. Timely implementation of reperfusion therapy is the optimal treatment for acute MI (AMI); restoring epicardial coronary flow via primary percutaneous coronary intervention (PCI) or coronary bypass grafting limits cardiomyocyte cell death. Since development of heart failure is influenced by the size of the infarct, prompt reperfusion therapy contributes to improving left ventricular function and ultimately patient outcome. Myocardial injury triggers a complex biological response, involving various molecular and cellular processes including a substantial inflammatory reaction. The inflammatory reaction is a natural response to tissue injury and crucial for healing of the infarcted myocardium. However, when the inflammatory response is excessive in duration and/or magnitude, it can result in exacerbated tissue damage and adverse remodeling contributing to the pathogenesis of heart failure. Various (pre-)clinical studies have shown correlations between elevated peripheral blood leukocyte counts and/or inflammatory cytokine levels following first MI and late stage cardiac function or 30-day mortality [1–3]. Moreover, adverse LV remodeling has been linked to an excessive or prolonged inflammatory reaction independent of initial infarct size [4]. Because of the apparent crucial role of post-MI inflammation on long-term patient outcome, treatment aimed at modulation of the inflammatory response is being widely pursued and investigated. Encouraging results have been obtained in preclinical as well as clinical studies, using non-steroidal anti-inflammatory drugs, anti-TNF- α therapy, and IL-1 modulating therapy. However, patient selection is crucial in such strategies since anti-inflammatory agents targeting the inflammatory response may also negatively affect wound healing. Better understanding of the dynamics of the post-MI inflammatory response and the ability to non-invasively monitor the processes involved is therefore crucial. Robust non-invasive imaging techniques are needed to ultimately predict adverse reactions and to monitor responses to anti-inflammatory therapy.

5.2 Biology of Ventricular Remodeling

The acute effect of myocardial infarction involves various molecular and mechanical alterations in the myocardium that instigate remodeling of the infarcted border zone and remote non-infarcted myocardium. Ventricular remodeling is characterized by changes in size, shape, structure, and function of the ventricle. Ventricular remodeling may continue for weeks or months with an overall decline in cardiac function. Clinically, this ultimately results in related symptoms, such as heart failure (HF) and arrhythmias that are associated with chronic disability and higher mortality.

5.2.1 Pathobiology of Ventricular Remodeling Post-MI

Myocardial infarction occurs when myocardial ischemia is of sufficient duration to cause cardiomyocyte death. The duration of ischemia and size of the ischemic area are critical determinants of infarct size, which in turn is a key factor in adverse remodeling of the myocardium and development of heart failure. Treatment of acute

MI is therefore principally aimed at reducing infarct size by opening of the obstruction as quickly as possible to limit the amount of irreversibly damaged myocardium [5]. However, reperfusion of ischemic myocardium also causes damage by itself, so-called reperfusion injury, which adds to the infarct size [6]. Cardiac tissue response following AMI can be divided into three, overlapping, phases: a pro-inflammatory phase (4 days in mice), a reparative (anti-inflammatory phase (4–14 days in mice) with proliferation of fibroblasts [7, 8], and maturation of the scar [3, 9].

Cardiomyocyte death triggers an acute pro-inflammatory response (Fig. 5.1) starting with the activation of several processes including activation of the complement cascade, reactive oxygen species (ROS) production, and release of damage-associated molecular patterns (DAMPs) which bind pattern recognition receptors (PRRs) (for more information on these processes we refer the reader to Prabdu and Frangogiannis [11], Ong et al. [10]). This subsequently results in the release of

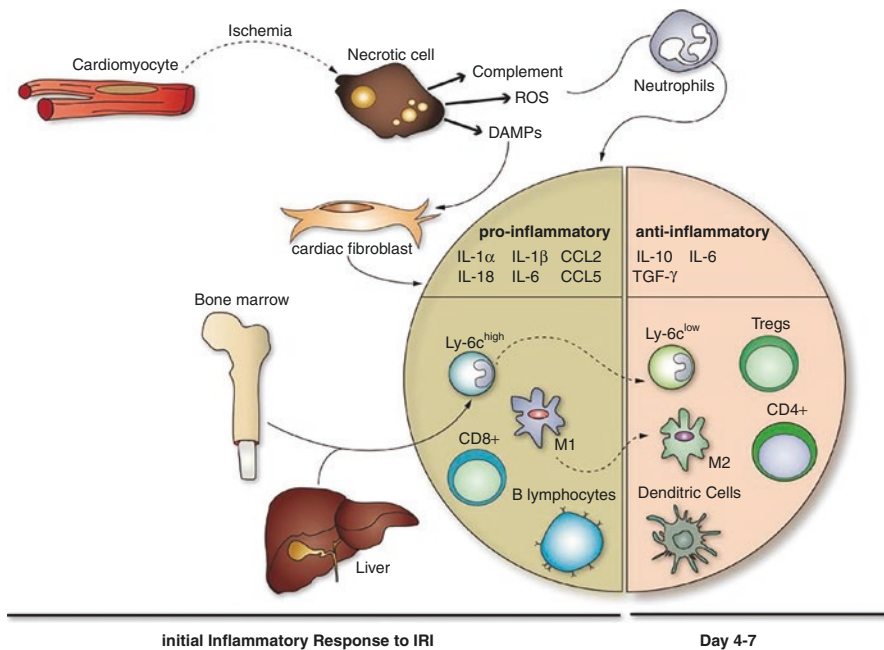


Fig. 5.1 The inflammatory response cascade. Following cardiomyocyte injury, an inflammatory response is induced through the release of danger-associated molecular patterns (DAMPs), reactive oxygen species (ROS), and complement elements that in turn induce production of pro-inflammatory cytokines in resident inflammatory cells and fibroblasts. These cytokines recruit pro-inflammatory cells into the infarct zone from circulation and remote depots, for clearance of dead cells and matrix debris. In the following anti-inflammatory reparative phase anti-inflammatory cytokines are produced and cells involved with inflammation mitigation appear and promote wound healing and scar formation. Reproduced without changes under Creative Commons license from Ong et al. [10]

cytokines and chemokines which in turn recruit inflammatory cells into the infarct region [11, 12].

It is important to note that both the proximal obstruction and reperfusion injury not only impact the cardiomyocytes but also the coronary microvasculature. The role of the microvasculature is underscored by a meta-analysis showing that microvascular obstruction was a better predictor for adverse outcome than infarct size [13]. The absence of flow and thus shear stress during the occlusion and the subsequent reperfusion with small debris from the proximal obstruction cause damage to, and dysfunction of, the microvascular endothelium [5, 14]. Endothelial dysfunction is accompanied by altered Ca^{2+} homeostasis and endothelial contraction which increases the gaps between endothelial cells, thereby increasing endothelial permeability to macromolecules and promoting edema formation and/or intramyocardial hemorrhage [5, 14]. Furthermore, endothelial activation promotes expression of adhesion molecules, thereby recruiting platelets and inflammatory cells, which causes plugging of the coronary microvasculature and no-reflow, and further add to the local inflammatory environment [5, 14]. In addition, inflammatory cell infiltration of the viable border zone of the infarct region induces the death of cardiomyocytes there, thus extending ischemic injury beyond the original MI zone.

5.2.2 The Inflammatory Response

The inflammatory response is initially aimed at clearing cellular debris and wound healing and encompasses extracellular matrix (ECM) degradation. This ECM is not only a scaffold that anchors the cardiomyocytes and myocardial vasculature but it also serves as a large reservoir for bioactive molecules, including proteolytic enzymes and growth factors [15]. ECM degradation has been found even prior to influx of inflammatory cells; the release of endogenous proteolytic enzymes is proposed to be the trigger for the influx of neutrophils and macrophages, followed by a vigorous inflammatory response that amplifies the proteolytic response [15].

The anti-inflammatory, pro-repair response encompasses proliferation and differentiation of fibroblasts into myofibroblasts and subsequent ECM deposition by these myofibroblasts to form scar tissue. The final step is crosslinking of ECM that further stabilizes the tissue and is accompanied by de-activation of the reparative cells [11, 12]. Immediately after infarct, there is an increase in collagen V, which presumably plays a role in stabilizing the type I and III fibers. In a murine model, collagen V decreases again 4 days after MI, at a time that type III peaks. Finally, the stiff type I collagen is the major collagen isoform in scar tissue [16]. Aberrant timing and/or resolution of the inflammatory processes is now thought to be one of the main factors determining ventricular remodeling after MI as excessive inflammation and insufficient scar maturation are related to scar thinning and adverse left ventricular remodeling [4, 11]. Furthermore, several studies have shown correlations between 30-day mortality and circulating leukocyte counts and cytokines [1–3]. Macrophages play a key role in orchestrating the wound healing response as macrophage depletion results in impaired wound healing and excessive LV dilation

[12]. Yet, it is important to realize that the principal macrophage subtype shifts from pro-inflammatory M1 to anti-inflammatory, pro-reparative M2 macrophages in the process of infarct healing, and that this shift is critical for a proper healing response [12]. The inflammatory cell populations that are recruited to the infarct area and play a role in the pro-inflammatory and/or in the reparative, anti-inflammatory phase are described below.

5.2.2.1 Resident Inflammatory Cells

Mast Cells

Mast cells are resident cells in the perivascular areas of the heart. Following cardiomyocyte death inflammatory mediators induce mast cell to degranulate, thereby creating a signal for initiation of the inflammatory response [17, 18].

Macrophages

In the myocardium of mice, two subsets of resident macrophages have been identified in the heart, a chemokine receptor 2-negative (CCR2-) subtype and a CCR2+ subset [19]. These subsets are assumed to play a, as of yet not fully understood, central role in orchestrating the inflammatory response [20]. Functional analogs of these subsets have also been identified in human myocardium [21].

5.2.2.2 Infiltrating Inflammatory Cells

Polymorphonuclear Leukocytes

Following release of danger signals from infarcted myocardium, an influx of polymorphonuclear leukocytes (PMNs) starts within hours after AMI peaking between days 1 and 3 post-AMI, followed by a decline in PMN count after day 5 [22]. Neutrophils predominantly infiltrate the border zone, and their influx is augmented by reperfusion [23]. They contribute to clearance of dead cells and matrix debris and can amplify the immune response [24]. It has been suggested that neutrophils can polarize to different functional states. Neutrophils harvested at day 1 were reported to be pro-inflammatory (N1), in contrast, neutrophils harvested at days 5–7 post-AMI, exhibited an anti-inflammatory (N2) profile [22]. Apoptosis of neutrophils and their subsequent clearing from the infarcted area by M2 macrophages are a hallmark of inflammation resolution during the reparative phase [25]. Excessive PMN infiltration, insufficient or delayed removal of PMN may exacerbate myocardial injury via a prolonged pro-inflammatory response.

Monocytes and Macrophages

Monocytes are recruited to the infarcted area in 2 phases. The first phase, peaking at day 3–4 post-MI, is dominated by inflammatory Ly6Chi monocytes and M1 macrophages, and the second phase, peaking at day 7, by anti-inflammatory Ly6Clo monocytes and M2 macrophages [8, 26]. Within the myocardium the infiltrated monocytes differentiate into pro-inflammatory M1 macrophages which secrete cytokines, chemokines, and growth factors and influence the transition to the

reparative phase which becomes coordinated by M2 macrophages [8, 26]. This transition in phenotype is an important step in the reparative phase and could even be a result of a switch in phenotype of recruited Ly6Chi monocytes to Ly6Clo anti-inflammatory macrophages [11, 27], rather than an influx of Ly6Clo monocytes.

Dendritic Cells

During the inflammatory phase, dendritic cells (CD11c+) infiltrate the myocardium peaking at 7 days. Dendritic cells may play an important role for the transition from the inflammatory phase to the anti-inflammatory, reparative phase, by release of anti-inflammatory cytokines that coincide with reduced infiltration of pro-inflammatory Ly6Chi monocyte and M1 macrophages and enhanced infiltration of anti-inflammatory Ly6Clo monocyte and M2 macrophages [28, 29]. In addition, dendritic cells may recruit CD4+ helper T cells [30].

T and B Lymphocytes

CD8+ T lymphocytes and B lymphocytes infiltrate the infarcted area during the inflammatory phase [29]. In rats, circulating cytotoxic T (CD8) lymphocytes increase 1 week following AMI, and were shown to have cytotoxic effects on healthy cardiomyocytes in vitro and could therefore exacerbate acute ischemic injury in vivo [31]. In STEMI patients, however, a reduction in circulating T cells (predominantly CD8+) was observed 90 min after reperfusion [32]. B lymphocyte infiltration peaks at day 5 and increases the pro-inflammatory response by recruiting Ly6Chi monocytes [33]. During the reparative phase, regulatory T lymphocytes (Tregs) may play an anti-inflammatory (immunosuppressive) role in the setting of AMI (reviewed in [34, 35]). Tregs constitute a specific subset of T lymphocytes with immunosuppressive capacity and make up 5–10% of circulating CD4+ T lymphocytes under physiological conditions [36]. Interestingly, patients presenting with an AMI have been demonstrated to have decreased levels of circulating Tregs, compared with control patients [37, 38]. Furthermore, it has been shown that low levels of Tregs at baseline are associated with a higher risk for future AMI [39]. The reduction in Tregs following AMI has been attributed to a number of factors including: (1) accumulation of Tregs in MI zone [40]; (2) attenuated production of Tregs by thymus [41]; and (3) increased apoptosis of Tregs [41]. These clinical studies suggest a protective role of Tregs in MI. CD4+ helper T cells contribute to resolution of inflammation and wound healing [42]. Invariant natural killer lymphocytes were shown to be activated following AMI, and were shown to have anti-inflammatory effects [43, 44].

Regarding inflammation targeted imaging, keep the following in mind:

- inflammation evoked by AMI also occurs systemically,
- the size of the different inflammatory cell populations differs considerably, e.g., following the early appearance of neutrophils, monocytes and macrophages comprise the most abundant cells in the infarcted heart [7, 8, 29],

- inflammatory cell polarization is not black and white, e.g., M1 or M2 activated cell subsets represent two polar extremes [45], while in vivo data strongly suggest a much broader range of macrophage subsets [46], and
- inflammatory cell surface markers can differ between species, e.g., the human equivalent of the Ly6Chi subset in mice is CD16⁻, while the Ly6Clo subset in mice is CD16⁺ in humans [47].

Ventricular remodeling goes beyond the infarcted tissue. Cardiomyocytes in the border zone between the infarcted and non-infarcted tissue undergo electrical remodeling that together with the increased interstitial fibrosis creates an arrhythmogenic substrate [48, 49]. This electrical remodeling is promoted by neurohumoral activation as well as cytokines derived from macrophages. Intriguingly, cardiomyocytes can electrically couple to macrophages, which increases their membrane potential [50, 51] and may further contribute to arrhythmogenesis.

5.2.2.3 Cardiomyocytes and ECM

Ventricular remodeling after MI is further characterized by hypertrophy and increased calcium sensitivity of the cardiomyocytes in the remote, non-infarcted myocardium, which contributes to impaired relaxation of the cardiomyocytes [52]. Furthermore, there is some evidence of edema, i.e., an increase in extracellular volume, in the remote zone that correlates with infarct size [53]. Edema is accompanied by both structural (reduced capillary density) and functional alterations (microvascular dysfunction), that resulted in a perturbation in myocardial oxygen balance [54]. These changes were accompanied by alterations in gene-expression, suggestive of alterations in metabolism as well as activation of inflammatory pathways [55]. Activation of inflammatory pathways is further suggested by increased interstitial fibrosis although interstitial fibrosis is less pronounced than in the border zone [15]. Similar to the ECM in scar tissue, collagen V is the predominant isoform early after infarct, but collagen III is higher expressed than collagen I between 4 and 14 days after infarct. Finally, the stiff collagen I becomes the dominant collagen type also in the remote myocardium, but total collagen volume is much smaller (~1%) as compared to the scar region (~25%) [16].

5.2.3 Animal Models to Study Post-AMI Inflammation

To study the natural history of the inflammatory response after AMI and to test new intervention and imaging strategies, we have to resort to animal models, in which newly developed methods can be validated with postmortem histological examination of the tissue. Importantly, ischemia in patients ranges from low coronary flow to total flow cessation and differs in its duration; in most cases flow can be restored, however sometimes reperfusion is unsuccessful. When choosing an animal model, one should therefore carefully consider factors that impact infarct development and

subsequent wound healing. These factors not only concern the duration of ischemia and whether-or-not perfusion is restored, but also the presence of other risk factors and occurrence of short episodes of ischemia prior to the main ischemic event (pre-conditioning) are of importance. Hence, a variety of animal models can be used to address this spectrum of ischemia with or without reperfusion [56]. Here we focus on models with coronary artery occlusion with or without subsequent reperfusion, i.e., non-reperfused (MI) and reperfused (MI/R) myocardial infarction. We will first discuss some considerations when deciding about the most suitable model to answer a research question as well as the pros and cons of several commonly used animal models.

The first important aspect to consider regarding post-AMI inflammation is whether the model should include reperfusion (MI or MI/R). Myocardial reperfusion significantly reduces cardiomyocyte death and mortality after acute STEMI but leads to an increased risk of adverse remodeling and subsequent development of heart failure [57, 58]. Chronic occlusion (MI) models mimic patients with acute STEMI who cannot receive timely reperfusion [59, 60]. These patients present with robust myocardial inflammation in the infarct and border zone regions in the first 2 weeks after occlusion.

In addition to salvaging cardiomyocytes, reperfusion induces oxidative stress and a strong inflammatory response, the so-called reperfusion injury (MI/R), which also affects cell responses concerning repair and remodeling [61–63]. Reperfusion injury depends on the duration of occlusion until reperfusion and differs per species. In mice, durations of coronary occlusion exceeding 60–90 min are considered to cause irreversible damage [64–67]. In large animal models, such as dog and pig, restoration of perfusion within 15 min of occlusion prevents cardiomyocyte death, whereas 20- to 30-min. Occlusion is necessary to generate irreversible changes in cardiomyocytes [68–70]. Reperfusion should preferably occur within 45–60 min after initiation of the occlusion. Reperfusion after an occlusion of >6 h is considered unsuccessful in salvaging myocardium in large animal models [71]. A wavefront of cardiomyocyte death occurs starting at the subendocardium, progressing towards the subepicardium with increasing duration of the occlusion [70, 72] as observed in canine models of MI, where the subendocardium appears more susceptible to ischemic injury than the midmyocardium and subepicardium [73]. In mouse, rat, and sheep, on the other hand, the midmyocardium is typically affected while the subendocardium and the subepicardium are relatively spared [74]. The pig model of coronary occlusion-reperfusion comes closest to human STEMI in its temporal and spatial development, but other models are nevertheless useful to study fundamental mechanisms of MI [75]. The second aspect to consider is that induction of MI can be performed using an open chest (coronary artery ligation with or without reperfusion) or intravascular (balloon occlusion) approach. Although open chest models are sensitive to infections, which can subsequently affect the AMI-related inflammatory responses, in rodents, open chest models are the only option. However, the quality of the open chest surgery has a direct impact on study outcome [67]. Thirdly, MI can be induced in an acute setting, in anesthetized animals or in conscious, chronically instrumented, animals without the presence of anesthesia. Anesthesia

affects hemodynamics and flow, in turn affecting coronary vasodilation and vasoconstriction, and some anesthetic agents may induce pre-conditioning and thereby directly impact infarct size [76]. Fourthly, humans and animals differ considerably in their anatomy, including size, heart rate, metabolism, and collateral circulation. A reduction or cessation of flow in a subject with little or no collateral circulation often results in massive cell death in the area at risk, while in a subject with an extensive collateral circulation cessation of flow results in unpredictable and largely variable infarct size. Most animals have little or no collateral circulation, resulting in a severe, but uniform infarct. However, guinea pigs exhibit a very well-developed collateral circulation that prevents infarction upon occluding a single main coronary artery and are therefore not suitable for occlusion studies [77]. Dogs display high variability in collateral circulation, which majorly affects reproducibility of infarct size. Swine on the other hand have a coronary anatomy, similar to that of humans with minimal preexisting coronary collateral vessels [77]. In addition, their, typically right-dominant, coronary system and their cardiac conduction system are very similar to humans [78]. However, due to their minimal preexisting coronary collaterals, they tolerate acute coronary occlusion poorly, with large areas of infarcted tissue and a high mortality rate, necessitating a gradual coronary occlusion and/or a smaller area at risk in most pig models. In imaging studies, it is also important to keep in mind that the delivery of imaging probes to the infarct region may be affected by the degree of collateral formation. Finally, logistics and finances can also affect the choice of animal model. Access to patients' scanners for large animals or to a small animal imaging equipment may play a role. Larger animal models are expensive to obtain and labor-intensive regarding care and handling and require larger amounts of probe. They, however, have the main advantage that they are eligible for closed-chest, catheter-based techniques. Illustration of the pathophysiological effects of MI induction in animal models is provided in Fig. 5.2.

5.2.3.1 Small Animal Models

Open Chest

Coronary Artery Ligation

Surgical ligation of the left coronary artery (LCA) or the left anterior descending artery (LAD) in mice and rats, classically including ventilation and a full thoracotomy [79], often results in extensive tissue damage and high mortality. Gao and colleagues [80] developed a much faster method (with a similar infarct size and post-MI cardiac function, without intubation, requiring just a small incision, resulting in reduced mortality rates and reduced inflammation indicated by reduced plasma concentrations of TNF- α and myeloperoxidase levels). Reperfusion can be obtained by removal of the ligature [80].

Topical Application of FeCl₃

The topical application of FeCl₃ on the LAD by means of a tissue strip produces several physiological and biochemical changes similar to arterial thrombus

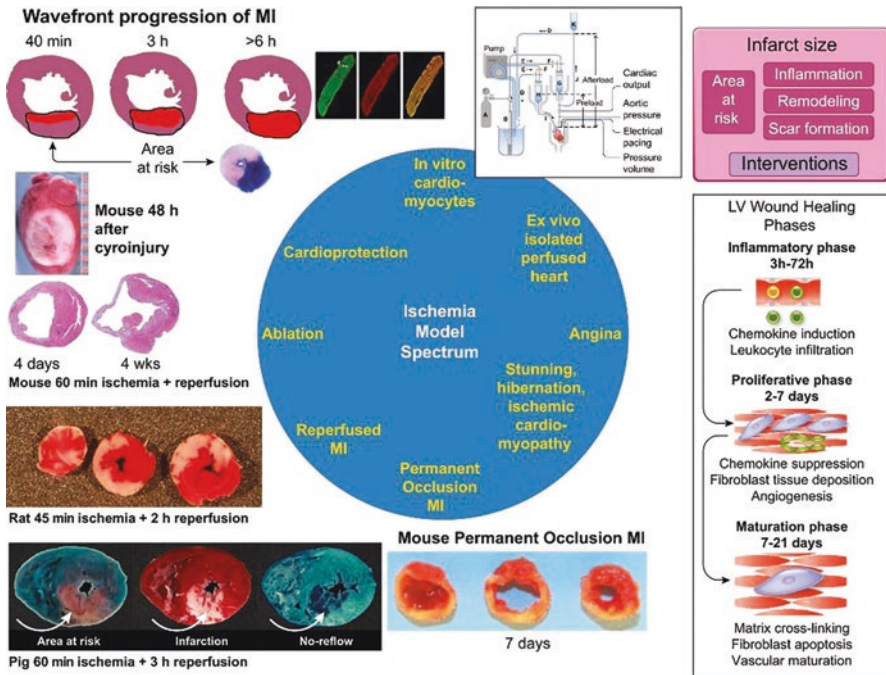


Fig. 5.2 Histological and schematic representation of animal models for myocardial infarction. Reproduced without changes under Creative Commons license from Lindsey et al. [56]

formation. This method of MI induction, performed in rats [81], is very simple to execute and does not require specialized surgical techniques or equipment.

Closed Chest

Isoproterenol Injection

Chemically induced AMI by isoproterenol [82] through β -adrenergic receptor stimulation has a low mortality rate, is simple compared to surgical techniques, and has no risk of postsurgical infections. However, the isoproterenol-induced inflammatory response might differ from the AMI-induced inflammatory response in humans.

5.2.3.2 Large Animal Models

Open Chest

Coronary Artery Ligation

Open chest ligation of the LAD or the left circumflex (LCx) [83] has the advantage of precise control of site of occlusion and direct visual assessment of contractile function of heart. The severity of the MI depends on occlusion location, i.e., proximal, midpoint, or distal, but is reproducible and consistent.

Gradual Constriction

Ameroid Constrictor

These constrictors are constructed of the hygroscopic material casein encased within a steel sleeve [84]. When the device is implanted around an artery, the constrictor absorbs water and swells, compressing the artery and producing total coronary occlusion over a period of 14–30 or more days [85], which can be prolonged by coating the ameroid with petrolatum, which slows the absorption of water by the constructor [86]. The induced external arterial compression also causes mechanical trauma, resulting in endothelial damage, platelet aggregation, and thrombus formation, as well as potentially inciting a foreign body reaction with local scar formation. This technique is most often used on the LCx. The LCx myocardial region in pigs has a greater innate collateral circulation than regions of the left ventricle supplied by the LAD or right coronary arteries [87]. Despite these collaterals and the gradual ameroid closure, there still is significant mortality, averaging nearly 30% in those studies reporting mortality rates [88]. Other limitations of this model include the large variation in the infarct size, likely caused by the non-uniform rate of ameroid closure [89], which depends on the size, shape, and stiffness of material encasing the ameroid as well as the temperature of the surrounding fluid. Because of the metal outer ring, the constructor will always be visible on X-rays of the chest.

Hydraulic Occluder

An adjustable hydraulic occluder [90] can be placed around an epicardial coronary artery (LAD or LCx) either alone or proximal or distal to a coronary flow probe. The diameter of the coronary artery can be gradually reduced via controlled percutaneous injections of fluid into a subcutaneous injection port of device, attached to a balloon. Furthermore, the occlusion can easily be reversed, allowing for the study of reperfusion injury (MI/R). An additional advantage is that the animals are allowed to recover from surgery for several days before inflating the hydraulic occluder, such that the stress response associated with surgery has had time to abate.

Topical Application of FeCl₃

The topical application of FeCl₃ on the LAD by means of a tissue strip, as described above, has also been used in pigs, resulting in thromboembolic coronary lesions [91].

Closed Chest

Balloon Inflation

This is a catheter-based technique used in pigs and dogs that provides reproducible LAD occlusion at a selected location and for a selected duration with subsequent MI including or excluding reperfusion (MI/R), through coronary catheterization followed by balloon inflation and possible deflation [92]. This method requires minimal surgical techniques and time and offers precise control over the location and duration of occlusion.

Embolization

Embolization to induce AMI in dogs or pigs can be realized in several ways. A self-embolus or blood clot can be injected into the middle segment of the LAD coronary artery via means of guiding catheter and coronary angiography [93]. A helical shaped, thrombogenic, platinum or stainless-steel coil can be precisely deployed in the LAD, LCx, or RCA, resulting in reproducible AMI [94]. Alternatively, one can inject a foreign body object under catheter guidance. These include microsphere(s) [95], a ball [96], a foam sponge [97], and gel microbeads [98]. Reperfusion is only possible in the case where a 2 mm diameter ball was used by retraction of the ball via a thin filament attached to it [96].

Endothelial Electrical Injury

In this method, a Teflon-coated stainless-steel electrode is implanted into the LCx with the uninsulated portion touching the endothelial surface. An anode current of 150 mA is applied to the endothelial surface to induce endothelial damage and subsequent thrombosis [99].

In experimental models of MI and MI/R, knowledge on the timing of the cellular and molecular events is critical for optimal study design. For example, rodents, opposed to large mammals, exhibit an accelerated time course of infiltration with inflammatory and reparative cells [64]. Detailed knowledge on the inflammatory responses of the different models is currently incomplete. Small animal models that are genetically modifiable are often used to study the cellular and molecular events, but large animal models are considered closer to the clinical situation for translational studies but have the disadvantage of incomplete characterization of inflammatory cell types. A general concern with respect to animal models is that most studies characterizing responses to myocardial ischemia/reperfusion have been performed in healthy, young animals. Comorbidities including aging, diabetes, obesity, atherosclerosis, and metabolic dysfunction are known to affect the inflammatory responses. These comorbidities are clinically very relevant and should be incorporated prior to translating experimental findings to the clinic.

5.3 The Role of Molecular Imaging

To better understand and monitor biological processes involved in cardiovascular disease, imaging has already played an important role for many years. Techniques like ultrasound imaging (USI), computed tomography (CT), magnetic resonance imaging (MRI), single-photon emission computed tomography (SPECT), and positron emission tomography (PET) have made it possible to assess anatomical, functional, and physiological features of the heart associated with MI. In recent years, a need for more detailed assessment of the biological processes involved in MI has emerged. Especially the ability to characterize and measure the post-MI inflammatory response at the molecular and cellular level is now considered a prerequisite for the design of inflammation modulating treatment strategies intended to promote infarcted tissue repair and prevent derailment of the inflammatory response.

However, since post-MI inflammation is a dynamic process, with involvement of numerous inflammatory cell types, imaging is challenging.

Recent progress in imaging technology and the development of specific imaging agents has vastly improved the ability to non-invasively visualize, characterize, and quantify which molecular and cellular processes and consequently specific aspects of the post-MI inflammatory reaction are involved. Especially techniques such as MRI, PET, and SPECT offer various new possibilities in this regard. Below a general description of these techniques is provided followed by specific discussions of imaging strategies for assessment of post-MI inflammation in Sect. 5.5.

5.3.1 Cardiac MRI

Cardiac MRI (CMR) is a well-established technique in the evaluation of myocardial disease. MRI is considered the gold standard for assessment of left ventricular functional parameters such as ejection fraction and systolic volumes [100].

Magnetic resonance images are created by the signals released from hydrogen ions (protons) in the human body. When placed in a large magnetic field, the protons also act like a magnet and align with the external magnetic field. Via the scanner a rapidly repeating sequence of radiofrequency pulses is generated that causes “excitation” and “resonance” of the protons creating a magnetic resonance signal that can be measured and spatially encoded to generate 3D images with high spatial resolution. Specific tissues characteristics can be rendered by measuring longitudinal (T1) and transverse (T2) relaxation times of the excited protons and form the basis of the excellent soft tissue contrast capabilities of MRI.

These characteristics make MRI specifically suitable to visualize myocardial injury using a variety of imaging techniques also in combination with systemically administered contrast agents, such as late gadolinium enhancement (LGE), T1, T2, T2*-weighted imaging, and parametric mapping [101, 102]. MRI can provide anatomical information regarding infarct size, myocardial edema, focal or diffuse myocardial necrosis and fibrosis, intramyocardial hemorrhage microvascular injury, and myocardial contractility [102].

After coronary occlusion, myocardial ischemia results in the development of edema. A linear relation between T2 relaxation time and tissue water content has been demonstrated in the setting of myocardial infarction in animal models [103]. Using T2-weighted imaging, the increased free water content of edematous myocardium considerably prolongs T2 relaxation time, as the relatively large space in between free water molecules together with the rapid movement of these small molecules results in less spin–spin interactions.

Late gadolinium enhancement (LGE) imaging, with acquisition of T1-weighted images after intravenous administration of a gadolinium-based contrast agent, is an essential technique in CMR. The wash-out of gadolinium is delayed in areas with increased extracellular/interstitial volume, such as areas of necrosis and/or fibrosis. In acute myocardial infarction, native T1 mapping images show prolonged T1 values and are associated with inflammation and edema following acute ischemic

damage [104]. Quantification of T1-values in remote myocardium has also been found to be relevant for risk stratification in patients with ST-elevation myocardial infarction [105]. High native T1 values in remote myocardium predict adverse LV remodeling and future cardiac events, which suggest that global LV inflammation is an important driver of LV remodeling. These types of imaging parameters, however, are a measure of physiological tissue alterations and do not represent actual presence of inflammatory cells. As further described in later sections, more specific CMR techniques used for visualization of the presence of inflammatory cells comprise tagging of inflammatory cells with contrast agents and hyperpolarized MRI. Alternatively, MRI can be used to interrogate altered physiological conditions, e.g., oxygen levels, extracellular matrix (ECM) degradation, and fibrosis, using smart or activatable probes [106]. These probes only accumulate or produce signals at sites where the predefined conditions occur (further described in later sections).

5.3.2 Single-Photon Emission Computed Tomography

Single-photon emission computed tomography has become a commonly used technique to assess myocardial viability [108]. SPECT imaging uses a gamma camera that rotates around the subject, sampling the radiation emitted from an injected radiotracer. The acquired data is processed into a number of images which can then be reconstructed to produce a 3D image showing tracer distribution within the body.

Imaging of myocardial viability with SPECT is based on uptake by cardiomyocytes of specific radioactive tracers such as thallium-201 (^{201}Tl) or technetium-99 m ($^{99\text{m}}\text{Tc}$) sestamibi and [$^{99\text{m}}\text{Tc}$]Tc tetrofosmin, also designated as myocardial perfusion test.

More recently, newly developed and repurposed tracers are being evaluated for their use in imaging specific components of the inflammatory process such as molecules (over-)expressed by inflammatory cells [108–110] or altered conditions in the extracellular space [107, 111, 112]. SPECT radionuclides offer specific advantages because of their longer half-life making them more suitable for distribution and for anti-body-based probes because of the long circulation times of antibodies [111]. In addition, due to the different energies of the different radionuclides, multispectral imaging is possible (Fig. 5.3). Moreover, the higher resolution capabilities in multipinhole preclinical imaging also make availability of SPECT tracers desirable.

5.3.3 Positron Emission Tomography

Positron Emission Tomography (PET) has a strong position in nuclear medicine and is now recommended in various cardiovascular diseases, such as prosthetic valve endocarditis [113]. Just like SPECT, PET uses radiolabeled tracers and cameras to detect the emitted radiation. Different from SPECT is that the cameras are positioned in a stationary ring around the subject and PET tracers traditionally consist

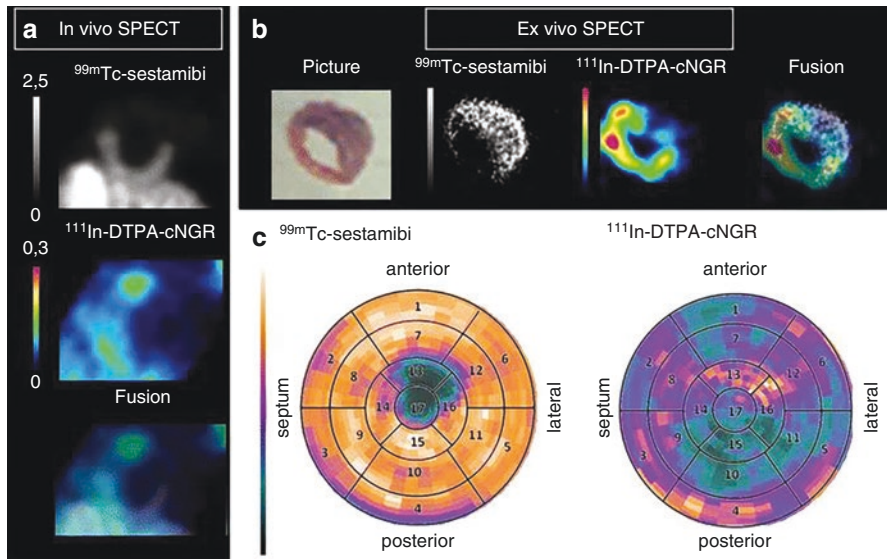


Fig. 5.3 Molecular imaging of angiogenesis after myocardial infarction by [^{111}In]In-DTPA-cNGR and [^{99m}Tc]Tc-sestamibi dual-isotope myocardial SPECT. (a) In vivo images of ^{111}In -DTPA-cNGR uptake, mainly in areas of ^{99m}Tc -sestamibi absence. Numerical values on the scale bars indicate the SUVmax and SUVmin. (b) Ex vivo images of ^{111}In -DTPA-cNGR uptake, mainly in areas of ^{99m}Tc -sestamibi absence. (c) Polar perfusion maps combined with the 17 segment model show that enhanced ^{111}In -DTPA-cNGR uptake (orange in areas 13, 16, and 17) occurred mainly in areas with low ^{99m}Tc -sestamibi uptake (green in areas 13, 16, and 17), signifying the anterolateral region in the infarcted myocardium. Reproduced without changes under Creative Commons license from Hendriks et al. [107]

of naturally occurring biologically active molecules that are labeled with positron-emitting radioisotopes (e.g. ^{11}C , ^{13}N , ^{15}O , ^{18}F), such as glucose ([^{18}F]FDG), [^{11}C]-methionine and [^{82}Rb]rubidium chloride. Alternatively, positron-emitting radionuclides can be coupled to or incorporated into molecules that can bind to receptors or other extracellular molecules.

After positron decay and annihilation, a pair of gamma rays are separated at an angle of 180 deg and captured on collinearly aligned detectors. Commercially available PET tracers have been used for imaging infection and inflammation. Fluorodeoxyglucose labeled with fluorine-18 ([^{18}F]FDG) is the best characterized and most widely applied tracer for targeting inflammatory cells. [^{18}F]FDG is a radiolabeled analog of glucose and is taken up by cells via cell membrane glucose transporters and subsequently incorporated into the first step of the normal glycolytic pathway. FDG accumulation in tissue is proportional to the amount of glucose utilization. [^{18}F]FDG imaging takes advantage of the elevated metabolic activity in activated leukocytes, with increased glucose uptake. Another metabolic target is the amino acid metabolism of leukocytes using [^{11}C]-methionine.

Targeting increased metabolism by FDG results in non-specific, broader range of cell types, to be imaged, thus increasing signal and detection. However, the

confounding uptake of [^{18}F]FDG by viable myocytes in the infarct region may also hamper the imaging of inflammatory cells [114]. Because of this lack of specificity of metabolic tracers, new PET radiopharmaceuticals for molecular imaging are pursued that target activated inflammatory cells or other specific aspects of inflammatory processes.

A widely studied alternative option for inflammatory cell imaging in CVD and other diseases concerns tracers targeting somatostatin receptors which are overexpressed by activated leukocytes [115]. These receptors can be targeted with radio-labeled somatostatin analogs such as [^{68}Ga]Ga-DOTA-TATE [116–118]. Also, for imaging of inflammation in cardiovascular disease there is an increasing interest in the use of SSTR-targeting tracers. In various studies, targeted imaging of somatostatin receptors seemed to be superior to [^{18}F]FDG for assessment of the inflammatory response in sarcoidosis and atherosclerotic plaque [116, 117].

Leukocyte infiltration following MI is mediated via increased expression of adhesion molecules on activated endothelium and recruited leukocytes. Therefore, the development and evaluation of tracers for imaging adhesion molecule expression in myocardium are also actively pursued. The CXCR4 receptor has recently drawn attention as a molecular target for imaging to identify activated inflammatory cells in myocardium post-MI. The CXCR4 receptor is expressed by leukocytes that infiltrate inflamed tissues and can be imaged using [^{68}Ga]Ga-pentixafor, a PET ligand for CXCR4.

An alternative approach to imaging myocardial inflammation is based on ex vivo cell labeling techniques, such as leukocytes scintigraphy for imaging of infections. Disadvantages are necessary blood handling, non-specific uptake and short physical half-life when using ^{18}F , making it unsuitable for late time imaging acquisition.

Although it is the most sensitive nuclear imaging technique, PET does not offer anatomical information. Fusion of imaging modalities, providing incremental diagnostic information on anatomical and physiological information is required.

5.4 Imaging Targets

Following AMI an inflammatory response is triggered that is aimed at removal of cellular debris, recruitment of reparative cells, and formation of scar tissue to stabilize the damaged muscle. However, increasing evidence is found that an excessive, uncontrolled inflammatory response may arise which subsequently contributes to additional myocardial damage, adverse LV remodeling, and ventricular arrhythmia. Given the central role of the inflammatory reaction in patient outcome post-AMI a need to elucidate and monitor the processes involved in the inflammatory reaction has arisen. In recent years this has boosted studies in which the use of molecular imaging techniques that can visualize, characterize, and quantify cellular and molecular processes underlying the inflammatory reaction is evaluated. The hope is that these techniques will aid in further elucidating and provide means to monitor the post-MI inflammatory response in view of myocardial repair, and to identify

patients at risk for late-phase complications and to monitor response to anti-inflammatory treatment in individual patients.

Expression of specific markers and/or altered biochemical profiles in the activated/recruited inflammatory cells and ECM can be used as imaging targets using specific probes. Alternatively, cells can be labeled with a variety of imaging compounds by which their distribution in the body can be followed.

5.4.1 Metabolic Activity

One of the most widely used techniques for imaging of inflammation is based on increased glucose consumption of activated leucocytes. Similar to glycolytic cancer cells, elevated glucose consumption in leukocytes can be imaged by PET using the positron-emitting analog of glucose, [^{18}F]FDG. This technique has been used in numerous studies in a variety of diseases including CVD. For endocarditis [^{18}F]FDG-PET is even the recommended imaging technique for suspected endocarditis within ESC guidelines. In various preclinical and clinical studies, uptake of [^{18}F]FDG within the infarct area was shown to be associated with local and/or systemic increase in leukocyte counts. Moreover, direct correlations between [^{18}F]FDG uptake and functional outcome in patients with AMI have been reported.

Based on observations that the cellular infiltrate in [^{18}F]FDG avid areas in inflamed tissues is dominated by macrophages/monocytes [119–121] and pro-inflammatory macrophages were found to exhibit preferential uptake of [^{18}F]FDG compared to other inflammatory cells, it is generally assumed that [^{18}F]FDG uptake in inflammatory lesions is mainly due to the presence of macrophages.

While broadly used for imaging of inflammation, [^{18}F]FDG-PET also suffers from some major limitations for the assessment of post-MI inflammation. Realistically, uptake of FDG is not specific. Any cell with an increased glucose demand will avidly incorporate the glucose analog. This includes other types of leukocytes, endothelial cells, and in case of ischemic heart disease also cardiomyocytes. In fact, myocardial uptake of [^{18}F]FDG is considered to reflect cardiomyocyte viability in ischemic myocardium [121–123]. Increased [^{18}F]FDG uptake of viable myocytes in the infarct region may therefore hamper imaging of inflammatory cells [114]. Results obtained from clinical as well as preclinical studies are not consistent regarding distribution and extent of FDG uptake in the myocardium. Reported hotspots of [^{18}F]FDG uptake may be found in the acute infarct area [124], the border zone [125], remote myocardial tissue [120], and remote peripheral tissue [126]. There is also no consistent relation between high focal uptake of the tracer and long-term cardiac function outcome, both negative correlations [2, 80, 122, 127, 128] as well as positive correlations have been reported [129].

Next to glucose metabolism, also amino acid metabolism has been proposed as a target for imaging inflammatory processes post-MI. In a study using the L-amino acid transporter-targeting PET tracer (L-[methyl- ^{11}C]-methionine) in patients within 2 weeks after MI in the infarcted area elevated uptake of this tracer in the

infarcted area was observed [130]. In subsequent studies indications were found that accumulated inflammatory cells were mainly the cells responsible for the elevated uptake [121, 131, 132]. As with [^{18}F]FDG-PET, [^{11}C]-methionine-PET is not a cell-type-specific marker, however, the tracer has a major advantage compared to [^{18}F]FDG in that there is no detectable normal physiological uptake in cardiomyocytes.

Continued studies have provided indications that [^{11}C]-methionine-PET may be a valuable tool to monitor response to anti-inflammatory treatment. Thackery et al. demonstrated that a decline in myocardial macrophage content, following blockage of integrins, coincided with lower [^{11}C]-methionine uptake [132], which was associated with larger infarct size in treated animals compared to sham-treated animals. This observation suggested that blocking of leucocyte trafficking via blockage of integrin interactions dampened the reparative function of the inflammatory response. In another setting, Taki et al. also reported on a relation between uptake of [^{11}C]-methionine over time in relation to response to treatment [133]. In this study, post-conditioning treatment [^{11}C]-methionine uptake had a negative correlation to functional outcome at a later stage in induced MI in rats. A disadvantage of this tracer is the short half-life of the Carbon-11. This limits the use of this imaging approach to locations that have an in-house radiochemistry facility and a cyclotron.

A potential alternative metabolic marker associated with activation of inflammatory macrophages is choline metabolism [134]. Choline is a precursor of phosphatidylcholine, a major component of cellular membranes and internalized in cells via choline transporters. Active and proliferating cells have high membrane turnover rates. Radiolabeled choline can therefore be used for imaging of increased membrane metabolism. Choline metabolism-based imaging has been used in tumor cell imaging and more recently for imaging of inflammatory cell activity in atherosclerotic plaques [134, 135]. Like methionine tracers, choline tracers also do not have detectable uptake in cardiomyocytes.

An emerging metabolic imaging technology that may be used to monitor the inflammatory process post-MI is hyperpolarized magnetic resonance spectroscopic imaging [136]. Hyperpolarized MR is based on dynamic nuclear polarization of ^{13}C -labeled compounds and used for spectroscopic analysis of metabolic conversions during glycolysis and tricarboxylic acid cycle. Hyperpolarization has increased the sensitivity of magnetic spectroscopic imaging (MRSI) by >10.000 fold [137]. The most prominently used substrate is [$1\text{-}^{13}\text{C}$]pyruvate [138] and has recently been introduced in clinical trials where its value as a diagnostic and prognostic tumor marker is being evaluated. Also in for cardiovascular applications [$1\text{-}^{13}\text{C}$]pyruvate, MRSI is regarded as a promising imaging technique [139]. In a recent study Lewis et al. [136] evaluated whether [$1\text{-}^{13}\text{C}$]pyruvate MRSI can be used to assess the local cardiac inflammatory response after MI. Using MI models in rats and pigs they were able to show that high [$1\text{-}^{13}\text{C}$]pyruvate conversion into [$1\text{-}^{13}\text{C}$]lactate at days 3 and 7 post-MI (Fig. 5.4) reflects the monocyte/macrophage inflammatory response. A major limitation of this technology is that very specialized expertise and equipment are needed to facilitate hyperpolarized ^{13}C -MRSI. Also, further validation is needed

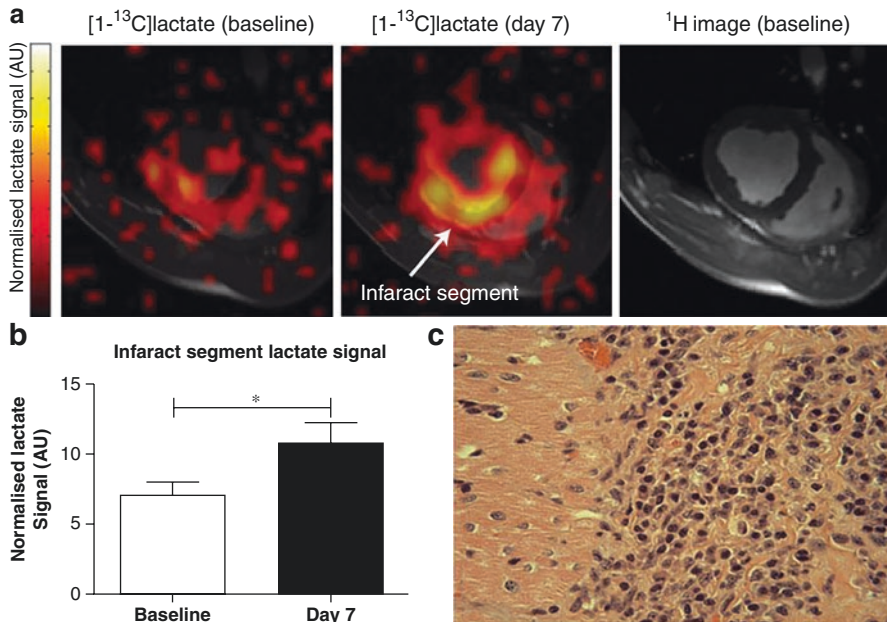


Fig. 5.4 Hyperpolarized [$1-^{13}\text{C}$]pyruvate MRSI of porcine heart. Measured [$1-^{13}\text{C}$]lactate signatures at baseline and 7 days post-MI are shown (**a** and **b**). Elevated [$1-^{13}\text{C}$]lactate signal reflects the monocyte/macrophage inflammatory response as verified by histological examination (**c**). Reproduced without changes under Creative Commons license from Lewis et al. [136]

to determine whether the technique has added value in comparison with other existing techniques.

5.4.2 Labeled Cells

An approach that is used with MRI, SPECT as well as PET is labeling of cells via endocytic pathways or passive diffusion of the compound over the cell membrane. Reinfusion of ex vivo labeled cells is a widely used technique for diagnostic imaging of infection-induced inflammation. This approach, known as leucocyte scintigraphy, is now also a clinically accepted method to image infection-related endocarditis [140]. In this approach, white blood cells are labeled ex vivo with radiolabeled compounds. Classically, compounds like $^{99\text{m}}\text{Tc}$ -HMPAO and ^{111}In -oxine $^{99\text{m}}\text{Tc}$ have been used to label leucocytes [141–143]. To enable more advanced image analyses, tracers suitable for PET imaging have been developed and evaluated. Initially, [^{18}F]FDG was the compound of choice for cell labeling and PET imaging [144]. However, due to its limited labeling efficiency and/or short half-life alternative options are now being explored including the use of compounds like [^{89}Zr]Zr-oxinate4 and [^{89}Zr]Zr-desferrioxamine-NCS [145, 146]. Specific utility of

these techniques in assessment of post-MI inflammation has not been established yet, but its potential value for assessing infarcted, obstructed tissue has been suggested. Based on studies using probes suitable for magnetic resonance imaging such as iron oxide particles or nanoparticles containing fluorine for in vivo tracking of stem cells, this approach may be further developed [147, 148]. However, ex vivo blood handling for radiopharmaceutical preparation requires additional safety precautions, and a longer duration of the procedure, limiting its use.

Alternatively, cells can also be labeled in vivo, using imaging compounds that can be taken up by resident and/or circulating leucocytes. Especially the behavior of cells with a propensity to take up foreign material such as dendritic cells, monocytes, and macrophages can be monitored using this approach. Various groups have used iron oxide nanoparticles to follow migratory behavior of phagocytic cells by MRI (Table 5.1). Due to the local concentration of iron oxide particles, proton relaxation is affected resulting in local signal loss in MR images. This approach is being tested in clinical settings [149–151]. However, interpretation of the images may be complicated because it is not evident whether signal loss in standard MR images is caused by these labeled cells or by other physiological phenomena [152]. To overcome this limitation the use of nanoparticles containing fluorine has shown promising results [152]. Fluorine is normally not present in the body, and therefore produces a highly specific signal in ^{19}F MRI. In addition, initial experiences with ^{19}F -labeled cells also proved the superior quantitative aspects of this technique compared to iron oxide labeled cells [153]. A major limitation of ^{19}F MRI is the limited sensitivity. However, technological improvements in both hardware and software are increasing the detection limit [153]. To overcome specificity as well as sensitivity issues as encountered with MRI of labeled cells radiolabeled nanoparticles are also being investigated for imaging of labeled cells. This includes particles

Table 5.1 Inflammation imaging in MI using cell labeling through endocytic uptake of imaging compounds

Imaging compound	Preclinical/clinical	Imaging technique	Characteristics
Iron oxide NP USPIO SPIO MPIO	Preclinical [147, 158, 159] Clinical [149–151, 160] Preclinical [160] Preclinical [161]	MRI: T2/T2* signal loss	High sensitivity, limited specificity. No linear relationship between concentration and signal in vivo. FDA-approved compounds May be with multiparametric MRI
^{19}F -NP Multicore NP PFC-nanoemulsion PFOB-NE	Preclinical [162] Preclinical: [152, 163] Preclinical [164]	MRI: ^{19}F chemical shift imaging	High specificity; no physiological background signals. High potential for quantification; linear relationship between concentration and signal. Potential for multispectral imaging; using compounds with different resonance frequencies

specifically for PET imaging as well as multimodal particles, suitable for visualization with both MRI and PET [148, 154, 155]. However, most of these studies concern inflammation imaging of AS or for monitoring in vivo behavior of cell transplants for immune therapy or stem cell therapy. A challenge in this setting is to match the signaling radionuclide to the purpose. Long circulating particles need radionuclides with a long half-life such as ^{89}Zr and ^{64}Cu , while shorter circulating nanoparticles can be labeled with ^{18}F [155]. The main challenge here is to get an optimal balance between long lasting signaling capability, efficient uptake of the nanoparticle, and limited radiation exposure. In a recently published study by Nahrendorf et al., a new class of radiolabeled nanoparticle was described that seem to fit most of the above-mentioned requirements [154]. The so-called macrophage sensor, Macrin, is a 20-nm dextran-based spherical nanoparticle labeled with ^{64}Cu was reported to have excellent performance in detecting macrophage accumulation in the hearts of mice, rabbit, and pigs with induced acute myocardial infarction. Blood half-life of ^{64}Cu -Macrin was 45 min and using mouse biodistribution data calculated human dose estimates for various organs and concluded that ^{64}Cu -Macrin could be a suitable nanotracer to survey spatiotemporal macrophage dynamics during various physiological and pathological conditions including post-MI inflammation.

The use of nanoparticles in CVD has received renewed interest especially in theragnostic settings. Of note, in recent studies various relations between nanoparticle uptake and macrophage polarization have been found. This includes changes in macrophage polarization following uptake of nanoparticles [156, 157].

5.4.3 Membrane Receptors

Many studies focused on imaging of the inflammatory response post-MI concern the use of imaging agents that target specific membrane receptors expressed by activated cells, and especially monocytic and granulocytic leucocytes which have been identified as major components and orchestrators of the inflammatory response post-MI. Generally, these strategies are aimed at monitoring the involvement of a specific cell type in the inflammatory process. A wide variety of receptors are being considered in this regard. A selection of promising candidates is described below and listed in Table 5.2, thereby mainly focusing on nuclear imaging tracers.

Of note; while generally, these receptors exhibit over-expression by a specific (functional) cell types this expression is often not exclusive for that cell type. Various other cell types may also express the targeted receptor, which may limit the specificity of the tracer.

5.4.4 Somatostatin Receptors

A clinically attractive imaging target is the family of somatostatin receptors (SSTRs) due to the availability of commercially available (FDA-approved) tracers. The

Table 5.2 Receptor-targeted imaging of inflammatory cells post-MI

Imaging target	Preclinical/ clinical	Imaging technique	Characteristics
SSTR2 [⁶⁸ Ga] Ga-DOTA-TATE [⁶⁸ Ga] Ga-DOTA-TOC	Preclinical [168]; Clinical [116, 118] Clinical [118]	PET: Radiolabeled substrate	Considered a marker for pro-inflammatory macrophages, however not exclusive. Variable affinity and specificity of different tracers for different SSTR subtypes. SPECT tracers also exist, but no known use in post-MI inflammation.
TSPO [¹¹ C]C-PK11195 [¹⁸ F]F-GE180 [¹⁸ F]F-LW223 [¹⁸ F]FDPA	Clinical [171] Preclinical [171, 184] Clinical [171] Preclinical [185] Preclinical [186]	PET: Radiolabeled substrate	Expression strongly associated with activated microglia, next to activated macrophages. Allelic variants of TSPO may influence tracer sensitivity. TSPO may be used as a marker to reveal connections between MI and cognitive impairment via concomitant brain inflammation.
CXCR4 [⁶⁸ Ga]Ga-Pentixafor [⁶⁸ Ga] Ga-mCXCL12 [⁶⁴ Cu] CuCB-bicyclam [¹²⁵ I]I-pentixather	Preclinical [187, 188] Clinical [188–192] Preclinical [193, 194]	PET: Radiolabeled substrate SPECT: Radiolabeled substrate	Next to expression by activated leucocytes, also known to be over-expressed in cardiomyocytes, endothelial cells, and myocardial fibroblasts under ischemic conditions. Species-dependent binding affinity for certain ligand scaffolds.
CCR2 [⁶⁸ Ga] Ga-DOTA-ECL1i	Preclinical [195]	PET: Radiolabeled substrate	Implicated as pro-inflammatory marker. Elevated expression associated with negative outcome regarding remodeling and myocardial function.
GLP-1R [¹⁸ F] F-FBEM-Cys40- exendin-4 [¹⁸ F] F-AIF-NOTAMAL- Cys40-Exendin-4 [⁶⁸ Ga] Ga -NODAGA- exendin-4	Preclinical: [196] Preclinical: [197] Preclinical: [198]	PET: Radiolabeled substrate	Potentially involved in protection of myocardium during post-MI inflammatory reaction. Potentially involved in the transition of macrophages from a pro- inflammatory state to an anti- inflammatory/repairative state.

somatostatin receptor family is a member of the G-protein-coupled receptor superfamily with five known somatostatin receptor subtypes (SSTR1–SSTR5). Somatostatin receptors are over-expressed by activated leucocytes [115], with differential expression of the subtypes between various subpopulations. The most widely studied receptor subtype is SSTR2, which has been designated as a marker for pro-inflammatory macrophages [165]. The natural ligand for the somatostatin

receptor is a peptide called somatostatin which functions as a paracrine regulator of signal transduction and hormone secretion. Due to SSTR2 over-expression on neuroendocrine tumors and some other malignancies, SSTR has become an established target for imaging and targeted therapy in oncology. Consequently, there is a variety of radiotracers consisting of radiolabeled somatostatin analogs commercially available [166, 167].

SSTR-targeting, nuclear imaging is currently being explored for use in a variety of inflammatory diseases [115] with tracers suitable for either PET imaging OR SPECT imaging. Also, some feasibility studies have been performed for inflammation imaging post-MI using PET tracers. In patients that suffered from MI, it was shown that uptake of SSTR-targeting tracers, [^{68}Ga]Ga-DOTA-TOC and [^{68}Ga]Ga-DOTA-TATE, was elevated in inflamed myocardium in areas with structural damage [116, 118]. In contrast, in a mouse model of myocardial infarction, no direct link between tracer uptake and myocardial inflammation was found. Myocardial uptake of the [^{68}Ga]Ga-DOTA-TATE tracer was overall very low, while blood pool levels were high [168]. A major limitation of the somatostatin-based tracers for inflammation imaging seems to be their short serum half-life [117, 168]. Due to the fast clearance from circulation, limited accumulation in targeted tissue can occur. Another concern is that SSTR2 expression is not exclusive to macrophages, (over-)expression also occurs on dendritic cells, certain types of tumor cells, and various cells throughout the central nervous system and peripheral tissue.

5.4.5 Mannose Receptor

Another potentially relevant target for macrophage-specific imaging in post-MI inflammation is the mannose receptor (MMR; CD206) [140, 169–171]. In contrast to the somatostatin receptor, the mannose receptor is associated with macrophages that exhibit the so-called M2 phenotype that is associated with anti-inflammatory processes as occur during the reparative post-MI [29, 172–174]. In several studies it was shown that recruitment and presence of CD206-positive macrophages correlated with improved myocardial status following anti-inflammatory treatment [172, 175, 176]. This marker therefore shows great promise for inflammation imaging in myocardial infarction, however, at the time of writing of this manuscript no such application has been reported yet.

5.4.6 Folate Receptor

The folate receptor (FR) is a cell surface glycosylphosphatidylinositol-anchored glycoprotein that is highly expressed on a variety of cells, including cancer cells, and activated macrophages. FR-targeting is therefore considered to be a valuable strategy for diagnostic and therapeutic purposes of cancers [177] and macrophage-mediated inflammatory diseases as atherosclerosis [178], myocarditis [179], and arthritis [180]. Like the mannose receptor, folate receptor expression by

macrophages is also associated with the M2-like phenotype [181]. However, in contrast to the positive association of the accumulation of MMR-positive macrophages with improved outcome in MI, accumulation of folate receptor-positive M2 macrophages has been implicated as promoting factor of the vulnerable stage of AS plaque. To our knowledge, no reported studies exist on using FR-targeted imaging in post-MI inflammation. Whether this strategy may still occur may depend on further validation of FR-imaging. Currently, there are some limitations associated with this approach. Folate receptor expression is not specific for inflammatory cells. High physiologic expression also occurs in various other cell types; especially expression in kidneys has been considered a limiting factor. Initial enthusiasm of folate receptor-targeting in oncological applications has been dampened by the less-than-optimal biodistribution profiles. Due to high kidney uptake unfavorable tumor-to-kidney ratios emerged, limiting the clinical potential of this approach [182]. Nonetheless, research is ongoing specifically for FR-targeted imaging in inflammatory disease where attention is also focused on the development of new tracers with more favorable biodistribution profiles [179, 180, 183].

5.4.7 Translocator Protein

The translocator protein (TSPO) is a mitochondrial membrane receptor involved in the translocation of cholesterol from the outer to the inner mitochondrial membrane. It is predominantly expressed in steroid-synthesizing tissues, and in response to injury it is strongly upregulated in Schwann cells, neurons, and macrophages. Because of the abundant expression of TSPO by macrophages, it has been evaluated as a marker for inflammation imaging, including post-MI inflammation (Table 5.2). Nuclear imaging using TSPO-targeting tracers has been widely explored in the field of neuroinflammation, during which activated microglia express this marker [199]. TSPO-targeting tracers have gone through development phases to improve specificity and practical use of the tracers [Werry, 2019 #341]. The widely used first-generation tracer [¹¹C]C-PK11195 suffered from these limitations. Second-generation tracers such as [¹²³I]I-CLINDE and [¹⁸F]F-DPA714 showed improved specificity, however, with lower reproducibility during clinical implementation. This most likely was a result of the existence of genetic polymorphism of TSPO with variable binding affinity to these second-generation tracers [200]. Initial data with the new third-generation tracers [¹⁸F]F-GE180 and [¹⁸F]F-LW223 indicate better specificity without loss of sensitivity and heterogenic binding to the TSPO allelic variants [201–203]. These third-generation tracers may also be a valuable option for inflammation imaging in peripheral disease including post-MI inflammation. Initial studies in animal models of MI [185, 204] and patients with MI [184, 204] revealed clear associations between TSPO tracer uptake in the infarct area and late stage functional outcome following anti-inflammatory treatment. In addition, in the studies by Thackery et al. and Borchert et al., elevated TSPO tracer uptake was also observed in the brain. These results are ascribed to a phenomenon called heart–brain inflammatory crosstalk where a link between myocardial inflammation and neuroinflammation seems to exist. Further

investigation into the use of TSPO-targeting tracers seems warranted. Of interest is the fact that in contrast to SSTR2 and FR there are no strong associations between elevated TSPO expression and macrophage polarized state. While SSTR is considered a pro-inflammatory macrophage marker (M1) and FR an anti-inflammatory macrophage (M2), contrasting reports on association of TSPO expression with M1 or M2 polarization exist. Generally, FR is considered a marker for pro-inflammatory microglial activation [205], however in other settings TSPO was reported to be downregulated in M1 pro-inflammatory macrophages [206].

5.4.8 Glucagon-like Peptide-1 Receptor (GLP-1R)

An emerging target for post-MI inflammation imaging is the GLP-1R, which binds Glucagon-like peptide-1 (GLP-1). GLP-1 is an intestinal hormone involved in glucose homeostasis [207]. In recent studies it was shown that GLP-1 also acts on inflammatory responses and treatment with GLP-1 antagonists or inhibitors can be useful in disease with chronic inflammatory conditions [208]. Also in cardiovascular disease beneficial effects of GLP-1-based therapies have been reported. In pre-clinical MI(/R) models, administration of GLP-1R agonists resulted in reduced infarct size, improved survival, and preservation of ventricular function [209]. The exact mechanisms of these effects are not known and further studies are warranted. To evaluate the role of GLP-1(R) in inflammatory disease several GLP-1R-targeting tracers have been developed by labeling the peptide agonist exendin-4, which is a peptide that was originally isolated from the saliva of the Gila monster. In studies by Goa et al. [196], Pan et al. [197] and [198] the feasibility of imaging of GLP-1R expression in infarcted myocardium was demonstrated (Fig. 5.5). In these studies, it was found that GLP-1R expression is focally upregulated, especially in the (peri-infarct) area, within hours after myocardial infarction gradually decreasing over time with still elevated expression 1 week post-MI. Moreover, Stähle et al. demonstrated that GLP-1R tracer uptake correlated with the presence of CD68+ macrophages during the healing phase of post-MI.

5.4.9 Chemokine Receptors

Inflammatory chemokines exert chemotactic effects on inflammatory cells thereby recruiting them to sites of inflammation. Chemokine receptors expressed by leukocytes have therefore received attention as imaging markers for inflammation. In the setting of myocardial inflammation imaging, the C-X-C Motif Chemokine Receptor 4 (CXCR4) has received considerable attention as a potential imaging target. The C-X-C Motif Chemokine Receptor 4 (CXCR4) and its ligand C-X-C Motif Chemokine Ligand 12 (CXCL12) also known as stromal cell-derived factor1 (SDF-1) are essential for homing of circulating cells to tissue, including stem/progenitor cells, inflammatory cells, and cancer cells [210–212]. Because of these findings, substantial attention has been given to enable non-invasive imaging of CXCR4

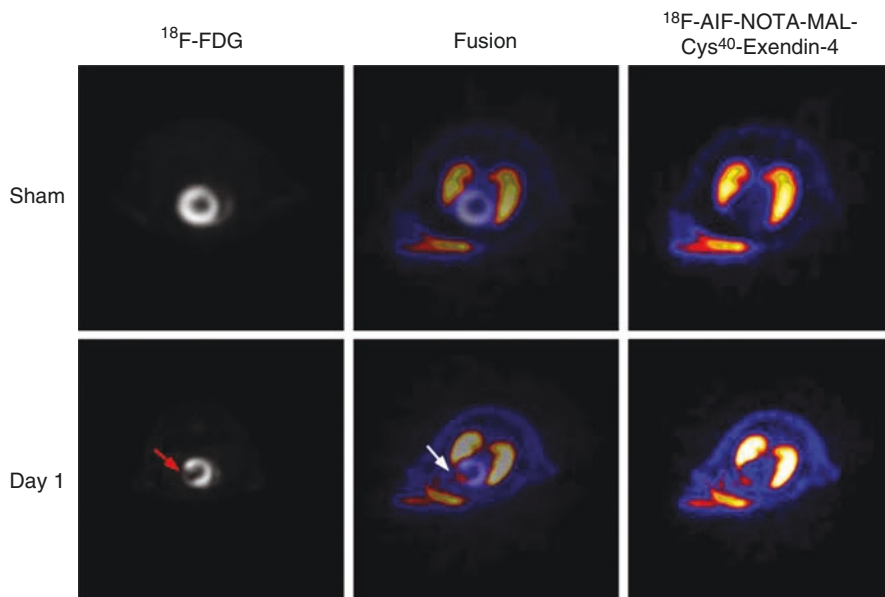


Fig. 5.5 Dual tracer PET imaging with [^{18}F]FDG and [^{18}F]F-AIF-NOTAMAL-Cys40-Exendin-4. Images acquired subsequently following injection of [^{18}F]FDG and [^{18}F]F-AIF-NOTAMAL-Cys40-Exendin-4 1 h apart were co-registered to show uptake of the GLP-1R-targeting tracer in FDG-defect area. Coronary artery ligation decreased ^{18}F -FDG accumulation (red arrow) and increased ^{18}F -AIF-NOTA-MAL-Cys40-exendin-4 accumulation (white arrow). Image reproduced without changes under Creative Commons license from Gao et al. [196]

expression [213]. Initial focus for CXCR4 as an imaging target originated from the oncological field, where it was found that CXCR4 is expressed by many different types of human cancers and its expression has been associated with tumor aggressiveness, poor prognosis, and resistance to chemotherapy. This had led to the development of a variety of tracers and theragnostic agents [214]. The most widely used tracer [^{68}Ga]Ga-pentixafor has in recent years also gained considerable attention for use in imaging of inflammation, especially in the field of cardiovascular disease [188, 192, 213], including inflammation imaging post-MI (Table 5.2). In initial studies, injury-related myocardial uptake of [^{68}Ga]Ga-pentixafor was demonstrated, and ascribed to an ongoing inflammatory reaction, however, without any clear clinical meaning [52, 192]. In more recent studies, correlations between [^{68}Ga]Ga-pentixafor uptake and functional outcome parameters were found [187, 190]. In the study by Reiter et al. performed in 22 patients suffering from (sub)acute MI, CXCR4 expression in the infarct area was negatively correlated with scar volume at follow-up in patients. In addition, uptake in remote organs, spleen, and bone marrow correlated with better infarct healing. Hess et al. recently described that early upregulation of CXCR4 expression, as also detected by PET imaging with [^{68}Ga]Ga-pentixafor, was predictive of acute rupture and chronic contractile

dysfunction in mice with R/I-MI. Blocking of the CXCR4 receptor with the inhibitor AMD3100 at peak time points improved survival and functional outcome that coincided with lower numbers of neutrophils and Ly6Chigh monocytes in the left ventricle. Subsequent application of CXCR4 imaging in patients with acute MI was reported to show high interindividual variability in tracer uptake, but nonetheless with significant correlation to myocardial damage and functional outcome parameters.

CXCR4 is also being considered as a target for therapeutic intervention. In various studies modulation of CXCR4 expression affected the post-MI inflammatory cascade and was reported to improve functional outcome [213, 215–218]. However, precise mechanisms are still under investigation. Positive effects of CXCR4 inhibitory interventions as well as upregulated myocardial CXCR4 expression on functional outcome have been reported [217–220]. Of note, also in atherosclerotic plaques both positive and negative correlations between upregulated CXCR4 expression and clinical outcome have been reported [181, 212, 221]. Factors to be considered in this respect are specificity of the tracer and issues regarding binding affinity and local tracer availability. Under inflammatory conditions, leukocytes have upregulated CXCR4 expression, however under ischemic conditions cardiomyocytes, endothelial cells, and myocardial fibroblasts can also abundantly express CXCR4 [219, 222]. In order to increase the understanding of the dynamics of CXCR4 expression during MI and its predictive value, additional studies are warranted. To further improve on CXCR4-targeted imaging, and enable more basic studies in animal models, several groups are developing new tracers with improved applicability. This includes alterations of the ligand with better affinity for murine CXCR4 and the use of other radionuclides better suited for micro-SPECT or PET imaging [193, 194, 223, 224].

Other chemokine receptors that have recently received attention as imaging target as well as for targeted therapy in CVD and other diseases are the structurally related C-C chemokine receptors type 2 (CCK2) and type 5 (CCK5) [225]. While CCR5 is broadly expressed on a variety of inflammatory cells and other cells including microglia, astrocytes, neurons, fibroblasts, epithelial cells, endothelium, and vascular smooth, CCR2 expression is more restricted and is mainly found on monocytes, NK cells, and T lymphocytes, and implicated as a pro-inflammatory cytokine.

The CCR2-CCL2 axis has been shown to be involved in the early stages of atherogenesis. Studies in CCR2-deficient mice revealed, reduced atherosclerotic lesion development, and expression of the CC chemokine monocyte chemoattractant protein-1 (MCP-1) is upregulated in human atherosclerotic plaques [20, 226]. In order to further study the role of CCR2 in CVD, a tracer based on an CCR2-inhibitor, called extracellular loop 1 in-verso (ECL1i), was developed [227]. Recently, Heo et al. modified the peptide to be labeled with ⁶⁸Ga and used it in two mouse MI/R models [195]. The investigators observed high uptake in MI lesions which was associated with CCR2 + -macrophage content.

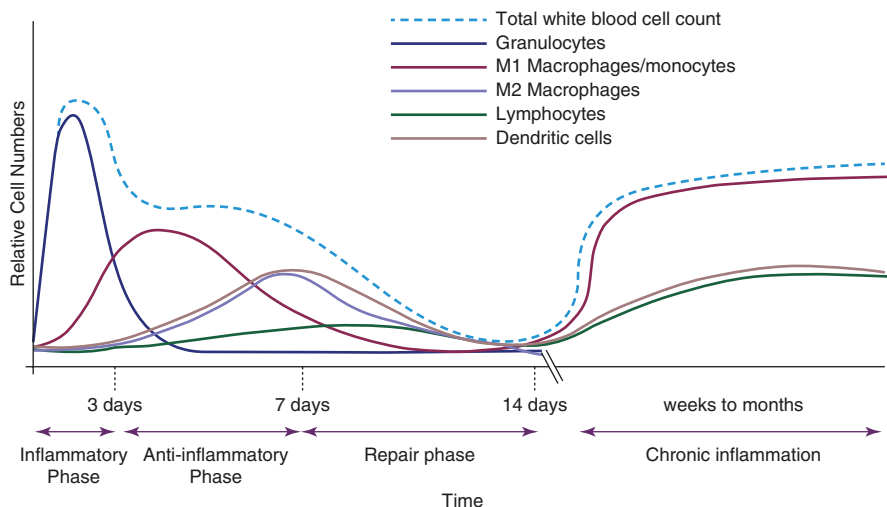


Fig. 5.6 Timeline of the inflammatory response cascade. Schematic representation of the presence and abundance of inflammatory cells over time following MI. Under normal circumstances, the inflammatory reaction resolves within 14 days. However, in case the post-MI inflammatory reaction remains unresolved or is exacerbated, the reaction may progress into a chronic inflammatory reaction

5.4.10 Lymphocyte Markers

In targeting inflammatory cells involved in post-MI inflammation, focus has been largely on monocytic/granulocytic leukocytes, which represent, in numbers, the main population that infiltrates infarcted myocardium (Fig. 5.6). However, T- and B lymphocytes are increasingly being recognized to also play an important role in the post-MI inflammatory cascade [31–35, 228, 229]. Therefore, imaging of lymphocytic cells in this process may also represent a relevant strategy. Imaging of lymphocyte trafficking, infiltration, and functionality received considerable interest in the fields of tumor immunology and chronic inflammatory diseases [230, 231]. For various markers specifically expressed by lymphocytes, e.g., CD2, CD3, CD4, CD20, CD25, and T cell receptor, antibody-based tracers have been developed and tested. However, while providing highly specific tracers, antibody-based imaging strategies suffer from some practical limitations such as limited tissue penetration, and long blood circulation times of antibodies, due to their relative high molecular weight and size [231]. Alternative approaches are being pursued such as targeting of the IL2-receptor (CD25) with radiolabeled IL-2 [232, 233]. However, the use of such tracers still needs extensive evaluation in the setting of post-MI inflammation. Especially since timing and context of tracer uptake may be crucial.

5.4.10.1 Adhesion Molecules

Another set of membrane molecules that are interesting as inflammation imaging markers concerns cell adhesion molecules (CAMs). Leukocyte infiltration to inflammatory sites is mediated via increased expression of adhesion molecules on activated endothelium and recruited leukocytes such as P-selectin, vascular endothelial adhesion molecule-1 (VCAM-1), intercellular adhesion molecule-1 (ICAM-1), and lymphocyte function associated antigen-1 (LFA-1) [242, 243]. Following MI, leukocyte infiltrates the infarcted tissue as a result from cardiomyocyte death. Because of vascular damage following reperfusion, remote myocardium may subsequently also become infiltrated with inflammatory cells.

Due to the central role of adhesion molecules in recruitment of inflammatory cells, CAMs have been studied as therapeutic targets for mitigating the inflammatory response [132, 216, 244–246]. Initial results have been encouraging; blocking of CAMs resulted in reduced scar size and/or improved ventricular function. However, further validation of these approaches is needed, with a requirement for tracers to image adhesion molecule expression.

P-selectin plays an essential role in the early phase of leukocyte recruitment to the site of injury during inflammation [247], and has been proposed both as molecular target for therapy and a relevant imaging target of post-MI inflammation [140, 244, 248, 249]. Some imaging strategies using P-selectin-targeting microbubbles [248] or radiolabeled fucoidan [234, 250], a P-selectin glycoprotein ligand mimic molecule, feasibility of imaging P-selectin expression in cardiovascular disease settings were recently demonstrated. From observations in a murine model for atherosclerosis Li et al. suggested that ^{68}Ga -labeled Fucoidan may be useful for identifying vulnerable plaque *in vivo*, since accumulation of the tracer was most pronounced in plaques with thin fibrous caps and co-localized with high-density macrophage infiltrate. Using $^{99\text{m}}\text{Tc}$ -labeled fucoidan, Chauvierre et al. demonstrated good performance of GMP-grade LMW fucoidan labeled with technetium-99 m for detecting of upregulated P-selectin expression in an ischemia/reperfusion model in rats [234].

The adhesion molecule LFA-1 and its counterpart ICAM-1 are also prominently involved in leukocyte recruitment to infarcted myocardium and have also been considered as targets for inflammation mitigating therapy in myocardial infarction and atherosclerosis [242, 246]. LFA-1 is expressed on activated inflammatory cells and has emerged as an imaging target of interest for prognostic and patient selection purposes in cardiovascular disease. The recently developed tracer [^{111}In]In-DANBIRT was shown to accumulate in plaque lesions *in vivo* in atherosclerotic mice [110, 251]. *Via in vitro* analysis it was shown that [^{111}In]In-DANBIRT uptake was associated with accumulation of CD68+ macrophages and LFA-1-expressing inflammatory cells [110, 252] in plaque lesions, including plaques in human carotid endarterectomy specimens. This tracer therefore holds promise for *in vivo* assessment of post-MI inflammation. Further investigation into its possible use as such is needed, including options to label the tracer with PET isotopes.

Also the integrin VCAM has been studied as an imaging target in cardiovascular disease, however this has also been mostly in the setting of AS plaque imaging [253], using peptides or nanobodies that bind to VCAM labeled with SPECT or

PET radionuclides or attached to microbubbles or iron oxide particles for US imaging or MR imaging, respectively. Nahrendorf et al., did report on the use of a VCAM-1-targeting, ^{18}F -labeled tetrameric peptide in a mouse MI model, with high in vivo PET signal in inflamed myocardium and good correlation with ex vivo measurement of VCAM-1 mRNA by quantitative polymerase chain reaction.

Another adhesion molecule markedly involved in ischemic heart disease is the integrin $\alpha\text{V}\beta3$. While mostly known as a marker of vasculogenesis and angiogenesis, expressed on activated endothelial cells, $\alpha\text{V}\beta3$ is also expressed by activated cardiomyocytes and leukocytes and contemplated as marker for the post-MI inflammatory process. Resulting from its central role in neo-angiogenesis during cancer development, various tracers have been developed that are suitable for PET, SPECT, or MR imaging [254]. In the setting of myocardial infarction various tracers targeting the integrin $\alpha\text{V}\beta3$ have been studied in preclinical models as well as in patients (Table 5.3). In a recent study, performed in 21 MI injected with the $\alpha\text{V}\beta3$ -targeting PET tracer, [^{18}F]-Fluciclatide, Jenkins et al. found increased uptake of [^{18}F]-Fluciclatide at sites of AMI with regional wall hypokinesis [239]. There was no correlation of tracer uptake with infarct size or C reactive protein levels, but [^{18}F]-Fluciclatide uptake was increased in segments displaying functional recovery and associated with increase in probability of regional recovery. Similarly, association between $\alpha\text{V}\beta3$ tracer uptake and infarcted tissue repair was found in a porcine model for ischemic myocardial damage using the ^{68}Ga -labeled tracer [^{68}Ga]-Ga-NODAGA-RGD [255]. Studies performed so far, therefore suggest that

Table 5.3 Imaging of adhesion molecules post-MI

Imaging target	Preclinical/ clinical	Imaging technique	Characteristics
P-selectin [$^{99\text{m}}\text{Tc}$] Tc-fucoidan MB _{RB40.34}	Preclinical [234] Preclinical	SPECT: Radiolabeled substrate Ultrasound microbubble functionalized with ab	Involved in leucocyte recruitment. Considered as target for inflammation mitigating therapies
VCAM-1 [^{18}F]F-4 V	Preclinical [235]	PET: Radiolabeled substrate	Tetrameric peptide designed for signal amplification potential via multivalent binding
$\alpha\text{V}\beta3$ [^{18}F] F-galacto-RGD [^{68}Ga] Ga-NODAGA- RGD [^{18}F]-Fluciclatide $^{99\text{m}}\text{Tc}$ -RAFT-RGD ^{111}In -RP748	Preclinical [236] Clinical ([237] Preclinical [238] Clinical [239] Preclinical [240] Preclinical [241]	PET: Radiolabeled substrate SPECT: Radiolabeled substrate SPECT: Radiolabeled substrate	Next to expression by activated endothelium also found on activated cardiomyocytes and leucocytes. Uptake in infarcted myocardium mostly associated with processes during the repair phase without direct connection to the inflammatory response. May be a marker for risk assessment of post-MI remodeling.

$\alpha V\beta 3$ expression is more associated with tissue repair processes than with actual inflammation in MI pathophysiology.

5.4.10.2 Extracellular (Matrix) Components

An alternative approach to imaging of post-MI inflammation processes is to target non-cellular components of the inflammatory process such as cytokines, proteases, and extracellular matrix (ECM) components. Such approaches are not aimed at assessing the presence of certain cell types but provide information on the activity of cells. Via the release of molecular mediators such as cytokines, chemokines, (degradative) enzymes, and reactive oxygen species, inflammatory cells exert their actions during the various phases of the post-MI cascade. There is increasing interest in the development of imaging tracers that target these molecular mediators of inflammatory processes, especially since inhibitors of these factors are also being considered as therapeutic options for mitigating post-MI adverse myocardial remodeling [270, 271]. Below and in Table 5.4 examples of such molecular targets and relevant imaging agents that have been used for imaging post-MI are described.

Following MI there is a substantial increase in intramyocardial cytokine levels within the first day, which depending on the further course of the inflammatory response may go down, persist, or undergo a second wave of upregulated expression corresponding to the progression into a chronic post-MI inflammatory condition. Cytokines are involved in cardiomyocyte survival, recruitment of circulating leukocytes, alterations in vascular endothelium and e ECM, and myocyte contractility [272]. Their effects can be favorable, stimulating tissue healing, or detrimental, promoting adverse remodeling. A variety of tracers targeting specific cytokines and cytokine receptors are being developed and investigated for their use in characterizing inflammatory responses [143, 272]. Cytokines and cytokine receptors that have been targeted for imaging in a post-MI setting include IL-8 [273], IL-1Ra, and TNF [274].

Matrix metalloproteinases (MMPs) are a type of proteolytic enzymes, produced by inflammatory cells that degrade multiple components of ECM and non-ECM molecules, thereby mediating tissue remodeling under pathological as well as physiological conditions. Because of their crucial role in human diseases, many MMP inhibitors (MMPIs) have been developed and are being investigated as novel therapeutics. To facilitate the evaluation of these novel molecular therapeutics, clinically relevant imaging techniques are required. As reviewed by Rangasamy et al., numerous MMPI-based imaging agents have emerged in recent years. MMPs are known to modulate left ventricular remodeling after MI, and the ability to image MMP activity following MI has been pursued (Table 5.4). Thorn et al. demonstrated the feasibility of imaging regional MMP activation in a porcine MI/R model using a ^{99m}Tc -labeled MMP inhibitor, [^{99m}Tc]Tc-RP805. Treatment-induced lowering of MMP activity could be visualized by SPECT imaging. Reduction in MMP activity was associated with an improvement in myocardial blood flow and improved myocardial strain in the MI region. Current MMP imaging tracers are based on known broad spectrum MMP inhibitors, and due to the side effects of these may induce research in ongoing in developing more specific targeting compounds.

Table 5.4 Imaging of extracellular components associated with post-MI inflammation

Imaging target Imaging tracer	Preclinical/ clinical	Imaging technique	Characteristics
MMP [^{99m} Tc] Tc-RP805 [⁶⁸ Ga] Ga-DOTA- peptide- MMP2/9 NAP9	Preclinical: [112, 256] Preclinical: [257] [258]	SPECT: Radiolabeled substrate PET: Radiolabeled substrate MRI: T1W imaging	Involved in myocardial repair and remodeling especially MMP2 and 9 (gelatinase). MMP uptake correlated to inflammatory cell infiltrate in infarct area.
Collagen EP-3533 [^{99m} Tc] Tc-collagenin [⁶⁴ Cu] cu- collagenin [⁶⁴ Cu]cu-CRPA	Preclinical: [259] Preclinical: [260] Preclinical: [261] Preclinical: [261]	MRI: T1W signal increase SPECT: Radiolabeled substrate PET: Radiolabeled substrate	Considered as indicator of fibrosis and/or (adverse) ventricular remodeling
Elastin Gd-ESMA	Preclinical: [163, 262]	MRI: T1/R1 value increase	Together with collagen a key element in ECM formation. Provides elasticity to connective tissue and may help preserve cardiac function after MI
Renin/ angiotensin system [^{99m} Tc] Tc-losartan [¹¹ C] C-KR31173	[263] [264, 265]	SPECT: Radiolabeled substrate PET: Radiolabeled substrate	Factors acting systemically and locally on cardiovascular homeostasis with modulating functions on ECM factors during post-MI inflammatory cascade.
Tenascin [¹¹¹ In]in-TNC fab') SPIO-anti- tenascin-C	Preclinical: [111, 266] Preclinical: [267]	SPECT: Radiolabeled substrate MRI: T2* susceptibility imaging	Physiologically expressed during embryonic development stages, with limited expression in normal adult tissue. Becomes highly expressed in myocardial tissue following tissue injury and inflammation
MPO MPO-Gd [¹⁸ F]F-MAPP	Preclinical: [155, 268] Preclinical: [269]	MRI: T1W signal increase PET: Radiolabeled substrate	MPO is indicative of inflammatory cell activation state instead being an indicator of just presence of inflammatory cells

Various studies have shown a clear link between the renin–angiotensin–aldosterone system (RAAS) and MMP activation and collagen production post-MI. Because of the important role of the RAAS system in cardiovascular homeostasis, imaging of components of this system is of interest. Some tracers consisting of radiolabeled angiotensin-converting enzyme (ACE) inhibitors have been developed and tested in *in vitro* settings for imaging ACE levels in infarcted myocardial [275, 276]. *In vivo* studies with targeted imaging of RAAS system components have been performed in mice, rats, and pigs using tracers targeting the Angiotensin II Type 1 Receptor

(AT₁R). These studies demonstrated the feasibility of such an approach, however, still needing further development and evaluation.

Instigated by inflammatory processes, reactive fibrosis may be induced thereby leading to ventricular stiffening, functional deterioration of the myocardium progressing into heart failure. The main component of fibrotic tissues is collagen 1 and various collagen-avid imaging agents have been developed and evaluated in the setting of MI (Table 5.4). Although fibrosis is an important prognostic factor in MI, clinical significance of molecular imaging-based diagnostics is still under investigation. Another key component in ECM formation is the protein elastin, which also was found to be over-expressed post-MI. Findings in several studies have indicated that elastin formation after MI leads to improved ejection fraction and decreased risk of myocardial rupture [170, 262]. In contrast, Ramos et al. found that increased elastin deposition within the scar tissue at 7 days post-MI was associated with detrimental cardiac remodeling as determined by EDV at day 21 post-MI. An emerging imaging target for assessment of inflammatory-induced fibrosis is fibroblast activation protein (FAP). FAP is expressed by activated fibroblasts in response to myocardial injury. From the oncological field FAP ligands have been introduced for PET imaging. In recent studies it was shown that FAP targeting tracers could be used to visualize fibroblast activation in infarcted myocardium [277, 278]. Diekman et al. applied a Ga-labeled FAP inhibitor as tracer in a group of 12 patients shortly after AMI. All patients exhibited FAP signal enrichment at the infarct site relative to blood, with considerable variation of uptake levels amongst patients. Within the patient group studied no correlation between tracer uptake and clinical outcome parameters was found. Further studies are needed to determine the value of FAP imaging in myocardial infarction monitoring.

Another ECM factor that may represent a relevant imaging target in post-MI inflammation is tenascin-C. Tenascin is an extracellular matrix molecule that normally is not expressed in myocardial ECM, but becomes strongly upregulated during active inflammation [111]. Using non-invasive imaging it has been found that tenascin is abundantly expressed early after MI peaking at day 3 with subsequent decline in the amount of tenascin with barely detectable presence on day 7 and beyond [266, 267, 279].

In the inflammatory cascade an important mediator of inflammatory processes is myeloperoxidase (MPO), produced by neutrophils and macrophages. Because of its important role in myocardial inflammation and adverse remodeling various attempts to image MPO activity have been undertaken. The group of Ralph Weissleder developed a so-called smart gadolinium-based contrast agent that targets MPO. The signaling capacity of the agent changes under the influence of MPO activity. In a study by Nahrendorf et al. using this MPO-Gd it was shown that myocardial MPO activity could be assessed by MR imaging and effects of atorvastatin therapy on MPO activity could be monitored over time [268]. Due to potential issues regarding sensitivity and potential toxicity of high amounts of Ga-based imaging agents alternative strategies for MPO imaging have been tried. Wang et al. developed and tested an activatable PET imaging probe to image MPO activity in vivo [269]. The developed probe has a short blood half-life and can be used to quantify changes in MPO activity in vivo, as demonstrated in mouse models.

5.5 Hybrid Imaging: The Added Value of Hybrid Imaging

Non-invasive imaging techniques play an important role in diagnostics, patient monitoring, and basic research in the biomedical field. As indicated above, various imaging technologies are available with each specific strengths and limitations in acquiring data on anatomical, functional, and/or molecular features in living subjects. Already early in the development stages of SPECT and PET, hybrid systems combining these techniques with CT became the standard. Due to the lack of anatomical reference information from SPECT and PET images, and the need for attenuation and scatter correction for reliable data, hybrid systems combining PET or SPECT with CT, quickly became the standard. Owing to the success of these hybrid systems in biomedicine, the desire to combine PET with MRI also quickly surfaced. However, realization of such a hybrid system faced many technical challenges, with initially largely incompatible physics of the separate technologies [280]. However, with the development of new detector technology, active MR shielding, and advanced image processing and analysis software, clinical integrated hybrid PET/MRI systems are now available.

With hybrid systems of SPECT or PET with CT, data sets are collected sequentially and subsequently co-registered. The added value of CT largely remains limited to providing anatomical context, with poor soft tissue contrast, photon attenuation maps, and scatter correction. In combinations with MRI more added value of hybrid systems can be obtained. Besides its excellent options for soft tissue contrast, MRI also offers many possibilities for functional imaging and to some extent also molecular imaging (see also sections above). This potential added value of MRI to PET image data has also attracted attention for use in post-MI inflammation imaging.

In contrast to hybrid systems with CT, systems with MRI exist where data acquisition of the different modalities occurs simultaneously [281]. Such fully integrated systems have several advantages compared to in-line systems with subsequent data acquisition. This includes reduced scan time and better spatial and temporal registration of the different data sets. In addition, better motion correction options via MR data with higher quality PET images can be obtained. Besides a number of advantages offered by MRI as an addition to PET there are also some limitations and challenges. One of the main challenges with PET/MRI has been the generation of robust attenuation maps. However, using segmented MR image data and a bone atlas, algorithms have been created by which reliable attenuation maps can be generated. And for cardiac imaging it has been shown that tracer uptake values obtained by PET/MRI were not significantly different from values determined with PE/CT [282]. An important limitation of MRI is the fact that patients with metal implants including pacemakers and defibrillators cannot be examined with MRI due to the interference of the MRI magnetic field with metal devices, which creates safety hazards for the patient (heating of the metal) as well as artifacts in the image data. For a detailed discussion of the (technical) options and challenges with hybrid PET/MRI systems the reader is referred to recent reviews by Nolte et al. [281], Rischpler et al. [283], and Wilk et al. [284].

In terms of the added value of PET/MRI for post-MI inflammatory imaging, main advantages may lie in the fact that the combined information with both spatial and temporal synchronization provides a higher level of informative value of imaging data. For instance, there is the option for cross-validation of available techniques such as myocardial perfusion, cell metabolism, and inflammation. Also, complementary information can be obtained providing the option to link image data that are informative on the presence of certain cell types, by targeting specific cell membrane markers, with information of actions of (inflammatory) cells such as MMP activity, or fibrosis (Fig. 5.7).

In a recent position statement from the European society of cardiovascular radiology the potential benefit of hybrid PET/MRI examinations for CVD has been discussed [285]. Concluding that PET/MRI is a feasible and robust technology strong potential for use in a variety of CVD conditions including myocardial inflammation. However, more in-depth studies and some technological developments are needed in order to establish its clinical value and cost-effectiveness. As a research tool for enhancing understanding of the processes underlying (detrimental) post-MI inflammation and in the evaluation and implementation of novel radiopharmaceuticals it seems to be of great scientific value.

5.6 Concluding Remarks

Visualization and characterization of the post-MI inflammatory response have become an urgent need for development and implementation of inflammation modulating treatments in patients with AMI. While survival of patients with AMI has

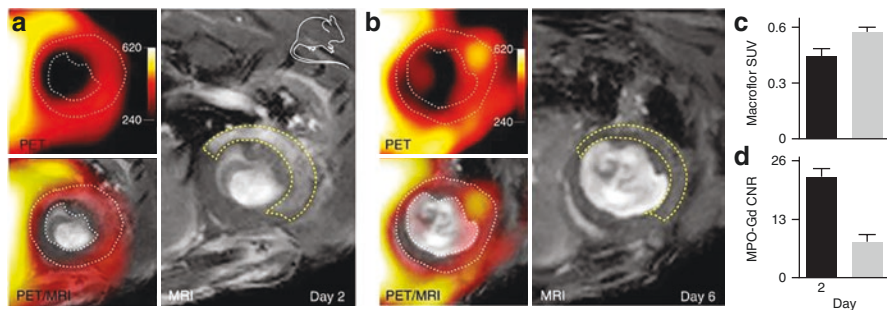


Fig. 5.7 Hybrid PET/MRI imaging of macrophage infiltration and MPO activity. Imaging macrophages and myeloperoxidase detect different inflammatory phenotypes. (a) PET/MRI on day 2 and (b) day 6 post-MI in wild-type mice. White dotted line on PET/MRI outlines myocardium. Yellow dashed line on MRI outlines the infarct identified by gadolinium enhancement and wall motion abnormality in cine loops. (c) In vivo PET standard uptake value (SUV) in infarct zone on days 2 and 6 post-MI ($n = 4$ per group, unpaired t-test). (d) In vivo MRI contrast to noise ratio (CNR) in infarct 90 min after IV MPO-Gd injection ($n = 4$ per group, unpaired t-test). Image reproduced in part without further changes under Creative Commons license from Keliher et al. [155] without changes

increased due to timely implementation of reperfusion therapy, later stage heart failure is still a major treat and has been linked to uncontrolled inflammatory processes. Various studies have shown promising results with anti-inflammatory treatment strategies; however, results have not been consistent or of limited impact. To reach full potential of such interventions, patient selection and precise timing and targeting of the treatment are crucial to reach the right balance in enhancing processes involved in tissue healing and attenuate processes leading to adverse remodeling. Several potential and promising imaging strategies have been discussed here, however, none of the described strategies has reached a level beyond proof-of-concept yet. Clear and consistent links between imaging data and patient outcome are still lacking. There is still a need to better understand the meaning of imaging data in the context of myocardial inflammatory status. None of the currently available tracers is unique for a specific cell type. Also, presence or absence of a given marker may be of limited value and has to be assessed in relation to other myocardial tissue features or markers of inflammation. The balance of various processes or effectors is decisive for the resulting effects, e.g., the balance between pro-inflammatory and anti-inflammatory cells. New developments regarding imaging technology and tracer/probe design enabling multi-parameter imaging may help in identifying the crucial parameters that dictate the balance between repair and adverse remodeling of myocardial tissue. Strategies like PET/MRI and multi-isotope imaging with SPECT or PET can contribute to a better understanding of inflammatory processes and states post-MI.

References

1. Thackeray JT. PET assessment of immune cell activity and therapeutic monitoring following myocardial infarction. *Curr Cardiol Rep.* 2018;20(3):13.
2. Rischpler C, Dirschinger RJ, Nekolla SG, Kossmann H, Nicolosi S, Hanus F, et al. Prospective evaluation of 18F-Fluorodeoxyglucose uptake in Postischemic myocardium by simultaneous positron emission tomography/magnetic resonance imaging as a prognostic marker of functional outcome. *Circ Cardiovasc Imaging.* 2016;9(4):e004316.
3. Bujak M, Dobaczewski M, Chatila K, Mendoza LH, Li N, Reddy A, et al. Interleukin-1 receptor type I signaling critically regulates infarct healing and cardiac remodeling. *Am J Pathol.* 2008;173(1):57–67.
4. Westman PC, Lipinski MJ, Luger D, Waksman R, Bonow RO, Wu E, et al. Inflammation as a driver of adverse left ventricular remodeling after acute myocardial infarction. *J Am Coll Cardiol.* 2016;67(17):2050–60.
5. Niccoli G, Montone RA, Ibanez B, Thiele H, Crea F, Heusch G, et al. Optimized treatment of ST-elevation myocardial infarction. *Circ Res.* 2019;125(2):245–58.
6. Yellon DM, Hausenloy DJ. Myocardial reperfusion injury. *N Engl J Med.* 2007;357(11):1121–35.
7. Frangogiannis NG. Regulation of the inflammatory response in cardiac repair. *Circ Res.* 2012;110(1):159–73.
8. Nahrendorf M, Pittet MJ, Swirski FK. Monocytes: protagonists of infarct inflammation and repair after myocardial infarction. *Circulation.* 2010;121(22):2437–45.

9. Dewald O, Zymek P, Winkelmann K, Koerting A, Ren G, Abou-Khamis T, et al. CCL2/monocyte chemoattractant Protein-1 regulates inflammatory responses critical to healing myocardial infarcts. *Circ Res*. 2005;96(8):881–9.
10. Ong SB, Hernandez-Resendiz S, Crespo-Avilan GE, Mukhametshina RT, Kwek XY, Cabrera-Fuentes HA, et al. Inflammation following acute myocardial infarction: multiple players, dynamic roles, and novel therapeutic opportunities. *Pharmacol Ther*. 2018;186:73–87.
11. Prabhu SD, Frangogiannis NG. The biological basis for cardiac repair after myocardial infarction: from inflammation to fibrosis. *Circ Res*. 2016;119(1):91–112.
12. Mouton AJ, Rivera OJ, Lindsey ML. Myocardial infarction remodeling that progresses to heart failure: a signaling misunderstanding. *Am J Physiol Heart Circ Physiol*. 2018;315(1):H71–H9.
13. van Kranenburg M, Magro M, Thiele H, de Waha S, Eitel I, Cochet A, et al. Prognostic value of microvascular obstruction and infarct size, as measured by CMR in STEMI patients. *JACC Cardiovasc Imaging*. 2014;7(9):930–9.
14. Hausenloy DJ, Chilian W, Crea F, Davidson SM, Ferdinandy P, Garcia-Dorado D, et al. The coronary circulation in acute myocardial ischaemia/reperfusion injury: a target for cardioprotection. *Cardiovasc Res*. 2019;115(7):1143–55.
15. Spinale FG. Myocardial matrix remodeling and the matrix metalloproteinases: influence on cardiac form and function. *Physiol Rev*. 2007;87(4):1285–342.
16. Rusu M, Hilse K, Schuh A, Martin L, Slabu I, Stoppe C, et al. Biomechanical assessment of remote and postinfarction scar remodeling following myocardial infarction. *Sci Rep*. 2019;9(1):16744.
17. Frangogiannis NG, Lindsey ML, Michael LH, Youker KA, Bressler RB, Mendoza LH, et al. Resident cardiac mast cells degranulate and release preformed TNF-alpha, initiating the cytokine cascade in experimental canine myocardial ischemia/reperfusion. *Circulation*. 1998;98(7):699–710.
18. Somasundaram P, Ren G, Nagar H, Kraemer D, Mendoza L, Michael LH, et al. Mast cell tryptase may modulate endothelial cell phenotype in healing myocardial infarcts. *J Pathol*. 2005;205(1):102–11.
19. Epelman S, Lavine KJ, Beaudin AE, Sojka DK, Carrero JA, Calderon B, et al. Embryonic and adult-derived resident cardiac macrophages are maintained through distinct mechanisms at steady state and during inflammation. *Immunity*. 2014;40(1):91–104.
20. Bajpai G, Bredemeyer A, Li W, Zaitsev K, Koenig AL, Lokshina I, et al. Tissue resident CCR2- and CCR2+ cardiac macrophages differentially orchestrate monocyte recruitment and fate specification following myocardial injury. *Circ Res*. 2019;124(2):263–78.
21. Bajpai G, Schneider C, Wong N, Bredemeyer A, Hulsmans M, Nahrendorf M, et al. The human heart contains distinct macrophage subsets with divergent origins and functions. *Nat Med*. 2018;24(8):1234–45.
22. Ma Y, Yabluchanskiy A, Iyer RP, Cannon PL, Flynn ER, Jung M, et al. Temporal neutrophil polarization following myocardial infarction. *Cardiovasc Res*. 2016;110(1):51–61.
23. Hansen PR. Role of neutrophils in myocardial ischemia and reperfusion. *Circulation*. 1995;91(6):1872–85.
24. Boufenzler A, Lemarie J, Simon T, Derive M, Bouazza Y, Tran N, et al. TREM-1 mediates inflammatory injury and cardiac remodeling following myocardial infarction. *Circ Res*. 2015;116(11):1772–82.
25. Horckmans M, Ring L, Duchene J, Santovito D, Schloss MJ, Drechsler M, et al. Neutrophils orchestrate post-myocardial infarction healing by polarizing macrophages towards a reparative phenotype. *Eur Heart J*. 2017;38(3):187–97.
26. Nahrendorf M, Swirski FK, Aikawa E, Stangenberg L, Wurdinger T, Figueiredo JL, et al. The healing myocardium sequentially mobilizes two monocyte subsets with divergent and complementary functions. *J Exp Med*. 2007;204(12):3037–47.
27. Hanna RN, Carlin LM, Hubbeling HG, Nackiewicz D, Green AM, Punt JA, et al. The transcription factor NR4A1 (Nur 77) controls bone marrow differentiation and the survival of Ly6C- monocytes. *Nat Immunol*. 2011;12(8):778–85.

28. Anzai A, Anzai T, Nagai S, Maekawa Y, Naito K, Kaneko H, et al. Regulatory role of dendritic cells in postinfarction healing and left ventricular remodeling. *Circulation*. 2012;125(10):1234–45.
29. Yan X, Anzai A, Katsumata Y, Matsuhashi T, Ito K, Endo J, et al. Temporal dynamics of cardiac immune cell accumulation following acute myocardial infarction. *J Mol Cell Cardiol*. 2013;62:24–35.
30. Liu H, Gao W, Yuan J, Wu C, Yao K, Zhang L, et al. Exosomes derived from dendritic cells improve cardiac function via activation of CD4(+) T lymphocytes after myocardial infarction. *J Mol Cell Cardiol*. 2016;91:123–33.
31. Varda-Bloom N, Leor J, Ohad DG, Hasin Y, Amar M, Fixler R, et al. Cytotoxic T lymphocytes are activated following myocardial infarction and can recognize and kill healthy myocytes in vitro. *J Mol Cell Cardiol*. 2000;32(12):2141–9.
32. Boag SE, Das R, Shmeleva EV, Bagnall A, Egred M, Howard N, et al. T lymphocytes and fractalkine contribute to myocardial ischemia/reperfusion injury in patients. *J Clin Invest*. 2015;125(8):3063–76.
33. Zouggari Y, Ait-Oufella H, Bonnin P, Simon T, Sage AP, Guerin C, et al. B lymphocytes trigger monocyte mobilization and impair heart function after acute myocardial infarction. *Nat Med*. 2013;19(10):1273–80.
34. Meng X, Yang J, Dong M, Zhang K, Tu E, Gao Q, et al. Regulatory T cells in cardiovascular diseases. *Nat Rev Cardiol*. 2016;13(3):167–79.
35. Wang YP, Xie Y, Ma H, Su SA, Wang YD, Wang JA, et al. Regulatory T lymphocytes in myocardial infarction: a promising new therapeutic target. *Int J Cardiol*. 2016;203:923–8.
36. Wang YM, Alexander SI. IL-2/anti-IL-2 complex: a novel strategy of in vivo regulatory T cell expansion in renal injury. *J Am Soc Nephrol*. 2013;24(10):1503–4.
37. Sardella G, De Luca L, Francavilla V, Accapezzato D, Mancone M, Sirinian MI, et al. Frequency of naturally-occurring regulatory T cells is reduced in patients with ST-segment elevation myocardial infarction. *Thromb Res*. 2007;120(4):631–4.
38. Mor A, Luboshits G, Planer D, Keren G, George J. Altered status of CD4(+)CD25(+) regulatory T cells in patients with acute coronary syndromes. *Eur Heart J*. 2006;27(21):2530–7.
39. Wigren M, Bjorkbacka H, Andersson L, Ljungcrantz I, Fredrikson GN, Persson M, et al. Low levels of circulating CD4+fox P3+ T cells are associated with an increased risk for development of myocardial infarction but not for stroke. *Arterioscler Thromb Vasc Biol*. 2012;32(8):2000–4.
40. Saxena A, Dobaczewski M, Rai V, Haque Z, Chen W, Li N, et al. Regulatory T cells are recruited in the infarcted mouse myocardium and may modulate fibroblast phenotype and function. *Am J Physiol Heart Circ Physiol*. 2014;307(8):H1233–42.
41. Zhang WC, Wang J, Shu YW, Tang TT, Zhu ZF, Xia N, et al. Impaired thymic export and increased apoptosis account for regulatory T cell defects in patients with non-ST segment elevation acute coronary syndrome. *J Biol Chem*. 2012;287(41):34157–66.
42. Hofmann U, Beyersdorf N, Weirather J, Podolskaya A, Bauersachs J, Ertl G, et al. Activation of CD4+ T lymphocytes improves wound healing and survival after experimental myocardial infarction in mice. *Circulation*. 2012;125(13):1652–63.
43. Homma T, Kinugawa S, Takahashi M, Sobirin MA, Saito A, Fukushima A, et al. Activation of invariant natural killer T cells by alpha-galactosylceramide ameliorates myocardial ischemia/reperfusion injury in mice. *J Mol Cell Cardiol*. 2013;62:179–88.
44. Sobirin MA, Kinugawa S, Takahashi M, Fukushima A, Homma T, Ono T, et al. Activation of natural killer T cells ameliorates postinfarct cardiac remodeling and failure in mice. *Circ Res*. 2012;111(8):1037–47.
45. Biswas SK, Mantovani A. Macrophage plasticity and interaction with lymphocyte subsets: cancer as a paradigm. *Nat Immunol*. 2010;11(10):889–96.
46. Xue J, Schmidt SV, Sander J, Draffehn A, Krebs W, Quester I, et al. Transcriptome-based network analysis reveals a spectrum model of human macrophage activation. *Immunity*. 2014;40(2):274–88.

47. Frodermann V, Nahrendorf M. Macrophages and cardiovascular health. *Physiol Rev.* 2018;98(4):2523–69.
48. Francis Stuart SD, De Jesus NM, Lindsey ML, Ripplinger CM. The crossroads of inflammation, fibrosis, and arrhythmia following myocardial infarction. *J Mol Cell Cardiol.* 2016;91:114–22.
49. Kung GL, Vaseghi M, Gahm JK, Shevtsov J, Garfinkel A, Shivkumar K, et al. Microstructural infarct border zone remodeling in the Post-infarct swine heart measured by diffusion tensor MRI. *Front Physiol.* 2018;9:826.
50. Hulsmans M, Clauss S, Xiao L, Aguirre AD, King KR, Hanley A, et al. Macrophages facilitate electrical conduction in the heart. *Cell.* 2017;169(3):510–22.
51. Fei YD, Wang Q, Hou JW, Li W, Cai XX, Yang YL, et al. Macrophages facilitate post myocardial infarction arrhythmias: roles of gap junction and KCa3.1. *Theranostics.* 2019;9(22):6396–411.
52. van der Velden J, Merkus D, de Beer V, Hamdani N, Linke WA, Boontje NM, et al. Transmural heterogeneity of myofilament function and sarcomeric protein phosphorylation in remodeled myocardium of pigs with a recent myocardial infarction. *Front Physiol.* 2011;2:83.
53. Carberry J, Carrick D, Haig C, Rauhalammi SM, Ahmed N, Mordi I, et al. Remote zone extracellular volume and left ventricular remodeling in survivors of ST-elevation myocardial infarction. *Hypertension.* 2016;68(2):385–91.
54. Duncker DJ, de Beer VJ, Merkus D. Alterations in vasomotor control of coronary resistance vessels in remodelled myocardium of swine with a recent myocardial infarction. *Med Biol Eng Comput.* 2008;46(5):485–97.
55. Kuster DW, Merkus D, Kremer A, van Ijcken WF, de Beer VJ, Verhoeven AJ, et al. Left ventricular remodeling in swine after myocardial infarction: a transcriptional genomics approach. *Basic Res Cardiol.* 2011;106(6):1269–81.
56. Lindsey ML, Bolli R, Canty JM Jr, Du XJ, Frangiannis NG, Frantz S, et al. Guidelines for experimental models of myocardial ischemia and infarction. *Am J Physiol Heart Circ Physiol.* 2018;314(4):H812–h38.
57. Heusch G, Gersh BJ. The pathophysiology of acute myocardial infarction and strategies of protection beyond reperfusion: a continual challenge. *Eur Heart J.* 2017;38(11):774–84.
58. Heusch G, Libby P, Gersh B, Yellon D, Bohm M, Lopaschuk G, et al. Cardiovascular remodelling in coronary artery disease and heart failure. *Lancet.* 2014;383(9932):1933–43.
59. Cohen M, Boiangiu C, Abidi M. Therapy for ST-segment elevation myocardial infarction patients who present late or are ineligible for reperfusion therapy. *J Am Coll Cardiol.* 2010;55(18):1895–906.
60. Gharacholou SM, Alexander KP, Chen AY, Wang TY, Melloni C, Gibler WB, et al. Implications and reasons for the lack of use of reperfusion therapy in patients with ST-segment elevation myocardial infarction: findings from the CRUSADE initiative. *Am Heart J.* 2010;159(5):757–63.
61. Hausenloy DJ, Botker HE, Engstrom T, Erlinge D, Heusch G, Ibanez B, et al. Targeting reperfusion injury in patients with ST-segment elevation myocardial infarction: trials and tribulations. *Eur Heart J.* 2017;38(13):935–41.
62. Hausenloy DJ, Yellon DM. Myocardial ischemia-reperfusion injury: a neglected therapeutic target. *J Clin Invest.* 2013;123(1):92–100.
63. Ibanez B, Heusch G, Ovize M, Van de Werf F. Evolving therapies for myocardial ischemia/reperfusion injury. *J Am Coll Cardiol.* 2015;65(14):1454–71.
64. Dewald O, Ren G, Duerr GD, Zoerlein M, Klemm C, Gersch C, et al. Of mice and dogs: species-specific differences in the inflammatory response following myocardial infarction. *Am J Pathol.* 2004;164(2):665–77.
65. Frantz S, Bauersachs J, Ertl G. Post-infarct remodelling: contribution of wound healing and inflammation. *Cardiovasc Res.* 2009;81(3):474–81.
66. Michael LH, Ballantyne CM, Zachariah JP, Gould KE, Pocius JS, Taffet GE, et al. Myocardial infarction and remodeling in mice: effect of reperfusion. *Am J Phys.* 1999;277(2 Pt 2):H660–8.

67. Michael LH, Entman ML, Hartley CJ, Youker KA, Zhu J, Hall SR, et al. Myocardial ischemia and reperfusion: a murine model. *Am J Phys.* 1995;269(6 Pt 2):H2147–54.
68. Jennings RB, Murry CE, Steenbergen C Jr, Reimer KA. Development of cell injury in sustained acute ischemia. *Circulation.* 1990;82(3 Suppl):II2.
69. Jennings RB, Reimer KA. Lethal myocardial ischemic injury. *Am J Pathol.* 1981;102(2):241–55.
70. Jennings RB, Sommers HM, Smyth GA, Flack HA, Linn H. Myocardial necrosis induced by temporary occlusion of a coronary artery in the dog. *Arch Pathol.* 1960;70:68–78.
71. Reimer KA, Jennings RB, Tatum AH. Pathobiology of acute myocardial ischemia: metabolic, functional and ultrastructural studies. *Am J Cardiol.* 1983;52(2):72a–81a.
72. Reimer KA, Lowe JE, Rasmussen MM, Jennings RB. The wavefront phenomenon of ischemic cell death. 1. Myocardial infarct size vs duration of coronary occlusion in dogs. *Circulation.* 1977;56(5):786–94.
73. Algranati D, Kassab GS, Lanir Y. Why is the subendocardium more vulnerable to ischemia? A new paradigm. *Am J Physiol Heart Circ Physiol.* 2011;300(3):H1090–100.
74. Yoshihara HA, Bastiaansen JA, Berthonneche C, Comment A, Schwitter J. An intact small animal model of myocardial ischemia-reperfusion: characterization of metabolic changes by hyperpolarized ¹³C MR spectroscopy. *Am J Physiol Heart Circ Physiol.* 2015;309(12):H2058–66.
75. Heusch G, Skyschally A, Schulz R. The in-situ pig heart with regional ischemia/reperfusion - ready for translation. *J Mol Cell Cardiol.* 2011;50(6):951–63.
76. Vatner SF. Effects of anesthesia on cardiovascular control mechanisms. *Environ Health Perspect.* 1978;26:193–206.
77. Maxwell MP, Hearse DJ, Yellon DM. Species variation in the coronary collateral circulation during regional myocardial ischaemia: a critical determinant of the rate of evolution and extent of myocardial infarction. *Cardiovasc Res.* 1987;21(10):737–46.
78. Swindle MM, Horneffer PJ, Gardner TJ, Gott VL, Hall TS, Stuart RS, et al. Anatomic and anesthetic considerations in experimental cardiopulmonary surgery in swine. *Lab Anim Sci.* 1986;36(4):357–61.
79. Johns TN, Olson BJ. Experimental myocardial infarction. I. a method of coronary occlusion in small animals. *Ann Surg.* 1954;140(5):675–82.
80. Gao E, Lei YH, Shang X, Huang ZM, Zuo L, Boucher M, et al. A novel and efficient model of coronary artery ligation and myocardial infarction in the mouse. *Circ Res.* 2010;107(12):1445–53.
81. Kurz KD, Main BW, Sandusky GE. Rat model of arterial thrombosis induced by ferric chloride. *Thromb Res.* 1990;60(4):269–80.
82. Garg M, Khanna D. Exploration of pharmacological interventions to prevent isoproterenol-induced myocardial infarction in experimental models. *Ther Adv Cardiovasc Dis.* 2014;8(4):155–69.
83. Munz MR, Faria MA, Monteiro JR, Aguas AP, Amorim MJ. Surgical porcine myocardial infarction model through permanent coronary occlusion. *Comp Med.* 2011;61(5):445–52.
84. Litvak J, Siderides LE, Vineberg AM. The experimental production of coronary artery insufficiency and occlusion. *Am Heart J.* 1957;53(4):505–18.
85. Elzinga WE. Ameroid constrictor: uniform closure rates and a calibration procedure. *J Appl Physiol.* 1969;27(3):419–21.
86. Vineberg A, Mahanti B, Litvak J. Experimental gradual coronary artery constriction by ameroid constrictors. *Surgery.* 1960;47:765–71.
87. White FC, Bloor CM. Coronary collateral circulation in the pig: correlation of collateral flow with coronary bed size. *Basic Res Cardiol.* 1981;76(2):189–96.
88. Hughes GC, Post MJ, Simons M, Annex BH. Translational physiology: porcine models of human coronary artery disease: implications for preclinical trials of therapeutic angiogenesis. *J Appl Physiol.* 2003;94(5):1689–701.

89. Inou T, Tomoike H, Watanabe K, Kikuchi Y, Mizukami M, Kurozumi T, et al. A newly developed X-ray transparent ameroid constrictor for study on progression of gradual coronary stenosis. *Basic Res Cardiol*. 1980;75(4):537–43.
90. Bolukoglu H, Liedtke AJ, Nellis SH, Eggleston AM, Subramanian R, Renstrom B. An animal model of chronic coronary stenosis resulting in hibernating myocardium. *Am J Phys*. 1992;263(1 Pt 2):H20–9.
91. Dogne JM, Rolin S, Petein M, Tchana-Sato V, Ghuysen A, Lambermont B, et al. Characterization of an original model of myocardial infarction provoked by coronary artery thrombosis induced by ferric chloride in pig. *Thromb Res*. 2005;116(5):431–42.
92. Krombach GA, Kinzel S, Mahnken AH, Gunther RW, Buecker A. Minimally invasive close-chest method for creating reperfused or occlusive myocardial infarction in swine. *Investig Radiol*. 2005;40(1):14–8.
93. Liu JX, Yu Z, Li XZ, Fu JH, Shang XH, Yan AG, et al. Cardioprotective effects of diltiazem reevaluated by a novel myocardial ischemic model in Chinese miniature swine. *Acta Pharmacol Sin*. 2007;28(1):52–7.
94. Dib N, Diethrich EB, Campbell A, Gahremanpour A, McGarry M, Opie SR. A percutaneous swine model of myocardial infarction. *J Pharmacol Toxicol Methods*. 2006;53(3):256–63.
95. Agress CM, Rosenberg MJ, Jacobs HI, Binder MJ, Schneiderman A, Clark WG. Prolonged shock in the closed-chest dog following coronary embolization with graded microspheres. *Am J Phys*. 1952;170(3):536–49.
96. Naslund U, Haggmark S, Johansson G, Pennert K, Reiz S, Marklund SL. Effects of reperfusion and superoxide dismutase on myocardial infarct size in a closed chest pig model. *Cardiovasc Res*. 1992;26(2):170–8.
97. Reffelmann T, Sensebat O, Birnbaum Y, Stroemer E, Hanrath P, Uretsky BF, et al. A novel minimal-invasive model of chronic myocardial infarction in swine. *Coron Artery Dis*. 2004;15(1):7–12.
98. Eldar M, Ohad D, Bor A, Varda-Bloom N, Swanson DK, Battler A. A closed-chest pig model of sustained ventricular tachycardia. *Pacing Clin Electrophysiol*. 1994;17(10):1603–9.
99. Hennen JK, Huang J, Barrett TD, Driscoll EM, Willens DE, Park AM, et al. Effects of selective cyclooxygenase-2 inhibition on vascular responses and thrombosis in canine coronary arteries. *Circulation*. 2001;104(7):820–5.
100. Epstein FH. MRI of left ventricular function. *J Nucl Cardiol*. 2007;14(5):729–44.
101. Demirkiran A, Everaars H, Amier RP, Beijinck C, Bom MJ, Gotte MJW, et al. Cardiovascular magnetic resonance techniques for tissue characterization after acute myocardial injury. *Eur Heart J Cardiovasc Imaging*. 2019;20(7):723–34.
102. Ibanez B, Aletras AH, Arai AE, Arheden H, Bax J, Berry C, et al. Cardiac MRI endpoints in myocardial infarction experimental and clinical trials: JACC scientific expert panel. *J Am Coll Cardiol*. 2019;74(2):238–56.
103. Garcia-Dorado D, Oliveras J, Gili J, Sanz E, Perez-Villa F, Barrabes J, et al. Analysis of myocardial oedema by magnetic resonance imaging early after coronary artery occlusion with or without reperfusion. *Cardiovasc Res*. 1993;27(8):1462–9.
104. Dastidar AG, Harries I, Pontecorboli G, Bruno VD, De Garate E, Moret C, et al. Native T1 mapping to detect extent of acute and chronic myocardial infarction: comparison with late gadolinium enhancement technique. *Int J Cardiovasc Imaging*. 2019;35(3):517–27.
105. Reinstadler SJ, Stiermaier T, Liebetrau J, Fuernau G, Eitel C, de Waha S, et al. Prognostic significance of remote myocardium alterations assessed by quantitative noncontrast T1 mapping in ST-segment elevation myocardial infarction. *JACC Cardiovasc Imaging*. 2018;11(3):411–9.
106. Uppal R, Caravan P. Targeted probes for cardiovascular MRI. *Future Med Chem*. 2010;2(3):451–70.
107. Hendrikx G, De Saint-Hubert M, Dijkgraaf I, Bauwens M, Douma K, Wierdsma R, et al. Molecular imaging of angiogenesis after myocardial infarction by (111)in-DTPA-cNGR and (99m)Tc-sestamibi dual-isotope myocardial SPECT. *EJNMMI Res*. 2015;5:2.

108. Abbott BG, Case JA, Dorbala S, Einstein AJ, Galt JR, Pagnanelli R, et al. Contemporary cardiac SPECT imaging-innovations and best practices: an information statement from the American Society of Nuclear Cardiology. *J Nucl Cardiol*. 2018;25(5):1847–60.
109. Meester EJ, Krenning BJ, de Blois E, de Jong M, van der Steen AFW, Bernsen MR, van der Heiden K. Imaging inflammation in atherosclerotic plaques, targeting SST2 with [¹¹¹In]In-DOTA-JR11. *J Nucl Cardiol*. 2020. <https://doi.org/10.1007/s12350-020-02046-y>. Epub ahead of print.
110. Meester EJ, Krenning BJ, de Blois RH, Norenberg JP, de Jong M, Bernsen MR, et al. Imaging of atherosclerosis, targeting LFA-1 on inflammatory cells with (111)in-DANBIRT. *J Nucl Cardiol*. 2019;26(5):1697–704.
111. Ageyama N, Kurosawa H, Fujimoto O, Uehara T, Hiroe M, Arano Y, et al. Successful inflammation imaging of non-human primate hearts using an antibody specific for tenascin-C. *Int Heart J*. 2019;60(1):151–8.
112. Su H, Spinale FG, Dobrucki LW, Song J, Hua J, Sweterlitsch S, et al. Noninvasive targeted imaging of matrix metalloproteinase activation in a murine model of postinfarction remodeling. *Circulation*. 2005;112(20):3157–67.
113. Swart LE, Scholtens AM, Tanis W, Nieman K, Bogers A, Verzijlbergen FJ, et al. 18F-fluorodeoxyglucose positron emission/computed tomography and computed tomography angiography in prosthetic heart valve endocarditis: from guidelines to clinical practice. *Eur Heart J*. 2018;39(41):3739–49.
114. Schwaiger M, Brunken R, Grover-McKay M, Krivokapich J, Child J, Tillisch JH, et al. Regional myocardial metabolism in patients with acute myocardial infarction assessed by positron emission tomography. *J Am Coll Cardiol*. 1986;8(4):800–8.
115. Anzola LK, Glaudemans A, Dierckx R, Martinez FA, Moreno S, Signore A. Somatostatin receptor imaging by SPECT and PET in patients with chronic inflammatory disorders: a systematic review. *Eur J Nucl Med Mol Imaging*. 2019;46(12):2496–513.
116. Tarkin JM, Calcagno C, Dweck MR, Evans NR, Chowdhury MM, Gopalan D, et al. (68) Ga-DOTATATE PET identifies residual myocardial inflammation and bone marrow activation after myocardial infarction. *J Am Coll Cardiol*. 2019;73(19):2489–91.
117. Bravo PE, Bajaj N, Padera RF, Morgan V, Hainer J, Bibbo CF, Harrington M, Park MA, Hyun H, Robertson M, Lakdawala NK, Groarke J, Stewart GC, Dorbala S, Blankstein R, Di Carli MF. Feasibility of somatostatin receptortargeted imaging for detection of myocardial inflammation: A pilot study. *J Nucl Cardiol*. 2021;28(3):1089–99.
118. Lapa C, Reiter T, Li X, Werner RA, Samnick S, Jahns R, et al. Imaging of myocardial inflammation with somatostatin receptor based PET/CT-A comparison to cardiac MRI. *Int J Cardiol*. 2015;194:44–9.
119. Satomi T, Ogawa M, Mori I, Ishino S, Kubo K, Magata Y, et al. Comparison of contrast agents for atherosclerosis imaging using cultured macrophages: FDG versus ultrasmall superparamagnetic iron oxide. *J Nucl Med*. 2013;54(6):999–1004.
120. Lee WW, Marinelli B, van der Laan AM, Sena BF, Gorbatov R, Leuschner F, et al. PET/MRI of inflammation in myocardial infarction. *J Am Coll Cardiol*. 2012;59(2):153–63.
121. Buonincontri G, Methner C, Carpenter TA, Hawkes RC, Sawiak SJ, Krieg T. MRI and PET in mouse models of myocardial infarction. *J Vis Exp*. 2013;82:e50806.
122. Xi XY, Zhang F, Wang J, Gao W, Tian Y, Xu H, et al. Functional significance of post-myocardial infarction inflammation evaluated by (18)F-fluorodeoxyglucose imaging in swine model. *J Nucl Cardiol*. 2019;27(2):519–31.
123. Giorgetti A, Marras G, Genovesi D, Filidei E, Bottoni A, Mangione M, et al. Effect of prolonged fasting and low molecular weight heparin or warfarin therapies on 2-deoxy-2-[18F]-fluoro-D-glucose PET cardiac uptake. *J Nucl Cardiol*. 2018;25(4):1364–71.
124. Perel-Winkler A, Bokhari S, Perez-Recio T, Zartoshti A, Askanase A, Geraldino-Pardilla L. Myocarditis in systemic lupus erythematosus diagnosed by (18)F-fluorodeoxyglucose positron emission tomography. *Lupus Sci Med*. 2018;5(1):e000265.
125. Thackeray JT, Bankstahl JP, Wang Y, Wollert KC, Bengel FM. Clinically relevant strategies for lowering cardiomyocyte glucose uptake for 18F-FDG imaging of myocardial inflammation in mice. *Eur J Nucl Med Mol Imaging*. 2015;42(5):771–80.

126. Wollenweber T, Roentgen P, Schafer A, Schatka I, Zwadlo C, Brunkhorst T, et al. Characterizing the inflammatory tissue response to acute myocardial infarction by clinical multimodality noninvasive imaging. *Circ Cardiovasc Imaging*. 2014;7(5):811–8.
127. Li B, Lento PA, Pan S. Inflammatory cardiomyopathy: case-based review on clinical presentation, diagnosis, and management. *Cardiol Rev*. 2021;29(5):230–7.
128. Kossman H, Rischpler C, Hanus F, Nekolla SG, Kunze KP, Götz K, et al. Monocyte-platelet aggregates affect local inflammation in patients with acute myocardial infarction. *Int J Cardiol*. 2019;287:7–12.
129. Vasudevan P, Gaebel R, Doering P, Mueller P, Lemcke H, Stenzel J, et al. 18F-FDG PET-based imaging of myocardial inflammation predicts a functional outcome following transplantation of mESC-derived cardiac induced cells in a mouse model of myocardial infarction. *Cells*. 2019;8(12):1613.
130. Morooka M, Kubota K, Kadowaki H, Ito K, Okazaki O, Kashida M, et al. 11C-methionine PET of acute myocardial infarction. *J Nucl Med*. 2009;50(8):1283–7.
131. Taki J, Wakabayashi H, Inaki A, Imanaka-Yoshida K, Hiroe M, Ogawa K, et al. 14C-methionine uptake as a potential marker of inflammatory processes after myocardial ischemia and reperfusion. *J Nucl Med*. 2013;54(3):431–6.
132. Thackeray JT, Bankstahl JP, Wang Y, Wollert KC, Bengel FM. Targeting amino acid metabolism for molecular imaging of inflammation early after myocardial infarction. *Theranostics*. 2016;6(11):1768–79.
133. Taki J, Inaki A, Wakabayashi H, Matsunari I, Imanaka-Yoshida K, Ogawa K, et al. Postconditioning accelerates myocardial inflammatory resolution demonstrated by (14)C-methionine imaging and attenuates ventricular remodeling after ischemia and reperfusion. *Circ J*. 2019;83(12):2520–6.
134. Voo S, Kwee RM, Sluimer JC, Schreuder FH, Wierts R, Bauwens M, et al. Imaging intra-plaque inflammation in carotid atherosclerosis with 18F-fluorocholine positron emission tomography-computed tomography: prospective study on vulnerable atheroma with immunohistochemical validation. *Circ Cardiovasc Imaging*. 2016;9(5):e004467.
135. DeGrado TR, Baldwin SW, Wang S, Orr MD, Liao RP, Friedman HS, et al. Synthesis and evaluation of (18)F-labeled choline analogs as oncologic PET tracers. *J Nucl Med*. 2001;42(12):1805–14.
136. Lewis AJM, Miller JJ, Lau AZ, Curtis MK, Rider OJ, Choudhury RP, et al. Noninvasive Immunometabolic cardiac inflammation imaging using hyperpolarized magnetic resonance. *Circ Res*. 2018;122(8):1084–93.
137. Schroeder MA, Atherton HJ, Ball DR, Cole MA, Heather LC, Griffin JL, et al. Real-time assessment of Krebs cycle metabolism using hyperpolarized 13C magnetic resonance spectroscopy. *FASEB J*. 2009;23(8):2529–38.
138. Serrao EM, Brindle KM. Potential clinical roles for metabolic imaging with hyperpolarized [1-(13)C]pyruvate. *Front Oncol*. 2016;6:59.
139. Lewis AJM, Tyler DJ, Rider O. Clinical cardiovascular applications of hyperpolarized magnetic resonance. *Cardiovasc Drugs Ther*. 2020;34(2):231–40.
140. Kircher M, Lapa C. Novel noninvasive nuclear medicine imaging techniques for cardiac inflammation. *Curr Cardiovasc Imaging Rep*. 2017;10(2):6.
141. de Vries EF, Roca M, Jamar F, Israel O, Signore A. Guidelines for the labelling of leucocytes with (99m)Tc-HMPAO. Inflammation/infection Taskgroup of the European Association of Nuclear Medicine. *Eur J Nucl Med Mol Imaging*. 2010;37(4):842–8.
142. Roca M, de Vries EF, Jamar F, Israel O, Signore A. Guidelines for the labelling of leucocytes with (111)in-oxine. Inflammation/infection Taskgroup of the European Association of Nuclear Medicine. *Eur J Nucl Med Mol Imaging*. 2010;37(4):835–41.
143. Tsopelas C. Radiotracers used for the scintigraphic detection of infection and inflammation. *Sci World J*. 2015;2015:676719.
144. Vaidyanathan S, Patel CN, Scarsbrook AF, Chowdhury FU. FDG PET/CT in infection and inflammation—current and emerging clinical applications. *Clin Radiol*. 2015;70(7):787–800.

145. Charoenphun P, Meszaros LK, Chuamsaamarkkee K, Sharif-Paghaleh E, Ballinger JR, Ferris TJ, et al. [(89)Zr]oxinate4 for long-term in vivo cell tracking by positron emission tomography. *Eur J Nucl Med Mol Imaging*. 2015;42(2):278–87.
146. Bansal A, Pandey MK, Demirhan YE, Nesbitt JJ, Crespo-Diaz RJ, Terzic A, et al. Novel (89)Zr cell labeling approach for PET-based cell trafficking studies. *EJNMMI Res*. 2015;5:19.
147. Lagan J, Naish JH, Simpson K, Zi M, Cartwright EJ, Foden P, et al. Substrate for the myocardial inflammation-heart failure hypothesis identified using novel USPIO methodology. *JACC Cardiovasc Imaging*. 2020;14(2):365–76.
148. Belderbos S, Gonzalez-Gomez MA, Cleeren F, Wouters J, Pineiro Y, Deroose CM, et al. Simultaneous in vivo PET/MRI using fluorine-18 labeled Fe₃O₄@Al(OH)₃ nanoparticles: comparison of nanoparticle and nanoparticle-labeled stem cell distribution. *EJNMMI Res*. 2020;10(1):73.
149. Alam SR, Shah AS, Richards J, Lang NN, Barnes G, Joshi N, et al. Ultrasmall superparamagnetic particles of iron oxide in patients with acute myocardial infarction: early clinical experience. *Circ Cardiovasc Imaging*. 2012;5(5):559–65.
150. Alam SR, Stirrat C, Spath N, Zamvar V, Pessotto R, Dweck MR, et al. Myocardial inflammation, injury and infarction during on-pump coronary artery bypass graft surgery. *J Cardiothorac Surg*. 2017;12(1):115.
151. Stirrat CG, Alam SR, Mac Gillivray TJ, Gray CD, Dweck MR, Raftis J, et al. Ferumoxtyl-enhanced magnetic resonance imaging assessing inflammation after myocardial infarction. *Heart*. 2017;103(19):1528–35.
152. Fogel U, Ding Z, Hardung H, Jander S, Reichmann G, Jacoby C, et al. In vivo monitoring of inflammation after cardiac and cerebral ischemia by fluorine magnetic resonance imaging. *Circulation*. 2008;118(2):140–8.
153. Wu L, Liu F, Liu S, Xu X, Liu Z, Sun X. Perfluorocarbons-based (19)F magnetic resonance imaging in biomedicine. *Int J Nanomedicine*. 2020;15:7377–95.
154. Nahrendorf M, Hoyer FF, Meerwaldt AE, van Leent MMT, Senders ML, Calcagno C, et al. Imaging cardiovascular and lung macrophages with the positron emission tomography sensor (64)Cu-Macrin in mice, rabbits, and pigs. *Circ Cardiovasc Imaging*. 2020;13(10):e010586.
155. Keliher EJ, Ye YX, Wojtkiewicz GR, Aguirre AD, Tricot B, Senders ML, et al. Polyglucose nanoparticles with renal elimination and macrophage avidity facilitate PET imaging in ischemic heart disease. *Nat Commun*. 2017;8:14064.
156. Khaled W, Piraquive J, Leporq B, Wan JH, Lambert SA, Mignet N, et al. In vitro distinction between proinflammatory and antiinflammatory macrophages with gadolinium-liposomes and ultrasmall superparamagnetic iron oxide particles at 3.0T. *J Magn Reson Imaging*. 2019;49(4):1166–73.
157. Reichel D, Tripathi M, Perez JM. Biological effects of nanoparticles on macrophage polarization in the tumor microenvironment. *Nano*. 2019;3(1):66–88.
158. Chen J, Yang J, Liu R, Qiao C, Lu Z, Shi Y, et al. Dual-targeting Theranostic system with mimicking apoptosis to promote myocardial infarction repair via modulation of macrophages. *Theranostics*. 2017;7(17):4149–67.
159. Pratti A, Dong X, Andia ME, Yu B, Dokukina K, Chaubey S, et al. Assessment of inflammation with a very small iron-oxide particle in a murine model of reperfused myocardial infarction. *J Magn Reson Imaging*. 2014;39(3):598–608.
160. Montet-Abou K, Daire JL, Hyacinthe JN, Jorge-Costa M, Grosdemange K, Mach F, et al. In vivo labelling of resting monocytes in the reticuloendothelial system with fluorescent iron oxide nanoparticles prior to injury reveals that they are mobilized to infarcted myocardium. *Eur Heart J*. 2010;31(11):1410–20.
161. Yang Y, Liu J, Yang Y, Cho SH, Hu TC. Assessment of cell infiltration in myocardial infarction: a dose-dependent study using micrometer-sized iron oxide particles. *Magn Reson Med*. 2011;66(5):1353–61.
162. Staal AHJ, Becker K, Tagit O, Koen van Riessen N, Koshkina O, Veltien A, et al. In vivo clearance of (19)F MRI imaging nanocarriers is strongly influenced by nanoparticle ultrastructure. *Biomaterials*. 2020;261:120307.

163. Ramos IT, Henningsson M, Nezafat M, Lavin B, Lorrio S, Gebhardt P, et al. Simultaneous assessment of cardiac inflammation and extracellular matrix remodeling after myocardial infarction. *Circ Cardiovasc Imaging*. 2018;11(11):e007453.
164. Nienhaus F, Colley D, Jahn A, Pfeiler S, Flocke V, Temme S, et al. Phagocytosis of a PFOB-nanoemulsion for (19)F magnetic resonance imaging: first results in monocytes of patients with stable coronary artery disease and ST-elevation myocardial infarction. *Molecules*. 2019;24(11):2058.
165. Tarkin JM, Joshi FR, Evans NR, Chowdhury MM, Figg NL, Shah AV, et al. Detection of atherosclerotic inflammation by (68)Ga-DOTATATE PET compared to [(18)F]FDG PET imaging. *J Am Coll Cardiol*. 2017;69(14):1774–91.
166. Bison SM, Konijnenberg MW, Melis M, Pool SE, Bernsen MR, Teunissen JJ, et al. Peptide receptor radionuclide therapy using radiolabeled somatostatin analogs: focus on future developments. *Clin Transl Imaging*. 2014;2:55–66.
167. Kwetkeboom DJ, Kam BL, van Essen M, Teunissen JJ, van Eijck CH, Valkema R, et al. Somatostatin-receptor-based imaging and therapy of gastroenteropancreatic neuroendocrine tumors. *Endocr Relat Cancer*. 2010;17(1):R53–73.
168. Thackeray JT, Bankstahl JP, Wang Y, Korf-Klingebiel M, Walte A, Wittneben A, et al. Targeting post-infarct inflammation by PET imaging: comparison of (68)Ga-citrate and (68)Ga-DOTATATE with (18)F-FDG in a mouse model. *Eur J Nucl Med Mol Imaging*. 2015;42(2):317–27.
169. Bakerman I, Wardak M, Nguyen PK. Molecular imaging of inflammation in ischemic heart disease. *Curr Cardiovasc Imaging Rep*. 2018;11(6):13.
170. Lavin Plaza B, Theodoulou I, Rashid I, Hajhosseiny R, Phinikaridou A, Botnar RM. Molecular imaging in ischemic heart disease. *Curr Cardiovasc Imaging Rep*. 2019;12(7):31.
171. Thackeray JT, Hupe HC, Wang Y, Bankstahl JP, Berding G, Ross TL, et al. Myocardial inflammation predicts remodeling and Neuroinflammation after myocardial infarction. *J Am Coll Cardiol*. 2018;71(3):263–75.
172. Kimbrough D, Wang SH, Wright LH, Mani SK, Kasiganesan H, LaRue AC, et al. HDAC inhibition helps post-MI healing by modulating macrophage polarization. *J Mol Cell Cardiol*. 2018;119:51–63.
173. Nahrendorf M, Swirski FK. Monocyte and macrophage heterogeneity in the heart. *Circ Res*. 2013;112(12):1624–33.
174. Gombozhapova A, Rogovskaya Y, Shurupov V, Rebenkova M, Kzhyshkowska J, Popov SV, et al. Macrophage activation and polarization in post-infarction cardiac remodeling. *J Biomed Sci*. 2017;24(1):13.
175. Weirather J, Hofmann UD, Beyersdorf N, Ramos GC, Vogel B, Frey A, et al. Foxp3+ CD4+ T cells improve healing after myocardial infarction by modulating monocyte/macrophage differentiation. *Circ Res*. 2014;115(1):55–67.
176. Zhou LS, Zhao GL, Liu Q, Jiang SC, Wang Y, Zhang DM. Silencing collapsin response mediator protein-2 reprograms macrophage phenotype and improves infarct healing in experimental myocardial infarction model. *J Inflamm*. 2015;12:11.
177. Muller C. Folate based radiopharmaceuticals for imaging and therapy of cancer and inflammation. *Curr Pharm Des*. 2012;18(8):1058–83.
178. Winkel LC, Groen HC, van Thiel BS, Müller C, van der Steen AF, Wentzel JJ, de Jong M, Van der Heiden K. Folate receptor–targeted single-photon emission computed tomography/computed tomography to detect activated macrophages in atherosclerosis: can it distinguish vulnerable from stable atherosclerotic plaques? *Mol Imaging*. 2014;13. <https://doi.org/10.2310/7290.2013.00061>.
179. Jahandideh A, Uotila S, Stahle M, Virta J, Li XG, Kyto V, et al. Folate receptor beta-targeted PET imaging of macrophages in autoimmune myocarditis. *J Nucl Med*. 2020;61(11):1643–9.
180. Verweij NJF, Yaqub M, Bruijnen STG, Pieplenbosch S, Ter Wee MM, Jansen G, et al. First in man study of [(18)F]fluoro-PEG-folate PET: a novel macrophage imaging technique to visualize rheumatoid arthritis. *Sci Rep*. 2020;10(1):1047.

181. Bot I, Daissormont IT, Zerneck A, van Puijvelde GH, Kramp B, de Jager SC, et al. CXCR4 blockade induces atherosclerosis by affecting neutrophil function. *J Mol Cell Cardiol.* 2014;74:44–52.
182. Radford LL, Fernandez S, Beacham R, El Sayed R, Farkas R, Benesova M, et al. New (55) co-labeled albumin-binding folate derivatives as potential pet agents for folate receptor imaging. *Pharmaceuticals.* 2019;12(4):166.
183. Chandrupatla D, Mollthoff CFM, Lammertsma AA, van der Laken CJ, Jansen G. The folate receptor beta as a macrophage-mediated imaging and therapeutic target in rheumatoid arthritis. *Drug Deliv Transl Res.* 2019;9(1):366–78.
184. Borchert T, Hess A, Lukačević M, Ross TL, Bengel FM, Thackeray JT. Angiotensin-converting enzyme inhibitor treatment early after myocardial infarction attenuates acute cardiac and neuroinflammation without effect on chronic neuroinflammation. *Eur J Nucl Med Mol Imaging.* 2020;47(7):1757–68.
185. MacAskill MG, Stadulyte A, Williams L, Morgan TEF, Sloan NL, Alcaide-Corral CJ, et al. Quantification of macrophage-driven inflammation during myocardial infarction with (18) F-LW223, a novel TSPO radiotracer with binding independent of the rs6971 human polymorphism. *J Nucl Med.* 2020;62(4):536–44.
186. Mou T, Tian J, Tian Y, Yun M, Li J, Dong W, et al. Automated synthesis and preliminary evaluation of [(18)F]FDPA for cardiac inflammation imaging in rats after myocardial infarction. *Sci Rep.* 2020;10(1):18685.
187. Hess A, Derlin T, Koenig T, Diekmann J, Wittneben A, Wang Y, et al. Molecular imaging-guided repair after acute myocardial infarction by targeting the chemokine receptor CXCR4. *Eur Heart J.* 2020;41(37):3564–75.
188. Thackeray JT, Derlin T, Haghikia A, Napp LC, Wang Y, Ross TL, et al. Molecular imaging of the chemokine receptor CXCR4 after acute myocardial infarction. *JACC Cardiovasc Imaging.* 2015;8(12):1417–26.
189. Koenig T, Sedding DG, Wester HJ, Derlin T. Seeing the unseen: post-infarction inflammation in an isolated right ventricular myocardial infarction visualized by combined cardiac magnetic resonance imaging and chemokine receptor CXCR4-targeted molecular imaging. *Eur Heart J.* 2018;39(11):966.
190. Reiter T, Kircher M, Schirbel A, Werner RA, Kropf S, Ertl G, et al. Imaging of C-X-C motif chemokine receptor CXCR4 expression after myocardial infarction with [(68)Ga]Pentixafor-PET/CT in correlation with cardiac MRI. *JACC Cardiovasc Imaging.* 2018;11(10):1541–3.
191. Rischpler C, Nekolla SG, Kossmann H, Dirschinger RJ, Schottelius M, Hyafil F, et al. Upregulated myocardial CXCR4-expression after myocardial infarction assessed by simultaneous GA-68 pentixafor PET/MRI. *J Nucl Cardiol.* 2016;23(1):131–3.
192. Lapa C, Reiter T, Werner RA, Ertl G, Wester HJ, Buck AK, et al. [(68)Ga]Pentixafor-PET/CT for imaging of chemokine receptor 4 expression after myocardial infarction. *JACC Cardiovasc Imaging.* 2015;8(12):1466–8.
193. Zacherl MJ, Todica A, Wängler C, Schirrmacher R, Hajebrahimi MA, Pircher J, Li X, Lindner S, Brendel M, Bartenstein P, Massberg S, Brunner S, Lehner S, Hacker M, Huber BC. Molecular imaging of cardiac CXCR4 expression in a mouse model of acute myocardial infarction using a novel 68Ga-mCXCL12 PET tracer. *J Nucl Cardiol.* 2020. <https://doi.org/10.1007/s12350-020-02262-6>. Epub ahead of print.
194. Burke BP, Miranda CS, Lee RE, Renard I, Nigam S, Clemente GS, et al. (64)cu PET imaging of the CXCR4 chemokine receptor using a cross-bridged Cyclam Bis-Tetraazamacrocyclic antagonist. *J Nucl Med.* 2020;61(1):123–8.
195. Heo GS, Bajpai G, Li W, Luehmann HP, Sultan DH, Dun H, et al. Targeted PET imaging of chemokine receptor 2+ monocytes and macrophages in the injured heart. *J Nucl Med.* 2020;62(1):111–4.
196. Gao H, Kiesewetter DO, Zhang X, Huang X, Guo N, Lang L, et al. PET of glucagonlike peptide receptor upregulation after myocardial ischemia or reperfusion injury. *J Nucl Med.* 2012;53(12):1960–8.

197. Pan X, Xu Q, Chen J, Wang T, Zhang M, Wang H, et al. Preliminary evaluation of ¹⁸F-FAIFNOTAMALCys40Exendin4 in rodent heart after myocardial ischemia and reperfusion. *Mol Med Rep.* 2019;20(3):2276–84.
198. Stahle M, Kyto V, Kiugel M, Liljenback H, Metsala O, Kakela M, et al. Glucagon-like peptide-1 receptor expression after myocardial infarction: imaging study using (68)Ga-NODAGA-exendin-4 positron emission tomography. *J Nucl Cardiol.* 2020;27(6):2386–97.
199. Werry EL, Bright FM, Piguot O, Ittner LM, Halliday GM, Hodges JR, et al. Recent developments in TSPO PET imaging as a biomarker of neuroinflammation in neurodegenerative disorders. *Int J Mol Sci.* 2019;20(13):3161.
200. Tronel C, Largeau B, Santiago Ribeiro MJ, Guilloteau D, Dupont AC, Arlicot N. Molecular targets for PET imaging of activated microglia: the current situation and future expectations. *Int J Mol Sci.* 2017;18(4):802.
201. Werner RA, Chen X, Rowe SP, Lapa C, Javadi MS, Higuchi T. Recent paradigm shifts in molecular cardiac imaging-establishing precision cardiology through novel (18)F-labeled PET radiotracers. *Trends Cardiovasc Med.* 2020;30(1):11–9.
202. Largeau B, Dupont AC, Guilloteau D, Santiago-Ribeiro MJ, Arlicot N. TSPO PET imaging: from microglial activation to peripheral sterile inflammatory diseases? *Contrast Media Mol Imaging.* 2017;2017:6592139.
203. MacAskill MG, Newby DE, Tavares AAS. Frontiers in positron emission tomography imaging of the vulnerable atherosclerotic plaque. *Cardiovasc Res.* 2019;115(14):1952–62.
204. Thackeray JT, Bengel FM. Molecular imaging of myocardial inflammation with positron emission tomography Post-ischemia: a determinant of subsequent remodeling or recovery. *JACC Cardiovasc Imaging.* 2018;11(9):1340–55.
205. Janssen B, Vugts DJ, Windhorst AD, Mach RH. PET imaging of microglial activation-beyond targeting TSPO. *Molecules.* 2018;23(3):607.
206. Narayan N, Mandhair H, Smyth E, Dakin SG, Kiriakidis S, Wells L, et al. The macrophage marker translocator protein (TSPO) is down-regulated on pro-inflammatory 'M1' human macrophages. *PLoS One.* 2017;12(10):e0185767.
207. Muller TD, Finan B, Bloom SR, D'Alessio D, Drucker DJ, Flatt PR, et al. Glucagon-like peptide 1 (GLP-1). *Mol Metab.* 2019;30:72–130.
208. Lee YS, Jun HS. Anti-inflammatory effects of GLP-1-based therapies beyond glucose control. *Mediat Inflamm.* 2016;2016:3094642.
209. Drucker DJ. The cardiovascular biology of glucagon-like Peptide-1. *Cell Metab.* 2016;24(1):15–30.
210. Askari AT, Unzek S, Popovic ZB, Goldman CK, Forudi F, Kiedrowski M, et al. Effect of stromal-cell-derived factor 1 on stem-cell homing and tissue regeneration in ischaemic cardiomyopathy. *Lancet.* 2003;362(9385):697–703.
211. De Filippo K, Rankin SM. CXCR4, the master regulator of neutrophil trafficking in homeostasis and disease. *Eur J Clin Invest.* 2018;48:e12949.
212. Doring Y, Noels H, van der Vorst EPC, Neideck C, Egea V, Drechsler M, et al. Vascular CXCR4 limits atherosclerosis by maintaining arterial integrity: evidence from mouse and human studies. *Circulation.* 2017;136(4):388–403.
213. Kircher M, Herhaus P, Schottelius M, Buck AK, Werner RA, Wester HJ, et al. CXCR4-directed theranostics in oncology and inflammation. *Ann Nucl Med.* 2018;32(8):503–11.
214. Weiss ID, Jacobson O. Molecular imaging of chemokine receptor CXCR4. *Theranostics.* 2013;3(1):76–84.
215. Hess A, Thackeray JT, Wollert KC, Bengel FM. Radionuclide image-guided repair of the heart. *JACC Cardiovasc Imaging.* 2019;13(11):2415–29.
216. Huang S, Frangogiannis NG. Anti-inflammatory therapies in myocardial infarction: failures, hopes and challenges. *Br J Pharmacol.* 2018;175(9):1377–400.
217. Jujo K, Hamada H, Iwakura A, Thorne T, Sekiguchi H, Clarke T, et al. CXCR4 blockade augments bone marrow progenitor cell recruitment to the neovasculature and reduces mortality after myocardial infarction. *Proc Natl Acad Sci U S A.* 2010;107(24):11008–13.

218. Wang Y, Dembowski K, Chevalier E, Stüve P, Korf-Klingebiel M, Lochner M, et al. C-X-C motif chemokine receptor 4 blockade promotes tissue repair after myocardial infarction by enhancing regulatory T cell mobilization and immune-regulatory function. *Circulation*. 2019;139(15):1798–812.
219. Mayorga M, Kiedrowski M, Shamhart P, Forudi F, Weber K, Chilian WM, et al. Early upregulation of myocardial CXCR4 expression is critical for dimethylallylglycine-induced cardiac improvement in acute myocardial infarction. *Am J Physiol Heart Circ Physiol*. 2016;310(1):H20–8.
220. Dong F, Harvey J, Finan A, Weber K, Agarwal U, Penn MS. Myocardial CXCR4 expression is required for mesenchymal stem cell mediated repair following acute myocardial infarction. *Circulation*. 2012;126(3):314–24.
221. Derlin T, Sedding DG, Dutzmann J, Haghikia A, König T, Napp LC, et al. Imaging of chemokine receptor CXCR4 expression in culprit and nonculprit coronary atherosclerotic plaque using motion-corrected [(68)Ga]pentixafor PET/CT. *Eur J Nucl Med Mol Imaging*. 2018;45(11):1934–44.
222. Scofield SLC, Daniels CR, Dalal S, Millard JA, Singh M, Singh K. Extracellular ubiquitin modulates cardiac fibroblast phenotype and function via its interaction with CXCR4. *Life Sci*. 2018;211:8–16.
223. Schottelius M, Ludescher M, Richter F, Kapp TG, Kessler H, Wester HJ. Validation of [(125)I]CPCR4.3 as an investigative tool for the sensitive and specific detection of hCXCR4 and mCXCR4 expression in vitro and in vivo. *EJNMMI Res*. 2019;9(1):75.
224. Osl T, Schmidt A, Schwaiger M, Schottelius M, Wester HJ. A new class of PentixaFor- and PentixaTher-based theranostic agents with enhanced CXCR4-targeting efficiency. *Theranostics*. 2020;10(18):8264–80.
225. Fantuzzi L, Tagliamonte M, Gauzzi MC, Lopalco L. Dual CCR5/CCR2 targeting: opportunities for the cure of complex disorders. *Cell Mol Life Sci*. 2019;76(24):4869–86.
226. Boring L, Gosling J, Cleary M, Charo IF. Decreased lesion formation in CCR2^{-/-} mice reveals a role for chemokines in the initiation of atherosclerosis. *Nature*. 1998;394(6696):894–7.
227. Liu Y, Li W, Luehmann HP, Zhao Y, Detering L, Sultan DH, et al. Noninvasive imaging of CCR2(+) cells in ischemia-reperfusion injury after lung transplantation. *Am J Transplant*. 2016;16(10):3016–23.
228. Ilatovskaya DV, Pitts C, Clayton J, Domondon M, Troncoso M, Pippin S, et al. CD8(+) T-cells negatively regulate inflammation post-myocardial infarction. *Am J Physiol Heart Circ Physiol*. 2019;317(3):H581–H96.
229. Hofmann U, Frantz S. Role of T-cells in myocardial infarction. *Eur Heart J*. 2016;37(11):873–9.
230. McCarthy CE, White JM, Viola NT, Gibson HM. In vivo imaging technologies to monitor the immune system. *Front Immunol*. 2020;11:1067.
231. Wei W, Jiang D, Ehlerding EB, Luo Q, Cai W. Noninvasive PET imaging of T cells. *Trends Cancer*. 2018;4(5):359–73.
232. Telenga ED, van der Bij W, de Vries EFJ, Verschuuren EAM, Timens W, Luurtsema G, et al. (99m)Tc-HYNIC-IL-2 scintigraphy to detect acute rejection in lung transplantation patients: a proof-of-concept study. *EJNMMI Res*. 2019;9(1):41.
233. Klein C, Waldhauer I, Nicolini VG, Freimoser-Grundschober A, Nayak T, Vugts DJ, et al. Cergutuzumab amunaleukin (CEA-IL2v), a CEA-targeted IL-2 variant-based immunocytokine for combination cancer immunotherapy: overcoming limitations of aldesleukin and conventional IL-2-based immunocytokines. *Onco Targets Ther*. 2017;6(3):e1277306.
234. Chauvierre C, Aid-Launais R, Aerts J, Chaubet F, Maire M, Chollet L, et al. Pharmaceutical development and safety evaluation of a GMP-grade fucoidan for molecular diagnosis of cardiovascular diseases. *Mar Drugs*. 2019;17(12):699.
235. Nahrendorf M, Keliher E, Panizzi P, Zhang H, Hembrador S, Figueiredo JL, et al. 18F-4V for PET-CT imaging of VCAM-1 expression in atherosclerosis. *JACC Cardiovasc Imaging*. 2009;2(10):1213–22.

236. Sherif HM, Saraste A, Nekolla SG, Weidl E, Reder S, Tapfer A, et al. Molecular imaging of early alphavbeta3 integrin expression predicts long-term left-ventricle remodeling after myocardial infarction in rats. *J Nucl Med*. 2012;53(2):318–23.
237. Makowski MR, Rischpler C, Ebersberger U, Keithahn A, Kasel M, Hoffmann E, et al. Multiparametric PET and MRI of myocardial damage after myocardial infarction: correlation of integrin $\alpha v \beta 3$ expression and myocardial blood flow. *Eur J Nucl Med Mol Imaging*. 2020;48(4):1070–80.
238. Lang CI, Doring P, Gabel R, Vasudevan P, Lemcke H, Muller P, et al. [(68)Ga]-NODAGA-RGD positron emission tomography (PET) for assessment of post myocardial infarction angiogenesis as a predictor for left ventricular remodeling in mice after cardiac stem cell therapy. *Cells*. 2020;9(6):1358.
239. Jenkins WS, Vesey AT, Stirrat C, Connell M, Lucatelli C, Neale A, et al. Cardiac $\alpha(V)\beta(3)$ integrin expression following acute myocardial infarction in humans. *Heart*. 2017;103(8):607–15.
240. Dimastromatteo J, Riou LM, Ahmadi M, Pons G, Pellegrini E, Broisat A, et al. In vivo molecular imaging of myocardial angiogenesis using the alpha(v)beta3 integrin-targeted tracer ^{99m}Tc -RAFT-RGD. *J Nucl Cardiol*. 2010;17(3):435–43.
241. Meoli DF, Sadeghi MM, Krassilnikova S, Bourke BN, Giordano FJ, Dione DP, et al. Noninvasive imaging of myocardial angiogenesis following experimental myocardial infarction. *J Clin Invest*. 2004;113(12):1684–91.
242. Meisel SR, Shapiro H, Radnay J, Neuman Y, Khaskia AR, Gruener N, et al. Increased expression of neutrophil and monocyte adhesion molecules LFA-1 and Mac-1 and their ligand ICAM-1 and VLA-4 throughout the acute phase of myocardial infarction: possible implications for leukocyte aggregation and microvascular plugging. *J Am Coll Cardiol*. 1998;31(1):120–5.
243. Ruparelina N, Digby JE, Jefferson A, Medway DJ, Neubauer S, Lygate CA, et al. Myocardial infarction causes inflammation and leukocyte recruitment at remote sites in the myocardium and in the renal glomerulus. *Inflamm Res*. 2013;62(5):515–25.
244. Seropian IM, Toldo S, Van Tassel BW, Abbate A. Anti-inflammatory strategies for ventricular remodeling following ST-segment elevation acute myocardial infarction. *J Am Coll Cardiol*. 2014;63(16):1593–603.
245. Ruparelina N, Chai JT, Fisher EA, Choudhury RP. Inflammatory processes in cardiovascular disease: a route to targeted therapies. *Nat Rev Cardiol*. 2017;14(3):133–44.
246. Lin QY, Lang PP, Zhang YL, Yang XL, Xia YL, Bai J, et al. Pharmacological blockage of ICAM-1 improves angiotensin II-induced cardiac remodeling by inhibiting adhesion of LFA-1(+) monocytes. *Am J Physiol Heart Circ Physiol*. 2019;317(6):H1301–H11.
247. Kourtzelis I, Mitroulis I, von Renesse J, Hajishengallis G, Chavakis T. From leukocyte recruitment to resolution of inflammation: the cardinal role of integrins. *J Leukoc Biol*. 2017;102(3):677–83.
248. Moccetti F, Brown E, Xie A, Packwood W, Qi Y, Ruggeri Z, et al. Myocardial infarction produces sustained Proinflammatory endothelial activation in remote arteries. *J Am Coll Cardiol*. 2018;72(9):1015–26.
249. Kaufmann BA, Lewis C, Xie A, Mirza-Mohd A, Lindner JR. Detection of recent myocardial ischaemia by molecular imaging of P-selectin with targeted contrast echocardiography. *Eur Heart J*. 2007;28(16):2011–7.
250. Li X, Bauer W, Israel I, Kreissl MC, Weirather J, Richter D, et al. Targeting P-selectin by gallium-68-labeled fucoidan positron emission tomography for noninvasive characterization of vulnerable plaques: correlation with in vivo 17.6T MRI. *Arterioscler Thromb Vasc Biol*. 2014;34(8):1661–7.
251. Mota R, Campen MJ, Cuellar ME, Garver WS, Hesterman J, Qutaish M, et al. (111) In-DANBIRT in vivo molecular imaging of inflammatory cells in atherosclerosis. *Contrast Media Mol Imaging*. 2018;2018:6508724.
252. Barrett HE, Meester EJ, van Gaalen K, van der Heiden K, Krenning BJ, Beekman FJ, et al. Imaging of inflammatory cellular protagonists in human atherosclerosis: a dual-isotope SPECT approach. *Eur J Nucl Med Mol Imaging*. 2020;47(12):2856–65.

253. Wang X, Peter K. Molecular imaging of Atherothrombotic diseases: seeing is believing. *Arterioscler Thromb Vasc Biol.* 2017;37(6):1029–40.
254. Debordeaux F, Chansel-Debordeaux L, Pinaquy JB, Fernandez P, Schulz J. What about alphavbeta3 integrins in molecular imaging in oncology? *Nucl Med Biol.* 2018;62-63:31–46.
255. Gronman M, Tarkia M, Kiviniemi T, Halonen P, Kuivanen A, Savunen T, et al. Imaging of alphavbeta3 integrin expression in experimental myocardial ischemia with [(68) Ga]NODAGA-RGD positron emission tomography. *J Transl Med.* 2017;15(1):144.
256. Thorn SL, Barlow SC, Feher A, Stacy MR, Doviak H, Jacobs J, et al. Application of hybrid matrix metalloproteinase-targeted and dynamic (201)Tl single-photon emission computed tomography/computed tomography imaging for evaluation of early Post-myocardial infarction remodeling. *Circ Cardiovasc Imaging.* 2019;12(11):e009055.
257. Kiugel M, Kyto V, Saanijoki T, Liljenback H, Metsala O, Stahle M, et al. Evaluation of (68) Ga-labeled peptide tracer for detection of gelatinase expression after myocardial infarction in rat. *J Nucl Cardiol.* 2018;25(4):1114–23.
258. Cuadrado I, Piedras MJ, Herruzo I, Turpin Mdel C, Castejon B, Reventun P, et al. EMMPRIN-targeted magnetic nanoparticles for in vivo visualization and regression of acute myocardial infarction. *Theranostics.* 2016;6(4):545–57.
259. Helm PA, Caravan P, French BA, Jacques V, Shen L, Xu Y, et al. Postinfarction myocardial scarring in mice: molecular MR imaging with use of a collagen-targeting contrast agent. *Radiology.* 2008;247(3):788–96.
260. Muzard J, Sarda-Mantel L, Loyau S, Meulemans A, Louedec L, Bantsimba-Malanda C, et al. Non-invasive molecular imaging of fibrosis using a collagen-targeted peptidomimetic of the platelet collagen receptor glycoprotein VI. *PLoS One.* 2009;4(5):e5585.
261. Kim H, Lee SJ, Kim JS, Davies-Venn C, Cho HJ, Won SJ, et al. Pharmacokinetics and micro-biodistribution of 64Cu-labeled collagen-binding peptides in chronic myocardial infarction. *Nucl Med Commun.* 2016;37(12):1306–17.
262. Wildgruber M, Bielicki I, Aichler M, Kosanke K, Feuchtinger A, Settles M, et al. Assessment of myocardial infarction and postinfarction scar remodeling with an elastin-specific magnetic resonance agent. *Circ Cardiovasc Imaging.* 2014;7(2):321–9.
263. Verjans JW, Lovhaug D, Narula N, Petrov AD, Indrevoll B, Bjurgert E, et al. Noninvasive imaging of angiotensin receptors after myocardial infarction. *JACC Cardiovasc Imaging.* 2008;1(3):354–62.
264. Higuchi T, Fukushima K, Xia J, Mathews WB, Lautamaki R, Bravo PE, et al. Radionuclide imaging of angiotensin II type 1 receptor upregulation after myocardial ischemia-reperfusion injury. *J Nucl Med.* 2010;51(12):1956–61.
265. Fukushima K, Bravo PE, Higuchi T, Schuleri KH, Lin X, Abraham MR, et al. Molecular hybrid positron emission tomography/computed tomography imaging of cardiac angiotensin II type 1 receptors. *J Am Coll Cardiol.* 2012;60(24):2527–34.
266. Odaka K, Uehara T, Arano Y, Adachi S, Tadokoro H, Yoshida K, et al. Noninvasive detection of cardiac repair after acute myocardial infarction in rats by 111 in fab fragment of monoclonal antibody specific for tenascin-C. *Int Heart J.* 2008;49(4):481–92.
267. Song J, Yu J, Li Y, Lu S, Ma Z, Shi H. MR targeted imaging for the expression of tenascin-C in myocardial infarction in vivo. *J Magn Reson Imaging.* 2017;45(6):1668–74.
268. Nahrendorf M, Sosnovik D, Chen JW, Panizzi P, Figueiredo JL, Aikawa E, et al. Activatable magnetic resonance imaging agent reports myeloperoxidase activity in healing infarcts and noninvasively detects the antiinflammatory effects of atorvastatin on ischemia-reperfusion injury. *Circulation.* 2008;117(9):1153–60.
269. Wang C, Keliher E, Zeller MWG, Wojtkiewicz GR, Aguirre AD, Buckbinder L, et al. An activatable PET imaging radioprobe is a dynamic reporter of myeloperoxidase activity in vivo. *Proc Natl Acad Sci U S A.* 2019;116(24):11966–71.
270. Anstensrud AK, Woxholt S, Sharma K, Broch K, Bendz B, Aakhus S, et al. Rationale for the ASSAIL-MI-trial: a randomised controlled trial designed to assess the effect of tocilizumab on myocardial salvage in patients with acute ST-elevation myocardial infarction (STEMI). *Open Heart.* 2019;6(2):e001108.

271. Rangasamy L, Geronimo BD, Ortin I, Coderch C, Zapico JM, Ramos A, et al. Molecular imaging probes based on matrix metalloproteinase inhibitors (MMPi). *Molecules*. 2019;24(16):2982.
272. Nian M, Lee P, Khaper N, Liu P. Inflammatory cytokines and postmyocardial infarction remodeling. *Circ Res*. 2004;94(12):1543–53.
273. Sun Y, Wang Y, Yang H, Lu Y, Zhu G, Yang L, et al. Interleukin 8 targeted contrast echocardiography is effective to evaluate myocardial ischemia-reperfusion injury in the rabbits. *Biomed Pharmacother*. 2019;109:1346–50.
274. Liu Z, Barber C, Wan L, Liu S, Hui MM, Furenli LR, et al. SPECT imaging of inflammatory response in ischemic-reperfused rat hearts using a ^{99m}Tc-labeled dual-domain cytokine ligand. *J Nucl Med*. 2013;54(12):2139–45.
275. Valenta I, Pacher P, Dilsizian V, Schindler TH. Novel myocardial PET/CT receptor imaging and potential therapeutic targets. *Curr Cardiol Rep*. 2019;21(7):55.
276. Shirani J, Dilsizian V. Imaging left ventricular remodeling: targeting the neurohumoral axis. *Nat Clin Pract Cardiovasc Med*. 2008;5(Suppl 2):S57–62.
277. Diekmann J, Koenig T, Zwadlo C, Derlin T, Neuser J, Thackeray JT, et al. Molecular imaging identifies fibroblast activation beyond the infarct region after acute myocardial infarction. *J Am Coll Cardiol*. 2021;77(14):1835–7.
278. Totzeck M, Siebermair J, Rassaf T, Rischpler C. Cardiac fibroblast activation detected by positron emission tomography/computed tomography as a possible sign of cardiotoxicity. *Eur Heart J*. 2020;41(9):1060.
279. Taki J, Inaki A, Wakabayashi H, Imanaka-Yoshida K, Ogawa K, Hiroe M, et al. Dynamic expression of tenascin-C after myocardial ischemia and reperfusion: assessment by 125I-anti-tenascin-C antibody imaging. *J Nucl Med*. 2010;51(7):1116–22.
280. Cal-Gonzalez J, Rausch I, Shiyam Sundar LK, Lassen ML, Muzik O, Moser E, et al. Hybrid imaging: instrumentation and data processing. *Front Phys*. 2018;6:47.
281. Nolte T, Gross-Weege N, Schulz V. (hybrid) SPECT and PET technologies. *Recent Results Cancer Res*. 2020;216:111–33.
282. Lau JMC, Laforest R, Sotoudeh H, Nie X, Sharma S, McConathy J, et al. Evaluation of attenuation correction in cardiac PET using PET/MR. *J Nucl Cardiol*. 2017;24(3):839–46.
283. Rischpler C, Siebermair J, Kessler L, Quick HH, Umutlu L, Rassaf T, et al. Cardiac PET/MRI: current clinical status and future perspectives. *Semin Nucl Med*. 2020;50(3):260–9.
284. Wilk B, Wisenberg G, Dharmakumar R, Thiessen JD, Goldhawk DE, Prato FS. Hybrid PET/MR imaging in myocardial inflammation post-myocardial infarction. *J Nucl Cardiol*. 2020;27(6):2083–99.
285. Nensa F, Bamberg F, Rischpler C, Menezes L, Poeppel TD, la Fougere C, et al. Hybrid cardiac imaging using PET/MRI: a joint position statement by the European Society of Cardiovascular Radiology (ESCR) and the European Association of Nuclear Medicine (EANM). *Eur Radiol*. 2018;28(10):4086–101.

Part IV
Infection



Tevfik F. Ismail, Philip Haaf, and Assuero Giorgetti

Contents

6.1 Pericardial Anatomy.....	163
6.2 Pericardial Pathologies.....	165
6.3 Aetiology and Pathophysiology.....	166
6.4 Clinical Manifestations and Diagnosis.....	168
6.5 Computed Tomography.....	169
6.6 Cardiovascular Magnetic Resonance (CMR).....	170
6.7 Molecular Imaging.....	184
6.8 Basics of Treatment.....	186
6.9 Conclusion.....	186
References.....	187

6.1 Pericardial Anatomy

The normal pericardium consists of two principal layers: an outer fibrous layer made up of collagen and to a lesser extent elastin and an inner serous layer of ciliated mesothelium that covers the myocardium and great vessels (visceral pericardium) and reflects back to form the serous inner surface of the fibrous layer (parietal pericardium) [1, 2]. The tough outer sac functions as a barrier to infection, prevents excessive cardiac motion, and helps to maintain interventricular dependence by

T. F. Ismail

King's College London & Guy's and St Thomas' NHS Foundation Trust, London, UK

P. Haaf

Clinic of Cardiology, University Hospital Basel and University of Basel, Basel, Switzerland

A. Giorgetti (✉)

Fondazione CNR/Regione Toscana "Gabriele Monasterio", Pisa, Italy

e-mail: asso@ftgm.it

limiting cardiac distension (Fig. 6.1). Histologically, the pericardium is typically 1 mm thick and therefore approaches the limits of the spatial resolution of cardiac imaging techniques. The parietal pericardium is often apposed with a variable amount of epicardial fat which serendipitously provides intrinsic contrast on cardiovascular magnetic resonance imaging (CMR, Fig. 6.2). However, the relative absence of epicardial fat over the lateral wall of the left ventricle in some individuals can make it challenging to differentiate the pericardium from surrounding lung tissue. The fibrous pericardium itself is attached to the sternum anteriorly, the diaphragm inferiorly, and to the thoracic vertebrae posteriorly by the pericardial ligaments. Superiorly, it extends to the proximal aortic arch just prior to the origin of the innominate, and to the level of the pulmonary artery bifurcation [1]. The

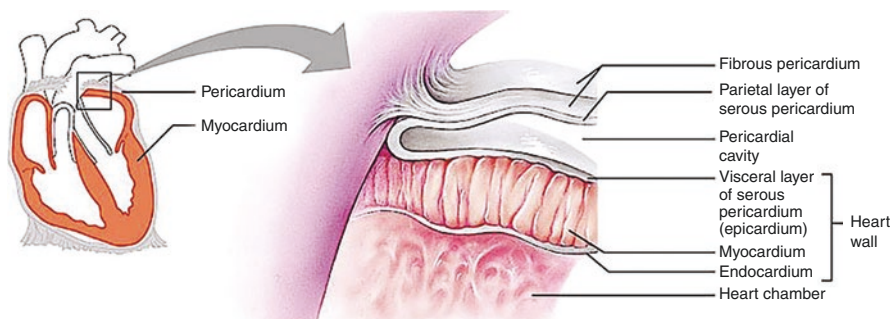


Fig. 6.1 The pericardial layers and layers of the heart wall. Note that the visceral layer of the pericardium and the epicardium of the heart are the same structure. From: Pearson Education 2013, Chapter 18, The cardiovascular system: The heart: Part A

Fig. 6.2 Axial Half-Fourier Acquisition Single-Shot Turbo Spin Echo (HASTE) commonly used as a pilot scout. The pericardium is a thin often barely perceptible structure (white arrows) best seen anteriorly where the contrast with RV epicardial fat can help render it visible. Over the lateral wall where there is a relative paucity of fat, and the pericardium is related to lung tissue, it can be challenging to discern

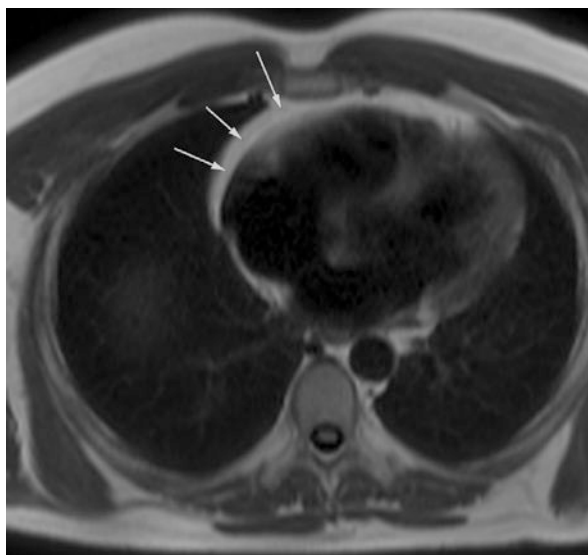
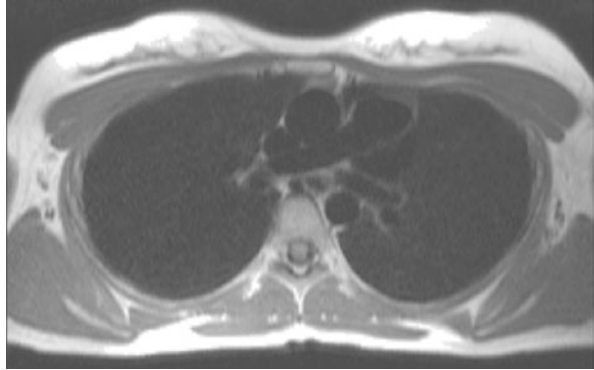


Fig. 6.3 Lung parenchyma interposed between the aorta and pulmonary trunk in a patient with congenital absence of the pericardium



presence of congenital absence of the pericardium can therefore be inferred by interposition of a tongue of lung parenchyma between the ascending aorta and the main pulmonary artery (which would normally be excluded by intact pericardium) or lung tissue between the inferior surface of the heart and the diaphragm [3] (Fig. 6.3). The inner serous layer is too thin to directly image in health. Its ciliated surface facilitates the synthesis and resorption of pericardial fluid which is a dynamic process and physiologically can reach up to 50 ml in volume. The fluid serves to reduce friction between the myocardium and surrounding structures. It tends to congregate around the atrioventricular grooves hinting at its role in lubricating the motion of the coronary arteries. In most patients who are imaged supine, it is not usually possible to see a complete layer of fluid surrounding the whole myocardium unless an effusion is present.

6.2 Pericardial Pathologies

Pericardial abnormalities include several pathological conditions (pericardial effusion, pericardial constriction, tamponade, pneumopericardium, fistulas, pericardial rupture, congenital abnormalities, pericardial tumours) but inflammation of pericardial layers is the most frequent disease of the pericardium worldwide. It often occurs in young and middle-aged subjects. Exact epidemiological data for acute pericarditis are lacking. In Italy, an incidence of about 28 cases/100,000/year has been reported [4]. In a Finnish national registry, the rate of hospitalisation for acute pericarditis was 3.32 per 100,000 person/years, with men more affected than women [5]. Non-specific symptoms, which may overlap with other diseases such as myocarditis, acute coronary syndrome or Takotsubo syndrome, may complicate the diagnosis of pericarditis. In the emergency department, pericarditis is diagnosed in about 5% of patients with non-ischaemic chest pain and the in-hospital mortality is relatively low (about 1.1%) [6, 7]. This could produce the misconception that pericarditis is a benign disease with low morbidity and mortality. However, the exact incidence of pericarditis is probably underestimated and if not diagnosed and properly treated, the disease tends to recur, it can become chronic and it can entail

serious complications. A recent database analysis in the USA (years 2016 and 2017), including 21,335 patients hospitalised for acute pericarditis, found a rate of 30-day readmission of 12.9% [8]. In-hospital mortality was significantly higher following readmission than for the index hospitalisation (3.4% vs 1.0%, $p < 0.001$). Therefore, a high level of clinical suspicion and multimodal imaging is crucial for the prompt identification of the disease and the correct management of the patient to minimise possible complications and to ameliorate the patient's outcome.

6.3 Aetiology and Pathophysiology

Inflammation of pericardial layers can have both an infectious and non-infectious aetiology. In developed countries, most cases (80–90%) are labelled as “idiopathic” and probably have a viral origin [6, 7]. Other relatively frequent infectious aetiologies are tuberculous pericarditis (about 4%) and purulent pericarditis (<1%). Non-infectious pericarditis can occur in primary or secondary metastatic tumours (5–10%), in systemic inflammatory diseases, and pericardial injury syndromes (2–7%) [9–11]. In a recent prospective cohort of 1162 patients, Gouriet et al. found a lower incidence of idiopathic cases (55%) and a higher number of autoimmune or post-cardiac injury syndromes (24%) [12]. It is likely that, in developed countries, ageing of the population increases cardiovascular invasive procedures and the risk of pericardial complications. Conversely, in developing countries the most frequent cause of pericarditis is tuberculosis (70%), often associated with human immunodeficiency virus and poor outcome (40% mortality) [13]. Common causes of acute pericarditis are summarised in Table 6.1.

Inflammation of pericardium may be an acute, subacute, or chronic fibrinous, “non-effusive” or exudative process that reflects the aetiology of the disease [14]. With infectious aetiologies, the response to injury is the exudation of fluid, fibrin, and inflammatory cells. Healing can lead to an obliteration of the pericardial space by adhesions between the pericardial layers and, sometimes, late focal or extensive calcification. Following acute coronary syndrome, trauma or pericardiectomy, a post-cardiac injury syndrome can occur. The damage of the pericardial layers is thought to release cardiac antigens that stimulate an immune response and sustain the inflammatory process.

When the amount of fluid in the pericardial space exceeds the normal 15–50 ml, a pericardial effusion is present. The amount and the rate of accumulation of pericardial effusion, the thickness and compliance of pericardium, and the coexistence of heart diseases influence the clinical presentation of the disease. Cardiac tamponade is a serious complication in which the pericardial effusion increases pericardial pressure and determines a compression of the cardiac chambers. Haemodynamic consequences are reduced cardiac filling, an exaggerated expiratory decrease in aortic systolic pressure (*pulsus paradoxus*) and arterial hypotension. Acute tamponade is sudden and life-threatening, and it requires a prompt diagnosis because pericardiocentesis may be life-saving. Persistence of pericarditis or recurrence of the disease, cardiac surgery or radiation therapy can result in a constrictive pericarditis.

Table 6.1 Aetiology of pericarditis

Infectious pericarditis	Prevalence	Non-infectious pericarditis	Prevalence
<i>Viral</i> (coxsackievirus; echovirus; influenza; Epstein-Barr virus; cytomegalovirus; parvovirus B19; human herpes virus 6; varicella; rubella; adenovirus; human immunodeficiency virus; hepatitis B, C viruses, COVID19)	Common in developed countries (80–90% labelled as “idiopathic” and probably of viral origin)	<i>Autoimmune</i> (post-myocardial infarction; post-pericardiectomy; posttraumatic; in systemic autoimmune diseases: Systemic sclerosis; lupus; vasculitis)	Relatively frequent (range 10–24%)
<i>Bacterial</i> (tuberculous; pneumococci; meningococci; <i>Coxiella burnetii</i> ; <i>Haemophilus</i> ; <i>chlamydia</i> ; <i>mycoplasma</i> ; staphylococci)	Frequent in developing countries (tuberculosis 70%), uncommon or rare in developed regions	<i>Neoplastic</i> (primary tumour: mesothelioma; metastatic tumours: lung cancer, breast cancer; lymphoma)	Relatively rare (5–10%)
<i>Fungal and parasitic</i> (histoplasmosis; candida; aspergillosis; echinococcus; toxoplasma)	Rare, more likely in immunosuppressed patients	<i>Metabolic</i> (myxoedema; uraemia)	Rare

Table 6.2 Aetiology of constrictive pericarditis and associated clinical features

Aetiology	Clinical features/diagnostic clues
Idiopathic	Absence of other positive features/findings, i.e., a diagnosis of exclusion
Tuberculosis	Cavitating lung lesions, pulmonary consolidation
Purulent bacterial pericarditis	Associated pulmonary consolidation, history of instrumentation/surgery/trauma
Surgery	Sternotomy wires or other features of cardiothoracic or other surgical intervention
Trauma	Bony injury, haemopericardium
Radiation	Features of radiation-associated RV disease or coronary disease
Neoplastic	Signs of underlying neoplasm, e.g., metastases, tumour deposits, pleural effusions
Autoimmune rheumatic disease	Multi-organ involvement, signs of associated myocarditis
Sarcoid	Mediastinal lymphadenopathy, pulmonary fibrosis, myocardial involvement (see Chap. 5)
Asbestosis	Pleural thickening, round atelectasis, mesothelioma, bronchogenic carcinoma, interstitial fibrosis

This is a condition in which a thickened-inelastic, inflamed, fibrotic and/or calcified pericardium limits cardiac diastolic filling, reduces ventricular volumes and stroke volumes. Table 6.2 summarises common causes of constrictive pericarditis and associated clinical features.

6.4 Clinical Manifestations and Diagnosis

Some red flags leading to clinical suspicion of inflammation of the pericardial layers include chest pain, pericardial friction rubs, electrocardiographic changes, and new or worsening of pericardial effusion.

The chest pain of acute pericarditis is sudden in onset, retrosternal, it changes with the position of the patient (improved by sitting up and leaning forward) and can be exacerbated by inspiration (pleuritic). Sometimes dull and oppressive, radiating to the neck, arms and shoulders, it mimics an acute coronary syndrome and patients may even be submitted to urgent coronary angiography [15]. An audible friction rub, reported in about one-third of cases and linked to increased friction of inflamed pericardial layers, is considered highly suggestive for pericarditis. Typical ECG changes in acute pericarditis include widespread upward concave ST-segment elevation and PR-segment depression and can evolve in four stages of abnormalities [16, 17]. Low QRS voltage and isolated ST-T abnormalities are common in constrictive pericarditis. In this case, peripheral oedema and exertional fatigue or dyspnoea are frequent and associated with an elevated jugular venous pressure.

Serological markers of inflammation confirm the presence of an active process but they provide little information on the aetiology. Considering the prevalence of “idiopathic” forms, viral cultures and antibody titres are often investigated but rarely useful [18]. For the same reason, routine serological tests for autoimmune disease are not recommended. Tuberculin skin test or QuantiFERON-TB assay needs to be assessed in the suspicion of tuberculous pericarditis, particularly in developing countries. Elevation of serum troponins raises the clinical suspicion of myopericarditis, and can be observed in about 20–30% of patients and is associated with a higher rate of complications [19].

Chest radiography has been used in the past but is often of limited value unless in the case of a massive pericardial effusion or if pericardial calcifications are present (25% of cases of constrictive pericarditis). However, a chest radiograph can detect concomitant lung, mediastinal, and pleural diseases of which pericarditis is a clinical manifestation (e.g., pulmonary tuberculosis, lung cancer). Transthoracic Doppler echocardiography is the first-line imaging modality because it is widely available and safe. Echocardiography allows the assessment of the presence and the amount of pericardial effusion, permits the identification of cardiac tamponade, can be used to guide pericardiocentesis and remains the method of choice for the follow-up of pericardial diseases [20]. An abnormal ventricular septal motion to the left in early diastole, in inspiration, due to the enhanced ventricular interdependence (septal bounce) should alert the cardiologist to consider the diagnosis of constriction. Other echocardiographic findings include normal ventricular systolic function and thickened pericardium, and vena cava dilatation with little respiratory variation (suggestive of elevated right atrial pressures).

Fever at presentation, leucocytosis, a subacute course, important pericardial effusion and lack of response to initial therapy are considered markers of adverse prognosis and identify patients that may need hospitalisation [21].

Table 6.3 Diagnostic criteria for pericarditis (modified from reference 22)

Pericarditis	Diagnostic criteria
Acute	Pericardial inflammation with at least 2 of the following criteria: 1. Chest pain (sudden in onset, changes with the position, exacerbated by inspiration). 2. Audible friction rub. 3. ECG changes (widespread upward concave ST-segment elevation, PR-segment depression) 4. New onset or worsening of pericardial effusion Additional criteria: a. Elevation of serological markers of inflammation b. Pericardial inflammation on CT and/or CMR
Incessant	Persistent pericarditis for 2–4 weeks without remission (<3 months)
Recurrent	Recurrence of the disease following an acute episode with a symptoms-free period >4–6 weeks
Chronic	Pericarditis lasting >3 months

The European Society of Cardiology (ESC) has established diagnostic criteria for the diagnosis of acute and recurrent pericarditis (level of evidence C) [22] (Table 6.3). Diagnosis of acute pericarditis requires the presence of at least two clinical criteria among chest pain, pericardial friction rubs, electrocardiographic changes and pericardial effusion. Diagnosis of recurrent pericarditis needs the presence of a documented first attack of acute pericarditis, a symptom-free interval of 4–6 weeks or longer, recurrent pain combined with other symptoms and serological findings. Evidence of inflammation of the pericardial layers by an imaging technique is considered as an additional supportive criterion. However, contemporary diagnosis and patient management cannot ignore a multimodal imaging approach, including second-level imaging techniques such as computed tomography, cardiovascular magnetic resonance and molecular imaging.

6.5 Computed Tomography

Cardiac CT is increasingly used in clinical practice, mainly to study coronary arteries but it is able to provide morphological information about all cardiac structures. Baseline non-contrast and contrast-enhanced CT images permit the identification of thickened pericardium by an inflammatory process or tumours [23, 24], and the presence of calcification of pericardial layers. Although thickened pericardium can be observed in constrictive pericarditis, it does not prove the presence of constriction [25]. Conversely, a “normal” pericardium on CT images does not exclude the presence of constriction [26]. Moreover, inflamed pericardium may show contrast enhancement. CT is superior to echocardiography for the characterisation of pericardial effusion [27]. Generally, pericardial effusion has a low density (0–20 HU) but a high protein concentration, such as in infective aetiology or when the effusion is haemorrhagic, can increase density up to 50HU. These data can be used to speculate about the aetiology of the disease as serous fluid is more common in viral

pericarditis while tuberculous, neoplastic, and purulent pericarditis tend to produce more haemorrhagic exudates. CT can also reveal valuable ancillary findings, such as the presence of mediastinal lymphadenopathy, enlargement of the atria and venae cavae in cases of pericardial constriction, and can be used for disease staging where neoplasia is the culprit.

ESC guidelines do not recommend CT in acute pericarditis with small or no effusion, while in presence of moderate to severe effusion, the use of CT could be reasonable. In cardiac tamponade, CT imaging is considered reasonable to confirm the clinical suspicion of aortic dissection or to confirm diagnosis in case of thoracic trauma. In constrictive pericarditis, a CT scan is reasonable if echocardiography is inconclusive or to plan a pericardiectomy. CT imaging of the pericardium is not recommended in patients with severely decreased renal insufficiency (eGFR < 30 ml/min/1.73 m²) and during pregnancy [22].

6.6 Cardiovascular Magnetic Resonance (CMR)

6.6.1 Typical CMR Protocol for the Evaluation of Pericardial Disease

The full gamut of sequences available for modern CMR needs to be used to comprehensively evaluate pericardial disease and refine differential diagnosis [28]. These are summarised in Table 6.4. Pericardial thickness should be evaluated on breath-held T1-weighted turbo spin echo sequences as these afford excellent tissue contrast and are less liable to motion and susceptibility effects that can result in overestimation of pericardial thickness. These are best done in an axial configuration to maximally leverage the intrinsic contrast afforded by pericardial fat which usually overlies the bulk of the right ventricle (RV) even in slim individuals. Comprehensive bright and black blood scouts in axial, sagittal, and coronal orientations can be invaluable for detecting extracardiac pathology that may give clues to the aetiology of the underlying pericardial disease. T2-weighted spin echo sequences with fat saturation (achieved either through inversion recovery or spectral pre-saturation techniques) performed in long axis (2 chamber, 4 chamber, 3 chamber) and short-axis orientations can be helpful for delineating acute myocardial and pericardial inflammation which results in increased extracellular water and increased mobility of intracellular water in injured cells. Balanced steady-state-free-precession (SSFP) cine sequences are being used to evaluate cardiac function (Fig. 6.4) and may also be used to visualise the pericardium. Tagging sequences in 4 chamber and representative short-axis orientations can be helpful to identify pericardial adhesions or confirm appropriate slippage between the myocardium and the surrounding pericardium or other structures [29] (Fig. 6.5). Late gadolinium enhancement (LGE) imaging is then conducted in the normal way and can reveal the concomitant presence of myocarditis or contrast uptake by the inflamed pericardium. The normal pericardium does not avidly take up contrast, however, LGE sequences (which are inversion recovery prepared heavily T1-weighted sequences) can be complementary to

Table 6.4 Summary of CMR protocol for the Evaluation of pericardial disease

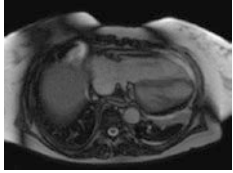
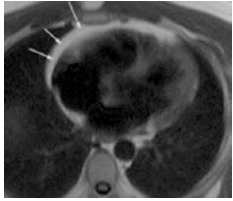
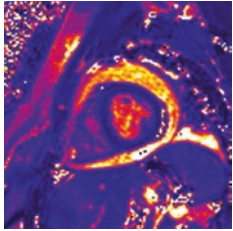
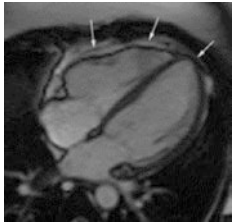


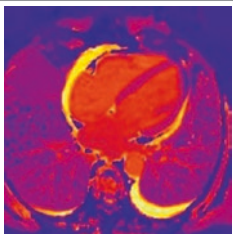
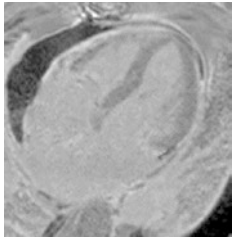
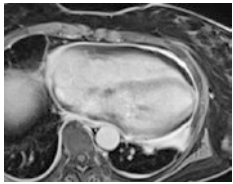
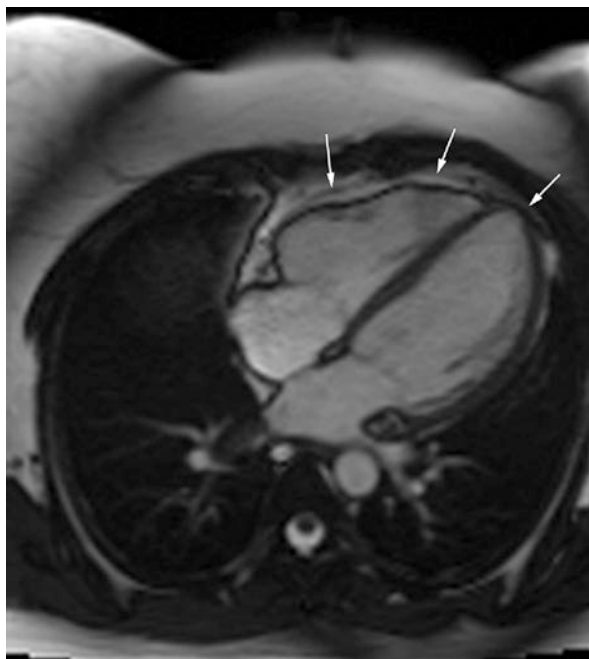
Sequence		Main findings
<i>Scouts/localisers (bright and black blood)</i>		Extracardiac findings <ul style="list-style-type: none"> • Pleural effusions, • Parenchymal lung abnormalities, • Lymphadenopathy
<i>Axial T1-Turbo spin Echo (without fat saturation)</i>		Morphological assessment <ul style="list-style-type: none"> • Pericardial thickness and effusion, • Pericardial lesions and tumours
<i>T2w-imaging/T2 mapping</i>		Oedema <ul style="list-style-type: none"> • Myocardial inflammation/oedema, • Pericardial inflammation/oedema
<i>Balanced SSFP cine sequences</i>		<u>Haemodynamic assessment</u> <ul style="list-style-type: none"> • Global and regional contractile dysfunction (concomitant myocarditis?) • Haemodynamic relevance of pericardial effusion (RV/RA collapse), loculation, fibrous stands in pericardial effusion, • Septal bounce (increased interventricular dependence)
<i>Tagging</i>		Constrictive pericarditis <ul style="list-style-type: none"> • Pericardial adhesions
<i>Real-time cine imaging</i>		Dynamic effects <ul style="list-style-type: none"> • Increased ventricular interdependence during deep inspiration

Table 6.4 (continued)

Sequence		Main findings
<i>Native T1 mapping</i>		Characterisation of pericardial effusion <ul style="list-style-type: none"> • Pericardial effusion vs. epi-/paracardial fat, • Transudative vs. exudative pericardial effusion vs. haemopericardium
<i>LGE with PSIR reconstruction</i>		Active pericardial inflammation <ul style="list-style-type: none"> • Pericardial inflammation and concomitant myocardial injury (myocarditis or infarction). • Confirm presence of pericardial effusions (black/signal poor on PSIR reconstructions)
<i>ECG-gated Dixon fat-water separation sequences</i>		Characterisation of pericardium <ul style="list-style-type: none"> • Pericardial thickness, • Pathological pericardial contrast uptake/active inflammation

SSFP steady-state-free-precession, *LGE* late gadolinium enhancement, *PSIR* phase-sensitive inversion recovery

Fig. 6.4 Balanced steady-state free precession cine sequence in the horizontal long-axis orientation. This sequence has high intrinsic T1 and T2 contrast and is best used to evaluate cardiac function. The pericardium can be seen as a thin black line (arrows)



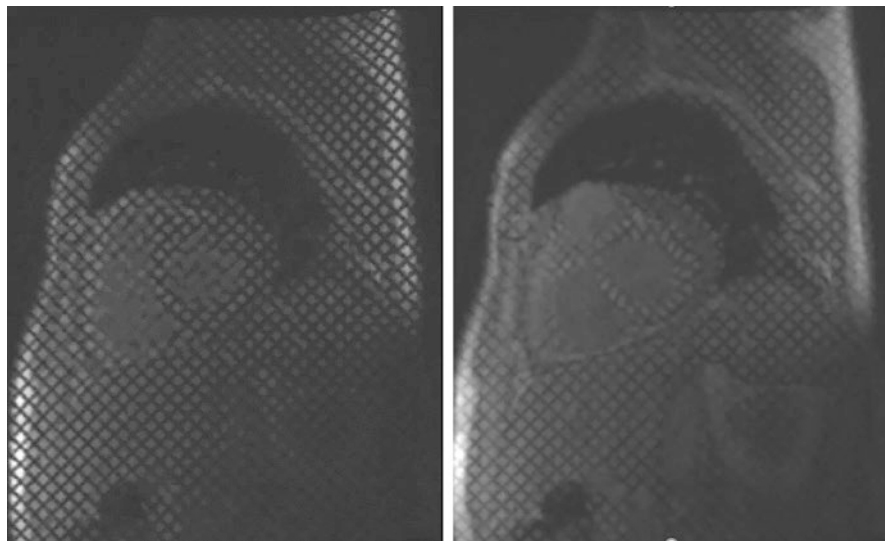


Fig. 6.5 Tagging sequence at mid-ventricular short-axis level demonstrating appropriate slippage between myocardium and surrounding pericardium

T1-TSE for evaluating pericardial anatomy (Fig. 6.6). ECG-gated Dixon fat-water separation sequences may be helpful for the assessment of pericardial thickness and confirm pericardial late enhancement of LGE sequences. Finally, real-time free breathing sequences (Fig. 6.7) are undertaken for assessment of pericardial constriction/constrictive pericarditis. Images are acquired over 10–20 s in a mid-ventricular short-axis orientation and/or 4-chamber orientation with the patient asked to take gentle breaths in and out [5, 6]. A breath hold should be avoided for this acquisition so as not to engender an inadvertent Valsalva manoeuvre that might confound the interpretation of septal motion.

6.6.2 CMR and Acute Pericarditis

Most cases of pericarditis are idiopathic and presumed viral in aetiology (see Table 6.1). Pericarditis can be categorised as acute (<4–6 weeks), incessant (>4–6 weeks), recurrent (with symptom-free interval of 4–6 weeks), or chronic (>3 months) [22, 30] (see Table 6.2). If required for diagnostic purposes, an effusion can usually be readily visualised by echocardiography. CMR or other advanced imaging is seldom required. However, CMR may play a role in the assessment of patients with “red flags” including a history of fever, trauma, a large effusion (>20 mm), history of systemic autoimmune disease, immunodeficiency or failure to respond to conventional anti-inflammatory therapy which usually consists of non-steroidal anti-inflammatory drugs (NSAIDs) and colchicine. CMR should also be considered in any patient with signs of accompanying myocardial contractile

Fig. 6.6 Late gadolinium enhancement sequences are heavily T1 weighted and so can be used to evaluate pericardial anatomy. With normal inversion times set to null the myocardium, in the late phase, normal pericardium appears black (arrows)

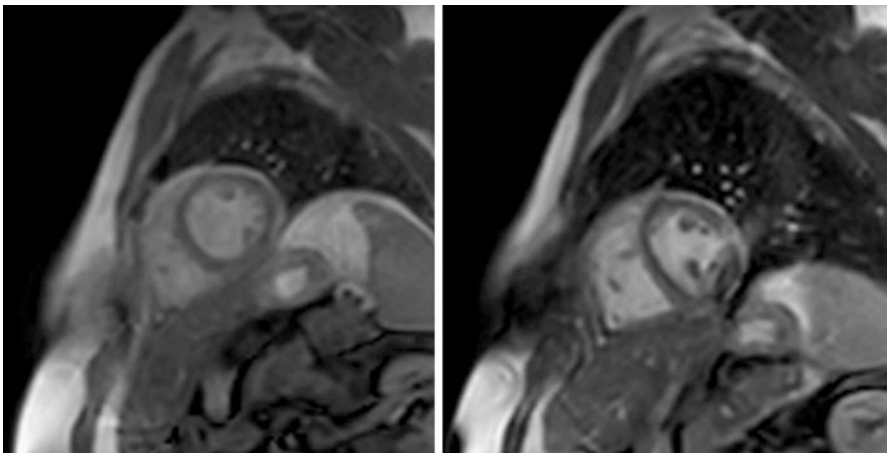
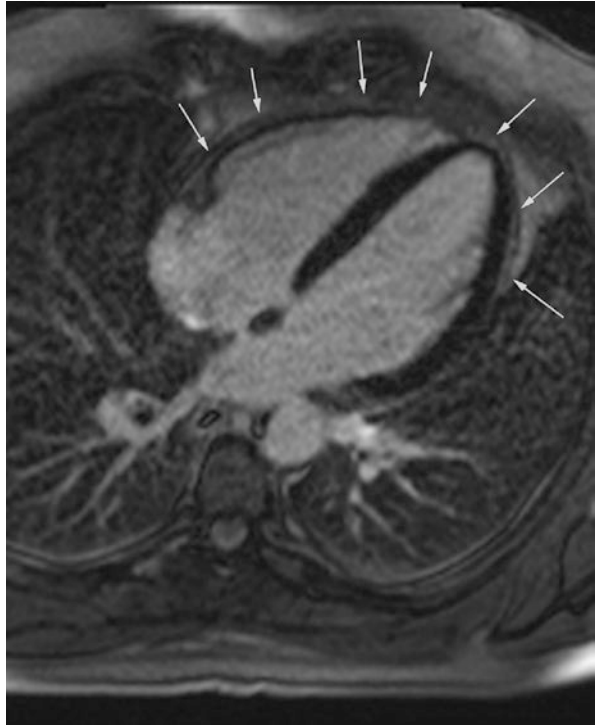


Fig. 6.7 Real-time free-breathing short-axis cine in a patient with pericardial constriction demonstrating increased inter-ventricular interdependence. At end-expiration (left) the left ventricle is circular with the septum convex to the left. During inspiration (note the position of the dome of the diaphragm), as RV filling increases, and LV filling falls, the interventricular septum is displaced towards the left

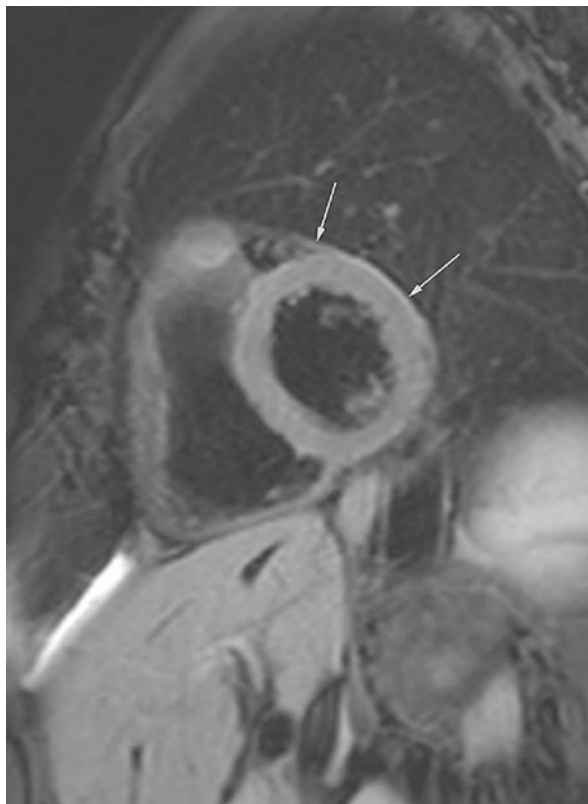
Fig. 6.8 Mid-ventricular short-axis T2-Weighted spin echo sequence in a patient with acute pericarditis. There is hyperintensity of the visceral and parietal pericardium reflecting pericardial inflammation and increased interstitial water content



dysfunction or biochemical evidence of necrosis which may point to the presence of a limited amount of myocarditis (myopericarditis) or to myocarditis being the dominant pathology (peri-myocarditis) [25] (see also Chap. 7/Myocarditis).

The acutely inflamed pericardium may be thickened. There may be an associated exudative effusion; however, the absence of this does not exclude active pericarditis as particularly in the early phases, the amount of fluid production can be balanced by resorption resulting in little or no new fluid accumulation. The pericardium may be high signal on T2W spin echo sequences, whereas healthy pericardium is not normally clearly seen (Figs. 6.8 and 6.9). Late enhancement sequences may reveal contrast uptake by the pericardium as inflammation causes expansion of the pericardial interstitium (Fig. 6.10). The pericardium is normally relatively avascular and does not readily enhance in the late phase with conventionally chosen inversion times. Although enhancement can signify inflammation [31], it can sometimes persist even after acute inflammation has settled owing to neovascularisation of the pericardium itself in response to chronic inflammation. This may suggest potential responsiveness to anti-inflammatory interventions to prevent the emergence of constriction [32]. Observational data has also suggested that CMR may be useful to

Fig. 6.9 Mid-ventricular short-axis T2-Weighted short-tau inversion recovery sequence in a patient with recovering pericarditis. The pericardium appears high signal (white arrows)



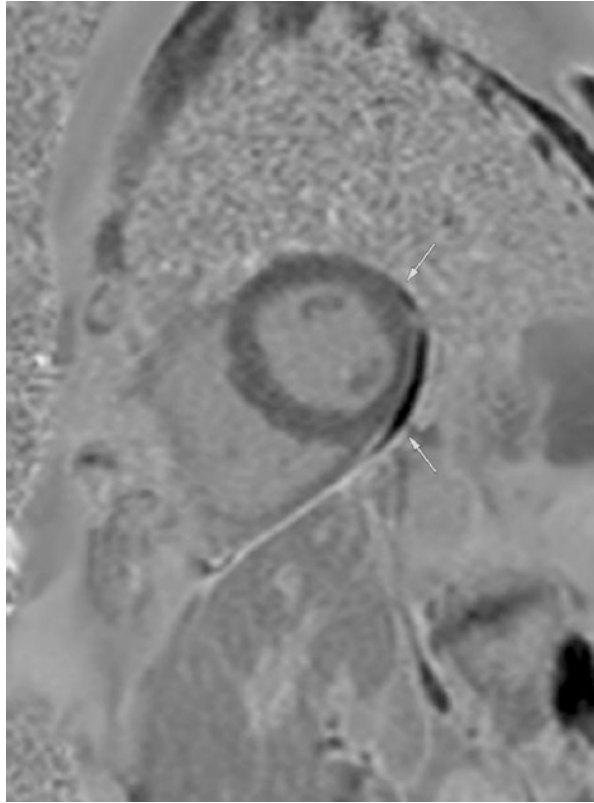
objectify response to therapy and guide the tapering of steroids in patients with recurrent pericarditis [33].

6.6.3 CMR and Pericardial Effusions

A pericardial effusion is the excess accumulation of fluid in the pericardial space as a result of pericardial fluid production exceeding resorption or the addition of extrinsic fluid to the pericardial space. As with pleural effusions, the aetiologies can be classified under two principal umbrellas: transudative and exudative. In both the latter situations, the fluid originates from the serosal pericardial layers. Fluid can also enter the pericardial space from extrinsic sources, e.g., blood from trauma, aortic dissection, or surgery giving rise to a haemopericardium and chyle from injury to the thoracic duct giving rise to chylopericardium.

Transudates occur due to an alteration in the balance of hydrostatic forces most commonly through impaired venous drainage. Normal pericardial venous drainage occurs into the superior vena cava via the azygos system. As a result, chronic elevations of systemic venous pressure, e.g., chronic right heart failure, tricuspid regurgitation, pulmonary hypertension, can give rise to transudative effusions. Increased

Fig. 6.10 Mid-ventricular short-axis late gadolinium enhancement sequence with phase-sensitive inversion recovery reconstruction in a patient with recovering pericarditis. The pericardium appears high signal/enhanced in contrast to the normal pericardium in Fig. 6.5. There is a thin rim of pericardial fluid next to the lateral wall which is black reflecting the comparatively long T1 of water



fluid shift can also occur in conditions such as nephrotic syndrome and in other states of systemic fluid overload. By definition, the protein content of transudates relative to their water content is low.

Exudates in contrast develop as a result of serosal pericardial inflammation or pericarditis and have a relatively high protein content. Their differential diagnosis therefore closely reflects that of pericarditis.

Echocardiography remains the first modality of choice for the diagnosis and evaluation of pericardial effusions. Especially where there is a clinical concern about haemodynamic instability or potential cardiac tamponade, it is rarely advisable to transfer the patient to the confines of the MR-environment. However, outside of this scenario, CMR can add considerable value by allowing: (1) rapid evaluation of the presence, size, and location of effusions, particularly if loculation is present, thereby guiding drainage; (2) detecting concomitant pericarditis and/or myocardial injury (see section on Pericarditis above); and (3) where diagnostic pericardiocentesis is not planned, evaluation of effusion signal characteristics in the wider clinical context may help with classification of the effusion as an exudate or transudate.

The haemodynamic importance of a pericardial effusion is determined not only by its size/volume but by its rate of formation or accumulation. A small but rapidly

developing effusion gives little time for the pericardium to stretch and accommodate the additional fluid and so can produce more significant effects than larger effusions that develop more slowly. The grading of effusion size (measured in end-diastole on b-SSFP cine sequences) is therefore somewhat moot, but in general, effusions ≤ 1 cm are considered small, 1–2 cm moderate, and > 2 cm in depth large [34]. The usual approaches to percutaneous drainage are sub-xiphoid or transapical. A description of the depth of the effusion at these potential access sites can therefore be helpful to referrers. The presence of loculation and complex septation of the effusion may point towards the need for a surgical approach.

On balanced SSFP sequences which have strong T1 and T2 weighting, pericardial fluid is usually high signal. It can usually be readily differentiated from pericardial fat which is also high signal by its greater intensity and uniformity. Native T1 sequences are also very helpful to clearly distinguish fat from fluid. If doubt persists however, heavily T1-weighted sequences such as those acquired for LGE imaging can be helpful, particularly where a phase-sensitive inversion recovery reconstruction is used. With conventional inversion times (designed to null the myocardium), on the latter, fat appears bright/high signal, whereas fluid is near black or signal void owing to its long T1 (Fig. 6.10). Balanced SSFP cine sequences can be used to evaluate the impact of an effusion on right ventricular filling in diastole and to look for right atrial or RV outflow tract compression.

The signal characteristics of an effusion can be used to help classify it. Transudates have a high water content relative to protein and so appear high signal on T2-weighted sequences and low signal on T1-weighted imaging. The presence of an exudate can sometimes be inferred by fibrin strands seen oscillating over the surface of the visceral pericardium, and the presence of pericardial thickening, which is usually absent with transudative effusions, particularly if this is seen on T2-weighted sequences (Fig. 6.11). Exudates tend to have more heterogeneous signal characteristics and by

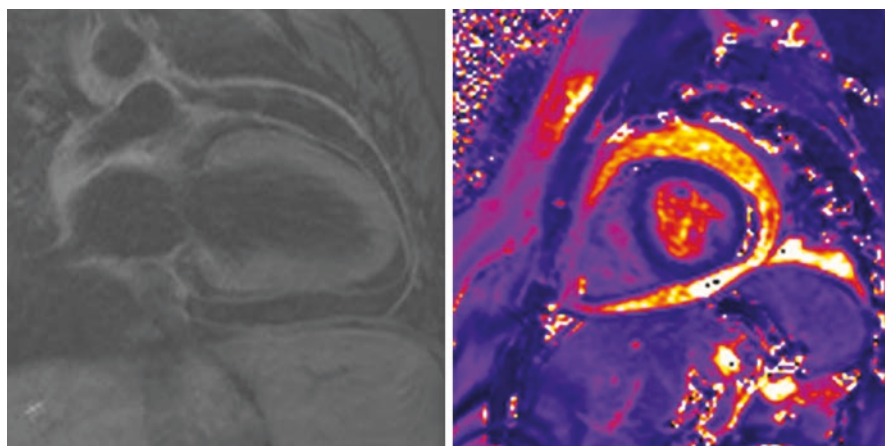
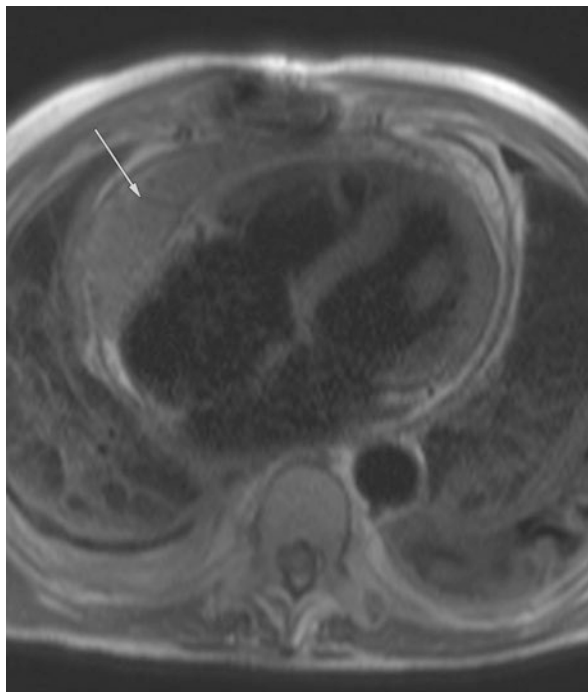


Fig. 6.11 T2W-short tau inversion recovery sequence (left) depicting pericardial high signal with an associated exudative global pericardial effusion. T2-maps (right) confirm pericardial inflammation and reveal heterogeneous T2 signal in the resulting pericardial effusion

Fig. 6.12 Axial Half-Fourier Acquisition Single-Shot Turbo Spin Echo (HASTE) sequence in a patient post mitral and tricuspid valve repair. Note the susceptibility artefact from the sternotomy wires. The pericardium is markedly thickened. There is a collection overlying the right atrium and right ventricle which is of intermediate signal intensity suggesting a serosanguinous exudate (arrow). There are bilateral pleural effusions and signs of pulmonary congestion



virtue of their high protein content relative to water, appearing intermediate or lower signal on T1 and T2-weighted sequences (Figs. 6.12, 6.13, 6.14). Chylous effusions are rare but owing to their lipid rich content, tend to be high signal on T1-weighted sequences. Native T1 mapping techniques may become another straightforward approach to differentiate between transudative effusions (low in protein with very high native T1 values similar to cerebrospinal fluid), exudative effusions (elevated protein with native T1 values lower than CSF but higher than ventricular blood pool) and haemopericardium (native T1 values similar to ventricular blood pool).

6.6.4 CMR and Pericardial Constriction

This is an important and underdiagnosed complication of acute and chronic inflammatory pericardial syndromes. It occurs as a result of thickening and fibrosis of the visceral and/or parietal pericardium which often also undergoes dystrophic calcification but this can also occur without pericardial thickening [26]. These changes reduce the normal compliance of the pericardium, rendering it rigid and inelastic. This causes the pericardium to become a barrier to normal cardiac filling. Pericardial constriction should be considered in the differential diagnosis of any patient with signs and symptoms of heart failure but normal ejection fraction, particularly where right-sided features predominate. Suspicion should also be heightened in any patient

Fig. 6.13 Balanced steady-state free precession sequence in the four-chamber orientation for patient described in Fig. 6.12. Note the heterogeneous signal in the collection in contrast to the left pleural effusion which is brighter and more uniform in signal intensity suggesting a lower protein content

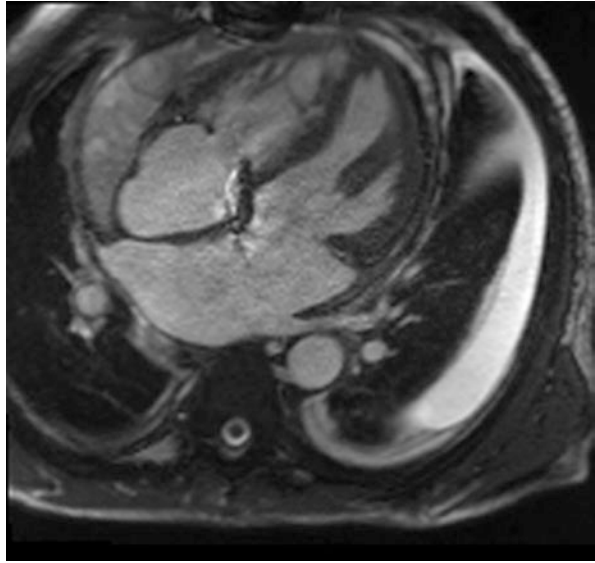


Fig. 6.14 Four chamber late gadolinium enhancement sequence with phase-sensitive inversion recovery reconstruction for patient in Fig. 6.12. The inflamed pericardium enhances with contrast and is high signal. The anterior pericardial collection is low signal but has a heterogeneous texture which is less evident in the more water rich left pleural effusion

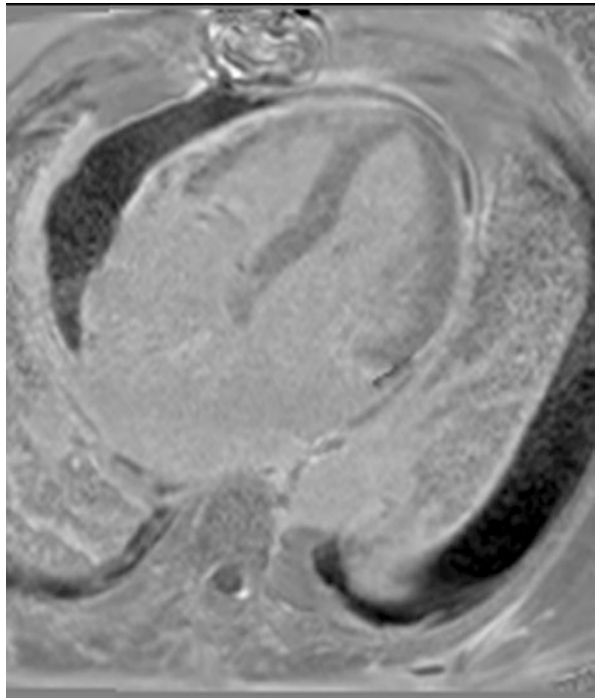
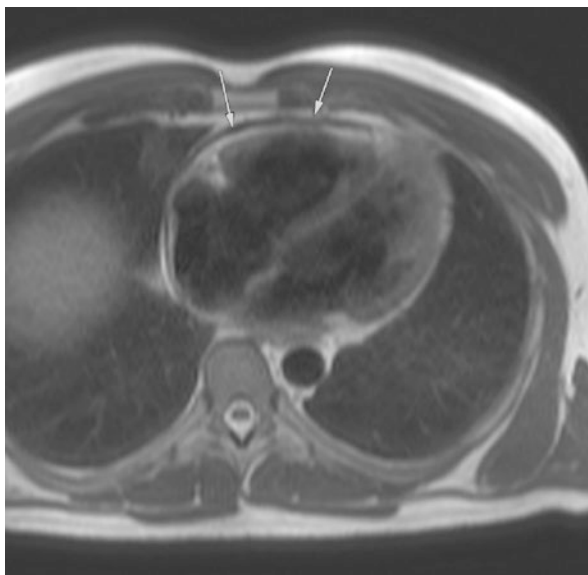


Fig. 6.15 Axial Half-Fourier Acquisition Single-Shot Turbo Spin Echo (HASTE) sequence in a patient with constrictive pericarditis. There is marked anterior pericardial thickening

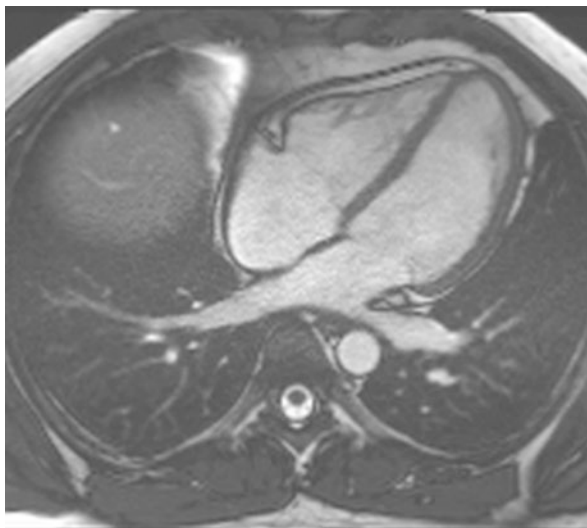


with a history of previous cardiac surgery or previous pericarditis due to a predisposing condition. Viral myocarditis can be but seldom is complicated by constriction; however, suppurative processes such as tuberculosis and other purulent bacterial infections pose a particular risk [35].

CMR can play a valuable role in non-invasive diagnosis [36]. Scout sequences may reveal signs of chronically elevated right-sided filling pressures and congestion. The superior and inferior vena cava may be dilated, together with the hepatic tributaries of the latter. There may be evidence of ascites. The patient's resting heart rate may be increased to preserve cardiac output as a means of compensating for the limited stroke volume. In chronic constriction, the atria are often enlarged. T1W-spin echo sequences may reveal pericardial thickening (Figs. 6.15 and 6.16), which can be significant and accompanied by areas of signal void where dystrophic calcification has occurred. However, it is important to note that normal pericardial thickness does not exclude a diagnosis of constriction and when present, can also be very localised. Approximately 20% of patients with constriction have an apparently normal pericardial thickness of 2 mm or less and the problem appears to be simply increased stiffness [26]. This may reflect altered pericardial compliance in the setting of acute inflammation (potentially signifying transient constriction) [37] or simply that current imaging techniques lack sufficient spatial resolution to accurately measure true pericardial thickness which physiologically is ~1 mm rather than 2 mm, a 50% relative difference.

On occasions, fibrosis and calcification of the visceral pericardium can directly alter the geometry of the right ventricle hinting at the presence of constriction. Tagging sequences can be used to demonstrate a failure of relative slippage between the myocardium and the surrounding pericardium. On SSFP cine

Fig. 6.16 Four chamber balanced steady-state free precession cine in a patient with pericardial constriction at early diastole. Note the increased pericardial thickness and the loss of the normal concavity of the LV septum in early diastole



sequence, biventricular size and systolic function are usually normal. In particular, RV long axis motion is either normal or increased, in contradistinction to the situation with primary restrictive cardiomyopathies which may mimic constriction clinically. Rarely, the two pathologies can coexist particularly where concurrent pericardial and right ventricular injury have occurred, e.g., radiotherapy-induced pericarditis and right ventricular injury. On occasions, it may be possible to see exaggerated early septal bounce which suggests increased interventricular dependence.

Under normal circumstances, the RV fills slightly earlier than the left ventricle (LV). As the RV blood volume increases during early diastole, the RV simply expands within the normally unrestricted pericardial space to readily accommodate the additional ingress of systemic venous return with no impact on LV filling. The septum may move at most slightly towards the left as the intracavitary pressure in the LV is usually close to that of the RV. However, with pericardial constriction, filling of the RV is limited by the rigid and non-compliant pericardium. Thus, as RV filling increases abruptly, the pressure transiently rises abruptly displacing the septum leftward (Fig. 6.16). As the LV eventually fills and intracavitary pressure increases, the septum is pushed back to its normal position giving rise to an exaggerated early septal bounce.

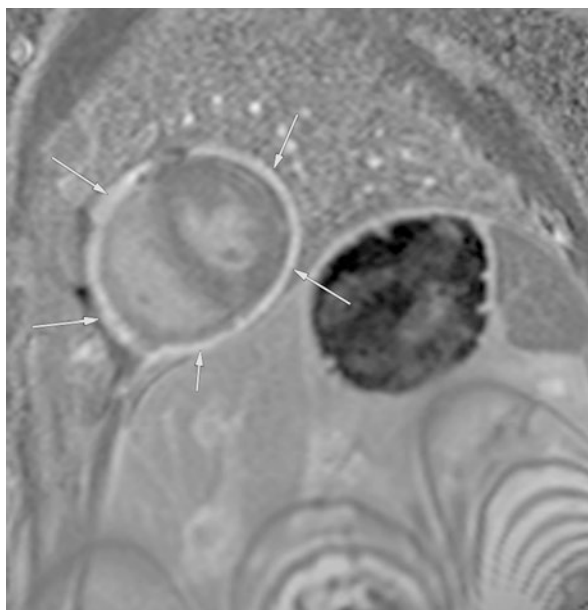
Increased ventricular interdependence can be demonstrated by observing septal motion usually in a basal or mid-ventricular short-axis view during free inspiration and expiration (Fig. 6.7) [38]. As the diaphragm descends, there is a fall in intrathoracic pressure which increases systemic venous return to the RV. At the same time, the fall in intrathoracic pressure commensurately reduces pulmonary venous return directly and by increasing pulmonary venous capacitance. Only a small portion of the pulmonary veins are within the pericardial sac, therefore the impact of the fall in intrapleural pressure on the pulmonary veins is significant. In the setting of constriction, this again forces the septum to displace towards the LV cavity as LV volumes

fall and RV pressures and volumes rise. Usually, two or three respiratory cycles are sufficient to demonstrate the phenomenon. Breath holds should be avoided as these may engender a Valsalva response if prolonged and performed at end-inspiration. Similarly, the phenomenon will not be seen in patients who are anaesthetised or receiving positive pressure ventilation as the latter increases rather than decreases intrapleural/intrathoracic pressure during inspiration.

Increased ventricular interdependence can also be seen in other settings where RV compliance is reduced directly, e.g., RV infarction, or indirectly through increased pericardial pressure, e.g., pericardial tamponade. However, these two circumstances are usually readily distinguished from constriction clinically by their acuity or from the history alone. Patients with suspected cardiac tamponade should not be subjected to CMR.

Late gadolinium enhancement imaging can play a valuable role in the evaluation of patients with suspected pericardial constriction. It may disclose the presence of myocardial disease, particularly in the setting of restrictive cardiomyopathy where imaging is being used to differentiate the latter from constriction. Where both pathologies are present, e.g., radiation-induced pericardial and RV disease, the presence of RV injury and fibrosis may highlight a subgroup of patients that may not respond to pericardial stripping surgery. Patients with increased signal on T2W-STIR sequences and prominent late enhancement may constitute an important subgroup that may potentially respond to anti-inflammatory treatments [32]. Similarly, simply the presence of pericardial late enhancement itself may signify the presence of neovascularisation of the pericardium and on-going organising pericarditis which may merit a trial of medical therapy targeting inflammation before considering pericardiectomy in patients who are symptomatic but not end-stage [39] (Fig. 6.17).

Fig. 6.17 Mid-ventricular short-axis late gadolinium enhancement sequence with phase-sensitive inversion recovery in a patient with pericardial constriction. Note the marked thickening and enhancement of the pericardium (arrows). This enhancement may highlight a subgroup of patients who may respond to medical therapy focussed on treating inflammation



CMR can therefore also be used to monitor response to such therapeutic trials [40], particularly where there is an underlying systemic autoimmune rheumatic disease (where alternative indications for immunosuppression may coexist) or there is clinical concern about concomitant myocardial involvement where again CMR may play a valuable role in diagnosing cardiac involvement and response to treatment.

6.6.5 Constrictive–Effusive Pericarditis

In this setting, there is the combined presence of features of pericardial constriction and a concomitant pericardial effusion [30]. The presentation can mimic cardiac tamponade, but usually atrial pressures remain elevated (assuming the absence of any primary RV failure) despite drainage of any associated effusion and the features of constriction persist post-drainage [41]. The phenomenon may represent an intermediate phase in the evolution of acute pericarditis to chronic constriction. In addition to identifying features of constriction, CMR can be of value in highlighting the presence of active/on-going inflammation (signified by increased pericardial signal on T2W-STIR imaging and enhancement in the late phase after gadolinium injection).

6.7 Molecular Imaging

Molecular imaging with 2-deoxy-2-[^{18}F]-fluoro-D-glucose (^{18}FDG) and positron emission tomography (PET) can study the entire heart revealing focal or diffuse patterns of inflammation and appears an appealing tool for the non-invasive diagnosis of the disease. Glucose is a normal metabolic substrate of myocardium and when the clinical question is the detection of an increased focal augmentation of myocardial glucose metabolism caused by an inflammatory process, the metabolic activity of the normal myocardium may disturb clinical interpretation of the images. Therefore, long fasting, a fatty meal or fractionated/unfractionated heparin administration before ^{18}FDG injection has been proposed to suppress physiological myocardial radiotracer uptake, a crucial requirement to identifying inflammation of the pericardial layers [42–44].

In infective pericarditis or myopericarditis, ^{18}FDG -PET/CT has been less used than echocardiography, cardiovascular magnetic resonance, or diagnostic CT (Figs. 6.18 and 6.19). Dong and colleagues studied 15 patients with acute tuberculous ($n = 5$) or idiopathic pericarditis ($n = 10$) [45]. Radiotracer uptake measured by using standardized uptake value (SUV) was more increased in both pericardium and mediastinal and supraclavicular lymph nodes affected by tuberculosis than in idiopathic lesions. Thus, the authors concluded that the degree of ^{18}FDG uptake is useful for differentiating acute tuberculous from idiopathic pericarditis. Moreover, ^{18}FDG PET can be more sensitive than CT in assessing lymph nodes involvement. Satheghe et al. reported a greater number of lymph nodes detected by dual phase ^{18}FDG -PET/CT than CT (18 sites vs 9) in nine patients affected by tuberculosis [46].

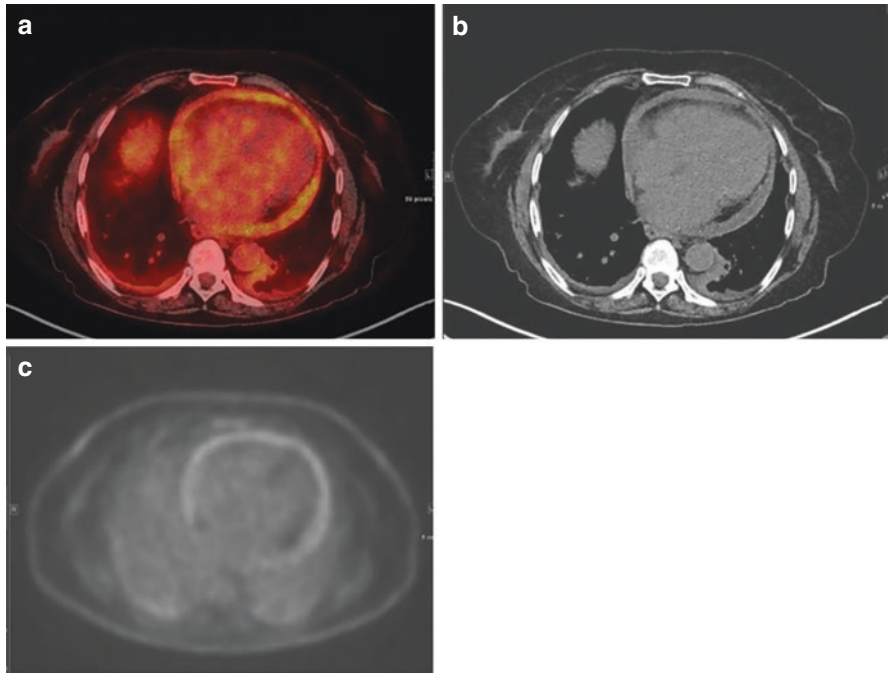


Fig. 6.18 Representative images of a 78 year-old woman diagnosed with pericarditis. Patient underwent a 72h dietary preparation prior to the investigation in order to suppress the physiological myocardial glucose metabolism. Fused PET/CT images (a) show a diffuse, moderately increased FDG uptake within the pericardium, corresponding to a moderate pericardial effusion as seen on CT images (b). The extent of the hypermetabolism, consistent with an infective pericarditis, is more evident on PET images (c), wherein the absence of myocardial uptake can be demonstrated, which can rule out a concomitant myocarditis

Recently, Chang et al. prospectively studied 16 patients with constrictive pericarditis [47]. ^{18}F FDG-PET/CT was performed at enrolment and at follow-up (after 3 months of steroid therapy). Using a SUV_{max} cut-off value of 3.0, the sensitivity and specificity of ^{18}F FDG-PET/CT for predicting responders were 100% and 71%, respectively. These data are encouraging, but further studies are needed to establish the clinical utility of the technique in this field. On the other hand, theoretically, and as for other malignant diseases, ^{18}F FDG-PET/CT could be used for the diagnosis of primary and metastatic pericardial lesions and for disease staging. Pericardial effusion of neoplastic aetiology can be a manifestation of pericardial mesothelioma [48] or associated with breast cancer, lung cancer, Hodgkin's lymphoma, and sarcoma. Sarcoma and lymphoma also can present as constrictive pericarditis. In the presence of a pericardial effusion, a whole body ^{18}F FDG-PET/CT scan could be helpful to find or exclude other malignant lesions, and to identify the origin of the neoplasm of which pericardial effusion is a primary or secondary manifestation (paraneoplastic syndrome). High accumulation of ^{18}F FDG in mediastinal or other lymph nodes can be used to speculate about malignancy or infective disease [49] although differentiation between benign and malignant pericardial disease remains challenging.

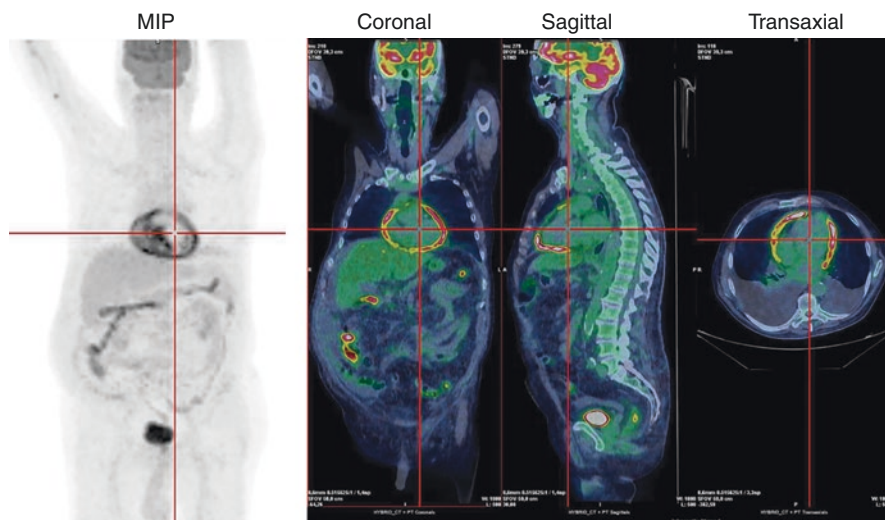


Fig. 6.19 PET/CT imaging in pericarditis. 1-month after a febrile prodromal syndrome followed by persistent asthenia and worsening dyspnoea, a 67 year old patient was admitted with atrial fibrillation. Serologic findings and echocardiographic/CMR images were suggestive of incessant pericarditis. PET/CT scan confirmed the diagnosis revealing diffuse uptake of ^{18}F FDG in the pericardial layers without myocardial involvement and associated large bilateral pleural effusions

6.8 Basics of Treatment

A detailed description of treatment of pericarditis is outside the framework of this book. To give a brief summary, anti-inflammatory therapy is the cornerstone of acute pericarditis: Non-steroidal anti-inflammatory drugs are recommended based on clinical experience [2]. The benefit of colchicine is well established in both acute and recurrent pericarditis [30]. Systemic corticosteroids have been used mostly as second- or third-line treatments. Recently, IL-1 blockers (i.e., anakinra) have proven beneficial in recurrent pericarditis [50]. In purulent pericarditis, a rare but potentially life-threatening disease, specific antimicrobial therapy according to the causative agent is indicated [51]. The indication of pericardiectomy should always be based on a multi-disciplinary heart-team approach when patients remain highly symptomatic and all medical therapies are deemed ineffective.

6.9 Conclusion

Pericarditis can be considered a relatively uncommon, often self-limiting disease. However, if not promptly diagnosed and treated, it tends to relapse, become chronic, and lead to re-hospitalisation. Diagnosis and differential diagnosis remain challenging because the accessibility of pericardial fluid and tissue is limited and pericardiocentesis is not without risk. Therefore, high levels of clinical suspicion and multimodal imaging are necessary for the correct management of patients and to prevent or diagnose long-term complications.

References

1. Rodriguez ER, Tan CD. Structure and anatomy of the human pericardium. *Prog Cardiovasc Dis.* 2017;59:327–40.
2. Ismail TF. Acute pericarditis: update on diagnosis and management. *Clin Med.* 2020;20:48–51.
3. Shah AB, Kronzon I. Congenital defects of the pericardium: a review. *Eur Heart J Cardiovasc Imaging.* 2015;16:821–7.
4. Imazio M, Cecchi E, Demichelis B, Chinaglia A, Ierna S, Demarie D, Ghisio A, Pomari F, Belli R, Trincherio R. Myopericarditis vs viral or idiopathic acute pericarditis. *Heart.* 2008;94(4):498–501.
5. Kytö V, Sipilä J, Rautava P. Clinical profile and influences on outcomes in patients hospitalized for acute pericarditis. *Circulation.* 2014;130(18):1601–6.
6. Imazio M, Spodick DH, Brucato A, Trincherio R, Adler Y. Controversial issues in the management of pericardial diseases. *Circulation.* 2010;121(7):916–28.
7. Le Winter MM. Acute pericarditis. *N Engl J Med.* 2014;371(25):2410–6.
8. Sreenivasan J, Khan MS, Hooda U, Khan SU, Aronow WS, Mookadam F, Krasuski RA, Cooper HA, Michos ED, Panza JA. Rate, causes, and predictors of 30-day readmission following hospitalization for acute pericarditis. *Am J Med.* 2020;133:1453–9.
9. Imazio M, Cecchi E, Demichelis B, Ierna S, Demarie D, Ghisio A, Pomari F, Coda L, Belli R, Trincherio R. Indicators of poor prognosis of acute pericarditis. *Circulation.* 2007;115(21):2739–44.
10. Permanyer-Miralda G, Sagristá-Sauleda J, Soler-Soler J. Primary acute pericardial disease. *Am J Cardiol.* 1985;56(10):623–30.
11. Zayas R, Anguita M, Torres F, Giménez D, Bergillos F, Ruiz M, Ciudad M, Gallardo A, Vallés F. Incidence of specific etiology and role of methods for specific etiologic diagnosis of primary acute pericarditis. *Am J Cardiol.* 1995;75(5):378–82.
12. Gouriet F, Levy PY, Casalta JP, Zandotti C, Collart F, Lepidi H, Cautela J, Bonnet JL, Thuny F, Habib G, Raoult D. Etiology of pericarditis in a prospective cohort of 1162 cases. *Am J Med.* 2015;128(7):784.
13. Mayosi BM. Contemporary trends in the epidemiology and management of cardiomyopathy and pericarditis in sub-Saharan Africa. *Heart.* 2007;93(10):1176–83.
14. Hoit BD. Pathophysiology of the pericardium. *Prog Cardiovasc Dis.* 2017;59(4):341–8.
15. Salisbury AC, Olalla-Gómez C, Rihal CS, Bell MR, Ting HH, Casaclang-Verzosa G, Oh JK. Frequency and predictors of urgent coronary angiography in patients with acute pericarditis. *Mayo Clin Proc.* 2009;84(1):11–5.
16. Troughton RW, Asher CR, Klein AL. Pericarditis. *Lancet.* 2004;363(9410):717–27.
17. Spodick DH. Acute pericarditis: current concepts and practice. *JAMA.* 2003;289(9):1150–3.
18. Permanyer-Miralda G. Acute pericardial disease: approach to the aetiological diagnosis. *Heart.* 2004;90(3):252–4.
19. Imazio M, Brucato A, Spodick DH, Adler Y. Prognosis of myopericarditis as determined from previously published reports. *J Cardiovasc Med.* 2014;15(12):835–9.
20. Tsang TS, Oh JK, Seward JB. Diagnosis and management of cardiac tamponade in the era of echocardiography. *Clin Cardiol.* 1999;22:446–52.
21. Imazio M, Gaita F, LeWinter M. Evaluation and treatment of pericarditis: a systematic review. *JAMA.* 2015;314(14):1498–506.
22. Adler Y, Charron P, Imazio M, Badano L, Barón-Esquivias G, Bogaert J, Brucato A, Guerot P, Klingel K, Lionis C, Maisch B, Mayosi B, Pavie A, Ristic AD, Sabaté Tenas M, Seferovic P, Swedberg K, Tomkowski W, ESC Scientific Document Group. 2015 ESC guidelines for the diagnosis and management of pericardial diseases: the task force for the diagnosis and Management of Pericardial Diseases of the European Society of Cardiology (ESC) endorsed by: the European Association for Cardio-Thoracic Surgery (EACTS). *Eur Heart J.* 2015;36(42):2921–64.
23. Wang ZJ, Reddy GP, Gotway MB, Yeh BM, Hetts SW, Higgins CB. CT and MR imaging of pericardial disease. *Radiographics.* 2003;23:S167–80.

24. Rajiah P, Kanne JP. Computed tomography of the pericardium and pericardial disease. *J Cardiovasc Comput Tomogr*. 2010;4:3–18.
25. Verhaert D, Gabriel RS, Johnston D, Lytle BW, Desai MY, Klein AL. The role of multimodality imaging in the management of pericardial disease. *Circ Cardiovasc Imaging*. 2010;3:333–43.
26. Talreja DR, Edwards WD, Danielson GK, Schaff HV, Tajik AJ, Tazelaar HD, Breen JF, Oh JK. Constrictive pericarditis in 26 patients with histologically normal pericardial thickness. *Circulation*. 2003;108(15):1852–7.
27. Kim JS, Kim HH, Yoon Y. Imaging of pericardial diseases. *Clin Radiol*. 2007;62:626–31.
28. Kramer CM, Barkhausen J, Flamm SD, Kim RJ, Nagel E, Society for Cardiovascular Magnetic Resonance Board of Trustees Task Force on Standardized Protocols. Standardized cardiovascular magnetic resonance (CMR) protocols 2013 update. *J Cardiovasc Magn Reson*. 2013;15:91.
29. Bogaert J, Francone M. Cardiovascular magnetic resonance in pericardial diseases. *J Cardiovasc Magn Reson*. 2009;11:14.
30. Chiabrando JG, Bonaventura A, Vecchié A, Wohlford GF, Mauro AG, Jordan JH, Grizzard JD, Montecucco F, Berrocal DH, Brucato A, Imazio M, Abbate A. Management of Acute and Recurrent Pericarditis: JACC state-of-the-art review. *J Am Coll Cardiol*. 2020;75(1):76–92.
31. Young PM, Glockner JF, Williamson EE, Morris MF, Araoz PA, Julsrud PR, Schaff HV, Edwards WD, Oh JK, Breen JF. MR imaging findings in 76 consecutive surgically proven cases of pericardial disease with CT and pathologic correlation. *Int J Cardiovasc Imaging*. 2012;28:1099–109.
32. Feng D, Glockner J, Kim K, Martinez M, Syed IS, Araoz P, Breen J, Espinosa RE, Sundt T, Schaff HV, Oh JK. Cardiac magnetic resonance imaging pericardial late gadolinium enhancement and elevated inflammatory markers can predict the reversibility of constrictive pericarditis after antiinflammatory medical therapy: a pilot study. *Circulation*. 2011;124:1830–7.
33. Alraies MC, AlJaroudi W, Yarmohammadi H, Yingchoncharoen T, Schuster A, Senapati A, Tariq M, Kwon D, Griffin BP, Klein AL. Usefulness of cardiac magnetic resonance-guided management in patients with recurrent pericarditis. *Am J Cardiol*. 2015;115:542–7.
34. Imazio M, Adler Y. Management of pericardial effusion. *Eur Heart J*. 2013;34:1186–97.
35. Imazio M, Brucato A, Rovere ME, Gandino A, Cemin R, Ferrua S, Maestroni S, Zingarelli E, Barosi A, Simon C, Sansone F, Patrini D, Vitali E, Belli R, Ferrazzi P, Trinchero R, Spodick DH, Adler Y. Colchicine prevents early postoperative pericardial and pleural effusions. *Am Heart J*. 2011;162:527–32.
36. Bolen MA, Rajiah P, Kusunose K, Collier P, Klein A, Popovic ZB, Flamm SD. Cardiac MR imaging in constrictive pericarditis: multiparametric assessment in patients with surgically proven constriction. *Int J Cardiovasc Imaging*. 2015;31:859–66.
37. Haley JH, Tajik AJ, Danielson GK, Schaff HV, Mulvagh SL, Oh JK. Transient constrictive pericarditis: causes and natural history. *J Am Coll Cardiol*. 2004;43:271–5.
38. Giorgi B, Mollet NR, Dymarkowski S, Rademakers FE, Bogaert J. Clinically suspected constrictive pericarditis: MR imaging assessment of ventricular septal motion and configuration in patients and healthy subjects. *Radiology*. 2003;228:417–24.
39. Zurick AO, Bolen MA, Kwon DH, Tan CD, Popovic ZB, Rajeswaran J, Rodriguez ER, Flamm SD, Klein AL. Pericardial delayed hyperenhancement with CMR imaging in patients with constrictive pericarditis undergoing surgical pericardiectomy: a case series with histopathological correlation. *JACC Cardiovasc Imaging*. 2011;4:1180–91.
40. Cremer PC, Tariq MU, Karwa A, Alraies MC, Benatti R, Schuster A, Agarwal S, Flamm SD, Kwon DH, Klein AL. Quantitative assessment of pericardial delayed hyperenhancement predicts clinical improvement in patients with constrictive pericarditis treated with anti-inflammatory therapy. *Circ Cardiovasc Imaging*. 2015;8(5):e003125.
41. Miranda WR, Oh JK. Effusive-constrictive pericarditis. *Cardiol Clin*. 2017;35:551–8.
42. Harisankar CN, Mittal BR, Agrawal KL, Abrar ML, Bhattacharya A. Utility of high fat and low carbohydrate diet in suppressing myocardial FDG uptake. *J Nucl Cardiol*. 2011;18:926–36.

43. Scholtens AM, Verberne HJ, Budde R, Lam M. Additional heparin pre-administration improves cardiac glucose metabolism suppression over low carbohydrate diet alone in 18F-FDG-PET imaging. *J Nucl Med.* 2016;57(4):568–73.
44. Giorgetti A, Marras G, Genovesi D, Filidei E, Bottoni A, Mangione M, Emdin M, Marzullo P. Effect of prolonged fasting and low molecular weight heparin or warfarin therapies on 2-deoxy-2-[18F]-fluoro-D-glucose PET cardiac uptake. *J Nucl Cardiol.* 2018;25(4):1364–71.
45. Dong A, Dong H, Wang Y, Cheng C, Zuo C, Lu J. (18)F-FDG PET/CT in differentiating acute tuberculous from idiopathic pericarditis: preliminary study. *Clin Nucl Med.* 2013;38(4):e160–5.
46. Sathekge MM, Maes A, Pottel H, Stoltz A, van de Wiele C. Dual time-point FDG PET-CT for differentiating benign from malignant solitary pulmonary nodules in a TB endemic area. *S Afr Med J.* 2010;100(9):598–601.
47. Chang SA, Choi JY, Kim EK, Hyun SH, Jang SY, Choi JO, Park SJ, Lee SC, Park SW, Oh JK. [(18)F]Fluorodeoxyglucose PET/CT predicts response to steroid therapy in constrictive pericarditis. *J Am Coll Cardiol.* 2017;69(6):750–2.
48. Restrepo CS, Vargas D, Ocazonez D, Martinez-Jimenez S, Betancourt Cuellar SL, Gutierrez FR. Primary pericardial tumors. *Radiographics.* 2013;33(6):1613–30.
49. Behnia FL, Leblond A, Vesselle H. A practical guide to interpreting FDG PET and CT nodal findings in lung cancer. *J Nucl Med Rad Ther.* 2016;8(1):319.
50. Brucato A, Imazio M, Gattorno M, Lazaros G, Maestroni S, Carraro M, Finetti M, Cumetti D, Carobbio A, Ruperto N, Marcolongo R, Lorini M, Rimini A, Valenti A, Erre GL, Sormani MP, Belli R, Gaita F, Martini A. Effect of Anakinra on recurrent pericarditis among patients with colchicine resistance and corticosteroid dependence: the AIRTRIP randomized clinical trial. *JAMA.* 2016;316(18):1906–12.
51. Rubin RH, Moellering RC Jr. Clinical, microbiologic and therapeutic aspects of purulent pericarditis. *Am J Med.* 1975;59(1):68–78.



Infection: Myocarditis

7

Tevfik F. Ismail, Alina Hua, Philip Haaf,
and Assuero Giorgetti

Contents

7.1	Introduction.....	192
7.2	Aetiology and Pathogenesis.....	192
7.3	From Acute Myocarditis to Chronic Inflammatory Cardiomyopathy and Heart Failure.....	194
7.4	Clinical Presentations and Diagnosis.....	195
7.5	Endomyocardial Biopsy.....	197
7.6	Cardiovascular Magnetic Resonance (CMR).....	198
7.7	Infectious Inflammatory Cardiomyopathy.....	205
7.8	Coronavirus Disease-2019 (COVID-19) and Myocarditis.....	205
7.9	Non-Infectious Inflammatory Cardiomyopathy.....	206
7.10	Eosinophilic Myocarditis/Endomyocardial fibrosis.....	213
7.11	Drug-Induced or Toxic Myocarditis.....	217
7.12	Inflammatory Myositis.....	219
7.13	Giant Cell Myocarditis.....	220
7.14	Genetic Causes.....	220
7.15	Molecular Imaging.....	223
7.16	Hybrid Imaging.....	224
7.17	Summary.....	225
	References.....	225

T. F. Ismail · A. Hua

King's College London & Guy's and St Thomas' NHS Foundation Trust, London, UK

P. Haaf (✉)

Clinic of Cardiology, University Hospital Basel and University of Basel, Basel, Switzerland

e-mail: philip.haaf@usb.ch

A. Giorgetti (✉)

Fondazione CNR/Regione Toscana "Gabriele Monasterio", Pisa, Pisa, Italy

e-mail: asso@ftgm.it

7.1 Introduction

Myocarditis is an inflammatory condition affecting the myocardium that can present as an acute, subacute, or chronic disease and as a focal or global process. It is variably caused by an infectious agent, autoimmune conditions, or reactions to exogenous/endogenous substances. Its incidence is usually estimated between 10 and 20 cases per 100,000 persons per year, and the majority of patients are young and healthy [1, 2]. The short-term prognosis of acute myocarditis is usually good but varies by aetiology and the disease may show late serious complications. It is estimated that approximately 10–20% of young adults with acute myocarditis develop chronic myocarditis, dilated cardiomyopathy, and congestive heart failure, and about half of these patients undergo cardiac transplantation [3]. The prevalence of myocarditis as a cause of heart failure varies by age and geographical regions and ranges from 0.4% to 4% [4]. In 2015, the global death rate for myocarditis and cardiomyopathy was 4.8/100,000 persons with 350,000 deaths [4]. Myocardial inflammation is considered responsible for sudden cardiac death in approximately 5–12% of young athletes, 5% of children, and in 2% of infants [5]. However, the exact incidence of myocarditis remains unknown. Myocarditis is probably underestimated, as the clinical presentation is often heterogeneous and diagnosis can be challenging.

Myocarditis is a heart muscle disease characterised histologically by myocyte injury or necrosis in the presence of an inflammatory infiltrate not triggered by myocardial ischaemia. Given that this diagnosis requires histology and often immunohistochemistry, endomyocardial biopsy is still regarded as the diagnostic gold standard by consensus guidelines [6]. However, endomyocardial biopsy as a diagnostic strategy has significant limitations. Firstly, it has imperfect sensitivity and may miss inflammation in at least a third of affected patients due to sampling issues, or ~20% even when both ventricles are sampled [7]. Many cases of myocarditis predominantly involve the epicardial and mid-myocardial walls, whereas percutaneous endomyocardial biopsy preferentially samples the endocardial aspect of the myocardium. Secondly, the technique is invasive and carries small but tangible risks of significant procedural complications [7]. Thirdly, the technical expertise required for undertaking biopsies and the expert pathology support for their interpretation is not widely available.

Given these limitations, there is growing interest in the use of imaging modalities as a means to diagnose myocarditis non-invasively and in some instances, guide endomyocardial biopsy where this may specifically change management [6, 7].

7.2 Aetiology and Pathogenesis

A complex interplay of genetic, epigenetic, and environmental factors causes inflammatory myocardial injury (Fig. 7.1).

The aetiology of myocarditis is summarised in Fig. 7.2 and can be classified into four broad groups: (1) infectious; (2) autoimmune; (3) toxic; and (4) genetic. However, these groupings are not mutually exclusive and there is growing evidence

Fig. 7.1 A complex interplay of genetic, epigenetic, and environmental factors causes inflammatory myocardial injury

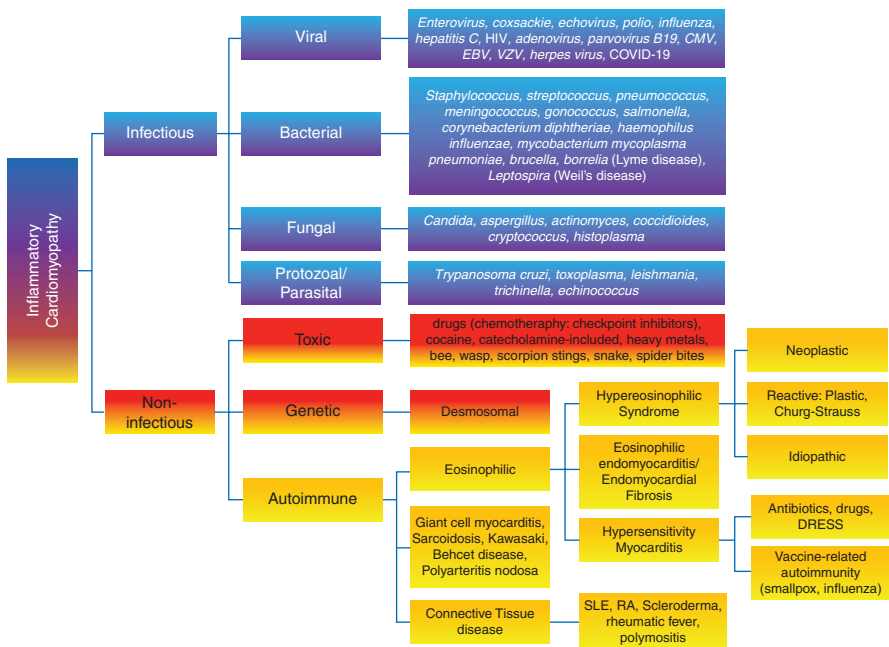
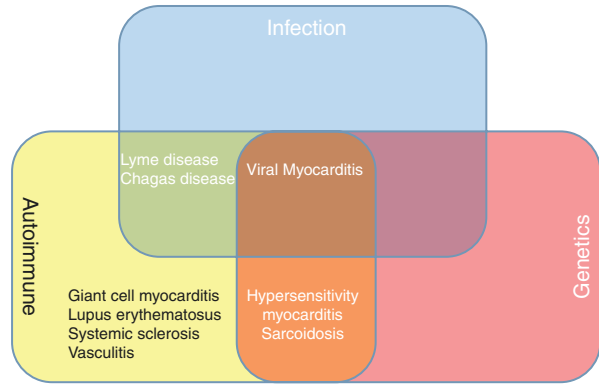


Fig. 7.2 Aetiology of inflammatory cardiomyopathies. *HIV* human immunodeficiency virus, *CMV* cytomegalovirus, *EBV* Epstein–Barr virus, *VZV* Varicella Zoster virus, *DRESS* drug reaction with eosinophilia and systemic symptoms, *SLE* systemic lupus erythematosus, *RA* rheumatoid arthritis

to support a role for autoimmunity in sustaining myocarditis triggered initially by viral infections, for instance, as well as a role for viruses including endogenous retroviruses in triggering systemic autoimmune disease [8]. In all categories, there is tissue injury and/or necrosis.

Virally mediated cardiac injury remains the most common cause in developed countries, and induces an immune response that leads to organ dysfunction and remodelling. The prevalent pathogen has changed over time from coxsackievirus

(1950s–1990s) to adenovirus (late 1990s), and more recently to parvovirus B19 and Human Herpesvirus 6 [9]. In Japan, Hepatitis C virus is associated with myocarditis and cardiomyopathy [10] while HIV is frequent in Africa [4]. Other infective causes of myocarditis are bacteria, such as diphtheria and *Borrelia burgdorferi* (Lyme disease), or parasites, such as *Trypanosoma cruzi* (Chagas disease) which are important causes of myocarditis in specific geographical regions of the world [11, 12]. Non-infectious causes of myocarditis include hypersensitivity myocarditis that may result from drug- or vaccine-related autoimmunity (e.g., smallpox, influenza) [13]. Myocardial inflammation can be observed in the context of systemic autoimmunity, such as in systemic lupus erythematosus, systemic sclerosis, vasculitis, and sarcoidosis [6]. Giant cell myocarditis (GCM) is a non-infectious form of myocarditis, sometimes associated with other autoimmune conditions (about 20% of cases), quite rare but rapidly progressive and clinically important [14].

7.3 From Acute Myocarditis to Chronic Inflammatory Cardiomyopathy and Heart Failure

The pathogenesis and progression of inflammatory cardiomyopathy to heart failure are believed to be a multiphase process and most of the current understanding derives from experimental animal models infected with viruses. In acute myocarditis, tissue injury derives from virus entry into myocardial cells via viral-specific receptors and this causes a direct inflammatory response [15]. Inflammation and muscle injury lead to cardiac protein (myosin) exposure that recruits the innate immune system as a first-line defence against the pathogen, followed by release of pro-inflammatory cytokines [16]. This is followed by an acquired immune system response, with the activation and expansion of T and B-cells which characterises a third phase with cellular cardiac infiltrates involving pathogen- and autoantigen-specific T cells, macrophages, and antibodies [17]. Therefore, different cellular compartments are participating in the inflammatory response: the bone marrow derived compartment, the endothelial compartment that controls the access of immune cells to the heart, the interstitial compartment, and the cardiomyocyte compartment, which interacts with the local microenvironment to modulate the inflammatory response [18]. Efficient clearance of the pathogen can lead to resolution and recovery of cardiac function. In the presence of a genetic susceptibility, a malfunction of immune system tolerance to cardiac antigens may occur and determines a chronic autoantigen-driven inflammatory process which can evolve in dilated cardiomyopathy and end-stage congestive heart failure [19]. The progression of the disease seems to be facilitated by the release of pro-inflammatory cytokines such as tumour necrosis factor alpha and interleukins, along with viral persistence in the myocardium and is characterised by cardiomyocyte hypertrophy, apoptosis, and fibrosis [20, 21]. In non-infectious aetiologies, autoimmune phases of inflammation, as described for viral myocarditis, can trigger the progression to heart failure and its complications. Furthermore, since myocarditis pathogenesis is a multiphase

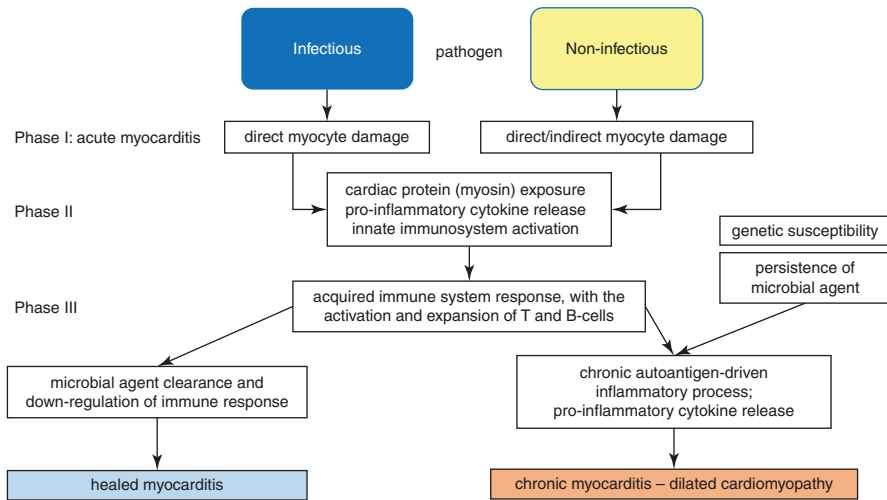


Fig. 7.3 Summary of the course of acute myocarditis to healed myocarditis vs. chronic myocarditis and dilated cardiomyopathy

process, cogent therapeutic strategies may need to change according to the stage of the disease. Figure 7.3 summarises the pathogenesis of the disease.

7.4 Clinical Presentations and Diagnosis

The clinical presentation of the disease is often heterogeneous, ranging from benign, subclinical manifestations to major clinical syndromes with severe complications. Acute myocarditis begins often insidiously with fever, asthenia, arthralgia, myalgia, loss of appetite, and abdominal pain, as prodromal symptoms that precede cardiac dysfunction by several days to weeks and may suggest a post-viral aetiology [22]. The European Study of the Epidemiology and Treatment of Inflammatory Heart Disease screened 3055 patients with suspected myocarditis and reported a high variability in the disease-related symptoms experienced by patients: 72% had dyspnoea, 32% had chest pain, and 18% had palpitations [23]. Chest pain may mimic pericarditis or an acute coronary syndrome, with or without an associated rise in troponin levels [24]. Angina may be due to coronary vasospasm or microvascular dysfunction. A position statement from the European Society of Cardiology (ESC) suggests that in all cases of suspected myocarditis, it is mandatory to exclude coronary artery disease or pre-existing conditions that could explain the clinical scenario [6]. Palpitations and syncope may result from atrioventricular (AV) block and ventricular arrhythmias. Therefore, a prodromal syndrome followed by dyspnoea/orthopnoea, chest pain, and palpitations and associated with sudden left ventricular dysfunction raises the suspicion of acute myocarditis and the need for appropriate investigations to identify its cause. If patient develops ventricular arrhythmias,

high-grade AV block, or fails to respond to standard heart failure treatment, the outcome is worse and a more serious form of myocarditis, such as giant cell myocarditis, should be considered, especially if associated with a history of thymoma or underlying autoimmune disease [25]. In these cases, endomyocardial biopsy is crucial because it allows histological typing and it can guide cause-specific treatment [26]. Sometimes, specific clinical features can point towards a specific aetiology. For example, diphtheria is frequently associated with bradyarrhythmias and heart block. High-grade AV block and ventricular arrhythmias may be observed in Chagas and Lyme diseases, sarcoidosis, and necrotizing eosinophilic myocarditis [27–29]. On average, men tend to have a more severe course with less complete recovery than women [30]. Moreover, myocarditis is an important cause of sudden death as well as childhood cardiomyopathy [31, 32].

Patients may come to medical attention with symptoms and signs of heart failure due to chronic dilated cardiomyopathy of unknown aetiology. Up to 40% of these patients show immunohistological pattern of myocarditis [33] and those with persistent cardiac inflammation, demonstrated by immunohistology, have a higher risk of death than those without inflammation [34].

Inflammatory biomarkers (erythrocyte sedimentation rate and C-reactive protein) are often elevated and can be used to monitor the evolution of inflammation but they do not confirm or exclude the diagnosis of myocarditis. Troponins are very sensitive markers of myocytes injury but non-specific and even normal levels of high-sensitivity cardiac troponin assays do not necessarily fully exclude myocarditis [35]. Circulatory IgG antibodies levels of cardiotropic viruses are often high in the general population and routine viral serology is not recommended [6]. Serum samples should be assessed for cardiac and muscle-specific autoantigens. Lack of viral genome on endomyocardial biopsy, in the presence of detectable serum autoantibodies, is highly suggestive of immune-mediated myocarditis and it allows the identification of patients who may benefit from specific immunosuppression and/or immunomodulatory treatment [19].

The electrocardiogram is a first-line investigation and is usually abnormal in myocarditis. Repolarisation abnormalities, with ST-T concave elevation (rather than convex as in ischaemic syndromes), are frequent. Atrioventricular block and/or ventricular arrhythmias associated with mild left ventricular dilatation may be suggestive of cardiac sarcoidosis or GCM. QRS prolongation is associated with a poor outcome. However, ECG changes have low diagnostic accuracy [36].

Echocardiography remains an essential tool in suspected myocarditis demonstrating left ventricular global or regional ventricular dysfunction with increased volumes, right ventricular involvement, and pericardial effusion [37]. Intense inflammation and interstitial oedema in fulminant myocarditis may result in a non-dilated, thickened, and diffusely hypocontractile left ventricle (LV). Transthoracic echocardiography at presentation is always recommended and can be used to monitor the evolution of the disease. Newer approaches such as tissue Doppler and strain rate imaging using speckle tracking appear promising but further studies are needed to establish their role in the diagnosis of myocarditis [38]. Table 7.1 illustrates diagnostic criteria to validate the clinical suspicion of myocarditis.

Table 7.1 Diagnostic criteria to validate the clinical suspicion of myocarditis (modified from reference [6])

Clinical presentation
Chest pain (ischaemia-like or pericarditic)
New onset (<3 months) or worsening of dyspnoea and/or fatigue
Subacute/chronic (>3 months) or worsening of dyspnoea and/or fatigue
Signs of left/right heart failure
Palpitations and/or arrhythmias and/or syncope; aborted cardiac sudden death
Unexplained cardiogenic shock
Diagnostic criteria
<i>ECG abnormalities (new)</i>
Low voltages; intraventricular conduction delay (wide QRS complex, bundle branch block); repolarisation abnormalities (ST elevation, T wave inversion); sinus arrest; atrioventricular blocks; asystole; frequent premature beats, supraventricular tachycardia; ventricular tachycardia or fibrillation
<i>Elevated markers of myocytolysis</i>
Elevation of high-sensitivity cardiac troponin
<i>Cardiac imaging (echocardiography/angiography/CMR)</i>
New onset: Left and/or right ventricular abnormalities; regional wall motion abnormalities; global systolic or diastolic dysfunction with or without ventricular dilatation; increased wall thickness; endocavitary thrombi; pericardial effusion
<i>CMR tissue characterisation</i>
Oedema and/or LGE in a non-ischaemic pattern

Clinical suspicion if ≥ 1 clinical presentation and ≥ 1 diagnostic criteria in the absence of significant coronary stenosis ($>50\%$) and pre-existing cardiac disease that could explain the findings (i.e., congenital heart diseases, valve disease, etc.). The higher the number of clinical/diagnostic criteria, the higher the suspicion of myocarditis. *LGE* late gadolinium enhancement.

7.5 Endomyocardial Biopsy

Endomyocardial biopsy (EMB) is still widely considered the diagnostic gold standard. EMB permits diagnosis and identifies the aetiology and the type of inflammation (e.g., lymphocytic, neutrophilic, eosinophilic, GCM, sarcoidosis) with important implications on the therapeutic approach and prognosis. If performed by experienced teams, EMB is relatively safe (rate of complications $<0.8\%$) and may be repeated to monitor response to therapy [6]. In 1987, the Dallas criteria for the histologic diagnosis were defined [39]. Patients with lymphocytic infiltration and myocytolysis were identified as having myocarditis. In the absence of myocytolysis, cases are classified as borderline or having on-going myocarditis. However, less than 10% of patients with suspected myocarditis meet the Dallas criteria, raising issues about technique sensitivity and inter-observer variability. The sensitivity of biopsy has been reported higher for GCM (80–93%) than for sarcoidosis (25%) and lymphocytic myocarditis (35%) [40, 41]. Moreover, the Dallas histopathologic criteria did not include immunohistochemistry and viral genome analysis that are now recommended to be performed on heart tissue samples [6]. Therefore, EMB may be

affected by sampling errors, variability in sampling interpretation, and it is not risk-free. For all these reasons, non-invasive second-level cardiac imaging is increasingly recommended in the management of patient with suspected myocarditis or in the evaluation of dilated cardiomyopathy of non-*ischaemic* origin.

7.6 Cardiovascular Magnetic Resonance (CMR)

CMR is unique in its ability to simultaneously allow the evaluation of cardiac structure, function, and tissue characteristics non-invasively and without ionising radiation. Multiparametric CMR is sensitive to many tissue changes that occur during myocardial inflammation, regardless of its aetiology (Table 7.2).

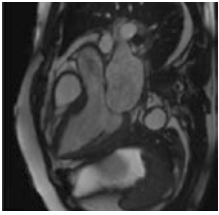
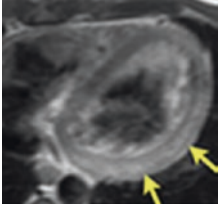
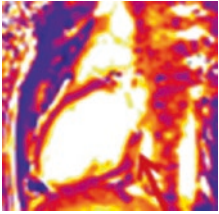
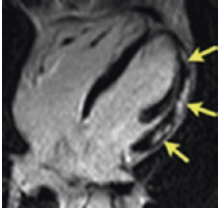
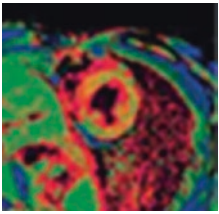
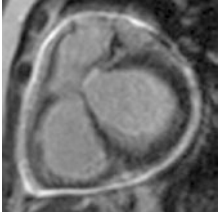
Reflecting clinical practice, although there has been some limited validation of CMR against histology, recommendations for its use and interpretation are driven by consensus guidelines (the “Lake Louise Criteria”) using a pragmatic evidence-base of imaging data derived from a population of patients with clinically suspected myocarditis [42]. This reflects the challenges of validating novel diagnostic techniques where there is an imperfect gold standard. The original Lake Louise Criteria have been modified and revised to incorporate recent developments in parametric mapping techniques (see below) [8].

Patients presenting with fulminant myocarditis, *i.e.*, myocardial inflammation with rapid onset (days to <2 weeks) and severe heart failure with cardiogenic shock or evidence of high-grade (second or third degree) AV block and/or malignant ventricular arrhythmias should be investigated by EMB in the first instance because of the need to exclude treatable causes such as GCM that can only be diagnosed histologically [43]. The procedure can usually be combined with coronary angiography if there is concurrent clinical need to exclude epicardial coronary disease as a trigger for cardiogenic shock.

CMR exploits differences in the relaxometry characteristics of inflamed and normal tissue. A central feature of myocardial inflammation is oedema. This can be both cellular and interstitial in origin and can be detected using T2 and T1-weighted sequences. Like most other cells, myocytes are predominantly made up of water. The water content of cells is very tightly regulated at the cell membrane level by active ion transport and tight homeostasis of the composition of interstitial fluid. These processes are energy dependent and therefore *ischaemia* or any inflammatory insult that alters the metabolic state of the cell or the permeability of the cell membrane, may allow influx of water into the cell as active ion transport fails to maintain the intracellular osmolality. Even small changes (~3%) in cellular water content can increase T2-times [44]. The combination of increased cellular water content and increased cellular free water in response to tissue injury therefore significantly prolongs T2 relaxation times [45].

In addition, capillary leak is a cardinal feature of inflammation as endothelial permeability is increased by the release of pro-inflammatory mediators to allow diapedesis of inflammatory cells and plasma into the interstitial space. This increase

Table 7.2 Multiparametric CMR is sensitive to many tissue changes that occur during myocardial inflammation, regardless of its aetiology

Tissue changes that occur during myocardial inflammation		
Dysfunction (“functio laesa”)	<i>Cine Sequence</i>	
<i>Hyperaemia</i> (increased vascular permeability, capillary leak)	<i>Early gadolinium enhancement (EGE)</i>	
<i>Oedema</i> (intracellular and interstitial)	<i>T2-mapping T2-weighted imaging</i>	
<i>Myocyte injury/necrosis</i> with loss of cell membrane integrity	<i>Late gadolinium enhancement</i>	
<i>Accumulation of debris, inflammatory cells, collagen deposition in the extracellular space</i>	<i>Extracellular volume (ECV) map</i>	
<i>Pericardial involvement</i> (effusion, thickening, fibrosis, constriction)	<i>Late gadolinium enhancement (LGE) Dixon fat-water separation sequences</i>	

in extracellular water content is also detected by T2W-imaging (Fig. 7.4) techniques but will also increase T1 relaxation times (Fig. 7.5).

Imaging early after the injection of gadolinium may reveal hyperintensity in areas of increased capillary leak or hyperaemia due to increased delivery and egress of contrast [42]. However, its use has not been shown to improve the diagnostic performance of the original Lake Louise Criteria which incorporated it. Despite attempts to standardise its interpretation using ratios of signal intensity to nearby

Fig. 7.4 T2W-spin echo sequence with fat saturation depicting increased signal in the basal lateral wall (arrow), which is one of the segments most frequently affected in acute myocarditis

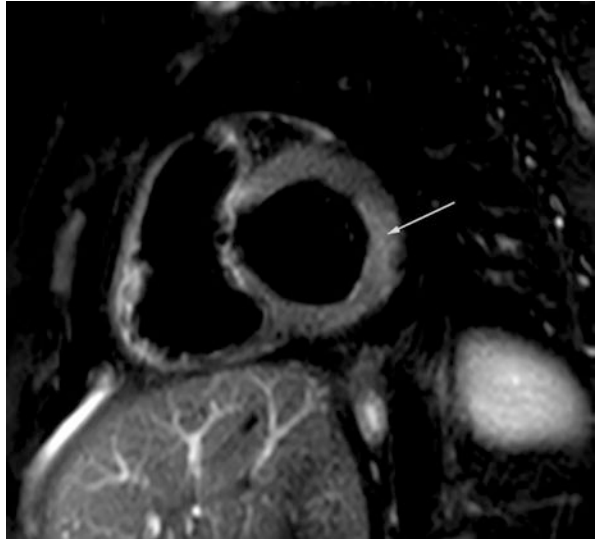


Fig. 7.5 T1-parametric map illustrating increased native T1 in a mid-wall (non-ischaemic) distribution, most striking in the lateral and inferior walls

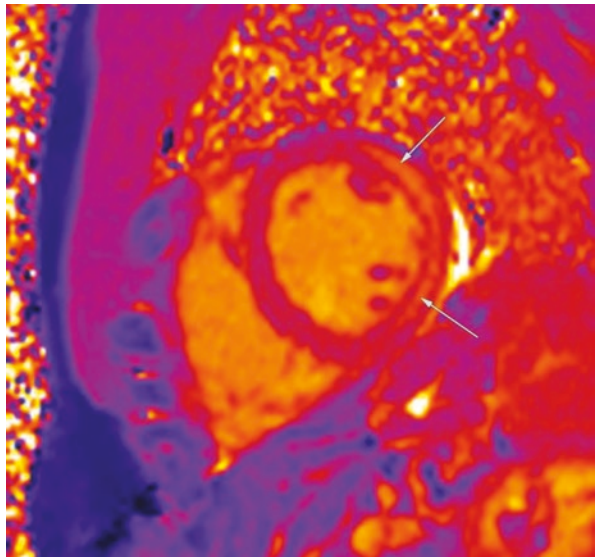
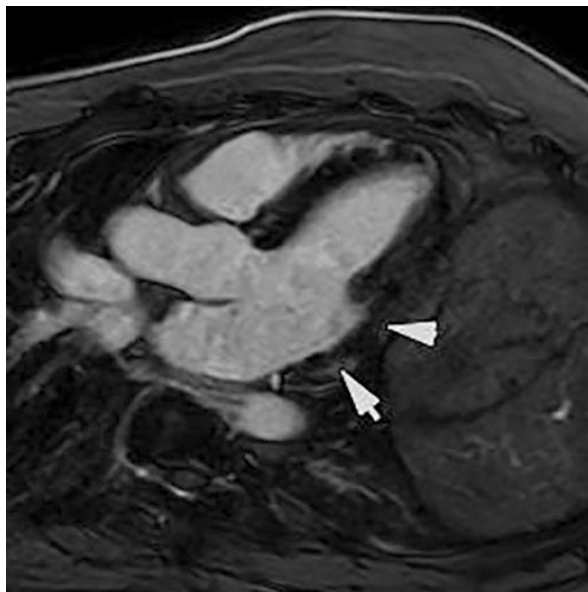


Fig. 7.6 Late gadolinium enhancement sequence in patient with acute myocarditis. The inversion time is set to null the normal myocardium which appears black. The areas of inflammation/fibrosis which attain higher contrast concentrations and therefore have shorter T1 relaxation times appear high signal or white (arrows). In this instance, there is focal patchy epicardial to mid-wall enhancement of the basal inferolateral wall which spares the endocardium, a typical distribution for myocarditis



skeletal muscle, its use remains fraught with subjectivity and it is therefore seldom employed in clinical practice.

However, imaging in the late phase after gadolinium contrast injection continues to play a critical role in diagnosis [46]. Late gadolinium enhancement imaging uses contrast to depict differences in tissue relaxation characteristics. Gadolinium chelates are large molecules that cannot penetrate the healthy intact cell membrane. Therefore, when contrast is given, it stays entirely extracellular and accumulates in areas of cell injury and fibrosis, while in healthy regions, contrast more readily washes out [47]. Gadolinium is paramagnetic and shortens T1 in proportion to its concentration. Thus, if imaging is performed after an interval to allow contrast washout (typically 10–15 min) using an inversion recovery prepared sequence, areas of tissue injury which harbour a higher gadolinium concentration will have a shorter T1 than surrounding healthy myocardium and so will recover signal more quickly. If the inversion time is set to null the normal myocardium, the areas of shortened T1 will appear to enhance (Fig. 7.6).

However, this enhancement may reflect expansion of the extracellular space through interstitial oedema, myocyte injury (with loss of cell membrane integrity) and in later phases, replacement fibrosis [46]. It is therefore not specific for inflammation per se and indeed, as the latter resolves, apparent fibrosis can appear to shrink reflecting resolution of interstitial oedema as well as contraction of scar tissue itself [48]. However, the pattern of tissue injury and fibrosis can be helpful in some instances for assessing the aetiology of myocarditis and in differentiating suspected myocarditis from infarction in patients with myocardial infarction and apparently unobstructed coronary arteries [49]. In the latter, there is usually a centrifugal pattern of tissue injury starting from the sub-endocardium (in a defined coronary

territory) and extending towards the epicardium, reflecting the greater vulnerability of the sub-endocardium to ischaemia. In contrast, most types of myocarditis with a few exceptions produce a more centripetal pattern of injury, starting from the epicardium and/or involving the mid-wall.

The advent of T1 mapping techniques now allows myocardial T1 to be directly measured. These techniques may afford good diagnostic accuracy if undertaken within 2 weeks of the index presentation [46], however, as T1 prolongation can occur due to a variety of other reasons, e.g., hypertensive heart disease, they may be less reliable in patients with pre-existing cardiovascular disease or heart failure. Furthermore, reliable values are generally obtained by drawing regions of interest excluding epicardial and endocardial voxels. The latter may be subject to blood pool contamination and partial volume effects from this. The former may be impacted by susceptibility effects from surrounding epicardial fat or other structures. Numerous other technical factors can influence the readings obtained [50]. Therefore, in addition to meticulous precautions during image acquisition, dedicated normal ranges are required specific to the actual sequence used as well as the scanner platform and vendor being utilised [51]. Depending on the sequence, these may vary with temperature, age, gender, heart rate, and segmental location in the myocardium [51]. Each centre therefore needs scanner-specific reference ranges which may limit the correct use of these techniques in clinical practice. Measurement of native T1 may afford improved sensitivity as it detects increased intracellular water, expansion of the extracellular space, hyperaemia, and fibrosis, but for the same reason, may lack specificity on its own.

T1-maps acquired 15 min or more after contrast can be combined with pre-contrast maps and knowledge of the patient's haematocrit to generate estimates of extracellular volume (ECV) [52]. This approach has the potential advantage of quantitatively identifying areas of tissue injury and minimising subjectivity. The late gadolinium enhancement (LGE) technique relies upon selection of an inversion time to null apparently normal myocardium. However, in doing so, signal from diffuse interstitial expansion may be rendered imperceptible. As with LGE, changes in ECV may be present due to underlying pre-existing cardiovascular disease and may be due to any of increased interstitial fluid/water, cell death, or fibrosis. Parametric maps of ECV are generated after non-rigid registration of pre- and post-contrast T1 maps [52]. They may have lower spatial resolution than LGE images and while their use has entered the revised Lake Louise Criteria [8], their precise role and added value over and above LGE in the setting of myocarditis remains to be defined.

T2-parametric mapping sequences are less liable to some of these limitations, but dedicated reference ranges are still required. It is likely that T2 prolongation will have greater specificity for myocardial inflammation and therefore may be of significant utility in the setting of acute myocarditis [8].

Traditionally, T2-weighted spin echo sequences have been used to evaluate changes in T2 signal in suspected myocarditis. However, only relative differences in signal intensity are depicted, rendering a degree of subjectivity to image interpretation. In addition, slow-flow artefacts and signal drop-out due to arrhythmia or cardiac motion may further decrease image quality [45] (Fig. 7.7a).

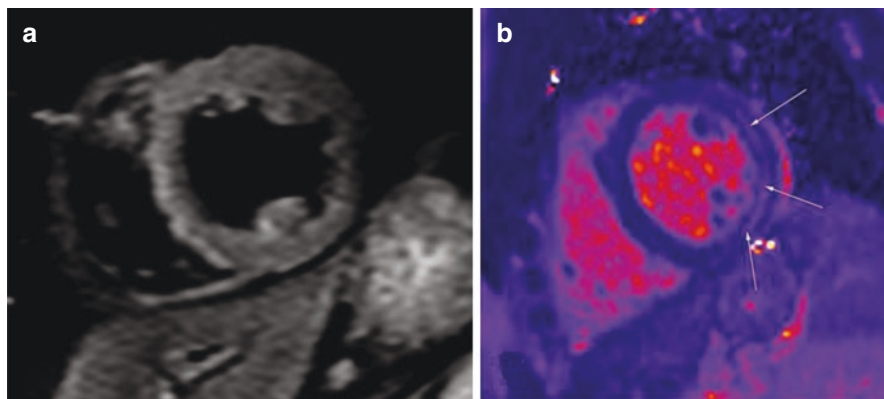


Fig. 7.7 (a) T2W-spin echo sequence with fat saturation illustrating the problem of signal drop-out in the lateral wall. The non-uniformity of signal intensity also illustrates the potential subjectivity involved in interpreting relative differences in signal with this approach. (b) T2-prepared Steady-State Free Precession (SSFP) parametric map depicting increased T2 times in the lateral and inferior walls (arrows) in a mid-wall distribution in a patient with acute myocarditis

This can usually be overcome by adjusting the acquisition to earlier in diastole. Finally, signal intensity can vary as a function of distance from the coils, introducing significant coil bias effects [45]. These effects can be partially abrogated by switching off surface coils (with a resulting signal to noise ratio (SNR) penalty) and/or by using nearby skeletal muscle to normalise signal intensity. Nevertheless, the reliance on relative differences in signal for image interpretation pre-supposes that the entire myocardium is not inflamed. Quantitative T2 mapping techniques measure actual T2 times and so are not subject to these limitations (Fig. 7.7b).

They require shorter breath holds and so may be both better tolerated and less liable to the effects of intermittent arrhythmia. However, they tend to have lower spatial resolution and may not adequately visualise thin structures such as the pericardium. In this setting, traditional spin echo sequences can still afford added value (Fig. 7.8).

The original Lake Louise criteria advocated an “any 2 out of 3” approach to diagnosing any two of *positive T2-weighted imaging, increased early gadolinium enhancement, and late gadolinium enhancement* in a non-ischaemic pattern [42]. As early gadolinium enhancement is not frequently used in most centres, in practical terms, the original criteria were operationalised as a “2 of 2” approach: one T2-weighted imaging technique (traditionally T2W-spin echo based imaging) and one T1-weighted technique post-contrast (LGE). The criteria have now been revised to acknowledge the growing use of parametric mapping retaining this de facto schema. The revised (2018) criteria now stipulate the use of any T2-based technique (T2W-spin echo as previously or T2-parametric mapping) and a T1 based technique (native T1 on its own, LGE, or ECV) [8]. The requirement for a T2-based imaging technique affords improved specificity for active inflammation. While these revised criteria reflect a pragmatic evolution of the original consensus guidelines, they are

Fig. 7.8 T2W-spin echo sequence with fat saturation in a patient with acute myocarditis illustrating increased signal in the lateral wall. In addition, the high spatial resolution allows the overlying inflamed pericardium to be visualised

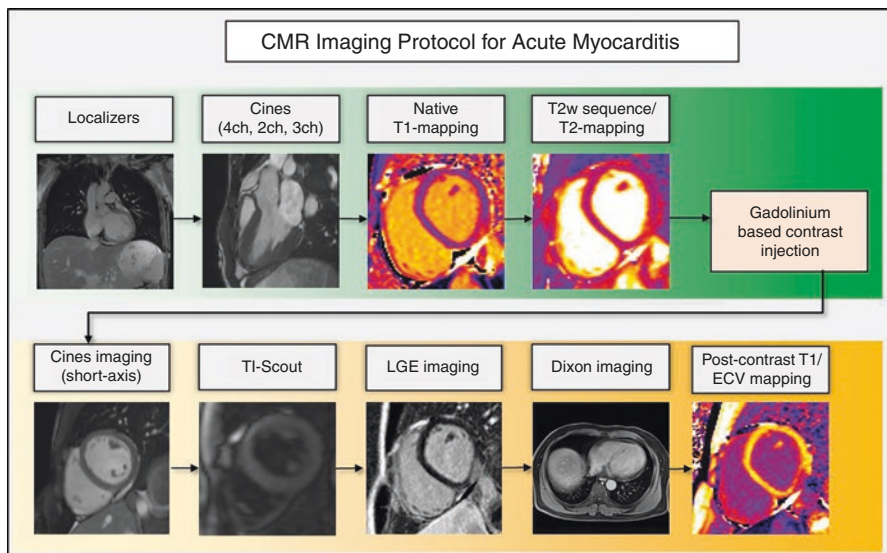
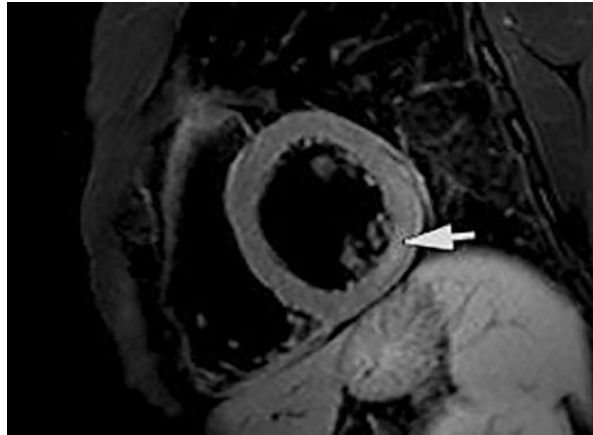


Fig. 7.9 Clinically feasible CMR imaging protocol for acute myocarditis

yet to be comprehensively validated in large cohorts in clinical practice. Initial data seems to suggest improved diagnostic accuracy [53].

A clinically feasible CMR protocol for assessment of myocarditis is shown in Fig. 7.9.

As with any other imaging findings, data particularly from parametric mapping needs to be interpreted in the appropriate clinical context. A diagnosis of myocarditis should only be made if there is sufficient pre-test probability in terms of clinical presentation to justify this. The original and updated Lake Louise Criteria recognise the presence of additional imaging findings that may support the diagnosis

including features consistent with concomitant pericarditis (see Chap. 5: Pericarditis) and the presence of regional or global LV systolic dysfunction in the absence of significant coronary artery disease [8, 42].

7.7 Infectious Inflammatory Cardiomyopathy

7.7.1 Idiopathic/Post-Viral Myocarditis

Most cases of myocarditis are either idiopathic or presumed viral. The diagnostic yield of viral serology is low and therefore not routinely recommended unless specific therapeutic interventions are likely to be offered, e.g., HIV [6]. The underlying pathophysiology may involve direct invasion of myocytes and tissue injury due to virally mediated cytotoxicity or to innate or virus-specific T-cell responses [54]. It is likely however that subsequent tissue injury is at least in part autoreactive in response to the release of previously private cardiac epitopes that may mimic viral antigens [18].

There is a predilection towards the basal to mid-inferolateral walls [8]. The reasons are unclear but may reflect direct spread of infection from the overlying serosal visceral pericardium. This is less likely to be undermined by epicardial fat along the lateral surface of the LV. T2W-imaging may reveal epicardial to mid-wall increases in signal intensity. LGE imaging characteristically also reveals epicardial to mid-wall enhancement, sparing the sub-endocardium. There may also be additional evidence of a concomitant pericarditis (see Chap. 5: Pericarditis). The other segments commonly involved are the basal to mid-septum, usually with fibrosis/tissue injury in a mid-wall distribution.

Active myocarditis may engender regional or global contractile dysfunction. However, often there can be extensive tissue injury with comparably minimal impact on cardiac contractility, as the endocardial myocytes which tend to be prime movers in normal ventricular function are relatively spared.

In the acute phase, areas of LGE may exhibit significant oedema as well as cell death and fibrosis. As oedema subsides, and necrotic cells are removed and replaced by collagen/fibrous tissue, the area of injury can appear to shrink [48].

7.8 Coronavirus Disease-2019 (COVID-19) and Myocarditis

A number of coronavirus disease-2019 (COVID-19) related myocarditis cases have been reported, but its true incidence is unclear [55]. Apart from clinical presentation, simple bedside tests such as serial ECG and cardiac biomarkers or echocardiography can raise the suspicion of acute-onset cardiac symptoms [56]. Presence of cardiovascular risk factors and pre-existing coronary atherosclerosis seems to be associated with a worse prognosis in patients with COVID-19 [57]. The pathophysiology of COVID-19-related myocarditis is thought to be a combination of direct viral injury, cytokine release, and cardiac damage due to the host's immune response

[56, 58]. Distinguishing between acute myocarditis, stress or sepsis-related cardiomyopathy, and acute coronary syndrome may be difficult, particularly in patients with more severe COVID-19 disease course [56]. CMR may play a role in differential diagnosis and detection of cardiac damage. In a prospective cohort study ($n = 100$) of recently recovered patients from COVID-19, CMR revealed apparent cardiac involvement in 32% (positive LGE) and 78% (abnormal parametric T1/T2 mapping), independent of pre-existing conditions, severity, and overall course of the acute illness [59, 60]. These findings seem to be partly supported by a certain correlation of T1/T2 measures with mild elevations of high-sensitivity cardiac troponin values [59]. Other smaller studies reported similar rate of cardiac involvement (positive LGE) and much higher rates of cardiac involvement after consideration of parametric T1/T2 mapping results [61, 62]. In general, applying the revised CMR Lake Louise criteria (including findings of T1 and T2 mapping) [8] seems to result in a much higher rate of potential cardiac involvement in COVID-19. In contrast, most myocardial histology from autopsy specimens of patients who died of COVID-19 illness have not conclusively established the presence of myocarditis in most of the patients [63, 64]. Therefore, it is possible that the prevalence of true myocarditis may have been overestimated in these early CMR studies, in particular when quantitative T1 and T2 mapping had been employed. There is still some way to go with standardisation of T1/T2 mapping methods, reference ranges, evaluation, and protocols [52, 65]. Therefore, further and also long-term imaging studies with clinical endpoints are needed to fully assess the association of COVID-19 and myocarditis and in particular their clinical significance.

7.9 Non-Infectious Inflammatory Cardiomyopathy

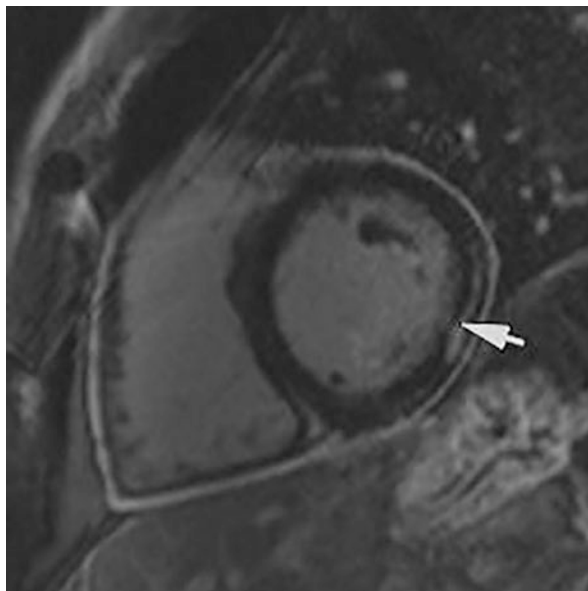
7.9.1 Connective Tissue Disease

7.9.1.1 Systemic Lupus Erythematosus

Systemic lupus erythematosus (SLE) is a systemic autoimmune disease with protean clinical manifestation. The pericardium is frequently involved resulting in pericarditis (Fig. 7.10), which forms part of the diagnostic criteria for the condition [66]. Patients experience accelerated atherosclerosis in the setting of the chronic inflammatory milieu engendered by the condition and therefore coronary heart disease remains a frequent cause of mortality. However, the myocardium and occasionally the endocardium can also become involved.

Myocarditis in SLE, like infectious myocarditis, can present with epicardial to mid-wall fibrosis of the basal to mid-lateral wall and mid-wall fibrosis of the inter-ventricular septum. However, equally, myocardial inflammation can occur and resolve without fibrosis detectable by conventional LGE imaging or can be subacute [67]. Parametric mapping techniques, and particularly T2-mapping, may play an important role in detecting inflammation in the latter settings [68, 69]. SLE can also present with a fulminant myocarditis [43].

Fig. 7.10 Mid-ventricular short-axis late gadolinium enhancement sequence in a patient with lupus peri-myocarditis. There is mid-wall enhancement of the lateral wall (arrow). In addition, there is global enhancement of the pericardium



Patients with SLE may also develop Libman–Sacks endocarditis which may manifest as a valvulitis with aseptic vegetations or as diffuse sub-endocardial enhancement. Valvular involvement however is better assessed by echocardiography which has higher temporal resolution allowing the movement of vegetations to be appreciated and is more adept at assessing the functional consequences of any resulting valvular dysfunction.

Patients with SLE frequently have associated or secondary antiphospholipid antibody syndrome. The latter can present with infarcts in multiple territories (Fig. 7.11). This can result in areas of sub-endocardial enhancement that involve entire segments supplied by a given epicardial coronary artery or in the setting of a thrombotic microangiopathy, in small focal punched out lesions reflecting the involvement of the more distal vasculature. Additional stress perfusion imaging should therefore be considered in all patients referred for potential cardiac involvement with SLE.

7.9.1.2 Rheumatoid Arthritis

Most patients with rheumatoid arthritis who develop cardiovascular complications are afflicted by coronary disease which occurs as a result of accelerated atherosclerosis in the inflammatory state generated by the condition [70]. One-third of patients develop pericarditis (Fig. 7.12) although only up to one-third of these are ever symptomatic [71]. Myocarditis is relatively rare but can present in the form of focal granulomatous inflammation with intramyocardial rheumatoid nodules, often in seropositive disease with high rheumatoid factor titres [72]. Rheumatoid nodules can also develop in the pericardium and rarely, also on valves, with potential functional consequences [73]. Some studies however have identified a high prevalence

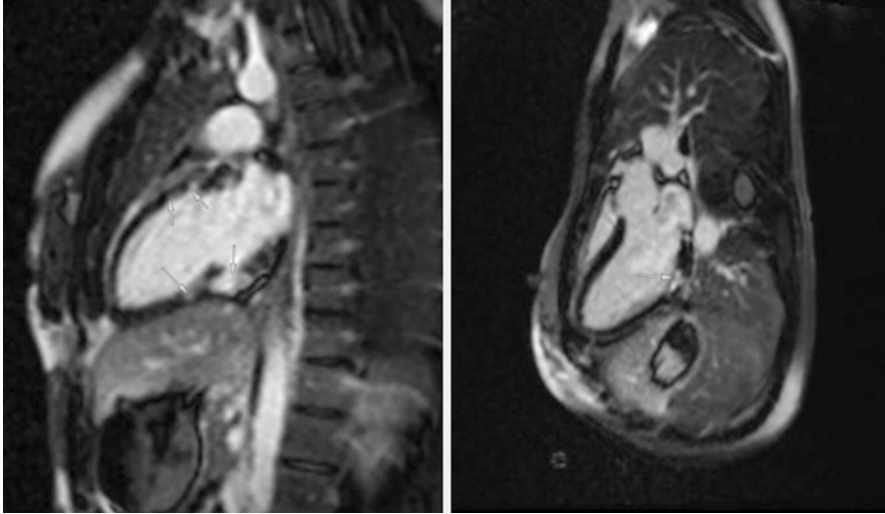
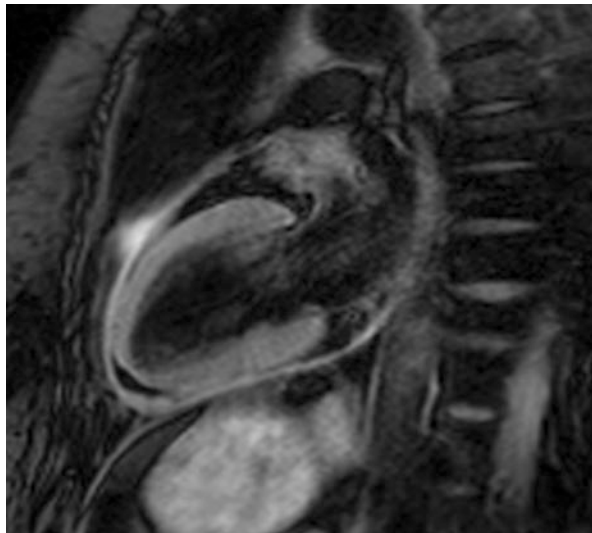


Fig. 7.11 Two chamber (left) and three chamber (right) late gadolinium enhancement sequences from a patient with SLE and secondary antiphospholipid antibody syndrome-associated thrombotic microangiopathy. There are multiple (arrows) small focal discrete partial thickness sub-endocardial areas of enhancement in the anterior wall, inferior, and inferolateral walls

Fig. 7.12 T2W-spin echo sequence in a patient with rheumatoid-associated pericarditis. The pericardium (normally inconspicuous on this sequence in the healthy state) is clearly visible and high signal. There is also an associated small pericardial effusion but no myocardial involvement in this instance



of non-ischaeamic patterns of LGE in patients with rheumatoid arthritis [74] and evidence of diffuse fibrosis on T1-parametric mapping [75]. This may suggest that many patients may develop myocarditis without ever manifesting clinical symptoms.

Patients can also develop a malignant necrotising small and medium vessel vasculitis which can occasionally involve the heart in a manner analogous to

polyarteritis nodosa [76]. This is again usually associated with high rheumatoid factor titres and erosive disease.

7.9.1.3 Systemic Sclerosis/Systemic Scleroderma

This disorder is a multisystem autoimmune disease characterised by vascular dysfunction and the deposition of fibrous tissue in different organs including the heart [77]. Patients may experience direct myocardial injury by way of deposition of fibrous tissue following myocarditis [78]. Areas of sub-endocardial injury and fibrosis (Fig. 7.13) may also result from the effects of severe microvascular dysfunction/ischaemia and can occasionally result in circumferential ring-like sub-endocardial fibrosis. However, the heart is also frequently impacted by the effects of systemic hypertension, particularly if there is renal involvement (manifesting as hypertensive heart disease with left ventricular hypertrophy and diffuse fibrosis), or pulmonary hypertension which can result in right ventricular pressure overload and failure (Fig. 7.14) [77].

The combination of these direct and indirect insults on the myocardium can also generate the development of focal [79] and diffuse myocardial fibrosis [80]. The latter can be detected through non-contrast T1 mapping techniques and with contrast, by estimating ECV [81]. Fibrosis may be driven by chronic low grade myocarditis which is otherwise clinically silent [82].

The pericardium can also become involved, resulting in sometimes moderate or large pericardial effusions (Fig. 7.15). Although most effusions are asymptomatic, patients can also present with tamponade or with features of acute pericarditis. Pericarditis can progress to constriction. The latter can be challenging to diagnose particularly if there is concomitant pulmonary arterial hypertension. Based on a

Fig. 7.13 Four chamber late gadolinium enhancement sequence in a patient with systemic sclerosis. There is a focal area of near-transmural enhancement in the basal lateral wall (arrow). This can be seen in systemic sclerosis even in the setting of unobstructed coronary arteries. Accelerated epicardial coronary artery disease, however, is also common. Note the diffuse contrast uptake in the lung reflecting associated interstitial lung disease

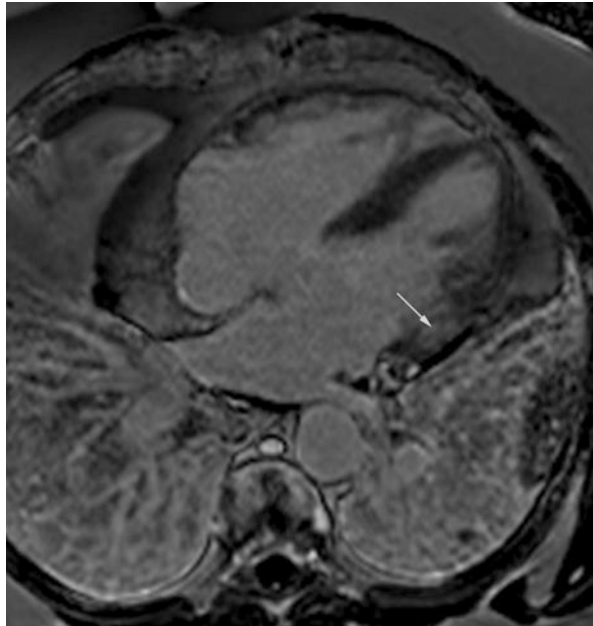
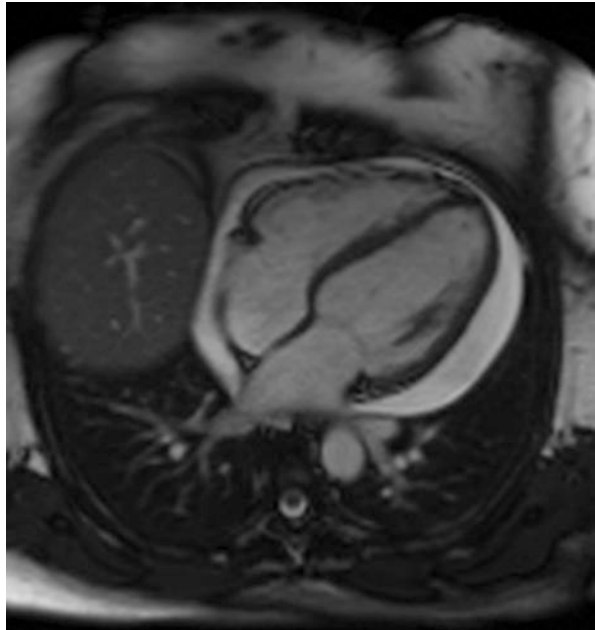


Fig. 7.14 Mid-ventricular short-axis late gadolinium enhancement sequence in a patient with pulmonary hypertension associated with systemic sclerosis. In common with other causes of pulmonary hypertension, there is enhancement of both the anterior and inferior LV/RV insertion points (arrows)



Fig. 7.15 Four chamber balanced steady-state free precession cine sequence in patient with a moderate pericardial effusion associated with systemic sclerosis



relatively small CMR study with histopathologically confirmed myocardial involvement of systemic sclerosis, a CMR-based pragmatic approach has been proposed: myocardial involvement in systemic sclerosis can be assumed in patients with pathological CMR findings in at least three of five categories: (1) pericardial effusion; (2) pathological LV or right ventricle (RV) contractility (hypokinesia, dyssynchrony,

diastolic restriction); (3) depressed left of right ventricular ejection fraction; (4) fibrosis (positive LGE) and/or inflammation; and (5) right ventricular dilatation [80].

7.9.1.4 Behçet's Disease

This is a rare systemic vasculitis of unknown aetiology. It can characteristically affect both arteries and veins but can also directly involve all layers of the heart with pericarditis, myocarditis, and aseptic endocarditis [83].

Venous involvement can manifest as a thrombophlebitis all the way through to thrombosis of the great veins. Patients can therefore present with the vascular consequences of this, e.g., Budd–Chiari syndrome, or with venous thromboembolism [84].

It can also characteristically result in an aseptic endomyocarditis, which can involve large parts of the right ventricle and generate large in situ RV thrombi (Fig. 7.16). As with thrombi in the systemic venous circulation, the latter can embolise resulting in pulmonary embolism and secondary thromboembolic pulmonary hypertension (Fig. 7.16). The pulmonary arteries can also be directly involved as part of the systemic vasculitis resulting in pulmonary arterial aneurysms, thrombosis, and pulmonary haemorrhage [84]. An acute aseptic endomyocarditis can heal with sub-endocardial fibrosis (Fig. 7.17). The myocardium can also be directly

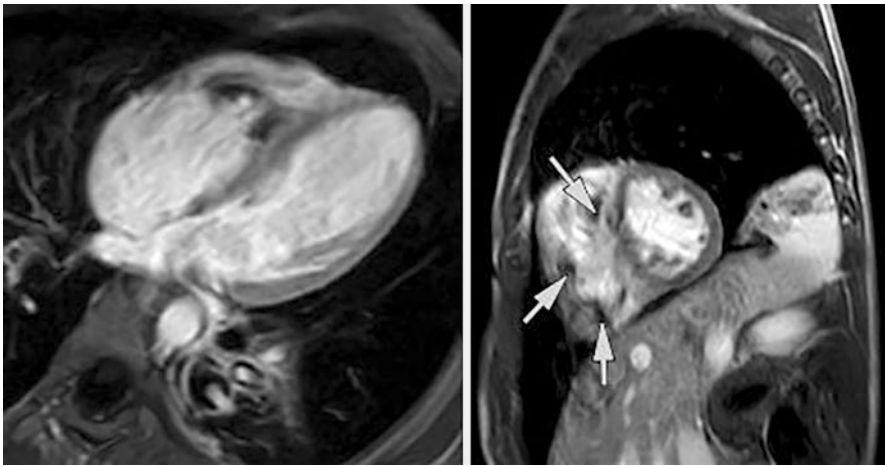
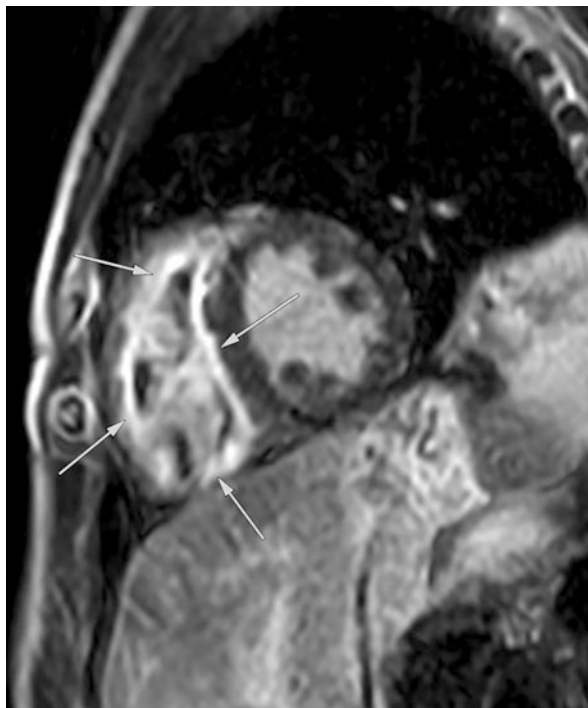


Fig. 7.16 Four chamber (left) and mid-ventricular short-axis (right) early gadolinium enhancement sequences in a patient with active Behçet's disease with cardiac involvement, acquired immediately after contrast injection with the inversion time set to 450 ms. This causes the myocardium to appear very bright as it is saturated with contrast. Thrombus on the other hand is not perfused and so does not take up contrast. It has a long intrinsic T1 and so therefore appears black. There is an aseptic endomyocarditis of the right ventricle (RV) resulting in thrombus formation (white arrows). These thrombi or those from associated pulmonary arterial vasculitis can embolise. Note the area of signal change in the left lung which reflects the consequences of pulmonary infarction

Fig. 7.17 Mid-ventricular short-axis late gadolinium enhancement sequence in a patient with active cardiac Behçet's disease. There is aseptic endomyocarditis of the right ventricle resulting in enhancement of the endocardial surface of the RV and the RV aspect of the septum (arrows). Several thrombi can be seen on the inflamed surface



involved resulting in mid-wall fibrosis as in many other types of acute myocarditis. Rarely, there may be inflammation of the coronary arteries themselves resulting in myocardial infarction with sub-endocardial to transmural enhancement in the relevant coronary territory [85].

7.9.1.5 Polyarteritis Nodosa

This is medium vessel vasculitis. It often involves the renal and mesenteric vascular beds; however, it can occasionally affect the coronary arteries. The resulting coronary arteritis can present as an acute myocardial infarction with often transmural infarction in the relevant territory (Figs. 7.18 and 7.19) [86, 87]. This results from dissection, thrombotic coronary occlusion, or embolization of thrombus within a more proximal coronary artery aneurysm to the distal vessel. As in other arteries, the arteritis can result in the formation of multiple stenoses which may generate angina pectoris.

As the kidneys are very frequently involved, patients often have significant systemic hypertension [88]. The myocardium can therefore be indirectly impacted by the effects of this, resulting in diffuse fibrosis and LVH. The combination of ischaemic myocardial injury and a persistent high afterload state may risk the development of chronic left ventricular dysfunction.

Fig. 7.18 Four chamber late gadolinium enhancement sequence in a patient with polyarteritis nodosa. There are multiple distinct areas of sub-endocardial infarction in this instance in the left anterior descending and right coronary artery territories

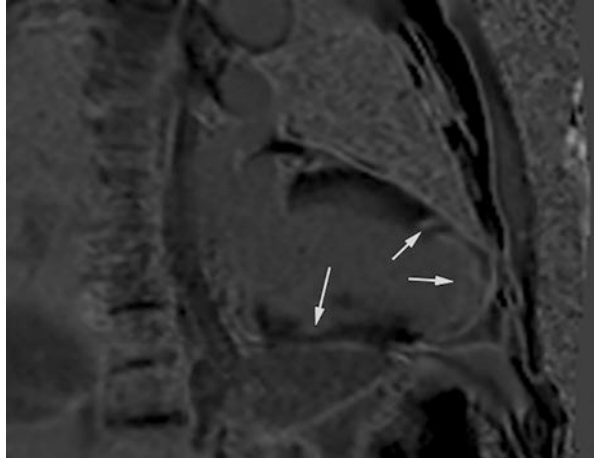
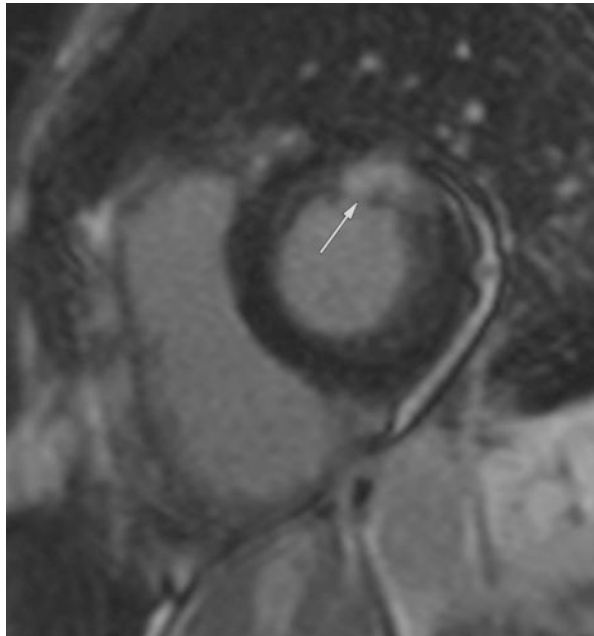


Fig. 7.19 Mid-ventricular short-axis late gadolinium enhancement sequence in a patient with polyarteritis nodosa with coronary involvement depicting a focal infarct in the circumflex territory



7.10 Eosinophilic Myocarditis/Endomyocardial fibrosis

In the Western world, this is a relatively uncommon cause of myocarditis where eosinophils play a cardinal role in inciting myocardial injury [89]. As such, endomyocardial biopsy plays an important role in diagnosis, particularly for fulminant presentations [53]. For non-fulminant presentations where CMR is safe to undertake, a scan may obviate the need for biopsy or may confirm the presence of

intraventricular thrombus which might increase the thromboembolic risks of this and inform decisions on timing. However, many different causes of eosinophilic myocarditis produce characteristic CMR findings which may allow diagnosis in the appropriate clinical context.

In addition to idiopathic hypereosinophilic syndromes, the principal causes are as follows:

1. Eosinophilic Granulomatous Polyangiitis (EGPA), formerly known as Churg-Strauss syndrome.
2. Infectious—particularly helminthic or parasitic which may generate a Loeffler's endomyocarditis and result in endomyocardial fibrosis.
3. Haematological.
4. Drug-induced—Drug Reaction with Eosinophilia and Systemic Symptoms (DRESS) or hypersensitivity myocarditis.

7.10.1 EGPA

This is characterised by asthma, allergic rhinosinusitis, and blood eosinophilia [90]. It can result in a small or medium vessel vasculitis which may be p-ANCA positive and is driven by eosinophil-mediated tissue injury. Patients with EGPA-associated small vessel vasculitis typically develop small highly localised focal sub-endocardial areas of late enhancement disseminated in different coronary territories (Fig. 7.20) [89]. This can sometimes even be appreciated on unenhanced cine sequences (Fig. 7.21). Patients with medium vessel vasculitis can develop a coronary arteritis

Fig. 7.20 Three chamber late gadolinium enhancement sequence in a patient with cardiac eosinophilic granulomatous polyangiitis. Note the discrete foci of sub-endocardial enhancement (arrows) as well as wider endocardial injury

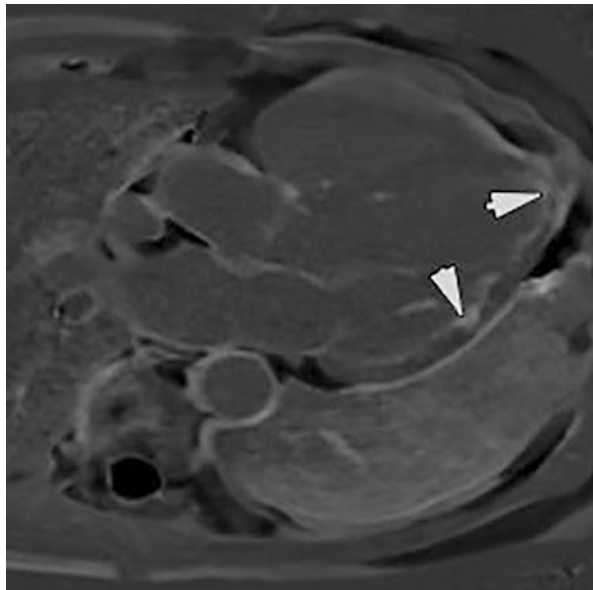


Fig. 7.21 Four chamber balanced steady-state free precession cine sequence in a patient with cardiac eosinophilic granulomatous polyangiitis. Typical small punched out defects are seen within the septum in this instance (arrows) typical of what is seen with this small vessel vasculitis

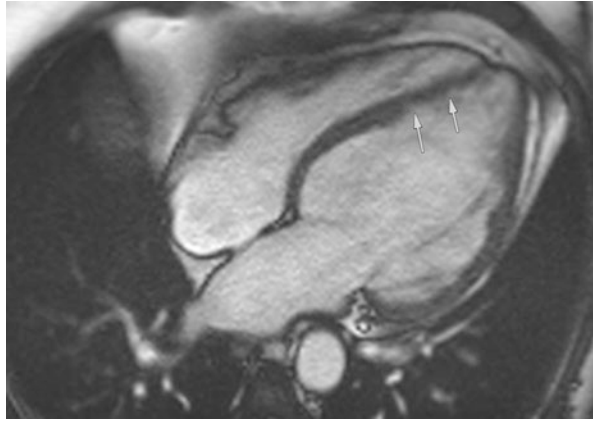
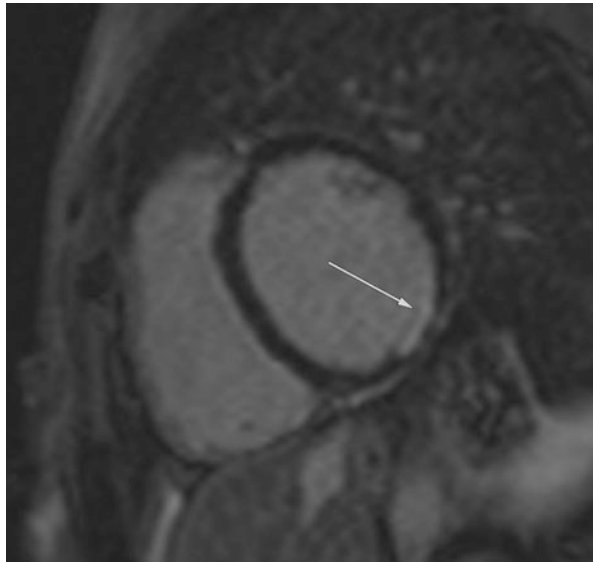


Fig. 7.22 Basal short-axis late gadolinium enhancement sequence in a patient with coronary arteritis secondary to EGPA depicting a near-transmural sub-endocardial infarct in the inferolateral wall



which can present as acute myocardial infarction and transmural myocardial enhancement within segments subtended by the relevant coronary artery (Fig. 7.22). The depth, extent, and regional restriction of such enhancement can therefore allude to the presence of coronary vasculitis. Patients may also develop an aseptic endomyocarditis which is characterised by diffuse sub-endocardial myocardial injury. The latter manifests as diffuse sub-endocardial enhancement, and particularly when there is acute endothelial injury, there may be superimposed LV thrombus formation [86, 91]. About 40% of EGPA patients are ANCA positive (predominantly p-ANCA) [90]. Cardiac complications in patients with EGPA remain the principal cause of death [92]. A high index of suspicion should be maintained as up to ~60% or more of patients with cardiac involvement or complications appear to be asymptomatic [93].

7.10.2 Infectious Endomyocarditis and Endomyocardial Fibrosis

The precise cause of endomyocardial fibrosis is often not clear. Chronic or recurrent parasitic infections can result in an eosinophilic endomyocarditis (Loeffler's endocarditis) and may ultimately be responsible for endomyocardial fibrosis in the tropics but it has also been postulated that environmental toxins such as linamarin, a cyanogenic glycoside found in Cassava roots, may be implicated in inciting initial tissue injury [94]. Whatever the ultimate trigger, endomyocardial fibrosis remains the leading cause of restrictive cardiomyopathy worldwide.

With tropical parasitic infections or toxoplasmosis, initial infection may result in a pancarditis with mural thickening secondary to inflammatory infiltrates. Patchy areas of sub-endocardial injury and fibrosis then develop, particularly at the apices, likely reflecting an underlying vasculitis, analogous to EGPA. The resulting endocardial fibrosis leads to a restrictive cardiomyopathy. Over time, this results in bi-atrial enlargement with the risk of atrial fibrillation [94]. Progression can also be accelerated by fibrosis of the papillary muscle which can result in tethering of the mitral valve or tricuspid valve leaflets and significant mitral and/or tricuspid regurgitation. As in other types of endomyocarditis, endothelial injury can predispose to mural thrombus which is often found at the apices. This can generate a so-called double V sign on post-enhancement studies made up of apical myocardium, sub-endocardial late enhancement, and intracavitary thrombus. Both the right and left ventricular apex can be involved and the apex can become obliterated. Other segments can also appear smoother in contour than normal as endocardial fibrosis effaces normal trabeculation (Fig. 7.23).

Fig. 7.23 Three chamber balanced steady-state free precession cine from a patient with eosinophilic endomyocarditis. Notice how inflammation and fibrosis of the endocardial surface have obliterated the normal trabeculation of the left ventricle and has caused apparent thickening of the apex

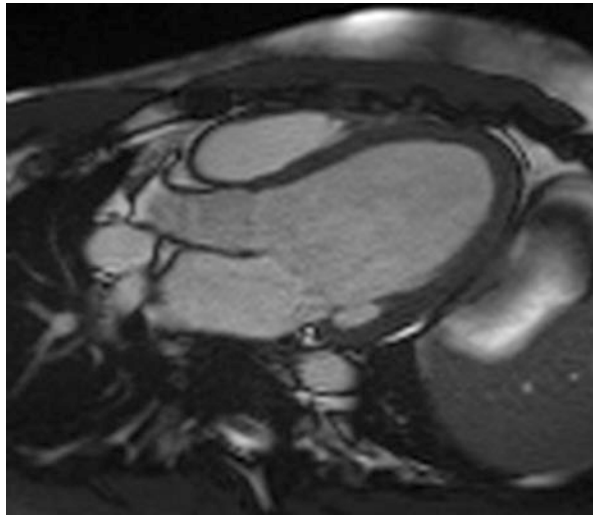
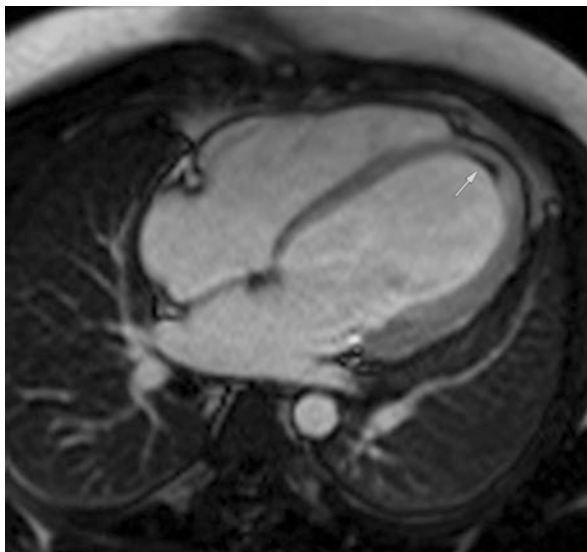


Fig. 7.24 Four chamber early gadolinium enhancement sequence in a patient with eosinophilic endomyocarditis depicting an apical mural thrombus (arrow)



7.10.3 Haematological

Eosinophilic endomyocarditis can also occur because of a primary haematological disorder. The underlying eosinophilia results from either clonal proliferation of eosinophils or in response to excess production of interleukin-5 [95]. The features on CMR are very similar to other causes of eosinophilic endomyocarditis. There is endocardial fibrosis often with super-added thrombosis (Fig. 7.24). This may extend throughout the endocardium. There may be focal sub-endocardial lesions, but these tend to be small and highly localised rather than involving entire segments as might be expected with epicardial coronary disease. These may result for the eosinophilic endomyocarditis itself or potentially from thromboembolism.

7.11 Drug-Induced or Toxic Myocarditis

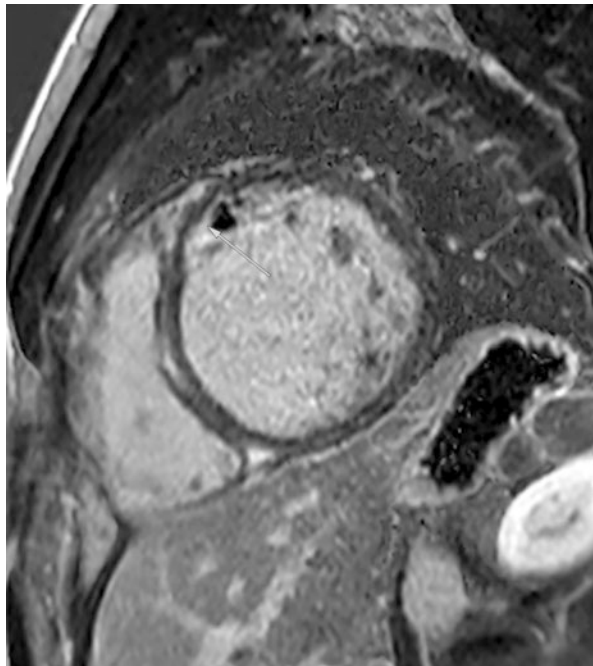
Myocardial inflammation can be incited by a myriad of different drugs. Cardiotoxic chemotherapy agents are particular culprits. The CMR findings vary with the agent but are often non-specific, i.e., epicardial or mid-wall late enhancement. Myocarditis can be an uncommon (1%) but potentially serious complication of immune checkpoint inhibitors, especially when these agents are used in combination [96]. This can present as a fulminant myocarditis, often with a wider myositis or in association with a myasthenic syndrome [97]. The CMR findings can vary depending on the time point of examination. Scans early in the course within a few days of onset may not exhibit any late enhancement or myocardial oedema. Scans can often be delayed

due to patient instability. Up to a quarter of patients in some series exhibit epicardial or mid-wall fibrosis and varying degrees of T2-positivity depending on timing and disease progression [96]. However, the absence of these features does not rule out cardiac involvement and if the clinical picture is still suggestive (e.g., elevation of high-sensitivity cardiac troponin and/or natriuretic peptides), endomyocardial biopsy may afford better sensitivity [98].

As with other forms of myocarditis, patients can also present with new onset heart failure or chest pain without evidence of a coronary cause. CMR can be helpful in this setting (if there is no pressing indication for emergency angiography) in ruling out a coronary aetiology and ruling-in myocarditis. It is likely that mild cases of toxicity do not come to clinical attention. Our understanding of the use and complications of this class of drugs is likely to improve in coming years as indications for their use continue to expand.

In addition to therapeutic drugs, several elicit substances can incite myocarditis. One of the most commonly encountered in clinical practice is cocaine. This can trigger acute myocardial infarction through a combination of profound vasospasm and platelet activation [99], resulting in regional areas of infarction/sub-endocardial enhancement (Fig. 7.25). In addition, however, it can also produce a non-ischaemic pattern of myocardial injury through direct myotoxicity (Fig. 7.25) [100]. Patients can therefore exhibit all three enhancement patterns: epicardial, mid-wall, and sub-endocardial in the same study.

Fig. 7.25 Mid-ventricular short-axis late gadolinium enhancement sequence in a patient with acute on chronic cocaine-induced cardiotoxicity. There is a partial thickness sub-endocardial infarct of the anteroseptum and anterior wall (arrow) with an overlying intraventricular thrombus (dark black). In addition, there is mid-wall fibrosis, particularly of the septum



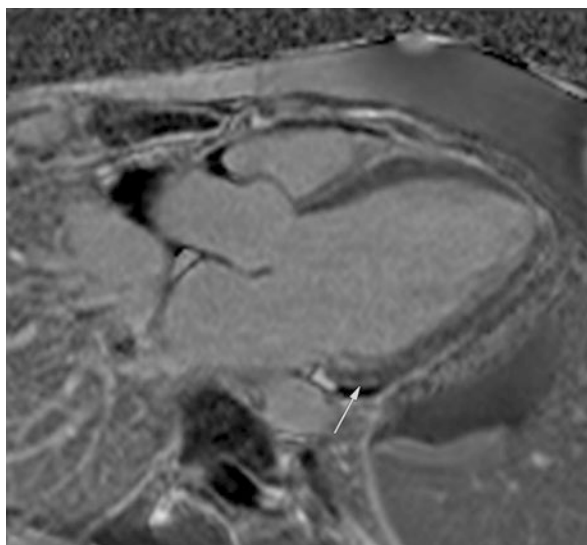
7.12 Inflammatory Myositis

This group of disorders includes dermatomyositis, polymyositis, inclusion body disease, and necrotising myositis. In common with other systemic autoimmune diseases, there is a heightened risk of myocardial infarction due to underlying coronary atherosclerosis [101]. However, cardiac involvement and myocarditis are also recognised complications. Many patients with inflammatory myositis have markedly raised CK levels. When inflamed skeletal muscle starts to regenerate, CK-MB fractions and cardiac isoforms of troponin T can be expressed, potentially giving the impression that there is myocardial injury [102]. In this setting, measurement of troponin I isoforms appears to be more reliable and specific for myocarditis [102]. Troponin T assays and CK-MB should therefore not be used on their own to either rule in or rule out an acute coronary syndrome in patients with significant skeletal muscle myositis.

The exact prevalence of cardiac involvement in dermatomyositis/polymyositis is not known. Data in the literature suggests it is between 9% and 72% but this almost certainly reflects differences in the timing and intensity of cardiac investigations used in different studies as well as heterogeneity in case definitions [103]. The limited CMR case series published suggest that ~56% to 62% may have LGE in a typical non-ischaemic pattern, i.e., epicardial or mid-wall fibrosis [104]. This appears to be more prevalent in patients with a polymyositis phenotype as opposed to dermatomyositis but can occur with the latter (Fig. 7.26).

Cardiac involvement in inclusion body disease is exceptionally rare and limited to isolated case reports and it is unclear whether the myositis is causally linked

Fig. 7.26 Three chamber late gadolinium enhancement sequence in a patient with dermatomyositis with cardiac involvement. There is limited epicardial fibrosis (arrow) of the basal inferolateral wall



[105]. The situation is similar with autoimmune acute necrotising myositis which in itself is a rare disease.

7.13 Giant Cell Myocarditis

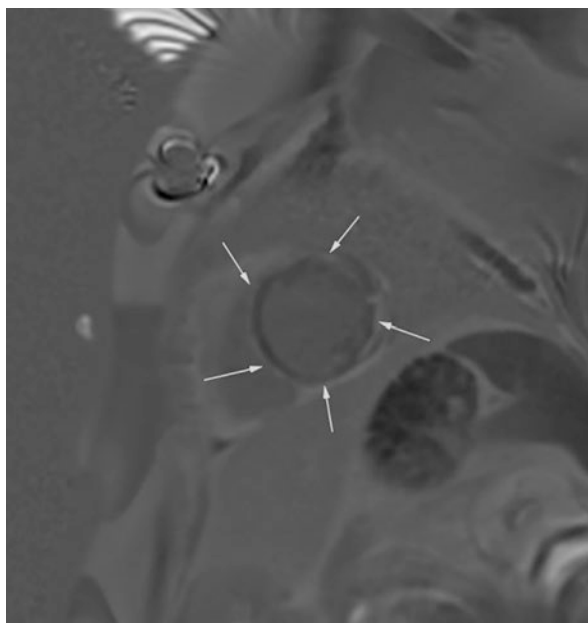
This is a rare cause of fulminant myocarditis of unknown aetiology [43]. It typically presents with acute heart failure complicated by ventricular arrhythmias or progressive AV block [6, 43]. As this often results in haemodynamic instability, patients are rarely stable enough to undergo cardiovascular magnetic resonance. Prompt endomyocardial biopsy is therefore rightly the first means by which diagnosis should be sought. Early diagnosis and prompt immunosuppressive treatment may help to reduce myocardial inflammation and to prevent cardiac complications such as heart failure and reduce the need for mechanical circulatory support or heart transplantation. Descriptions of consistent typical CMR findings are scarce. The few patients that have been scanned have exhibited fibrosis in all patterns and locations, including sub-endocardial injury which is traditionally regarded as ischaemic or embolic in origin [106]. However, the typical multinucleated giant cells may not appear on biopsy specimens until 1–2 weeks into the course of the illness resulting in delayed diagnosis or confusion with fulminant necrotising eosinophilic myocarditis as eosinophil infiltration can be a prominent early feature [43].

7.14 Genetic Causes

It is increasingly recognised that single gene or oligogenic inherited heart muscle diseases responsible for arrhythmogenic cardiomyopathy have a natural history punctuated by episodes of myocarditis. These disorders have traditionally been highlighted as representing a myocarditis mimic on CMR with epicardial to mid-wall late enhancement. Affected individuals have been described as having been incorrectly diagnosed with myocarditis [107]. However, these diagnoses are not mutually exclusive, and it is likely that both are correct with myocardial inflammation playing a key role in the chronic and saltatory progression of these disorders [108].

Mutations in desmoplakin represent a prototypical case for the role of inflammation in the expression of a cardiomyopathy phenotype [108]. Desmoplakin plays a key role maintaining myocyte structural integrity and in force transduction, linking the desmosome to cellular intermediate filaments [109]. It is likely that defects in desmoplakin reduce the resilience of the myocyte to repetitive stress and strain, eventually resulting in loss of cell–cell connections and myocyte apoptosis. This may account for the predilection of susceptible athletic individuals or those who are subject to prolonged or intense bouts of exercise to express the phenotype or experience earlier or more severe disease phenotypes. It is likely that cell injury and cell death incite myocardial inflammation which leads to myocardial fibrosis. Over time, fibroblasts may undergo metaplasia and differentiate to adipocytes and induce

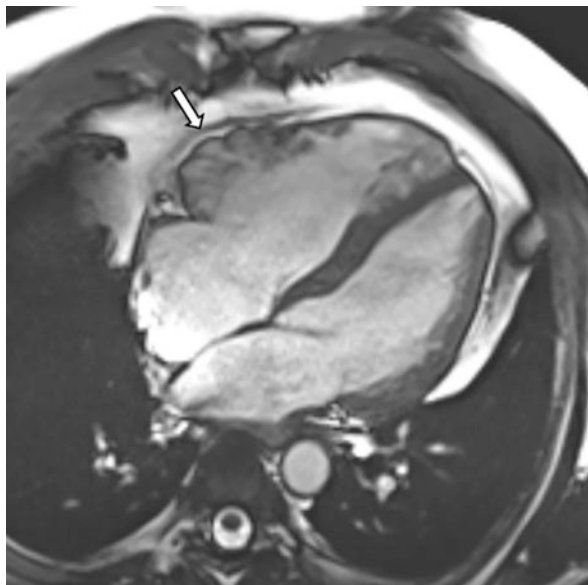
Fig. 7.27 Mid-apical short-axis late gadolinium enhancement sequence from a patient with a confirmed desmoplakinopathy. There is circumferential epicardial to mid-wall enhancement (arrows) forming a ring-like pattern. Also note the susceptibility artefact in the precordial region from an implantable loop recorder



lipomatous transformation of areas of fibrosis and yielding the fibrofatty replacement tissue that is often regarded as a histopathological hallmark of these conditions. Speculatively, the process of myocyte injury and inflammation may expose private myocardial epitopes to the immune system and trigger more on-going inflammation beyond the immediate area of tissue injury. These conditions often present on CMR as extensive circumferential or ring-like late enhancement (Fig. 7.27) [108]. It is also possible that by affecting cell–cell adhesion and integrity, these disorders may make the myocyte more vulnerable to cardiotropic viruses and therefore acute viral myocarditis. It may be that specific modes of inflammatory injury release unique combinations of chemokines and cytokines that mediate fibrofatty differentiation of local mesenchymal progenitor cells [109]. However, there may also be direct differentiation of cardiac progenitor cells to an adipogenic phenotype via suppression of the canonical Wnt (Wingless and Int-1) pathway [110]. The precise mechanisms involved require further elucidation and may provide insights into potential therapeutic approaches aimed at halting the progression of these disorders that are focused on treating myocardial inflammation.

The RV is usually also affected as it is a relatively thin-wall structure and as a result, not able to withstand loads or strain as well as the LV. As in other forms of desmosomal arrhythmogenic cardiomyopathy diseases, there may be RV aneurysms (regions which protrude or bulge in diastole and which fail to contract with systole), particularly in the basal sub-tricuspid region (Fig. 7.28). The presence of typical RV involvement and fibrofatty change may allow differential diagnosis from other variants of arrhythmogenic cardiomyopathy that can produce LV ring enhancement and inflammatory conditions such as sarcoidosis.

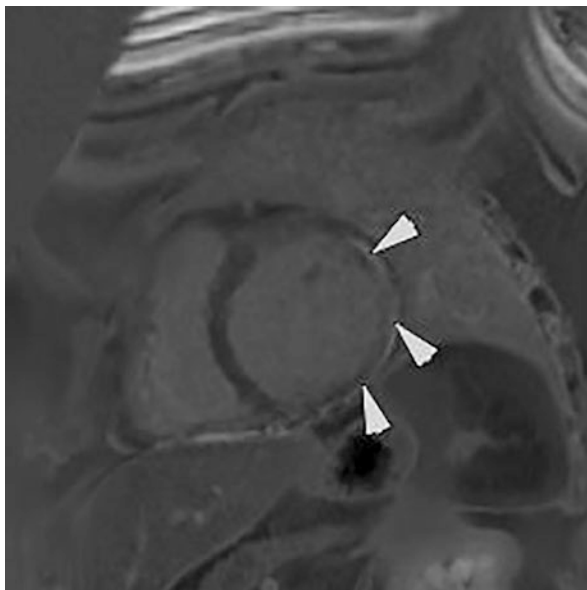
Fig. 7.28 Four chamber balanced steady-state free precession cine image from a patient with a desmoplakin mutation and arrhythmogenic cardiomyopathy phenotype. There is an aneurysmal dyskinetic area (accordion sign) in the basal sub-tricuspid region (arrow)



The contemporary management of patients with X-linked muscular dystrophies provides support for this paradigm. These disorders are also characterised by cellular injury, inflammation, and reparative fibrofatty replacement. The outcomes for these patients have been significantly ameliorated in recent years by the increasing use of oral glucocorticoids. Although part of the mechanism of action of these drugs may involve their anabolic properties, and direct effects on dystrophin expression, their anti-inflammatory properties may also play an important role in their efficacy [111]. The dystrophinopathies typically also involve the heart and on CMR typically manifest as epicardial to mid-wall enhancement of the lateral wall although fibrosis can occur in other segments too (Fig. 7.29). This can be severe enough to produce regional thinning and even regional wall motion abnormalities that may mimic a previous infarct outside of the clinical context.

From an imaging perspective, ^{18}F FDG-PET is frequently used to look for evidence of inflammation as a means of differentiating heritable arrhythmogenic cardiomyopathies from what are through to be primary inflammatory pathologies such as sarcoidosis. However, this approach may require reappraisal given growing appreciation of the role of inflammation in the pathogenesis of arrhythmogenic right ventricular cardiomyopathy. Indeed, patients with arrhythmogenic cardiomyopathy presenting in hot phases of their illness have been found to have evidence of active myocardial inflammation on positron emission tomography [112]. In the absence of extracardiac disease, or other specific clinical features, this may make differential diagnosis very challenging.

Fig. 7.29 Mid-ventricular short-axis late gadolinium enhancement sequence from a female Duchenne carrier. There is dense epicardial to mid-wall enhancement of the lateral and inferior walls (arrows). This pattern is very analogous to that seen as a sequela to a myriad of different inflammatory cardiomyopathies



7.15 Molecular Imaging

Nuclear medicine represents a non-invasive, targeted, in vivo approach of assessing myocardial inflammation using specific radiotracers. Radiolabelled leukocytes with Technetium-99m (^{99m}Tc) or Indium-111 (^{111}In) have been employed in inflammation/infection imaging but the technique is complex and some concerns about its specificity have limited clinical use [113, 114]. Gallium-67 (^{67}Ga) is a radioisotope used in the past to identify chronic inflammatory reactions. In a study including 68 patients with dilated cardiomyopathy, cardiac ^{67}Ga uptake showed a close correlation with myocarditis on biopsy suggesting the possibility of a clinical use [115]. Furthermore, injury to myocytes leads to the release of myosin heavy chain. Anti-myosin antibodies radiolabelled with ^{111}In have been used to detect myocardial injury in both myocardial infarction and myocarditis. Two studies reported the incremental diagnostic value of anti-myosin scans in patients with acute myocarditis who present with severe chest pain masquerading as acute myocardial infarction [116, 117]. Subsequently, Narula and co-workers demonstrated that radiolabelled anti-myosin scintigraphy has a high sensitivity and negative predictive value and may be an effective screening procedure for obviating biopsies in patients with suspected myocarditis [118].

Despite interesting results, the low quality of the images obtained, the variable diagnostic accuracy provided, and the paucity of data on their use have limited the clinical utilisation of these radiotracers.

Conversely, molecular imaging with 2-deoxy-2-[^{18}F]-fluoro-D-glucose (^{18}F -FDG) and positron emission tomography (PET) can study the entire heart revealing focal or diffuse patterns of inflammation and appears an appealing tool for the non-invasive diagnosis of the disease, to guide EMB, and for monitoring treatment response. Glucose is a normal metabolic substrate of myocardium and glucose loading protocols are employed in clinical practice for exploring myocardial viability [119]. On the other hand, when the clinical question is the detection of an increased focal augmentation of myocardial glucose metabolism caused by an inflammatory process, the metabolic activity of the normal myocardium may disturb clinical interpretation of the images. Therefore, long fasting, fatty meal or fractionated/unfractionated heparin administration before ^{18}F -FDG injection has been proposed to suppress physiological radiotracer uptake [120, 121]. However, with the exclusion of sarcoidosis, data on the performance of ^{18}F -FDG PET/CT in the diagnosis and management of patients with myocarditis are scarce. Tanimura and Moriwaki reported two case reports of patients with myocarditis (one patient with lymphocytic and one with eosinophilic myocarditis) in which ^{18}F -FDG-PET/CT was used for diagnosis and to successfully monitor response to treatment [122, 123]. Ozawa retrospectively evaluated 29 subjects with symptoms or left ventricular dysfunction that underwent both ^{18}F -FDG-PET and EMB from left ventricular posterior wall within 3 months. ^{18}F -FDG-PET showed excellent agreement with EMB for detecting active inflammatory disease and the best timing of imaging was within 14 days after the onset of the clinical symptoms [124]. Moreover, myocardial inflammation is probably underestimated in various autoimmune diseases. Perel-Winkler et al. studied eight patients with systemic lupus erythematosus using ^{18}F -FDG-PET/CT [125]. Most patients had chest pain or dyspnoea, half had a reduction in left ventricular ejection fraction, and all patients showed diffuse myocardial ^{18}F -FDG uptake consistent with myocardial inflammation. Similarly, Besenyi et al. studied 16 patients with systemic sclerosis and nine control subjects [126]. Half of the patients were PET-positive at visual analysis, and showed higher myocardial ^{18}F -FDG standardised uptake value ratios and heterogeneity indices, as compared to the control group. The authors concluded that myocardial inflammation can be identified early by ^{18}F -FDG PET/CT in a considerable percentage of systemic sclerosis patients presenting without cardiac symptoms.

7.16 Hybrid Imaging

Recent advances in technology have implemented hybrid PET-CMR as an attractive imaging modality for the evaluation of myocarditis. PET-CMR has the advantage of allowing simultaneous acquisition of both CMR and PET combining the morphological data, tissue characterisation, and metabolic information in the same examination [127]. Nensa et al. prospectively studied 65 patients with suspected myocarditis [128]. Compared with CMR (LGE and/or T2), sensitivity and specificity of PET were 74% and 97%, respectively, demonstrating a good agreement between the two techniques and feasibility of hybrid imaging. In patients with

chronic myocarditis ^{18}F -FDG could improve the diagnostic accuracy of CMR through the metabolic assessment of inflammation. Obviously, the hybrid approach has limitations in patients with severe renal insufficiency, metal devices and in those suffering from claustrophobia. All these findings suggest the potential utility of ^{18}F -FDG PET-CMR in the early clinical assessment of patients with suspected myocardial inflammation, but structured prospective clinical trials are needed to expand it into clinical practice. Therefore, ^{18}F -FDG PET/CT is not routinely recommended for the diagnosis of myocarditis, with the possible exception of sarcoidosis [6].

7.17 Summary

Myocarditis has a range of different aetiologies and management is often supportive or driven by the underlying cause. While endomyocardial biopsy is still regarded as the gold standard for diagnosis, the advent of advanced multiparametric CMR and PET has meant that the majority of patients can now be diagnosed and managed non-invasively with biopsy being reserved for those with a fulminant presentation or where diagnosis remains unclear or remission cannot be induced by standard supportive measures.

It is increasingly being recognised that myocardial inflammation, autoimmunity, and myocarditis may play an important role in the pathogenesis and natural history of what have traditionally been regarded as genetic cardiomyopathies. Similarly, genetic factors are likely to underlie susceptibility to myocardial inflammation due to infectious agents and autoimmune rheumatic disease. It is likely that further advances in multimodality imaging and our understanding of human genetics will shed more light on the complex interplay between genetic factors, environmental conditions, and pathogens.

References

1. Drory Y, Turetz Y, Hiss Y, Lev B, Fisman EZ, Pines A, et al. Sudden unexpected death in persons less than 40 years of age. *Am J Cardiol.* 1991;68(13):1388–92.
2. Roth GA, Huffman MD, Moran AE, Feigin V, Mensah GA, Naghavi M, et al. Global and regional patterns in cardiovascular mortality from 1990 to 2013. *Circulation.* 2015;132(17):1667–78.
3. Rose NR. Viral myocarditis. *Curr Opin Rheumatol.* 2016;28(4):383–9.
4. Cooper LT, Keren A, Sliwa K, Matsumori A, Mensah GA. The global burden of myocarditis: part 1: a systematic literature review for the global burden of diseases, injuries, and risk factors 2010 study. *Glob Heart.* 2014;9(1):121–9.
5. Maron BJ, Udelson JE, Bonow RO, Nishimura RA, Ackerman MJ, Estes NAM, et al. Eligibility and disqualification recommendations for competitive athletes with cardiovascular abnormalities: task force 3: hypertrophic cardiomyopathy, Arrhythmogenic right ventricular cardiomyopathy and other cardiomyopathies, and myocarditis: a scientific statement from the American Heart Association and American College of Cardiology. *J Am Coll Cardiol.* 2015;66(21):2362–71.

6. Caforio ALP, Pankuweit S, Arbustini E, Basso C, Gimeno-Blanes J, Felix SB, et al. Current state of knowledge on aetiology, diagnosis, management, and therapy of myocarditis: a position statement of the European Society of Cardiology Working Group on myocardial and pericardial diseases. *Eur Heart J*. 2013;34(33):2636–48.
7. Yilmaz A, Kindermann I, Kindermann M, Mahfoud F, Ukena C, Athanasiadis A, et al. Comparative evaluation of left and right ventricular endomyocardial biopsy: differences in complication rate and diagnostic performance. *Circulation*. 2010;122(9):900–9.
8. Ferreira VM, Schulz-Menger J, Holmvang G, Kramer CM, Carbone I, Sechtem U, et al. Cardiovascular magnetic resonance in nonischemic myocardial inflammation: expert recommendations. *J Am Coll Cardiol*. 2018;72(24):3158–76.
9. Andréoletti L, Lévêque N, Boulagnon C, Brasselet C, Fornes P. Viral causes of human myocarditis. *Arch Cardiovasc Dis*. 2009;102(6–7):559–68.
10. Matsumori A, Yutani C, Ikeda Y, Kawai S, Sasayama S. Hepatitis C virus from the hearts of patients with myocarditis and cardiomyopathy. *Lab Invest*. 2000;80(7):1137–42.
11. Karatolios K, Maisch B, Pankuweit S. Suspected inflammatory cardiomyopathy. Prevalence of *Borrelia burgdorferi* in endomyocardial biopsies with positive serological evidence. *Herz*. 2015;40:91–5.
12. Marin-Neto JA, Cunha-Neto E, Maciel BC, Simões MV. Pathogenesis of chronic Chagas heart disease. *Circulation*. 2007;115(9):1109–23.
13. Engler RJM, Nelson MR, Collins LC, Spooner C, Hemann BA, Gibbs BT, et al. A prospective study of the incidence of myocarditis/pericarditis and new onset cardiac symptoms following smallpox and influenza vaccination. *PLoS One*. 2015;10(3):e0118283.
14. Maleszewski JJ, Orellana VM, Hodge DO, Kuhl U, Schultheiss H-P, Cooper LT. Long-term risk of recurrence, morbidity and mortality in giant cell myocarditis. *Am J Cardiol*. 2015;115(12):1733–8.
15. Shi Y, Chen C, Lisewski U, Wrackmeyer U, Radke M, Westermann D, et al. Cardiac deletion of the Coxsackievirus-adenovirus receptor abolishes Coxsackievirus B3 infection and prevents myocarditis in vivo. *J Am Coll Cardiol*. 2009;53(14):1219–26.
16. Zhang P, Cox CJ, Alvarez KM, Cunningham MW. Cutting edge: cardiac myosin activates innate immune responses through TLRs. *J Immunol*. 2009;183(1):27–31.
17. Noutsias M, Rohde M, Göldner K, Block A, Blunert K, Hemaïdan L, et al. Expression of functional T-cell markers and T-cell receptor Vbeta repertoire in endomyocardial biopsies from patients presenting with acute myocarditis and dilated cardiomyopathy. *Eur J Heart Fail*. 2011;13(6):611–8.
18. Heymans S, Eriksson U, Lehtonen J, Cooper LT. The quest for new approaches in myocarditis and inflammatory cardiomyopathy. *J Am Coll Cardiol*. 2016;68(21):2348–64.
19. Caforio ALP, Marcolongo R, Jahns R, Fu M, Felix SB, Iliceto S. Immune-mediated and autoimmune myocarditis: clinical presentation, diagnosis and management. *Heart Fail Rev*. 2013;18(6):715–32.
20. Cain BS, Meldrum DR, Dinarello CA, Meng X, Joo KS, Banerjee A, et al. Tumor necrosis factor- α and interleukin-1 β synergistically depress human myocardial function. *Crit Care Med*. 1999;27(7):1309–18.
21. Kühl U, Pauschinger M, Seeberg B, Lassner D, Noutsias M, Poller W, et al. Viral persistence in the myocardium is associated with progressive cardiac dysfunction. *Circulation*. 2005;112(13):1965–70.
22. Elamm C, Fairweather D, Cooper LT. Pathogenesis and diagnosis of myocarditis. *Heart*. 2012;98(11):835–40.
23. Hufnagel G, Pankuweit S, Richter A, Schönian U, Maisch B. The European study of epidemiology and treatment of cardiac inflammatory diseases (ESETCID). First epidemiological results. *Herz*. 2000;25(3):279–85.
24. Bozkurt B, Colvin M, Cook J, Cooper LT, Deswal A, Fonarow GC, et al. Current diagnostic and treatment strategies for specific dilated cardiomyopathies: a scientific statement from the American Heart Association. *Circulation*. 2016;134(23):e579–646.

25. Cooper LT, Berry GJ, Shabetai R. Idiopathic giant-cell myocarditis--natural history and treatment. Multicenter Giant cell myocarditis study group investigators. *N Engl J Med*. 1997;336(26):1860-6.
26. Cooper LT, Baughman KL, Feldman AM, Frustaci A, Jessup M, Kuhl U, et al. The role of endomyocardial biopsy in the management of cardiovascular disease: a scientific statement from the American Heart Association, the American College of Cardiology, and the European Society of Cardiology. *Circulation*. 2007;116(19):2216-33.
27. Patel RAG, DiMarco JP, Akar JG, Voros S, Kramer CM. Chagas myocarditis and syncope. *J Cardiovasc Magn Reson*. 2005;7(4):685-8.
28. Costello JM, Alexander ME, Greco KM, Perez-Atayde AR, Laussen PC. Lyme carditis in children: presentation, predictive factors, and clinical course. *Pediatrics*. 2009;123(5):e835-41.
29. Kandolin R, Lehtonen J, Kupari M. Cardiac sarcoidosis and giant cell myocarditis as causes of atrioventricular block in young and middle-aged adults. *Circ Arrhythm Electrophysiol*. 2011;4(3):303-9.
30. Fairweather D, Cooper LT, Blauwet LA. Sex and gender differences in myocarditis and dilated cardiomyopathy. *Curr Probl Cardiol*. 2013;38(1):7-46.
31. Maron BJ, Doerer JJ, Haas TS, Tierney DM, Mueller FO. Sudden deaths in young competitive athletes: analysis of 1866 deaths in the United States, 1980-2006. *Circulation*. 2009;119(8):1085-92.
32. Nugent AW, Daubeney PEF, Chondros P, Carlin JB, Cheung M, Wilkinson LC, et al. The epidemiology of childhood cardiomyopathy in Australia. *N Engl J Med*. 2003;348(17):1639-46.
33. Wojnicz R, Nowalany-Kozielska E, Wojciechowska C, Glanowska G, Wilczewski P, Niklewski T, et al. Randomized, placebo-controlled study for immunosuppressive treatment of inflammatory dilated cardiomyopathy: two-year follow-up results. *Circulation*. 2001;104(1):39-45.
34. Kindermann I, Kindermann M, Kandolf R, Klingel K, Bültmann B, Müller T, et al. Predictors of outcome in patients with suspected myocarditis. *Circulation*. 2008;118(6):639-48.
35. Heymans S. Myocarditis and heart failure: need for better diagnostic, predictive, and therapeutic tools. *Eur Heart J*. 2007;28(11):1279-80.
36. Ukena C, Mahfoud F, Kindermann I, Kandolf R, Kindermann M, Böhm M. Prognostic electrocardiographic parameters in patients with suspected myocarditis. *Eur J Heart Fail*. 2011;13(4):398-405.
37. Felker GM, Boehmer JP, Hruban RH, Hutchins GM, Kasper EK, Baughman KL, et al. Echocardiographic findings in fulminant and acute myocarditis. *J Am Coll Cardiol*. 2000;36(1):227-32.
38. Escher F, Kasner M, Kühl U, Heymer J, Wilkenschhoff U, Tschöpe C, et al. New echocardiographic findings correlate with intramyocardial inflammation in endomyocardial biopsies of patients with acute myocarditis and inflammatory cardiomyopathy. *Mediat Inflamm*. 2013;2013:875420.
39. Aretz HT, Billingham ME, Edwards WD, Factor SM, Fallon JT, Fenoglio JJ, et al. Myocarditis. A histopathologic definition and classification. *Am J Cardiovasc Pathol*. 1987;1(1):3-14.
40. Shields RC, Tazelaar HD, Berry GJ, Cooper LT. The role of right ventricular endomyocardial biopsy for idiopathic giant cell myocarditis. *J Card Fail*. 2002;8(2):74-8.
41. Hauck AJ, Kearney DL, Edwards WD. Evaluation of postmortem endomyocardial biopsy specimens from 38 patients with lymphocytic myocarditis: implications for role of sampling error. *Mayo Clin Proc*. 1989;64(10):1235-45.
42. Friedrich MG, Sechtem U, Schulz-Menger J, Holmvang G, Alakija P, Cooper LT, et al. Cardiovascular magnetic resonance in myocarditis: a JACC White paper. *J Am Coll Cardiol*. 2009;53(17):1475-87.
43. Kociol RD, Cooper LT, Fang JC, Moslehi JJ, Pang PS, Sabe MA, et al. Recognition and initial Management of Fulminant Myocarditis: a scientific statement from the American Heart Association. *Circulation*. 2020;141(6):e69-92.

44. Higgins CB, Herfkens R, Lipton MJ, Sievers R, Sheldon P, Kaufman L, et al. Nuclear magnetic resonance imaging of acute myocardial infarction in dogs: alterations in magnetic relaxation times. *Am J Cardiol.* 1983;52(1):184–8.
45. Eitel I, Friedrich MG. T2-weighted cardiovascular magnetic resonance in acute cardiac disease. *J Cardiovasc Magn Reson.* 2011;13:13.
46. Ferreira VM, Piechnik SK, Dall'Armellina E, Karamitsos TD, Francis JM, Ntusi N, et al. Native T1-mapping detects the location, extent and patterns of acute myocarditis without the need for gadolinium contrast agents. *J Cardiovasc Magn Reson.* 2014;16:36.
47. Ismail TF, Prasad SK, Pennell DJ. Prognostic importance of late gadolinium enhancement cardiovascular magnetic resonance in cardiomyopathy. *Heart.* 2012;98(6):438–42.
48. Mahrholdt H, Goedecke C, Wagner A, Meinhardt G, Athanasiadis A, Vogelsberg H, et al. Cardiovascular magnetic resonance assessment of human myocarditis: a comparison to histology and molecular pathology. *Circulation.* 2004;109(10):1250–8.
49. Assomull RG, Lyne JC, Keenan N, Gulati A, Bunce NH, Davies SW, et al. The role of cardiovascular magnetic resonance in patients presenting with chest pain, raised troponin, and unobstructed coronary arteries. *Eur Heart J.* 2007;28(10):1242–9.
50. Kellman P, Hansen MS. T1-mapping in the heart: accuracy and precision. *J Cardiovasc Magn Reson.* 2014;16:2.
51. Moon JC, Messroghli DR, Kellman P, Piechnik SK, Robson MD, Ugander M, et al. Myocardial T1 mapping and extracellular volume quantification: a Society for Cardiovascular Magnetic Resonance (SCMR) and CMR working Group of the European Society of cardiology consensus statement. *J Cardiovasc Magn Reson.* 2013;15:92.
52. Haaf P, Garg P, Messroghli DR, Broadbent DA, Greenwood JP, Plein S. Cardiac T1 mapping and extracellular volume (ECV) in clinical practice: a comprehensive review. *J Cardiovasc Magn Reson.* 2016;18(1):89.
53. Kotanidis CP, Bazmpani MA, Haidich AB, Karvounis C, Antoniadis C, Karamitsos TD. Diagnostic accuracy of cardiovascular magnetic resonance in acute myocarditis: a systematic review and meta-analysis. *JACC Cardiovasc Imaging.* 2018;11(11):1583–90.
54. Fung G, Luo H, Qiu Y, Yang D, McManus B. Myocarditis. *Circ Res.* 2016;118(3):496–514.
55. Ho JS, Sia C-H, Chan MY, Lin W, Wong RC. Coronavirus-induced myocarditis: a meta-summary of cases. *Heart Lung.* 2020;49(6):681–5.
56. Siripanthong B, Nazarian S, Muser D, Deo R, Santangeli P, Khanji MY, et al. Recognizing COVID-19-related myocarditis: the possible pathophysiology and proposed guideline for diagnosis and management. *Heart Rhythm.* 2020;17(9):1463–71.
57. Dillinger JG, Benmessaoud FA, Pezel T, Voicu S, Sideris G, Chergui N, et al. Coronary artery calcification and complications in patients with COVID-19. *JACC Cardiovasc Imaging.* 2020;13(11):2468–70.
58. Garot J, Amour J, Pezel T, Dermoch F, Messadaa K, Felten M-L, et al. SARS-CoV-2 fulminant myocarditis. *JACC Case Rep.* 2020;2(9):1342–6.
59. Puntmann VO, Carerj ML, Wieters I, Fahim M, Arendt C, Hoffmann J, et al. Outcomes of cardiovascular magnetic resonance imaging in patients recently recovered from coronavirus disease 2019 (COVID-19). *JAMA Cardiol.* 2020;5(11):1265–73.
60. Nagel E, Puntmann VO. Errors in statistical numbers and data in study of cardiovascular magnetic resonance imaging in patients recently recovered from COVID-19. *JAMA Cardiol.* 2020;5(11):1307–8.
61. Huang L, Zhao P, Tang D, Zhu T, Han R, Zhan C, et al. Cardiac involvement in patients recovered from COVID-2019 identified using magnetic resonance imaging. *JACC Cardiovasc Imaging.* 2020;13(11):2330–9.
62. Esposito A, Palmisano A, Natale L, Ligabue G, Peretto G, Lovato L, et al. Cardiac magnetic resonance characterization of myocarditis-like acute cardiac syndrome in COVID-19. *JACC Cardiovasc Imaging.* 2020;13(11):2462–5.
63. Basso C, Leone O, Rizzo S, De Gaspari M, van der Wal AC, Aubry M-C, et al. Pathological features of COVID-19-associated myocardial injury: a multicentre cardiovascular pathology study. *Eur Heart J.* 2020;41(39):3827–35.

64. Sengupta PP, Chandrashekar YS. Cardiac involvement in the COVID-19 pandemic. *JACC Cardiovasc Imaging*. 2020;13(11):2480–3.
65. Messroghli DR, Moon JC, Ferreira VM, Grosse-Wortmann L, He T, Kellman P, et al. Clinical recommendations for cardiovascular magnetic resonance mapping of T1, T2, T2* and extracellular volume: a consensus statement by the Society for Cardiovascular Magnetic Resonance (SCMR) endorsed by the European Association for Cardiovascular Imaging (EACVI). *J Cardiovasc Magn Reson*. 2017;19(1):75.
66. Petri M, Orbai AM, Alarcon GS, Gordon C, Merrill JT, Fortin PR, et al. Derivation and validation of the systemic lupus international collaborating clinics classification criteria for systemic lupus erythematosus. *Arthritis Rheum*. 2012;64(8):2677–86.
67. Mavrogeni S, Bratis K, Markussis V, Spargias C, Papadopoulou E, Papamentzelopoulos S, et al. The diagnostic role of cardiac magnetic resonance imaging in detecting myocardial inflammation in systemic lupus erythematosus. Differentiation from viral myocarditis. *Lupus*. 2013;22(1):34–43.
68. Burkard T, Trendelenburg M, Daikeler T, Hess C, Bremerich J, Haaf P, et al. The heart in systemic lupus erythematosus - a comprehensive approach by cardiovascular magnetic resonance tomography. *PLoS One*. 2018;13(10):e0202105.
69. Hinojar R, Foote L, Sangle S, Marber M, Mayr M, Carr-White G, et al. Native T1 and T2 mapping by CMR in lupus myocarditis: disease recognition and response to treatment. *Int J Cardiol*. 2016;222:717–26.
70. Maradit-Kremers H, Nicola PJ, Crowson CS, Ballman KV, Gabriel SE. Cardiovascular death in rheumatoid arthritis: a population-based study. *Arthritis Rheum*. 2005 Mar;52(3):722–32.
71. Kitis G, Banks MJ, Bacon PA. Cardiac involvement in rheumatoid disease. *Clin Med*. 2001;1(1):18–21.
72. Turiel M, Sitia S, Atzeni F, Tomasoni L, Gianturco L, Giuffrida M, et al. The heart in rheumatoid arthritis. *Autoimmun Rev*. 2010;9(6):414–8.
73. Chand EM, Freant LJ, Rubin JW. Aortic valve rheumatoid nodules producing clinical aortic regurgitation and a review of the literature. *Cardiovasc Pathol*. 1999;8(6):333–8.
74. Kobayashi Y, Giles JT, Hirano M, Yokoe I, Nakajima Y, Bathon JM, et al. Assessment of myocardial abnormalities in rheumatoid arthritis using a comprehensive cardiac magnetic resonance approach: a pilot study. *Arthritis Res Ther*. 2010;12(5):R171.
75. Ntusi NAB, Piechnik SK, Francis JM, Ferreira VM, Matthews PM, Robson MD, et al. Diffuse myocardial fibrosis and inflammation in rheumatoid arthritis: insights from CMR T1 mapping. *JACC Cardiovasc Imaging*. 2015;8(5):526–36.
76. van Albada-Kuipers GA, Brujijn JA, Westedt ML, Breedveld FC, Eulerink F. Coronary arteritis complicating rheumatoid arthritis. *Ann Rheum Dis*. 1986;45(11):963–5.
77. Denton CP, Khanna D. Systemic sclerosis. *Lancet*. 2017;390(10103):1685–99.
78. Pieroni M, De Santis M, Zizzo G, Bosello S, Smaldone C, Campioni M, et al. Recognizing and treating myocarditis in recent-onset systemic sclerosis heart disease: potential utility of immunosuppressive therapy in cardiac damage progression. *Semin Arthritis Rheum*. 2014;43(4):526–35.
79. Mousseaux E, Agoston-Coldea L, Marjanovic Z, Stanciu R, Deligny C, Perdrix L, et al. Left ventricle replacement fibrosis detected by CMR associated with cardiovascular events in systemic sclerosis patients. *J Am Coll Cardiol*. 2018;71(6):703–5.
80. Krumm P, Mueller KA, Klingel K, Kramer U, Horger MS, Zitzelsberger T, et al. Cardiovascular magnetic resonance patterns of biopsy proven cardiac involvement in systemic sclerosis. *J Cardiovasc Magn Reson*. 2016;18(1):70.
81. Ntusi NA, Piechnik SK, Francis JM, Ferreira VM, Rai AB, Matthews PM, et al. Subclinical myocardial inflammation and diffuse fibrosis are common in systemic sclerosis—a clinical study using myocardial T1-mapping and extracellular volume quantification. *J Cardiovasc Magn Reson*. 2014;16:21.
82. Mavrogeni S, Koutsogeorgopoulou L, Karabela G, Stavropoulos E, Katsifis G, Raftakis J, et al. Silent myocarditis in systemic sclerosis detected by cardiovascular magnetic resonance using Lake Louise criteria. *BMC Cardiovasc Disord*. 2017;17(1):187.

83. Geri G, Wechsler B, Thi Huong du L, Isnard R, Piette JC, Amoura Z, et al. Spectrum of cardiac lesions in Behcet disease: a series of 52 patients and review of the literature. *Medicine*. 2012;91(1):25–34.
84. Calamia KT, Schirmer M, Melikoglu M. Major vessel involvement in Behcet's disease: an update. *Curr Opin Rheumatol*. 2011;23(1):24–31.
85. Demirelli S, Degirmenci H, Inci S, Arisoy A. Cardiac manifestations in Behcet's disease. *Intractable Rare Dis Res*. 2015;4(2):70–5.
86. Raman SV, Aneja A, Jarjour WN. CMR in inflammatory vasculitis. *J Cardiovasc Magn Reson*. 2012;14:82.
87. Wi J, Choi HH, Lee CJ, Kim T, Shin S, Ko YG, et al. Acute myocardial infarction due to Polyarteritis Nodosa in a young female patient. *Korean Circ J*. 2010;40(4):197–200.
88. Holsinger DR, Osmundson PJ, Edwards JE. The heart in periarteritis nodosa. *Circulation*. 1962;25:610–8.
89. Brambatti M, Matassini MV, Adler ED, Klingel K, Camici PG, Ammirati E. Eosinophilic myocarditis: characteristics, treatment, and outcomes. *J Am Coll Cardiol*. 2017;70(19):2363–75.
90. Greco A, Rizzo MI, De Virgilio A, Gallo A, Fusconi M, Ruoppolo G, et al. Churg-Strauss syndrome. *Autoimmun Rev*. 2015;14(4):341–8.
91. Greulich S, Kitterer D, Kurmann R, Henes J, Latus J, Gloekler S, et al. Cardiac involvement in patients with rheumatic disorders: data of the RHEU-M(a)R study. *Int J Cardiol*. 2016;224:37–49.
92. Comarmond C, Pagnoux C, Khellaf M, Cordier JF, Hamidou M, Viallard JF, et al. Eosinophilic granulomatosis with polyangiitis (Churg-Strauss): clinical characteristics and long-term followup of the 383 patients enrolled in the French Vasculitis study group cohort. *Arthritis Rheum*. 2013;65(1):270–81.
93. Szczeklik W, Miszalski-Jamka T, Mastalerz L, Sokolowska B, Dropinski J, Banys R, et al. Multimodality assessment of cardiac involvement in Churg-Strauss syndrome patients in clinical remission. *Circ J*. 2011;75(3):649–55.
94. Grimaldi A, Mocumbi AO, Freers J, Lachaud M, Mirabel M, Ferreira B, et al. Tropical endomyocardial fibrosis: natural history, challenges, and perspectives. *Circulation*. 2016;133(24):2503–15.
95. Ackerman SJ, Bochner BS. Mechanisms of eosinophilia in the pathogenesis of hypereosinophilic disorders. *Immunol Allergy Clin N Am*. 2007;27(3):357–75.
96. Mahmood SS, Fradley MG, Cohen JV, Nohria A, Reynolds KL, Heinzerling LM, et al. Myocarditis in patients treated with immune checkpoint inhibitors. *J Am Coll Cardiol*. 2018;71(16):1755–64.
97. Wang DY, Salem JE, Cohen JV, Chandra S, Menzer C, Ye F, et al. Fatal toxic effects associated with immune checkpoint inhibitors: a systematic review and meta-analysis. *JAMA Oncol*. 2018;4(12):1721–8.
98. Palaskas N, Lopez-Mattei J, Durand JB, Iliescu C, Deswal A. Immune checkpoint inhibitor myocarditis: pathophysiological characteristics, diagnosis, and treatment. *J Am Heart Assoc*. 2020;9(2):e013757.
99. Eged M, Davis GK. Cocaine and the heart. *Postgrad Med J*. 2005;81(959):568–71.
100. Rijal S, Cavalcante JL. Acute cocaine myocarditis: a word of caution. *Eur Heart J*. 2015;36(15):946.
101. Rai SK, Choi HK, Sayre EC, Avina-Zubieta JA. Risk of myocardial infarction and ischaemic stroke in adults with polymyositis and dermatomyositis: a general population-based study. *Rheumatology*. 2016;55(3):461–9.
102. Schmid J, Liesinger L, Birner-Gruenberger R, Stojakovic T, Scharnagl H, Dieplinger B, et al. Elevated cardiac troponin T in patients with skeletal myopathies. *J Am Coll Cardiol*. 2018;71(14):1540–9.
103. Zhang L, Wang GC, Ma L, Zu N. Cardiac involvement in adult polymyositis or dermatomyositis: a systematic review. *Clin Cardiol*. 2012;35(11):686–91.

104. Rosenbohm A, Buckert D, Gerischer N, Walcher T, Kassubek J, Rottbauer W, et al. Early diagnosis of cardiac involvement in idiopathic inflammatory myopathy by cardiac magnetic resonance tomography. *J Neurol*. 2015;262(4):949–56.
105. Cox FM, Delgado V, Verschuuren JJ, Ballieux BE, Bax JJ, Wintzen AR, et al. The heart in sporadic inclusion body myositis: a study in 51 patients. *J Neurol*. 2010;257(3):447–51.
106. Sujino Y, Kimura F, Tanno J, Nakano S, Yamaguchi E, Shimizu M, et al. Cardiac magnetic resonance imaging in giant cell myocarditis: intriguing associations with clinical and pathological features. *Circulation*. 2014;129(17):e467–9.
107. Sen-Chowdhry S, Syrris P, Prasad SK, Hughes SE, Merrifield R, Ward D, et al. Left-dominant arrhythmogenic cardiomyopathy: an under-recognized clinical entity. *J Am Coll Cardiol*. 2008;52(25):2175–87.
108. Smith ED, Lakdawala NK, Papoutsidakis N, Aubert G, Mazzanti A, McCanta AC, et al. Desmoplakin cardiomyopathy, a fibrotic and inflammatory form of cardiomyopathy distinct from typical dilated or Arrhythmogenic right ventricular cardiomyopathy. *Circulation*. 2020;141(23):1872–84.
109. Vermij SH, Abriel H, van Veen TA. Refining the molecular organization of the cardiac intercalated disc. *Cardiovasc Res*. 2017;113(3):259–75.
110. Gao S, Chen SN, Di Nardo C, Lombardi R. Arrhythmogenic cardiomyopathy and skeletal muscle dystrophies: shared histopathological features and pathogenic mechanisms. *Front Physiol*. 2020;11:834.
111. Angelini C, Peterle E. Old and new therapeutic developments in steroid treatment in Duchenne muscular dystrophy. *Acta Myol*. 2012;31(1):9–15.
112. Protonotarios A, Wicks E, Ashworth M, Stephenson E, Guttman O, Savvatis K, et al. Prevalence of (18)F-fluorodeoxyglucose positron emission tomography abnormalities in patients with arrhythmogenic right ventricular cardiomyopathy. *Int J Cardiol*. 2019;284:99–104.
113. Peters AM, Danpure HJ, Osman S, Hawker RJ, Henderson BL, Hodgson HJ, et al. Clinical experience with 99mTc-hexamethylpropylene-amineoxime for labelling leucocytes and imaging inflammation. *Lancet*. 1986;2(8513):946–9.
114. Peters AM, Saverymuttu SH. The value of indium-labelled leucocytes in clinical practice. *Blood Rev*. 1987;1(1):65–76.
115. O’Connell JB, Henkin RE, Robinson JA, Subramanian R, Scanlon PJ, Gunnar RM. Gallium-67 imaging in patients with dilated cardiomyopathy and biopsy-proven myocarditis. *Circulation*. 1984;70(1):58–62.
116. Narula J, Khaw BA, Dec GW, Palacios IF, Southern JF, Fallon JT, et al. Brief report: recognition of acute myocarditis masquerading as acute myocardial infarction. *N Engl J Med*. 1993;328(2):100–4.
117. Lambert K, Isaac D, Hendel R. Myocarditis masquerading as ischemic heart disease: the diagnostic utility of antimyosin imaging. *Cardiology*. 1993;82(6):415–22.
118. Narula J, Khaw BA, Dec GW, Palacios IF, Newell JB, Southern JF, et al. Diagnostic accuracy of antimyosin scintigraphy in suspected myocarditis. *J Nucl Cardiol*. 1996;3(5):371–81.
119. Dilsizian V, Bacharach SL, Beanlands RS, Bergmann SR, Delbeke D, Dorbala S, et al. ASNC imaging guidelines/SNMMI procedure standard for positron emission tomography (PET) nuclear cardiology procedures. *J Nucl Cardiol*. 2016;23(5):1187–226.
120. Manabe O, Yoshinaga K, Ohira H, Masuda A, Sato T, Tsujino I, et al. The effects of 18-h fasting with low-carbohydrate diet preparation on suppressed physiological myocardial (18)F-fluorodeoxyglucose (FDG) uptake and possible minimal effects of unfractionated heparin use in patients with suspected cardiac involvement sarcoidosis. *J Nucl Cardiol*. 2016;23(2):244–52.
121. Giorgetti A, Marras G, Genovesi D, Filidei E, Bottoni A, Mangione M, et al. Effect of prolonged fasting and low molecular weight heparin or warfarin therapies on 2-deoxy-2-[18F]-fluoro-D-glucose PET cardiac uptake. *J Nucl Cardiol*. 2018;25(4):1364–71.

122. Tanimura M, Dohi K, Imanaka-Yoshida K, Omori T, Moriwaki K, Nakamori S, et al. Fulminant myocarditis with prolonged active lymphocytic infiltration after hemodynamic recovery. *Int Heart J.* 2017;58(2):294–7.
123. Moriwaki K, Dohi K, Omori T, Tanimura M, Sugiura E, Nakamori S, et al. A survival case of fulminant right-side dominant eosinophilic myocarditis. *Int Heart J.* 2017;58(3):459–62.
124. Ozawa K, Funabashi N, Daimon M, Takaoka H, Takano H, Uehara M, et al. Determination of optimum periods between onset of suspected acute myocarditis and ¹⁸F-fluorodeoxyglucose positron emission tomography in the diagnosis of inflammatory left ventricular myocardium. *Int J Cardiol.* 2013;169(3):196–200.
125. Perel-Winkler A, Bokhari S, Perez-Recio T, Zartoshti A, Askanase A, Geraldino-Pardilla L. Myocarditis in systemic lupus erythematosus diagnosed by 18F-fluorodeoxyglucose positron emission tomography. *Lupus Sci Med.* 2018;5(1):e000265.
126. Besenyi Z, Ágoston G, Hemelein R, Bakos A, Nagy FT, Varga A, et al. Detection of myocardial inflammation by 18F-FDG-PET/CT in patients with systemic sclerosis without cardiac symptoms: a pilot study. *Clin Exp Rheumatol.* 2019;37(4):88–96.
127. Nazir MS, Ismail TF, Reyes E, Chiribiri A, Kaufmann PA, Plein S. Hybrid positron emission tomography-magnetic resonance of the heart: current state of the art and future applications. *Eur Heart J Cardiovasc Imaging.* 2018;19(9):962–74.
128. Nensa F, Kloth J, Tezgah E, Poeppel TD, Heusch P, Goebel J, et al. Feasibility of FDG-PET in myocarditis: comparison to CMR using integrated PET/MRI. *J Nucl Cardiol.* 2018;25(3):785–94.



Cardiac Devices Infection

8

Ismaheel O. Lawal, Andor W. J. M. Glaudemans,
and Mike M. Sathekge

Contents

8.1 Introduction.....	233
8.2 Scintigraphy in Cardiac Devices Infection.....	235
8.3 FDG PET/CT Imaging of Cardiac Devices Infection.....	242
8.4 Comparative Performance of Radionuclide WBC Scintigraphy and FDG PET/CT in Cardiac Devices Infection.....	253
8.5 Conclusion.....	253
References.....	254

8.1 Introduction

There has been a rise in the number of cardiac devices implanted globally for ailing hearts [1, 2]. These devices include cardiac implantable electronic devices (CIED) and ventricular assist devices. CIED are devices implanted to treat cardiac arrhythmias and include pacemakers, implantable cardioverter-defibrillators, and cardiac resynchronization therapy devices. The rise in the number of cardiac devices implanted worldwide is related to the aging population and associated growing demand for these devices in managing cardiac disorders.

I. O. Lawal · M. M. Sathekge (✉)
Department of Nuclear Medicine, University of Pretoria & Nuclear Medicine Research
Infrastructure (NuMeRI), Steve Biko Academic Hospital, Pretoria, South Africa
e-mail: mike.sathekge@up.ac.za

A. W. J. M. Glaudemans
Department of Nuclear Medicine & Molecular Imaging, University Medical Center
Groningen & University of Groningen, Groningen, The Netherlands
e-mail: a.w.j.m.glaudemans@umcg.nl

© The Author(s), under exclusive license to Springer Nature
Switzerland AG 2021

F. Caobelli (ed.), *Imaging of Inflammation and Infection in Cardiovascular
Diseases*, https://doi.org/10.1007/978-3-030-81131-0_8

233

Infection is a rare but dreaded complication of implanted cardiac devices [3]. The rate of increase in cardiac device-related infection (CDI) has far outstripped the rate of rise in the number of implanted devices [1, 2]. There has been a continued rise in the CDI rate despite improved device design, surgical techniques, and preventive measures. The factors that predispose to CDI include diabetes mellitus, underlying heart disease, organ failure, device with more than one lead, repeat surgery for device replacement, male gender, and device complexity [4–6]. Established infection of a cardiac device warrants its extraction. Therefore, infection involving a cardiac device is associated with increased morbidity and mortality and the burden of cost due to prolonged antibiotic therapy, hospitalization, and repeat surgery [7, 8].

The basic anatomy of a CIED consists of a subcutaneously implanted generator and leads that traverse the vascular lumen to reach the heart. Infection can involve any of these components of the device. Based on the component of the device involved by infection, CDI can be classified as follows:

- Superficial incisional infection: this is an infection that involves the skin and subcutaneous tissues overlying the generator without an extension to the generator pocket itself. Antibiotic therapy with local wound care is sufficient for treatment without device extraction [9].
- Pocket infection: here, the infection involves the generator pocket. Clinical manifestation may be in the form of an erythema, warmth, and fluctuant mass. The infection may progress to manifest as deformation of the pocket, adherence, or erosion of the device generator [10]. Pocket infection may extend to the device leads and the endocardium, causing lead infections, CIED systemic infection, and infective endocarditis.
- CIED systemic infection and infective endocarditis: here, the infection involves the device's intravascular and intracardiac components. CIED systemic infection and infective endocarditis may occur in isolation without associated generator pocket infection. This isolated CIED systemic infection presents a diagnostic challenge as symptoms may be non-specific and may present long after device implantation [10].

The clinical presentation of CIED systemic infection is variable depending on the virulence of the causative organism. The presentation may, therefore, be acute, subacute, or chronic. The commonest symptom at presentation is fever, which may be associated with chills, poor appetite, and weight loss [9]. Other common symptoms of CIED systemic infection are heart murmur and signs and symptoms of embolic events. Laboratory investigations and imaging play essential roles in the diagnosis of CIED systemic infection. Elevated levels of C-reactive protein and erythrocyte sedimentation rate, leucocytosis, anemia, and microscopic haematuria may be seen during patients' workup. Blood culture is an important test for establishing the diagnosis and for guiding the choice of antibiotic. Despite the important role of blood culture in establishing CIED infection, it is negative in up

to 31% of patients [11, 12]. A negative blood culture may be due to prior antibiotic use, infection due to fastidious or non-culturable organisms, or non-bacterial microbial infection. Echocardiography plays a critical role in establishing the presence of endocardial or lead infection and its complications. Findings suggestive of CIED infection on echocardiography include valve or lead vegetations, new valve regurgitation, and formation of abscess, pseudoaneurysm, or intracardiac fistula [10]. Transthoracic echocardiography has a lower sensitivity for detecting these findings compared with transoesophageal echocardiography (TOE). Despite its superior sensitivity, TOE cannot differentiate masses caused by infection from thrombus or fibrosis. Masses are present in up to 10% of patients without CIED infection [13].

None of the clinical symptoms, laboratory investigations, or echocardiographic findings is significantly accurate on their own for the diagnosis of CIED infection. Hence, a combination of these three is employed for diagnosis. The difficulty associated with CIED infection has led to the recommendation that patient management must be done in a multidisciplinary setting involving infectious disease specialists, cardiologists, microbiologists, radiologists, and nuclear medicine physicians [11]. The modified Duke criteria [14] and the 2015 European Society of Cardiology criteria [11], which were validated for the diagnosis of infective endocarditis, are generally used for this purpose. Recently, the European Heart Rhythm Association proposed the 2019 International CIED Infection Criteria as a specific tool for diagnosing CIED infection [10]. These new diagnostic criteria included abnormal tracer accumulation on radiolabelled white blood cell scintigraphy or ^{18}F -fluorodeoxyglucose (FDG) positron emission tomography/computed tomography (PET/CT) at the pocket/generator site, along the leads, or at the valve site to constitute a major criterion for the diagnosis of CIED infection. This chapter will discuss the diagnostic performances of these two radionuclide techniques in patients evaluated for CIED infection. Left ventricular assist device is another cardiac device with increasing use as a bridge to transplant, bridge to candidacy, or destination therapy in patients with heart failure. We will discuss the data emerging on the diagnostic utility of FDG PET/CT and radiolabelled white cell scintigraphy in the evaluation of infection in patients with left ventricular assist device infection.

8.2 Scintigraphy in Cardiac Devices Infection

Infection is characterized by chemotaxis of white blood cells (WBC) towards the site of infection. Radiolabelled white blood cell scintigraphy (WBC scintigraphy), therefore, explores a physiologic *in vivo* process to detect the site of infection with high specificity [15]. Technological improvement in gamma camera design has led to the widespread availability of single-photon emission tomography/computed tomography (SPECT/CT) as a form of hybrid tomographic imaging with improvement in contrast resolution leading to an improved sensitivity for disease detection [16].

8.2.1 Radiolabelling of White Blood Cells with ^{99m}Tc -HMPAO or ^{111}In -oxine

For WBC scintigraphy, the patient own WBC is separated from a whole blood sample and labelled with either Technetium-99 m hexamethylpropyleneamine oxime (^{99m}Tc -HMPAO) or Indium-111 oxine. ^{99m}Tc can be eluted from a Molybdenum-99/Technetium-99 m generator available in most nuclear medicine centers and can be easily complexed to HMPAO for onward use for WBC radiolabelling. ^{99m}Tc decays by isomeric transition with a physical half-life of 6 h, emitting a gamma photon of 140 KeV photopeak, making it suitable for imaging with the gamma camera. ^{111}In is a cyclotron-produced radionuclide. This limits its availability and making it an expensive alternative to ^{99m}Tc for WBC radiolabelling. It decays by electron capture with a physical half-life of 2.8 days and emitting two photopeaks of 173 and 245 KeV. Its long physical half-life means that only small activity (18.5 MBq compared with 370–740 MBq for ^{99m}Tc -HMPAO) can be used for the radiolabelling of WBC to reduce radiation burden to patients. This low injected activity and the relatively higher energies of its gamma photons make ^{111}In -oxine WBC scintigraphy of poorer resolution than ^{99m}Tc -HMPAO WBC scintigraphy. Detailed procedure guidelines and quality control measures for the radiolabelling of WBC with either ^{99m}Tc -HMPAO or ^{111}In -oxine have been published by the European Association of Nuclear Medicine [17, 18]. About 50ml of the patient's blood is collected, and a WBC count of at least $2 \times 10^8/\text{L}$ is required to achieve an optimum labeling efficiency. Labeling efficiency of 40–80% is desirable.

8.2.2 Image Acquisition

To obtain useful images required for correct scan interpretation, attention must be paid to the imaging acquisition protocol. For both ^{99m}Tc -HMPAO and ^{111}In -oxine-labelled WBC scintigraphy, imaging is obtained at multiple time-points. For ^{99m}Tc -HMPAO WBC scintigraphy, early images at 30 min post-injection (pi), delayed images at 3–4 h pi, and late images at 20–24 h pi are necessary. Due to the relatively short physical half-life of ^{99m}Tc compared with ^{111}In , decay corrected acquisition of the delayed, and late imaging is mandatory. For ^{111}In -oxine WBC scintigraphy, imaging at two-time-points (4–5 pi hours and 20–24 pi hours) is necessary. Images acquired should include chest imaging to evaluate for infection in the generator pocket, leads, or heart and whole-body imaging to assess for possible septic emboli. SPECT/CT imaging at 4–5 h pi performed for anatomic co-localization is mandatory. Addition SPECT/CT at 20–24 h pi may be performed if a new focus of radio-labelled WBC accumulation is seen on the delayed imaging. A detailed protocol for image acquisition has been recently published by the infection committee of the European Association of Nuclear Medicine [19].

8.2.3 Image Interpretation

Image interpretation must be done on a dedicated nuclear medicine workstation with all images acquired at the different time-points displayed with the same intensity scale in absolute counts [19]. Both attenuation corrected and non-corrected images should be reviewed during interpretation as attenuation correction can introduce artifacts in the processed images, which may be misinterpreted as increased radiolabelled WBC accumulation caused by infection. The early images are most useful for *in vivo* quality control to confirm the viability of the reinjected WBC. Diffusely increased bilateral lung activity on the early images is a normal finding. It results from the activation of WBC due to their contact with glasswares used during radiolabelling. Activated WBCs are less deformable and are sluggish in transiting through the pulmonary microcirculation. The diffuse lung activity is not visualized beyond 1-h pi. The persistence of lung activity may be indicative of damage to the WBC during radiolabelling. Attention must be paid to the relative radiolabelled WBC accumulation in the liver and spleen. The spleen is normally the more intense organ of the two. Intense liver activity greater than the spleen is abnormal and may indicate damaged WBC before reinjection into the patient. High background blood-pool activity may indicate red blood cells' radiolabelling due to a sub-optimal whole blood separation technique. This high background activity can reduce the signal-to-noise ratio and compromise diagnostic sensitivity.

Infection is seen as areas of increased radiotracer accumulation seen on the delayed images acquired at 3–4 h pi with an increase in the intensity of accumulation seen in the late images acquired at 20–24 h pi. This diagnostic criterion reflects the time-dependent accumulation of radiolabelled WBC at the site of infection. The study is negative for infection where there is no definite area of increased radiolabelled WBC accumulation or an area of increased radiolabelled WBC accumulation seen on the delayed images with a clear decrease in intensity on the late images.

The whole-body images should be reviewed for extra-cardiac radiolabelled WBC accumulation areas that may suggest foci of septic emboli or portal of entry of infection. Septic emboli may occur as an area of photopenic in organs with intense physiologic radiolabelled WBC accumulation such as the spleen [20]. The spine is a frequent site of septic embolization in patients with CIED infection. Infection of the spine has a variable appearance of radiolabelled WBC scintigraphy as it may present as an area of photopenia, increased accumulation, or normal uptake comparable to background activity [21].

8.2.4 Radiolabelled WBC Scintigraphy of CIED Infection

Radiolabelled WBC scintigraphy is an overly sensitive and specific technique in the detection of CIED infection. This excellent diagnostic performance was confirmed in one of the earliest studies including 63 patients with a pacemaker or ICD

evaluated for suspected infection [21]. CIED infection was confirmed in 32 patients while 31 patients had no CIED infection. Radiolabelled WBC scintigraphy correctly identifies 30 of 32 patients with CIED infection giving a diagnostic sensitivity of 94%. Radiolabelled WBC SPECT/CT imaging was more accurate (correctly identified 30 of 32 patients with CIED infection) and able to localize the site of infection compared with planar (correctly identified 15 of 32 patients with CIED infection) or SPECT-only imaging (correctly identified 21/32 patients with CIED infection). Two cases of CIED infection that were falsely negative on radiolabelled WBC SPECT/CT were due to *Candida* and *Enterococci* species, two organisms that do not induce intense WBC chemotaxis. These two patients with falsely negative radiolabelled WBC SPECT/CT were on antibiotic treatment at imaging time. Radiolabelled WBC SPECT/CT correctly identified all patients without CIED infection, giving a specificity of 100% [22]. This study was important in establishing the diagnostic accuracy of radiolabelled WBC scintigraphy in CIED infection and the added value of SPECT/CT imaging. It also shows the potential impact of the causative agent or prior antibiotic therapy on the diagnostic accuracy of radiolabelled WBC scintigraphy.

Before the recently proposed criteria by the European Heart Rhythm Association [10], the modified Duke criteria have been used for the diagnosis of CIED infection [14]. In a recent study, Holcman and colleagues showed the superior accuracy of radiolabelled WBC scintigraphy with ^{99m}Tc -HMPAO-labelled SPECT/CT imaging compared with the modified Duke criteria in a group of 40 patients with suspect cardiac device-related infection [23]. Radiolabelled WBC scintigraphy had a sensitivity, specificity, and accuracy of 93%, 88%, and 90%, respectively, compared with 43%, 96%, and 76%, respectively, for modified Duke criteria (when a positive result for the test was defined as a definite category). Also, radiolabelled WBC scintigraphy was associated with a less false-positive rate compared with transthoracic echocardiography. Despite the superior accuracy reported for radiolabelled WBC scintigraphy compared with the modified Duke criteria in this study [23], the specificity of scintigraphy (88%) was lower compared with the specificity (100%) reported earlier by Erba et al. [22]. It is difficult to adduce any reason for this lower specificity in this latter study since the authors did not present the characteristics of the patients with false-positive scintigraphy in their study. However, it is worthy of note that the study by Holcman et al. was more heterogeneous, including patients with suspected prosthetic valvular endocarditis (20% of the study population) rather than patients with suspected CIED infections alone [23].

CIED infection that is limited to the device leads is difficult to diagnose. This lead infection carries an important complication of septic embolization. Infective vegetation can dislodge from the intravascular or cardiac leads, embolize to a distant site, and establish a foothold of infection at a distant site. Vegetations larger than 10 mm have the greatest risk for embolization [9]. Early diagnosis of leads infection is, therefore, critical to prevent associated mortality and morbidity. There is a justifiable concern that radiolabelled WBC scintigraphy may be less sensitive for detecting lead infection. This concern was evaluated in a recent study by Małecka and colleagues who evaluated the diagnostic performance of ^{99m}Tc -HMPAO-labelled WBC SPECT/

CT in 40 patients admitted with lead vegetations detected on echocardiography and evaluated for lead-dependent infective endocarditis (LDIE) [24]. LDIE was eventually confirmed in 19 patients while it was ruled-out in 21 patients. The diagnostic sensitivity, specificity, and accuracy of radiolabelled WBC SPECT/CT for LDIE were 73.7%, 81.0%, and 77.5%, respectively. Like the findings by Erba et al. [22], SPECT/CT imaging was false negative in five patients, all of whom were on antibiotics at the time of imaging. This study is important because it shows a high diagnostic performance of radiolabelled WBC SPECT/CT imaging in LDIE and the negative impact of prior antibiotic therapy on its diagnostic performance. It also confirms the preponderance of vegetations in patients with an implanted cardiac device but without CIED infection limiting the diagnostic accuracy of echocardiography that relies on the demonstration of vegetation in the diagnosis of LDIE.

The modified Duke criteria continued to be an important tool for the diagnosis of CIED infection. Recently Calais and colleagues evaluated the value ^{99m}Tc -HPO-^{99m}Tc-labelled WBC SPECT/CT imaging in patients with a long-standing implanted device with suspected infection [25]. In a group of 48 patients with suspected CIED infection, a final diagnosis of CIED infection was definite in 15, rejected in 22 patients, and remained possible in 11 patients. Based on modified Duke criteria, patients were classified as definite, rejected, or possible CIED infections in 13, 14, and 21, respectively. Radiolabelled WBC scintigraphy had no added value to diagnosis if patients were classified as infection definite or rejected. The added value of scintigraphy was in the gray zone in patients classified by modified Duke criteria as possible for infection. In this sub-category, radiolabelled WBC SPECT/CT imaging had a sensitivity, specificity, and specificity of 80%, 100%, 90%, respectively, in reclassifying patients as either infection definite or rejected. In the study, a longer duration of antibiotic therapy before scintigraphy was associated with a high likelihood of a false-negative scan finding. All five patients with CIED infection who received antibiotic therapy for less than 9 days had true negative scan findings [25]. This study advanced knowledge by defining the category of patients with suspected CIED infection in whom radiolabelled WBC scintigraphy was most useful and giving clarity on the need not to delay imaging in patients who had been commenced on antibiotic therapy.

8.2.5 Radiolabelled WBC Imaging of Left Ventricular Assist Devices Infection

Left ventricular assist devices (LVAD) are increasingly being used in the management of heart failure. LVAD represents a recent improvement in heart failure management by contributing to the reduction in morbidity and mortality associated with this condition [26]. Use of LVAD as either a destination therapy or as a bridge-to-heart transplantation intervention is on the increase due to a rise in the population of patients with heart failure refractory to medical therapy [26]. A ventricular assist device may be placed into either or both ventricles. Ventricular assist devices are mostly placed in the left ventricle. Based on perfusion pattern, LVAD can be

pulsatile or continuous flow devices. The continuous-flow devices are the most used of the two types as they provide superior organ perfusion compared with the pulsatile pump design [27]. The basic design of an LVAD consists of a pumping chamber that receives blood from the patient's left ventricle via an inflow cannula and pumps out blood to the patient's general circulation via an outflow cannula, and percutaneous drivelines that serve as the conduit for wiring connecting the pump to the system controller. Infection is one of the commonest complications of LVAD [26, 28]. Infection most commonly affects the drivelines or the pump pocket [28]. The exit site of the driveline on the skin surface is a potential entry point for microbial organisms. LVAD infection not only increases the mortality of patients but also predisposes to other complications, including thrombosis, stroke, and gastrointestinal bleeding [28]. In patients with suspected LVAD infection, blood culture and echocardiography are considered for initial assessment [29]. Radiolabelled WBC scintigraphy may play a role in patients in whom initial assessment remained inconclusive for infection.

In an early pilot study of ^{99m}Tc -HMPAO-labelled WBC SPECT/CT imaging in eight patients evaluated with 13 scans for LVAD infection at different intervals, scintigraphy correctly identified infection in all eight scans of patients with LVAD infection and was true negative in all five scans of patients without LVAD infection [30]. The addition of SPECT/CT imaging improved diagnostic sensitivity and helped in localizing the site of infection. In five scans, SPECT/CT localized percutaneous drivelines infection while deep infection was seen in three scans. In four out of five patients without LVAD infection, alternative sources of infection were localized, and the patients received antibiotic treatment without the need for device extraction. This pilot study provided the early evidence of the potential of radiolabelled WBC scintigraphy in the diagnostic assessment of patients with suspected LVAD infection, the added value of SPECT/CT imaging in the localization of the site of infection, and the role of this imaging in detecting an alternative source of infection in patients without LVAD infection [30].

Infections in patients with LVAD can belong to one of three categories: (a) LVAD-specific infections are device-specific infections and involve components of the device; (b) LVAD-related infections are infections that can be seen in patients without LVAD but occur with greater frequency in LVAD patients including mediastinitis, endocarditis, and bacteremia; and (c) non-LVAD infections such as pneumonia and urinary tract infection are independent or not directly related to the presence of LVAD but are known to be prevalent among sick people with compromised immune status and underlying co-morbid conditions such as diabetes, prolonged hospitalization, and renal impairment. A recent study has shown the diagnostic performance of ^{99m}Tc -HMPAO-labelled WBC SPECT/CT in assessing different types of infections seen in 24 patients with LVAD imaged evaluated for infection [31]. In 15, six, and three patients, the infection was LVAD-specific, LVAD-related, and non-LVAD infection, respectively. ^{99m}Tc -HMPAO-labelled SPECT/CT imaging was true positive in 14 of the 21 patients with either LVAD-specific or LVAD-associated infection. Five of the seven patients with LVAD-specific or LVAD-associated infection but had false-negative scintigraphy were on

antibiotic treatment at imaging time. This finding, again, is consistent with the negative impact of prior antibiotic treatment on imaging outcomes.

8.2.6 Merits and Limitations of Radiolabelled WBC Scintigraphy in Cardiac Devices Infection: Alternative SPECT Tracers

The most important strength of radiolabelled WBC scintigraphy lies its excellent specificity. The technique is modeled on a physiologic process that is highly specific for infection. Time-dependent accumulation of radiolabelled WBC at the site of suspected infection has an excellent positive predictive value. When the diagnostic criteria for interpreting radiolabelled WBC scintigraphy are applied with utmost fidelity [19], false-positive interpretation due to sterile inflammation can be prevented.

Unlike echocardiography that is cardiac-focussed imaging, radiolabelled WBC scintigraphy is whole-body imaging. The whole-body sweep provides an additional benefit of detecting septic embolization sites or portal of entry of infection. Infected vegetation can dislodge from cardiac device infection and embolize to a distant site via the pulmonary or systemic circulation. Infected vegetations that embolize via the pulmonary circulation commonly end up in the lungs, causing a septic pulmonary embolism. In contrast, septic emboli traversing the systemic circulation may cause distant infection in various organs, including the brain, the spleen, the spine, etc. Septic embolization is seen in up to 80% of patients with infected cardiac devices [12]. In different radiolabelled WBC scintigraphy reports, septic embolization was reported in 25–47.5% of patients with suspected CIED infection [22, 23, 25]. The septic embolization sites detected on radiolabelled WBC scintigraphy include the lungs, spleen, musculoskeletal system, gastrointestinal tract, and urinary system. It is important to detect the sites of distant embolization or portal of entry of infection. These sites may require a longer duration of antibiotic therapy or additional local surgical care. Non-optimal treatment of septic embolization or the portal of entry of infection is a potential cause of device reinfection.

Not all patients evaluated will have device infection. Some patients are evaluated for suspected device infection because of signs and symptoms of systemic infection and a positive blood culture. When the cardiac device is not the infection site, whole-body imaging in radiolabelled WBC scintigraphy has an added advantage of detecting the site of alternative infection [22]. These alternative infections can be given the standard care, including antibiotic therapy, without the need to extract an uninfected cardiac device.

A major drawback of radiolabelled WBC scintigraphy is the labor-intensive, time-consuming, and technically demanding process of *in vitro* labeling of WBC with either ^{99m}Tc -HMPAO or ^{111}In -oxine. The procedure, which requires a skilled technician to perform it, exposes the technicians to blood-borne infectious pathogens. Also, patients with leukopenia may not benefit from this imaging modality since a minimum WBC count of $2 \times 10^8/\text{L}$ is required to obtain a satisfactory labeling efficiency. Due to these limitations associated with *in vitro* radiolabeling of

WBC, radiotracers *for in vivo* labeling of WBC have been tested for their diagnostic performance in different human infections. ^{99m}Tc -Sulesomab (monoclonal antibody Fab' fragment that targets NCA-90 expressed on granulocytes and their precursors) and ^{99m}Tc -Besilesomab (a monoclonal IgG1 antibody that targets NCA-95 expressed on granulocytes and their precursors) are two of the radiopharmaceuticals for *in vivo* labeling of WBC. Most of the experience with these agents is with their use for imaging peripheral bone infections [32–34]. Their use in the assessment of suspected cardiac device infection is limited [35].

Gallium-67 (^{67}Ga) citrate is an alternative tracer for scintigraphic assessment of human infections. Its uses have declined significantly since the availability of more effective means of radionuclide imaging of infection. It continued to be used, in a limited sense, in climes where FDG PET/CT is not widely available or FDG PET/CT done for infection imaging is not reimbursed. In recent years, two small studies have evaluated the diagnostic performance of ^{67}Ga citrate SPECT/CT in the assessment of infection in VAD patients [36, 37]. In the earlier of the two studies reporting data on five patients, ^{67}Ga citrate SPECT/CT was true positive in three patients with infection and true negative in the two patients without infection [36]. In a more recent study, Kimura and colleagues evaluated the diagnostic performance of ^{67}Ga citrate SPECT/CT in the diagnosis of driveline infection in 36 patients with continuous-flow LVAD and reported a diagnostic sensitivity of 61% [37]. Based on this limited data, ^{67}Ga citrate SPECT/CT should be considered for assessing suspected cardiac device infection only when more accurate radionuclide techniques such as radiolabelled WBC scintigraphy and FDG PET/CT are not available. This is based not only on the high background activity that characterizes ^{67}Ga citrate SPECT imaging but also on the high radiation burden it confers on patients.

The gamma camera's limited spatial resolution is a limitation shared by all SPECT tracers used in the assessment of suspected cardiac device infection. This limited spatial resolution implied that small lesions due to cardiac device infection like those associated with device lead or driveline infection may be missed during a scintigraphic assessment. The need for delayed imaging at 24–48 h post-tracer injection is another common limitation encountered in the clinical use of scintigraphy for cardiac device infection imaging. This delay in obtaining imaging results may delay the effective management of patients who may be critically ill.

8.3 FDG PET/CT Imaging of Cardiac Devices Infection

FDG PET/CT is most successful for its use in the staging and re-staging different solid human tumors. Its use for clinical imaging of inflammation and infection is increasing. FDG PET/CT has found multiple cardiology applications, especially for the determination of viable myocardium in patients with coronary artery disease and for infection and inflammation imaging. In the clinical imaging of cardiac devices infection, the success with the use of FDG PET/CT in the diagnostic workup of patients relates to the better resolution of the PET system compared with the SPECT system and the rapidity with which imaging results are available for patients management.

The better resolution of the PET system is a useful improvement over the SPECT system. This may improve the detection of small lesions occurring in the context of cardiac device infection. Infections involving the leads of CIED are commonly associated with vegetations on the leads. These vegetations may be small (sub-centimeter) and may be easily missed when the imaging system has a poorer resolution. The results of FDG PET/CT imaging are available within 2 h post-tracer injection. This contrasts with radiolabelled WBC scintigraphy where imaging result is available only after 24- or 48-h post-tracer injection. This quick availability of imaging results with FDG PET/CT helps make prompt treatment decisions in patient management.

Physiologic FDG accumulation in the myocardium is an important drawback of FDG PET/CT for imaging cardiac device infection. The high physiologic FDG uptake within the myocardium can mask the detection of the infection site that manifests as a focus of increased FDG accumulation. Specific dietary and pharmacologic manipulations need to be carried out to reduce the physiologic myocardial FDG uptake [38].

8.3.1 Patient Preparation

Specific patient preparation must be observed to obtain an optimum image requisite to arrive at the correct image interpretation.

8.3.1.1 Suppression of Myocardial FDG Uptake

Relevant strategies to suppress physiological myocardial FDG-uptake are extensively described in Chap. 1. The myocardium utilizes different energy substrates for its metabolism. In the presence of high circulating glucose and insulin levels, as seen in the postprandial state, the myocardium utilizes glucose for its energy metabolism. In conditions causing high circulating fatty acid level and low blood level of insulin as seen in the fasting state, the myocardium utilizes free fatty acid for energy metabolism [39]. This knowledge of the factors driving myocardial use is utilized in patient preparation to ensure suppression of physiologic FDG uptake by the myocardium and thereby improve its diagnostic sensitivity for infection (Fig. 8.1). The most important step in patient preparation appears to be a prolonged fasting for 12–18 h before FDG PET/CT imaging. Dietary modification in the form of low carbohydrate, high fat, and protein permitted diet in the 24–48 h before imaging has a contributory effect to suppressing myocardial FDG uptake. Unfractionated heparin given as an intravenous bolus 15 min before FDG administration at 50 IU/kg body weight activates lipoprotein lipase, which increases the circulating levels of free fatty acid and has also been found to improve suppression of FDG uptake by the normal myocardium [40]. The detailed protocols for myocardial FDG suppression have been recently published by different professional organizations [41, 42].

8.3.1.2 Withdrawal of Medications

Although many reports have shown the prevalence of long-term antibiotic use in patients with false-negative FDG PET/CT scan findings, it is not recommended at

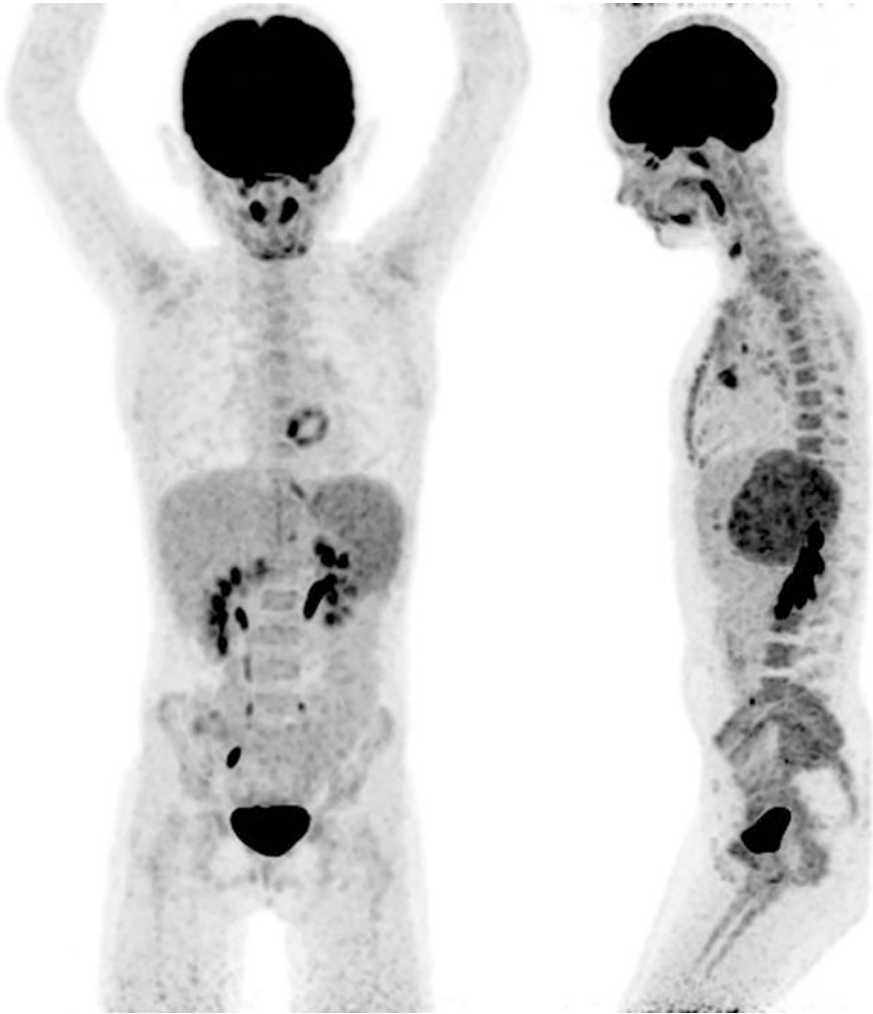


Fig. 8.1 FDG PET/CT images of a patient with heart valve-related infective endocarditis. Good suppression of myocardial FDG uptake ensures the detection of the site of infection with an excellent contrast. Apart from the organs such as brain, liver, spleen, and the urinary system with intense physiologic FDG uptake, there is low background activity which allows for the sensitive detection of portal of entry of infection and sites of septic embolization

this time that antibiotic treatment be withdrawn solely for imaging purposes [43]. When FDG PET/CT is contemplated for use in evaluating patients with suspected cardiac device infection, imaging must be done promptly without undue delay to reduce the impact of prolonged antibiotic use on the diagnostic sensitivity of FDG PET/CT.

Steroid induces gluconeogenesis and inhibits the peripheral utilization of glucose, thereby causing hyperglycemia [44]. Elevated plasma glucose competes with

FDG for uptake at the infection site and may reduce diagnostic sensitivity. Hyperglycemia induces endogenous insulin secretion, which increases FDG uptake by insulin-sensitive tissues such as skeletal muscle, thereby increasing the background activity. This resultant reduction in signal-to-noise ratio may reduce the diagnostic sensitivity of FDG PET/CT for cardiac device infection. Given this impact of steroids on FDG uptake at disease site and in normal tissues, steroids should be withheld or reduced to the minimum before FDG PET/CT imaging in patients with suspected cardiac device infection [43]. Hyperglycemia, by itself, as seen in diabetic patients is not a contraindication to FDG PET/CT imaging since high blood glucose level has been reported not to have a significant impact on the diagnostic sensitivity of FDG PET/CT obtained for inflammation and infection imaging [45].

8.3.2 Image Acquisition and Interpretation

Image acquisition is commenced 60 min post-intravenous administration of FDG. While delaying imaging till 120 min or beyond post-tracer administration has been found to improve vascular FDG uptake and decrease background activity [46], the impact of delayed imaging in improving the diagnostic sensitivity of FDG PET/CT in the evaluation of cardiac infection is still controversial at present [47, 48].

Post-acquisition processing and image interpretation should be done on a dedicated nuclear medicine workstation. Image reconstruction should be done with and without attenuation correction. Similarly, for image interpretation, both attenuated corrected and uncorrected images should be reviewed to prevent false-positive interpretation due to reconstruction artifacts [49]. The application of a metal artifact reduction algorithm may help reduce the severity of this reconstruction artifact [50].

FDG PET images should be reviewed for areas of pathologic FDG uptake around the device components and elsewhere in the body. Any focus of pathologic FDG uptake should be assessed for pattern (focal, linear, diffuse), intensity, and relationship with areas of physiologic FDG uptake [43]. A correlation should be made between pathologic FDG uptake and corresponding morphologic changes on the CT images.

8.3.3 FDG PET/CT Imaging of CIED Infection

FDG PET/CT has been reported in many studies to have a high diagnostic performance in assessing CIED infection with a pooled sensitivity and specificity of 80–89% and 86–100%, respectively [51–53]. Device infection may affect different components of CIED (Fig. 8.2). The diagnostic performance of FDG PET/CT for infection varies significantly by the component of the CIED involved [52, 53]. FDG PET/CT has the highest diagnostic performance in CIED infection involving the generator pocket with a pooled sensitivity and specificity of 96% (95% CI, 86–99%) and 97% (95% CI, 86–99%), respectively [54–56]. The diagnostic performance of

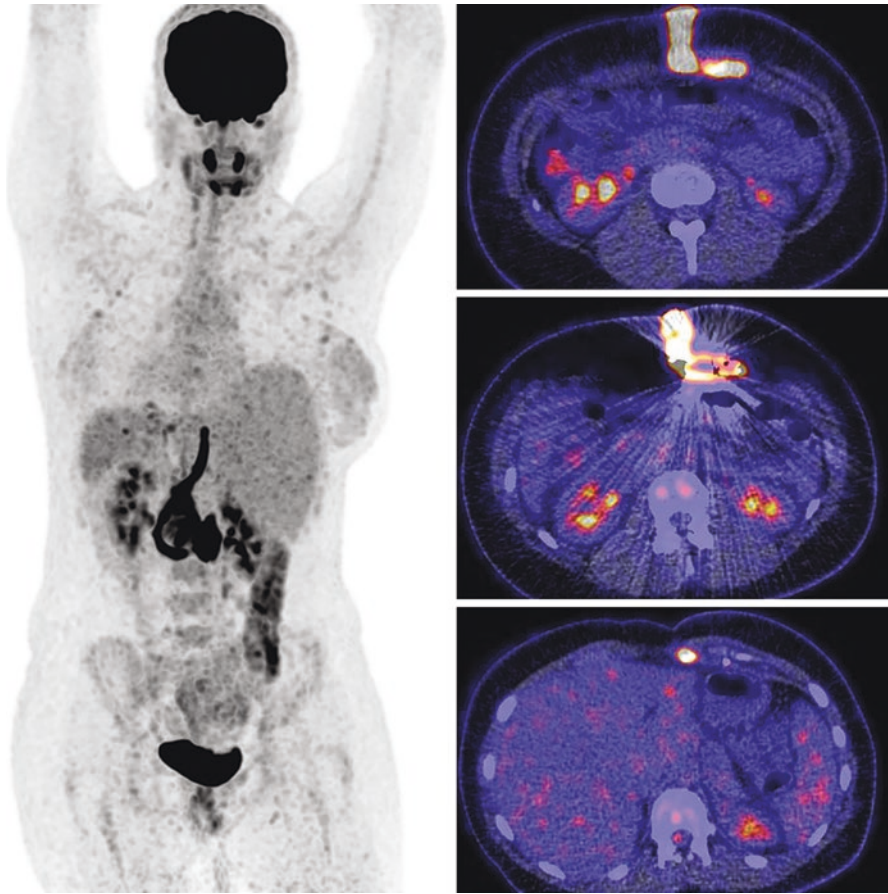


Fig. 8.2 FDG PET/CT images obtained in a patient with pacemaker evaluated for CIED-related infection. Images show intense FDG uptake in the deep pocket of the device generator implanted in the anterior abdominal wall as well as around the device lead, consistent with infection of these components of the device

FDG PET/CT for CIED lead infection is lower with a pooled sensitivity and specificity of 76% (95%CI, 65–85%) and 83% (95%CI, 72–90%), respectively [54, 55, 57–61]. The lower diagnostic accuracy of FDG PET/CT for CIED lead infection than generator pocket infection may be related to the small size of the leads and the associated lesions in an infection that may be below PET camera resolution. When infection involves the intracardiac portion of the CIED lead causing infective endocarditis, FDG PET/CT has a low diagnostic accuracy for detecting this CIED-related infective endocarditis with a sensitivity and specificity of 31% and 63%, respectively [55]. This poor diagnostic performance, which has been replicated in a more recent study [62], may be related to small vegetations and correspondingly low FDG avidity in this type of infection [63]. FDG PET/CT is accurate in

distinguishing superficial pocket site infections from deep pocket infection [55, 64]. This differentiation is significant since both entities are treated differently; superficial pocket site infection requires antibiotic therapy and local wound care while deep pocket infection requires CIED system extraction, a procedure fraught with morbidity and mortality [9, 63].

A few factors may reduce the diagnostic accuracy of FDG PET/CT in the evaluation of CIED-related endocarditis (CIEDIE). Failure to suppress myocardial uptake of FDG is a crucial confounder that may impair the detection of pathologic FDG accumulation due to CIED infection. There is variability in the methods of myocardial FDG suppression utilized in different studies [55]. This may be related to the lack of consensus on the most effective way to suppress myocardial FDG uptake. More so, the application of protocols for the suppression of myocardial FDG uptake is not consistent across studies, especially regarding fasting duration, which is shorter than what is recommended in some studies [55].

The interval between device implantation and FDG PET/CT imaging is another potential confounder in image interpretation of infection. FDG is accumulated at the site of sterile inflammation that occurs within the first few weeks after surgical implantation of cardiac devices, the intensity of which can be of limited value in differentiating sterile inflammation from infection. A recent study evaluated the performance of FDG PET/CT in two groups of patients with suspected CIED infection [65]. The first group of patients was imaged within 8 weeks of device implantation. In this group, FDG PET/CT performed poorly in discriminating between superficial pocket site infection and CIED (deep pocket and/or lead) infection. The intensity of FDG uptake in the generator pocket and around the leads was similar between patients with isolated superficial pocket site infection and patients with CIED (deep pocket/lead) infection. FDG PET/CT was acquired beyond 8 weeks after device implantation in the other group of patients. FDG uptake was limited to the component of the device involved in infection in this latter group, with no abnormal FDG uptake seen in the patient without CIED infection. In an earlier study, mild or no FDG uptake was seen around the CIED of patients without infection in whom FDG PET/CT imaging was obtained between 4- and 8-week post-device implantation [66].

There is no consensus regarding the optimum waiting period between cardiac surgery/device implantation and the application of FDG PET/CT for suspected cardiac infection imaging. In the 2015 European Society of Cardiology guidelines on the management of infective endocarditis, a three-month waiting time was recommended [11]. This contrasts with the one-month wait recommended in the joint guidelines on FDG PET imaging of inflammation and infection by the European Society of Nuclear Medicine and the Society of Nuclear Medicine and Molecular Imaging [67]. In a recent meta-analysis including studies evaluating the diagnostic performance of FDG PET/CT in suspected cardiac devices infection, Gomes and colleagues proposed a diagnostic algorithm for evaluating CIED infection in which they also recommended a one-month wait between device implantation/cardiac surgery and FDG PET/CT imaging [52]. In a recent study from the same group where they applied their proposed diagnostic algorithm, FDG PET/CT had a sensitivity,

specificity, positive predictive value, and negative predictive value of 83%, 86%, 91%, and 75%, respectively, in a group of patients with cardiac device in situ who were evaluated for infective endocarditis [68]. When interpreting FDG PET/CT images obtained within three-month of device implantation, the possibility of false-positive image findings must be borne in mind to avoid a diagnostic pitfall.

Until the 2019 International CIED Infection criteria recently proposed by the European Heart Rhythm Association become widely applied in the evaluation of patients, the modified Duke criteria remain the most used diagnostic criteria in patients with suspected CIED infection. The modified Duke criteria classify patients into definite CIED infection, CIED infection possible, or CIED infection rejected. The patients classified as CIED infection possible represent a group with a diagnostic conundrum that requires further evaluation to either confirm or reject CIED infection. It is in this group of patients with uncertainty regarding CIED infection that FDG PET/CT is most useful in reclassifying patients as either definite for CIED infection or CIED infection rejected [59]. The modern PET/CT camera can acquire diagnostic quality CT scans, including CT angiography (CTA). The addition of CTA to FDG PET (rather than non-contrast-enhanced CT) has been shown to improve the diagnostic performance of FDG PET/CT [59, 68]. CTA was reported to be superior to echocardiography in the detection of abscesses. Patients with falsely negative FDG PET may have abnormality demonstrated on the CTA component of the study leading to improved diagnosis of CIED infection [68].

There has been an improvement in the survival of patients with congenital heart diseases (CHD), with more than 90% of children born with heart defects now surviving well into adulthood [69]. This improvement in survival presents a new challenge for adults with complex anatomy of the heart and who may require cardiac devices for acquired heart diseases. Previous surgical interventions and implanted cardiac devices predispose to infection. The distortion in cardiac anatomy resulting from previous surgical interventions may limit the utility of echocardiography for evaluating cardiac device infection. Pizzi and colleagues reported the added value of FDG PET/CTA in a group of patients with CHD with multiple prosthetic materials in situ, including 36% of patients with CIED [70]. The addition of FDG PET/CTA to Duke criteria leads to a reclassification of 86% of patients initially classified as possible infective endocarditis/CIED infection. There was a significant improvement in sensitivity (from 39% to 87%) without a change in specificity (83% for Duke criteria alone and combined Duke criteria and FDG PET/CTA) when the findings of FDG PET/CT were added to Duke criteria in the diagnosis of cardiac infection. Improvement in sensitivity due to the addition of FDG PET/CTA was due to better detection of abscesses and pseudoaneurysms missed by echocardiography [70]. This study shows the challenges with the diagnosis of cardiac infection in patients with CHD due to the limited diagnostic performance of echocardiography and the added benefit of including multimodal imaging with FDG PET/CTA. The extent of the added value of CTA over non-contrast-enhanced CT in this study is unknown. It is important to determine the real contribution of CTA to diagnostic accuracy as the radiation burden associated with it is much higher than

non-contrast-enhanced CT. There is an additional risk of kidney damage with intravenous contrast use during CTA.

8.3.4 FDG PET/CT Imaging of LVAD Infection

Fewer studies report the utility of FDG PET/CT for LVAD infection compared with those on CIED infection. In the last 2–3 years, there has been an increase in the interest in the use of FDG PET/CT in the clinical assessment of patients with suspected LVAD infection, manifesting as an increase in the number of reports on this subject in the literature. In a 2018 meta-analysis including qualifying studies published through March 2018, the pooled sensitivity and specificity of FDG PET/CT for the diagnosis of LVAD infection were 92% (95% CI, 82–97%) and 83% (95% CI, 24–99%), respectively [71]. In a more recent pooled analysis of studies published between 2016 and 2019, the pooled sensitivity and specificity of FDG PET/CT for detecting LVAD infection were 95% (95% CI, 89–97%) and 91% (95% CI 54–99%), respectively [72]. While both meta-analyses show excellent sensitivity, there is much variability in the specificity of FDG PET/CT in the diagnosis of LVAD infection, suggesting that it is less consistent in ruling in LVAD infection. False-positive scan interpretation due to the wrong allocation of FDG uptake due to sterile inflammation to infection is a significant cause of the variability seen in the specificity of FDG PET/CT for LVAD infection [71]. Physiologic FDG accumulation may persist around the device components for a variable time after its implantation and should not be misconstrued to be due to infection.

The exit site of the driveline serves as the potential entry site for microbial agents. Infection involving the exit site of the driveline is easily accessible for definite microbiological diagnosis. Infection can spread from the exit site to involve the percutaneous driveline and, eventually, the deeper components of the device, including the inflow cannula, the outflow cannula, and the pump/pocket site. It is important to delineate the extent of infection as this delineation impacts treatment modality and prognosis. Patients with infection localized to the exit site of the driveline on the skin surface may benefit from local wound care and antibiotic therapy. In contrast, patients with superficial driveline infections may benefit from an additional replacement of the driveline (Fig. 8.3). When the infection involves the deeper components of the device, complete system extraction may be indicated (Fig. 8.4). FDG PET/CT has a pooled sensitivity and specificity of 97% (95% CI, 88–99%) and 99% (95% CI, 13–100%), respectively, for percutaneous driveline infection [72]. For pump/pocket infection, the corresponding pooled sensitivity and specificity are 97% (70–100%) and 93% (95% CI, 64–99%), respectively [72]. In both cases, the specificities show wider variability indicating the variable performance of FDG PET/CT in ruling in driveline infection and pump/pocket infection.

Beyond contributing to the diagnosis of CIED infection, determining the device component involved by infection, and quantifying the whole-body extent of the infection, findings on FDG PET/CT imaging can guide therapy and provide useful prognostic information. Patients with a positive FDG PET/CT are more likely to die

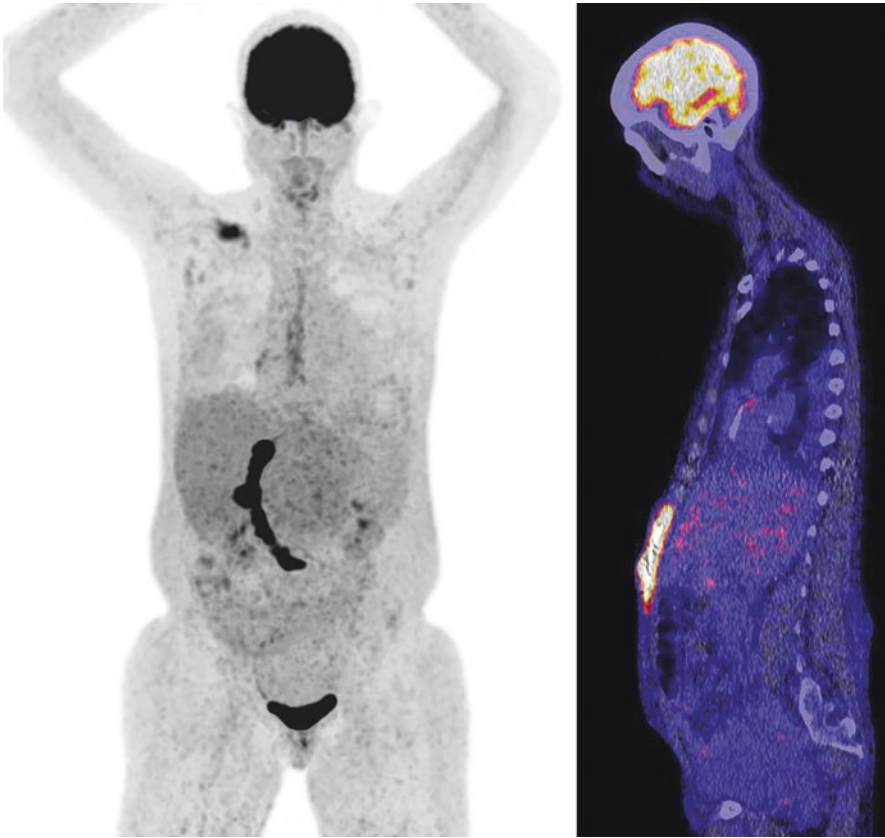


Fig. 8.3 FDG PET/CT images obtained in a patient with left ventricular assist device suspected with device-related infection. There is intense FDG uptake around the driveline with involvement of deeper device components. This is consistent with an isolated driveline infection

than patients with negative FDG PET/CT findings [73]. Also, the involvement of central device components, especially the pump or its pocket, has a higher risk of mortality compared with the infection involving the peripheral components of the device [73]. The involvement of central device components such as the inflow and outflow cannulae and the pump/pocket indicates a severe infection requiring device extraction for infection control. Device removal is associated with significant morbidity and mortality. Findings on FDG PET/CT may guide the selection of appropriate therapy for patients [74]. For example, in a study, findings on FDG PET/CT informed the decision to list some patients for urgent heart transplantation and others to surgical revision [75]. Patients with FDG-avid thoracic nodes on PET/CT have been reported to have poorer survival [76]. FDG-avid lymph nodes reported in patients on antibiotics in this study may represent severe infection with significant reactive changes in the lymph nodes draining the infection sites.

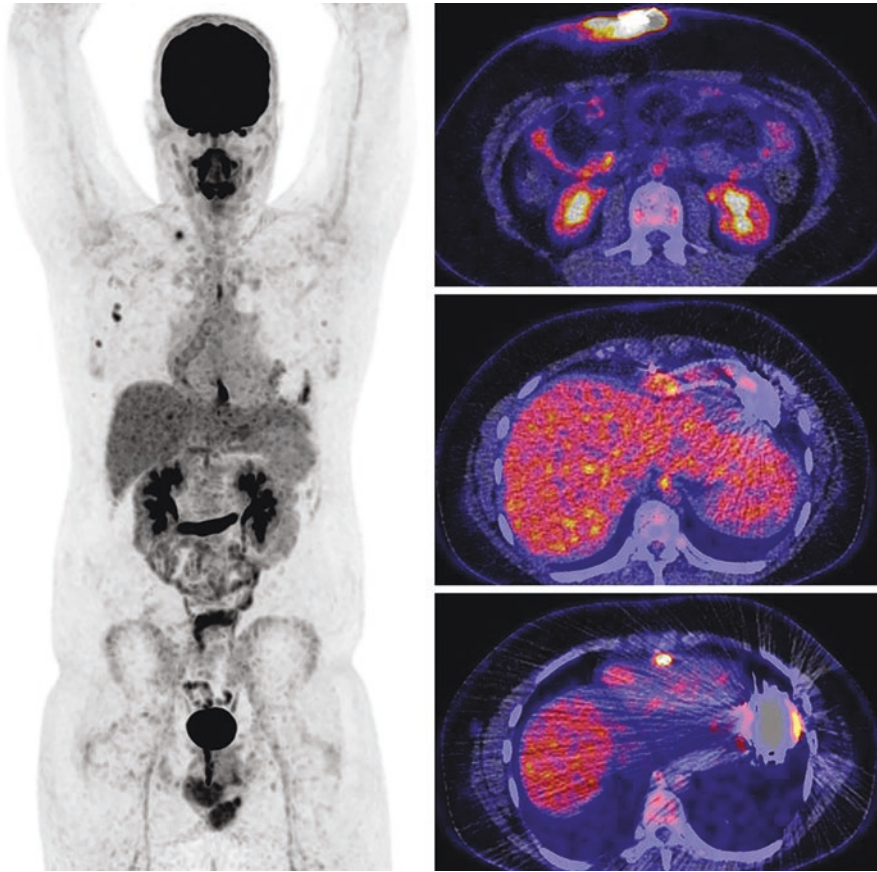


Fig. 8.4 FDG PET/CT images of a patient with left ventricular assist device (LVAD). Imaging was performed to confirm the presence of LVAD infection and delineate its extent. Images show intense FDG accumulation around the driveline with a lower intensity level of uptake around the device cannula, consistent with infection of the driveline and deeper components of the device

8.3.5 FDG PET/CT for Extra-Cardiac Disease in Patients Assessed for Cardiac Devices Infection

Whole-body imaging in FDG PET/CT allows assessing for foci of septic embolization and portal of entry of infection in a single imaging session (Fig. 8.5). Detection of the portal of entry and its treatment helps prevent the recurrence of infection. The brain is one of the commonest sites of septic embolization. The brain is an obligate user of glucose for its metabolism and traps FDG avidly. This high physiologic brain FDG uptake may mask the detection of septic embolism in the brain. Given this, a dedicated brain imaging, preferably with MRI, may be indicated for the assessment of septic embolism in the brain when clinically indicated. Other

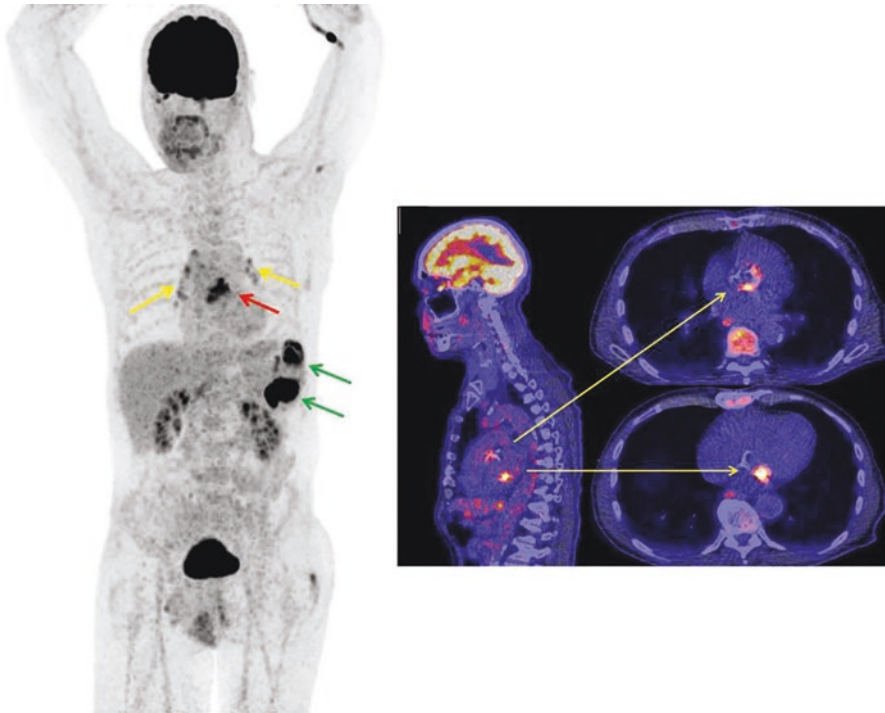


Fig. 8.5 FDG PET/CT images obtained in a patient evaluated for valve-related infective endocarditis. Images show multi-focal sites of infection involving the heart valves (yellow and red arrows). In addition, there are multiple sites of intense FDG accumulation in the spleen consistent with septic embolization causing the formation of splenic abscesses

common sites of septic embolization in patients with cardiac devices include the lungs and the musculoskeletal system [77]. At the time of diagnosis of cardiac device infection, metastatic infection due to septic embolization may be asymptomatic. FDG PET/CT is sensitive in determining these sites of asymptomatic distant infections [77].

Patients requiring cardiac devices are generally older. This age group is at increased risk of malignancies. Associations have been established between some of the aetiological agents of infective endocarditis and cancers [78, 79]. Patients with endocarditis, with or without cardiac devices, are known to be at a higher risk for malignancies [80]. In a recent study assessing occult cancer detected in patients with suspected endocarditis with or without cardiac devices, FDG PET/CT was useful in detecting occult cancers, including colorectal cancer, lung cancer, prostate cancer, among others [81]. During FDG PET/CT image interpretation, attention must, therefore, be paid not only to finding suggestive of device infection, septic embolism, and portal of entry of infection, but also to findings that may suggest occult malignancy.

8.4 Comparative Performance of Radionuclide WBC Scintigraphy and FDG PET/CT in Cardiac Devices Infection

There is limited data on the comparative performance of radiolabelled WBC scintigraphy and FDG PET/CT in the assessment of patients with suspected cardiac device infection. In a recent study of 48 patients evaluated for suspected CIED infection with combined radiolabelled WBC SPECT/CT and FDG PET/CT, radiolabelled WBC scintigraphy had a lower sensitivity of 60% compared with 80% for FDG PET/CT but a better specificity of 100% compared with 91% for FDG PET/CT [25]. FDG PET/CT detected foci of septic emboli in 25% of the study population, whereas radiolabelled WBC SPECT/CT imaging missed all the cases of septic emboli. These findings are like those of another study where the two imaging modalities were evaluated in patients with suspected LVAD infection [31]. In this study involving prospectively recruited 24 patients, 15 of whom had LVAD-specific infection (five with pump and/or cannula infections and ten with superficial percutaneous driveline infections), six with LVAD-related infections, and three with non-LVAD infections, radiolabelled WBC SPECT/CT imaging had a sensitivity and specificity of 71% and 100%, respectively, compared with 95% and 67%, respectively, for FDG PET/CT with visual image analysis [31]. The results from these two studies are consistent in showing higher sensitivity for FDG PET/CT in cardiac device infection and better specificity for radiolabelled WBC scintigraphy. The relative performances indicate that FDG PET/CT performs better at ruling out infection, while radiolabelled WBC scintigraphy is better at ruling in infection of cardiac devices. In clinical decision making, this information is important in selecting the right test for the right indication. FDG PET/CT is selected for its high sensitivity when it is more clinically meaningful to rule out infection. In contrast, radiolabelled WBC scintigraphy is selected when ruling in infection is more clinically impactful.

8.5 Conclusion

Radiolabelled WBC scintigraphy and FDG PET/CT imaging are functional imaging modalities useful in the diagnostic workup of patients with suspected cardiac device infection. Both imaging modalities are most useful in reclassifying patients in whom the presence of infection remained uncertain after standard clinical workup, including echocardiography and blood culture. Being whole-body imaging techniques, both imaging modalities can detect foci of septic embolization and portal of entry of infection, which may be asymptomatic at the time of workup for cardiac device infection. Determination of these distant sites of infection is necessary for optimum therapy as a failure to adequately control infection at these sites is a common cause of recurrence of infection. Radiolabelled WBC scintigraphy has an exquisite specificity as time-dependent radiolabelled WBC accumulation is consistent with infection. This attribute makes it suitable for ruling in infection. FDG PET/

CT has excellent sensitivity for infection detection, hence most suitable for ruling out infection. In the early post-operative/post-intervention period, FDG accumulation at the surgical site due to reparative changes and associated sterile inflammation may be a confounder during assessment for infection, contributing to reducing the specificity of this imaging test. In view of this limitation, infection-specific PET tracers are needed in the future to exploit the high sensitivity of the PET system combined with the specificity offered by a tracer that accumulates at sites of infection and not in sterile inflammation for an improved diagnosis of cardiac device infection.

References

1. Cabell CH, Heidenreich PA, Chu VH, Moore CM, Stryjewski ME, Corey GR, et al. Increasing rates of cardiac device infections among Medicare beneficiaries: 1990-1999. *Am Heart J.* 2004;147:582–6.
2. Voigt A, Shalaby A, Saba S. Continued rise in rates of cardiovascular implantable electronic device infections in the United States: temporal trends and causative insights. *Pacing Clin Electrophysiol.* 2010;33:414–9.
3. Ann HW, Ahn JY, Jeon YD, Jung IY, Jeong SJ, Joung B, et al. Incidence of and risk factors for infectious complications in patients with cardiac device implantation. *Int J Infect Dis.* 2015;36:9–14.
4. Hercé B, Nazeyrollas P, Lesaffre F, Sandras R, Chabert JP, Martin A, et al. Risk factors for infection of implantation cardiac devices: data from a registry of 2496 patients. *EP Europace.* 2013;15:66–70.
5. Polyzos KA, Konstantelias AA, Falagas ME. Risk factors for cardiac implantable electronic device infection: a systematic review and meta-analysis. *Europace.* 2015;17:767–77.
6. Nery PB, Fernandes R, Nair GM, Sumner GL, Ribas CS, Menon SM, et al. Device-related infection among patients with pacemakers and implantable defibrillators: incidence, risk factors, and consequences. *J Cardiovasc Electrophysiol.* 2010;21:786–90.
7. Clémenty N, Carion PL, Léotoing L, Lamarsalle L, Wilquin-Bequet F, Brown B, et al. Infections and associated costs following cardiovascular implantable electronic device implantations: a nationwide cohort study. *Europace.* 2018;20:1974–80.
8. Daneman N, Homenauth E, Saskin R, Ng R, Ha A, Wijeyesundera HC. The predictors and economic burden of early-, mid- and late-onset cardiac implantable electronic device infections: a retrospective cohort study in Ontario, Canada. *Clin Microbiol Infect.* 2020;26:255.
9. Bongiorni MG, Burri H, Deharo JC, Starck C, Kennergren C, Saghy L, et al. 2018 EHRA expert consensus statement on lead extraction: recommendations on definitions, endpoints, research trial design, and data collection requirements for clinical scientific studies and registries: endorsed by APHRS/HRS/LAHS. *Europace.* 2018;20:1217.
10. Blomström-Lundqvist C, Traykov V, Erba PA, Burri H, Nielsen JC, Bongiorni MG, et al. European Heart Rhythm Association (EHRA) international consensus document on how to prevent, diagnose, and treat cardiac implantable electronic device infections – endorsed by the Heart Rhythm Society (HRS), the Asia Pacific Heart Rhythm Society (APHRS), the Latin American Heart Rhythm Society (LAHS), International Society for Cardiovascular Infectious Diseases (ISCVID) and the European Society of Clinical Microbiology and Infectious Diseases (ESCMID) in collaboration with the European Association for Cardio-Thoracic Surgery (EACTS). *Eur J Cardiothorac Surg.* 2020;22:514–49.
11. Habib G, Lancellotti P, Antunes MJ, Bongiorni MG, Casalta JP, Del Zotti F, et al. 2015 ESC Guidelines for the management of infective endocarditis. *Eur Heart J.* 2015;21(36):3075–128.

12. Habib G, Erba PA, Iung B, Donal E, Cosyns B, Laroche C, et al. Clinical presentation, aetiology and outcome of infective endocarditis. Results of the ESC-EORP EURO-ENDO (European infective endocarditis) registry: a prospective cohort study. *Eur. Heart J.* 2019;40:3222–33.
13. Downey BC, Juselius WE, Pandian NG, Estes NA 3rd, Link MS. Incidence and significance of pacemaker and implantable cardioverter-defibrillator lead masses discovered during transesophageal echocardiography. *Pacing Clin Electrophysiol.* 2011;34:679–83.
14. Li JS, Sexton DJ, Mick N, Nettles R, Fowler VG Jr, Ryan T, et al. Proposed modifications to the Duke criteria for the diagnosis of infective endocarditis. *Clin Infect Dis.* 2000;30:633–8.
15. Lawal IO, Zeevaart JR, Ebenhan T, Ankrah A, Vorster M, Kruger HG, et al. Metabolic imaging of infection. *J Nucl Med.* 2017;58:1727–32.
16. Israel O, Pellet O, Biassoni L, De Palma D, Estrada-Lobato E, Gnanasegaran G, et al. Two decades of SPECT/CT - the coming of age of a technology: an updated review of literature evidence. *Eur J Nucl Med Mol Imaging.* 2019;46:1990–2012.
17. Roca M, de Vries EF, Jamar F, Israel O, Signore A. Guidelines for the labelling of leucocytes with (111) in-oxine. inflammation/infection taskgroup of the European association of nuclear medicine. *Eur J Nucl Med Mol Imaging.* 2010;37:835–41.
18. de Vries EF, Roca M, Jamar F, Israel O, Signore A. Guidelines for the labelling of leucocytes with (99m)Tc-HMPAO. Inflammation/infection taskgroup of the European Association of Nuclear Medicine. *Eur J Nucl Med Mol Imaging.* 2010;37:842–8.
19. Signore A, Jamar F, Israel O, Buscombe J, Martin-Comin J, Lazzeri E. Clinical indications, image acquisition and data interpretation for white blood cells and anti-granulocyte monoclonal antibody scintigraphy: an EANM procedural guideline. *Eur J Nucl Med Mol Imaging.* 2018;45:1816–31.
20. Lawal IO, Kleynhans J, Mokoala KMG, Vorster M, Ebenhan T, Zeevaart JR, et al. Single photon emission tomography in the diagnostic assessment of cardiac and vascular infectious diseases. *Curr Radiopharm.* Epub ahead of print on 21 June 2020. <https://doi.org/10.2174/1874471013666200621190001>.
21. Palestro CJ, Kim CK, Swyer AJ, Vallabhajusula S, Goldsmith SJ. Radionuclide diagnosis of vertebral osteomyelitis: Indium-111-leukocyte and technetium-99m-methylene diphosphonate bone scintigraphy. *J Nucl Med.* 1991;32:1861–5.
22. Erba PA, Sollini M, Conti U, Bandera F, Tascini C, De Tommasi SM, et al. Radiolabeled WBC scintigraphy in the diagnostic workup of patients with suspected device-related infections. *J Am Coll Cardiol Imaging.* 2013;36:1075–86.
23. Holcman K, Szot W, Rubiś P, Leśniak-Sobelga A, Hlawaty M, Wiśniowska-Śmiałocka B, et al. 99mTc-HMPAO-labeled leucocyte SPECT/CT and transthoracic echocardiography diagnostic value in infective endocarditis. *Int J Cardiovasc Imaging.* 2019;35:749–58.
24. Małocka BA, Ząbek A, Dębski M, Szot W, Holcman K, Boczar K, et al. The usefulness of SPECT-CT with radioisotope-labeled leukocytes in diagnosing lead-dependent infective endocarditis. *Adv Clin Exp Med.* 2019;28:113–9.
25. Calais J, Touati A, Grall N, Laouénan C, Benali K, Mahida B, et al. Diagnostic impact of ¹⁸F-fluorodeoxyglucose positron emission tomography/computed tomography and white blood cell SPECT/computed tomography in patients with suspected cardiac implantable electronic device chronic infection. *Circ Cardiovasc Imaging.* 2019;12:e007188.
26. de By TMMH, Mohacsi P, Gahl B, Zittermann A, Krabatsch T, Gustafsson F, et al. The European registry for patients with mechanical circulation support (EUROMACS) of the European Association of Cardio-Thoracic Surgery (EACTS): second report. *Eur J Cardiothorac Surg.* 2018;53:309–16.
27. Feldman D, Pamboukian SV, Teuteberg JJ, Birks E, Lietz K, Moore SA, et al. The 2013 International Society for Heart and Lung Transplantation guidelines for mechanical circulatory support: executive summary. *J Heart Lung Transplant.* 2013;32:157–87.
28. Long B, Robertson J, Koyfman A, Brady W. Left ventricular assist devices and their complications: a review for emergency clinicians. *Am J Emerg Med.* 2019;37:1562–70.

29. Hannan MM, Husain S, Mattner F, Danziger-Isakov L, Drew RJ, Corey GR, et al. Working formulation for the standardization of definitions of infections in patients using ventricular assist devices. *J Heart Lung Transplant.* 2011;30:375–84.
30. Litzler PY, Manrique A, Etienne M, Salles A, Edet-Sanson A, Vera P, et al. Leukocyte SPECT/CT for detecting infection of left-ventricular-assist devices: preliminary results. *J Nucl Med.* 2010;51:1044–8.
31. de Vaugelade C, Mesguich C, Nubret K, Camou F, Greib C, Dourmes G, et al. Infections in patients using ventricular-assist devices: comparison of the diagnostic performance of ^{18}F -FDG PET/CT scan and leucocyte-labeled scintigraphy. *J Nucl Med.* 2019;26:42–55.
32. Sousa R, Massada M, Pereira A, Amorim FF, I, Oliviera A. Diagnostic accuracy of combined $^{99\text{m}}\text{Tc}$ -sulesomab and $^{99\text{m}}\text{Tc}$ -nanocolloid bone marrow imaging in detecting prosthetic joint infection. *Nucl Med Commun.* 2011;834–9.
33. Sathekge M, Garcia-Perez O, Paez D, El-Haj N, Kain-Godoy T, Lawal I, et al. Molecular imaging in musculoskeletal infections with $^{99\text{m}}\text{Tc}$ -UBI 29-41 SPECT/CT. *Ann Nucl Med.* 2018;32:54–9.
34. Richter WS, Ivancevic V, Meller J, Lang O, Le Guludec D, Szilvazi I, et al. $^{99\text{m}}\text{Tc}$ -besilesomab (Scintimun®) in peripheral osteomyelitis: comparison with $^{99\text{m}}\text{Tc}$ -labelled white blood cells. *Eur J Nucl Med Mol Imaging.* 2011;38:899–910.
35. Schiavo R, Ricci A, Pontillo D, Bernardini G, Melacrinis FF, Maccafeo S. Implantable cardioverter-defibrillator lead infection detected by $^{99\text{m}}\text{Tc}$ -sulesomab single-photon emission computed tomography/computed tomography ‘fusion’ imaging. *J Cardiovasc Med.* 2009;10:883–4.
36. Levy DT, Minamoto GY, Da Silva R, Puius YA, Peck N, Goldstein D, et al. Role of gallium SPECT-CT in the diagnosis of left ventricular assist device infections. *ASAIO J.* 2015;61:e5–e10.
37. Kimura Y, Seguchi O, Mochizuki H, Iwasaki K, Toda K, Kumai Y, et al. Role of Gallium-SPECT-CT in the management of patients with ventricular assist device-specific percutaneous driveline infection. *J Cardiac Fail.* 2019;25:795–802.
38. Lawal IO, Stoltz AC, Sathekge MM. Molecular imaging of cardiovascular inflammation and infection in people living with HIV. *Clin Transl Imaging.* 2020;8:141–55.
39. Scholtens AM. ^{18}F -fluorodeoxyglucose PET/computed tomography in endocarditis. *PET Clin.* 2020;15:187–95.
40. Scholtens AM, Verberne HJ, Budde RPJ, Lam MGEH. Additional heparin preadministration improves cardiac glucose metabolism suppression over low-carbohydrate diet alone in ^{18}F -FDG PET imaging. *J Nucl Med.* 2016;57:568–73.
41. Kumita S, Yoshinaga K, Miyagawa M, Momose M, Kiso K, Kasai T, et al. Recommendations for ^{18}F -fluorodeoxyglucose positron emission tomography imaging for diagnosis of cardiac sarcoidosis-2018 update: Japanese Society of Nuclear Cardiology recommendations. *J Nucl Cardiol.* 2019;26:1414–33.
42. Chareonthaitawee P, Beanlands RS, Chen W, Dorbala S, Miller EJ, Murthy VL, et al. Joint SNMMI-ASNC expert consensus document on the role of ^{18}F -FDG PET/CT in cardiac sarcoid detection and therapy monitoring. *J Nucl Cardiol.* 2017;24:1741–58.
43. Erba PA, Lancellotti P, Vilacosta I, Gaemperli O, Rouzet F, Hacker M, et al. Recommendations on nuclear and multimodality imaging in IE and CIED infections. *Eur J Nucl Med Mol Imaging.* 2018;45:1795–815.
44. Kuo T, McQueen A, Chen TC, Wang JC. Regulation of glucose homeostasis by glucocorticoids. *Adv Exp Med Biol.* 2015;872:99–126.
45. Rabkin Z, Israel O, Keidar Z. Do hyperglycemia and diabetes affect the incidence of false-negative ^{18}F -FDG PET/CT studies in patients evaluated for infection or inflammation and cancer? a comparative analysis. *J Nucl Med.* 2010;51:1015–20.
46. Lawal IO, Mokoala KG, Popoola GO, Lengana T, Ankrah AO, Stoltz AC, et al. Impact of optimized PET imaging conditions on ^{18}F -FDG uptake quantification in patients with apparently normal aortas. *J Nucl Cardiol.* Epub ahead of print on 6 August 2019. <https://doi.org/10.1007/s12350-019-01833-6>.

47. Leccisotti L, Perna F, Lago M, Leo M, Stefanelli A, Calcagni ML, et al. Cardiovascular implantable electronic device infection: delayed vs standard FDG PET-CT imaging. *J Nucl Cardiol*. 2014;21:622–32.
48. Scholtens AM, Swart LE, Verberne HJ, Budde RPJ, Lam MGEH. Dual-time-point FDG PET/CT imaging in prosthetic heart valve endocarditis. *J Nucl Cardiol*. 2018;25:1960–7.
49. DiFilippo FP, Brunken RC. Do implanted pacemaker leads and ICD leads cause metal-related artifact in cardiac PET/CT? *J Nucl Med*. 2005;46:436–43.
50. Ahmed FZ, James J, Tout D, Arumugam P, Mamas M, Zaidi AM. Metal artefact reduction algorithms prevent false positive results when assessing patients for cardiac implantable electronic device infection. *J Nucl Cardiol*. 2015;22:219–20.
51. Juneau D, Golfam M, Hazra S, Zuckier LS, Garas S, Redpath C, et al. Positron emission tomography and single-photon emission computed tomography imaging in the diagnosis of cardiac implantable electronic device infection: A systematic review and meta-analysis. *Circ Cardiovasc Imaging*. 2017;10:e005772.
52. Gomes A, Glaudemans AWJM, Touw DJ, van Melle JP, Willems TP, Maass AH, et al. Diagnostic value of imaging in infective endocarditis: a systematic review. *Lancet Infect*. 2017;17:e1–14.
53. Mahmood M, Kendi AT, Farid S, Ajmal S, Johnson GB, Baddour LM, et al. Role of ¹⁸F-FDG PET/CT in the diagnosis of cardiovascular implantable electronic device infections: A meta-analysis. *J Nucl Cardiol*. 2019;26:958–70.
54. Bensimhon L, Lavergne T, Hugonnet F, Mainardi JL, Latremouille C, Maunoury C, et al. Whole body [(18) F] fluorodeoxyglucose positron emission tomography imaging for the diagnosis of pacemaker or implantable cardioverter defibrillator infection: a preliminary prospective study. *Clin Microbiol Infect*. 2011;17:836–44.
55. Cautela J, Alessandrini S, Cammilleri S, Giorgi R, Richet H, Casalta JP, et al. Diagnostic yield of FDG positron-emission tomography/computed tomography in patients with CEID infection: a pilot study. *Europace*. 2013;15:252–7.
56. Ahmed FZ, James J, Cunningham C, Motwani M, Fullwood C, Hooper J, et al. Early diagnosis of cardiac implantable electronic device generator pocket infection using ¹⁸F-FDG-PET/CT. *Eur Heart J Cardiovasc Imaging*. 2015;16:521–30.
57. Graziosi M, Nanni C, Lorenzini M, Diemberger I, Bonfiglioli R, Pasquale F, et al. Role of ¹⁸F-FDG PET/CT in the diagnosis of infective endocarditis in patients with an implanted cardiac device: a prospective study. *Eur J Nucl Med Mol Imaging*. 2014;41:1617–23.
58. Jiménez-Ballvé A, Pérez-Castejón MJ, Delgado-Bolton RC, Sánchez-Enrique C, Vilacosta I, Vivas D, et al. Assessment of the diagnostic accuracy of ¹⁸F-FDG PET/CT in prosthetic infective endocarditis and cardiac implantable electronic device infection: comparison of different interpretation criteria. *Eur J Nucl Med Mol Imaging*. 2016;43:2401–12.
59. Pizzi MN, Roque A, Fernández-Hidalgo N, Cuéllar-Calabria H, Ferreira-González I, González-Alujas MT, et al. Improving the diagnosis of infective endocarditis in prosthetic valves and intracardiac devices with ¹⁸F-fluorodeoxyglucose positron emission tomography/computed tomography angiography: initial results at an infective endocarditis referral center. *Circulation*. 2015;132:1113–26.
60. Ploux S, Riviere A, Amraoui S, Whinnett Z, Barandon L, Lafitte S, et al. Positron emission tomography in patients with suspected pacing system infections may play a critical role in difficult cases. *Heart Rhythm*. 2011;8:1478–81.
61. Granados U, Fuster D, Pericas JM, Llopis JL, Ninot S, Quintana E, et al. Diagnostic accuracy of ¹⁸F-FDG PET/CT in infective endocarditis and implantable cardiac electronic device infection: a cross-sectional study. *J Nucl Med*. 2016;57:1726–32.
62. Jerónimo A, Olmos C, Vilacosta I, Ortega-Candil A, Rodríguez-Rey C, Pérez-Castejón MJ, et al. Accuracy of ¹⁸F-FDG PET/CT in the suspicion of cardiac implantable electronic device infections. *J Nucl Cardiol*. Epub ahead of print on 03 August 2020. <https://doi.org/10.1007/s12350-020-02285-z>.

63. Galea N, Bandera F, Lauri C, Autore C, Laghi A, Erba PA. Multimodality imaging in the diagnostic workup of endocarditis and cardiac implantable electronic device (CIED) infection. *J Clin Med*. 2020;9:2237.
64. Lawal I, Sathekge M. F-18 FDG PET/CT imaging of cardiac and vascular inflammation and infection. *Br Med Bull*. 2016;120:55–74.
65. Salomäki SP, Saraste A, Kempainen J, Hurme S, Knuuti J, Nuutila P, et al. ¹⁸F-FDG positron emission tomography/computed tomography of cardiac implantable electronic device infections. *J Nucl Cardiol*. Epub ahead of print on 31 July 2020. <https://doi.org/10.1007/s12350-020-02256-4>.
66. Sarrazin JF, Philippon F, Tessier M, Guimond FM, Champagne J, Nault I, et al. Usefulness of fluorine-18 positron emission tomography/computed tomography for identification of cardiovascular implantable electronic device infections. *J Am Coll Cardiol*. 2012;59:1616–25.
67. Jamar F, Buscombe J, Chiti A, Christian PE, Delbeke D, Donohoe KJ, et al. EANM/SNMMI guideline for 18F-FDG use in inflammation and infection. *J Nucl Med*. 2013;54:647–58.
68. Gomes A, van Geel PP, Santing M, Prakken NHJ, Ruis ML, van Assen S, et al. Imaging infective endocarditis: Adherence to a diagnostic flowchart and direct comparison of imaging techniques. *J Nucl Cardiol*. 2020;27:592–608.
69. Brida M, Gatzoulis MA. Adult congenital heart disease: past, present and future. *Acta Paediatr*. 2019;108:1757–64.
70. Pizzi MN, Dos-Subirà L, Roque A, Fernández-Hidalgo N, Cuéllar-Calabria H, Pijuan Domènech A, et al. ¹⁸F-FDG-PET/CT angiography in the diagnosis of infective endocarditis and cardiac device infection in adult patients with congenital heart disease and prosthetic material. *Int J Cardiol*. 2017;248:396–402.
71. Tam MC, Patel VN, Weinberg RL, Hulten EA, Aaronson KD, Pagani FD, et al. Diagnostic accuracy of FDG PET/CT in suspected LVAD infections: a case series, systematic review, and meta-analysis. *JACC Cardiovasc Imaging*. 2020;13:1191–202.
72. Ten Hove D, Treglia G, Slart RHJA, Damman K, Wouthuyzen-Bakker M, Postma DF, et al. The value of ¹⁸F-FDG PET/CT for the diagnosis of device-related infections in patients with a left ventricular assist device: a systematic review and meta-analysis. *Eur J Nucl Med Mol Imaging*. Epub ahead of print on 27 June 2020. <https://doi.org/10.1007/s00259-020-04930-8>.
73. Kim J, Feller ED, Chen W, Liang Y, Dilsizian V. FDG PET/CT for early detection and localization of left ventricular assist device infection. *J Am Coll Cardiol Imaging*. 2019;12:722–9.
74. Bernhardt AM, Pamirsad MA, Brand C, Reichart D, Tienken M, Barten MJ, et al. The value of fluorine-18 deoxyglucose positron emission tomography scans in patients with ventricular assist device specific infections. *Eur J Cardiothorac Surg*. 2017;51:1072–7.
75. Dell'Aquila AM, Mastrobuoni S, Alles S, Wenning C, Henryk W, Schneider SRB, et al. Contributory role of fluorine 18-fluorodeoxyglucose positron emission tomography/computed tomography in the diagnosis and clinical management of infections in patients supported with a continuous-flow left ventricular assist device. *Ann Thorac Surg*. 2016;101:87–94.
76. Sohns JMS, Kröhn H, Schöde A, Derlin T, Haverich A, Schmitto JD, et al. ¹⁸F-FDG PET/CT in left-ventricular assist device infection: initial results supporting the usefulness of image-guided therapy. *J Nucl Med*. 2020;61:971–6.
77. Amraoui S, Tlili G, Sohal M, Berte B, Hindié E, Ritter P, et al. Contribution of PET imaging to the diagnosis of septic embolism in patients with pacing lead endocarditis. *JACC Cardiovasc Imaging*. 2016;9:283–90.
78. Boleij A, van Gelder MM, Swinkels DW, Tjalsma H. Clinical importance of *Streptococcus gallolyticus* infection among colorectal cancer patients: systematic review and meta-analysis. *Clin Infect Dis*. 2011;53:870–8.
79. Balamurugan R, Rajendiran E, George S, Samuel GV, Ramakrishna BS. Real-time polymerase chain reaction quantification of specific butyrate-producing bacteria, *Desulfovibrio* and *Enterococcus faecalis* in the feces of patients with colorectal cancer. *J Gastroenterol Hepatol*. 2008;23:1298–303.

-
80. Thomsen RW, Farkas DK, Friis S, Sværke C, Ording AG, Nørgaard M, et al. Endocarditis and risk of cancer: a Danish nationwide cohort study. *Am J Med.* 2013;126:58–67.
 81. Gouriet F, Tissot-Dupont H, Casalta JP, Hubert S, Cammilleri S, Riberi A, et al. FDG-PET/CT incidental detection of cancer in patients investigated for infective endocarditis. *Front Med.* 2020;7:535.



Antti Saraste and Federico Caobelli

Contents

9.1 Introduction.....	261
9.2 Single Photon Emission Tomography (SPECT).....	262
9.3 Positron Emission Tomography (PET).....	269
9.4 Concluding Remarks.....	272
References.....	273

9.1 Introduction

Infectious Endocarditis (IE) is a life-threatening condition with various clinical presentations, which affects either the damaged endocardial surface of the heart valve or the surface of an indwelling cardiac device [1]. While IE is a relatively rare disease, with a prevalence ranging from 1.5 to 11.6 cases per 100,000 subjects yearly [2], still its impact on the patients' survival remains dramatic. In fact, despite improvements in diagnosis and therapy, the mortality rate remains up to 25% [3].

The diagnosis of IE is challenging. It may present with very different clinical patterns depending on organs involved, the underlying cardiac disease, the microorganisms involved, the presence or absence of complications, and the patient's characteristics. The diagnosis of IE relies on the clinical definition by the Duke criteria (DC) [4] that stratifies patients with suspected IE into three categories: definite,

A. Saraste (✉)
Heart Center, Turku University Hospital, Turku, Finland
e-mail: antti.saraste@utu.fi

F. Caobelli
Clinic of Radiology and Nuclear Medicine, Department of Nuclear Medicine, University Hospital of Basel and University of Basel, Basel, Switzerland
e-mail: federico.caobelli@usb.ch

possible, and rejected IE. The Duke classification is mainly based on the results of blood cultures and either transthoracic echocardiography (TTE) or transesophageal echocardiography (TEE), because positive blood culture and echocardiogram positive for IE are defined as the two major criteria for IE. The most recent guidelines of the European Society of Cardiology (ESC) suggest a multimodality approach, wherein the confirmative role of molecular imaging plays a pivotal role [5].

The need for integrating clinical and instrumental findings was driven by the desire of improving diagnostic accuracy. In fact, it was reported that DC alone lead to about 24% misclassification of patients with proven IE, especially by negative blood culture endocarditis or negative echocardiogram in patients with a prosthetic valve IE [6]. A recent study demonstrated the increased sensitivity in diagnosis prosthetic valve IE if data from molecular imaging is added to the diagnostic workup [7].

A prompt diagnosis remains of clinical importance, since any delay in the initiation of an appropriate treatment results in poorer clinical outcome [8]. Therefore, improved strategies for prompt and accurate diagnosis are highly warranted.

In this chapter, we will discuss the new advances in cardiovascular molecular imaging, which may aid in reducing the number of equivocal diagnosis at an early stage and possibly lead to reduced morbidity and death rate in patients with IE.

9.2 Single Photon Emission Tomography (SPECT)

Radionuclide techniques using SPECT tracers allow for an effective and accurate diagnosis of cardiac infection. Among the different SPECT tracers for infection imaging, radiolabelled leucocytes scintigraphy is currently the most useful tool in the diagnosis and management of patients with suspected cardiac and vascular infection. The advantage of radiolabelled leucocytes scintigraphy over other techniques relies in its higher specificity, due to the ability of the leucocytes to migrate and selectively accumulate in the sites of infection [9], while being absent in sites of sterile inflammation as can be observed early after a surgical procedure or in the granulation tissue due to the presence of a prosthetic implant.

Hence, the use of labelled autologous leucocytes may be a preferred technique for the trafficking of inflammatory cells, due to their more specific bindings to the site of active infection. However, the suboptimal sensitivity of leucocyte SPET can be a serious drawback in the delineation of small foci due to small infectious vegetations [10]. As such, new advances in SPECT imaging of infection have been investigated in the latest years, capitalizing on the introduction of new camera systems able to provide improved spatial, temporal, and energy resolution [11].

9.2.1 ⁶⁷Ga-citrate Scintigraphy

A few data on the use of ⁶⁷Ga-citrate in the diagnostic workup of IE can be found in literature. This imaging agent has been widely used in the past due to its ability to localize in the sites of inflammation and infection [12]. One of the advantages

of ^{67}Ga -citrate over labelled leukocytes imaging is that no handling of blood products is needed, and imaging can be also performed in patients with leukopenia, which represents an important limitation in many clinical situations [13]. Unfortunately, along with its advantages also evident limitations of this radio-tracer should be acknowledged: non-ideal dosimetry, a prolonged delay between administration and imaging, suboptimal image quality, and a lack of specificity [14]. The introduction of hybrid scanners with a computed tomography (CT) component (SPECT/CT), partly overcame the drawback of poor image quality, allowing a three-dimensional re- construction and a more precise localization of the infection sites [15].

9.2.2 Labelled Leukocytes Scintigraphy

The use of radiolabelled leukocytes (WBC) scintigraphy in infection is supported by the recruitment of inflammatory cells in the sites of active infection. Typically, WBC can be labelled either using $^{99\text{m}}\text{Tc}$ -HMPAO or ^{111}In -oxine. Each labelling method has advantages and disadvantages in clinical practice. Summarizing, an advantage of $^{99\text{m}}\text{Tc}$ -HMPAO-WBC relies in the most favorable dosimetry and the higher image quality in modern cameras, whose collimators are optimized for $^{99\text{m}}\text{Tc}$ -labelled imaging. On the other hand, the longer half-life of ^{111}In allows for acquiring delayed imaging also after 48 h, thus representing an improvement in the sensitivity. In fact, the leukocyte accumulation within the site of infection follows a time-dependent increase in radioactivity from early to delayed images; as such, some small foci of infection may be missed if delayed imaging is not available [16].

While $^{99\text{m}}\text{Tc}$ -HMPAO can specifically label granulocytes (which are the predominant inflammatory cells in acute infection), ^{111}In -oxine can be used to label all categories of leucocytes (granulocytes, monocytes, and nonnuclear lymphocytes). As such, it was suggested that $^{99\text{m}}\text{Tc}$ -HMPAO-labelled leucocytes will perform better in the setting of acute infections while ^{111}In -oxine will be useful in acute and chronic phases of infections [17]. However, the two labelling methods generally prove equivalent in clinical practice with regard to diagnostic accuracy.

The procedure to label leucocytes with either $^{99\text{m}}\text{Tc}$ -HMPAO or ^{111}In -oxine has been defined in guidelines published by the European Association of Nuclear Medicine (EANM) [18, 19]. The in-vitro labelling requires that approximately 50 ml of patients own blood is required, with a count of at least 2×10^8 in the collected sample. This is mandatory to achieve an adequate labelling efficiency, which ranges between 40% and 80%.

Both $^{99\text{m}}\text{Tc}$ -HMPAO and ^{111}In -oxine WBC scintigraphy consist of sequential acquisition of whole-body scan and spot planar images of any region of interest in three time points: at 30 min (early images), 4–6 h (late images), and 24 h (delayed images, if needed). Imaging at a time point >24 h is typically not performed with $^{99\text{m}}\text{Tc}$ -HMPAO leukocytes scintigraphy, because of the very low count statistics due to the relatively short half-life of $^{99\text{m}}\text{Tc}$ (about 6 h).

Generally, a three-dimensional SPECT/CT acquisition of the thorax is performed at 4–6 h after the injection and repeated after 24 h if needed, in order to allow for an anatomical correlation of the revealed foci of increased uptake (Fig. 9.1).

Infection appears as single or multiple foci of radiolabelled leucocytes accumulation seen on early and late images (30 min or 4–6 h images) with typically increasing intensity on the delayed imaging (24 h images), reflecting the above-mentioned time-dependent leucocytes trafficking into the sites of active infection [16].

The sensitivity of radiolabelled leucocytes SPECT/CT imaging for IE range is between 64% and 91% with relatively great variability across different studies. On the contrary, specificity remains consistently high across different reports (87–100%) [10, 16, 20, 21]. The inherent limitations of radiolabelled leucocytes SPECT/CT imaging concerning the reduced sensitivity have been partly overcome by the use of new heart-dedicated camera systems equipped with cadmium-zinc-telluride (CZT) solid state detectors, which yield significant improvements in image quality, temporal, and spatial resolution over standard SPECT [11].

In this regard, a preclinical and clinical study was recently published by Caobelli et al. [22], wherein the feasibility of a double-radioisotope approach using a CZT camera was investigated. The authors simultaneously injected ^{111}In -oxine WBC and $^{99\text{m}}\text{Tc}$ -sestamibi (a perfusion agent, able to identify valve plan). Firstly, the authors tested this approach in phantoms, showing that a CZT camera system can effectively discriminate the signal coming from ^{111}In and $^{99\text{m}}\text{Tc}$ in a wide range of activities, consistent with a normal clinical setting. Then, 34 consecutive patients with equivocal diagnosis of IE were scanned. All underwent whole-body planar acquisitions at 24 h after the injection of ^{111}In -oxine WBC, followed by a standard SPECT-CT. Following conventional imaging, $^{99\text{m}}\text{Tc}$ -sestamibi was injected, and dual isotope CZT SPECT was started 30 min later. A significant improvement in image quality, diagnostic accuracy, and reader's confidence was rated for CZT imaging (sensitivity 83%, specificity 95%, positive Likelihood ratio 17.14, negative likelihood ratio 0.15, diagnostic odd ratio 114, Figs. 9.2, 9.3 and 9.4). The results of this study support the usefulness of this novel approach to increase sensitivity and overall accuracy of WBC imaging in endocarditis.

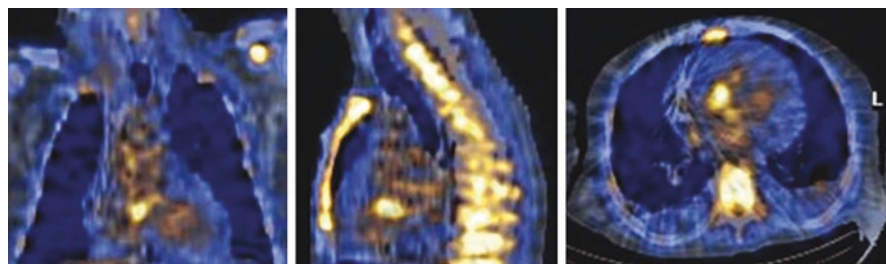


Fig. 9.1 Example of $^{99\text{m}}\text{Tc}$ -HMPAO labelled leukocyte scintigraphy in a patient with native valve endocarditis: from left to right, superimposed coronal, sagittal and transaxial SPECT/CT. Reprinted from Habib G (ed.). Infective Endocarditis. Springer 2016

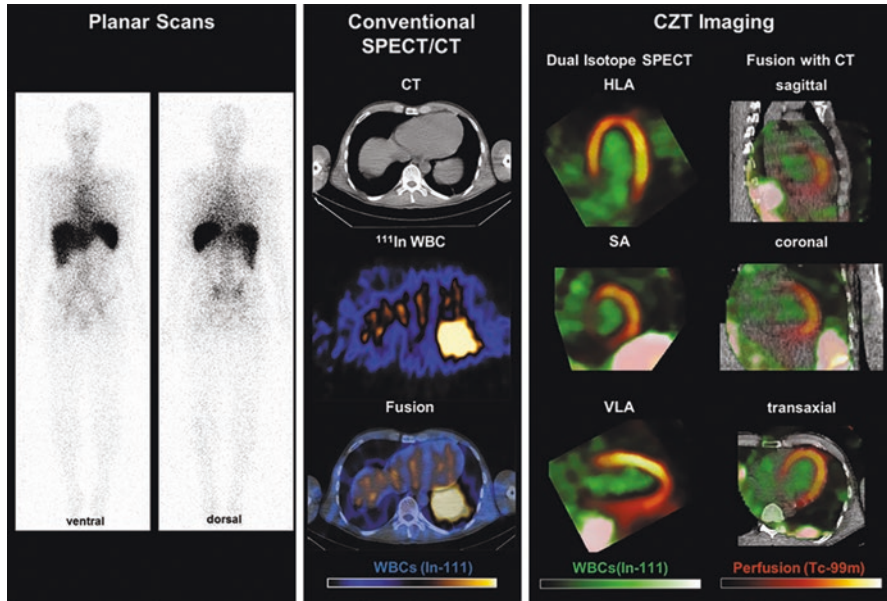


Fig. 9.2 Representative images of a patient with initially suspected endocarditis. Planar white blood cell scans, conventional SPECT/CT and cadmium-zinc-telluride dual radioisotope images (with and without fusion with external CT) show blood pool activity but no focal accumulation in the valve region. Higher image quality and more accurate localization of valve plane on cadmium-zinc-telluride images facilitate confident rule-out. Due to severe aortic insufficiency, the patient underwent valve replacement in due course. Based on negative microbiological examination on explanted material and Duke Criteria, absence of endocarditis was confirmed. Reprinted with permission of Oxford Academic from Caobelli et al. *Eur Heart J.* 2017; 38: 436–443 [22]. No changes were made

Using a conventional SPECT/CT system, Hyafil et al. investigated the role of radiolabelled leucocytes scintigraphy as a tool for guiding patients' management in 42 patients [20], showing that the degree of uptake within the infectious sites well correlated to the need of a more invasive strategy. In fact, while sites of infection with higher uptake required surgical intervention, a mild tracer accumulation at the site of infection identified patients who recovered after receiving an antibiotic therapy. The same authors also performed a follow-up study showing in this case a suboptimal sensitivity for the scintigraphy with labelled WBC (64%) but an excellent specificity (100%), therefore reporting positive and negative predictive values of 81% and 86%, respectively [10].

It should be noted that the evaluation of an infection on a native valve is typically less challenging than on valvular prostheses. While echocardiography can in most cases detect an infection of native valves, the role of labelled leucocytes scintigraphy is more pronounced in case of equivocal findings on prosthetic valves. This concept was recently confirmed in a systematic review featuring studies including a large fraction of patients with prosthetic valves [23]. A recent study by Holcman

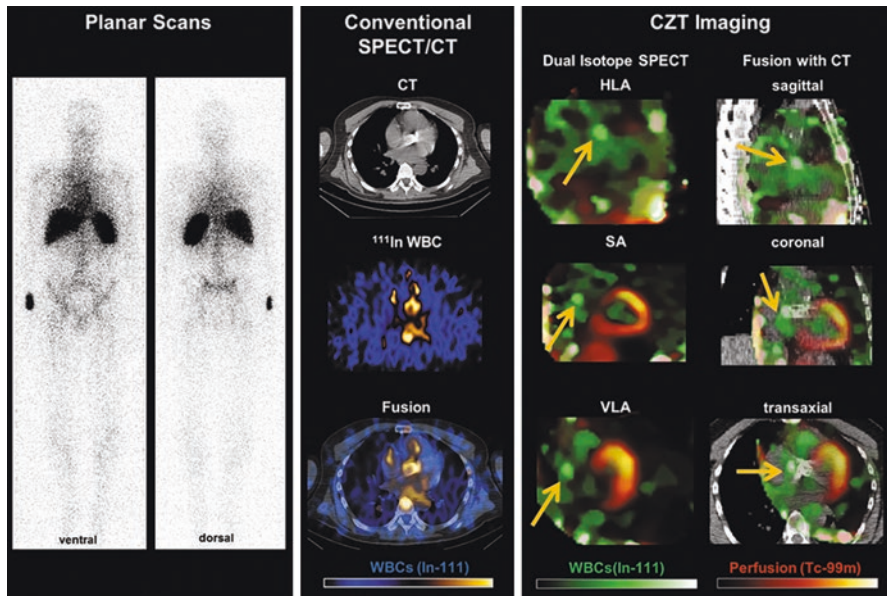


Fig. 9.3 Representative images of a patient with initially suspected endocarditis after aortic valve replacement. Planar white blood cell scans show blood pool, with uncertainty about a valvular focus. Conventional SPECT/CT images suggest a potential hot spot in the region of the artificial valve, but are limited by low counts and noise. Dual isotope cadmium-zinc-telluride images show reduced noise and a focal accumulation adjacent to the implant, read as positive for endocarditis (arrows). Due to persistent fever and clinical symptoms, the valvular prosthesis was replaced. At surgery, an abscess was identified under the right coronary artery ostium, matching the hot spot on the cadmium-zinc-telluride scan and confirming the diagnosis of endocarditis. Reprinted with permission of Oxford Academic from Caobelli et al. *Eur Heart J.* 2017; 38: 436–443 [22]. No changes were made

et al. investigated the additive role of ^{99m}Tc -HMPAO-granulocytes SPECT/CT over transthoracic echocardiography [24], reporting 90% accuracy, 93% sensitivity, 88% specificity, 96% negative predictive value, and 81% positive predictive value. Thus, SPECT/CT allowed to reduce the number of misdiagnosed IE by 27% (Fig. 9.5).

The evaluation of infection associated with cardiac implantable electronic devices (CIED) represents another challenge in clinical practice. Erba et al. [9] provided evidence supporting the use of radiolabelled leucocytes scintigraphy in patients with suspected CIED infection. In their study, 63 patients with equivocal diagnosis were investigated and underwent ^{99m}Tc -HMPAO-WBC SPECT/CT imaging. Sensitivity, specificity, positive predictive value, negative predictive value, and accuracy were 93.7%, 100%, 100%, 93.9%, and 96.8%, respectively. Similarly to what reported by Caobelli et al. [22], combined SPECT/CT imaging yielded superior diagnostic performance over planar imaging alone.

Infections affecting the intravascular and intracardiac leads are the most challenging entities among the various types of endocarditis and they account for the highest rate of mortality in affected patients [25]. The performance of SPECT/CT with

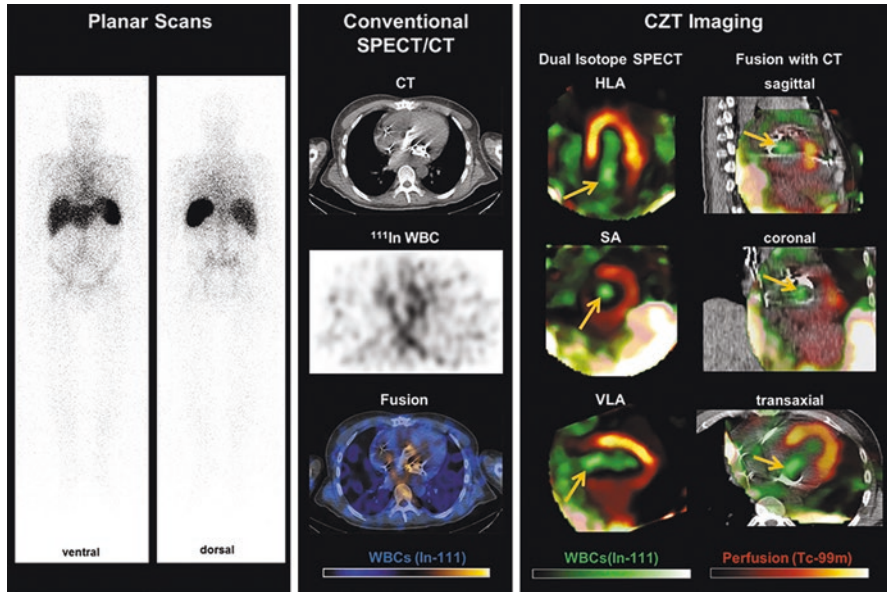


Fig. 9.4 Representative images of a patient with confirmed endocarditis affecting a mitral valve prosthesis. Planar white blood cell scans, conventional SPECT/CT and cadmium-zinc-telluride dual radioisotope images are shown. Only cadmium-zinc-telluride images show a discernible mild focal accumulation in the valve plane, adjacent to the mitral implant, consistent with focal endocarditis (yellow arrows). Reprinted with permission of Oxford Academic from Caobelli et al. *Eur Heart J.* 2017; 38: 436–443 [22]. No changes were made

radiolabelled leucocytes was investigated in a recent work by Malecka et al., wherein sensitivity and specificity of 73.7% and 81.0%, respectively, were reported [26].

Finally, infection is also a rare but serious complication of vascular graft (VG) placement [27]. While computed tomographic angiography (CTA) is considered the gold standard imaging for VG infections, able to determine its extent, radiolabelled leucocytes SPECT/CT is expected to play also an important role in this regard. Liberatore et al. [28] reported an important role for WBC SPECT/CT in the early post-operative setting, a period when CTA may be less reliable to diagnose VG infection. A comparison between CTA and SPECT with ^{111}In -oxine-WBC was performed by Khaja et al., wherein highest accuracy was yielded when both modalities were combined (sensitivity 94%, specificity 50%, accuracy 67%) [29]. The diagnostic accuracy further improves if a hybrid SPECT/CT system is used, as reported by Erba et al. (100% for sensitivity, specificity, PPV, NPV, and accuracy) [30].

9.2.3 Other SPECT Tracers

As the in-vitro labelling of leucocytes can be time-consuming and requires skilled technicians, other probes have been investigated for the imaging of cardiac

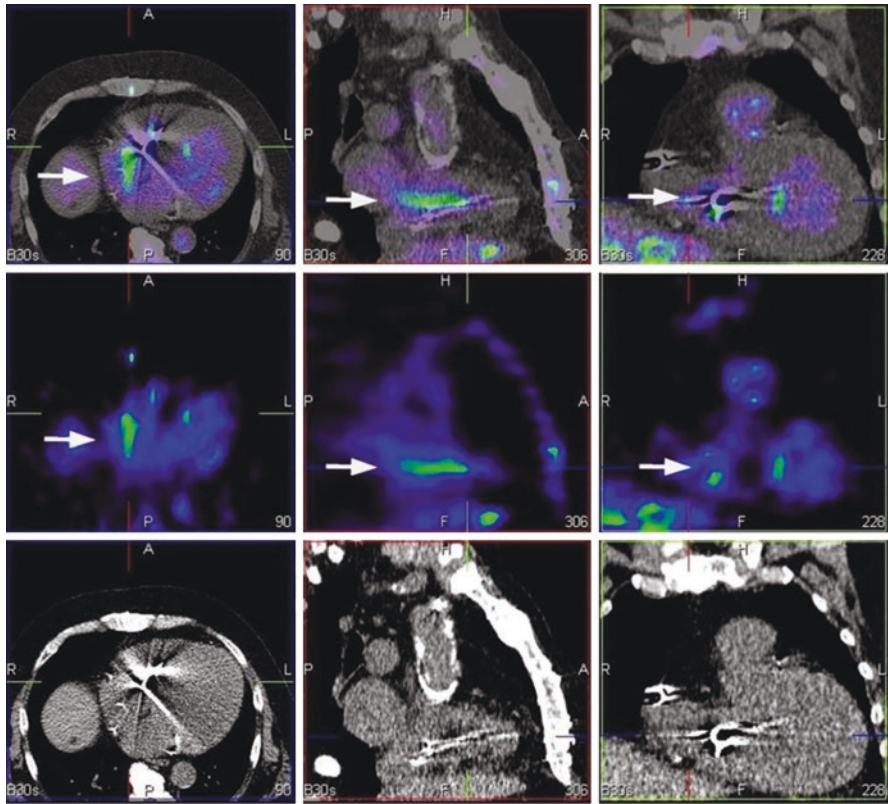


Fig. 9.5 ^{99m}Tc -HMPAO-SPECT/CT—study in three projections axial (left), sagittal (middle) and coronal (right). Bottom panel presents CT scans. Corresponding SPECT sections are presented in middle row and fusion images (^{99m}Tc -HMPAO-SPECT/CT) are placed in upper row. ^{99m}Tc -HMPAO-SPECT/CT shows an accumulation of radiolabelled leucocytes in the vicinity of an implanted electrode (arrows). Reprinted under the terms of the Creative Commons Attribution License (CC BY) from Holcman et al. *Int. J Cardiovasc. Imaging.*, 2019, 35, 749–758 [24]. No changes were made

infection. Monoclonal murine antibodies like Sulesomab, labelled with ^{99m}Tc have affinity for a 42 kDa glycoprotein expressed on granulocytes [31]. There are a few reports in literature on the use of ^{99m}Tc -Sulesomab SPECT/CT in the diagnostic workup of IE, generally reporting lower performance compared to those of in-vitro labelled leucocytes, like in the study by Gratz et al. [32], wherein sensitivity and specificity were 66% and 79%, respectively.

Besilesomab is another monoclonal IgG antibody, binding to the protein NCA-95 expressed on granulocytes [33]. A limited clinical experience is available for ^{99m}Tc -Besilesomab SPECT imaging. In a group of 72 patients with suspected subacute endocarditis (33 with confirmed and 39 with ruled-out condition), ^{99m}Tc -Besilesomab SPECT showed 79% sensitivity and 82 specificity [34]. In another study capitalizing on SPECT/CT imaging of ^{99m}Tc -besilesomab in patients with suspected IE,

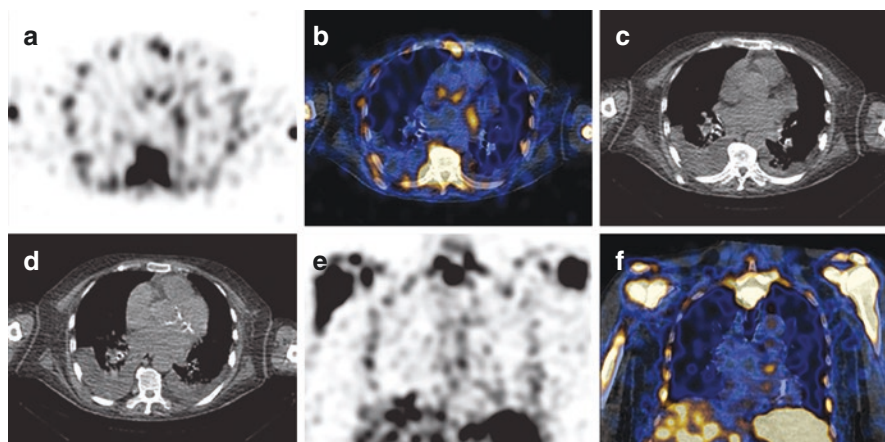


Fig. 9.6 Besilesomab-SPECT/CT in a patient with suspected prosthetic valve infection. Blood cultures detected *Enterococcus faecalis* and TEE was negative. SPECT showed a trifocal uptake at the aortic valve level (a). This focal uptake was localized slightly cranial of the prosthetic valve in fused images (b). (c) Non-fused CT image at the same level as (b). (d) Non-fused CT image of the prosthetic valve caudal of (d). Focal uptake was also visible in coronal view (e, f). The patient had a fever above 38 °C for 4 weeks. Clinical inspection detected Osler's nodes on the hands. Endocarditis was clinically confirmed according to Duke criteria. Reprinted under the under the terms of the Creative Commons Attribution License (CC BY) from Bouter et al. *Front. Med.*, 2019, 6, 40. No changes were made

better diagnostic performance was demonstrated (sensitivity 86–100% and specificity 100%, Fig. 9.6) [35].

9.3 Positron Emission Tomography (PET)

Positron emission tomography (PET) with ^{18}F -fluorodeoxyglucose (^{18}F -FDG) is evolving as an important imaging modality for patients with suspected IE and diagnostic difficulties, particularly in patients with suspected prosthetic valve endocarditis (PVE) [5, 36, 37]. Multimodality imaging may improve identification of endocardial involvement and extracardiac complications of IE.

The most recent guidance on the use of imaging in the evaluation and management of IE provided by the European Society of Cardiology (ESC) considered that the published data are sufficiently strong and convincing to propose new diagnostic criteria [5]. The addition of three further points in the diagnostic criteria of IE was proposed: (1) The identification of paravalvular lesions by cardiac CT should be considered a major criterion; (2) In suspected PVE, abnormal activity around the site of implantation detected by ^{18}F -FDG PET/CT (only if the prosthesis was implanted for >3 months earlier) or WBC SPECT/CT should be considered as a major criterion; (3) The identification of recent embolic events or infectious aneurysms by imaging only (silent events) should be considered a minor criterion.

When ^{18}F -FDG PET/CT is used to diagnose cardiac infection, patient preparation is very important in order to suppress physiological tracer uptake in the myocardium. To suppress physiological myocardial glucose utilization, it is recommended to use patient preparation protocols including a fat-enriched diet lacking carbohydrates for 12–24 h prior to the scan, a fast of 12–18 h, and/or the administration of intravenous heparin approximately 15 min prior to ^{18}F -FDG injection [37–39]. Strenuous exercise should be avoided for at least 12 h prior to the exam. Furthermore, following ^{18}F -FDG injection, and before the images are obtained, the patients should continue to fast and should restrain from any physical activity, as both will enhance myocardial glucose uptake. Image quality should be continuously evaluated to ensure that adequate suppression of tracer uptake is achieved in more than 80% of scans.

The administered tracer activity is not crucial for the results of the exam, but should be within a certain range depending also on the type of PET scanner. The EANM guidelines on ^{18}F -FDG PET imaging in inflammation/infection suggest an administered activity of 2.5–5.0 MBq/kg [37].

For image acquisition, reconstruction, and post-processing, similar protocols are recommended for imaging IE as tumor imaging. It is recommended that reconstructions be performed both with and without attenuation correction to identify potential reconstruction artifacts [37]. Such artifacts may be present in the presence of dense objects, such as implantable devices, pacing leads, or valve prostheses.

Several reports have shown promising results for ^{18}F -FDG PET/CT imaging in IE summarized in recent meta-analyses of published studies [23, 40]. With adequate cardiac preparation a meta-analysis including 407 patients found that the overall pooled sensitivity of ^{18}F -FDG PET/CT in patients with suspected IE is 81%, increasing to 85% when only PVE is considered [40]. The overall pooled specificity was 90%, and 81% when only PVE was considered [40]. Notably, studies have included mainly patients with suspected PVE [23, 40] and the diagnostic performance of ^{18}F -FDG PET/CT imaging in native valve IE has been studied less extensively.

There are some possible confounders that may influence accuracy of ^{18}F -FDG PET in the detection of IE, including myocardial ^{18}F -FDG uptake as discussed earlier, low inflammatory activity (e.g., attributable to prolonged antibiotic therapy), prior use of surgical adhesives, and recent valve implantation [41–44]. A recent retrospective multicenter study including 160 patients with suspected PVE and 77 controls with a prosthetic valve who underwent ^{18}F -FDG PET/CT imaging for other indications, evaluated possible confounders in the interpretation of ^{18}F -FDG PET/CT images [45]. The study found that low inflammatory activity defined as CRP < 40 mg/L at the time of imaging was a significant predictor of a false-negative scan, whereas the use of surgical adhesives during the surgery was a significant predictor of a false-positive scan [45]. After exclusion of patients with significant confounders, the sensitivity and specificity of ^{18}F -FDG PET/CT in the detection of PVE were 91% and 95%, respectively. Post-operative inflammation may lead to a false-positive scan and therefore, guidelines recommend the use of ^{18}F -FDG PET/CT only >3 months after the operation [5]. However, recent studies indicate that a scan <3 months after surgery can also be considered [43, 45, 46].

An infectious process is typically associated with a focal, heterogeneous increase in ^{18}F -FDG signal at or adjacent to the valve/prosthesis that is present in both attenuation corrected and non-corrected images and corresponds to an area of suspected infection on echocardiography or CT [37, 42] (Figs. 9.7 and 9.8). The probability of infection increases with the intensity of ^{18}F -FDG signal at the valve/prosthesis [37, 42].

Several parameters have been tested to quantify the ^{18}F -FDG signal in IE. The easiest semiquantitative parameter to measure is the highest standardized uptake value (SUVmax) in the valvular region. Another semiquantitative parameter that has been proposed is the valvular to background ratio (target-to-background ratio or TBR) that takes into account the variability of the signal related to residual blood pool activity and image noise. Reported cutoff value for the detection of IE varies between studies depending on scanner, and image processing techniques [45, 47–49].

Additional benefit of nuclear imaging is that extracardiac complications, such as septic embolism and metastatic infection, can be detected by whole-body ^{18}F -FDG PET/CT. The findings of whole-body scan can contribute to the diagnosis of IE and have therapeutic implications [50–53]. Septic emboli appear as focal ^{18}F -FDG uptake in organs with low background uptake, such as the spleen, the liver, the lungs, and the kidneys. Finding of ^{18}F -FDG uptake in vertebral bone and/or intervertebral disks suggests metastatic infection (spondylodiscitis), which can also be found in muscles and joints. In one study, extracardiac findings were seen in 60% of patients, and in 15% these lesions were previously unknown and considered of clinical relevance [50].

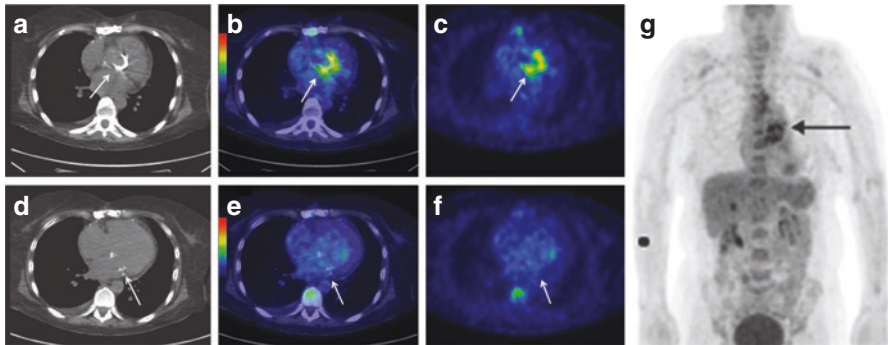


Fig. 9.7 ^{18}F -fluorodeoxyglucose (^{18}F -FDG) positron emission tomography (PET)/computed tomography (CT) in infective endocarditis of a prosthetic valve implanted several years earlier caused by *Staphylococcus epidermidis*. Initial transesophageal echocardiography showed no sign of endocarditis. ^{18}F -FDG PET/CT study showed strong tracer uptake (arrows in panels **b**, **c**, and **g**, maximum standardized uptake value 8.4) that co-localizes with the aortic valve prosthesis (arrows in PET/CT fusion image in panel **b** and non-contrast CT image in panel **a**). No uptake was visible in the region of mitral valve prosthesis (maximum SUV 3.6, arrows in panels **d**, **e**, and **f**). Myocardial uptake had been suppressed by overnight fasting and low-carbohydrate diet on the day preceding imaging

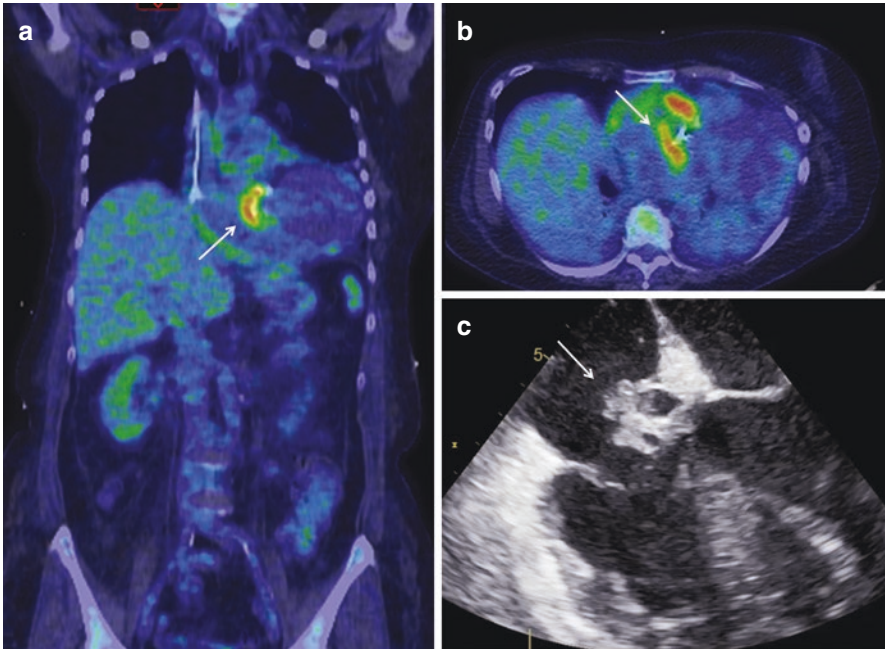


Fig. 9.8 ^{18}F -fluorodeoxyglucose (^{18}F -FDG) positron emission tomography (PET)/computed tomography (CT) in infective endocarditis of a native aortic valve caused by *Staphylococcus aureus*. PET/CT images (arrows in panels **a** and **b**) show strong tracer uptake that co-localizes with the aortic valve. Transesophageal echocardiography shows large vegetation and a paravalvular abscess in a modified four-chamber view (arrow in panel **c**). Myocardial uptake had been suppressed by overnight fasting and low-carbohydrate diet on the day preceding imaging

A cardiac CT scan with intravenous contrast agent is possible to combine with ^{18}F -FDG PET for evaluation of IE, unless there are contraindications to the use of iodine contrast agent. In a series of patients with suspected PVE, Pizzi et al. showed that the addition of contrast-enhanced CT to ^{18}F -FDG PET resulted in a high rate of patients reclassified from possible IE to definite IE, thus improving the overall diagnostic accuracy as compared with the ^{18}F -FDG PET alone [47]. The additional information provided by CT includes accurate discrimination of the origin of ^{18}F -FDG uptake between the valve and the myocardium, identification of anatomical abnormalities related to the IE, such as perivalvular abscess, and exclusion of coronary artery disease.

9.4 Concluding Remarks

In summary, the most recent clinical guidelines on the management of IE propose findings of multimodality imaging, including nuclear imaging with SPECT/CT or PET/CT, as part of the diagnostic criteria and diagnostic flowchart of IE,

particularly in patients with suspected PVE. Current data indicate that multimodality imaging may contribute to early diagnosis of IE. However, there is need for data on the diagnostic accuracy and the risks of false positive and negative findings in different patient groups. Furthermore, studies should assess whether multimodality imaging results in a better prognosis for patients and is cost-effective.

References

1. Holland TL, Baddour LM, Bayer AS, Hoen B, Miro JM, Fowler VG Jr. Infective endocarditis. *Nat Rev Dis Primers*. 2016;2:16059.
2. Bin Abdulhak AA, Baddour LM, Erwin PJ, Hoen B, Chu VH, Mensah GA, Tleyjeh IM. Global and regional burden of infective endocarditis, 1990–2010: a systematic review of the literature. *Glob Heart*. 2014;9:1311–43.
3. Habib G, Erba PA, Iung B, Donal E, Cosyns B, Laroche C, Popescu BA, Prendergast B, Tornos P, Sadeghpour A, et al. Clinical presentation, aetiology and outcome of infective endocarditis. Results of the ESC-EORP EURO-ENDO (European infective endocarditis) registry: a prospective cohort study. *Eur Heart J*. 2019;40:32223–32.
4. Li JS, Sexton DJ, Mick N, Nettles R, Fowler VG Jr, Ryan T, Bashore T, Corey GR. Proposed modifications to the Duke criteria for the diagnosis of infective endocarditis. *Clin Infect Dis*. 2000;30:633–8.
5. Habib G, Lancellotti P, Antunes MJ, Bongiorni MG, Casalta JP, Del Zotti F, Dulgheru R, El Khoury G, Erba PA, Iung B, et al. 2015 ESC guidelines for the management of infective endocarditis: the task force for the Management of Infective Endocarditis of the European Society of Cardiology (ESC). Endorsed by: European Association for Cardio-Thoracic Surgery (EACTS), the European Association of Nuclear Medicine (EANM). *Eur Heart J*. 2015;36:30753–128.
6. Habib G, Derumeaux G, Avierinos JF, Casalta JP, Jamal F, Volot F, Garcia M, Lefevre J, Biou F, Maximovitch-Rodaminoff A, et al. Value and limitations of the Duke criteria for the diagnosis of infective endocarditis. *J Am Coll Cardiol*. 1999;33:20232–029.
7. Philip M, Tessonier L, Mancini J, Mainardi JL, Fernandez-Gerlinger MP, Lussato D, Attias D, Cammilleri S, Weinmann P, Hagege A, Arregle F, Martel H, Oliver L, Camoin L, Casalta AC, Casalta JP, Gouriet F, Riberi A, Lepidi H, Raoult D, Drancourt M, Habib G. Comparison Between ESC and Duke criteria for the diagnosis of prosthetic valve infective endocarditis. *JACC Cardiovasc Imaging*. 2020;13(12):2605–15. <https://doi.org/10.1016/j.jcmg.2020.04.011>.
8. Fukuchi T, Iwata K, Ohji G. Failure of early diagnosis of infective endocarditis in Japan—a retrospective descriptive analysis. *Medicine*. 2014;93:e237.
9. Erba PA, Sollini M, Conti U, Bandera F, Tascini C, De Tommasi SM, Zucchelli G, Doria R, Menichetti F, Bongiorni MG, Lazzari E, Mariani G. Radiolabeled WBC scintigraphy in the diagnostic workup of patients with suspected device-related infections. *JACC Cardiovasc Imaging*. 2013;6:1075–86.
10. Rouzet F, Chequer R, Benali K, Lepage L, Ghodbane W, Duval X, Iung B, Vahanian A, Le Guludec D, Hyafil F. Respective performance of 18F-FDG PET and radiolabeled leukocyte scintigraphy for the diagnosis of prosthetic valve endocarditis. *J Nucl Med*. 2014;55:1980–5.
11. Imbert L, Poussier S, Franken PR, et al. Compared performance of high-sensitivity cameras dedicated to myocardial perfusion SPECT: a comprehensive analysis of phantom and human images. *J Nucl Med*. 2012;53:1897–903.
12. Lavender JP, Lowe J, Barker JR, Burn JI, Chaudhri MA. Gallium 67 citrate scanning in neoplastic and inflammatory lesions. *Br J Radiol*. 1971;44:361–6.
13. Palestro CJ. Molecular imaging of infection: the first 50 years. *Semin Nucl Med*. 2020;50:23–34.
14. Palestro CJ, Love C. Nuclear medicine imaging in fever of unknown origin: the new paradigm. *Curr Pharm Des*. 2018;24:814–20.

15. McWilliams ET, Yavari A, Raman V. Aortic root abscess: multimodality imaging with computed tomography and gallium-67 citrate single-photon emission computed tomography/computed tomography hybrid imaging. *J Cardiovasc Comput Tomogr*. 2011;5:122–4.
16. Erba PA, Conti U, Lazzeri E, Sollini M, Doria R, De Tommasi SM, et al. Added value of ^{99m}Tc-HMPAO-labeled leukocyte SPECT/CT in the characterization and management of patients with infective endocarditis. *J Nucl Med*. 2012;53:1235–43.
17. Lawal IO, Kleyhans J, Mokoala KMG, Vorster M, Ebenhan T, Zeevaart JR, Sathekge MM. Single photon emission tomography in the diagnostic assessment of cardiac and vascular infectious diseases. *Curr Radiopharm*. 2020; <https://doi.org/10.2174/1874471013666200621190001>. Online ahead of print.
18. de Vries EFJ, Roca M, Jamar F, Israel O, Signore A. Guidelines for the labelling of leucocytes with ^{99m}Tc-HMPAO. *Eur J Nucl Med Mol Imaging*. 2010;37:842–8.
19. Roca M, de Vries EFJ, Jamar F, Israel O, Signore A. Guidelines for the labelling of leucocytes with ¹¹¹In-oxine. *Eur J Nucl Med Mol Imaging*. 2010;37:835–41.
20. Hyafil F, Rouzet F, Lepage L, Benali K, Raffoul R, Duval X, Hvass U, Iung B, Nataf P, Lebtahi R, Vahanian A, Le Guludec D. Role of radiolabeled leucocyte scintigraphy in patients with a suspicion of prosthetic valve endocarditis and inconclusive echocardiography. *Eur Heart J*. 2013;14:586–94.
21. Juneau D, Golfam M, Hazra S, Erthal F, Zuckier LS, Bernick J, Wells GA, Beanlands RSB, Chow BJW. Molecular imaging for the diagnosis of infective endocarditis: a systematic literature review and meta-analysis. *Int J Cardiol*. 2018;253:183–8.
22. Caobelli F, Wollenweber T, Bavendiek U, Kühn C, Schütze C, Geworski L, Thackeray JT, Bauersachs J, Haverich A, Bengel FM. Simultaneous dual-isotope solid-state detector SPECT for improved tracking of white blood cells in suspected endocarditis. *Eur Heart J*. 2017;38:436–43.
23. Gomes A, Glaudemans AWJM, Touw DJ, van Melle JP, Willems TP, Maass AH, Natour E, Prakken NHJ, Borra RJH, van Geel PP, Slart RHJA, van Assen S, Sinha B. Diagnostic value of imaging in infective endocarditis: a systematic review. *Lancet Infect Dis*. 2017;17:e1–e14.
24. Holcman K, Szot W, Rubiś P, Leśniak-Sobelga A, Hlawaty M, Wiśniowska-Śmiałek S, Małecka B, Zabek A, Boczar K, Stepień A, Podolec P, Kostkiewicz M. ^{99m}Tc-HMPAO-labeled leukocyte SPECT/CT and transthoracic echocardiography diagnostic value in infective endocarditis. *Int J Cardiovasc Imaging*. 2019;35:749–58.
25. Blomström-Lundqvist C, Traykov V, Erba PA, Burri H, Nielsen JC, Bongiorno MG, Poole J, Boriani G, Costa R, Deharo JC, Epstein LM, Sághy L, Snygg-Martin U, Starck C, Tascini C, Strathmore N. European Heart Rhythm Association (EHRA) international consensus document on how to prevent, diagnose, and treat cardiac implantable electronic device infections-endorsed by the Heart Rhythm Society (HRS), the Asia Pacific Heart Rhythm Society (APHRS), the Latin American Heart Rhythm Society (LAHRS), International Society for Cardiovascular Infectious Diseases (ISCVID), and the European Society of Clinical Microbiology and Infectious Diseases (ESCMID) in collaboration with the European Association for Cardio-Thoracic Surgery (EACTS). *Eur Heart J*. 2020;41:2012–32.
26. Małecka BA, Zabek A, Dębski M, Szot W, Holcman K, Boczar K, Ulman M, Lelakowski J, Kostkiewicz M. The usefulness of SPECT-CT with radioisotope-labeled leukocytes in diagnosing lead-dependent infective endocarditis. *Adv Clin Exp Med*. 2019;28:113–9.
27. Shiraev T, Barrett S, Heywood S, Mirza W, Hunter-Dickson M, Bradshaw C, Hardman D, Neilson S, Bradshaw S. Incidence, management, and outcomes of aortic graft infection. *Ann Vasc Surg*. 2019;59:73–83.
28. Liberatore M, Misuraca M, Calandri E, Rizzo L, Speziale F, Iurilli AP, Anagnostou C. White blood cell scintigraphy in the diagnosis of infection of endovascular prostheses within the first month after implantation. *Med Sci Monit*. 2006;12:MT5–9.
29. Khaja MS, Sildiroglu O, Hagspiel K, Rehm PK, Cherry KJ, Turba UC. Prosthetic vascular graft infection imaging. *Clin Imaging*. 2013;37:239–44.
30. Erba PA, Leo G, Sollini M, Tascini C, Boni R, Berchiolli RN, Menichetti F, Ferrari M, Lazzeri E, Mariani G. Radiolabelled leucocyte scintigraphy versus conventional radiological imaging

- for the management of late, low-grade vascular prosthesis infections. *Eur J Nucl Med Mol Imaging*. 2014;41:357–68.
31. Becker W, Borst U, Fischbach W, Pasurka B, Schäfer R, Börner W. Kinetic data of in-vivo labeled granulocytes in humans with a murine Tc-99m-labelled monoclonal antibody. *Eur J Nucl Med*. 1989;15:361–6.
 32. Gratz S, Schipper ML, Dörner J, Höffken H, Becker W, Kaiser JW, Béhé M, Behr TM. LeukoScan for imaging infection in different clinical settings: a retrospective evaluation and extended review of the literature. *Clin Nucl Med*. 2003;28:267–76.
 33. Palestro CJ. Radionuclide imaging of musculoskeletal infection: a review. *J Nucl Med*. 2016;57:1406–12.
 34. Morguet AJ, Munz DL, Ivančević V, Werner GS, Sandrock D, Bökemeier M, Kreuzer H. Immunoscintigraphy using technetium-99m-labeled anti-NCA-95 antigranulocyte antibodies as an adjunct to echocardiography in subacute infective endocarditis. *J Am Coll Cardiol*. 1994;23:1171–8.
 35. Bouter C, Meller B, Sahlmann CO, Meller J. 99mTc-besilesomab-SPECT/CT in infectious endocarditis: upgrade of a forgotten method? *Front Med*. 2019;6:40.
 36. Saby L, Laas O, Habib G, Cammilleri S, Mancini J, Tessonnier L, Casalta JP, Gouriet F, Riberi A, Avierinos JF, Collart F, Mundler O, Raoult D, Thuny F. Positron emission tomography/computed tomography for diagnosis of prosthetic valve endocarditis: increased valvular 18F-fluorodeoxyglucose uptake as a novel major criterion. *J Am Coll Cardiol*. 2013;61:2374–82.
 37. RHJA S, AWJM G, Gheysens O, Lubberink M, Kero T, Dweck MR, Habib G, Gaemperli O, Saraste A, Gimelli A, Georgoulas P, Verberne HJ, Bucierius J, Rischpler C, Hyafil F, Erba PA, 4Is Cardiovascular Imaging: a joint initiative of the European Association of Cardiovascular Imaging (EACVI) and the European Association of Nuclear Medicine (EANM). Procedural recommendations of cardiac PET/CT imaging: standardization in inflammatory-, infective-, infiltrative-, and innervation- (4Is) related cardiovascular diseases: a joint collaboration of the EACVI and the EANM. *Eur J Nucl Med Mol Imaging*. 2020;48:1016–39. <https://doi.org/10.1007/s00259-020-05066-5>.
 38. Dorbala S, Di Carli MF, Delbeke D, Abbara S, DePuey EG, Dilsizian V, et al. SNMMI/ASNC/SCCT guideline for cardiac SPECT/CT and PET/CT 1.0. *J Nucl Med*. 2013;54:1485–507.
 39. Osborne MT, Hulten EA, Murthy VL, Skali H, Taqueti VR, Dorbala S, et al. Patient preparation for cardiac fluorine-18 fluorodeoxyglucose positron emission tomography imaging of inflammation. *J Nucl Cardiol*. 2017;24:86–99.
 40. Juneau D, Golfam M, Hazra S, Erthal F, Zuckier LS, Bernick J, et al. Molecular imaging for the diagnosis of infective endocarditis: a systematic literature review and meta-analysis. *Int J Cardiol*. 2018;253:183–8.
 41. Scholtens AM, van Aarnhem EE, Budde RP. Effect of antibiotics on FDGPET/CT imaging of prosthetic heart valve endocarditis. *Eur Heart J Cardiovasc Imaging*. 2015;16:1223.
 42. Scholtens AM, Swart LE, Verberne HJ, Tanis W, Lam MG, Budde RP. Confounders in FDG-PET/CT imaging of suspected prosthetic valve endocarditis. *JACC Cardiovasc Imaging*. 2016;9:1462–5.
 43. Swart LE, Scholtens AM, Tanis W, Nieman K, Bogers AJJC, Verzijlbergen FJ, Krestin GP, Roos-Hesselink JW, Budde RPJ. 18F-fluorodeoxyglucose positron emission/computed tomography and computed tomography angiography in prosthetic heart valve endocarditis: from guidelines to clinical practice. *Eur Heart J*. 2018;39:3739–49.
 44. Scholtens AM, Budde RPJ, Lam MGEH, Verberne HJ. FDG PET/CT in prosthetic heart valve endocarditis: there is no need to wait. *J Nucl Cardiol*. 2017;24:1540–1.
 45. Swart LE, Gomes A, Scholtens AM, Sinha B, Tanis W, Lam MGEH, van der Vlugt MJ, Streukens SAF, Aarntzen EHJG, Bucierius J, van Assen S, Bleeker-Rovers CP, van Geel PP, Krestin GP, van Melle JP, Roos-Hesselink JW, Slart RHJA, Glaudemans AWJM, Budde RPJ. Improving the diagnostic performance of 18F-Fluorodeoxyglucose positron-emission tomography/computed tomography in prosthetic heart valve endocarditis. *Circulation*. 2018;138:1412–27.

46. Mathieu C, Mikäil N, Benali K, Iung B, Duval X, Nataf P, Jondeau G, Hyafil F, Le Guludec D, Rouzet F. Characterization of (18) F-Fluorodeoxyglucose uptake pattern in noninfected prosthetic heart valves. *Circ Cardiovasc Imaging*. 2017;10:e005585.
47. Pizzi MN, Roque A, Fernández-Hidalgo N, Cuéllar-Calabria H, Ferreira-González I, González-Alujas MT, et al. Improving the diagnosis of infective endocarditis in prosthetic valves and intracardiac devices with 18F-fluorodeoxyglucose positron emission tomography/computed tomography angiography: initial results at an infective endocarditis referral center. *Circulation*. 2015;132:1113–26.
48. Scholtens AM, Swart LE, Kolste HJT, Budde RPJ, Lam MGEH, Verberne HJ. Standardized uptake values in FDG PET/CT for prosthetic heart valve endocarditis: a call for standardization. *J Nucl Cardiol*. 2018;25:2084–91.
49. Salomäki SP, Saraste A, Kemppainen J, Bax JJ, Knuuti J, Nuutila P, Seppänen M, Roivainen A, Airaksinen J, Pirilä L, Oksi J, Hohenthal U. 18F-FDG positron emission tomography/computed tomography in infective endocarditis. *J Nucl Cardiol*. 2017;24:195–206.
50. Asmar A, Ozcan C, Diederichsen AC, Thomassen A, Gill S. Clinical impact of 18F-FDG-PET/CT in the extra cardiac work-up of patients with infective endocarditis. *Eur Heart J Cardiovasc Imaging*. 2014;15:1013–9.
51. Van Riet J, Hill EE, Gheysens O, Dymarkowski S, Herregods MC, Herijgers P, et al. (18) F-FDG PET/CT for early detection of embolism and metastatic infection in patients with infective endocarditis. *Eur J Nucl Med Mol Imaging*. 2010;37:1189–97.
52. Bonfiglioli R, Nanni C, Morigi JJ, Graziosi M, Trapani F, Bartoletti M, et al. 18F-FDG PET/CT diagnosis of unexpected extracardiac septic embolisms in patients with suspected cardiac endocarditis. *Eur J Nucl Med Mol Imaging*. 2013;40:1190–6.
53. Kestler M, Munoz P, Rodriguez-Creixems M, Rotger A, Jimenez-Requena F, Mari A, et al. Role of (18)F-FDG PET in patients with infectious endocarditis. *J Nucl Med*. 2014;55:1093–8.